The scale free and scale - bound properties of land surfaces: fractal analysis and specific geomorphometry from digital terrain models

Colin John McClean

Abstract

Colin John McClean

The scale - free and scale - bound properties of land surfaces:

Fractal analysis and specific geomorphometry from digital terrain models.

The scale-bound view of landsurfaces, being an assemblage of certain landforms, occurring within limited scale ranges, has been challenged by the scale-free characteristics of fractal geometry. This thesis assesses the fractal model by examining the irregularity of landsurface form, for the self-affine behaviour present in fractional Brownian surfaces.

Different methods for detecting self-affine behaviour in surfaces are considered and of these the variogram technique is shown to be the most effective. It produces the best results of two methods tested on simulated surfaces, with known fractal properties. The algorithm used has been adapted to consider log (altitude variance) over a sample of log (distances) for: complete surfaces; subareas within surfaces; separate directions within surfaces.

Twenty seven digital elevation models of landsurfaces are re-examined for self-affine behaviour. The variogram results for complete surfaces show that none of these are self-affine over the scale range considered. This is because of dominant slope lengths and regular valley spacing within areas. For similar reasons subarea analysis produces the non-fractal behaviour of markedly different variograms for separate subareas. The linearity of landforms in many areas, is detected by the variograms for separate directions. This indicates that the roughness of landsurfaces is anisotropic, unlike that of fractal surfaces.

Because of difficulties in extracting particular landforms from their landsurfaces, no clear links between fractal behaviour, and landform size distribution could be established.

A comparative study shows the geomorphometric parameters of fractal surfaces to vary with fractal dimension, while the geomorphometry of landsurfaces varies with the landforms present. Fractal dimensions estimated from landsurfaces do not correlate with geomorphometric parameters.

From the results of this study, real landsurfaces would not appear to be scale-free. Therefore, a scale-bound approach towards landsurfaces would seem to be more appropriate to geomorphology than the fractal alternative.

The scale - free and scale - bound properties of land surfaces:

Fractal analysis and specific geomorphometry from digital terrain models.

Colin John McClean

Ph.D Thesis

UNIVERSITY OF DURHAM

Department of Geography

September 1990

Table of Contents

List of Tables and Illustrations

Declaration and Copyright Statement

The material contained in this thesis has not been previously submitted for a degree in this or any other university.

Signed

Date

Acknowledgements

My first thanks must go to Jim Waddington for his remarkable skill at wielding a Macintosh and his patience with my slow progress over the past month.

Second thanks must go to my father for putting me in touch with Jim, and also a few diagrams and a bit of printing he helped me with.

Thirdly I must thank my sister for being a better dictionary than most commercially available word processing packages.

My mother, as usual, fed me.

Further thanks must go to my family for encouraging me in all the activities I have been involved in over the years.

Ian Evans and Nick Cox must be thanked for being patient supervisors who have always been available for advice.

Sinclair Sutherland, Simon Hook and other remote sensors from Durham must be thanked for their initial help with the computing facilities in Durham.

All the past occupants of 3 Union Place (and at least one of the present ones) should be blamed for any mistakes in this thesis. However they must also be thanked for making my stay in Durham a very enjoyable one.

Finally, my current colleagues and housemates in Cardiff must be thanked for their understanding of my situation.

Chapter 1: Introduction

1.1 Introduction.

This thesis looks at the appropriateness of using fractal geometry in one field of the geosciences, geomorphology. Over the past decade fractal geometry has increasingly been hailed as an important base to chaos theory: a new way of looking at the irregularities of phenomena from subjects "*spanning the breadth of science*" (The Independent,5/6/89). However, at the heart of this thesis lies a series of dichotomies that has disturbed geomorphologists for a much longer period of time. The most important of these dichotomies is that between the use of stochastic models based on random processes and the use of deterministic models based on physical processes.

"*...many patterns of nature are so irregular and fragmented, that, compared with Euclid - a term used in this work to denote all of standard geometry - nature exhibits not simply a higher degree but an altogether different level of complexity.*" (Mandelbrot, 1982, p.1). Most geomorphologists would agree that landsurfaces and forms are indeed complex. Furthermore graphical representations of landscapes using fractal geometry have a definite visual resemblance to real landscapes. However should a model based on stochastic rather than physical processes be adopted to describe the surfaces and forms geomorphology studies?

This dichotomy if considered further, and in the direction of form rather than process, leads to the discussion of whether or not landsurfaces should be subdivided into separate landforms. Ideally geomorphologists would like to be able to state that a certain set of physical processes produces a particular landform type. However because of the complexities of geomorphic systems, in both form, process and time, subclassification of landforms has had to involve at least some degree of subjectivity on the part of the interested geomorphologist. An extreme reaction to the complexities of geomorphic systems would be to turn away from the geomorphologist's ideal situation and treat landscapes as continuous rough surfaces and use whatever statistical methods become available to describe and model them. The bulk of modern geomorphological study lies somewhere between these two extremes. Deterministic models have been used alongside stochastic models in the study of many geomorphic systems. However, the use of fractal geometry, championed by Mandelbrot(1977,1982), lies towards the stochastic extreme of this debate.

1.2 Random Landsurfaces versus Deterministic Landforms.

Chorley reviews the dichotomy as early as 1967. In his discussion of the methodological issues raised by the new techniques being increasingly introduced to geomorphology, he looked at both deterministic and stochastic mathematical models (Chorley 1967). His definition of deterministic models refers to the main attractions of this type of model: "*deterministic mathematical models are based on classical mathematical notations of exactly predictable relationships between independent and dependent variables (i.e. between cause and effect), and consist of a set of exactly specified mathematical assertions (derived from experience or intuition) from which unique consequences can be derived by logical mathematical argumentation. Such models are thus intimately concerned with relationships and 'driving forces' between factors identified in the simplified model.*" (Chorley, 1967, p. 69).

It is the disadvantages of deterministic models, however, which led to the development of chaos theory and fractal geometry. The disadvantages of these models in geomorphology are again well appreciated in Chorley's discussion: "*However few deterministic statements can completely specify all the variables included in a complex natural situation, so that discrepancies occur which, together with the random unpredictable effects inherent in natural processes, combine to produce 'noise' which tends to obscure the simpler deterministic relationships. Often these random effects are so important in determining the result of natural processes that partly or wholly statistical (stochastic) models have to be constructed to take account of them.*" (Chorley, 1967, p.72).

By the early 1980s the dichotomy was still cause for discussion in geomorphology, although as Thornes and Ferguson (1981) pointed out, in their review of the adoption of quantitative methods in the subject, there had been work where parts of a system were modelled deterministically while other parts of the system were modelled stochastically. Thornes and Ferguson (1981) structure their discussion by looking at progress made in handling three categories of system. The first are simple systems which involve a maximum of three or four variables and tend to lend themselves to deterministic approaches. The other two system types, systems of complex disorder and systems of complex order, are where the use of stochastic models becomes important. In the case of models of complex disorder there are three areas which have led to the adoption of probabilistic ways of looking at landform development: the behaviour of ideal closed and open systems (Chorley, 1962); the randomness of geomorphic processes at the particle scale (Culling, 1963); and the apparent randomness caused by a large number of deterministic relationships interacting to produce a complex landscape system (Leopold and Langbein, 1963).

The classification of Thornes and Ferguson allows each type of system to merge into the other two and although stochastic processes may be used to add input into the more deterministically modelled parts of a system (Kirkby,1986), the major need for stochastic processes in modelling remains clear. Complexity, whether ordered or disordered, provides the reason for the attractiveness of stochastic modelling. The complexity of a system at its least extreme may, as Thornes and Ferguson suggest, demand the use of stochastic constraints to allow a solution when modelling using predominantly deterministic methods. At the other extreme the stochastic process may be used at the heart of the explanation of a process such as with Culling's work on soil creep at the scale of individual soil particles. The major problem of using these processes is testing the results of the subsequent simulations. Simulated results should be compared with empirically observed results.

Before discussing the ideas behind the fractal model it is interesting to note the comments of two geomorphologists at around the time the use of fractal geometry was beginning to become widespread, "*...but there is still ample scope in geomorphology for the development or importation of new techniques and there is certainly willingness to recognise the complexity of earth surface systems.*" (Thornes and Ferguson, 1981, p.285).

1.3 Fractals

Fractal geometry is a new technique in geomorphology, mainly imported from outside the discipline, but partially inspired by exactly the complexity of earth surface systems described above. Although Mandelbrot has developed the mathematical basis of fractal geometry from classical geometry and some of the long standing puzzles in it, the complexity of nature seems to have provided much of the inspiration for his new approach. "*Why is geometry often described as 'cold' and 'dry'? One reason lies in its inability to describe the shape of a cloud, a mountain, a coastline, or a tree. Clouds are not spheres, mountains are not cones, coastlines are not circles...*" (Mandelbrot, 1982, p.1). As a result of such questioning Mandelbrot has developed certain concepts that challenge the geomorphologist to look at the same complex systems in a different light. The fractal approach accepts the irregularity in the forms found in nature and seeks to quantify that irregularity.

There are two main themes in the fractal geometry which will be used in this thesis. One is irregularity. Mandelbrot suggests that the lines found in nature, for example coastlines and contours, are not 'rectifiable'. That is they are so irregular that to try and measure their length in the same way as the line understood in classical mathematics is pointless. A straight line or the circumference of a circle have an easily found precise length. If an irregular coastline's length is measured the result will depend

on the scale at which the coastline is considered. If the coastline is considered at a larger scale, more irregularity in its form must be taken into account than at a smaller scale, and the resulting length will be longer than the result found at a smaller scale (fig. 1.1).

Although fractals do not have to be irregular shapes, Mandelbrot himself states that the most useful fractals involve chance. It is therefore the irregularity of the fractal surfaces which have been created as simulations of real landsurfaces that is of interest in this study. The second theme of interest in fractal geometry in this work is the peculiar way in which the irregularity of such fractals behave.

Perhaps the most concise and simple definition of a fractal is provided by Mandelbrot in Feder (1988, p.11), "*A fractal is a shape made of parts similar to the whole in some way*". It is the similarity of the parts to the whole which makes the irregularity of the fractals considered here to be peculiar. This scaling behaviour of the irregularity or self-similarity as it has become known will be discussed more fully in Chapter 2, but it is relevant to explain the idea simply at this stage so that its likely implications for geomorphology can be discussed.

If a fractal line is considered, its irregularity at one scale is the same as the irregularity of part of that line magnified. Mandelbrot's early discussion of coastlines as possible fractals implies that the shape of a coastline viewed at one scale is similar to the shape of a smaller part of that coastline viewed at a greater magnification (Mandelbrot, 1967). Mandelbrot also suggests that this applies to cross-sections of the earth's relief and indeed the surfaces from which such cross sections come (Mandelbrot, 1975). It would therefore be difficult to distinguish the whole surface from smaller parts of it viewed at a larger scale.

This implies that if a real landsurface such as the one shown in Figure 1.2 is fractal, and it is then studied at a higher resolution, the irregularity revealed at that resolution should be statistically self-similar to the irregularity displayed in Figure 1.2. Figure 1.2 shows the surface at 300m grid mesh resolution. Figure 1.3 shows the same surface at a 100m grid mesh resolution. The question is, does the surface viewed at higher resolution reveal added irregularity to the degree necessary to be self-similar?

Figure 1.1 (a) Coastline at large scale.

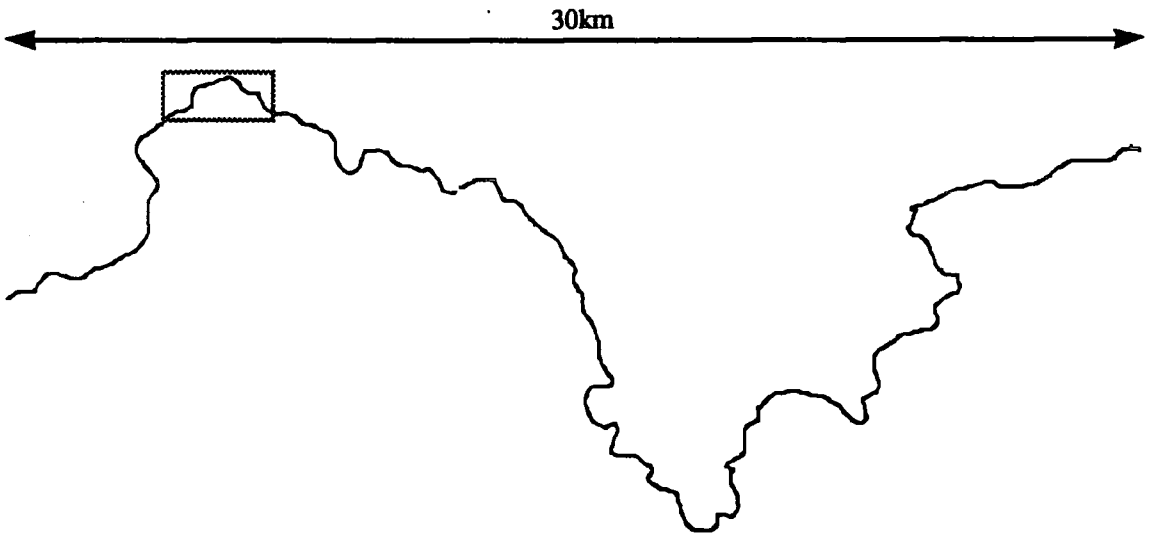

(b) Segment of coastline from box in (a) at a smaller scale. Similar irregularities are shown at both scales.

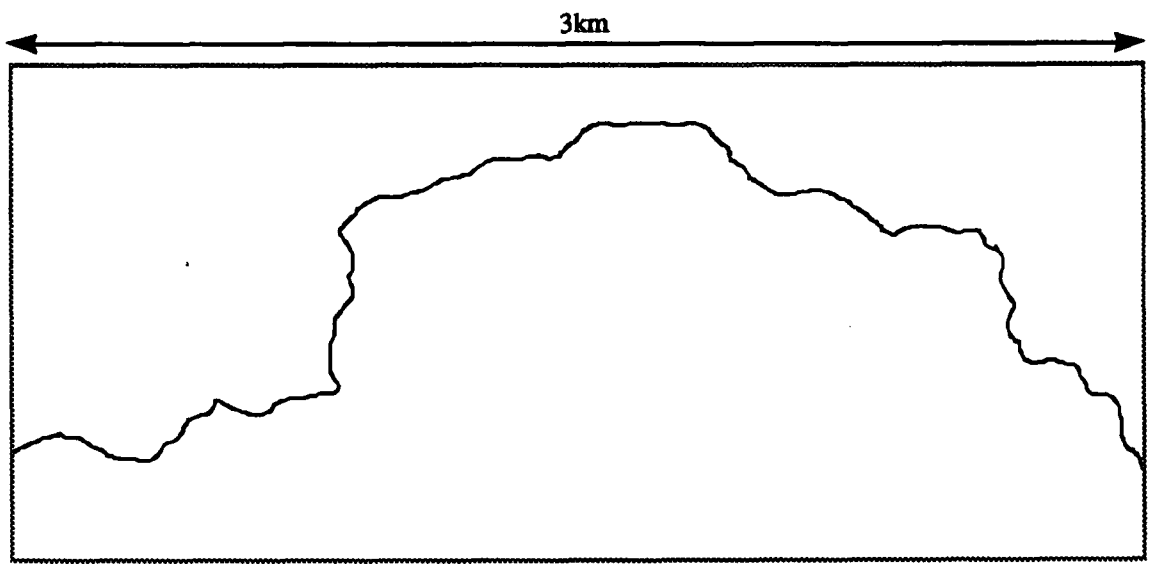

Figure 1.2 Representation of a landsurface using 300m grid mesh resolution.

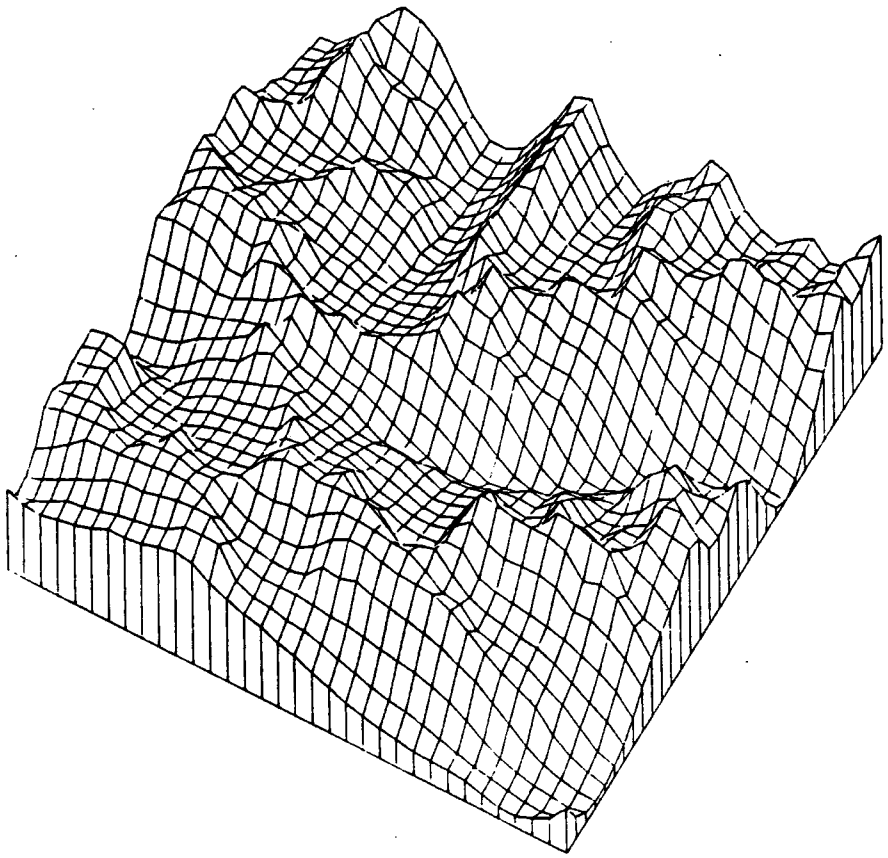

Figure 1.3 Representation of a landsurface using 100m grid mesh resolution.

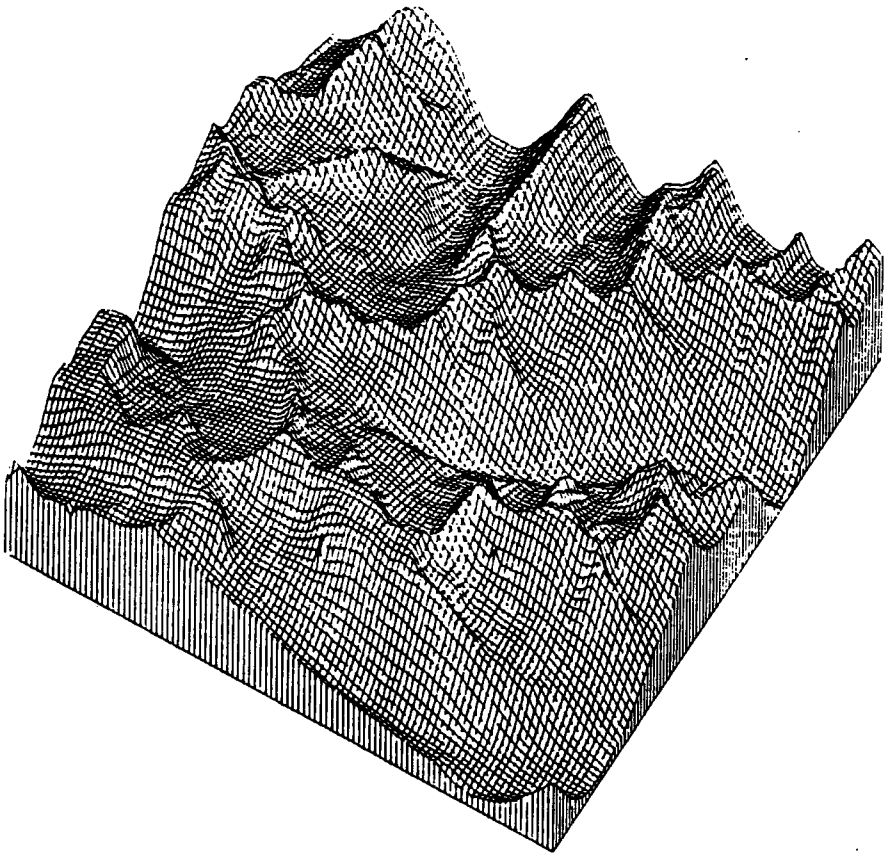

At this point it can already be seen that the concept of self-similarity challenges many ideas in geomorphology. Certainly it is in conflict with the geomorphologist's practice of landform delimitation. Most geomorphologists would agree that landforms such as cirques or drumlins exist within a limited scale range. Therefore from their perspective it is difficult to see landforms as being elements of surface roughness which are similar in roughness to landscape features at different scales. As a result a closer look at geomorphologists' treatment of scale must be taken to see if there is any agreement between the concept of self-similarity and the classification of subunits in landsurfaces into landforms.

1.4 Scale in Geomorphology.

Mark (1980) makes several interesting comments about the scales at which geomorphologists have traditionally worked. He mentions a dichotomy between 'landscape-scale geomorphology' and 'process geomorphology'. On elaboration, this dichotomy can be seen to have similar roots to the dichotomy already discussed. The 'landscape scale' referred to is the scale at which landforms can be identified from medium scale topographic maps. The map scale of 1:50000 is used as Mark's example, although landforms identified from 1:25000 or 1:10000 maps would also fall into this category and indeed such maps have been used in this study to create digital elevation models (DEMs).

Process geomorphology on the other hand has tended to focus on smaller sized features, Mark (1980) uses the example of channel cross sections. As its title suggests 'process' geomorphology often attempts to understand physical processes. In this respect it is closely linked to deterministic models.

Examples of areas where work is currently carried out at the landscape scale are given by Mark as glacial geomorphology and drainage basin morphometry. This is interesting because many of the landsurfaces which will provide empirical data for this study have been received from workers in the two fields mentioned.

Much of the work at the landscape scale has been 'descriptive' as Mark puts it. Although Mark does except drainage basin morphometry from this classification it must be noted that morphometry in general is 'describing' forms by using numbers. Therefore, although it is intuitively thought that many of the variables measured in geomorphometry have an important effect on processes as studied in process geomorphology, the two separate areas of work have "*not yet been successfully linked*" (Mark, 1980, p.81).

The final interesting comment made by Mark is that the quantitative techniques used at the landscape scale have often been based on models with a 'randomness' component. This of course brings the discussion back to the use of stochastic models and all the problems associated with the previously discussed dichotomy. Initial and boundary conditions are generally not known for real landsurfaces thus at least a certain random component is often added when considering such conditions. On the other hand, Mark suggests that individual physical processes place narrow constraints on the possible forms at the landscape-scale. Therefore limitations in the understanding of process geomorphology mean that it cannot, as yet, explain the complexity of form measured in the landscape scale. Although there is a difference of scale between these two sides of this dichotomy there is a general desire to bridge the gap. This dichotomy is not, therefore, necessarily evidence against the concept of self similarity, and it certainly takes into account the complexity of form.

The closest geomorphologists came to applying concepts of self-similarity before the emergence of fractal geometry was the use of allometric analysis (Bull, 1975; Cox,1977; Church and Mark, 1980). Allometric analysis is the study of how forms in a system vary in comparison with one another with size. Although Cox (1977) has cited several problems when using allometric analysis in geomorphology, it is of interest here as it considers the effect of scale in geomorphology. It detects 'scale-related' distortions of geometry. Church and Mark suggest that this is the opposite of what they call 'self-similarity', a state of constant proportion between the forms of parts of a system. They also describe this as 'isometry' which may be a more appropriate term as certain allometric relationships have subsequently been discussed as exhibiting self-similarity in fractal terms.

In their discussion Church and Mark use the abundant work on the relationships between the dimensions associated with alluvial fans and their source drainage basin characteristics (e.g. Bull, 1975) as examples. They also refer to work on the relationships between the different measures of drainage basin dimension (e.g. Hack, 1957). This study of the unbalanced change of such forms with scale is carried out with the eventual aim of uncovering possible mechanisms, physical processes, which cause the non-linearity of these relationships between form.

Of the two types of allometric analysis described by Church and Mark (1980), dynamic and static, it is static allometry which is of most interest in this discussion. Dynamic allometry looks at the change in form relationships of one individual landform with scale over time. This is clearly rather difficult in the case of many landforms because of the nature of the geomorphic time scale. Static allometry takes data from as large a sample of a particular landform type as possible and then looks at the changes of form with scale. This approach expects the phenomenon under examination to exist

over a wide enough range of scales to justify any relationship obtained. For example, Church and Mark (1980) discover from looking at several different works on alluvial fan gradient that the associated basins range in area from 0.11km^2 to 760km^2. This possibility that landforms of similar shape can occur in a wide range of sizes seems intuitively to be evidence in support of Mandelbrot's concept of landsurfaces displaying self-similarity. However it must be remembered that in the cases where landforms exist over a wide scale range, the sample of landforms may be from several diverse areas. The above example of drainage basins involves a sample from a very large area of North America. The range in size of a certain landform type in one limited area may be much smaller.

Allometric analysis in geomorphology is another example of quantitative research at the landscape scale and indeed much of the analysis in this study will also take place at this scale. This is because the resolutions of DEMs used in this study are in general at the landscape scale. It is therefore appropriate to look at the way geomorphology has described form at this scale.

1.5 Geomorphometry

Workers in the field of geomorphometry have accepted when dealing with landsurfaces rather than landforms, general rather than specific geomorphometry, that landsurfaces are rough. As a result a number of indices have been developed to consider surface roughness. Many workers have, as Mark (1975) points out, realised that roughness cannot be completely defined by any single measure. It must be represented by a 'roughness vector' (Mark, 1975) or by a set of parameters considered jointly. This appreciation of irregularity in geomorphometry is an immediate point of agreement between fractal concepts and attempts to quantitatively describe landscape form. However geomorphologists have clearly sought to provide reasons for why such surfaces have different degrees and types of roughness. Mark (1975) mentions reasons such as irregularity of ridge spacing and differing sharpness of ridges.

Another point of agreement between geomorphometry's attempts to characterise landsurfaces and Mandelbrot's view on landsurfaces is the use of spectra, at least as an analogy, in dealing with ridges and valleys as crests and troughs of wave forms. Evans (1972; 1979) suggested that spectral analysis of landsurfaces has not been particularly successful because of the valleys' curved courses and the convergence of valleys down stream. Mark (1975) points out that the analogy between waves, ridges and valleys is useful for structuring discussion of geomorphometry. Mandelbrot (1975) uses the electrical engineering terms signal and noise in considering landsurfaces. Chapter 2 will explain how important noises are to the fractal model. Following the example of Wood and Snell (1960), Mark (1975) associated the geomorphometric concepts of 'grain' and

'texture' to wavelength. The concept of relief is linked to the idea of wave amplitude. The first two of these parameters, grain and texture, illustrate the way in which geomorphometry treats scale.

Texture, as considered by Mark, is the "*shortest significant wavelength in the topography*" (Mark, 1975, p.166). He also states "*Texture is related to the smallest landform element one wishes to detect*" (Mark, 1975, p.166). This view clearly points at the idea of landform delimitation determining the scale of study, by reference to the probable processes working.

The 'texture ratio' is also a specific geomorphometric parameter (Smith, 1950) and is defined as

$$T = \frac{N}{P}$$

where N is the number of contour crenulations on a particular contour and P is the perimeter of the drainage basin under consideration in miles. As a parameter it also deals with smaller features of the surface, taking into account small crenulations. This parameter does not require the definite subjective decision of what size of landform should be the lower limit of the study; however it would be affected by the scale of map chosen for the analysis.

Grain, as defined by Mark (1975, p.166), is the "*longest significant wavelength*" in the topography. He discusses the method of Wood and Snell (1960) to calculate the grain of the topography. They used the change of local relief with increasing area to detect the grain. Local relief is the difference between the highest and lowest altitudes of any given area. To obtain a plot of local relief against increasing distance Wood and Snell used concentric circles around a randomly-located point within their area of interest. When the local relief for each concentric circle was plotted against the diameter of the circle, Wood and Snell found that in general there was a 'knick-point' where the rate of increase in local relief with distance would slow. This distance was taken as the 'grain' of the topography. They did acknowledge that this method is not very precise; however their method does anticipate that for most landsurfaces the increase in local relief with distance will decrease after a distance related to the average slope length of the valleys in the area. This search for a knick-point assumes that for a given area there will be a certain limited distribution of slope lengths which would not be in agreement with the fractal model's requirement of self-similarity.

The measure of local relief discussed above is just one of many measures of relief. Relief is a term applied to the description of the vertical extent of topography. Mark (1975) suggests that it can be considered as the amplitude of the topography.

Ahnert (1984, p.1035) points out that it is "*a crude indicator of potential gravitational energy available for denudation*". There is an appreciation within the field of geomorphometry that the scale at which relief is measured has an important influence on its value. Evans (1972) points out that local relief must be measured over a large enough area to avoid merely estimating the gradient of one large slope. This corresponds to Mark's (1975) assertion that most parameters, such as local relief, must be calculated for areas containing distances greater than the grain of the topography. This is again a scale bound view based on the geomorphologist's empirical observation that local topography will have a noticeable grain.

Probably the most important quantity studied in geomorphometry is slope. Evans (1980) explains that slope is a vector quantity, with both a magnitude and a direction. He logically describes the magnitude as gradient and the direction as aspect. Slope is the geomorphometric quantity that can be seen immediately to have some control on geomorphic processes. As Evans (1972, p.36) points out "*slope angles control the gravitational force available for geomorphic work*".

Theoretically, gradient is a continuous variable. However, unless a mathematical surface is fitted to the area, gradient must be measured as the change in altitude over some finite horizontal distance. This means that the only theoretical scale limitations to the use of slope are the contour interval used on a map from which gradient is estimated or the grid mesh of a DEM from which gradient is measured.

Evans (1972,1979,1980) also proposes the use of the first derivative of slope. This gives a measure of the landsurface curvature. There are two components of this curvature. One is the rate of change of gradient with distance, termed profile convexity; the other is the rate of change of aspect with distance, termed plan convexity. These measures are also continuous and are subject to the same scale limitations as the slope measurements. Slope and its derivative will be more fully discussed in Chapter 7 where they will be used in a geomorphometric study of the surfaces used in this thesis.

The study of the distribution of landmass with elevation is described as hypsometry and several relationships and parameters can be calculated to describe various aspects of this. All of these are obtained by initially determining what area of landsurface lies at a particular elevation.

Most of the parameters briefly discussed here are measurements of changes in altitude with reference to changes in some other dimension of the landsurface. It will be seen in Chapter 2, when the fractal model is discussed at length, that such relationships for fractal surfaces are limited by certain constraints. The question arises, do real landsurfaces exhibit the same constraints and behaviour?

Ahnert (1984) has brushed against this question from the side of geomorphometry as opposed to from the fractal geometry side. Studying the local relief of 25 topographic maps from Germany, Austria, Switzerland, Scotland and Kenya, he makes some discoveries which have bearing on this study. He first looked at the relationship between local relief and the diameter of the area over which local relief was measured. As expected local relief increases with diameter. The form of the relationship for each area was a power function

$$H = aL^b$$

where H is local relief and L is the diameter of the area under consideration. He calculated local relief with various shapes of area and also along linear profiles. Comparing the various regression lines fitting the form of the above equation, he found that all the regression lines crossed each other near a common point. He described the relief at this point as the 'characteristic relief' of the area, and the diameter or length at this point as the characteristic length. This prompted further investigation of the coefficients and parameters obtained form the above relationship and although some of the analysis seems inappropriate it led Ahnert to follow one further line of investigation.By referring to the heights of the highest summits of major mountain ranges and their distance from their nearest forelands, he found that, as might be expected, wide mountain ranges can become higher than narrow ones. He attempts to explain this "*height-limit rule*" (Ahnert, 1984, p.1050) with reference to tectonic and denudational process rates. However, in this study it is the form of the height-limit rule itself that is of interest as it bears remarkable similarity to some of the relationships exhibited by certain fractal processes which will be discussed in subsequent chapters.

Clearly much geomorphometric analysis involves quite laborious algorithms. Computers have been used quite widely in the field to automate as many of these algorithms as possible. One specific program calculating gradient, aspect and their derivatives is described in Chapter 7 where it is used in a geomorphometric study of the surfaces considered in this thesis.

Reference has already been made to digital elevation models (DEMs). These are merely computer-readable representations of the landsurface. Altitudes of selected points from the landsurface are recorded as numbers in a computer file. Chapter 3 gives some discussion of the different types of DEM which can be produced as well as explaining the process of creating a gridded DEM. Gridded DEMs are the preferred type of model in this study. The elevations are held as a regular grid of points interpolated from the landsurface. These models can be easily manipulated to search for signs within them of self-similarity and are also compatible with models simulated using fractal process.

1.6 Questions Raised.

The fractal model has been introduced as an extreme of stochastic modelling techniques with which to model landsurface form. This has been presented against a background of the geomorphologist's desire to explain form in terms of physical processes and therefore, to a degree, the geomorphologist's preference for deterministic modelling. However in discussing geomorphology's progress in modelling, and views towards scale and approaches taken in geomorphometry, certain common concepts can be found between the fractal model and previous geomorphic thought.

The complexity of geomorphic forms and systems is clearly appreciated by geomorphologists and this irregularity is at the heart of the fractal model. Scale has for a long time been seen as an important variable in studying form and process and there is an appreciation that some landforms may be found over quite a wide range of scales and therefore the idea of self-similarity is not completely alien to geomorphology. However, self-similarity is still the obvious problem area when considering the appropriateness of the fractal model in geomorphological study.

The major question that must be asked in this study, therefore, becomes: are real landsurfaces self-similar? This question may be weakened to: are there any signs of self-similarity in any real landsurface? This is almost the inverse of a question about fractal surfaces which must also be studied. Do fractal surfaces exhibit the same geomorphometric properties as real landsurfaces?

The first of these questions is initially more approachable, as the statistical properties of fractals are well defined. Therefore it can be envisaged that devising tests for the same statistical properties in real landsurfaces should be relatively simple. Several studies have done this already (Goodchild,1982; Mark and Aronson, 1984; Roy et al.,1987). However the number of surfaces actually studied is small and they are mainly in North America. Mark and Aronson (1984) actually cite the need for further empirical analysis. There is still ample room in the field for studying different surfaces. In fact, this is the major limitation of this approach. There are many different landsurface types on the Earth's surface and to obtain models of them all and to test them all for fractal behaviour would be a very sizeable task.

The second question mentioned therefore becomes interesting. The processes which may be used to simulate fractal surfaces are now well defined (Feder, 1988; Peitgen and Saupe, 1988) and many programs and readily implementable algorithms exist for geomorphometric study. This means that the full range of fractal surfaces of varying degrees of roughness can be simulated and then analyzed as real landsurfaces have been in geomorphometry. The limitations of this approach would also be that the

geomorphometry of all landsurface types is not fully understood. Attempts will be made in this study to look at both of these questions because regardless of the limitations discussed, any work in this direction provides further evidence for or against the appropriateness of the fractal model to geomorphology.

A further issue that can be addressed is that of how the concept of self-similarity relates to the size distributions of individual landforms. Do landforms exist as a continuum through a wide range of scales? Can a surface dominated by one type of landform show any signs of fractal behaviour? Again, to test size distributions for all landform type would be impossible, so in this study empirical tests will only be carried out on certain landsurfaces.

As Chapter 2 will go on to explain, the properties of fractal surfaces are such that certain parameters associated with them can be calculated. One of these is of particular importance. The fractal dimension, as it is termed, is related to the complexity and roughness of the surface. In some respects it is similar to the geomorphometric parameters discussed above. It would therefore be interesting to see what use this parameter is in describing the form of real landsurfaces. This will of course depend on how close real landsurfaces are to fractal surfaces.

1.7 Thesis Structure

Having outlined the main questions which this work must address, the approach can now be discussed along with an explanation of the structure of this thesis.

Chapter 2 as has already been mentioned will deal in depth with the fractal geometry necessary to this study. This includes a more rigorous and mathematical explanation of self-similarity. The concept of fractal dimension will be fully explained. A class of fractal processes that are of the most use to the study of landsurfaces, fractional Brownian noises, will be introduced. Throughout the chapter a discussion of some of the relevant empirical studies carried out in the earth sciences will be given.

Before explaining the methods and algorithms to be used in this study it is necessary to introduce the way in which landsurfaces have been modelled in this study. As well as an introduction to digital elevation models, Chapter 3 will look closely at how a landsurface of drumlins was captured and converted into a DEM using the best method available given certain resource limitations.

The properties of fractals having been fully explained, Chapter 4 gives an introduction to the algorithms which can be used to study self-similarity and fractal dimension in the study of landsurfaces. The usefulness of the variogram will become apparent as will the limitations of some other methods. This is followed by a description

of the implementation of these algorithms in the programs used in the thesis. Algorithms for actually simulating fractal surfaces will also be discussed and a program to apply one of these algorithms will be explained.

The programs described in Chapter 4 can now be tested and used on the simulated fractal surfaces both as a check on the assessment techniques and as a source of information on the simulation algorithm. Chapter 5 discusses the results of using the above programs on simulated fractal surfaces.

Chapter 6 discusses the fractal nature of real landsurfaces. This chapter follows a similar pattern to the previous chapter, the difference being that the results being discussed are for real landsurfaces. This chapter attempts to answer the first major question mentioned above (are real landsurfaces self-similar?) in the light of the finer detail of the fractal model explained in Chapter 2.

The second question posed above was, do fractal surfaces exhibit the same geomorphometry as real landsurfaces? Chapter 7 deals with this question by looking at both the geomorphometry of fractal surfaces and the real surfaces studied. As well as attempting to answer this question a study of the geomorphometry of the real landsurfaces may cast light on any discrepancies between the fractal model and real landsurfaces revealed in Chapter 6. The geomorphometric parameters calculated for both real and simulated surfaces are also compared with the fractal dimensions from these surfaces in an attempt to assess the usefulness of fractal dimension as a geomorphometric parameter.

To assess whether or not landsurfaces dominated by one landform type can display self-similarity and to see if the landform type of the surface displays a wide range of sizes of the landform the DEM of an area of drumlins created in Chapter 3 and two other landsurfaces are analysed. Chapter 8 looks at the geomorphometry and size distribution of individual landforms identified from these DEMs. Comparison of these results with the fractal model allows a discussion of how well the concept of individual landform types may fit with the fractal model.

The conclusions are presented in Chapter 9, where an overview of the relevance of all the results obtained and discussed can be brought together for a debate based on the questions proposed above.

Chapter 2: Fractals

2.1 Introduction

'Fractal' has become a familiar word in many branches of science as the uses of fractal geometry are evaluated. As a result most papers dealing with fractals have started off with some definition of what a fractal is before a more rigorous examination of the particular phenomenon that seems to lend itself to analysis using fractal geometry. Many of these papers use the definition of Mandelbrot (1982, p.15): "*A fractal is by definition a set for which the Hausdorff-Besicovitch dimension strictly exceeds the topological dimension*". This is then followed by its explanation in relatively simple terms, normally involving an introduction to fractal dimension and self-similarity. However with the increase of investigation into the uses of fractal geometry, there has been an increase in the number of books which explain fractals and the development of ideas about them (Mandelbrot, 1977 and 1982; Falconer, 1985; Barnsley, 1988; Feder, 1988). This background coverage of fractals frees this study to focus on the concepts relevant to the examination of landsurfaces, landforms and other geophysical phenomena with a direct bearing on the subject of this thesis.

The definition of a fractal which is most relevant to this study is the one by Mandelbrot mentioned in Chapter 1: "*A fractal is a shape made of parts similar to the whole in some way*" (Feder, 1988, p.11). This chapter shall introduce the concept of fractal dimension via an explanation of the Hausdorff-Besicovitch dimension. Then Brownian motion and random walks will be considered, introducing the possibility of self-similar and self-affine fractals. This leads to a discussion of fractional Brownian motions which are the processes which have been proposed as realistic models of landsurfaces, coastlines and many other geophysical phenomena (Mandelbrot, 1975; Mandelbrot and Wallis 1968 and 1969a-e). The rest of the chapter shall be given over to a discussion of the work which has been carried out on investigating the applicability of these processes in various fields of research close to this study.

2.2 Fractal Dimension

As Feder (1988) demonstrates it is perhaps easiest to investigate the concepts of dimension by considering the size of a set of points in space. The size of a set of points might in the case of a line be its length or in the case of a surface its area. Figure 2.1 shows some measures of the size of a line and a surface to illustrate the following discussion.

Figure 2.1: Measuring the size of: (a) lines ,(b) surfaces (after Feder,1988).

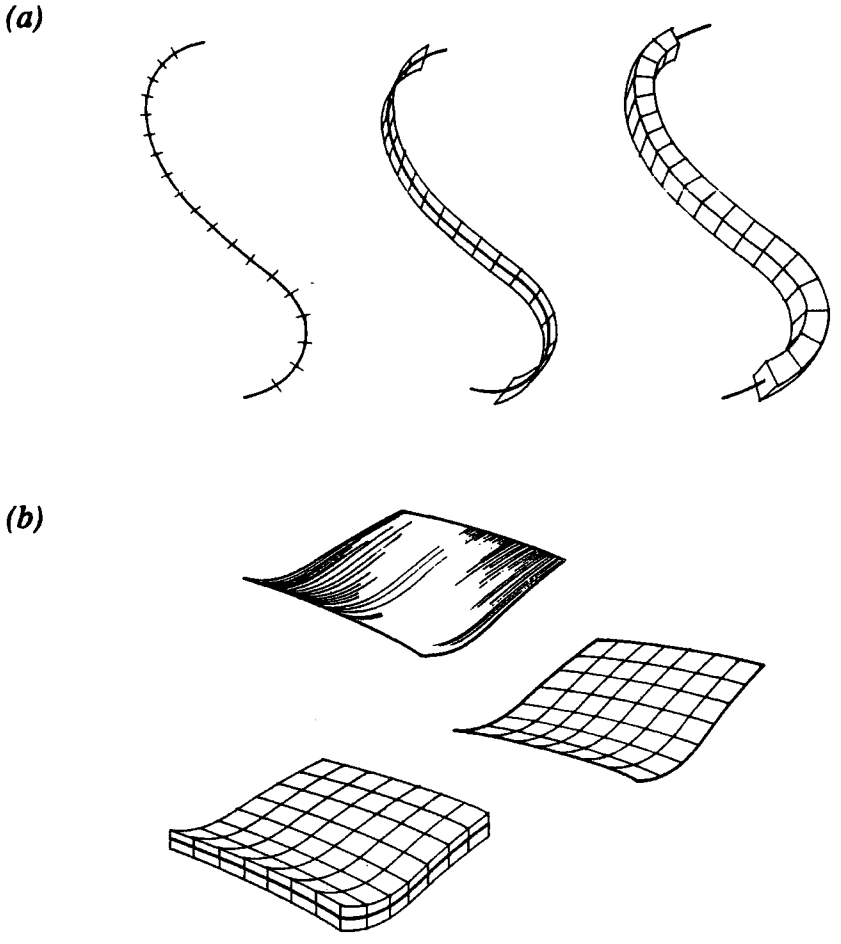

One measure of the size of a smooth curve is its length which can be measured in the following way. Using a line segment of a known length δ, the number $N(\delta)$ of such segments needed to cover the curve can be found. A measure of the curve's length is therefore:

$$L = N(\delta)\delta$$

as δ tends towards zero the measure of the length becomes asymptotically equal to the curve's true length L_0 and is independent of δ. Therefore:

$$L = N(\delta)\delta \xrightarrow[\delta \to 0]{} L_0\delta^0 \tag{2.1}$$

Another measure of the size of the set of points could be to associate an area with the curve. To measure the area of the curve a line segment of known area δ^2 could be used. The number of these segments $N(\delta)$ could again be found, providing a measure of the curve's area, A:

$$A = N(\delta)\delta^2 \xrightarrow[\delta \to 0]{} L_0\delta^1 \tag{2.2}$$

This time the measure of the area becomes asymptotically equal to the true length times δ as δ tends to zero.

Following the same logic a volume, V, can be measured using the segment δ^3 and the following relationships hold:

$$V = N(\delta)\delta^3 \xrightarrow[\delta \to 0]{} L_0\delta^2 \tag{2.3}$$

However, both the area and the volume tend to zero as δ itself tends to zero, leaving the only convenient measure of the set of points as the length of the curve.

Using exactly the same arguments for a set of points that describes a surface it is easy to see that the measure of area is still as for (2.2) but this time as δ vanishes A tends to the true area of the surface A_0:

$$A = N(\delta)\delta^2 \xrightarrow[\delta \to 0]{} A_0\delta^0 \tag{2.4}$$

similarly:

$$V = N(\delta)\delta^3 \xrightarrow[\delta \to 0]{} A_0\delta^1 \tag{2.5}$$

in this case, as for the A and V of the curve, the measure V vanishes as δ tends to zero.

If an attempt is made to go in the opposite direction and find a length for the set of points describing the surface the relationships from the reasoning above would be

$$L = N(\delta)\delta \xrightarrow[\delta \to 0]{} A_0\delta^{-1} \tag{2.6}$$

here L will tend towards infinity as δ vanishes. It is clear from this that the only sensible measure of the size of the set of points defining the surface is the area.

When considering the set of points describing the line, the length was a measure in space of dimension one, and the area was a measure in space of dimension two. Likewise for the set of points defining the surface the area is a measure in two dimensions while the volume is a measure in three dimensions. The Hausdorff-Besicovitch dimension, D, is the dimension of the measure which lies between the dimensions, d, of the measures which tend to zero on one side and infinity on the other:

$$M_d = N(\delta)\delta^d \xrightarrow[\delta \to 0]{} \begin{cases} 0, & d > D; \\ \infty, & d < D. \end{cases} \tag{2.7}$$

where M_d is the measure in the dimension d.

In the cases explained above this concept is relatively straightforward. For the set of points describing the line the appropriate measure has the Hausdorff-Besicovitch dimension 1. The Hausdorff-Besicovitch dimension for the area of the surface is 2. However when considering irregular curves and irregular surfaces as opposed to smooth ones the dimension suggested by the relationship in (2.7) may be a fraction rather than a whole number, hence the term fractal dimension.

Mandelbrot (1967) considered irregular, complicated lines such as the curves found in nature, showing that such curves could be thought of as having fractional dimensions. The example he used following the empirical research of Richardson (1961) was the dimension of a coastline. If such a curve is measured using a line segment of known length as in (2.1) an estimate of the curve's length L is obtained.

Unlike the smooth curve, the measured length L does not tend towards L_0 as δ vanishes. This is because as the curve is measured using smaller and smaller segment lengths more and more details of the line's irregularities are considered and the length estimate therefore increases for smaller δ. It follows from (2.7) that in the limit of small δ (Feder, 1988)

$$N(\delta) \sim \frac{1}{\delta^d} \tag{2.8}$$

Having calculated $N(\delta)$ for a range of values of δ the fractal dimension, D, of the curve can be found by plotting the log of $N(\delta)$ against the log of δ: the slope of the resulting line is therefore $-D$.

2.3 Brownian Motion.

It has been shown that as a result of the irregularity they display at all resolutions natural curves can be thought of as having a fractal dimension. The behaviour of this irregularity is important to the further definition of a fractal and is of particular interest to this study. The statistical properties of Brownian motion are well known and therefore it provides a convenient process to examine in terms of the irregular curves it produces. Mandelbrot (1968, 1969a-e, 1975) suggests that the behaviour of the curves which Brownian motion produces provides a first approximation to the behaviour of the kind of natural curves found in geomorphology.

One of the first science lessons learnt in school is how a pollen grain in water moves continually as it collides with water and other molecules which are all in motion due to thermal energy. It is, however, not the physics of this process that is of interest to the study of irregular curves but the path taken by the particles during Brownian

motion. Ignoring interactions with other particles the pollen grain moves in a series of random steps. It takes what is often referred to as a random walk. Again Feder (1988) gives a good explanation of random walks.

If such a random walk is thought of as taking place in only one dimension the particle moves by jumping by a random amount ξ_i during every increment i of time τ_i. The probability distribution of the variable ξ is Gaussian. The position of the particle $X(t)$ at time t is

$$X(t) = \sum_{i=1}^{n} \xi_i \tag{2.9}$$

When τ tends to zero $X(t)$ becomes a random function described by Mandelbrot (1982) as a Brown function denoted by $B(t)$. If the function is considered at two different resolutions, that is two different values of time interval, τ, important information about the scaling properties of the function is revealed. Feder (1988) suggests that the random steps ξ should be taken from a Gaussian probability distribution

$$p(\xi,\tau) = \frac{1}{\sqrt{4\pi\mathcal{D}\tau}} \exp\left(-\frac{\xi^2}{4\mathcal{D}\tau}\right) \tag{2.10}$$

where $\mathcal{D}$ is what Feder describes as the diffusion coefficient. Here the mean is zero while the variance is $2\mathcal{D}\tau$. If the time increment is doubled each jump τ considered becomes the sum of ξ' and ξ'', which are two values taken from the distribution in (2.10). The probability of obtaining a specified value for ξ' and a specified value for ξ'' to produce the value ξ is therefore the product of their two probability densities

$$p(\xi';\xi'',\tau) = p(\xi',\tau)p(\xi'',\tau) \tag{2.11}$$

The values of ξ' and ξ'' must add up to ξ and therefore by integrating over all combinations of the two values, the probability density for increment ξ is obtained:

$$p(\xi,2\tau) = \frac{1}{\sqrt{4\pi\mathcal{D}\tau}} \exp\left(-\frac{\xi^2}{4\mathcal{D}2\tau}\right) \tag{2.12}$$

This time the mean is still zero while the variance has increased to $4\mathcal{D}\tau$. This argument holds when the time interval is multiplied by any factor.

The probability density of Brownian motion at one time resolution is the same as the probability density at a time resolution multiplied by a factor b if the new increments or jumps are scaled by the factor $b^{1/2}$

$$p\left(\hat{\xi} = b^{1/2}\,\xi, \hat{\tau} = b\,\tau\right) = b^{1/2}\,p\left(\hat{\xi}, \tau\right) \tag{2.13}$$

This is described as an affine transformation and as a result the curves which exhibit such scaling properties are described as self-affine.

The scaling relation for the increments in (2.13) also holds for the Brown function and can be rewritten:

$$p\left(b^{1/2}\left[B(bt)-B(bt_0)\right]\right) = b^{-1/2}\,p\left(B(t)-B(t_0)\right) \tag{2.14}$$

where $B(t)$ and $B(t_0)$ are the positions of a random walk at the times t and t_0 respectively. Therefore the Brown function is a self-affine Gaussian random process with zero mean and a variance which is divergent with time interval. The position of the Brownian particle is related to the increments of the process by the following relationship

$$B(t)-B(t_0) \sim \xi\left|t-t_0\right|^{H} \quad (t \geq t_0) \tag{2.15}$$

where H equals $1/2$ for ordinary Brownian motion.

2.4 Fractional Brownian motion

Varying the exponent H in (2.15) between 0 and 1 provides a generalization to a family of processes Mandelbrot and Van Ness (1968) describe as fractional Brownian motions. These processes, of which Brownian motion is an example where the value $H=1/5$, produce curves with self-affine properties as discussed above. They have average increments of zero and the variances of their increments all diverge with time:

$$\left\langle\left[B_H(t) - B_H(t_0)\right]^2\right\rangle \sim \left|t-t_0\right|^{2H} \tag{2.16}$$

The correlation between past and future values of these functions varies with the parameter H. If τ is equal to one,

$$C(t) = \frac{\langle -B_H(-t)\, B_H(t) \rangle}{\langle B_H(t)^2 \rangle} = 2^{2H-1} - 1 \qquad (2.17)$$

where $-B_H(-t)$ are past increments of the process, $B_H(t)$ are future increments, and the present increment is zero (Feder, 1988). If $H=1/2$ then $C(t)$ equals zero suggesting that past increments are independent of future increments. However if $H > 1/2$ the correlation between past and future increments will be positive. This suggests that there is persistence of positive or negative increment values. A trend, either positive or negative in the past will on average be followed by the same sort of trend in the future. When $H < 1/2$, $C(t)$ becomes negative implying antipersistence. This suggests that a positive trend in the past, will on average, be followed by a negative trend in the future or vice versa.

When $H > 1/2$ fractional Brownian motion is characterised by dominant long term fluctuations. $\mathcal{D}$ or $H < 1/2$ values of the fractional Brownian motion alternate between positive and negative yielding curves dominated by short term noise.

2.5 The Dimension of Self-Affine Fractals.

In many of the earlier papers dealing with fractals, referred to in the introduction of this chapter, the concept of the scaling nature of fractals is often discussed using the example of a self-similar regular fractal. Examples of this can be seen in Mandelbrot (1967) and Burrough (1983a).

In the case of self-similar fractal functions, the variables of the functions are scaled by the same factor. This is not the case for Brownian motion, a self-affine fractal, where the variables are scaled by two different but closely related factors. This difference in scaling properties has an influence on the extent to which the concept of dimension can be taken when dealing with self-affine fractals.

From the discussion in part 2.2 about the fractal dimension of an irregular curve it can be seen that the measured length of such a line is

$$L(\delta) = a\delta^{1-D} \qquad (2.18)$$

if that curve was a self-affine fractal like the curves produced by Brownian motion. Consideration must then be taken of the different scaling factors for the X and Y

directions. When measuring such a curve by using a step size as mentioned in part 2.2, the contribution made to the length estimate by one step would be

$$\delta = \left(b^2\tau^2 + b^{2H}\left[\Delta B_H(\tau)/a\right]^2 \right)^{1/2} \tag{2.19}$$

where $b\tau$ is the time step or step in the X-direction and $\Delta B_H(\tau)$ is the step in the Y-direction. The last term of (2.19) will dominate if a has a very small value or if the magnification of the steps in the Y-direction is large. In these cases $\delta \sim b^H$. The number of segments of length δ, in the X- direction is

$$T/b\tau \sim b^{-1} \sim \delta^{-1/H} \tag{2.20}$$

where T is the extent of the curve in the X-direction. This leads to the length of the curve being

$$L \sim \delta^{1-1/H} \sim \delta^{1-D} \tag{2.21}$$

giving a fractal dimension of $D = 1/H$ when the magnification in the Y-direction is sufficient or the value of a is small enough to allow increasing amounts of irregularity in the curve to be measured.

If, alternatively, the X-direction was magnified the fluctuations in the Y-direction would appear very small and when measured using a segment length δ, the first term in (2.18) would dominate and $\delta \sim b$, then

$$L \sim \delta \cdot \left(T/b\right) \tag{2.22}$$

This yields a fractal dimension of 1.

It is these conflicting values of fractal dimension which must be appreciated when dealing with self-affine fractals. The fractal dimension $D = 1$, which is produced when measurement ceases to take account of irregularity in the curve is described as the 'global' fractal dimension (Mandelbrot, 1985, 1986; Feder, 1988). The fractal dimension estimated when measurements take into account irregularity at different scales is called the 'local' fractal dimension by Feder (1988) or the 'latent' fractal dimension by Mandelbrot (1983, 1985).

This section of the chapter has discussed the fractals necessary to understand the way in which they may begin to be related to landsurfaces and landforms. Before any

analysis is described, it is necessary to review the way fractal concepts have been put to use or examined in fields related to this study.

2.6 The Hurst Phenomenon.

Hurst (1951) showed that the rescaled range, of some geophysical time series, varied as a function of the period of the record, but not in the way expected. This phenomenon has been examined by many workers since Hurst but is still referred to as the Hurst phenomenon and takes the following form:

$$R_n/S_n \sim n^H \tag{2.23}$$

where R_n is the sample range of cumulative departures from the mean of a time series over the period n and S_n is the Standard deviation of the time series over the period n. Using the notation introduced previously in the chapter, the mean of the time series over a period n, where $x(t)$ is the value of the time series for each interval of time t, is

$$\langle x(t) \rangle_n = \sum \frac{x(t)}{n} \tag{2.24}$$

The cumulative departure from that mean for a time period n is

$$\sum \left[\frac{x(t) - \langle x(t) \rangle}{n} \right]$$

If the minimum value that this sum attains is subtracted from the maximum value reached Rn is obtained.

The unexpected result that this form of analysis yields for certain time series is that the exponent H in (2.23) takes a value greater than 0.5, which is the expected value for a time series where there is an absence of long-run statistical dependence or persistence as described in part 2.4. The Hurst phenomenon is therefore present in time series which seem to have the properties of fractional Brownian motions and because of this time series can be simulated with any desired value of the Hurst exponent, H, between 0 and 1.

Hurst (1965) found the time series he studied to have values of H typically of about 0.7 (Table 2.1). Table 2.1 shows the range of records used by Hurst. Mandelbrot and Wallis (1969d) (Table 2.2) provide values of H for more of the same kind of data sets and indeed for one set of Canadian varves used by Hurst as well. For this data set Hurst obtained $H = 0.77$ whereas Mandelbrot and Wallis obtain the much higher value

of 0.96. This may be because Mandelbrot and Wallis redefined Hurst's original way of looking at the data sets

Table 2.1: Table of H(= K) for various natural phenomena (from Feder, 1988).

Properties of K from Natural Phenomena

Phenomenon	Range of N Years	Number Pheno-mena	Number Sets	K Mean	K Std. devn.	K Range	Coeff. of auto-correl-ation
River discharges	10–100	39	94	0·72	0·091	0·50–0·94	
Roda Gauge	80–1,080	1	66	0·77	0·055	0·58–0·86	$0·025 \pm 0·26$
River and lake levels	44–176	4	13	0·71	0·082	0·59–0·85	$n=15$
Rainfall	24–211	39	173	0·70	0·088	0·46–0·91	$0·07 \pm 0·08$* $n=65$
Varves							
Lake Saki	50–2,000	1	114	0·69	0·064	0·56–0·87	$-0·07 \pm 0·11$ $n=39$
Moen and Tamiskaming	50–1,200	2	90	0·77	0·094	0·50–0·95	
Corintos and Haileybury	50–650	2	54	0·77	0·098	0·51–0·91	
Temperatures	29–60	18	120	0·68	0·087	0·46–0·92	
Pressures	29–96	8	28	0·63	0·070	0·51–0·76	
Sunspot numbers	38–190	1	15	0·75	0·056	0·65–0·85	
Tree-rings and spruce index	50–900	5	105	0·79	0·076	0·56–0·94	
Totals and means of sections							
Water statistics		83	346	0·72	0·08	0·46–0·94	
Varves		5	258	0·74	0·09	0·50–0·95	
Meteorology and trees		32	268	0·72	0·08	0·46–0·94	
Grand totals and means	10–2,000	120	872	0·726	0·082	0·46–0·95	

* Includes also river discharges.

To analyse each data set Mandelbrot and Wallis (1969d) selected a sequence of values of n for which calculations of R_n were performed. The sequence was selected in order to avoid redundancy in the results generated and the unmanageable amount of values of R_n that could have been calculated. For each value of n selected the entire period of the time series, T, can be divided into nonoverlapping subsamples of n. As n gets closer to T and the number of nonoverlapping subsamples becomes small, overlapping subsamples must be taken. If the values of R_n calculated from these subsamples are then plotted on doubly logarithmic paper a series of points for each selected value of n is produced (fig. 2.2). The mean of the R_n values calculated for each n is also plotted in fig. 2.2 as a square box. Mandelbrot and Wallis (1969d, p.324) state "*An empirical record is said to satisfy Hurst's law if, save perhaps for very small and very large values of s, the pox diagram of R(t,s)/S(t,s) is tightly aligned along a straight trendline, the slope of which will be designated by H*". The s of their notation is the same as the n of the notation used here. The reasons for the care Mandelbrot and Wallis take when considering the extreme ends of the plot are: at the bottom end, very small n gives rise to a large scatter of points for each n; at the top end, either the small number of subsegments available or the strong correlation between subsamples which overlap produces an artificial tightening of the scatter.

Figure. 2.2: Rescaled Range (R/S) versus time interval over which rescaled range is measured (Time) for Monthly Sunspot Activity, 1749–1948 (from Mandelbrot and Wallis,1969d).

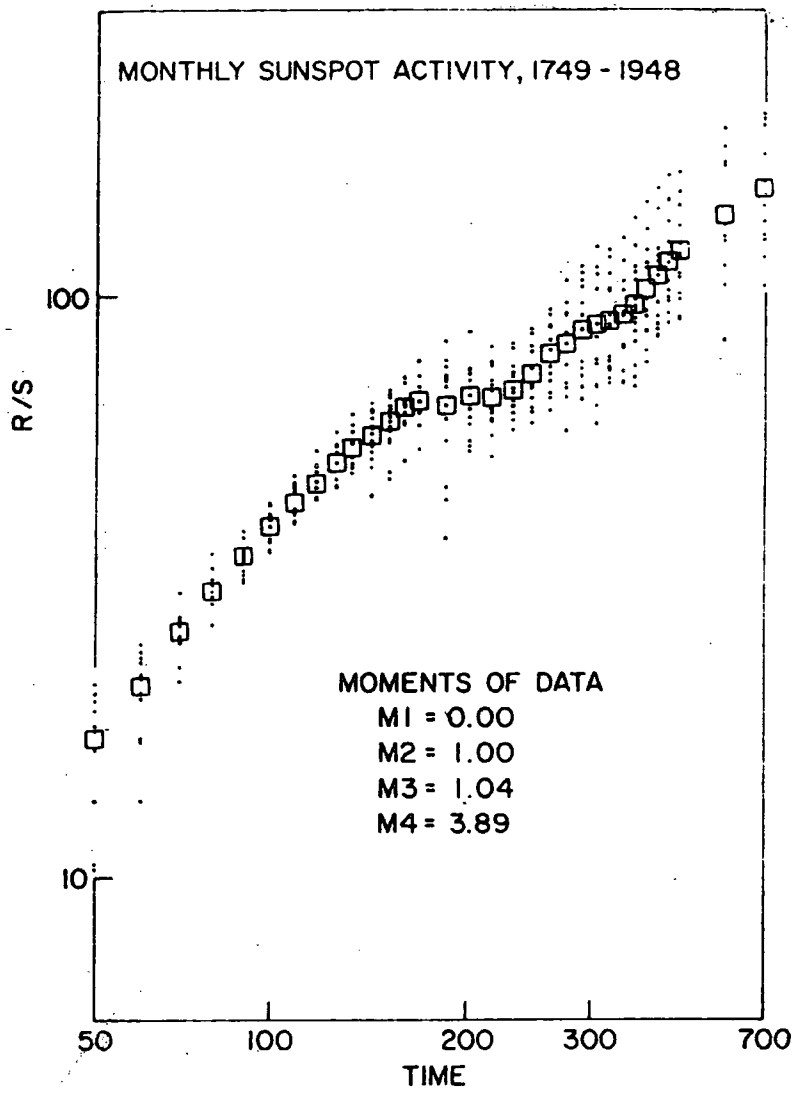

Table 2.2 : H values, calculated by Mandelbrot and Wallis, for some observed geophysical data. The Tamiskaming varve records were also studied by Hurst. (from Mandelbrot and Wallis,1969d).

Description	Apparent H	Moments 3rd	Moments 4th
Varve Data from De Geer [1940] Swedish Time Scale			
Haileybury, Canada, +310 to −369	0.80	0.74	4.41
Timiskaming, Canada, +1321 to −588	0.96	1.03	6.33
Sirapsbacken, Sweden, +576 to +257	≈1.00	0.95	3.52
Degeron, Sweden, +499 to 0	0.97	1.10	3.65
Omnas, Sweden, +1399 to +1162	0.65	3.39	23.01
Resele, Sweden, +1399 to +1132	0.67	4.00	26.02
Hammerstrand, Sweden +2000 to +1767	0.85	2.10	9.05
Ragunda, Sweden, +1933 to +1800	0.99	1.59	5.21
Lago Corintos, Argentina, −801 to −1168	0.89	0.85	3.58
Biano, Himalaya Mountains, −1180 to −1279	0.50	1.84	7.82
Sesko, Himalaya Mountains, −1293 to −1374	0.99	0.31	2.20
Enderit River, E. Africa, −406 to −546	0.91	1.07	4.10
Schulman [1956] Tree ring indices			
Table 28, Douglas Fir and Ponderosa Pine, Fraser River, Brit. Col., 1420–1944	0.70	0.19	2.84
Table 30, Douglas Fir, Jasper, Alberta 1537–1948	0.75	0.60	3.34
Table 31, Douglas Fir, Banff, Alberta 1460–1950	0.65	0.32	2.76
Table 33, Douglas Fir and Ponderosa Pine, Middle Columbia River Basin 1650–1942	0.75	0.10	3.20
Table 36, Douglas Fir, Snake River Basin, 1282–1950	0.77	0.24	3.60
Table 38, Limber Pine, Snake River Basin, 1550–1951	0.60	−0.06	3.47
Table 40, Douglas Fir, Upper Missouri River Basin, 1175–1950	≈0.5	0.33	3.14
Table 41, Limber Pine, Upper Missouri River Basin, 978–1950	0.63	0.29	3.71
Table 43, Douglas Fir, North Platte River Basin, 1336–1946	0.70	0.65	3.88
Table 44, Douglas Fir, South Platte River Basin, 1425–1944	0.62	0.21	2.77
Table 45, Douglas Fir, Arkansas River Basin, 1427–1950	0.66	0.03	2.86
Table 49, Mixed species, 3 year means, Colorado River Basin 70 B.C. to 1949 A.D.	0.55	0.25	3.07
Table 50, Douglas Fir, Colorado River Basin, 1450–1950	0.64	−0.15	2.82
Table 52, Pinyon Pine, Colorado River Basin, 1320–1948	0.68	−0.43	3.32
Table 65, Ponderosa Pine, Upper Gila River, 1603–1930	0.69	−0.07	3.25
Table 66, Douglas Fir, Southern Arizona, 1414–1950	0.69	−0.03	3.11
Table 70, Douglas Fir, Upper Rio Grande, 1375–1951	0.65	0.21	2.88
Table 71, Pinyon Pine, Upper Rio Grande, 1356–1951	0.68	−0.23	2.76
Table 72, Douglas Fir, Middle Rio Grande, (Guadalupe), 1650–1941	0.59	0.24	2.87
Table 73, Douglas Fir, Middle Rio Grande, (Big Bend), 1645–1945	0.71	0.59	3.13
Table 75, Ponderosa Pine, S. E. Oregon, 1453–1931	0.58	0.04	3.27
Table 76, Ponderosa Pine, N. E. Calif., 1485–1931	0.78	0.11	3.12
Table 77, Jeffrey Pine, E. Central Calif., 1353–1941	0.72	−0.15	2.93

Table 2.2 continued

Description		Apparent H	Moments 3rd	Moments 4th
Table 78, Big-cone Spruce, S. Calif., 1385–1950		0.56	0.11	3.62
Table 79, Ponderosa Pine, S. Calif., 1350–1931		0.72	−0.40	2.89
Table 80, Douglas Fir, W. Central Mexico, 1640–1943		0.86	−0.10	2.40
Table 85, Cipres at Cerro Leon, Argentina, 1572–1949		0.91	0.41	3.41
Data from Statistical History of the United States [1965]				
Annual Precipitation				
Albany, N. Y., 1826–1962		0.87	0.56	3.46
Baltimore, Md., 1817–1962		0.75	−0.06	2.64
Charleston, S. C., 1832–1962		0.89	0.65	3.53
New Haven, Conn., 1873–1962		0.73	0.30	2.33
New York, N. Y., 1826–1962		0.65	0.59	2.89
Philadelphia, Pa., 1820–1962		0.81	0.21	2.85
San Francisco, Calif., 1850–1963		0.64	0.45	3.11
St. Louis, Mo., 1857–1962		0.64	0.63	4.20
St. Paul, Minn., 1837–1962		0.67	0.49	5.15
Data from Ruth B. Simon (personal communication)				
Weekly Derby earthquake frequencies, April 1962–June 1967		0.93	3.99	24.45
Munro [1948] Sunspot data				
Monthly sunspot frequency, 1749–1948		0.96	1.04	3.88
Data from V. M. Yevdjevich [1963], U = Unadjusted for overyear carryover; Y = Adjusted for overyear carryover				
Gota River near Sjotrop-Vanersburg, Sweden, 1807–1957	U	≈0.5	−0.06	2.35
	Y	≈0.5	0.42	2.94
Neumunas River at Smalininkai, Lithuania, U.S.S.R., 1811–1943	U	0.61	0.47	3.15
	Y	0.48	0.61	3.31
Rhine River near Basle, Switzerland, 1807–1957	U	≈0.5	0.14	2.80
	Y	≈0.5	0.23	2.89
Danube River at Orshawa, Romania, 1837–1957	U	≈0.5	0.27	2.26
	Y	≈0.5	0.22	2.53
Mississippi River near St. Louis, 1861–1957	U	0.79	0.29	2.75
	Y	0.68	0.18	2.45
St. Lawrence River near Ogdensburg, N. Y., 1860–1957	U	0.98	−0.26	2.70
	Y	0.69	0.14	2.70
Professor J. C. Mann (personal communication) Data from Paleozoic Era Sediments				
Wolfcampian Section, Kansas	Thickness of beds	0.75	4.60	32.27
	Lithology of beds	0.71	0.25	2.97
Virginian–Desmoinesian Section, Superior, Arizona	Lithology of beds	0.55	0.78	3.27
	Bedding type	0.67	0.19	2.21
Missourian–Atokan Section, Honacker Trail, Utah	Thickness of beds	0.70	3.51	24.81
	Lithology of beds	0.61	−0.05	2.06
	Bedding type	0.58	0.47	2.11
Data from J. de Beauregard [1968]				
Rhine River, Monthly flows, 1808–1966		0.55	0.65	3.01
Loire River, Monthly flows, 1863–1966		0.69	1.53	5.47

Such rigorous care was not taken by Hurst, who suggested that the trend lines all passed through the point with X-coordinate log 2 and Y-coordinate log 1. He then calculated H from the supposed relationship

$$H = \frac{\log\left(\frac{R(t,n)}{S(t,n)}\right)}{\log n - \log 2}$$

where t is the starting point of a subsegment of length n.

Mandelbrot and Wallis (1969a) found that the trendlines did not, in general, pass through the point mentioned and therefore the estimate of H tended to be too low when $H > 0.72$ and too high when $H < 0.72$. This, they suggest, lead to Hurst's typical value of around H=0.7.

Feder (1988) has performed a small rescaled range study on sea wave height data from Tromsøflaket, Norway. The time series used was for the three year period, 1980-1983. Wave heights were recorded at 2 second intervals, 2045 times every 3 hours. The 'significant wave height' for each 3 hourly period was calculated by taking the average of the largest third of the wave heights recorded. R/S analysis was then performed on the significant wave height time series yielding a value for H of 0.87 +or– 0.01.

Visual investigation of the plot of the R/S analysis reveals some apparent structure (fig. 2.3). This structure in the curve is found at a lag of one year which suggested to Feder that it is the result of some seasonal variation. This poses the problem of how to deal with data sets which have some periodicity within them. Feder (1988) normalised the data set to zero mean and unit variance by taking the cumulative sum of significant wave heights, just as in (2.9) the cumulative sum of increments was used to define the position of the Brownian particle.

Figure 2.3: R/S *as a function of the lag* τ, *for a process where the significant wave-height* h_S *for Tromsøflaket is considered to be the random process* $\{\xi\}$. *The line represents a fit of the Hurst law* $R/S \sim \tau^H$ *to the data with* $H = 0.87 \pm 0.01$ *(from Feder, 1988).*

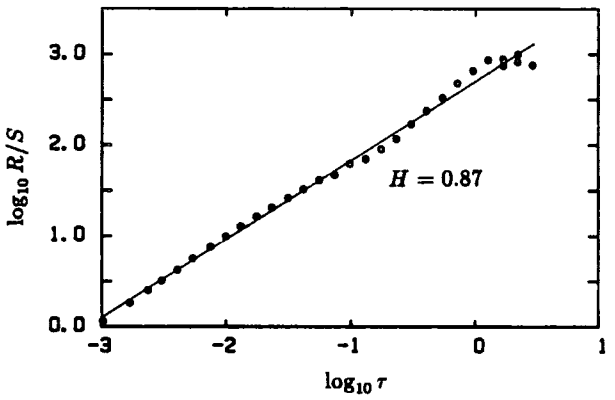

R/S analysis was then repeated, this time on the adjusted time series. The plot from the analysis (fig. 2.4) now shows two straight regions. For lags up to around 10 days a value for H of 0.92 ± 0.02 was calculated, while for lags greater than 20 days the curve had changed to yield a value of $H = 0.52 \pm 0.02$. This suggests that there is persistence in the wave statistics over periods of up to 10 days, but statistics separated by 20 days have become independent of each other.

Figure 2.4: *R/S as a function of the lag* τ *(in years), for a process where the seasonally adjusted and normalized significant wave-height* ξ *for Tromsøflaket is considered to be the step in a (fractional) random walk. The lines are fits of the Hurst law* $R/S \sim \tau^H$. *The fit for* $\tau < 10$ *days gives* $H = 0.92 \pm 0.02$, *and the fit for* $\tau > 20$ *days gives* $H = 0.52 \pm 0.02$ *(from Feder, 1988).*

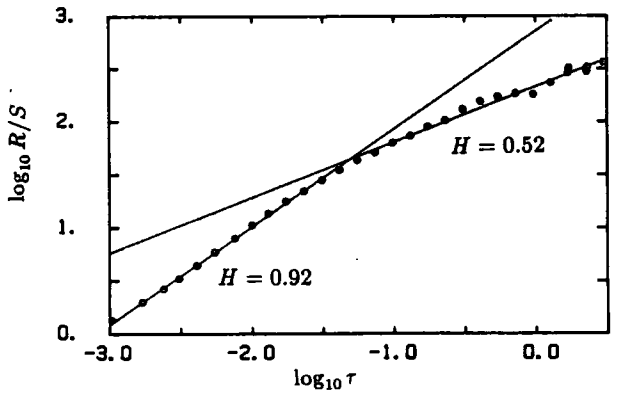

If the value of $H > 0.5$, obtained for the many geophysical time series studied using R/S analysis, is a result of the type of behaviour found in fractional Brownian motion the interesting issue is raised of why long-term dependence is exhibited. For the studies summarised by the results of Mandelbrot and Wallis (1969) in Table 2.2, the log-log plots revealed a linear relationship for all time lags and no breaks in the slope of the relationships were found, unlike the case of Feder's wave statistics. This led Mandelbrot and Wallis (1969, p.321) to claim: "*Thus, for practical purposes, geophysical records must be considered to have an 'infinite' span of statistical interdependence*". They did however qualify this statement by suggesting 'infinite' in the above usage means "*longer than the longest records so far examined*" (Mandelbrot and Wallis, 1969, p.335).

The suggested cause of such memory effects in these records varies slightly with the type of record studied. In the case of river discharge time series, clearly, the storage of water in a drainage basin, in its soils and so on, produces a memory effect in that several different episodes of precipitation will all be affecting the discharge of the river at a particular time. In the case of actual rainfall records feedback systems within the climate of an area might cause some sort of autocorrelation of records. However for many phenomena which produce $H > 0.5$ it is not easy, even intuitively, to see why such long-term persistence should be present.

Such problems have led to certain workers proposing alternative viewpoints as to the type of numerical process which can be used to simulate time series to imitate the geophysical time series exhibiting the Hurst phenomenon. Klemes (1974) draws attention to the intuitive weaknesses of fractional Brownian noises as models for long run geophysical records. He asks what physical mechanism can transmit the influence of, for example, a temperature at a particular time in one particular place over decades and centuries. This leads him to question the idea that a stationary stochastic process as proposed by Mandelbrot and Wallis can be used to model phenomena which could, quite feasibly be nonstationary. Klemes goes on to show by various numerical experiments that time series exhibiting the Hurst phenomena can be simulated by a process where the mean fluctuates with time.

To elaborate, Klemes (1974), first showed that performing R/S analysis on a Gaussian random series with unit variance in which the mean value alternates between 0.5 and -0.5 at regular time intervals gave results interestingly different to similar analysis of a stationary Gaussian random series which produces a value of 0.5 for H. During the first time interval H is clearly going to be equal to 0.5, however as the influence of the second time period with a different mean is considered the value of H rises. After the second change of the mean H returns to 0.5 before falling more sharply

until gradually converging to 0.5 again. This shows that a change in the mean can indeed increase the Hurst exponent to a value above 0.5.

Unlike natural time series, these series show very obvious structure starting with H=0.5 and returning to H=0.5. Klemes, therefore, developed the process by which the mean oscillates in order to make the simulated series have a constant H greater than 0.5. He did this by allowing the time period of each alternating mean to vary. Each time period was drawn from an exponential distribution of the logarithm of the time period. Time periods were allowed to vary between 1 and the some very large number. This process produces straight plots except at very large and very small values of τ where the plot converges on and diverges from $H = 0.5$, respectively.

The concept of a real time series exhibiting the Hurst phenomenon being produced by nonstationarity in the series mean is further supported by empirical evidence collected by Potter (1976). Using precipitation records from the eastern seaboard of the United States, Potter selected subsegments of the complete records which showed means substantially different to the total record. He then performed R/S analysis on the subsegments and the total record. The results of the subsegment analyses were compared to the expected results from a comparable Markovian series. Potter claims that the H exponent estimated from the real records are statistically near the exponents for the Markovian series and therefore suggests that nonstationarity can be an alternative to infinite memory as a numerical mechanism by which the Hurst phenomenon can occur.

2.7 Other Fractals in Geophysics.

One other relationship which is derived from (2.7) and (2.8) must be introduced and has been used in the investigation of Lunar and Martian morphometry (Woronow, 1981), cloud forms (Lovejoy, 1982; Rys and Waldvogel, 1986; Hentschel and Procaccia, 1984; Lovejoy and Schertzer, 1985; Lovejoy and Mandelbrot, 1985) and drainage basin indices (Tarboton et al., 1988). This is the perimeter- area relationship. It is derived from applying fractal concepts of irregularity to the well established ratio P between their perimeter lengths and the areas of regular polygons of the same shape,

$$P = \frac{\text{perimeter}}{\sqrt{\text{area}}} \tag{2.25}$$

However for a fractal polygon the perimeter length $L(\delta)$ tends to infinity as δ tends to zero. The area $A(\delta)$ remains finite, however, being measured by tiles of δ^2 in area. This leads to the ratio (Mandelbrot, 1977; Feder, 1988)

$$P(\delta) = \frac{L(\delta)^{1/D}}{\sqrt{A(\delta)}} \tag{2.26}$$

However $P(\delta)$ depends on the yardstick length δ and some arbitrary factor C such that the perimeter relationship is in fact

$$L(\delta) = C\,\delta^{(1-D)} \cdot \left(\sqrt{A(\delta)}\right)^{D}$$

where C is a constant.

Lovejoy (1982) used this ratio to study the scaling properties and the fractal dimensions of clouds and rain areas. Using remotely sensed radar images, areas containing large rain drops in quantities large enough to produce a rain rate of 0.2mm/hour, or over, could be detected as rain areas. The area A of these rain areas was simply taken as the number of pixels in the rain area (each pixel is $1km^2$). The length of the perimeter was taken as the number of rain area pixels which were bordered by a pixel not attaining the above requirements. Each rain area was plotted on a graph of area versus perimeter length.

Lovejoy measured clouds in the Indian Ocean from infrared images obtained from the Geostationary Operational Environment Satellite. Cloud areas were defined as groups of pixels where the temperature was less than -10 degrees centigrade. This definition of cloud therefore took no account of height in the atmosphere and both cumulus and cirrus clouds were included in the study. Areas and perimeters were calculated and plotted as for rain areas.

The result was that the perimeter-area ratio was near constant for all clouds and rain areas measured giving a fractal dimension of around 1.35 for areas between $1km^2$ and 1.2×10^6 km^2, three linear orders of magnitude. Lovejoy and Schertzer (1985) claim that the lower area limit has been extended to $0.026km^2$ by Cahalan et al., in an unpublished manuscript, using landsat imagery.

The fractal nature of atmospheric turbulence is generally considered to be the reason for the scaling behaviour of such meteorological phenomena. Hentschel and Procaccia (1984) extended their work on turbulence to the study of clouds. They considered atmospheric parameters such as temperature to be transported by a fractal turbulent field. Their theory produces an estimate of fractal dimension for cloud

perimeters in the range 1.37 to 1.41. This is clearly in good agreement with Lovejoy's empirical results and lends strong support for the scaling nature of turbulence leading to scaling phenomena such as clouds.

Lovejoy and Schertzer (1985) have since developed the concept of general scale invariance in the atmosphere. This considers the atmosphere to be influenced by fractal turbulence in that the statistical properties of the atmosphere at the small scale are related to the properties at large scales by a magnification. However on top of this magnification a differential stratification must be included due to the effects of gravity, while a differential rotation must be included to take into account the Coriolis force. This line of investigation has yielded very successful simulations of clouds.

Perhaps the reasonably good understanding which exists, of atmospheric physics and of turbulence has allowed the intuitive jump to a fractal description of meteorological phenomena. However, just as it was difficult to see reasons for infinite memory in some geophysical time series, it is difficult to explain the apparent fractal behaviour of such things as drainage basin morphology.

Mandelbrot (1977) referred to the results of Hack (1957) in his proposal that the fractal form of the perimeter-area relationship might hold for drainage basins. Here Mandelbrot substituted Hack's 'length of longest stream' for perimeter and suggests that the relationship Hack found, where L is proportional to $A^{0.6}$ can be translated to

$$L = 1.4\sqrt{A}^{D}$$

with D from Hack's empirical evidence equal to 1.2.

Tarboton et al. (1988) looked at the scaling properties of river networks, linking them to the indices devised by Horton (1945). Using U.S.G.S. DEM data they calculated the number of pixels which drained into each pixel of the DEM. This is equivalent to finding the area which drains into each pixel. They then used different threshold values of drainage area to select sets of pixels which defined channel networks. If the threshold drainage area was decreased, the product was a finer-resolution channel network. They then used three methods which can operate on the channel networks, for each resolution, to estimate fractal dimension. For each method they found that D was near to 2. This suggests that the networks are space filling.

Therefore, although many would question why Hack and Gray obtained the apparently scaling relationships they did, the idea that a drainage network should fill the plane in order to operate optimally is easily understood. Perhaps, then, some sort of scaling, nested structure hinted at by Hack's law could best allow drainage networks to fill the plane.

2.8 Conclusions.

When studying a phenomenon in terms of its possible fractal nature, its irregularity must be studied to see if it shows signs of self-similar or self-affine behaviour. If this self-similar or self-affine behaviour is present over a sufficient range of scales within the phenomenon, the scale free nature of the phenomenon can give rise to an estimable fractal dimension.

The fractional Brownian noise processes developed by Mandelbrot and Van Ness (1968) and Mandelbrot and Wallis (1969) provide methods for simulating fractal time series or if distance is substituted for time, fractal surface profiles. The properties of these simulations can be looked for, to some extent, in natural time series or profiles and so on. Investigation into the fractal properties of some of these time series have shown behaviour analogous to fractal Brownian motion. However properties such as infinite memory in fractional Brownian motions cannot always be easily reconciled with the possible physical mechanisms which seem to affect the natural time series exhibiting apparent fractal behaviour.

In this study the possible scaling behaviour of landsurfaces and the landforms which contribute to these surfaces is being investigated. Therefore it will be necessary to analyse landsurfaces to find: (a) what if any scaling properties they show; (b) over what distance range do these properties hold; (c) whether a fractal dimension can be estimated; (d) how closely do landsurfaces relate to fractional Brownian processes. The next chapter discusses various methods and algorithms which allow this analysis to begin.

Chapter 3: Creating DEMs From Contour Maps

3.1 Introduction

Data capture processes vary in applicability for different landforms. However, this study is looking both at landsurfaces and at the individual landforms which contribute toward those landsurfaces. Landsurface data, when it is required for geomorphometric analysis is often held in the form of digital elevation models (DEMs). DEMs allow manipulation by computer to provide graphical representation of the surfaces. More importantly to this study they also allow the calculation of morphometric parameters (Evans, 1981; Frederickson et al., 1985; O'Neill and Mark, 1987).

Likewise, landforms can also be stored as DEMs to allow both graphical display and the automation of the calculation of geomorphometric parameters (Evans, 1987). It is true that certain parameters in the study of particular landforms cannot be obtained from DEMs and must be measured in the field or from aerial photographs. However, this study is looking at the parameters related to size distribution of landforms. As a result of the geomorphologist's belief, as discussed in Chapter 1, that certain landforms occur within a certain size range, geomorphologists have perhaps focused attention on clearly defined examples of landforms which seem to be at a certain scale. This study objectively seeks to find scale thresholds within which landforms types may exist. The automation of processes used to measure parameters of landsurface form and landform morphology is therefore desirable in order to add objectivity. DEMs are clearly the base upon which this automation can begin.

It follows that in this study data capture of both landsurfaces and landforms should occur at the same time, individual landforms being components of the landsurfaces studied. As a result digital elevation models will be used for studying both surfaces and forms in this study. Digital elevation models (DEMs) must at this point be distinguished from digital terrain models (DTMs). Doyle (1978, p. 1481) suggests: *"A digital terrain model (DTM) is an ordered array of numbers that represents the spatial distribution of terrain characteristics"*. DEMs represent specifically the spatial distribution of elevation, one particular characteristic of terrain (Burrough, 1986).

3.2 Types of DEM

There are essentially two groups of method by which a DEM can be constructed (Burrough, 1986). Mathematical methods fit some form of three dimensional function either globally to the whole area or locally to smaller patches of the surface. The second

group consists of image methods which can be subdivided into two further groups. Line models include digitised contours or profiles while point models include regular grid networks or models comprised only of critical features such as pits, peaks, ridges and talweg lines.

Different methods have different applications. Mathematical methods to fit some global function to the surface, such as trend surface modelling are more appropriate where there is some recognition of a deterministic trend of interest in the surface rather than where the surface is being treated as possibly being random (Lam, 1983).

Chapter 1 briefly mentioned DEMs in the form of regular matrices of heights. In these DEMs the X and Y positions on the surface are implicit within the matrix while only the altitude Z is explicit. This form of DEM has also been described by the term 'altitude matrix' by Evans(1972, 1980).

Altitude matrices, or 'gridded' DEMs, are not the only form of DEM based on image methods. One of the most common alternatives to the gridded DEM is the triangular irregular network (TIN).

As its name implies the triangular irregular network method of modelling surfaces represents a surface by linking together, as a network of triangles, random altitude points or preferably information rich altitude points such as pits, peaks, ridges and valleys. An advantage of this type of model over the gridded DEM is that it can represent a surface by storing altitude information for fewer points. This is because large triangles are sufficient for representing areas of little relief while smaller triangles are used in area of more complex relief. However the reason for the TIN method's storage advantage also produces a major disadvantage. Where large triangles representing areas of low relief meet a major break of slope followed by a rougher slope which must be represented by smaller triangles the transition between large and small triangles is by way of long, thin, elongated triangles. Not only do the effects of these elongated triangles inevitably show up in graphical products from TIN models, but these long, thin triangles may often have the incorrect area for the surface which they are trying to represent (Douglas, 1986).

Clearly it is desirable to use comparable techniques in all stages of the study. As a result there are several reasons why gridded DEMs should be the standard data structure used here. One reason is the ease with which the data can be processed. TINs, as well as possessing the problem given above, are slightly more difficult to process than gridded DEMs. Another reason for chosing gridded DEMs is that the existing computer programs of Evans (1979) which are used in this study and the programs of Depraetere (1989) deal with altitude data in this format. The final consideration which

points towards the choice of regular grid DEMs is that national mapping agencies such as the O.S., the U.S.G.S., and the I.G.N. are producing these commercially; some of these are used in this investigation.

There are three groups of methods by which an altitude matrix can be produced: manual; automatic; and semi-automatic. Manual field survey is clearly time consuming and can only realistically be used in situations where only small areas are being considered. Furthermore surveying is often based on developing an irregular network of points and an altitude matrix must then be interpolated from this. A more practical manual solution for larger areas is to interpolate an altitude matrix from a contour map of the surface. This involves overlaying the map sheet of interest by an acetate sheet with points describing the necessary grid printed on it. The altitude at each point is then interpolated from the surrounding contours. The obvious advantage of this method is that the human interpolator can intelligently act on the information which the contours give him. The obvious disadvantage of this method is that it is tedious for the interpolator and time consuming. 10,000 points must be interpolated to represent a $5km^2$ Ordnance Survey 1:10,000 map sheet at a grid resolution of 50m. Once the interpolation is complete these 10,000 points must then be entered into a computer.

The most attractive methods are automatic. Stereoscopic aerial photographs can have elevation measurements sampled from them by analytical stereo-plotters. However hardware such as this is not available in Durham. This leaves semi-automation as the only practicable alternative to the manual interpolation of points from contour maps. Semi- automatic methods involve the digitising of contours from map sheets followed by some form of automatic interpolation from these to a regular grid.

3.3 Which Semi-Automated Method?

It was decided on the basis of hardware and software availability in Durham to investigate some of the possible semi-automated methods of creating a DEM of an area of drumlins. The purpose of this is to illustrate some of the difficulties involved when creating DEMs, highlighting the fact that DEMs from what ever source are subject to error. The process will also provide another landsurface for study. The full relevance of a landsurface of drumlins will be explained in Chapter 8.

The area of drumlins chosen for analysis was the area covered by the Ordnance Survey 1:10000 map series, sheets NY61NE and NY62SE, the southwest corner with grid coordinates 365000,517000; the northeast corner with coordinates 370000, 525000. Every contour, at 5m intervals, within this area was digitised on a A0 Summographics microgrid tablet using the pcARC/INFO digitising facility (ESRI, 1989).

Interpolation of a regular grid of values from an irregular spatial distribution of values has been widely discussed in the literature (Lam, 1983; Yoeli, 1986; Davis, 1986). Many methods of interpolation and algorithms for those methods exist. Sampson (1978) states *"There are many different ways in which the control points in a neighbourhood can be combined to create an estimate. Unfortunately little comparative work has been done on the relative merits of these alternatives"*. Many commercial packages exist which have routines for a so called 'random-to-grid' interpolation. Most of them use some distance weighting method. However, as many of these packages have been developed for use in a wide variety of applications where graphical products such as contour plots are the desired end product, the gridding algorithms may not be optimal for producing a matrix of one particular surface.

3.4 Surface II

Of the packages available in Durham 'Surface II' was found to provide the best facilities for creating DEMs. *"Surface II provides one of the most thoroughly tested grid interpolation routines commercially available"* (McCullagh and Sampson 1972; Walden 1972; and Grassie 1982). In addition, the Surface II package was designed primarily for topographic and geologic isometric mapping and is probably *"the most commonly used routine for these topics"*. (MacEachren et al., 1987, p.311). Most packages for contouring provide only one or two random-to-grid interpolation methods. Surface II provides three basic methods, and control over the parameters which determine the operation of each of these methods is facilitated, allowing a large number of possible interpolated grids. As different surfaces provide different problems for interpolation this flexibility is highly desirable if the product required is the actual DEM as opposed to a graphical representation. Table 3.1 presents the three methods and their relevant parameters.

The first and most simple method is a one-phase local fit method, this is the most basic distance weighting method Surface II provides. One of the search methods listed in table 3.1 is used to select an operator-defined number of data points around the grid point to be interpolated. A distance-based weight is calculated for each data point selected, the weight depending on one of the operator- defined weighting functions mentioned in table 3.1. The value interpolated for the grid point is then taken as a weighted average of the selected data values (fig. 3.1).

Table 3.1 Random-to-grid interpolation methods available in SurfaceII

User Defined Parameters		Method		
		1 Phase Local Fit	2 Phase Local Fit	Kriging
Types of search for Neighbouring Points	Nearest Neighbour	✓	✓	✗
	Quadrant	✓	✓	✓
	Octant	✓	✓	✓
Distance (D) Weighting Functions	Default	✓	✓	✗
	$1/D$	✓	✓	✗
	$1/D^2$	✓	✓	✗
	$1/D^4$	✓	✓	✗
	$1/D^6$	✓	✓	✗
	Semi-Variogram Slope	✗	✗	✓

Figure 3.1 One-phase local fit (after Sampson, 1978)

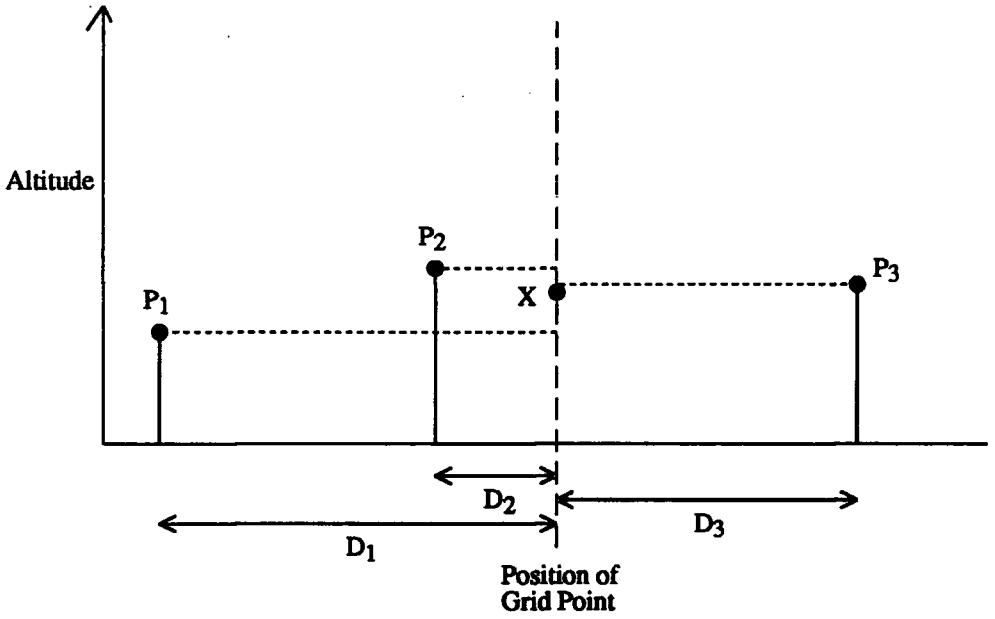

X Interpolated Point
P_n Data Point
D_n Distances Used for Weights

Figure 3.2 Two-phase local fit (after Sampson, 1978)

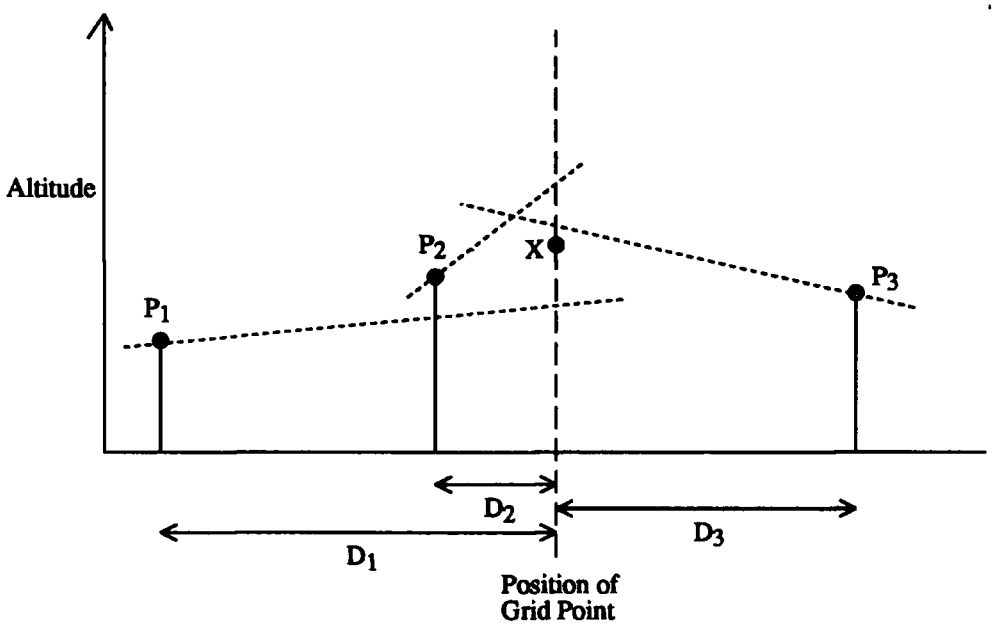

X Interpolated Point
P_n Data Point with Trend Surfaces Fitted
D_n Distances Used for Weights

A two-phase local fit is the next step up in complexity. During the first phase the nearest n neighbours to each data point are used to fit a weighted trend surface to each data point. The surface is constrained so that the plane passes exactly through the data points. The second phase is the same as the more simple one-phase method. Data points surrounding each grid point to be estimated are selected as before, and weights are allocated by the chosen weighting function. However it is the value of the trend surface passing through the selected data point extrapolated to the position of the grid point to be estimated that is used to give a weighted average value for the grid point (fig. 3.2). The Surface II command 'GRID' is used with its different parameters for both the one- and two-phase methods.

Universal kriging is the third method available. Assuming that a land surface can be treated as a regionalized variable, showing spatial autocorrelation over short distances while over larger distances points tend to be statistically independent of one another, kriging can provide a DEM estimated from random points that has *"certain statistically optimal properties"* (Davis, 1986, p. 383). Using kriging the weighting of points is based on the geostatistical properties of the random points. That is, weights for the data points depend on the spatial continuity of the random points expressed in the form of a semivariogram:

$$\gamma_n = \sum_{h=i}^{n} \frac{\left(Z_i - Z_{i+h}\right)^2}{2n}$$

where Z_i and Z_{i+h} are altitudes at different locations separated by the distance h, and n is the number of observations of altitude difference at this separation.

Therefore before Surface II can be used for kriging the semivariogram of the surface must be estimated in some way and if the surface is nonstationary the drift or trend in the surface must be estimated. The properties of the semivariogram are communicated to Surface II in the 'KRIG' command. The semivariogram's slope is input for a standard or more local neighbourhood and for a wider neighbourhood. This allows a less exhaustive but quicker calculation of weights as the number of simultaneous equations which must be solved is n+1 where n is the number of data points being used in the estimation. KRIG also allows a choice of three drift values: a first- or second-order polynomial or the subtraction of the mean from every observation. The number of points to be used in each neighbourhood search can be specified in calls to the same routines which select neighbouring points for the one- and two-phase local fits. Sampson (1978, p.) states *"In theory, no other method of grid generation can produce more accurate estimates of the form of a mapped surface. In practice, the effectiveness of kriging depends upon the proper selection of several parameters, including the slope of the semivariogram. However, even with naive estimates of these*

parameters, kriging will do no worse than arbitrary estimating procedures such as those of 'GRID'".

To obtain the highest possible quality DEM of the Eden Vale drumlins it was decided to compare the three different Surface II methods, with different combinations of values for their parameters. In order to save computer resources and time, only a small portion of the total area digitised was used to test the interpolation methods (fig. 3.3).

3.5 An Alternative

A possible drawback of using Surface II or any other package which allows a random-to-grid interpolation is that the package assumes that the data points provided are random. The package treats each point as a spot height rather than part of a contour line. A nearest neighbour analysis of the contour data using the Surface II routine yields a nearest neighbour statistic of 1.01, suggesting that the points are randomly distributed spatially when considered as points. However the nature of the digitising process means that points which are closest to one another are points on the same contour. This may affect the interpolation if data points selected by the various options are from the same contour line. As well as this practical problem there is the more theoretical problem of wasting all the available topological data contained in the contours by treating them as a series of random points.

As a result it was decided to write a Fortran 77 program based on an existing algorithm of Yoeli(1986) to interpolate a regular grid from digital contours. There are several stages to the algorithm.

The first is the calculation of profiles at each grid interval in the X and Y directions of the grid and for two 45 degree diagonal directions (fig. 3.4). Each profile is formed by calculating the positions along the profile line where it is cut by a contour. In the program written, DEM.FOR (Appendix 1), this is achieved in two steps. Each digitised point belonging to a contour is compared to the point next to it and a check is made for the presence of a grid interval between them in the X and Y directions and the directions 45 degrees to these. To find out if a diagonal interval lies between the two points, the points are rotated through 45 degrees so that the grid intervals are now equivalent to the diagonals of the unrotated grid (fig 3.4).

If for instance, as in figure 3.5, a grid interval with a value of $X=n$ is between the values $X1$ and $X2$ of the contour points $P1$ and $P2$, then the contour involved intersects the grid interval. The point of intersection will be part of a profile of the area in the Y direction with a constant X value.

Figure 3.3: Area used in tests of random-to-grid interpolation methods. National Grid coordinates are given. The contours are plotted from the DEM produced by kriging with no polynomial drift.

(368000,521000)

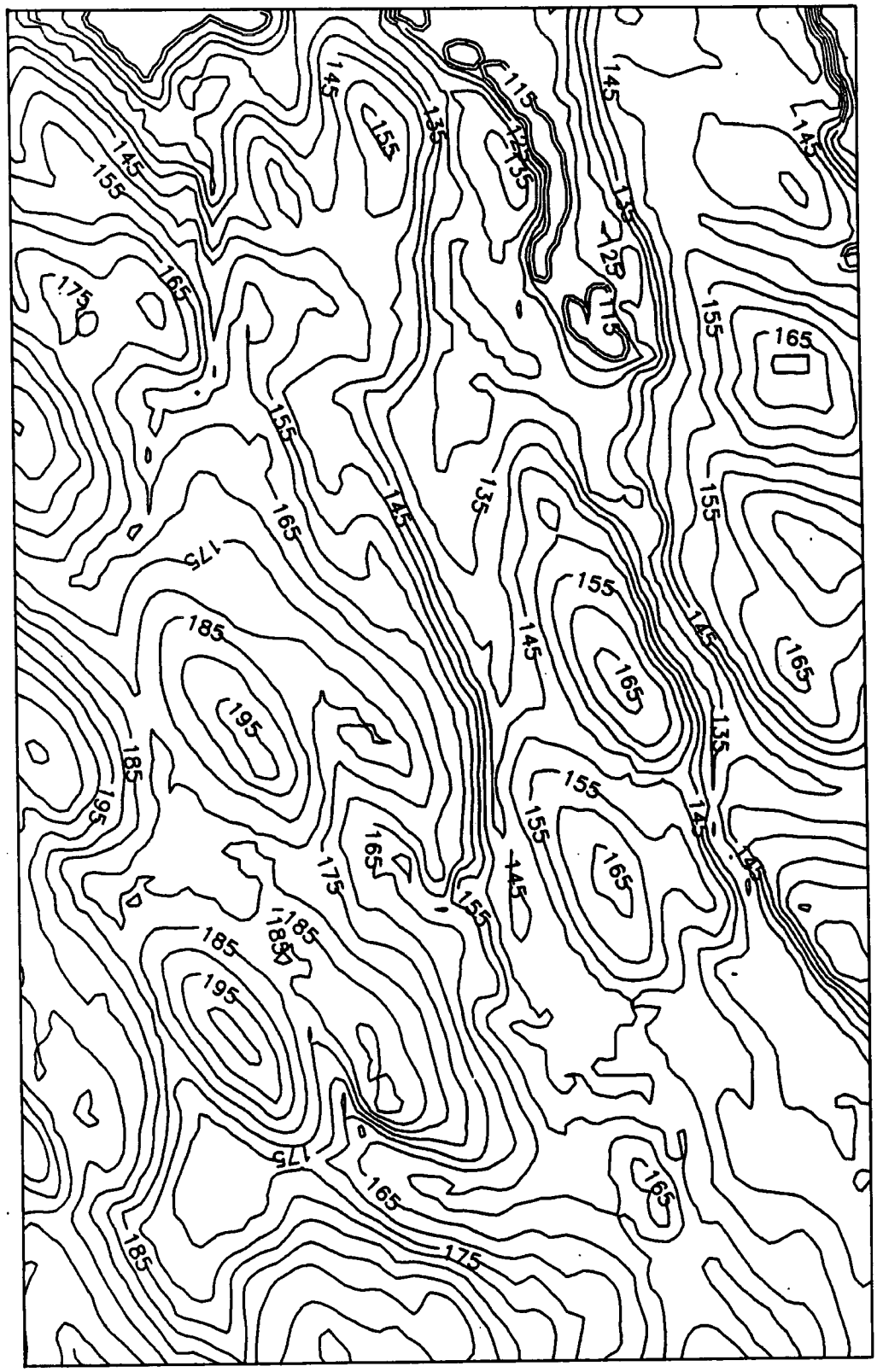

(365000,517000)

Figure 3.4 Profiles calculated from contour maps by DEM.FOR

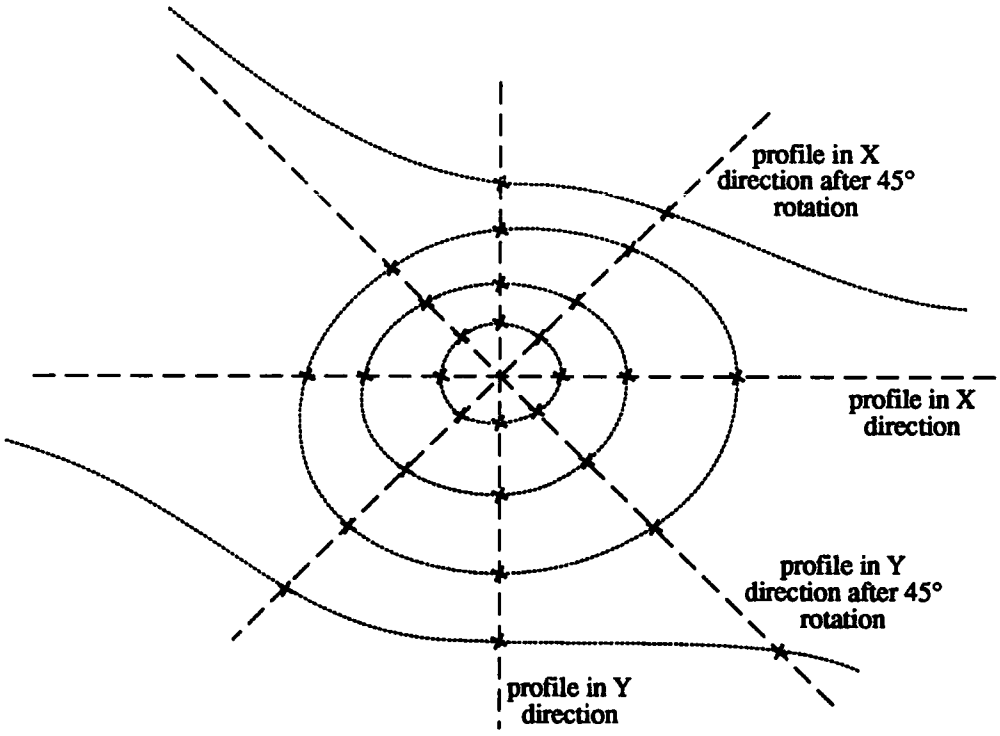

Figure 3.5 Intersection of contour line with grid.

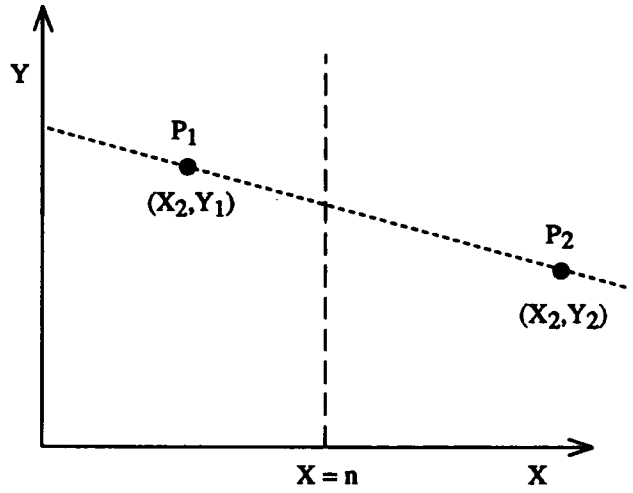

The Y value of the intersection point is simply found by linear interpolation between the point $P1$ and $P2$. Intersections in the X and diagonal directions are calculated in exactly the same way except that for the X direction and its rotated equivalent it is the X value of the intersection point which must be calculated.

Once each point pair has been checked for intersecting grid intervals and the X,Y,Z values of the intersections have been recorded in an array for each profile direction, the arrays for each profile direction are sorted. If the profiles are in the Y direction, as in figure 3.5, the intersections are sorted by X values to place all the intersection points on one profile together. If the profiles are in the X direction then the array is sorted by Y values. The arrays must then be partially sorted once more, to place the points on each profile in order.

The next stage of the algorithm is to fit a spline through the profile intersection points. In DEM.FOR the splines are used directly to estimate a value for the altitude at each grid node on a profile. A weight associated with this estimate can also be found by calculating the distance between the grid node and the two intersection points on either side of it. Any distance weighting function can then be used within the program.

Fitting the splines yields from zero up to four estimates of altitude at each grid node in the matrix to be interpolated, and a weight for each of these estimates, from each profile direction. A final DEM can be calculated from these different estimates by taking a weighted average for every grid point.

3.6 Quality Assessment

In assessing the quality of the DEM produced by each method and combination of values there are several indicators which can be taken into account. The most obvious indicator is the visual appearance of the DEM when it is run through a contouring package in relation to the original contours. Yoeli (1986) used contour threading, where the contours derived from the DEM are threaded through the original contours to see how closely they correspond. The closest operation to contour threading allowed by Surface II is to overlay the posting of the digitised points which make up the input contours with the derived contours. This approach has been used in this investigation.

Surface II contains a routine for error analysis 'ERAN'. This is provided because the averaging processes used to produce grids may fail to honour the data points exactly. An indication of the error in the calculated surface at the data points can be obtained by back-calculating the value of the calculated surface at the data points from the grid matrix values. The back-calculated values can then be compared to the

original data values to produce various statistics. The grid nodes which enclose a particular data point are used in a double linear interpolation to estimate the back-calculated value. The DEM.FOR matrix can be read into Surface II along with the contour points and 'ERAN' will perform an error analysis back-calculating from the DEM.FOR matrix to the contour points.

One problem of interpolating a matrix from digitised contour values is that using the wrong weighting factor may lead to a bias of grid values being estimated at or near contour interval values. An obvious way of checking for this bias is to plot a detailed histogram of calculated grid values and visually checking for spikes at contour altitudes.

3.7 Results

There are eleven statistics examined: the maximum positive error, maximum negative error, absolute mean error, and absolute standard deviation should obviously be as low as possible. Absolute skewness being calculated for a one-tailed distribution should produce as high a positive value as possible with all the values being clustered near the minimum possible value of zero. Likewise kurtosis should be high. The percentage of points with less than 3m error and the Pearsonian correlation coefficient between the original data points and the back- calculated values from the estimated grid nodes should be as high as possible. The mean, standard deviation and skewness of the two-tailed distribution of errors should both be as close to zero as possible.

Figures 3.6 to 3.16 are scatter plots for each statistic with methods classified in terms of their number of phases and search algorithms. The adaptation of Yoeli's contour-to- grid method (referred to as 'contour' in the method classification in the figures) provides by far the worst maximum positive and negative errors, -22.2m and 17m respectively; for ease of display these have been left off the figures. Although the range of maximum negative errors for all the other methods is only 1.114m, the methods exhibiting the smallest maximum negative errors are the two-phased local fits using octant searches except for the one using a $1/D^6$ weighting function (fig. 3.6). For maximum positive error the same pattern of results can be seen (fig. 3.7), one- and two-phase local fits with octant searches giving the lowest maximum errors while the worst results are those methods using a $1/D^6$ weighting function.

The smallest absolute mean errors (fig. 3.8) are given by the kriging methods using a first order polynomial drift and having a minimum of 6 sectors which must contain a data point, and the kriging method with 0 polynomial drift. The worst absolute mean errors are again given by the Yoeli method followed by the one- and two-phase local fits using nearest neighbour searches with $1/D$ weighting. Absolute standard deviation in figure 3.9 shows the same order.

Figures 3.10 and 3.11 display absolute skewness and absolute kurtosis respectively. Both reveal the same pattern with the two previously mentioned kriging methods producing the highest values indicating that the error values for the grids interpolated by these methods are clustered near zero.

Similarly, the methods producing the lowest positive skew and kurtosis are the one- and two-phase local fits using nearest neighbour searches with $1/D$ weighting, Yoeli's method performs slightly better according to these statistics.

The same basic order is shown in the Pearsonian correlation coefficients (fig. 3.12) and the percentage of points with less than 3m errors (fig. 3.13), except that the Yoeli method is again the worst while in the latter all kriging methods perform equally as well.

Statistics for the two-tailed distribution of errors show basically the same pattern as the absolute statistics.

However when considering skewness (fig. 3.14), for which all methods produce negative values, the lowest values are for the kriging methods. The highest values are for the Yoeli method and the one- and two-phase local fits, with nearest neighbour searches and $1/D$ weighting. This suggests that the errors associated with the kriging methods are more commonly overestimates than underestimates while the errors for the one- and two-phase methods are more evenly distributed between over and under estimates.

Mean error against case number in figure 3.15 reveals that the kriging method with 0 polynomial drift gives the closest mean error to zero. However the worst mean error results, after Yoeli's method, are in this case the two-phase method with octant searches and the one-phase method with quadrant search, both with $1/D^6$ weighting. The standard deviation of errors follows the usual pattern (fig. 3.16).

From these statistics it would seem that the worst method tried is the contour-to-grid method, while the best results are usually obtained by the kriging methods. Reference to figure 3.17, which is a scatterplot where the weighting factor has been used to classify the cases, indicates the apparent order of usefulness of the weighting functions. In the case of this drumlinised landsurface $1/D$ weighting would appear to give the worst results. This suggests that more importance must be placed on the points closer to the grid node being estimated. Indeed $1/D^4$, $1/D^6$ and the default weighting, which is very similar to the $1/D^4$ weighting seem to give better results respective to the limitations imposed upon them by the method and search technique being used.

3.8 Limitations of Surface II Error Analysis

The question must be raised of how realistic an indication of grid quality does the Surface II error analysis facility provide. This is because the back-calculation procedure is itself a form of interpolation procedure and will be in error to some extent.

A simple way to assess this was to read a gridded DEM into Surface II as a series of *X*,*Y* and *Z* values, as if the DEM were a series of measurements of *Z*, randomly distributed in the *X* and *Y* directions on a surface. A small increment (5m) was made to each *X* value so that the procedure would not fail due to the number of operations which would have to be performed on this unrealistic number of zero errors.The DEM was then read in as a matrix with its *X* and *Y* values implicitly contained in the data structure. 'ERAN' was then used to back-calculate from the matrix to the supposedly random 'original' data.

The results of this assessment were reasonably pleasing with statistics such as absolute mean error, absolute standard deviation, and standard deviation being around one order of magnitude better than for the kriging method with the zero degree polynomial drift. The percentage of points with less than 3m error was 100 and the correlation between original values and back-calculated values was 0.999. These statistic therefore suggest that 'ERAN' provides a useful tool to assess DEM interpolation quality.

Figure 3.6

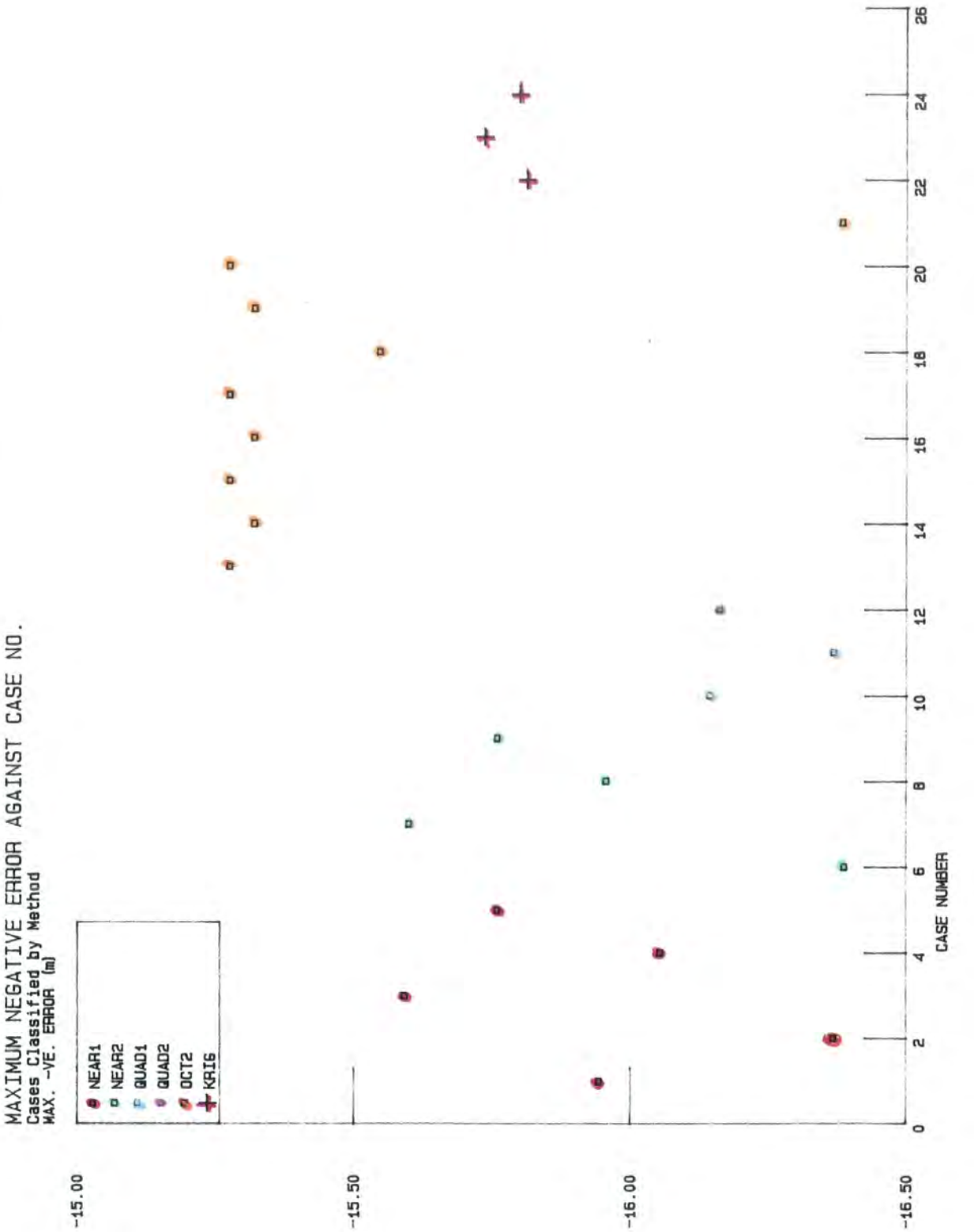
MAXIMUM NEGATIVE ERROR AGAINST CASE NO.
Cases Classified by Method
MAX. -VE. ERROR (m)
NEAR1
NEAR2
QUAD1
QUAD2
OCT2
KRIG
-15.00
-15.50
-16.00
-16.50
0
2
4
6
8
10
12
14
16
18
20
22
24
26
CASE NUMBER

Figure 3.7

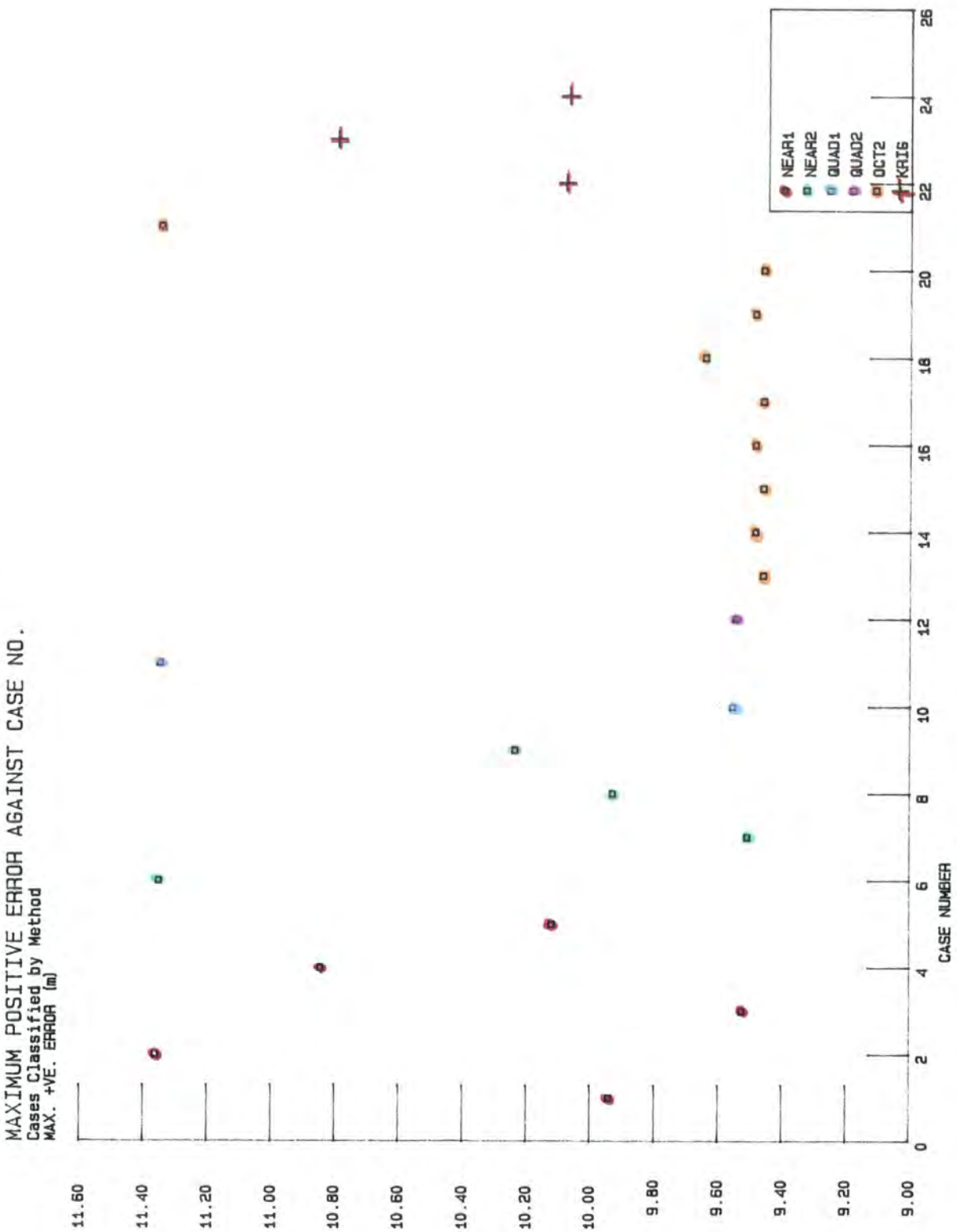
MAXIMUM POSITIVE ERROR AGAINST CASE NO.
Cases Classified by Method
MAX. +VE. ERROR (m)
11.60
11.40
11.20
11.00
10.80
10.60
10.40
10.20
10.00
9.80
9.60
9.40
9.20
9.00
0
2
4
6
8
10
12
14
16
18
20
22
24
26
CASE NUMBER
NEAR1
NEAR2
QUAD1
QUAD2
OCT2
KRIG

Figure 3.8

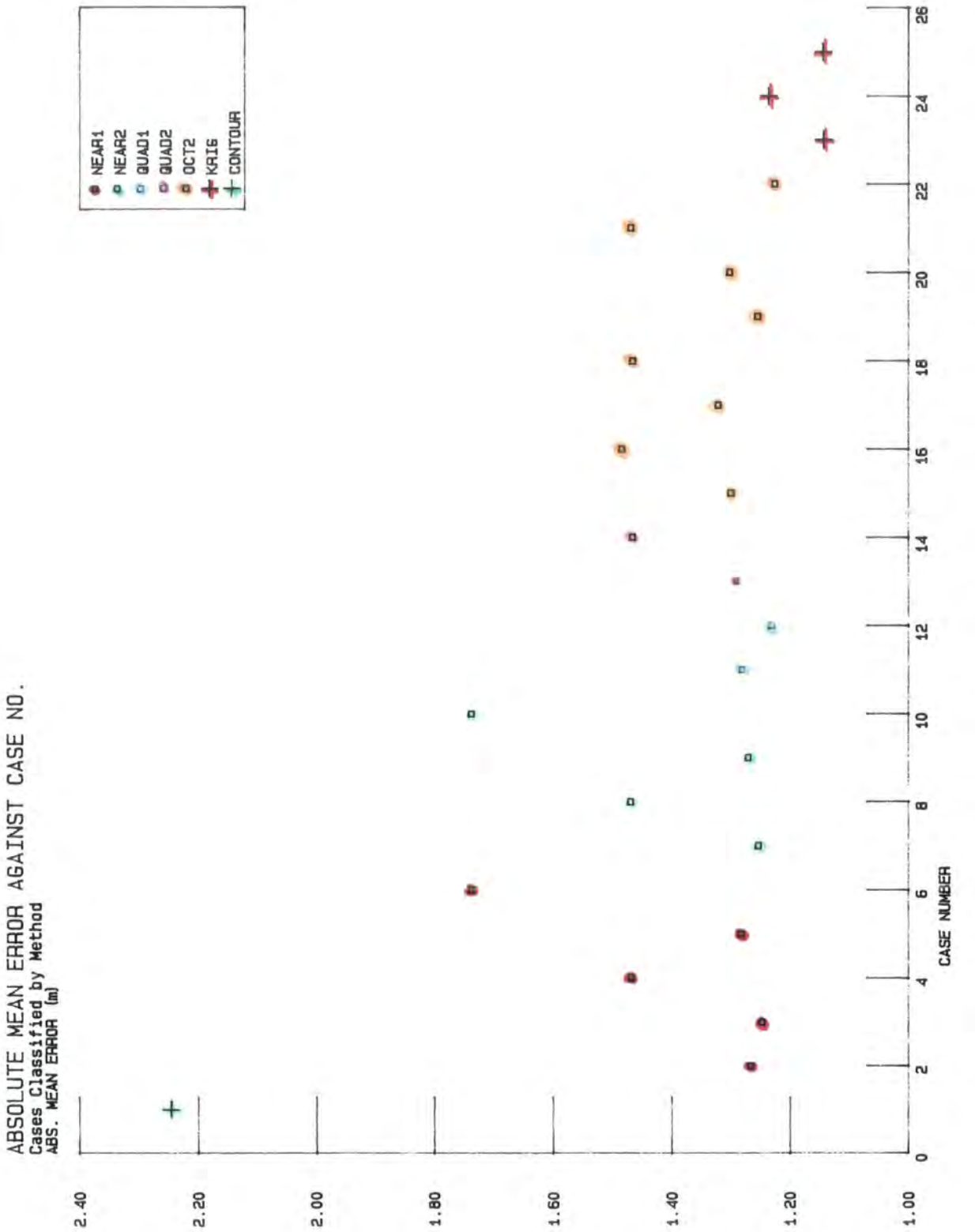
ABSOLUTE MEAN ERROR AGAINST CASE NO.
Cases Classified by Method
ABS. MEAN ERROR (m)
NEAR1
NEAR2
QUAD1
QUAD2
OCT2
KRIG
CONTOUR
2.40
2.20
2.00
1.80
1.60
1.40
1.20
1.00
0
2
4
6
8
10
12
14
16
18
20
22
24
26
CASE NUMBER

Figure 3.9

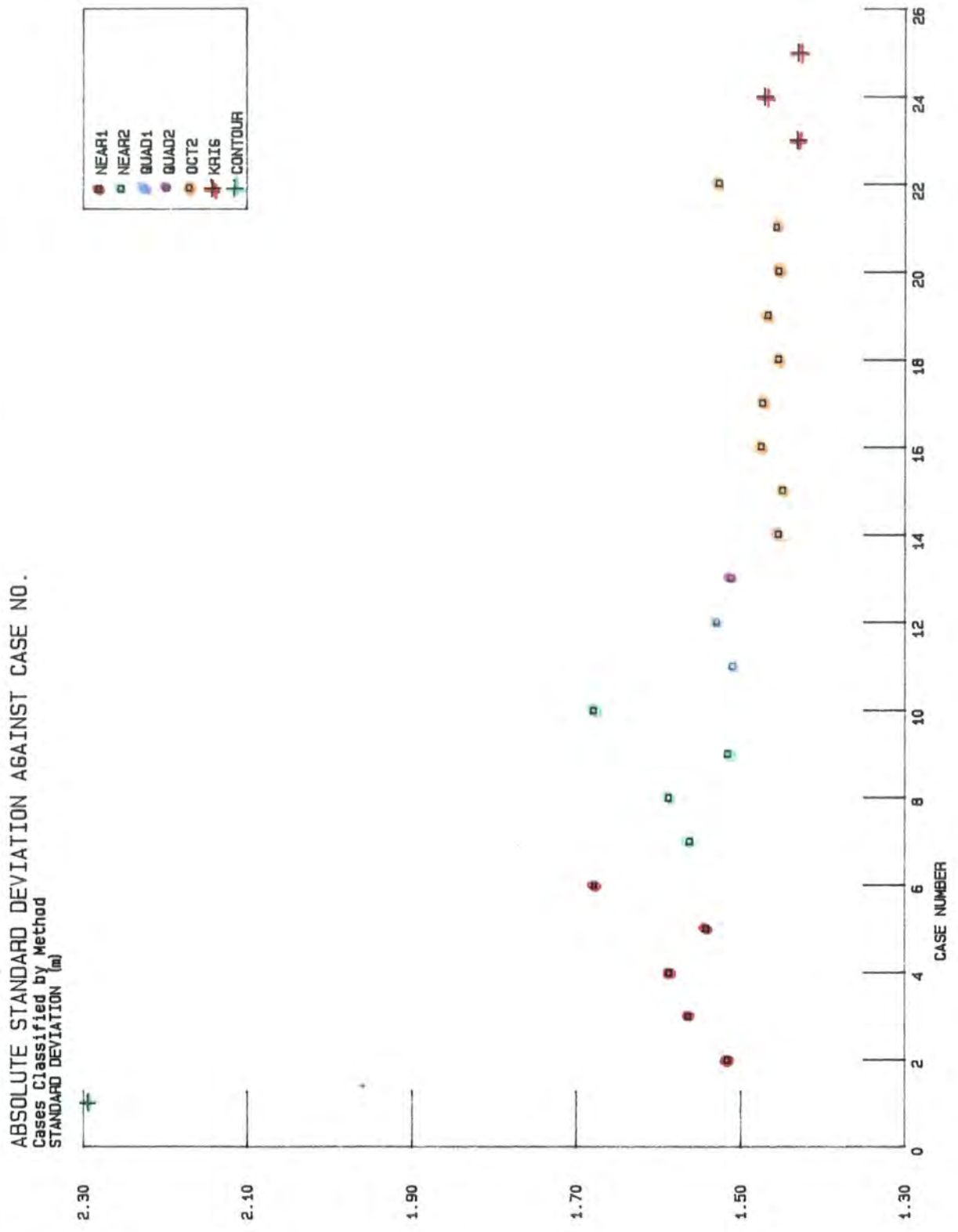
ABSOLUTE STANDARD DEVIATION AGAINST CASE NO.
Cases Classified by Method
STANDARD DEVIATION (m)
NEAR1
NEAR2
QUAD1
QUAD2
OCT2
KRIG
CONTOUR
2.30
2.10
1.90
1.70
1.50
1.30
0
2
4
6
8
10
12
14
16
18
20
22
24
26
CASE NUMBER

Figure 3.10

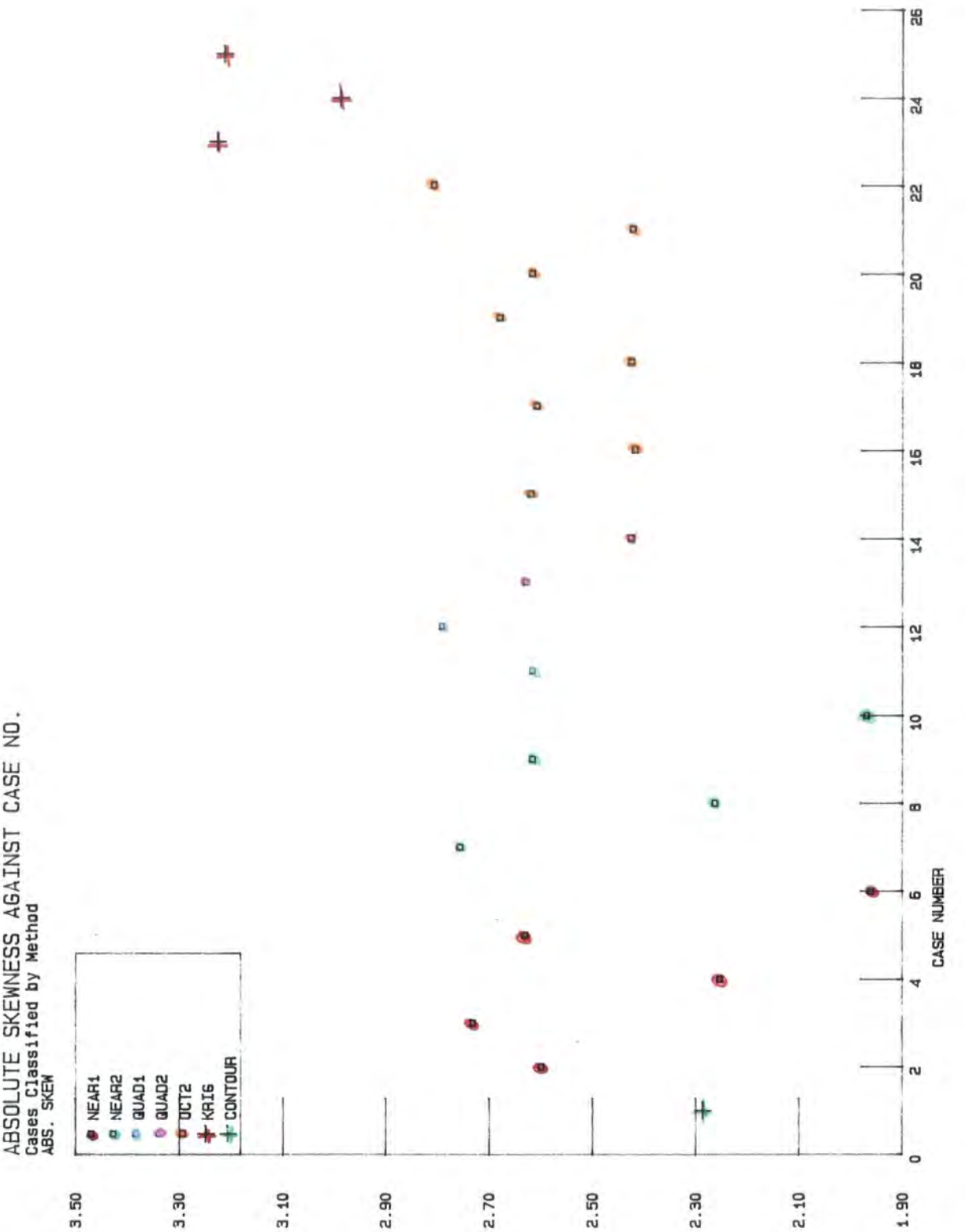
ABSOLUTE SKEWNESS AGAINST CASE NO.
Cases Classified by Method
ABS. SKEW
NEAR1
NEAR2
QUAD1
QUAD2
OCT2
KRI6
CONTOUR
3.50
3.30
3.10
2.90
2.70
2.50
2.30
2.10
1.90
0
2
4
6
8
10
12
14
16
18
20
22
24
26
CASE NUMBER

Figure 3.11

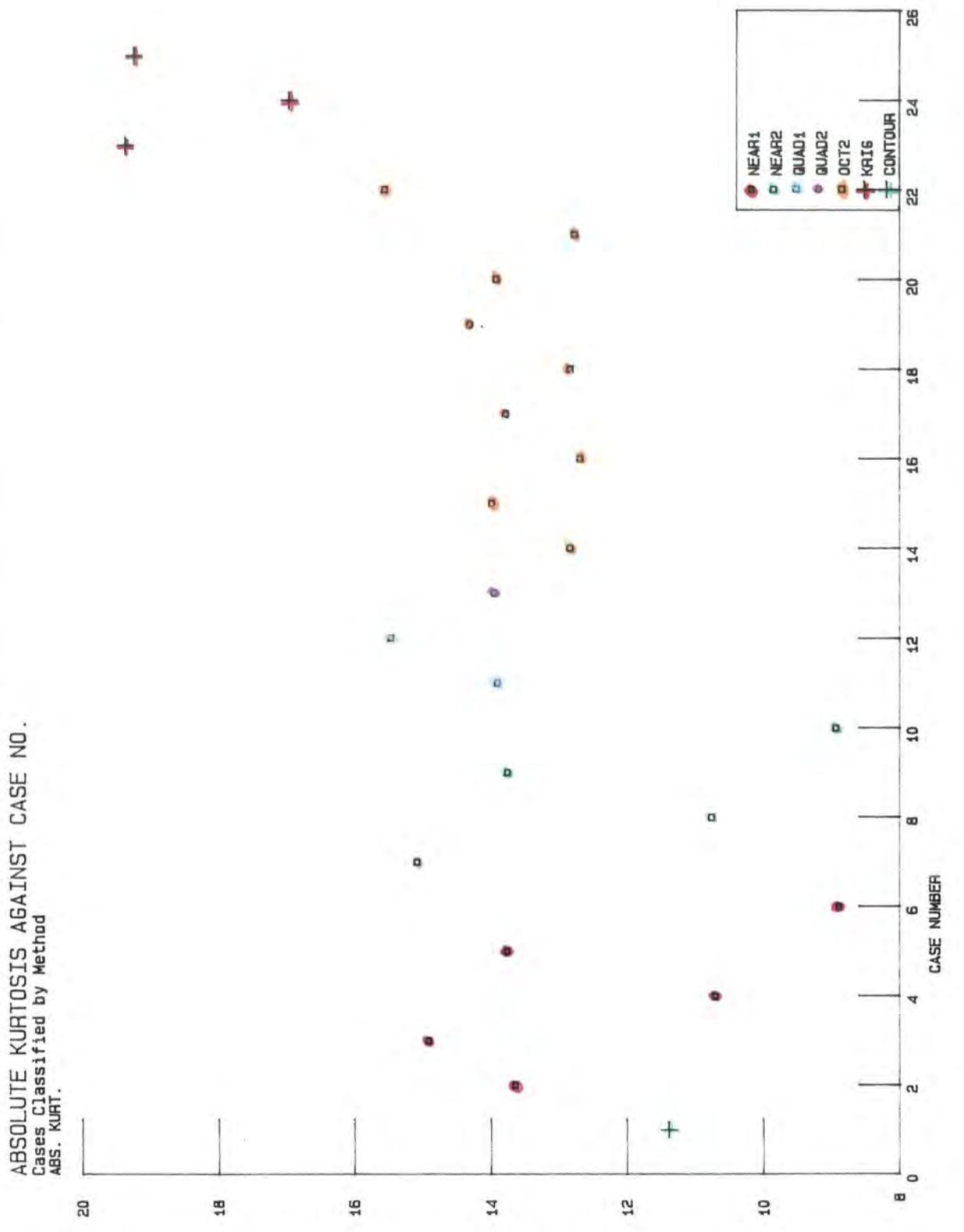
ABSOLUTE KURTOSIS AGAINST CASE NO.
Cases Classified by Method
ABS. KURT.
20
18
16
14
12
10
8
0
2
4
6
8
10
12
14
16
18
20
22
24
26
CASE NUMBER
NEAR1
NEAR2
QUAD1
QUAD2
OCT2
KRIG
CONTOUR

Figure 3.12

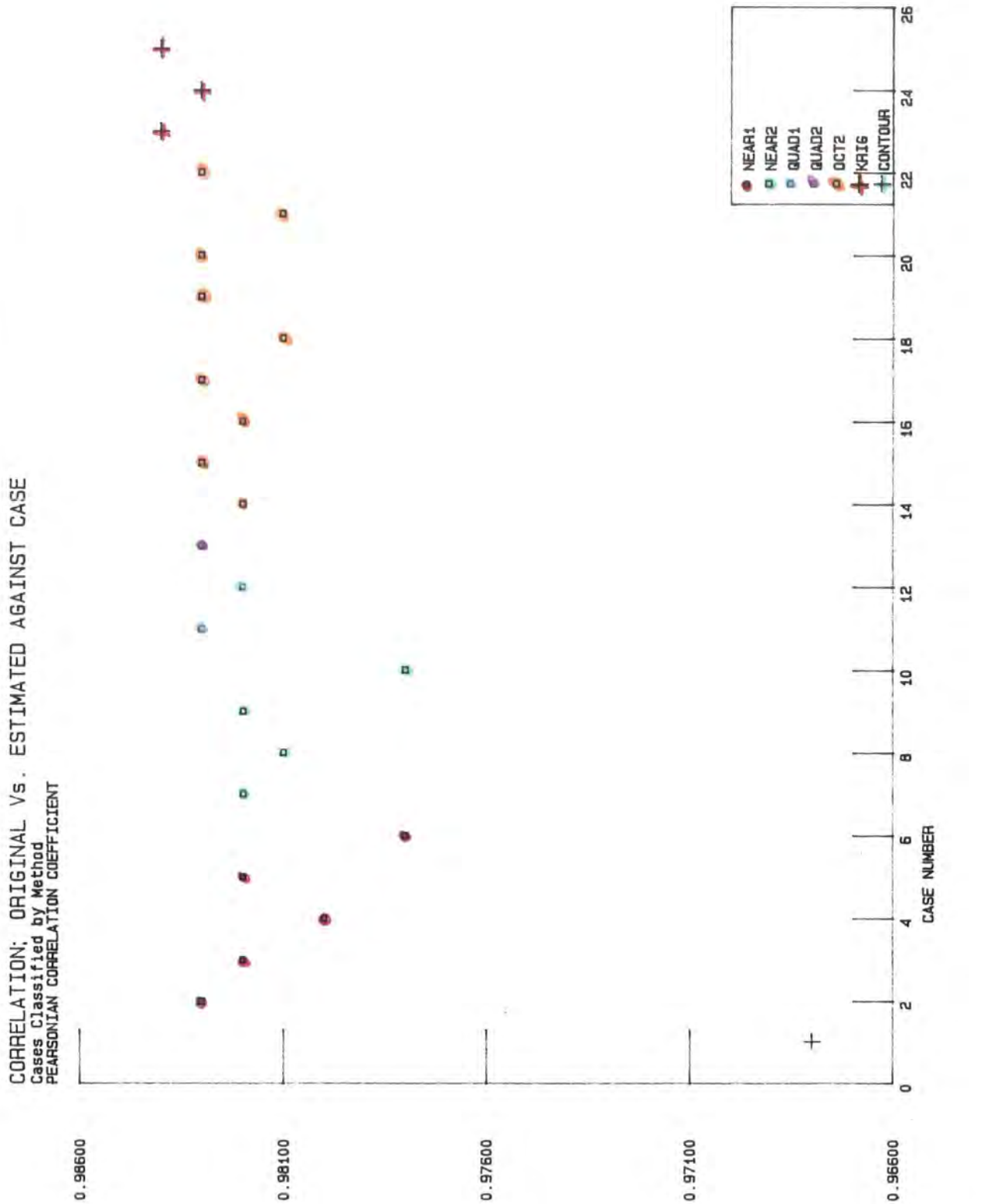
CORRELATION; ORIGINAL Vs. ESTIMATED AGAINST CASE
Cases Classified by Method
PEARSONIAN CORRELATION COEFFICIENT
0.98600
0.98100
0.97600
0.97100
0.96600
0
2
4
6
8
10
12
14
16
18
20
22
24
26
CASE NUMBER
NEAR1
NEAR2
QUAD1
QUAD2
OCT2
KRIG
CONTOUR

Figure 3.13

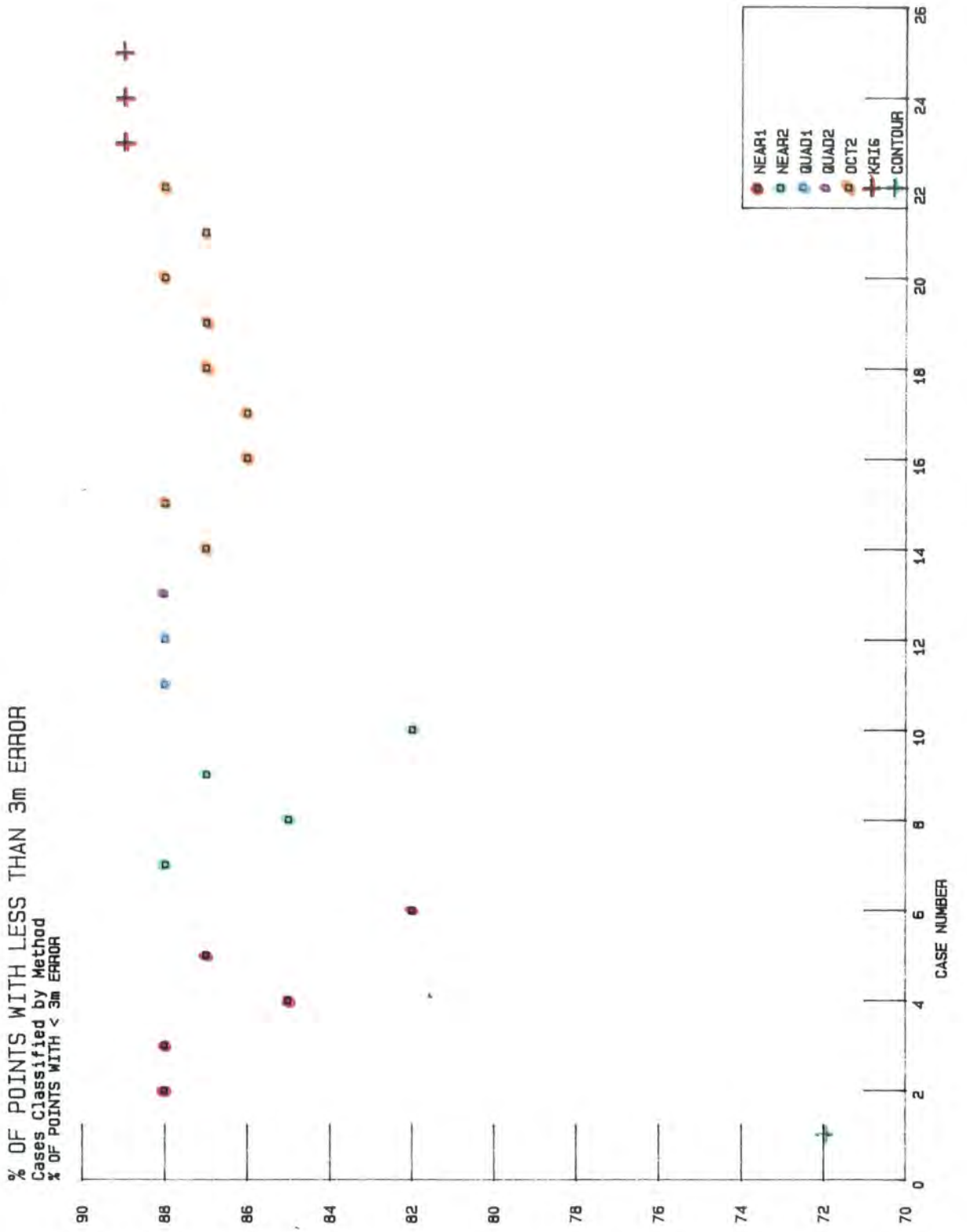
% OF POINTS WITH LESS THAN 3m ERROR
Cases Classified by Method
% OF POINTS WITH < 3m ERROR
90
88
86
84
82
80
78
76
74
72
70
0
2
4
6
8
10
12
14
16
18
20
22
24
26
CASE NUMBER
NEAR1
NEAR2
QUAD1
QUAD2
OCT2
KRIG
CONTOUR

Figure 3.14

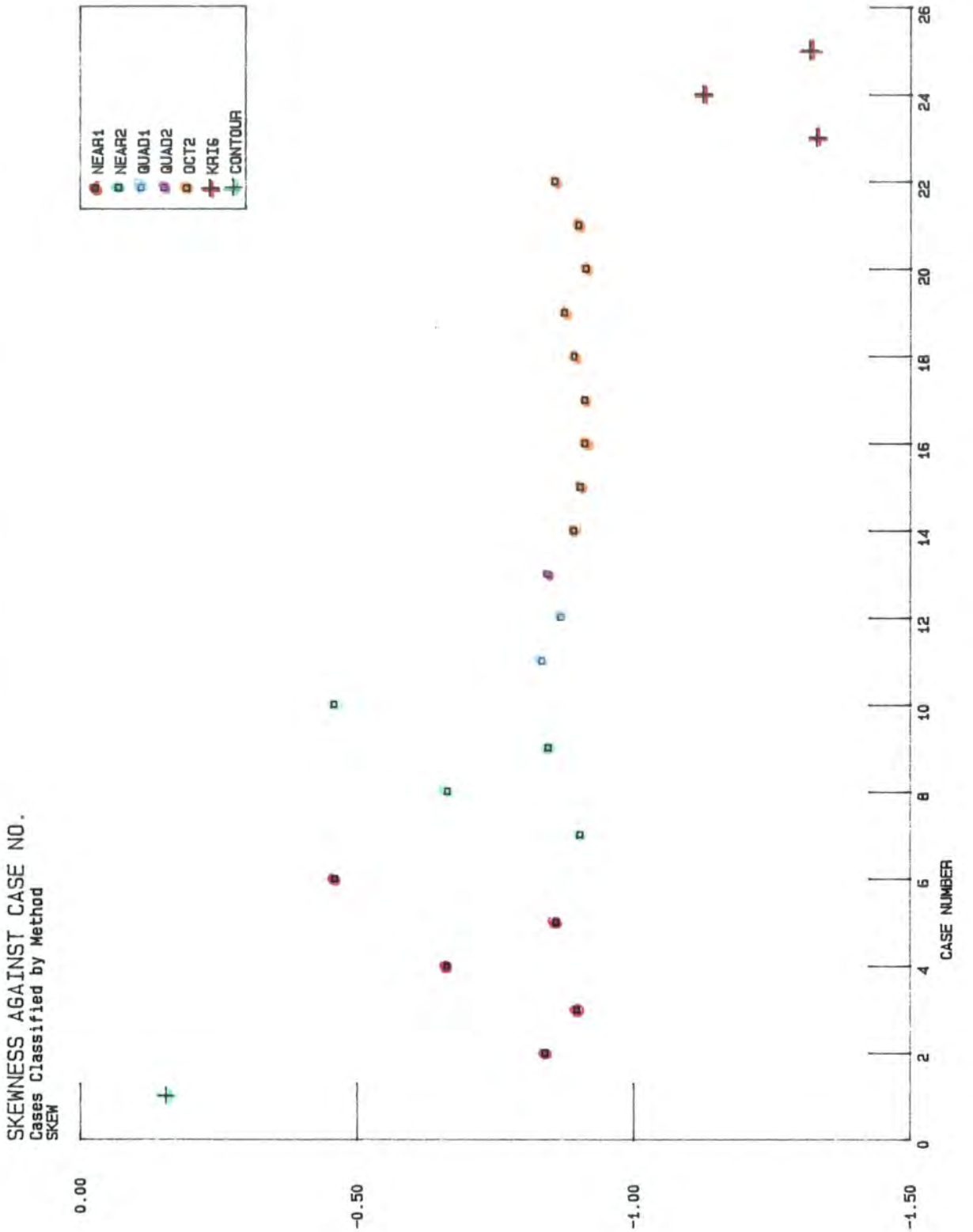
SKEWNESS AGAINST CASE NO.
Cases Classified by Method
SKEW
NEAR1
NEAR2
QUAD1
QUAD2
OCT2
KRIG
CONTOUR
0.00
-0.50
-1.00
-1.50
0
2
4
6
8
10
12
14
16
18
20
22
24
26
CASE NUMBER

Figure 3.15

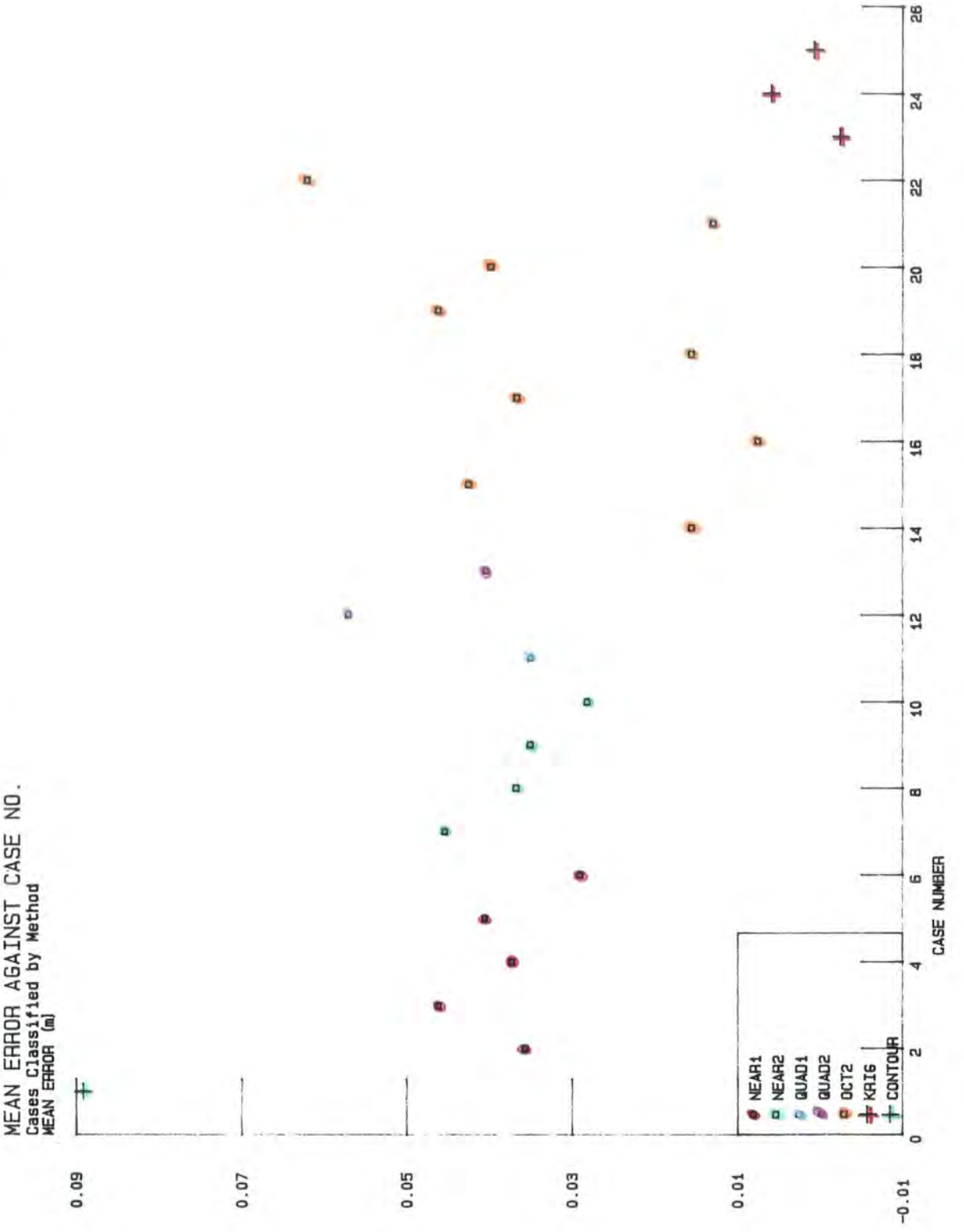
MEAN ERROR AGAINST CASE NO.
Cases Classified by Method
MEAN ERROR (m)
0.09
0.07
0.05
0.03
0.01
-0.01
0
2
4
6
8
10
12
14
16
18
20
22
24
26
CASE NUMBER
NEAR1
NEAR2
QUAD1
QUAD2
OCT2
KRIG
CONTOUR

Figure 3.16

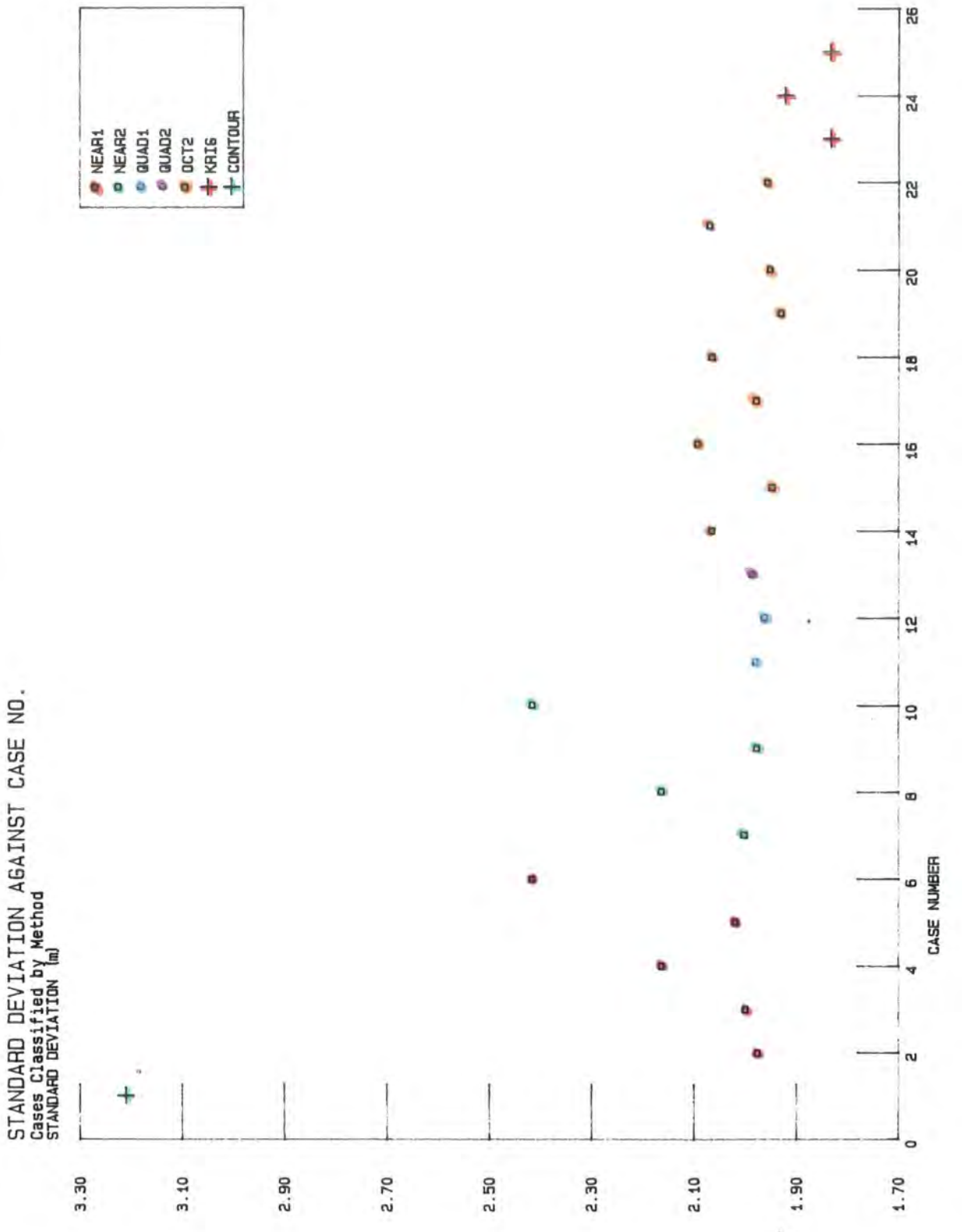
STANDARD DEVIATION AGAINST CASE NO.
Cases Classified by Method
STANDARD DEVIATION (m)
NEAR1
NEAR2
QUAD1
QUAD2
DCT2
KRIG
CONTOUR
3.30
3.10
2.90
2.70
2.50
2.30
2.10
1.90
1.70
0
2
4
6
8
10
12
14
16
18
20
22
24
26
CASE NUMBER

Figure 3.17

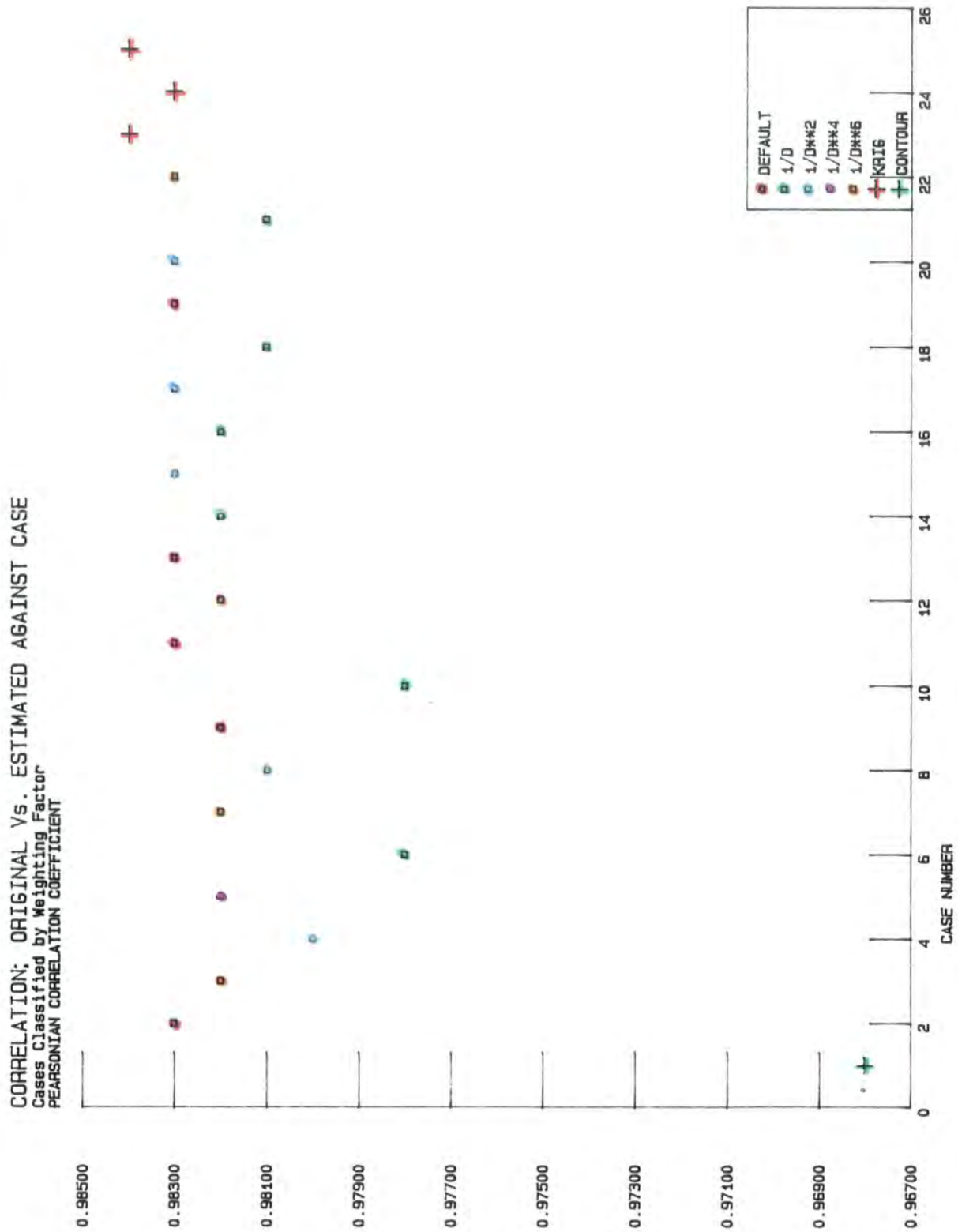
CORRELATION: ORIGINAL Vs. ESTIMATED AGAINST CASE
Cases Classified by Weighting Factor
PEARSONIAN CORRELATION COEFFICIENT
0.98500
0.98300
0.98100
0.97900
0.97700
0.97500
0.97300
0.97100
0.96900
0.96700
0
2
4
6
8
10
12
14
16
18
20
22
24
26
CASE NUMBER
DEFAULT
1/D
1/D**2
1/D**4
1/D**6
KRIG
CONTOUR

3.9 The Spatial Distribution of the Errors.

The back-calculated error values were read back into Surface II and contour plots of error were produced for a number of the methods used. All plots show that the worst errors are found in the flood plain of the Eden, the main river through the area.

This is easily explained by the fact that there are fewer contours over these level areas, in comparison to the drumlinised areas, and as a result the difficulty of interpolation in these areas where control points at different heights are separated by greater distances than for the rest of the surface cause problems for all the methods used. This is a problem common to all automated methods and only methods which can mimic the decision criteria used by a manual interpolator can begin to solve the problem. These decision criteria are reasonably complicated and the development of algorithms which successfully mimic the human interpolator would provide subject matter for several theses. Fortunately it is not the flood plains of this area which are of primary interest to this study; the drumlins of the area seem to suffer from less interpolation error.

3.10 Bias Toward Contour Levels.

As previously mentioned a bias of interpolated grid node values toward contour intervals can result when creating DEMs from contour maps. The frequency histograms of interpolated altitudes show this up clearly as spikes of high frequency at each contour level altitude in extreme cases. In cases where bias is slight, frequency of altitude increases up to, and then declines from, the contour level altitude. In the extreme cases, the usually near normal distribution of landsurface altitudes is almost obscured by spikedness.

The main influence on this bias is the use of an inappropriate weighting function. The worst case of spikedness encountered in this study was produced by the one-phase local fit using a nearest neighbour search with $1/D^6$ weighting. This is understandable because firstly the nearest neighbour search will tend to find points close together on the same contour line. Secondly, the weighting function has the strongest distance decay available in Surface II so points further away on other contours will be given very little weight.

The least biased DEM produced was in fact the one produced by DEM.FOR. This is for two reasons. Firstly, and least importantly, the topological information about the contours used by the program ensures that points which are adjacent to one another on the same contour line cannot be used in the interpolation as they are in the random-to-grid methods such as the one using the nearest neighbour search just mentioned.

Instead, the two contours which the grid node encloses are used in the interpolation. However the weighting of the estimates from these different contours is again a function of distance and this provides the major reason why the DEM.FOR method gives the least biased DEM. DEM.FOR used a $1/\sqrt{D}$ weighting function to produce this least biased DEM. This weighting function makes weight decay more slowly with distance and is not available with SURFACE II.

The next least biased DEM was produced using kriging with 0 polynomial drift. As mentioned previously the weights used in this interpolation are based on the spatial continuity of the surface as expressed by the slope of the semi-variogram, and so the weights are related to the actual surface being interpolated and not just a distance weighting function subjectively chosen by the user.

3.11 Visual Assessment.

So far, the kriging method with no polynomial drift has seemed to perform best over all the assessments used. However, since the back-calculating error analysis routine is itself an interpolation procedure and subject to some error, and, as there is some trade-off between bias in the interpolated values towards contour levels and the error analysis results ($1/D^6$ gives the largest bias but in general gives better error statistics than, for example, $1/D$ weighting) it seems prudent to go back to a visual comparison between the original data and the DEM produced.

Using Surface II, contour plots of the DEMs created by different methods were overlayed with the original data points, that is the points digitised along each of the original contours. The hard copy output of these plots was sufficiently large to be able to see both data points and contour lines clearly and as a result were too large to be included here.

The spatial distribution of error suggested by the 'ERAN' command was confirmed by all the plots, with the worst discrepancies between original points and derived contours occurring in the river flood plain and other relatively flat areas with a lack of control points. These areas often had spurious contour loops present. The Eden valley, for example is broken up into a number of closed basins by each method.

From a visual perspective, the best DEM was again the one constructed using kriging with no polynomial drift. DEMs produced using octant searches were the next best visually (the kriging method also uses the octant search methods). The nearest neighbour methods produced the worst visual results. Their contour plots showed jagged contours compared to the smoother octant search contours. This can be explained by the bias already mentioned toward adjacent points on the same contour

the nearest neighbours to the grid node being interpolated. The contours of the interpolated surface therefore lurch between the original contour lines. The octant search allows this to be overcome by forcing the selection of points in several different directions and as a result it is more probable that more than one original contour line will be considered in the interpolation.

3.12 Conclusions.

The limitations imposed by time and software availability in Durham have directed the study towards the creation of DEMs from contour maps by one out of a choice of several possible semi-automated methods.

The most appropriate method considered on the basis of the quality assessment criteria used is universal kriging, with the drift being dealt with by subtracting the mean from every data point. It has proved to perform better than the other Surface II random-to-grid methods because it uses octant searches to select data points to be used in the kriging process and the weightings used in this process are directly related to the statistical properties of the surface being worked on. As a result this kriged DEM will be the one used in the rest of this study..

This work has encountered most of the problems generally associated with semi-automated interpolation of DEMs. Perhaps the creation of DEMs is best achieved by manual interpolation from contour maps. However, as mentioned previously, to produce a DEM of an equivalent area completely by eye and hand would take days of tedium furthermore there are levels of subjectivity in the process of manual interpolation which it may be desirable to avoid.

The search for algorithms which reflect some of the desirable interpolation criteria of a manual interpolation continues. The IGN are still using a Yoeli-type method with a slightly more complicated curve fitting process and no doubt superior coverage of contour and spot height data than is available to this study. They are still encountering exactly the same problems as in this study (Breard 1989). The IGN have also looked at the random-to-grid procedures supplied with packages such as Uniras and have found them less satisfactory.

The decision must be made in the light of these short comings as to the wisdom of using semi-automated products in this study. In the case of the drumlins DEM it is worth using this surface because as mentioned previously the major source of error is in the main flat areas predominantly in the Eden river flood plain. The drumlins themselves are the most accurately depicted areas in the DEM. Knowledge of the limitations of DEM production makes their use reasonable.

Chapter 4: Detecting Scaling Behaviour in Landsurfaces

4.1 Introduction

As the range of phenomena which seem to display fractal behaviour is very large, there is perhaps an equally large range of techniques for assessing scaling behaviour and estimating fractal dimension. Two techniques and some of their applications have already been mentioned; rescaled range analysis and the perimeter-area relationship.

Mandelbrot (1975) described in some detail his view of the fractal behaviour of the Earth's relief, linking it to the fractal nature of coastlines and size distribution of islands. This has provided geomorphology the task of examining these ideas by empirically studying landsurfaces and by theoretically trying to reconcile fractal concepts with possible physical mechanisms which might allow such fractal behaviour in landsurfaces.

There has been some response from geomorphologists, and they can also refer to work which has been carried out on other types of surface and even to work on the description of particle shape. The majority of this work has analysed contours taken from surfaces or profiles across surfaces, using one-dimensional techniques. The methods used in these studies and some of the results will be discussed in this chapter.

The use of two-dimensional techniques, considering the whole surface at once, has been much less widespread but is obviously attractive when investigating Mandelbrot's (1975,1982) claim that any contour or profile taken from a fractal surface should have the same fractal dimension as that of the surface, minus one. If Mandelbrot's claim is incorrect for real surfaces, as has been suggested by Goodchild (1982), then an assessment of the relevance of scaling behaviour in the surface as a whole still needs to be looked for and geomorphological equivalents to the general scale invariance of clouds need to be considered. The various two-dimensional techniques and algorithms proposed and their results will be introduced in this chapter. Adaptations of these techniques to consider anisotropic effects in landsurfaces and areal distribution of different processes will also be discussed.

4.2 One-dimensional Techniques.

Most of the one-dimensional techniques used to assess scaling behaviour of perimeters and profiles of geomorphic features, and other surfaces and shapes, have

been based on Richardson's (1961) divider-walking method, referred to in Chapter 2. The equation (2.18) describes the relationship which this is based on

$$L(\delta) = a.\delta^{(1-D)}$$

Richardson (1961) manually walked a set of dividers along atlas map representations of coastlines and international boundaries to study the relationship between divider spacing and length estimates of these features. He started by measuring the entire length in one step. Then the length was remeasured using two steps and so on. The length measurements were then plotted, along logarithmic axes, against divider step length. This type of plot has subsequently become referred to as a 'Richardson's plot' by many workers. Richardson drew attention to several of the problems in his method. He found that because of the irregularity of the boundaries *"the fitting of a whole number of sides can only be done by troublesome successive approximations"* (Richardson, 1961, p.170). The final step to be measured was allowed to be a fraction of the step length being used. For similar reasons Richardson discovered that the total polygonal length, including the estimated fraction, when measuring the length of a closed line depends slightly on the starting point of the walk.

The method of manually walking dividers and the way in which it should be performed has been reassessed as recently as 1984 by Kaye (1984). Kaye describes the process of measuring line length at different step sizes as a 'structured' walk. He stresses the need to detail the algorithm used carefully when writing about the results obtained from such a structured walk. Variations, such as which way the divider swings, clockwise or anticlockwise or alternately between the two, can produce different results. Kaye is in agreement with Richardson on adding the fractional final step required in many walks to the estimate of length. He suggests normalising the magnitude of measurements by dividing measurements by the 'ferets' diameter of the closed shape being analysed. The ferets diameter is the fine particle science term for the maximum projected length of a polygon.

Kaye (1984) discusses the need for a multifractal approach when dealing with fine particle boundaries. He suggests that *"it is necessary to use different fractals to describe different aspects of the boundary structure when examined at different levels of scrutiny"* (Kaye, 1984, p.17). Kaye writes of a 'structural' fractal which describes the general irregularity of the shape as a whole, and a 'textural' fractal which describes the irregularity of the packing of the material which makes up the fine particle. He speculates as to how this method would apply when looking at coastlines (fig. 4.1) but provides no empirical evidence for examination.

Figure 4.1 *Kaye's hypothetical coastline: as it includes certain man-made features and would have different fractal dimensions depending on the scale at which it was examined. P is the length of the coastline; λ is the resolution of examination. (From Kaye, 1984)*

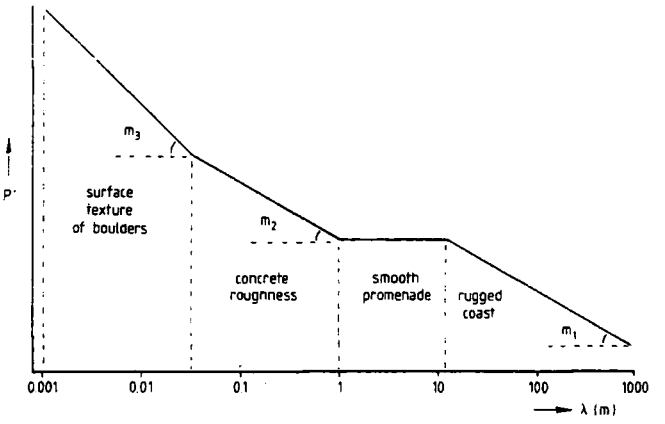

Clearly, if a large number of lines or maps at larger than atlas scale are going to be studied, it would be advantageous to automate this manual method to work on digitised data. Indeed, most of the one-dimensional work carried out since Richardson's has turned to automated adaptations of the manual walking-dividers technique.

Some of the earliest investigations of fractal ideas by geomorphologists using Mandelbrot's (1967) development of Richardson's work includes the work of Hakanson (1978) and Goodchild (1980). However this early work is focused more on examining the accuracy of geographical line lengths and surface areas with respect to map scales and measurement techniques used rather than empirically studying scaling behaviour and fractal dimension in such features.

Goodchild (1982) returned to fractal concepts in his study of fractional Brownian motion's contribution as a model for terrain. He used three methods to estimate the fractal dimension of: the shoreline; 250ft contour; 500ft contour; and lake outlines taken from 1:50,000 maps of Random Island, Newfoundland.

The first method used was a computer simulation of the manual walking-dividers method upon which Goodchild does not elaborate. The second method was developed for Goodchild's (1980) analysis of geographical line length. In it, a grid cell system is overlaid on the digitised line set. Line length is then estimated by counting the number of boundary grid cells which have neighbours both above and below the given line set. Equation (2.18) is then used to work out D from the relationship between line length and grid cell size. The third method used is based on the area-perimeter relationship, discussed in Chapter 2, although Goodchild did not explain how he measured area for this analysis.

Goodchild's results are very interesting and will be discussed more fully in later chapters. His results show that all the methods used give the same ranking of line sets when this ordering is based on the value of *D*. The shoreline has the lowest values of *D* for each method, and *D* increases for each method with altitude. This suggests that landsurfaces cannot be thought of as being like fractional Brownian surfaces where a contour line or profile taken from the surface will have the same fractal dimension as the surface, minus one. For a given line set, however, each method gives a slightly different estimate of *D*. The methods when applied to the shoreline give a small range from 1.11 to 1.14; for the 500ft contour this range has risen with *D* varying from 1.19 to 1.54. This range is unacceptably large as on the basis of Chapter 2 a dimension of 1.19 indicates quite a strong interdependence of altitude values separated by quite some distance, whereas a *D* of 1.54 suggests statistical independence between points.

The grid cell method is also used in a study by Shelberg et al. (1983). Goodchild (1980) had used the contour of the mean value of the maximum and minimum altitudes from simulated fractal surfaces to estimate fractal dimension using the grid cell method. Shelberg et al. (1983) appreciated the possibility that if a surface being analysed was composed of a mountain range and a plain, a contour with a low altitude which only occupies the plain, or a high altitude which only occurs in the mountains might give a biased view of the *"overall fracticality"* (Shelberg et al., 1983, p.322) of the surface. To overcome this possible bias they apply the grid cell method to a large sample (up to 200) of different contours from the surface. *D* is estimated for each one and the average value for *D* of the sample is considered to be what they call the surface's 'fracticality'. Three surfaces are analysed in their study. Two are fractal simulations and one is a DEM from southern Nevada. The results for the real surface show a variation of only 0.02 for different contour intervals used; however they do not state to what extent the real surface might be related to their hypothesised plain and mountain range situation.

Kennedy and Lin (1986) discuss three automated methods to estimate fractal dimension as an aid to shape analysis. The first which they call the 'exact' method is a direct automation of the manual Richardson walking divider method.

The algorithm is simple. A starting point on the digitised outline of the shape is selected. A minimum step length is selected for the first walk, δ. The straight line distance, *d*, between the starting point and the next digitised point in a selected direction from it (clockwise or anticlockwise) is calculated. This procedure occurs until *d* exceeds δ. When this occurs the point at which straight line distance equals δ is linearly interpolated between the point where *d* first exceeds δ and the previous digitised point. The interpolated point is then used as the new starting point for the next step. A length estimate from the walk can be made by multiplying the number of steps plus the fractional step which may have been required to complete the walk by the step length.

This produces one point for a Richardson's plot and obviously the process is repeated over the range of step sizes permitted by the data's resolution.

The second method discussed by Kennedy and Lin (1986) is the 'fast' method introduced by Schwarz and Exner (1980).

This method overcomes the time-consuming process in the 'exact' method of interpolating the point at which a step arrives. Instead of using a fixed length step size in each walk a step size which is a fixed number of boundary points is used. A walk proceeds by stepping a specified number of points from the starting point, again in a specified direction.The distance between the starting point and the point walked to is then calculated and stored. The point walked to becomes the new starting point and the walk continues. Once the walk has been completed an average step length is calculated from the stored distances. This average distance is then used in the Richardson's plot along with the results from other walks to calculate the fractal dimension. This method has the disadvantage of resulting in smaller step lengths where the line being measured is more irregular and there are more points digitised to describe the shape.

Kennedy and Lin's third method is called the 'FAENA' method (FAENA is for Fractal Analysis by Estimation - Normalised Approach) and is similar to Clark's (1986) 'Hybrid' method. In the FAENA method the digitised points are searched until ∂ is exceeded and the point where that occurs becomes the new point to step from. The distance of each step is again recorded so that an average can again be used in the Richardson's plot. Clark (1986) also reviews the 'exact' and 'fast' methods and proposes what he calls the 'hybrid' method where the point is searched out that has the straight line distance from the starting point which is closest to, either greater than or less than, δ. Both the Hybrid and FAENA methods are faster than the exact method but more accurate than the Fast method.

These methods are all clearly-defined algorithms, an advantage and quality which Kaye (1984) suggested should be looked for. Kennedy and Lin point out that these methods can be used for shapes which do not possess scaling behaviour over wide scale ranges, which may be multifractals.

One other method which can be used to estimate the fractal dimension of one-dimensional data is spectral analysis. A fractional Brownian function has a power spectrum which decays with frequency, k, in the form $k^{-(2H+1)}$ (Mandelbrot, 1975). That is the slope of the power spectrum on a log-log plot is $-(5-2D)$. Brown and Scholz (1985) use this relationship on the power spectra of several natural rock surfaces. They measured profiles of the surface topography of eight different rock surfaces in the field and laboratory over a scale range of 1m to 10 microns.

They then computed the power spectra of the profiles by a fast Fourier transform technique. The power spectra plotted on log axes reveal convex relationships and when split into narrower bands of frequency ranges the values of the slopes of the spectra change from band to band. They conclude from this *"that for fractals to be quantitatively useful in the study of rock surfaces, one must explicitly include the variation of the fractal dimension with spatial frequency"* (Brown and Scholz, 1985, p.12581).

The next section deals with the obvious idea of extending the popular and simple 'walking-dividers' methods to two-dimensions. As will be seen this is more difficult than it would appear.

4.3 The Triangular Prism Surface Area Method.

Clarke (1986) advocates mimicking the walking divider method in two dimensions. The algorithm he suggests deals with surface area instead of line length and instead of divider step size he proposes resolution at which surface area is measured.

In Clarke's method surface area is calculated by interpolation from DEMs. Surface area for a particular resolution is calculated by taking four elevations from the DEM which form a square with the required resolution. The average of these four elevations is then taken as the elevation of a fifth point which is allocated the position at the midpoint of the square. The surface described by the five points is composed of four triangles (fig. 4.2). The combined area of these triangles is an estimate of the surface area within the square.

Figure 4.2 A triangular prism composed of four triangles (afterClarke,1986)

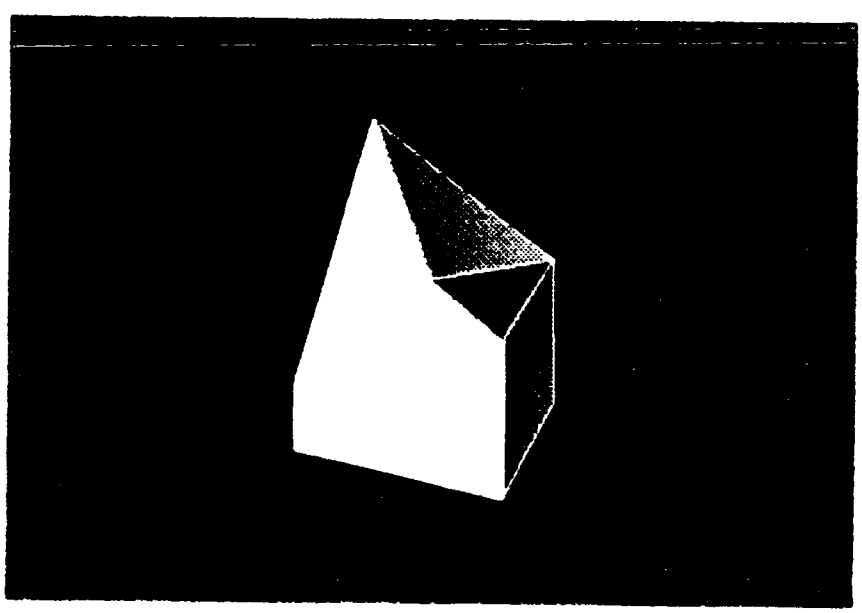

This process is repeated for the number of squares of that particular resolution required to tile the necessary part of the DEM. Clearly, the combined surface area within these squares of given resolution is an estimate of the surface area of that part of the DEM.

To obtain an estimate of the fractal dimension of the surface it is necessary to repeat this process for a number of resolutions. The part of the DEM tiled at different resolutions must obviously be the same. Clarke achieved this by using squares which increase in area as the lengths of their sides increase as powers of two. The number of powers of two which can fit into the shortest side of the DEM is the number of resolutions for which surface area can be calculated by this method.

Least-squares regression of log (surface area) on log (resolution) yields a value for the gradient of the relationship. This negative value can be subtracted from the topological dimension of the surface, 2, to give a supposed fractal dimension between 2 and 3.

One immediate drawback of this method, which is mentioned by Clarke himself and is shared by the one dimensional divider techniques, is that the least-squares regression is based on a small number of observations. The r^2 value for the relationship only gives a very rough indication of fit in this situation and, as in all other methods, individual values must be examined and visual reference made to a scatterplot of the relationship to check for linearity (Mark and Church, 1977).

However this method raises more serious theoretical questions. How closely does the method mimic the one dimensional walking-divider methods? To suggest that surface area is the two dimensional equivalent of line length is perfectly sensible. However is resolution the equivalent in two dimensions of divider step size or its computer algorithm approximations?

The manual method of walking dividers along a line does just that; the dividers are walked along the line following the line in whatever direction it turns. Likewise, in computer algorithm approximations to divider step size (Schwarz and Exner, 1980; Clark, 1986; Kennedy and Lin, 1986), the step, be it a number of digitised points or the closest point to a predefined distance, follows the direction set by the line. Each step is not just the scalar length of the step size, but is a vector with its direction determined by the geographical line it is walking. Even in cell counting methods (Hakanson, 1978; Goodchild, 1980, 1982; Shelberg et al., 1983) the way in which the cells are classified by the way in which the line crosses them adds a less direct but nevertheless directional component to the final estimate of line length. In the triangular prism surface area method, however, the resolution area is scalar.

A true two dimensional divider method would tile the surface as closely as possible with tiles of a given area (step size). The number of tiles it takes to cover the surface, times the tile area would give an estimate of surface area. Small tiles would fit the shape of the surface more exactly thus giving larger estimates of surface area, while larger tiles would generalise the surface to a greater extent thus yielding smaller estimates of surface area. Quite understandably, given the complexity of the problem, this type of analysis does not seem to have been attempted. Is the triangular prism surface area method analysing the actual surface under investigation? Reference to results given in Clarke's paper (fig. 4.3) raises initial doubts about this and studying his program reveals what is happening. The maximum resolution is the horizontal area covered by the landsurface and is given as 16384, with no units. The maximum value of surface area, again unitless, is given as 224729. This suggests that the surface area of the land surface is some 13 times the horizontal area which the landsurface covers. For surface area to be double horizontal area the average slope angle involved would be 60 degrees (fig. 4.4). Likewise an average slope angle of over 85 degrees would be necessary to make surface area 13 times horizontal area. These slope angles are clearly not representative of real landsurface.

Figure 4.3 Results produced by Clarke (1986) for Bell Canyon, California.

```
Minumum elevation :          509
Maximum elevation :         1084
** Data input complete **
Processing rows     2 to  130
 and columns     2 to  130
Step  Resolution  Area
   1        1.00   224729.93
   2        4.00   209515.99
   3       16.00   179843.68
   4       64.00   144139.61
   5      256.00    95409.38
   6     1024.00    64495.08
   7     4096.00    47874.59
   8    16384.00    42987.63
 ** Fractional Dimension =    2.192772
    r - squared =    0.965388
    with     8 observations
    ln(resolution) 0.00000  1.38629  2.77259
    ln(area)      12.32265 12.25256 12.09984

                   4.15888  5.54518  6.93147
                  11.87854 11.46593 11.07434

                   8.31777  9.70406
                  10.77634 10.66867
```

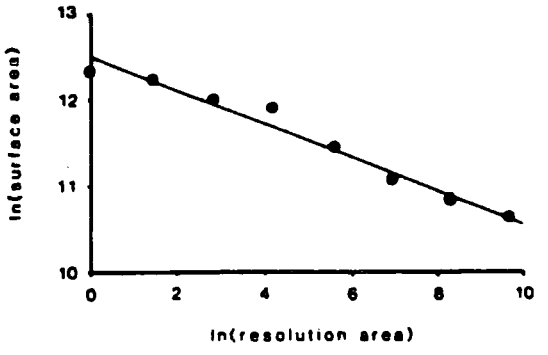

Figure 4.4 Relationship between surface area, horizontal area, and slope angle.

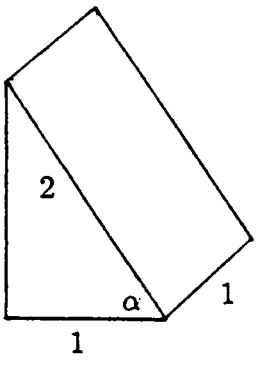

$$cos\alpha = \frac{1}{2}$$

$$\alpha = 60°$$

Studying Clarke's program reveals that no account of the grid mesh size of the DEM is taken. Grid mesh is always treated as the unitless value 1. All horizontal measurements are made on the basis of this value. Vertical values however are in units; in the case of Bell Canyon these are in metres. Elevation in a DEM might, therefore,

change from 60m to 40m in a distance of 30m but this is treated in the program as a change in elevation of 20m in a distance of only 1m. In the case of Bell Canyon it is therefore a distorted surface with an average slope angle of 85 degrees that yields a supposed fractal dimension of 2.193.

This distortion of the surface is easily remedied, if distances are calculated in the program taking grid mesh size into account. Not having access to the U.S.G.S. DEMs which Clarke analysed three different DEMs were studied both ignoring grid mesh and including grid mesh. It can be seen from Table 4.1 that the supposed fractal dimensions of the real, undistorted surfaces are too low to describe glaciated mountain areas such as Nupur, Thvera, and Torridon. In fact fractal dimensions of that order imply that the surfaces are very nearly regular and differentiable.

Table 4.1 *Fractal dimensions calculated from distorted (1m mesh) and undistorted (100m Mesh) DEMs.*

		Thvera		Nupur		Torridon
Grid Mesh	D	r^2	D	r^2	D	r^2
1m	2.465	.908	2.597	.841	2.586	.908
100m	2.013	.978	2.017	.965	2.011	.963

It would seem from this evidence that a more theoretically sound technique should be used to study self- similarity and to estimate fractal dimension.

4.4 The Variogram

It was stated in Chapter 2 that fractional Brownian motions have an average increment of zero and variance which diverges with time (2.16). Thus if a landsurface is considered as a fractional Brownian motion its variance should be

$$E=\left[\left(Z_p-Z_q\right)^2\right] = k d_{pq}^{6-2D} \tag{4.1}$$

where Z_p and Z_q are elevation values of the surface at points p and q and d_{pq} is the horizontal distance between them. This states that the expected value of the squared elevation difference between two points on a surface is a function of the distance separating them. D, fractal dimension, can be estimated from a surface by constructing a variogram; the mean squared elevation differences for different horizontal distances are computed and their logs plotted against the logs of horizontal distances. The slope of the plot, b, gives:

$$D = 3 - (b/2) \tag{4.2}$$

Mark and Aronson (1984) used the variogram as the basis of their method for estimating fractal dimension from U.S.G.S. DEMs. 32000 pairs of points were selected from within the largest circle that could be drawn in the area covered by the DEM. The points were chosen using a call to a pseudo-random number generator. Random selection of point pairs and selection from within a circle were performed to avoid directional bias in the sampling. The possible distance range was divided into 100 equal classes and then variance for the point pairs within these classes was calculated. A log-log plot of variance against distance was then made. Log (variance) values based on fewer than 64 point pairs were omitted.

The variogram was also used to study surfaces by Roy et al. (1987). They suggested that Mark and Aronson's sampling plan within the circle is biased towards the selection of points separated by middle and long distances. This results in the emphasis being put on the part of the variogram which is some distance from the origin. Analysis of variograms, they suggest, relies on the proximal part of the plot. This sampling bias may therefore distort the short range contribution to the fractal dimension estimate.

Roy et al. therefore used a different method to sample points. They also started with the largest circle which the DEM would accommodate. A point was then randomly selected from within the circle. However the distance to separate the next point selected from the random point was predefined. The direction in which that point lies was randomly chosen and the predefined distance was then walked to find it. If the end point of the walk was outside the circle the pair of points were ignored. The number of points per class and the distance classes could therefore be predefined as desired.

Both Mark and Aronson and Roy et al. obtain very reasonable and similar results. These have encouraged the development of the Fortran program FASTFRAC which also uses the variogram to examine surfaces for fractal behaviour.

4.5 FASTFRAC

FASTFRAC was developed at around the same time as Roy et al. were introducing their algorithm and is also developed in the light of Mark and Aronson's method. This method avoids checking for the occurrence of points within a circle and avoids the random selection of point pairs.

A rectangular DEM contains points which are related to one another in one of three ways: row neighbours; column neighbours; or diagonal neighbours. Row

neighbours and column neighbours cover four directions and distances separating them are multiples of the grid mesh size. Diagonally neighbouring points can cover many more directions and provide distances that are between multiples of grid mesh size. By sampling a number of these neighbour relationships systematically across the DEM a representative sample of directions and distances can be obtained from which a variogram can be constructed. Using a systematic sample can give a greater number of log variance against log distance points than the random sample used by Mark and Aronson, however a larger number of point pairs is used to construct the variogram. The systematic sample does not really create any directional bias, as to obtain a sufficient number of distances for which to calculate variance a wide range of diagonal relationships is used. It should be noted that the directions obtainable from a random sample are exactly the same as those obtainable in a systematic sample.

FASTFRAC calculates log (mean squared elevation difference) over a number of log (distances); the information necessary to create a variogram from a two dimensional data source stored within a file as a matrix. The variogram data can then be used to estimate the fractal dimension of the data source, an operation which can easily be performed using facilities for linear regression widely available in statistical packages.

4.5 (i) Input

Five variables are read in by individual read statements from either the terminal or a command file. These variables contain the necessary information to manipulate the matrix.The variable 'CONV' stores the factor by which the matrix data must be multiplied to convert it to metres. 'NROW' is the number of rows in the matrix. Likewise 'NCOL' is the number of columns in the matrix. The grid mesh size of the matrix is read in as 'GR'. The only character variable is 'FMT' which reads in the string which contains the format of the file containing the matrix. Once this information is available to the program the matrix can be read from an input file. The data are stored in the two dimensional array 'HT'.

4.5 (ii) Calculations

The two results required are log (mean squared elevation difference) and log (distance) for which the former is calculated. Squared elevation differences are calculated between neighbouring points which can be related by row, column or diagonally as mentioned previously. A point has NROW-1 neighbours in the same column, NCOL-1 neighbours in the same row and (NROW-1) x (NCOL-1) diagonal neighbours. To obtain a selection of different distances over which to measure mean

squared elevation difference (or variance) all three types of neighbours can be used. However, it is obvious that the greatest number of different distances can be obtained from diagonal relationships.

4.5 (iii) The subroutine ABSOL

One subroutine, ABSOL, forms most of the calculations for row and column neighbours. The subroutine ABSOL containing two sets of nested do loops allows squared altitude differences to be calculated for distances which are multiples of GR, that is distances obtained from row and column relationships. In the first set of loops the calculations are as follows: an array element is subtracted from the first array element which is a certain distance to its left, the distance between the points being determined outside the subroutine; the result is then squared; the process is then repeated for two more array elements, the addresses of which are determined by the value of the loop increment variable 'INCB'; the sum of the squared differences is kept in the variable 'HR'; the process continues in this way until the loop terminating value is reached; the variable 'CM' counts the number of calculations performed.

Finding the difference between every point in each matrix row would obviously take a large amount of time. This is why the variable INCB is employed. If the value of the inner loop variable is less than half the number of columns in the matrix then INCB is equal to some value greater than one, so that not every point and its relevant neighbour are sampled. To ensure a large enough sample to estimate the variance for any particular distance, INCB becomes equal to one when the inner loop variable is greater than or equal to half the number of columns in the matrix.

The second nest of loops performs in the same way except that it deals with column neighbours. The loop increment variable is called INCC. However, since the distance over which variance is being calculated is the same throughout each subroutine call, HR is the sum of the calculations in both sets of loops and CM is the total number of calculations performed in each call. At the end of the call the log variance is calculated for that distance by dividing HR by CM and storing the log10 result in the array 'HV'.

4.5 (iv) The subroutine DIAGO

DIAGO is the subroutine which deals with differences between diagonal neighbours. The subroutine performs a downwards left to right comparison of point pairs (fig. 4.5) and also a downwards right to left comparison. The particular diagonal distance which is used in any particular call to the subroutine is selected outside the subroutine in the main program. The numerical value of the distance is calculated

during the subroutine call however. INCD is similar to the variables INCB and INCC in ABSOL and ensures a sensible sample size from which to calculate variance . HV is again calculated in the same way.

45 **(v) Main program block**

This is split into two sets of nested loops. The first set of loops ensures that a sensibly-sized sample is used to estimate variance for smaller row/column and smaller diagonal distances, controlled by the variable INCA as well as ensuring a good range of smaller distances. The second set of loops takes a sample of the larger distances rather than using all possible distances which would, again, take to much time. This process is controlled by the variable INC. If these loops were not included the differences between each point pair, separated by each of the possible distances, would be calculated wasting large amounts of processor time even if a reasonably moderately sized DEM of 100 by 100 points was to be processed.

Figure 4.5 Diagonal comparison of point neighbours – example of downward left to right comparison and downward right to left comparison.

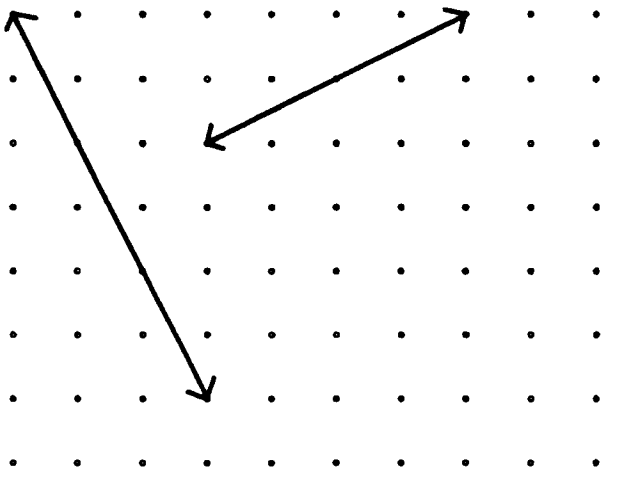

As well as calling ABSOL and DIAGO, the main program also contains calls to the subroutines SORT and AVWRIT. SORT is a standard sorting routine which is set up to sort HV and the array containing distances, DIST, by increasing distance. Output is prepared by the subroutine AVWRIT which uses the sorted distances to check for multiple occurrences of the same distance. If it finds a multiple occurrence it calculates an average variance for that distance.

4.5 (vi) Output

Distance and variance are written to an output file. Each row of output contains log distance and log variance for that distance. Also included in each row is the sample size used to obtain the variance. This output file is of a format compatible with many statistical packages.

4.5 (vii) Possible adaptations

As the program is fairly time consuming, it is designed to be run via a batch queue and is not particularly interactive. One major adaptation, which may often be desirable, is to change the initial values of the variables INC, INCB, INCC and INCD. To increase the number of distances sampled INC can be reduced. Likewise to increase the sample size for each variance estimation, INCB, INCC and INCD can be reduced.

Indeed while FASTFRAC was being developed these increment values were added only after several runs of the program where a completely exhaustive sample was taken up to large distances. It was on the basis of the near redundancy of many of the very similar distances over which variance was calculated that the more elaborate sampling method was introduced. In Chapter 6 the results from exhaustive and more careful sampling will be seen to be of the same quality.

4.6 Adaptations of FASTFRAC.

When studying the scaling behaviour of landsurfaces the question arises, from the geomorpological acceptance of such concepts as 'grain' in topography (Wood and Snell, 1960; Mark, 1975; Evans, 1972): how acceptable is a model which assumes topography to be isotropic? A simulated fractional Brownian surface should be isotropic as will be illustrated in the next chapter. Do real surfaces show anisotropy in any possible scaling behaviour? This question should be answerable by adapting FASTFRAC to calculate the variance over a range of different distances in four directions.

As FASTFRAC works on systematically sampling rows, columns and diagonals, it was relatively simple to adapt it to store the squared elevation differences it calculates in groups corresponding to certain directions. Within the subroutine ABSOL two loops deal with row neighbours ('East- West' direction) and column neighbours ('North-South' direction) separately. It is a simple task to store the results from each loop separately giving separate 'East-West' variances and 'North-South' variances.

Within the subroutine DIAGO it is two IF statements which control the left to right diagonals and the right to left diagonals. It is again simple to store the results from within these two IF statements separately. The major change to FASTFRAC which is needed for keeping separate the results for different directions is in the control structure of the main block. Again there are two loops dealing with larger and smaller distances in order to give a sensible sample size. INC is the variable which still controls the multiple of grid size which is being studied and is used in both ABSOL and DIAGO: however, the loops incrementing by INCA which are responsible for ensuring a selection of different diagonals are no longer used and as a result calls to DIAGO only refer to 'Northwest-Southeast' and 'Northeast-Southwest' relationships. These adaptations to FASTFRAC are completed by the need to sort and write out each set of directional results which is obviously achieved by using four sets of calls to SORT and AVWRIT.

As discussed in Chapter 1, another conceptual problem which geomorphologists should have with landsurfaces is the idea that a landsurface should possess a fractal dimension for the entire area. However in a landsurface a geomorphologist will recognise and classify certain areas in terms of the differing processes which have formed them and so on. These areas can often be at least partially delimited on the basis of form. How robust, therefore, is a fractal dimension obtained from a surface as a whole? Will smaller portions of the whole surface all have the same fractal characteristics as the whole? A first step to answering this question is to simply split each landsurface up into smaller sub-areas. This has been done in this study by dividing each surface into nine sub areas, as equal in horizontal area as possible. These sub-areas were then run through the programs discussed above. In summary the variogram method as implemented by FASTFRAC has been applied to whole DEMs of areas defined either on the basis of the areas' interest to the hydrologist or geomorphologist who made them, or purely on the mapping agency's need for coverage of an area. It has also been used to study the variation of scaling behaviour with orientation. Finally it has been used on smaller sub-areas of the DEMs to assess the areal limits of the overall results on scaling and fractal dimension.

4.7 Rescaled Range Analysis

It would obviously be of benefit to this study to use another estimation techniques to give results to compare with the results of the variogram method. In the light of the debate on the results of rescaled range analysis discussed in Chapter 2, it was decided to treat landsurfaces in a similar way to time series and perform rescaled range (R/S) analysis on them.

The first problem encountered when attempting R/S analysis of landsurfaces is how to make a suitable one-dimensional series out of a DEM. Unravelling a DEM into one long profile similar to a time series can be done in several ways. The main consideration as to which of these ways is most appropriate is the avoidance of a periodicity at which one segment of the unravelled DEM is nearly repeated because the next segment is composed of the row or column beside the row or column just unravelled in the last segment. This problem is discussed together with the results of the rescaled range analysis in chapters 5 and 6.

What properties of the landsurface represented by the DEM must be used in the rescaled range analysis? This is the second problem encountered when trying to treat landsurfaces in a similar way to time series. Equation (2.23) describes the relationship found by Hurst,

$$R_n/S_n \sim n^H \tag{2.23}$$

where R_n was the sample range of cumulative departures from the mean of a time series over the period n, and S_n was the standard deviation of the time series over the period n. When dealing with a DEM, grid mesh size becomes the base unit for n and distance is substituted for time. R_n and S_n must be dealt with more carefully. It is not the mean and its cumulative departures of the actual altitudes recorded in the DEM that are required but the mean and departures from it of the increments of altitudes between one point and another.

These two problems set the constraints for the FORTRAN program RS.FOR which using a DEM as input produces the $\log_{10}$ rescaled range value for a number of different $\log_{10}$ distances. The first part of this simple program reads the information about the DEM to be studied: the DEM filename; the number of columns; the number of rows; the grid mesh of the DEM; and the format of the DEM file. The DEM is then read into an array. A set of IF statements then allows the DEM array (HT) to be 'spiralled' through. That is, the first row of the DEM is stored in another array (OUT), then the last column of the DEM is stored in OUT followed by the last row reversed and the first column and so on until the middle of the DEM is reached. OUT eventually

holds the complete DEM 'time series'. The increments of elevation can easily be found in a loop where the elevation of one point is subtracted from the elevation of the next point.

The R/S analysis can now begin. The two outermost loops in this part of the program control the series of distances for which rescaled range is being calculated. The series starts with n equal to 5 grid cells and n is incremented in the inner of these two loops by 1 until n is equal to 10. This leads to the next iteration of the outer loop and with a ten-fold increase in the increment for n so that the series progresses: 20; 30; 40; and on until 100 is reached. The outer loop is again repeated with the increment value 100 and finally with 1000. The final possible number of grid cells used is 10000 but the maximum value of grid cells used is limited to half the total number of points in the DEM.

The third loop in is repeated as many times as n fits into the total number of points in the DEM, and it is within this loop that the mean and the maximum and minimum departures from it are calculated, for each section of the 'time series' n grid cells long. This means that for every value of n several values of rescaled range are calculated. As a result the average value of rescaled range can be calculated outside the third loop. In order to assess the dispersion around these average values of rescaled range the standard deviation is also calculated. The results are then written to a file in an format easily readable by most statistical packages.

4.8 Conclusions

This chapter has looked at the earliest one-dimensional techniques used in geomorphology to search for the presence of self-similarity and estimate fractal dimensions. The more recent adaptations of these techniques have also been discussed.

Some of the advantages of looking at surfaces as a whole have been mentioned and the value to this study of two-dimensional methods is clear. Unfortunately, the conceptually straightforward one-dimensional structured walk technique has not been adapted to work in two dimensions, and indeed it cannot be. This has led to the use in this study of the variogram method.

FASTFRAC uses a new sampling approach which allows as much of the data available in a DEM to be used as is desired. This is somewhat different to the approaches of Mark and Aronson (1984) and Roy et al. (1987) which sample randomly. FASTFRAC has also been easily adaptable, because of the way it works, to keep the variance measured over a range of distances separate for four different directions.

Even when tested on simulated surfaces of known fractal dimensions, the results of only one method have their limitations. With the variogram method some of the behaviour of the results will be explainable by the method and not just by real characteristics of landsurfaces studied. It is for this reason that the use of more than one method to study scaling behaviour in landsurfaces is desirable. Correspondence between results from two methods can be used more safely as information on scaling rather than effects of the analysis technique.

As a result of the amount of discussion on rescaled range analysis it seems appropriate to mimic this sort of analysis when studying landsurfaces. Although it is one-dimensional it has proved to be an easily used technique.

Having established the methods to be used to study the fractal nature of landsurfaces the next chapters go on to discuss the results produced by these methods. The next chapter is a short one on the results obtained from FASTFRAC and RS.FOR when simulated fractal surfaces were used as input. Chapter 6 will go into detail about the results obtained when a variety of real landsurfaces are analysed.

Chapter 5: The Fractal Nature of Simulated Fractal Surfaces

5.1 Introduction

Assessing the fractal nature of real landsurfaces by using the variogram method programmed in FASTFRAC and rescaled range analysis as it is implemented in RS.FOR are not the only ways of comparing real landsurfaces with the fractal model. By studying simulated surfaces which are supposedly fractional Brownian surfaces a comparison can be made between their properties, both fractal and traditional geomorphometric, and the properties of real landsurfaces. A useful by-product of this process is that the performance of FASTFRAC and RS.FOR can be assessed while studying surfaces that are already defined by their simulation and whose parameters are already known.

This chapter briefly discusses simulated fractal surfaces before elaborating on the method used in this study. The surfaces simulated have been processed through: FASTFRAC; its adaptation for the study of anisotropic effects in surfaces; and RS.FOR. The results of this analysis will be presented and discussed in this chapter.

5.2 Simulating Fractal Surfaces.

There are three basic algorithms for generating fractal surfaces. Two of these developed under Mandelbrot's guidance while the third was proposed by Fournier et al. (1982). They are: the shear displacement method; the fast Fourier transform filtering method; and the random midpoint displacement or recursive subdivision algorithm.

The first of these, the shear displacement method, was introduced by Mandelbrot (1975a). This algorithm is simple and easily visualised from Mandelbrot's first description of it:

"Start with an earth of zero altitude, then break it along a succession of straight faults, and in each case displace the two sides vertically to form a cliff. The terms 'fault' and 'cliff' are to be understood in purely geometrical terms, with no tectonic implication" (Mandelbrot, 1975a, p.3826). The difference between the 'geometrical' meanings of fault and cliff and the 'tectonic' meanings, touches upon some of the issues raised in Chapter 1, the latter term suggesting faults as landforms rather than geometrical parts of a rough surface.

To produce the irregularity necessary to make the simulated surfaces fractal, the positions of the faults must be randomly chosen so as to be mutually independent of one another and be isotropic, that is the direction of stike of the faults must also be random. The heights of the cliffs must also be randomly chosen and have zero mean and finite variance. If the cliffs are vertical Mandelbrot (1975a,b) explains how the relief obtained is a Brownian surface with the properties described in Chapter 2. A Brownian surface has the fractal dimension, D=2.5 and a Hurst exponent, H=0.5.

Mandelbrot (1975a) hints at how this algorithm can be adapted by varying the profile of faults so as to produce surfaces with values of H from 0 to 1. He explains in much more difficult and rigorous style how the profiles must change in Mandelbrot (1975b). Fortunately many of the recent books on fractals and their graphical applications explicitly describe the adaptation required to vary the fractal dimension of the surfaces generated (Feder, 1988; Peitgen and Saupe, 1988; Barnsley, 1988).

In the special case where H=0.5, on one side of the fault the altitude is incremented by the random cliff height selected, the other side of the fault stays at the original level. This ensures the independence of the points at any distance from the fault. If, however, H is not equal to 0.5 the effect of the increment must continue away from the actual line of the fault. The algorithm used is: every point on one side of the fault is incremented by the points distance from the fault raised to the power of H - 1/2, all of which is then multiplied by the random cliff height selected; every point on the other side of the fault is incremented by the negative of this. Figure 5.1 illustrates the shape of faults with different values of H.

The other methods of generating fractal surfaces are conceptually more difficult but take less computer time during the actual simulation and are therefore more popular with those involved with producing high resolution computer graphics. The fast Fourier transform filtering technique starts with a surface of Gaussian white noise and then filters this using fast Fourier transform techniques. This filtering produces a surface where the different frequencies are present in the amount necessary to give the form of power spectrum referred to in Chapter 4.

The third method, random midpoint displacement, recursively subdivides an area calculating a random value at the midpoint the randomness of which is again controlled by H. Clearly the amount of displacement scales with the number of recursions. Fournier et al. (1982) admit that the surface produced is neither fully stationary, isotropic, nor self-similar. It is however the fastest method and is commonly used as an approximation of a fractional Brownian motion.

Figure 5.1 *Shape of faults used in the Shear Displacement Method*

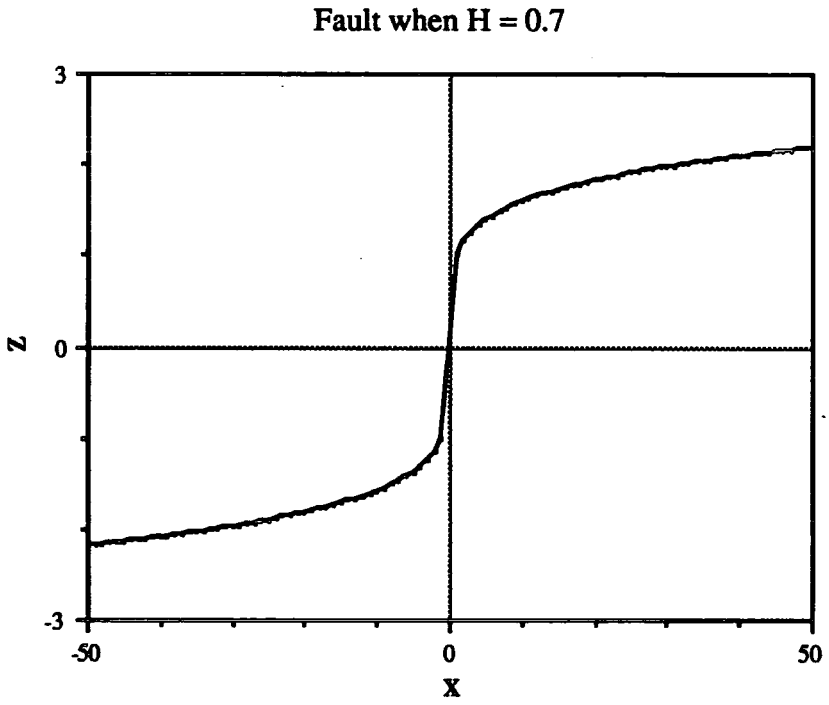

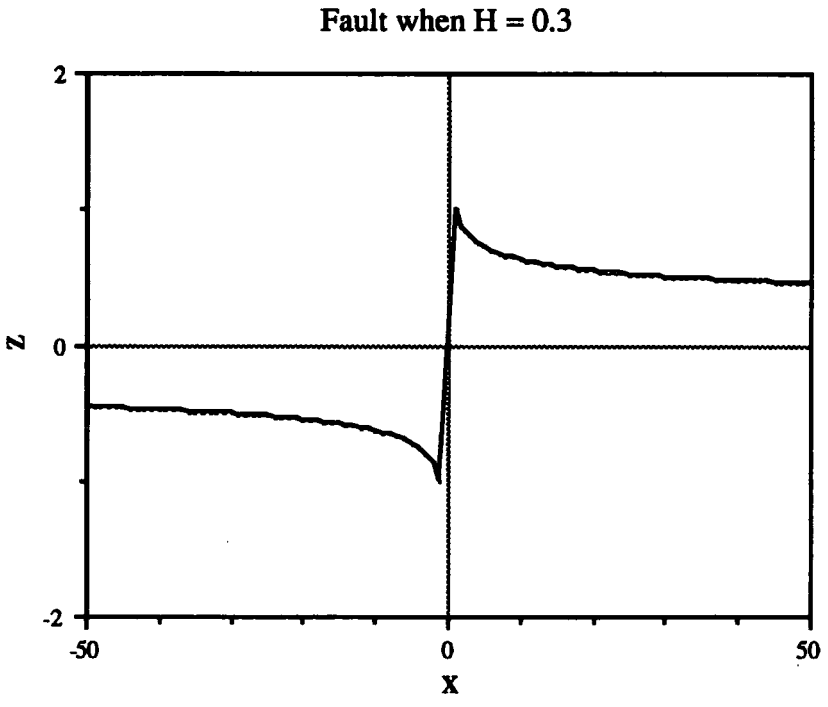

The requirements of this study are fractional Brownian surfaces at a similar type of resolution as the DEMs of real landsurfaces that will be looked at. As a result the detail obtainable from the latter two methods is not required. Furthermore the shear displacement method is conceptually simple as far as the process which generates a shear displacement surface goes and bears some resemblance at least to very simplified tectonic processes.

For these reasons the simple program FRACSIM.FOR (appendix 1) was written. It firstly initialises an array with zero values as a flat earth of zero relief. Inside a loop controlling how many shear displacements will be made, four random numbers within the dimension of the 'earth' array are obtained from a NAG function call. Pairs of these four numbers are then used as coordinates of points through which a fault shall pass. The 'earth' array's row index is taken as the *Y* direction of the flat earth while the *X* direction is obviously the column index. The variable B is the gradient of the fault line selected by the random number function in the *X Y* plane of the 'earth' array: variable A is its intercept. A set of nested DO loops now allows a pass through the array. Each point is checked to see if its *Y* co-ordinate is greater or less than the *Y* co-ordinate of the fault line at that *X* co-ordinate position. If the *Y* co-ordinate is less, then the distance of the point from the fault line is raised to the power of H - 0.5 and then multiplied by the altitude which was randomly selected earlier in the program from a Gaussian distribution with zero mean and variance equal to 1. If the *Y* co-ordinate was greater then the negative is taken.

Eleven surfaces where generated with H increasing by 0.1 from 0.0 to 1.0.

5.3 The Visual Appearance of the Surfaces.

Mandelbrot (1977) refers to the benefits of using visual evidence as a first judgement on the appropriateness of some of his theories. Therefore it is appropriate that when analysing the surfaces simulated by FRACSIM.FOR a visual inspection of the surfaces should be used as a starting point. Although all the comments here are based on subjective visual investigation, the comments are made in the light of experience of looking at similar representations of real landsurfaces; indeed, reference will be made to some of the real landsurfaces studied in this project. Full details of the real surfaces will be given in later chapters, perspective block diagrams of each of these surfaces are presented in Chapter 6. The surfaces generated are presented in figures 5.2 to 5.12 as perspective block diagrams.

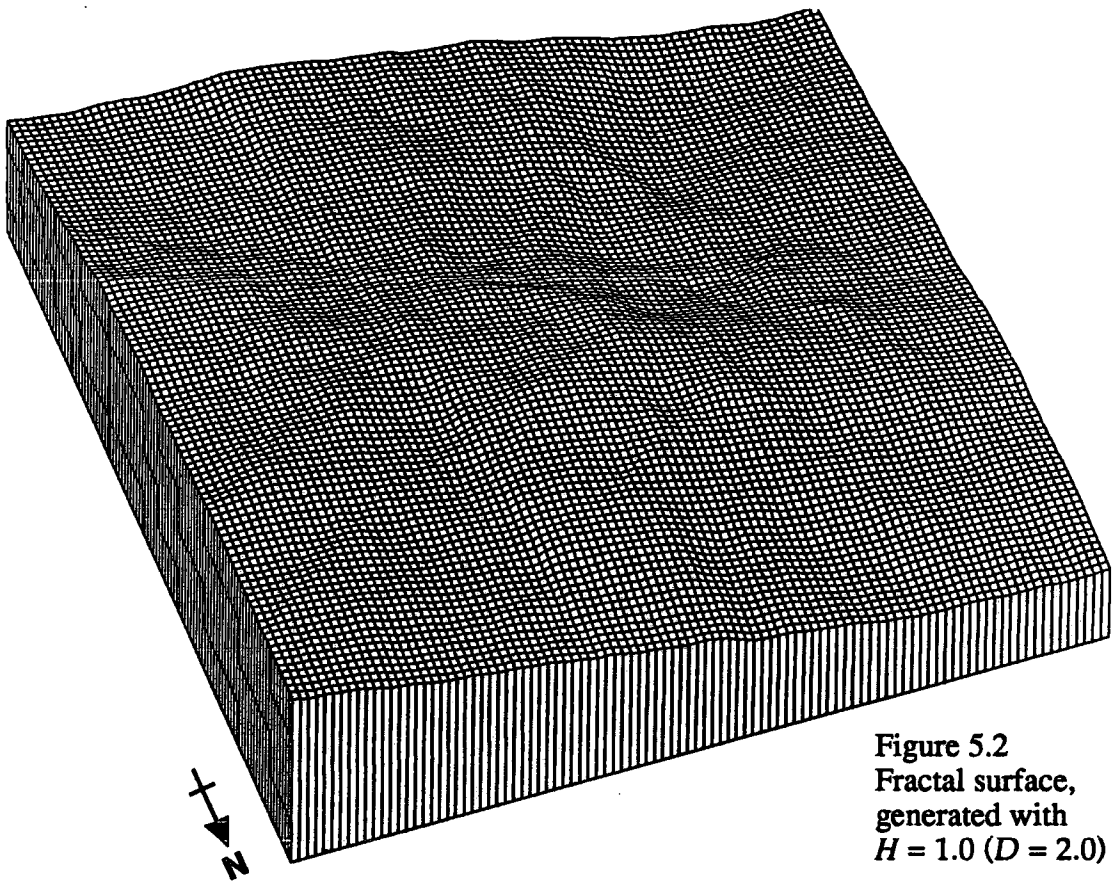

Figure 5.2
Fractal surface, generated with $H = 1.0$ ($D = 2.0$)

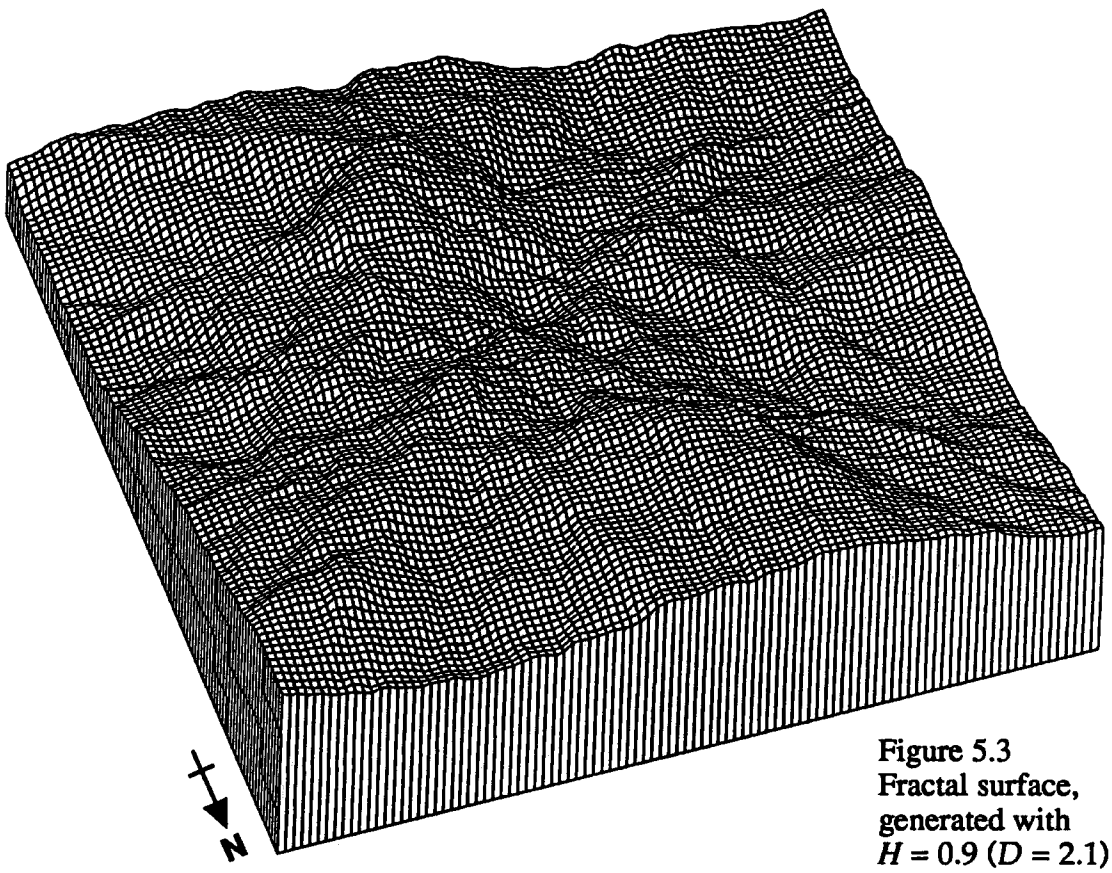

Figure 5.3
Fractal surface, generated with $H = 0.9$ ($D = 2.1$)

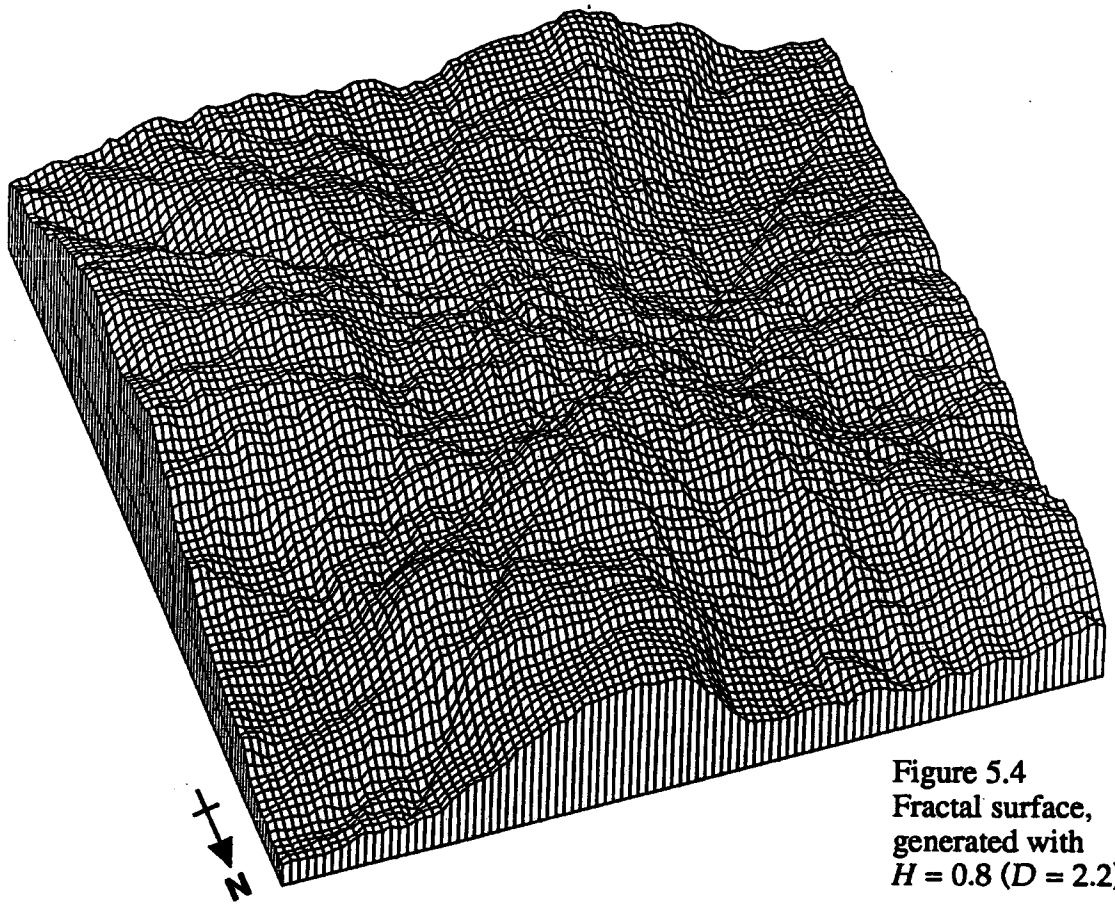

Figure 5.4
Fractal surface, generated with $H = 0.8$ ($D = 2.2$)

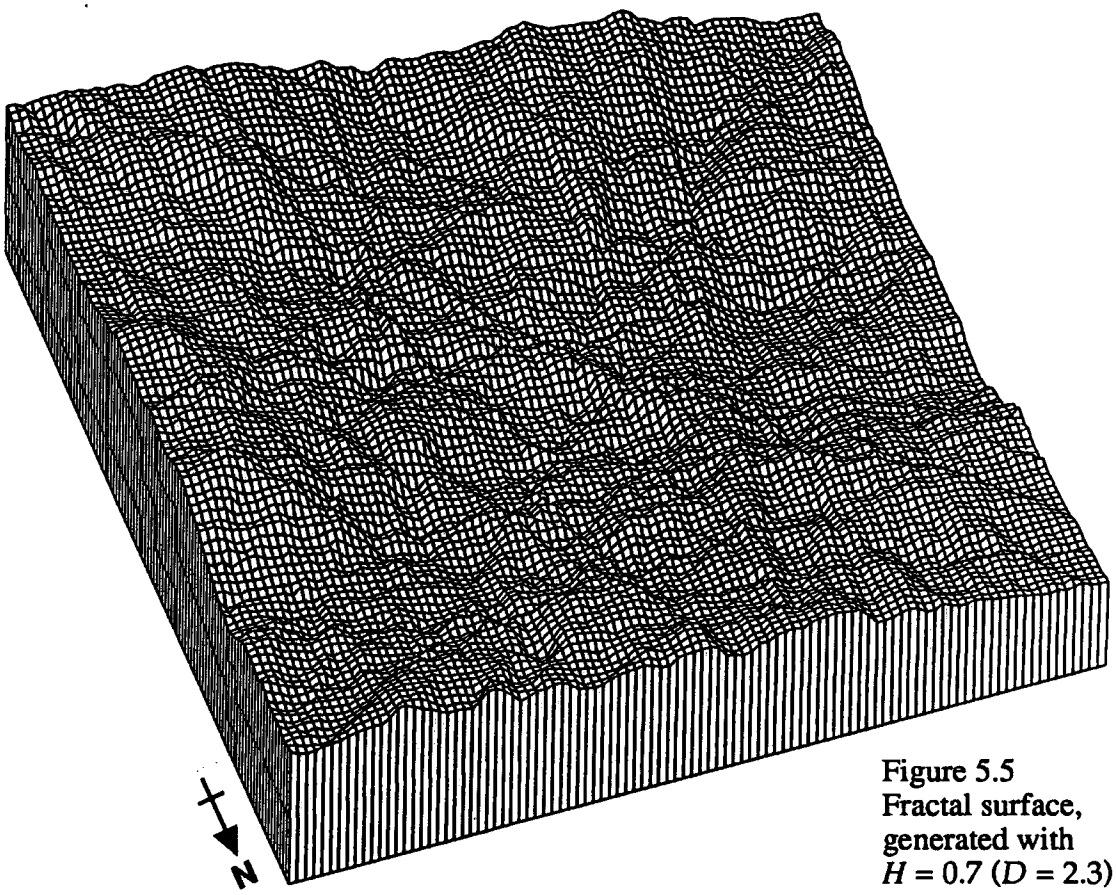

Figure 5.5
Fractal surface, generated with $H = 0.7$ ($D = 2.3$)

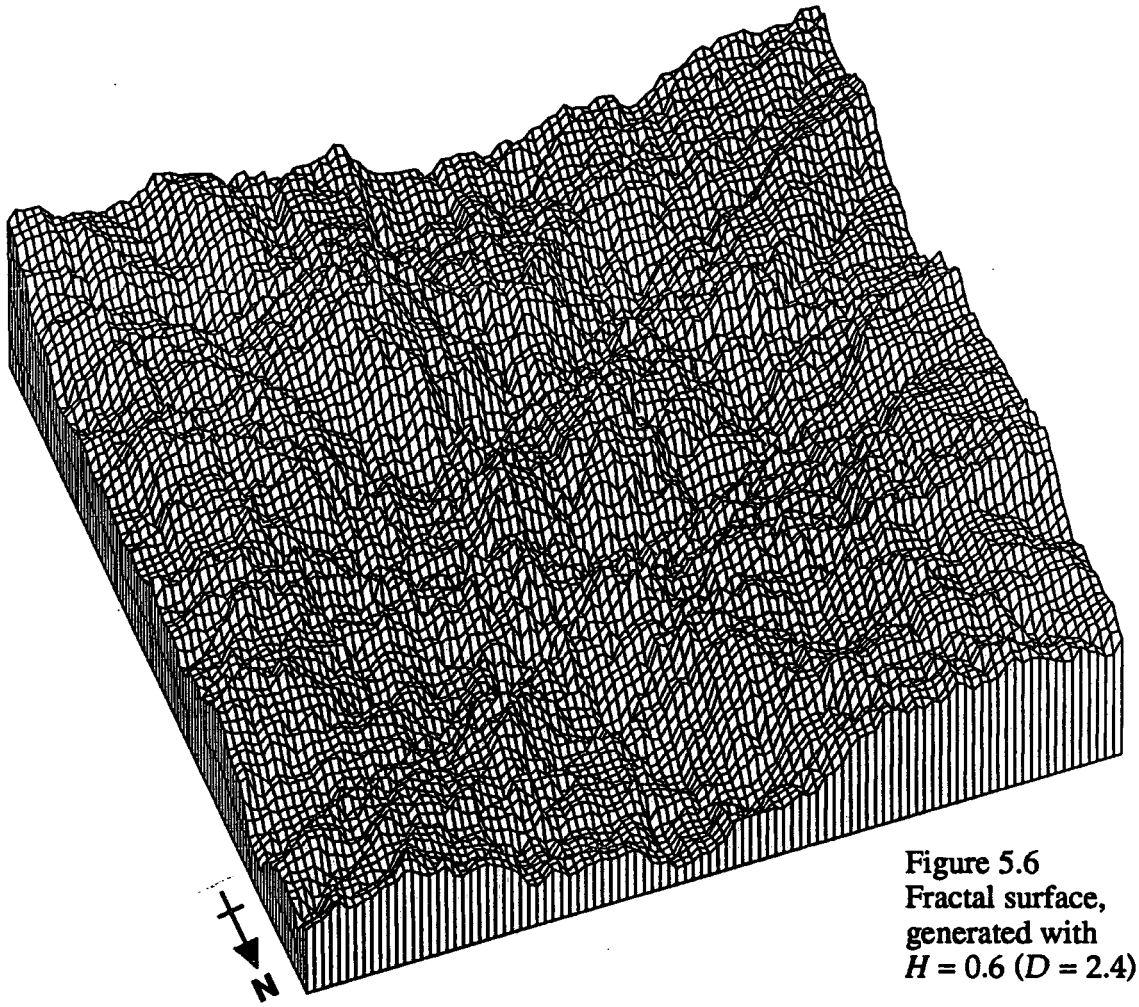

Figure 5.6
Fractal surface, generated with $H = 0.6$ ($D = 2.4$)

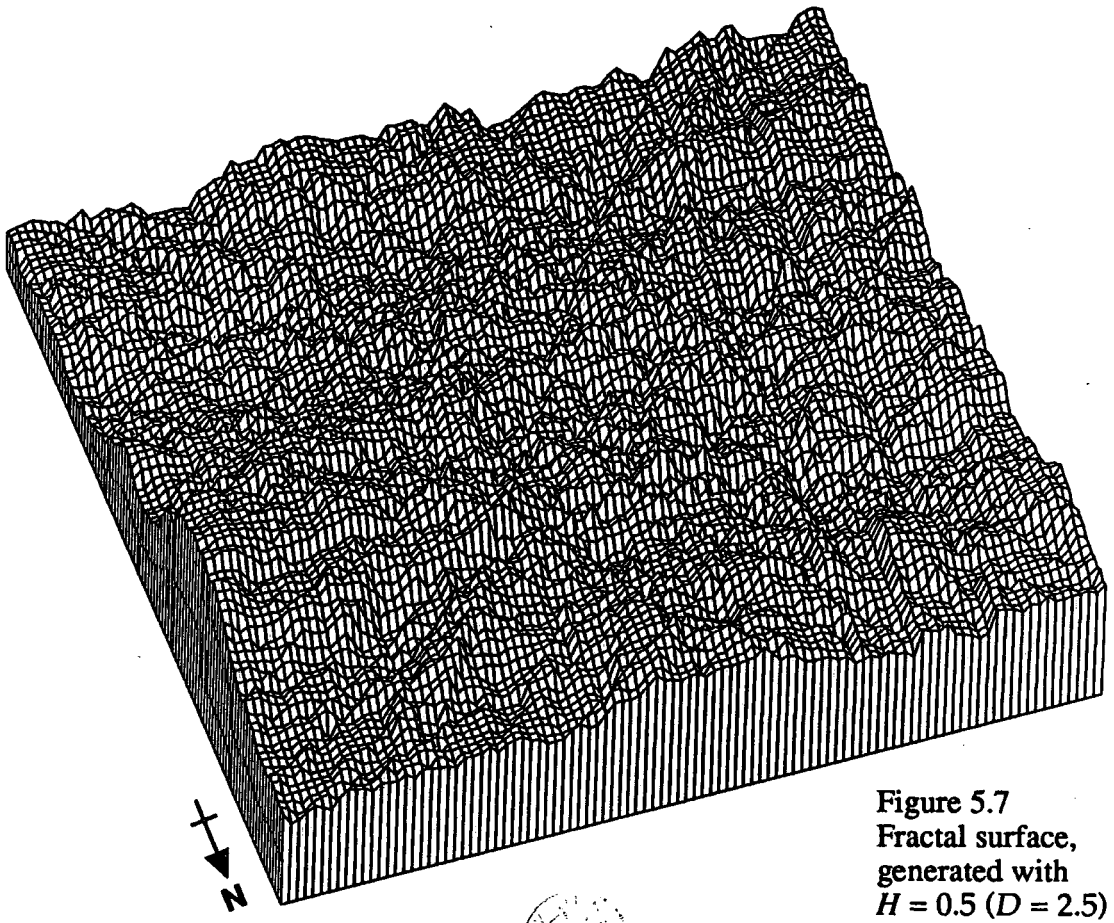

Figure 5.7
Fractal surface, generated with $H = 0.5$ ($D = 2.5$)

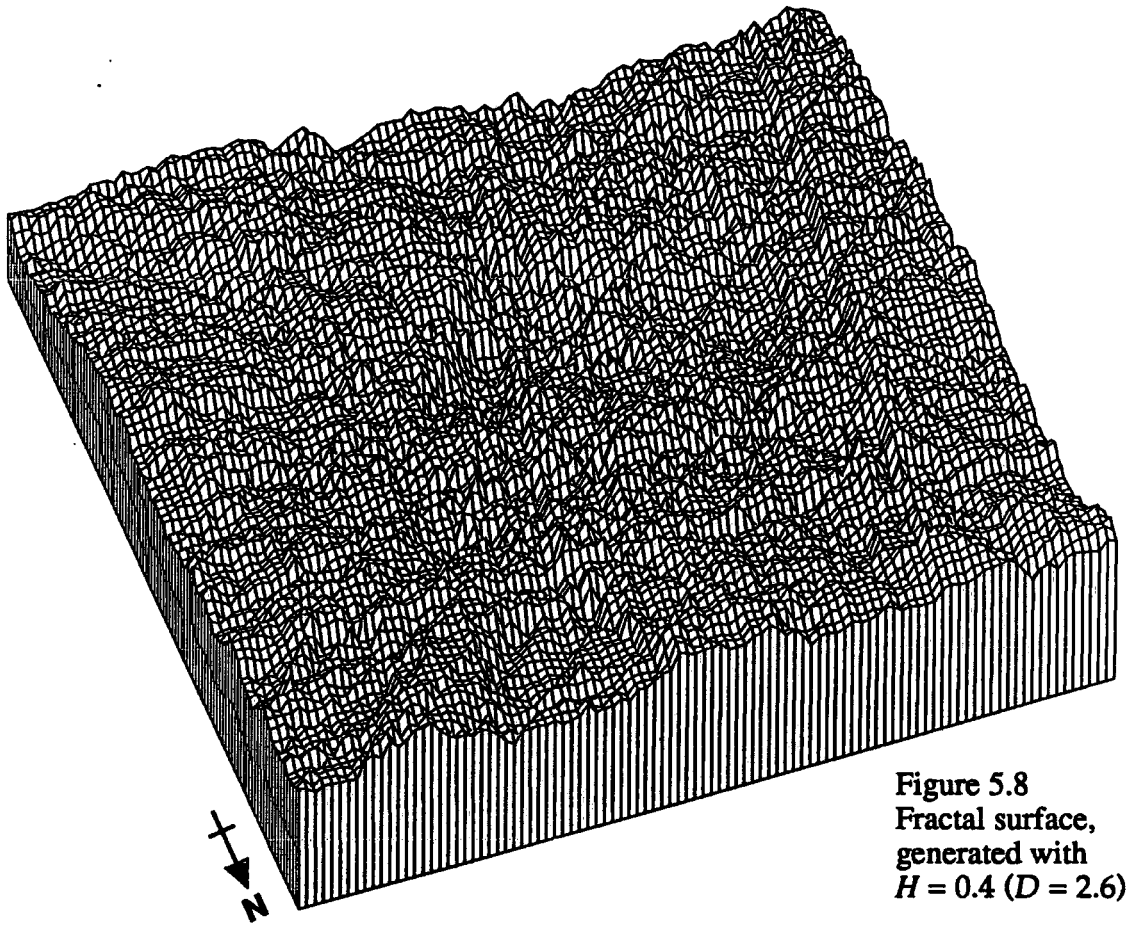

Figure 5.8
Fractal surface, generated with $H = 0.4$ ($D = 2.6$)

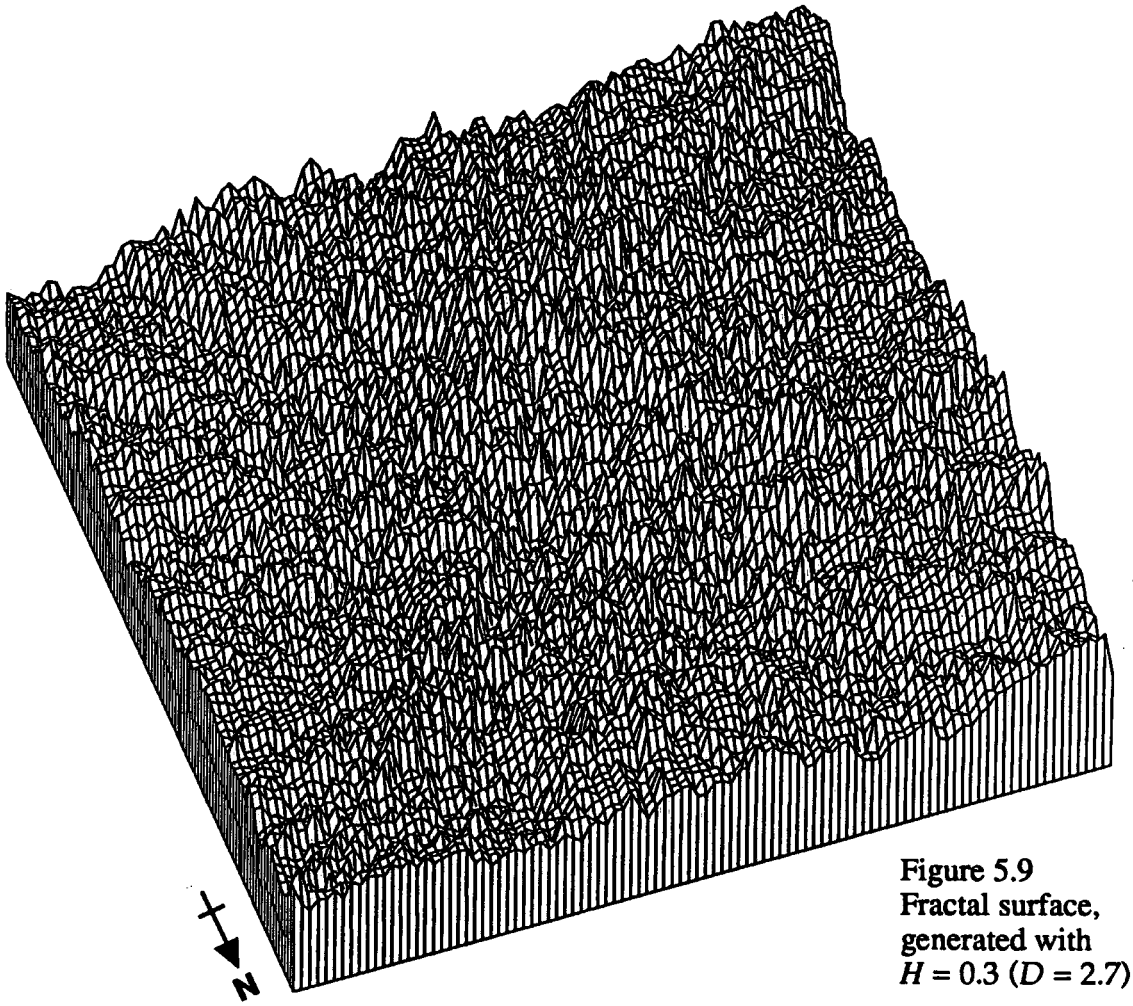

Figure 5.9
Fractal surface, generated with $H = 0.3$ ($D = 2.7$)

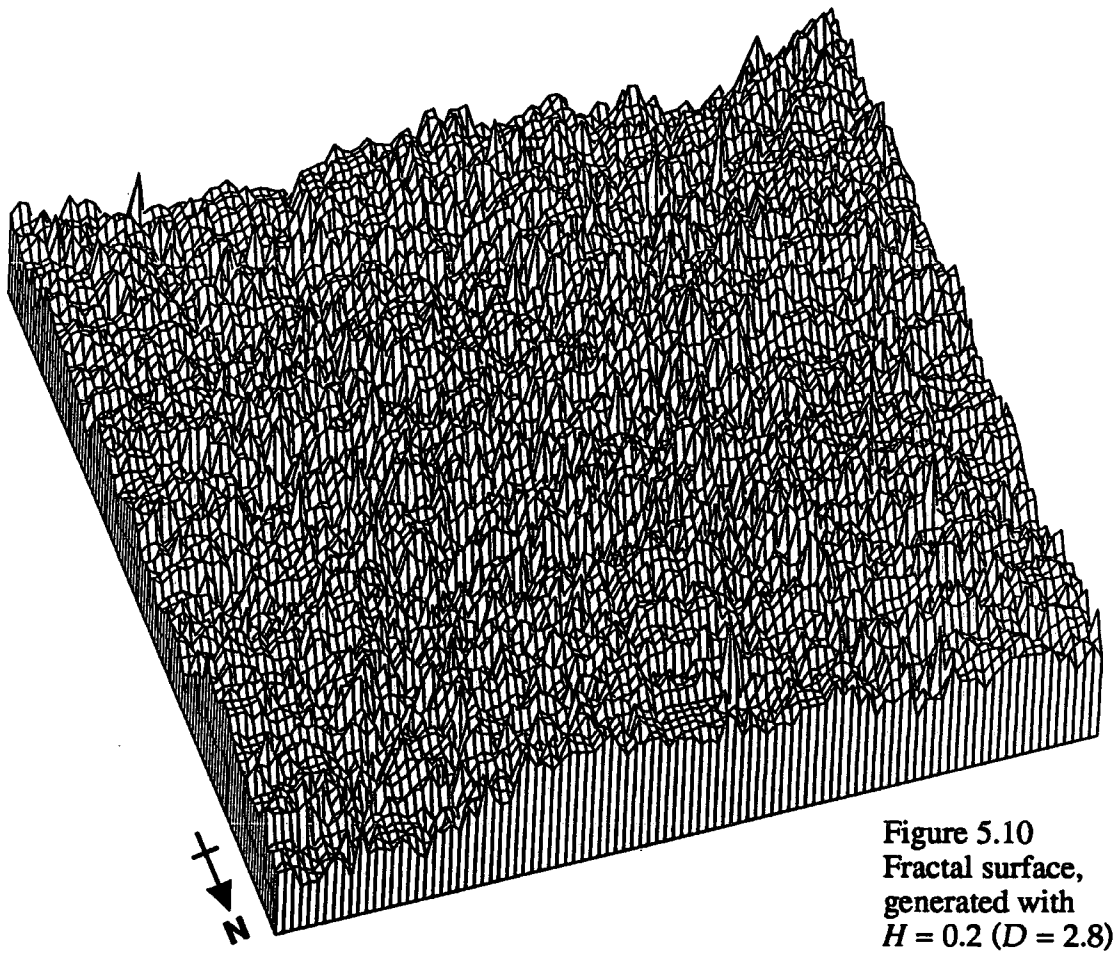

Figure 5.10
Fractal surface, generated with $H = 0.2$ ($D = 2.8$)

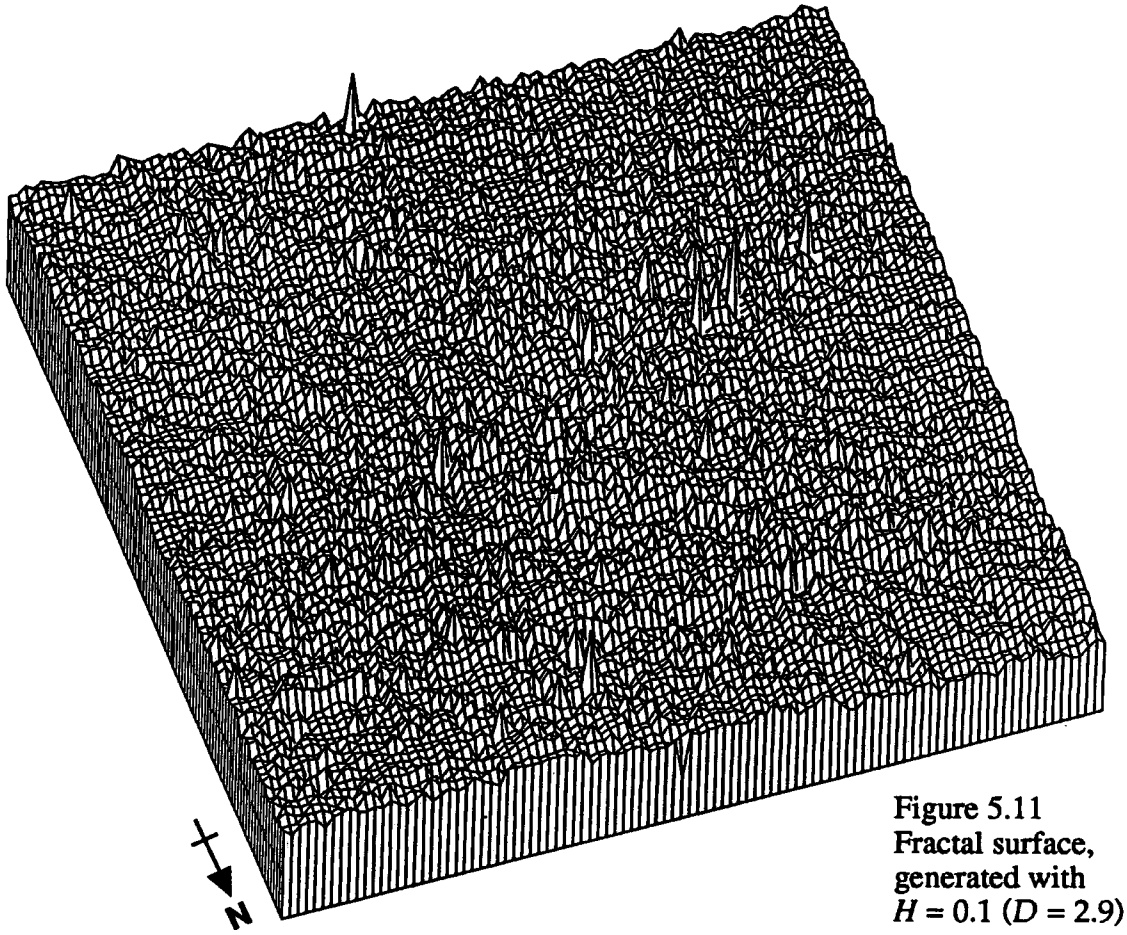

Figure 5.11
Fractal surface, generated with $H = 0.1$ ($D = 2.9$)

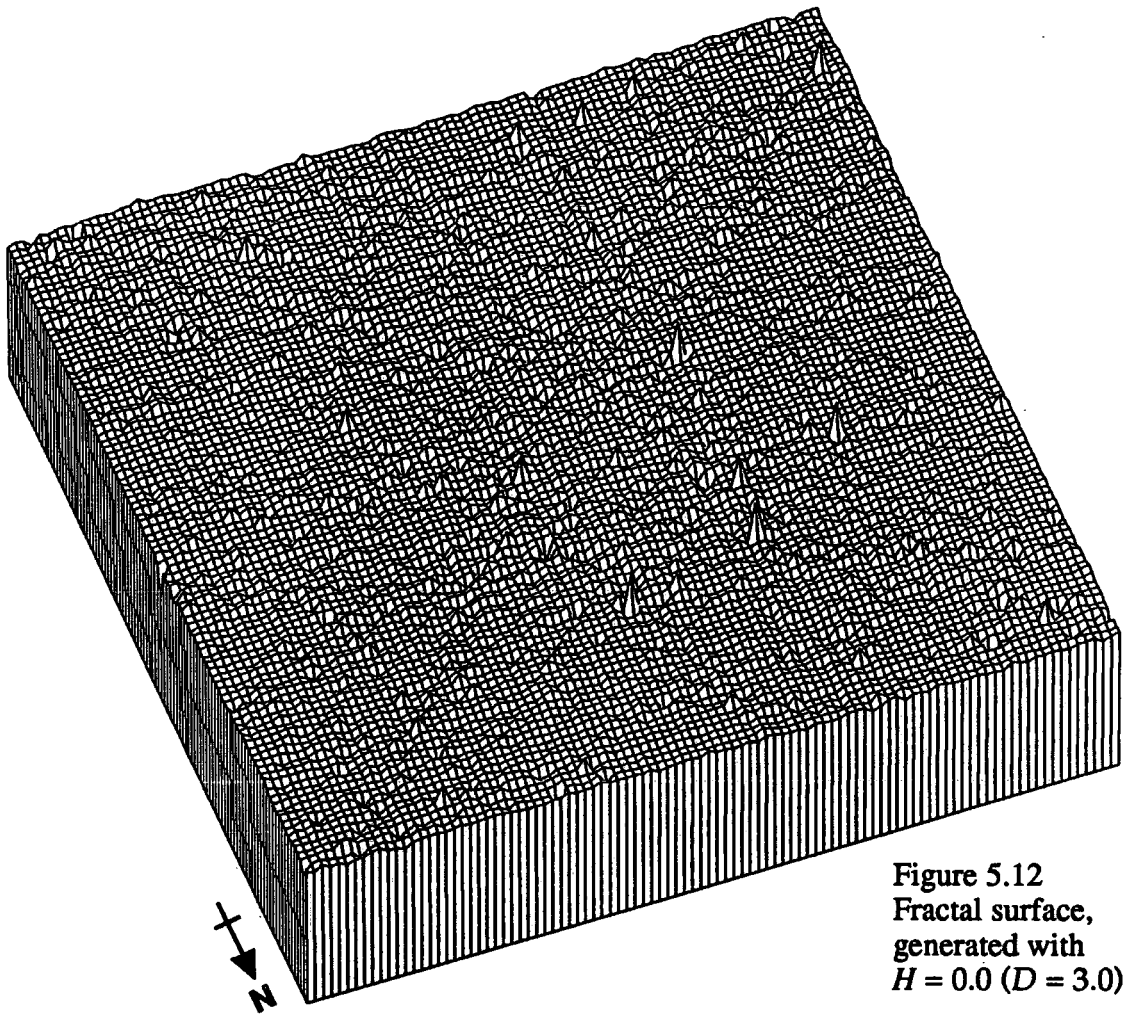

Figure 5.12
Fractal surface, generated with $H = 0.0$ ($D = 3.0$)

Starting with the surface simulated with the parameter H=1.0, which means D is equal to 2.0 (fig. 5.2), it is clear that the surface is very smooth . However there are several perturbations visible where large faults have stayed dominant in the generation procedure. The slopes that are present appear generally long and gentle. The real surfaces that are studied in this project that are most similar visually to this surface are those of the drainage basin areas of Wheeldale and Glaisdale.

The surface with H=0.9 and D=2.1 (5.3) seems, immediately, much rougher than the H=1.0 surface. The effects of more of the faults have become obvious. The surface looks quite realistic with some definite ridges. There are one or two features that look something like valleys. Visually the nearest real landsurfaces to it are Canigou and the Uinta Mountains.

The surface generated with H=0.8 (fig. 5.4) does bear some resemblance to real landsurfaces. The two cross sections visible on the diagram are for example quite realistic. There are however too many obvious linear features associated with the faults of the generation process. The simulated surface is visually closest to such surfaces as Devoluy, Nupur, and Galloway, although the vertical exaggeration in the diagrams of these surfaces is greater.

Mandelbrot (1982) refers to surfaces generated with the exponent H set at 0.7 (D=2.3) as being most similar to real landsurfaces based on the limited empirical evidence available to him. The generated surface (fig. 5.5) is obviously becoming rougher than the previous surfaces but again the cross sections look realistic. The number of faults visible divide the surface into depressions separated by narrow ridges. The closest real landsurface similar to the simulated surface is probably Devon, but this is purely from the point of view of dissection.

With H=0.6 the generated surface begins to look rougher than most natural landsurfaces (fig. 5.6). Some of the masses of higher points look quite like mountains with very steep slopes reminiscent of rock slabs. The effects of the process used in generation can still be seen however and no coherent drainage pattern like those found on real landsurfaces can be found. The cross sections look too rough to be real. Any apparent valleys are occupied by scaled down versions of the major ridges which seem to be present. This surface visually portrays the scaling concepts of fractal Brownian surfaces. The closest real surface in this study would be the Mount Aigoual area of the Cevennes or Alarta, Saudi Arabia.

The surface generated with H=0.5 definitely looks too rough to be real (fig. 5.7). It again demonstrates the concept of self -similarity well. From the cross section it can be seen that the variation in altitude over longer distances would seem realistic but there is too much short-distance variation. It seems clear from this surface that it is formed by

superimposing noises on top of one another. None of the real landsurfaces studied really resemble the simulated surface.

Figure 5.8 shows the surface generated with H=0.4. Again this surface appears too rough to be real. Some of the 'cliffs' appear as near vertical linear features. With reference to the cross sections the short-distance variation in altitude is more evident than in the last surface. There seems to be less long- distance variation.

When H is set equal to 0.3 the surface can be seen to be composed of knife sharp ridges and troughs (fig. 5.9). The ridges and troughs have many spike-like summits and pits. The cross sections show yet more influence of short term variations in altitude.

The H=0.2 surface, the surface that should have a fractal dimension of 2.8 (fig. 5.10), shows similar features to those seen in figure 5.9. However the ridges and troughs are even more dissected by sharp spikes and pits. This progression from ridges and troughs being noticeable to spikes and pits being dominant can be seen continuing through figure 5.11, which is the H=0.1 surface, and reaches its logical conclusion in figure 5.12. In this diagram short term variation is completely dominant; summits and pits alternate. The fractal dimension of 3.0 implies that the surface is space filling. This cannot be seen from the diagram but the process of generation has meant that the surface is full of short term but also small in altitude changes from pits to summits. As a result the relief of the surface appears small even though the surface is very rough.

5.4 Results of Non-Directional Variogram Analysis.

When using FASTFRAC to study whole surfaces in this project two runs of the program are used. In general the part of the variogram over shorter distances is the most linear part of the plot. Therefore a run of FASTFRAC is made using the first ten diagonals for the first ten multiples of grid mesh size. This gives an exhaustive sample over the sixty shortest possible distances given the grid mesh. The resulting variogram allows least-squares linear regression to be performed on the linear part of the whole variogram. The second run of FASTFRAC uses the dimensions of the array necessary to store the surface to regulate the sampling method to produce a variogram which goes up to much larger distances.

The results of the linear regressions performed on the output from the first runs are presented in table 5.1. It can be seen from this table that the values of D estimated from the surface by FASTFRAC are either over or under estimates according to the value of D that was specified during the generation of these surfaces.

Table 5.1: Results from regressions of 60 distance variograms and R/S analysis.

Expected	60 Distance Variograms				R/S Analysis			
D	D Output	Difference	R^2	SE	D Output	Difference	R^2	SE
2.0	2.0480	0.0480	1.0000	0.0022	2.0310	0.0310	1.0000	0.0102
2.1	2.1910	0.0910	1.0000	0.0086	2.1600	0.0600	0.9970	0.0278
2.2	2.2450	0.0450	0.9900	0.0114	2.2160	0.0160	0.9930	0.0389
2.3	2.3220	0.0220	1.0000	0.0028	2.2850	-0.0150	0.9990	0.0142
2.4	2.4370	0.0370	0.9980	0.0129	2.3620	-0.0380	0.9910	0.0357
2.5	2.5350	0.0350	0.9980	0.0091	2.4050	-0.0950	0.9990	0.0129
2.6	2.5600	-0.0400	0.9990	0.0061	2.4480	-0.1520	0.9980	0.0154
2.7	2.6740	-0.0260	0.9980	0.0072	2.4500	-0.2500	0.9980	0.0155
2.8	2.7600	-0.0400	0.9970	0.0064	2.7800	-0.0200	0.9870	0.0281
2.9	2.8600	-0.0400	0.9940	0.0056	2.8130	-0.0870	0.9820	0.0288
3.0	2.9540	-0.0460	0.9700	0.0039	2.5970	-0.4030	0.9970	0.0137

However they are, with the exception of the surface generated to have D=2.1, not far out. The absolute mean difference between estimated D and programmed D is 0.043.

Having discovered that the variogram method does not estimate exactly the expected dimension for the fractal Brownian surfaces it is necessary to try and discover why. Studying the scatterplots of log (variance) against log (distance), for the 60 distance runs of FASTFRAC presented in Appendix 2 it can be seen that many of them show some slight curvature. In Chapter 2 the concepts of scaling and calculating fractal dimensions were explained and for a completely self-affine fractal Brownian surface a perfect linear relationship of its variance to distance would be expected (2.16). Therefore, does the amount of curvature in these scatterplots show up in the error statistics associated with the least-squares linear regression equations fitted?

Looking at the r^2 values from the regressions of log (variance) against log (distance) for the surfaces it can be seen that they are all above 0.994 except that for the surface generated with H=0.0. These high values would all seem indicative of linearity. However using $r^2 = 0$ as a reference level to measure the linearity of a relationship is not particularly relevant when the minimum hypothesis in this situation would seem to be that there is a monotonic relationship. It has been shown that r^2 for perfect non-linear monotonic relationships will often be very high (Good, 1972). Standard error, due to its sensitivity to small changes in r^2, would seem to be a useful supplement to the indication of fit in this case and as a result standard errors are included in Table 1. However, from the variation in these statistics the magnitude of the difference between supposed and estimated fractal dimension can still not be explained.

On closer reference to Table 5.1 it can be seen that all the estimates of D for generated surfaces with supposed fractal dimensions of up to 2.5 are over-estimates. Surfaces with supposed fractal dimensions of more than 2.5 have all yielded under-estimates when run through FASTFRAC. For the first run of FASTFRAC the residuals of the regression were plotted against both distance and against the fitted values using 'Minitab'.

It is from these residuals that the relationship between the slight curvature of the scatter for the surfaces, the error statistics related to the regressions and the magnitude of discrepancy between estimated and supposed fractal dimension becomes apparent.

The residuals show that all the scatterplots up to and including the plot for the surface with D=2.5 are slightly convex while all the surfaces with fractal dimension above 2.5 have slightly concave plots. The surface with D supposedly equal to 2.5 has in fact much less obvious curvature in its residuals than all the other surfaces except that with expected D of 2.3.

The residuals from the regression of the 2.5 surface are mainly grouped around zero in a cloud except for a small group of about five points about three quarters of the way along the scatter and also the first two points. It can be seen from the scatterplots in Appendix 2 that there is slightly wider scatter of points in the plot for the 2.5 surface about three quarters of the way along its length. At the distal end of the plot the scatter has decreased again and the plot appears linear with the original gradient. This widening of the scatter is probably the reason for the lower r^2 value of .998.

All this evidence suggests that it is the curvature present in the relationship which makes the estimates of *D* either too large when the desired *D* is less than 2.5 or too small when the desired *D* is greater than 2.5. When *D* should be less than 2.5 the convexity means that the gradient of the plot is reduced as distance increases and as a result *D* is overestimated. If on the other hand *D* is greater than 2.5 the concavity increases gradient thus producing an under-estimate of *D*. In producing the simulated surface 500 faults were used. This relatively small number of iterations was chosen as a result of considering computer time and expense. Mandelbrot (1975a) goes only as far as to say that the number of faults should have high average density. In the light of the slight curvature of the variograms obtained from the surfaces generated from these runs of FRACSIM.FOR it would seem that more iterations are required to make the surface tend to fractal Brownian surfaces. In the cases where *D* was meant to be less than 2.5 low frequency effects were meant to dominate. It would seem that the smallish number of faults used has meant that variance over longer distances is not large enough. Where *D* was meant to be more than 2.5, high-frequency effects were meant to dominate; however the smallish number of faults has resulted in the variance over small distances not being great enough.

The findings from the second set of runs of FASTFRAC where variance is sampled at longer distances confirm the findings from the 60 distance variograms. The convexity of plots for surfaces with expected *D* of less than 2.5 can be detected visually as can the concavity of plots for surfaces expected to have $D > 2.5$. It is what happens at the distal ends of the variograms that is most interesting. In all the plots there is either a widening of scatter or a maximum variance. Where widening of the scatter is the only thing that happens the way in which it widens is important. Although some of the points continue in line with the same gradient as the trend of points before the widening most of the wider scatter is caused by points being below the trendline. This effect that can be roughly equated with the variance reaching a maximum value at a certain distance.The maxima occur at distances between about 50 grid cells and 90 grid cells. Obviously these surfaces must have a maximum possible variance. Depending on the positions of the highest and lowest groups of points the maximum variance can occur from 50 grid cells upwards. If the lowest points are in a corner while the highest points are in a diagonally opposite corner sampling will not go past a distance at which a maximum is

followed by a decrease in variance. The maximum can be around 50 grid cells if the lowest features in the surface are in the middle of the surface while the highest features are around the edges of the surface or vice versa.

5.6 Directional Variogram Results

The adaptation of FASTFRAC which writes the log (variance) and log (distance) for the row, column and two main diagonal directions to separate files was used with the simulated fractal surfaces as input. This section discusses the resulting variograms. Fractional Brownian surfaces are meant to be isotropic with the same order of irregularity and scaling in every direction. The method used to generate the fractal surfaces here would be expected to create an isotropic surface, as the strike directions of the faults used are randomly chosen. Table 5.2 presents the results of the 60 distance runs of the FASTFRAC adaptation in a similar form to the results presented in Table 5.1.

It can be seen from the estimated values of D in Table 5.1 that there is some variation in the fractal dimensions estimated for the four directions studied in each surface. However the row averages of difference between estimated and supposed D show a similar pattern to that found when treating the surfaces non-directionally. The row averages give an average absolute deviation of 0.041 compared with the average difference between estimated and supposed fractal dimensions for the surfaces treated non-directionally of 0.043. The directional and non-directional studies leave the surfaces in the same order as far as difference between estimated and supposed fractal dimension go, except for the surface with a supposed D of 2.5. For the directional variograms the absolute average difference is 0.047 which is greater than the difference obtained from the non-directional study. However the 2.5 surface has one directional estimate which is an underestimate of D and not an overestimate like all the other directions. If this is taken into account the average difference becomes 0.034 which is in line with the difference obtained in the non-directional study.

The directional study also agrees with the findings of the non-directional study as far as curvature goes. Surfaces with supposed fractal dimensions less than 2.5 consistently give overestimates of D from their variograms regardless of direction, while surfaces with expected fractal dimensions of greater than 2.5 give underestimates of D from their variograms.

Therefore, although there are differences in the estimated fractal dimensions of the surfaces for different directions, they are only slight. This suggests that the surfaces are indeed isotropic.

Table 5.2

Expected D	Direction Of Rows				Direction Of Rows				Direction Of Rows				Direction Of Rows				Row Averages Of Differences
	D Output	Diff	R^2	SE	D Output	Diff	R^2	SE	D Output	Diff	R^2	SE	D Output	Diff	R2	SE	
2.0	2.0430	0.0430	1.0000	0.0012	2.0550	0.0550	1.0000	0.0022	2.1050	0.1050	1.0000	0.0061	2.0240	0.0240	1.0000	0.2500	0.0540
2.1	2.1780	0.0780	1.0000	0.0077	2.1720	0.0720	1.0000	0.0086	2.2440	0.1440	0.9990	0.0191	2.1550	0.0550	1.0000	0.0540	0.0870
2.2	2.2180	0.0180	1.0000	0.0022	2.2310	0.0310	1.0000	0.0052	2.2790	0.0790	0.9990	0.0111	2.2270	0.0270	0.9990	0.0122	0.0390
2.3	2.3250	0.0250	1.0000	0.0058	2.3220	0.0220	1.0000	0.0031	2.3250	0.0250	1.0000	0.0068	2.3210	0.0210	1.0000	0.0350	0.0230
2.4	2.4030	0.0030	1.0000	0.0070	2.4350	0.0350	1.0000	0.0081	2.4160	0.0160	0.9990	0.0122	2.4650	0.0650	0.9950	0.0264	0.0300
2.5	2.6010	0.1010	0.9920	0.0240	2.4730	-0.0270	1.0000	0.0032	2.5400	0.0900	0.9990	0.0118	2.5210	0.0210	1.0000	0.0048	0.0470
2.6	2.5820	-0.0180	1.0000	0.0045	2.5660	-0.0370	0.9990	0.0104	2.5520	-0.0480	0.9990	0.0080	2.5690	-0.0310	0.9990	0.0068	-0.0340
2.7	2.6720	-0.0280	0.9990	0.0072	2.6900	-0.0100	1.0000	0.0034	2.6630	-0.0370	0.9980	0.0102	2.6810	-0.0190	0.9960	0.0130	-0.0240
2.8	2.7700	-0.0230	0.9990	0.0050	2.7720	-0.0280	0.9990	0.0045	2.7330	-0.0660	0.9960	0.0112	2.7920	-0.0080	0.9990	0.0037	-0.0310
2.9	2.8600	-0.0400	0.9960	0.0057	2.8710	-0.0290	0.9980	0.0042	2.8730	-0.0270	0.9900	0.0088	2.8460	-0.0540	0.9920	0.0094	-0.0380
3.0	2.9560	-0.0440	0.9920	0.0027	2.9640	-0.0360	0.9400	0.0061	2.9500	-0.0500	0.9600	0.0067	2.9570	-0.0430	0.9670	0.0054	-0.0430
Averages (Absolute) of Differences		0.0380				0.0350				0.0580				0.0340			

Results from regressions of 60 distance directional variograms.

5.7 Rescaled range analysis results.

When the scatterplots produced from the results of RS.FOR are studied (Appendix 2) it can be seen that relationship between log (rescaled range) and log (distance) is linear to start with and then curves convexly until it almost levels out. The convex curvature and levelling out at longer distances is easily explained as a product of the algorithm used to calculate these points.

As was explained in Chapter 4, RS.FOR 'spirals' through the DEM being processed. The spiral starts by considering the first row of the DEM. It then considers the last column, then the last row (last column to first column) and then the first column (last row to second row). Beyond the distance made up by these sides the series being studied almost repeats itself as the next set of two rows and two columns are geographically very close to the previous set. Rescaled range ceases to increase as rapidly beyond this distance and as a result the variograms produced by this algorithm begin to curve convexly and level off.

Therefore when using this method to estimate fractal dimension, least-squares linear regression is performed on only the observations which make up the linear segments of the scatterplots. The estimated fractal dimensions for the simulated surfaces obtained from this process are presented along with the difference between them and the expected fractal dimension, the r^2 and standard error values in Table 5.1.

When rescaled range analysis is used to estimate fractal dimension from the surfaces generated with supposed fractal dimensions of 2.0 to 2.4 it yields estimates that are less than 0.07 different from the input values. The surface with a supposed fractal dimension of 2.8 also yields an estimate which is fairly close. However the other surfaces' supposed and estimated fractal dimensions vary by quite wide margins. The surfaces generated with fractal dimensions of 2.6 and 2.7 yield particularly inaccurate estimates. It would seem that the rescaled range method may have difficulties with the rougher surfaces. There seems to be no obvious reason for this.

5.8 Conclusions.

Simulated fractal surfaces are necessary in this study so that comparisons between simulated and real landsurfaces can be made in two ways: fractal surfaces can be compared visually with real landsurfaces; and real and fractal geomorphometry can be compared. The simulated fractal surfaces also provide surfaces with certain expected properties that can be used to test the analysis programs which are being used in this study.

The most suitable method for simulating fractal Brownian surfaces for this study would seem to be the shear displacement method. Although it is not as suitable as its alternatives for high resolution graphics, it produces surfaces of the required resolution by an easily understood process. The simplicity of the process means that the behaviour of the surfaces when subjected to analysis can be more easily explained in terms of that process.

Visually the simulated surfaces with fractal dimensions of more than 2.4 are much too rough to be real landsurfaces. Even the surface with a fractal dimension of 2.4 would be an unusually rough real landsurface. The faults which were used to produce the surfaces show through as linear features in the smoother surfaces. Although real landsurfaces often have linear elements, they are often orientated in the same direction. This is not the case with the fractal surfaces. The major visual difference between fractal surfaces and real landsurfaces is the lack of drainage networks in the simulated surfaces.

The variogram method, employing FASTFRAC, yields estimated fractal dimensions which are close to the supposed fractal dimensions of the surfaces. More random faults would make the estimated and supposed values closer. Variance may reach a maximum value before the largest distance sampled due to the fact that the simulated surfaces are of finite area: variance must reach a maximum. The spatial distribution of the highest and lowest points determines at what distance variance reaches its maximum.

Rescaled range analysis does not seem to be an effective method of assessing the possible self-affine nature of a surface. Results obtained from it do provide a rough guide to the relative roughness of surfaces but the major use of the method here is to indicate the benefits of using the apparently accurate variogram method.

Chapter 6: The Fractal Nature of Real Landsurfaces

6.1 Introduction

Testing the variogram and rescaled range analysis programs on surfaces with certain expected properties has revealed some of their possible limitations. For example, the inability of the rescaled range analysis program to estimate the fractal dimension of surfaces with expected fractal dimensions of greater than 2.5 means that results obtained from this method of analysis must be closely scrutinized and compared with those from the variogram method which seems to be more consistently reliable.

With these limitations recognised it is possible to widen the study to examine digital elevation models of real landsurfaces. It is in this chapter that the results of variogram and rescaled range analysis are used to answer one of the original questions raised in Chapter 1: that is, whether or not landsurfaces are scale free.

The concepts behind the ways in which this can be done have been developed in Chapters 2 and 4. To recap, perfect fractional Brownian surfaces would, if submitted to variogram or rescaled range analysis, produce perfectly linear plots of log variance versus log distance and log rescaled range versus log distance.

This would apply to all orientations and all sub-areas. Real landsurfaces must therefore be exposed to the same examination to see whether they produce linear plots or some other sort of structure. Other sorts of structure might include plots with linear sections of different gradients separated by steps or, as seen in the fault displacement surfaces of Chapter 5, convex or concave curvature. If, as previous geomorphological observation would seem to suggest, the fractional Brownian model should break down when considering real landsurfaces, any structures revealed in the plots should suggest possible reasons for this break down. The more traditional geomorphometric approaches of Chapters 7 and 8 may shed further light on these possible reasons.

This chapter will therefore begin with a basic description of the 27 DEMs of real landsurfaces used. Chapter 7 gives details of the DEMs' geomorphometry. After the DEMs are introduced this chapter will follow a similar format to that of Chapter 5. The results of the non-directional 60 distance variograms will be presented first, followed by a comparison with the rescaled range analysis results. The non-directional variograms for larger distance ranges will then be discussed. After this, directional variogram results will be considered, and finally the analysis of subareas of the surfaces.

6.2 The Digital Elevation Models (DEMs)

Table 6.1 presents some of the details about the DEMs used in the study. Due to the cost of purchasing ready-made DEMs from mapping agencies and the complexity and time involved in creating them, as was mentioned in Chapter 3, this study has used DEMs from several different sources. Fourteen of these DEMs existed in Durham at the beginning of the project, many having been used in geomorphometry studies included in the references by I.S.Evans. The other thirteen DEMs have been acquired since the beginning of the project and therefore less is known about the geomorphology of some of the areas covered by these new DEMs. As a result the areas covered by the DEMs have not been chosen to try and represent as many types of geomorphologically different landscapes as possible but rather to give as large a sample as possible with the least input of expense and effort. Fortunately the sample does cover quite a number of different landsurface types.

Table 6.1 DEM details

Name	Grid Mesh	Area
Torridon	100m	10.000km × 10.000km
Keary	100m	5.000km × 5.000km
Wind	200m	9.000km × 9.400km
Nupar	100m	8.200km × 8.200km
Thvera	100m	10.200km × 10.600km
Dumfries	100m	7.100km × 15.100km
Galloway	100m	7.100km × 15.100km
Uinta	30m	13.950km × 10.620km
Devoluy	50m	10.050km × 10.050km
Canigou	50m	10.050km × 10.050km
Aigoual	50m	16.700km × 16.700km
Montoire	50m	10.050km × 10.050km
Le Puy	50m	10.000km × 10.050km
Le Porge	50m	10.050km × 10.050km
Reunion	300m	66.300km × 51.600km
St. Paul	50m	3.950km × 4.150km
Booro Borotou	7m	1.505km × 1.358km
Auchwick	30m	14.220km × 11.070km
Belleville	30m	14.190km × 11.010km
Allenville	30m	14.220km × 11.040km
Netherhearth Sike	10m	1.500km × 2.350km
Glaisdale	15m	0.750km × 0.750km
Wheeldale	15m	0.750km × 0.750km
Devon	100m	10.100km × 10.100km
Gara	50m	8.000km × 8.100km
Appleby	50m	8.000km × 5.000km
Alarta	100m	10.100km × 10.100km

There is a bias however of nine surfaces from glaciated mountain or upland areas due to the interests of the researchers who created or acquired them. Five of these have been produced by manual interpolation from contour maps in Durham. The file TORR contains a DEM, created by Iain Bain, of part of the Torridon area, N.W.

Scotland. The perspective block diagram (fig. 6.1) shows three north-south orientated ridges separated by well defined glacial troughs. The corner of mountain in the southeast belongs to Beinn Eighe, while the summits in the southwest make up part of Beinn Alligin.

KEARY is a file containing a DEM, created by I.S.Evans, of part of the Keary and Nosebag drainage basins, on the northeast slope of the Bendor range, British Columbia. The glaciated nature of this area is clearly visible in figure 6.2.

The file WIND contains a small DEM produced by Don Alford of an area in the Wind River mountains, Wyoming. This DEM has a grid mesh resolution of 200m which is one of the coarsest resolutions used in this study. Figure 6.3 shows that despite this resolution the glaciated nature of the area can still be seen with well defined cirques clearly visible.

NUPUR and THVERA are two DEMs of areas in Iceland, both produced by Jasbir Gill. Nupur is part of the West fjords penninsula, northwest Iceland. The DEM represents a glacially dissected plateau (fig 6.4). Thvera is in the central part of northern Iceland, southwest of Akureyri. Figure 6.5 shows the glacial landscape well including cirques, arêtes, and troughs.

Two areas of glaciated upland in the southwest of Scotland are used in the study. The DEMs DUMFRIES and GALLOWAY (fig. 6.6 and fig. 6.7 respectively) were produced by a semi-automated method involving the digitising of contours on 1/50000 maps and then some interpolation routine from these to a regular grid. They are both long thin rectangular matrices.

DUMFRIES (Evans, 1982) covers the area from Annandale to Nithsdale with its long axis parallel to the southern margin of the Southern Uplands of Scotland. The northern half of the DEM covers the glacially smoothed uplands dissected by the glacial troughs of Kinnel Water, the Water of Ae, Glenkill and Mollin Burns. The upland here is formed from Ordovician shales and Silurian shales and greywackes uplifted as an accretionary prism. The southern half of the matrix extends into lowlands of Permian sandstone and upper Carboniferous sequences.

GALLOWAY (Evans 1982) is a DEM of an area in Galloway south of Girvan running northwest-southwest. Completely in the Southern Uplands this relatively low plateau of upper Ordovician greywackes, siltstones and shales is dissected by the troughs of the Duisk and Stinchar valleys. The geology of the northwest corner is complicated by submarine volcanism of lower Ordovician age.

UINTA is a U.S.G.S. produced DEM, interpolation to a regular grid being made automatically during the photogrammetry stage of the mapping process. UINTA represents the northern slope of the Uinta mountains, Wyoming. The area covered by the DEM is about 10.6km by 14km which is relatively large for this study and no features associated with glaciated mountains can be easily discerned from figure 6.8. There is some doubt as to whether the area was glaciated or not.

DEVOLUY, in the extreme south western French Alps, is the final sizeable glaciated upland area studied (fig. 6.9). It is one of several French DEMs used and has been produced by a semi-automated interpolation routine from digitized contours using a Yoeli (1986) type method (as described in Chapter 3) with a slightly more complex spline fitting procedure (Breard, 1989).

Five other diverse landsurface types from France are also studied. Two of these are mountain areas in the south of France. CANIGOU (fig. 6.10) is a DEM covering 100km^2, near the eastern extreme of the French - Spanish border and is part of the glaciated Pyrennes. The second mountain landsurface is of a larger area 280km^2 in the Cevennes surrounding Mont Aigoual. The south-eastern corner of this DEM contains the upper part of the catchment of the river Gardon (fig. 6.11). The DEM AIG is produced using an Yoeli type method but has been made by hydrologists in Montpellier who use the Gardon as an instrumented catchment.

All three of the remaining French DEMs are produced in a similar manner; of these MONTOIRE is situated the furthest north. The area it represents is in the Loir valley around the town of Montoire-sur-Loir, near Vendome, and figure 6.12 shows clearly that it includes two incised meanders.

Moving south the next French DEM, PUY, is of the Puy de Dôme. The peaks in figure 6.13 illustrate the volcanic plugs of the Auvergne. The final DEM located in France is Le PORGE situated on the Atlantic coast, south of the Gironde estuary and north of Cap Ferret. The surface represented is made up of coastal dunes and then a flat forest area (fig. 6.14).

Two other French produced DEMs are of volcanic islands. One is REUNION island in the Indian Ocean (fig. 6.15), the other ST.PAUL (fig. 6.16). The former is dominated by two volcanic peaks with several collapsed craters in their sides while the later is formed completely by a flooded crater. Another DEM with French origins is BOBOL, which is of the small Booro Borotou catchment in the Ivory Coast, West Africa (fig. 6.17). This DEM has the finest grid mesh (7m) used in this study.

There is a set of three DEMs of Ridge and Valley type topography from the Appalachian mountains in Pennsylvania. AUGH, BELLE, and ALLEN (figures 6.18 to

6.20) are all USGS produced DEMs with a grid mesh of 30m representing the areas of Aughwick, Belleville, and Allenville. Aughwick is of particular interest as it is the same DEM as one of those Mark and Aronson (1984) studied in their assessment of the fractal nature of landsurfaces.

Three further DEMs which existed previously to this study in Durham include NETHER, GLAIS, and WHEEL (figs. 6.21 to 6.23). All three are of small areas of glaciated upland drainage basins. The first mentioned is of Netherhearth Sike in Teesdale, Co. Durham; the second, Glaisdale, and third, Wheeldale, are both from the North York Moors. Each shows only a small part of the landsurface

Unlike the others matrices DEVON and GARA (figures 6.24 and 6.25) are of areas not recently glaciated, and therefore widen the sample of areas studied from the British Isles.

The final British landsurface included in the study is of an area of Drumlins in the Vale of Eden, Cumbria. The DEM APPLEBY is almost centred on the town of Appleby. The process of making this DEM was detailed in Chapter 3. Figure 6.26 shows the drumlins quite clearly.

The last DEM to be discussed is from Saudi Arabia. ALARTA represents an area of ephemeral drainage, with a very dissected nature. The apparent irregularity can be seen from figure 6.27. This DEM was manually interpolated by Hoda Al-Mazrooa (1989).

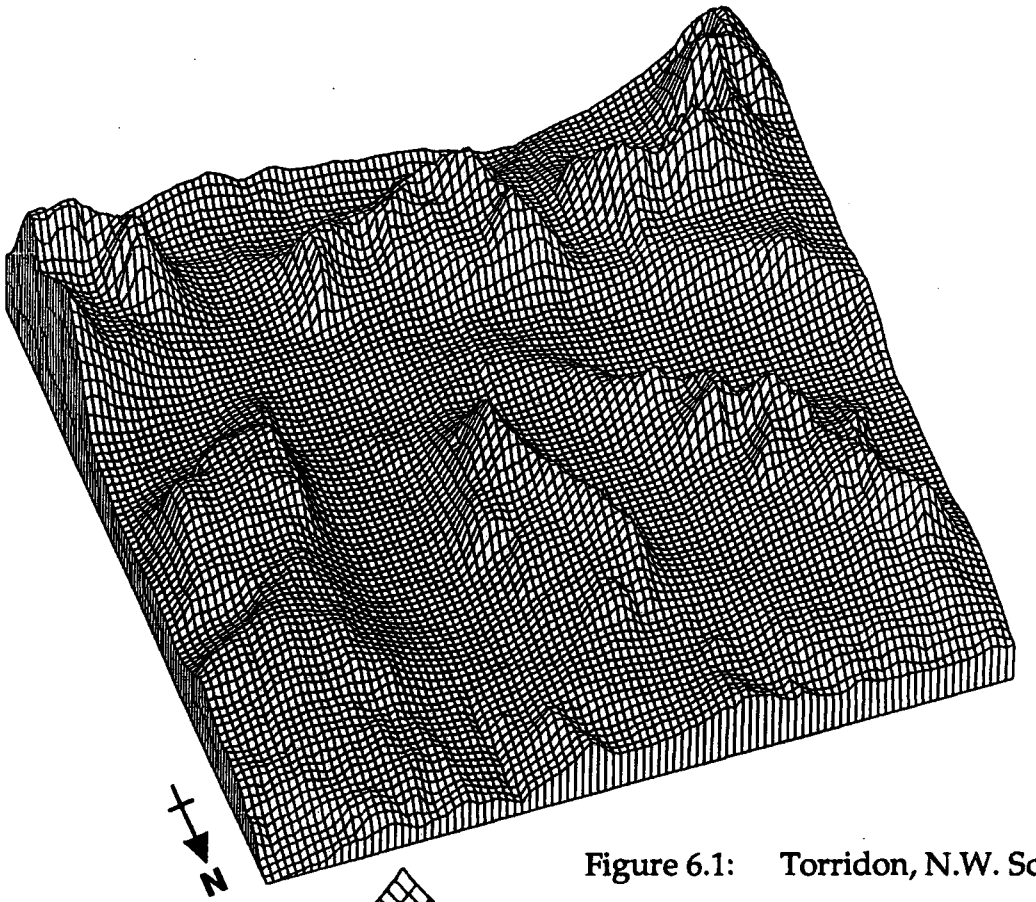

Figure 6.1: Torridon, N.W. Scotland.

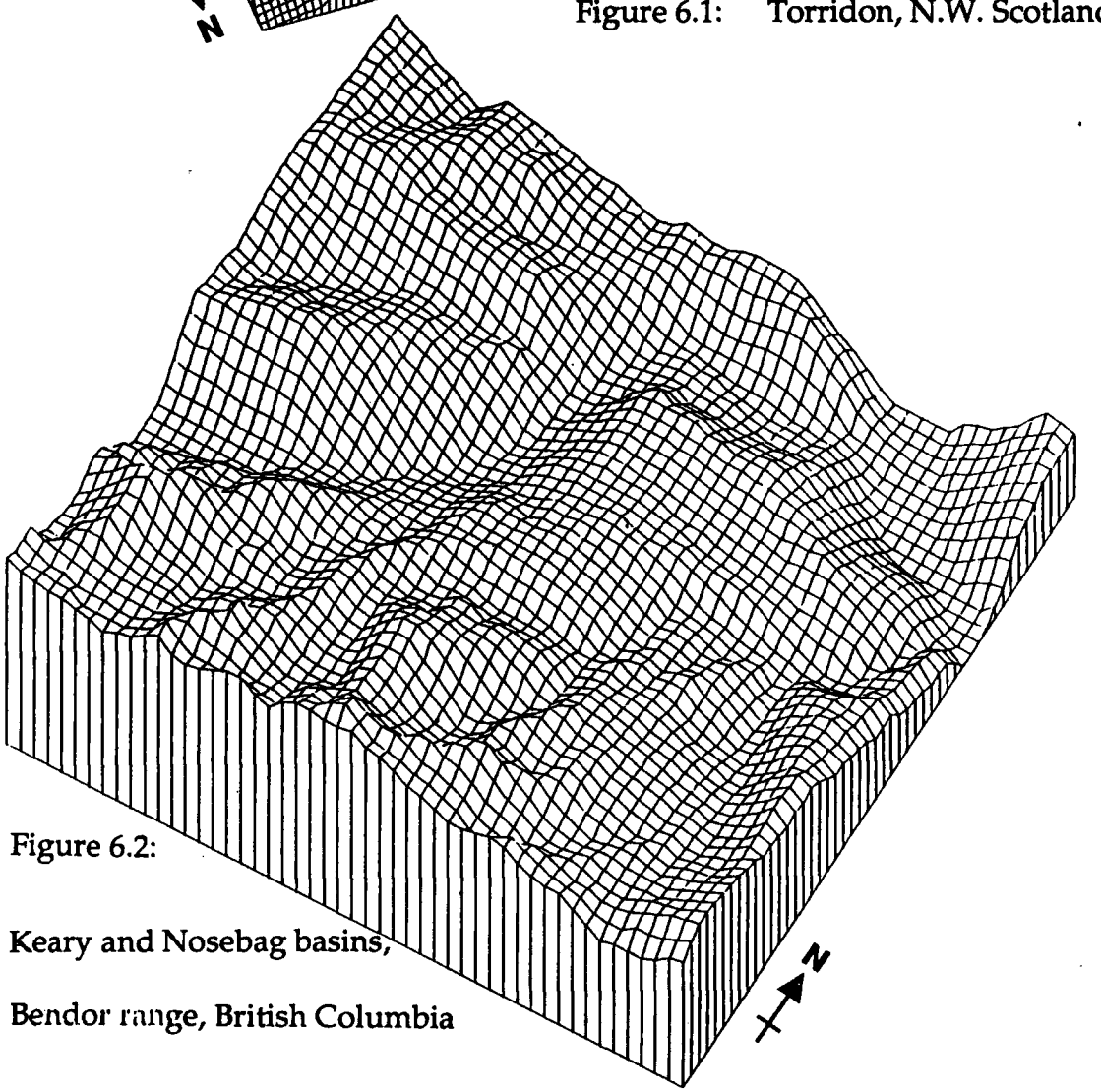

Figure 6.2:

Keary and Nosebag basins,

Bendor range, British Columbia

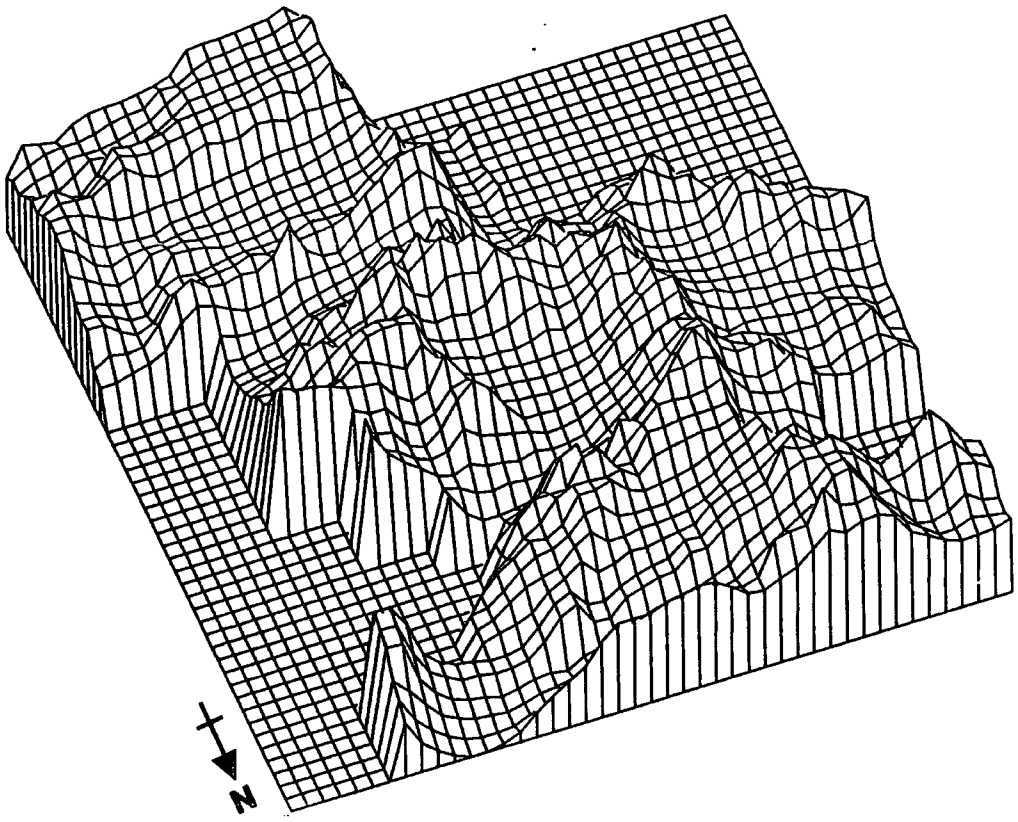

Figure 6.3: Wind River Mountains, Wyoming, USA.

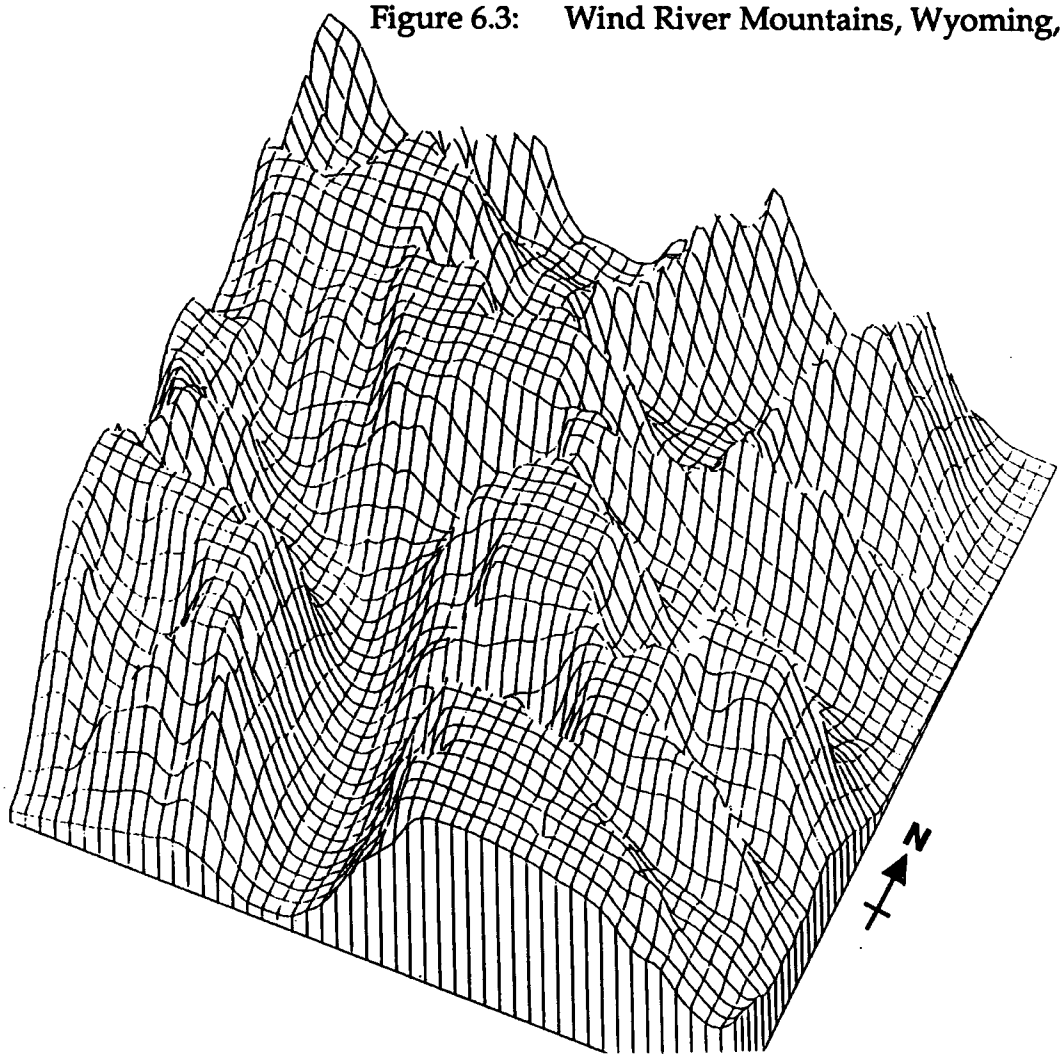

Figure 6.4: Nupur, West Fjords penninsula, N.W. Iceland.

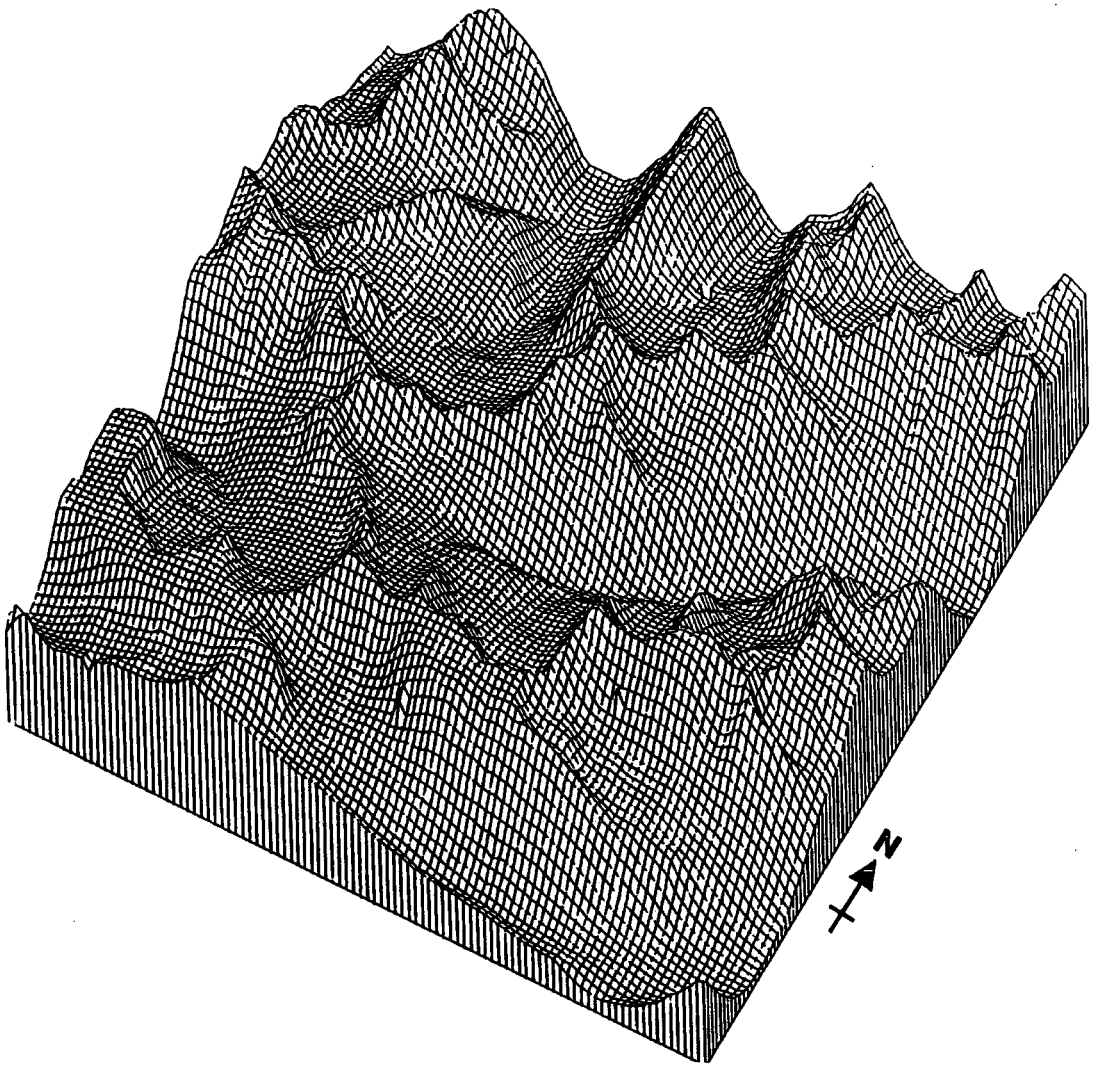

Figure 6.5: Thvera, North-Central Iceland.

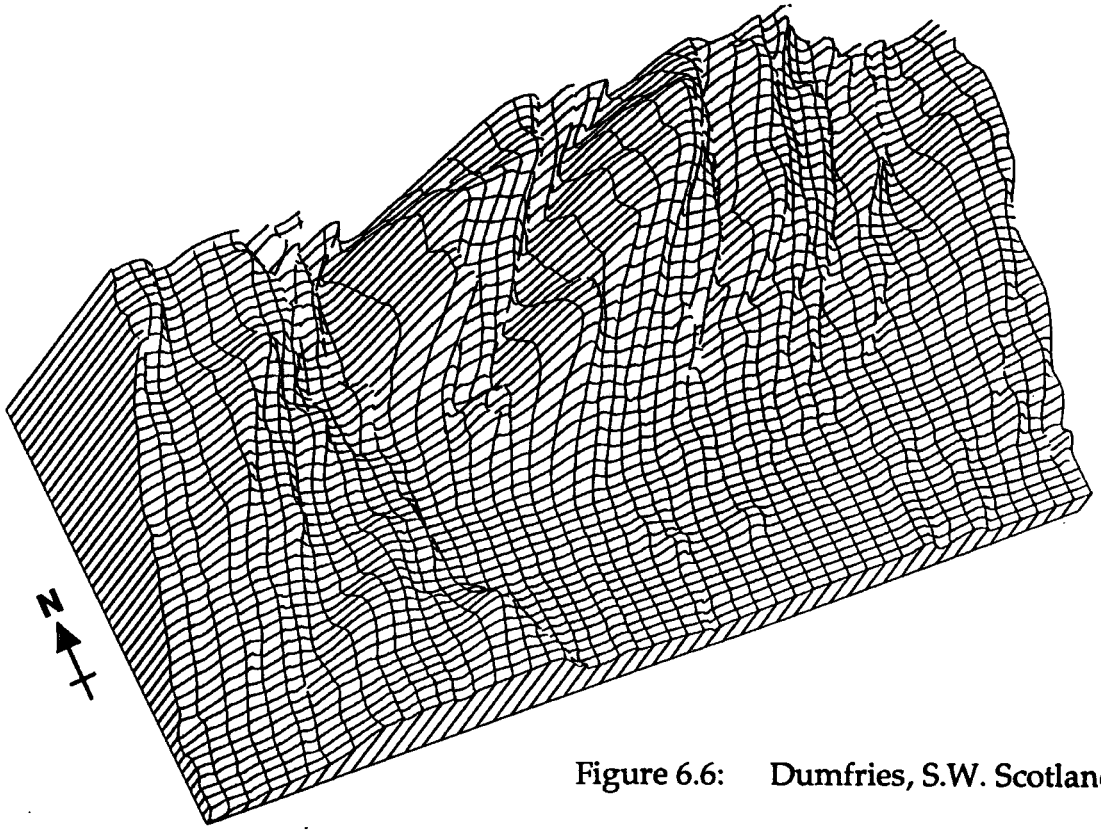

Figure 6.6: Dumfries, S.W. Scotland.

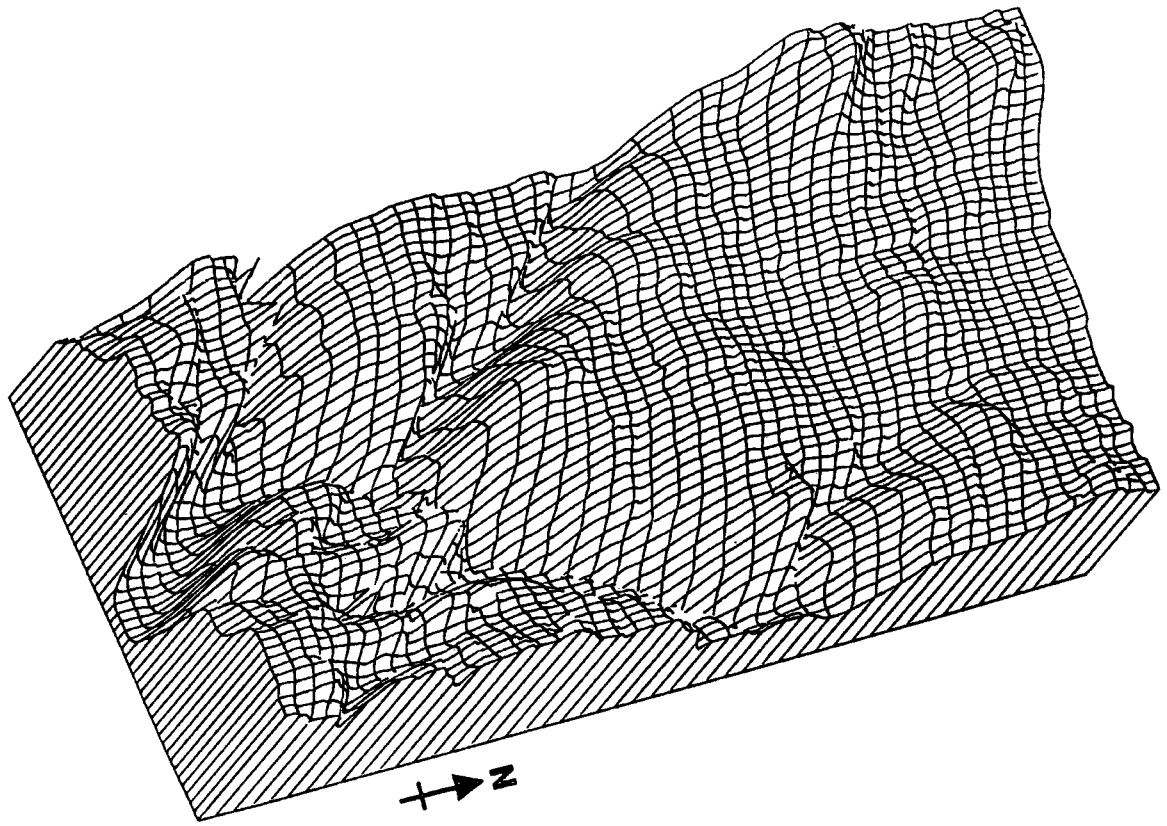

Figure 6.7: Galloway, S.W. Scotland.

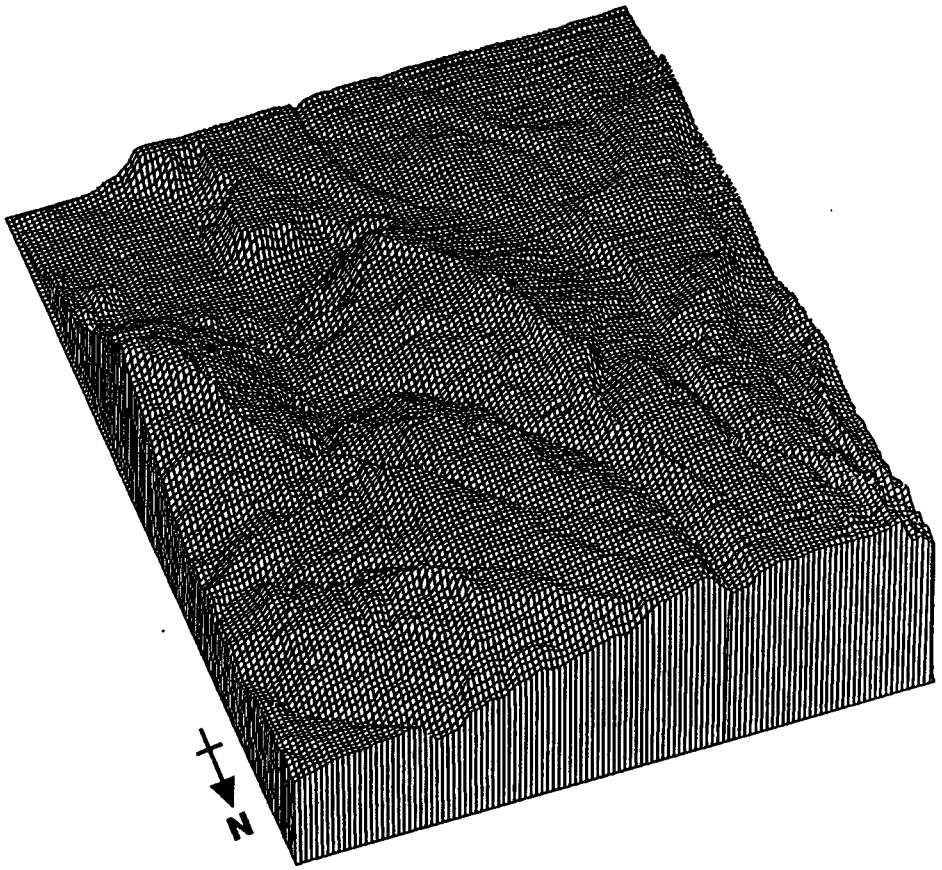

Figure 6.8: Northern slopes of Uinta Mountains, Wyoming, USA.

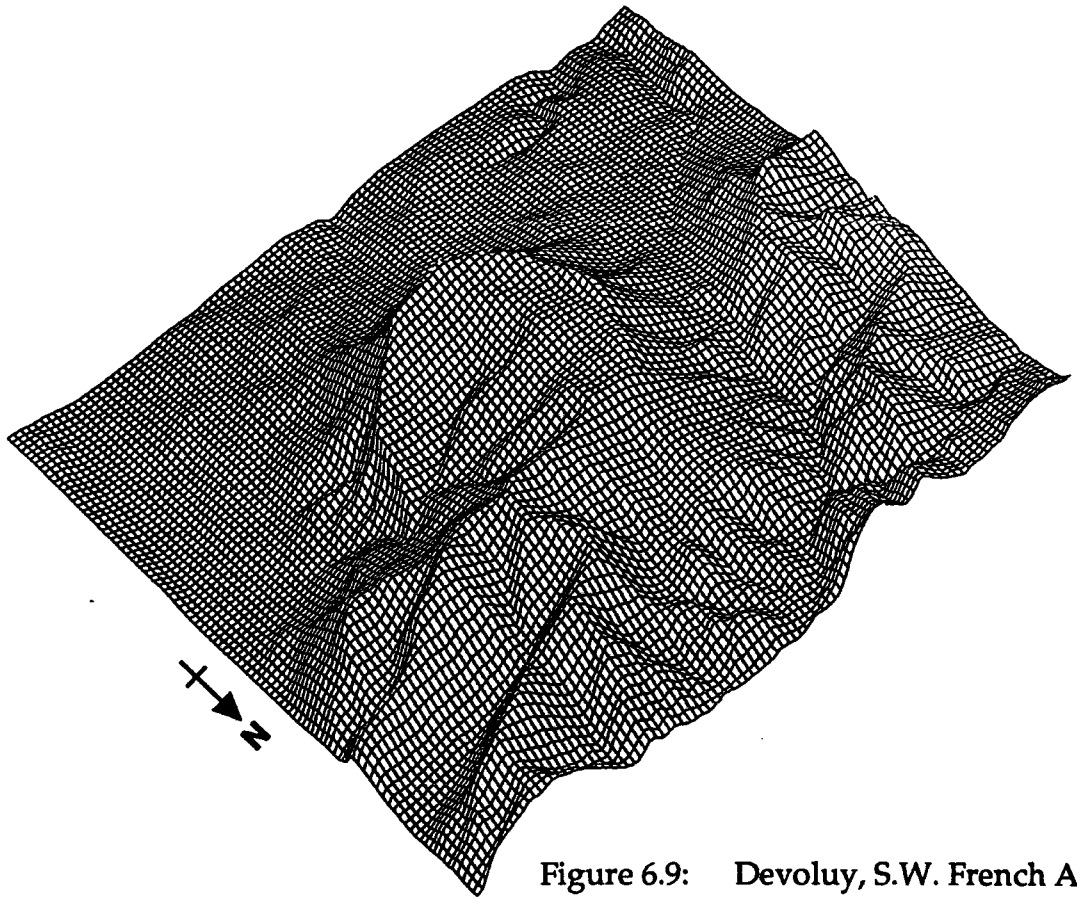

Figure 6.9: Devoluy, S.W. French Alps.

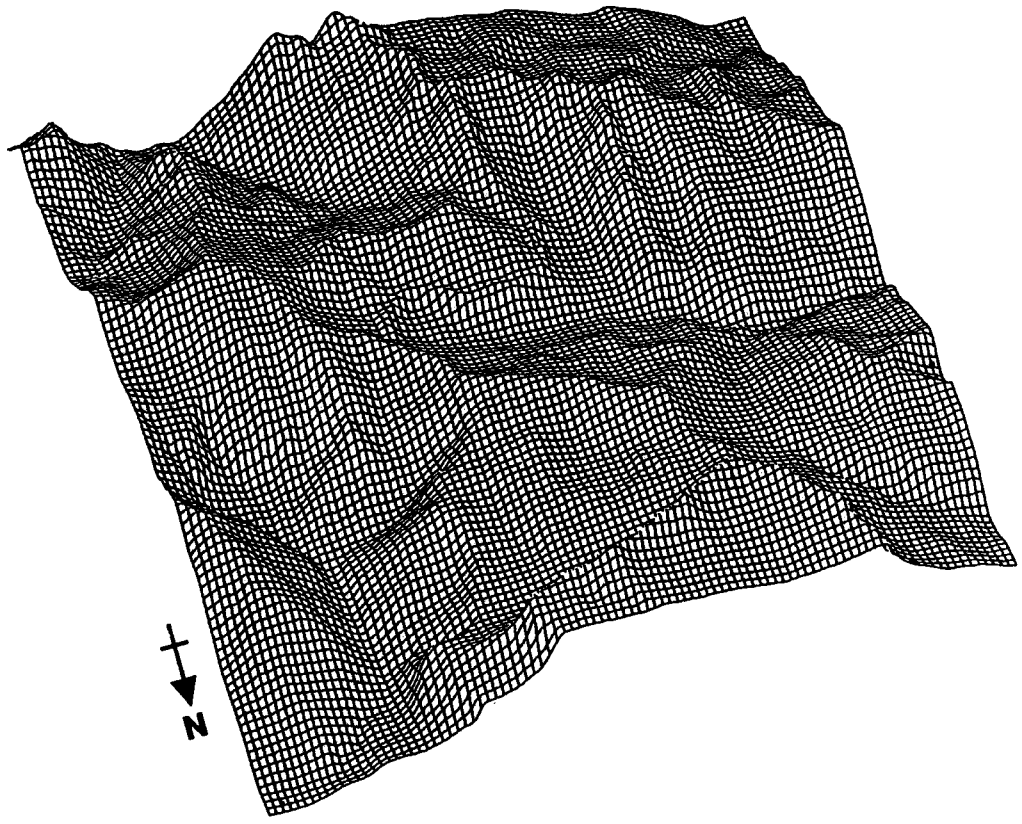

Figure 6.10: Canigou, N.E. Pyrennes, France.

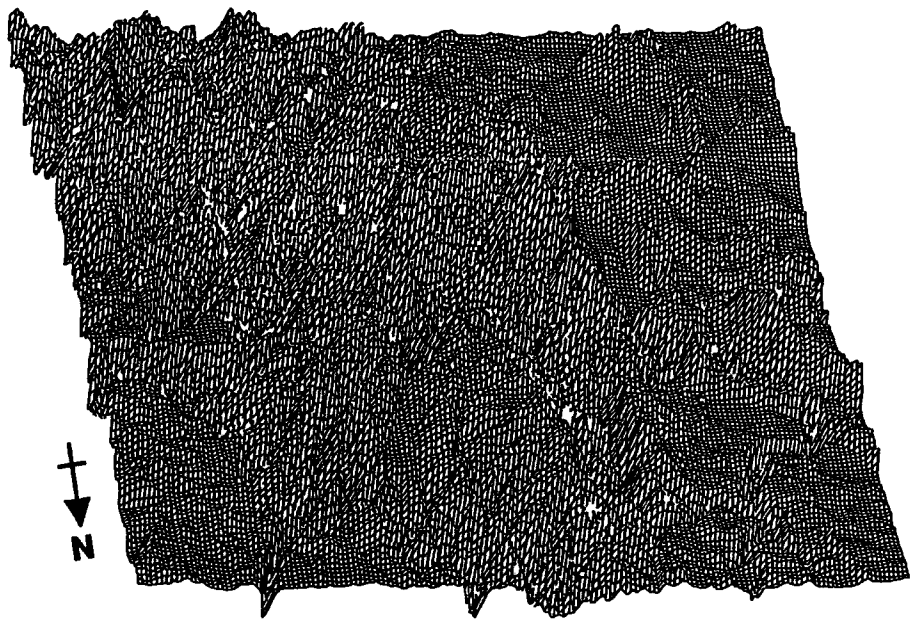

Figure 6.11: Mont Aigoual, Cevennes, S. France.

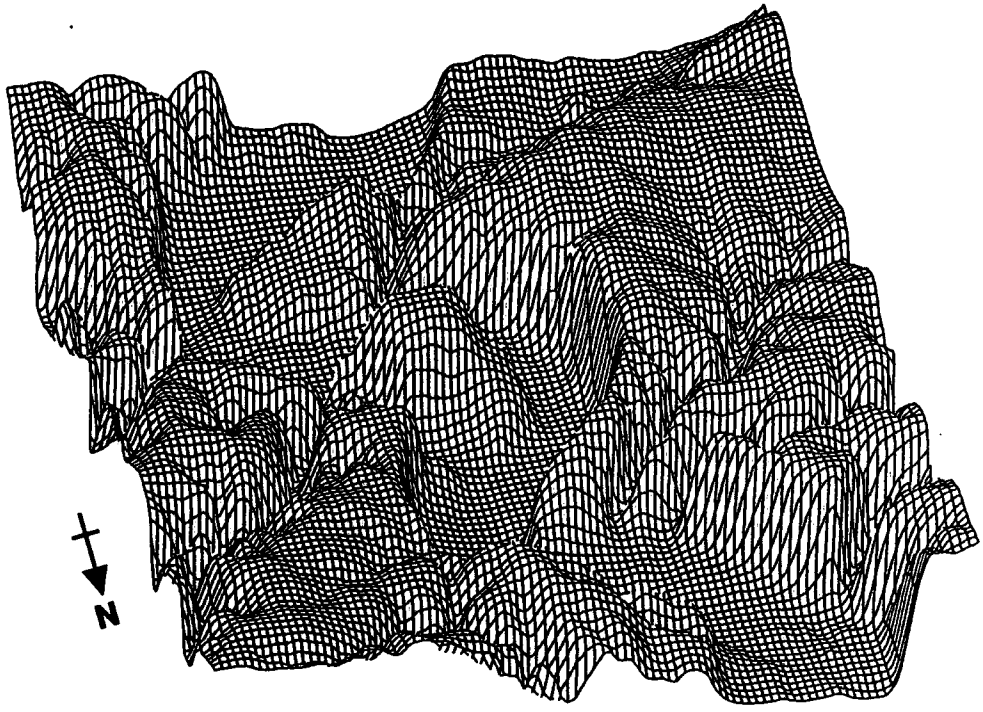

Figure 6.12: Montoire, Montoire-sur-loir, France.

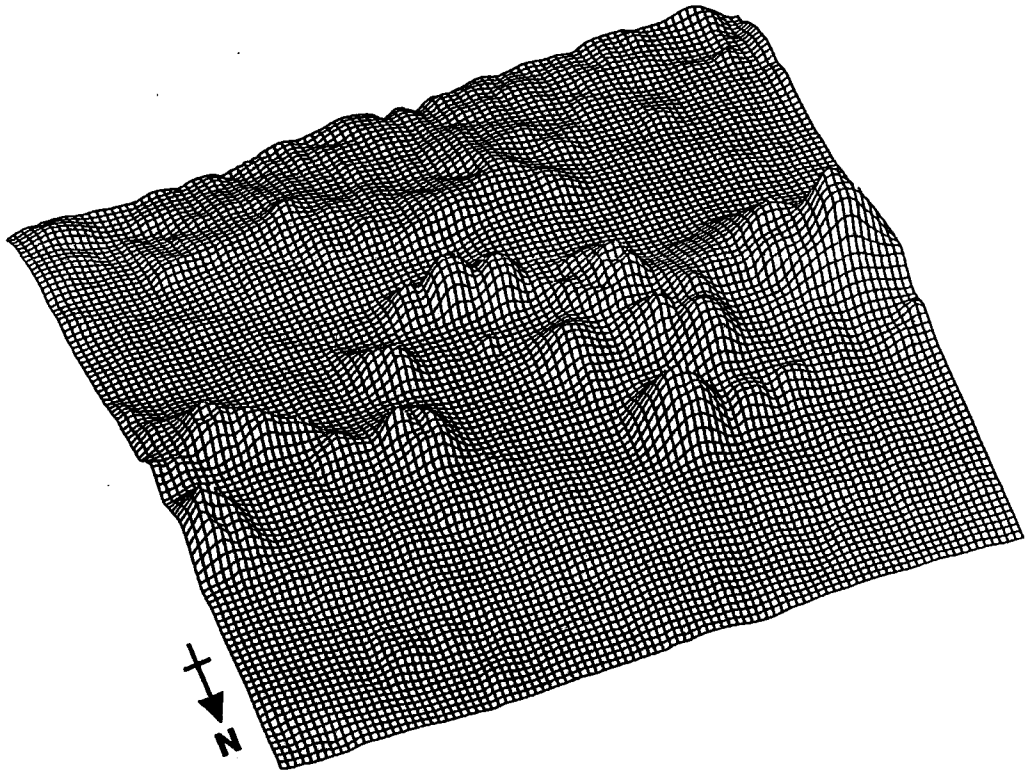

Figure 6.13: Le Puy, Puy de Dôme, Auvergne, France.

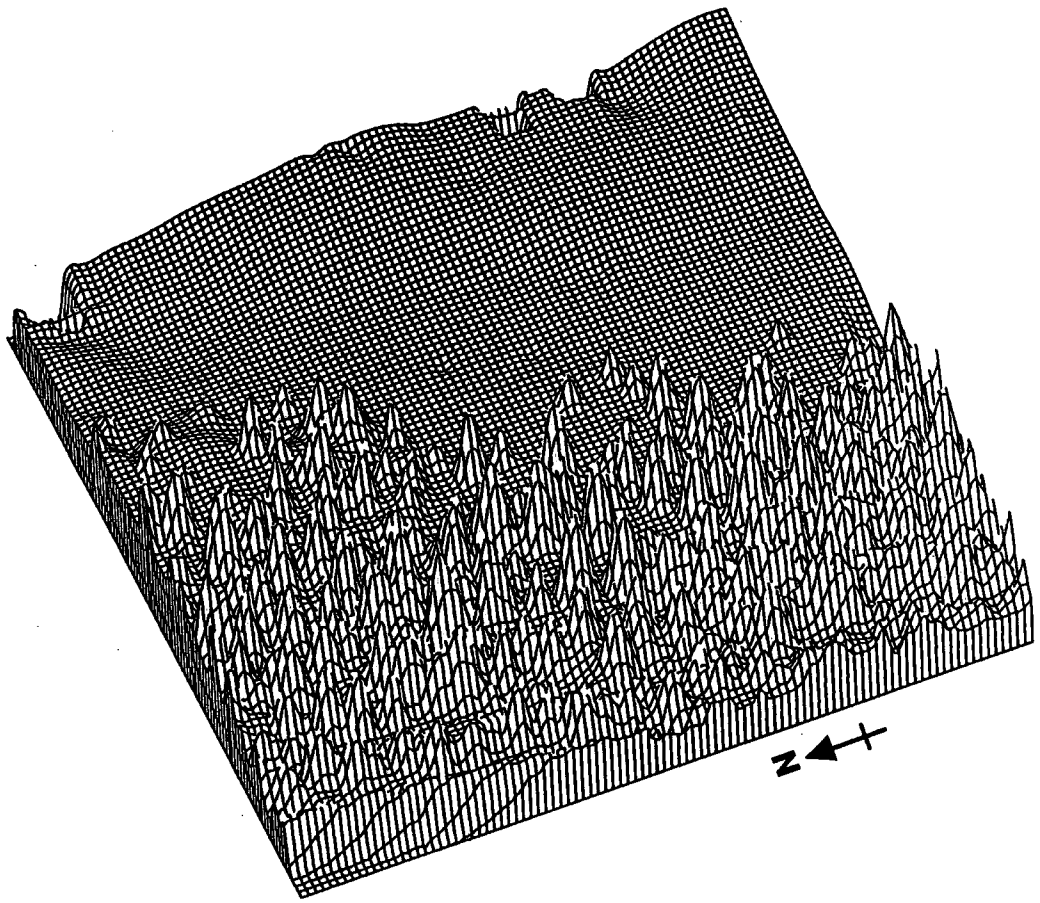

Figure 6.14: Le Porge, W. France.

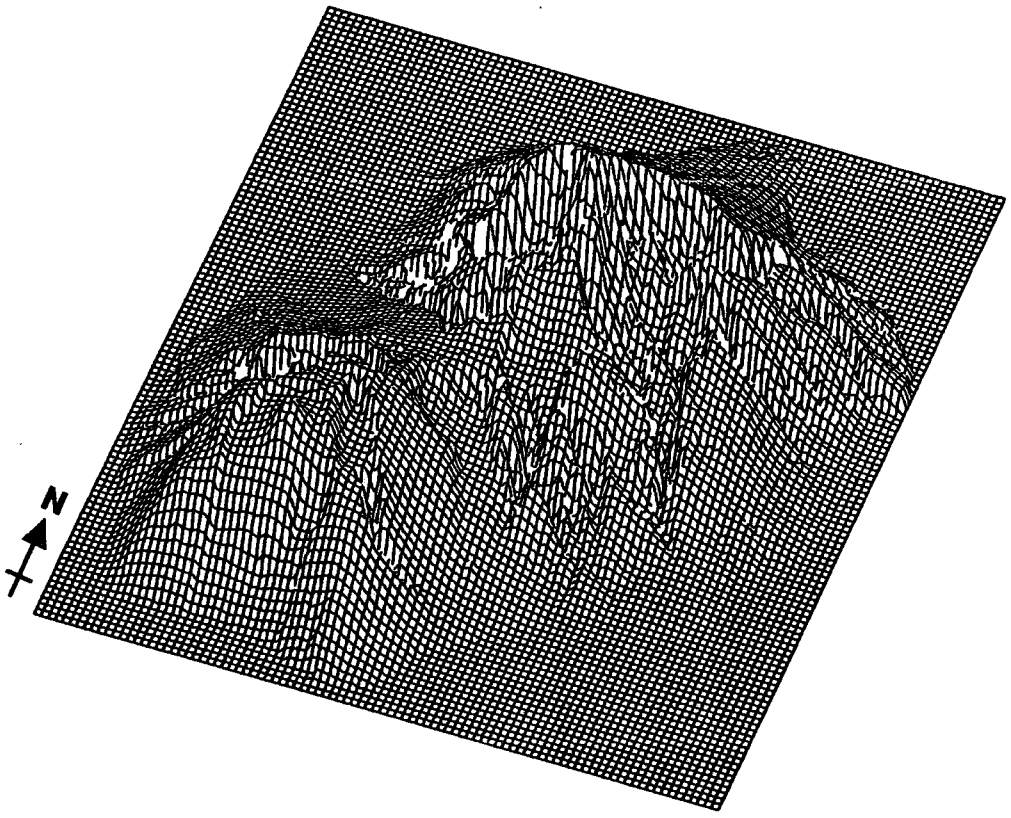

Figure 6.15: Réunion Island, Indian Ocean.

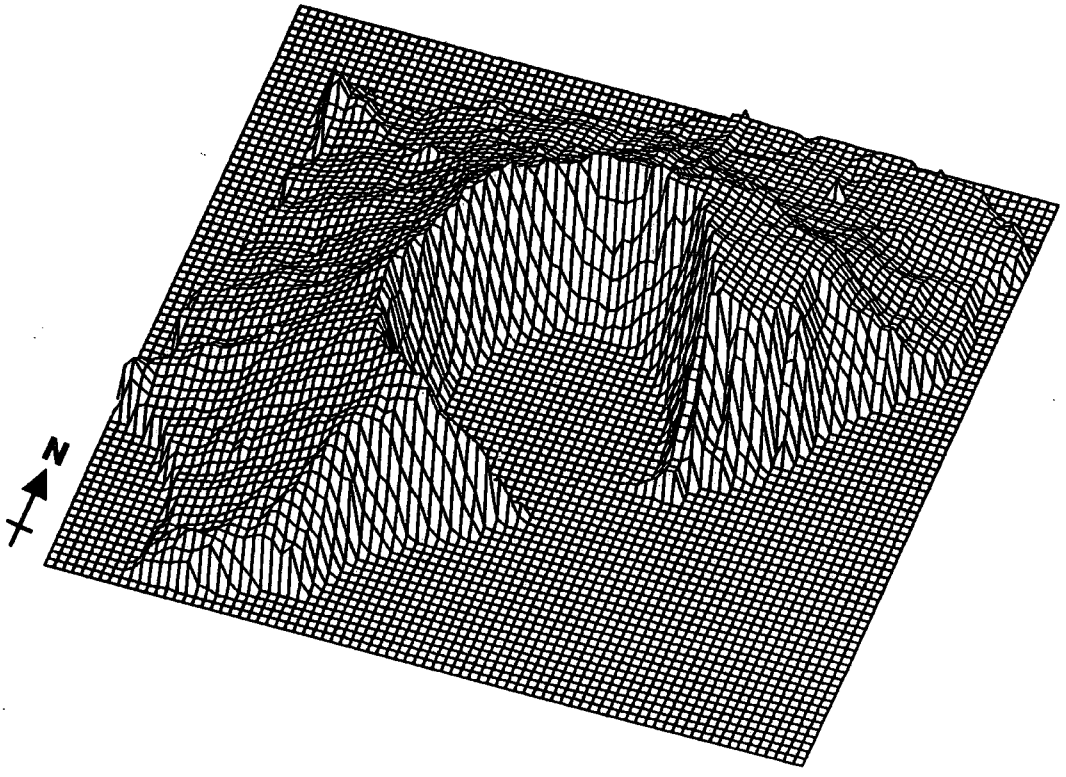

Figure 6.16: St Paul Island.

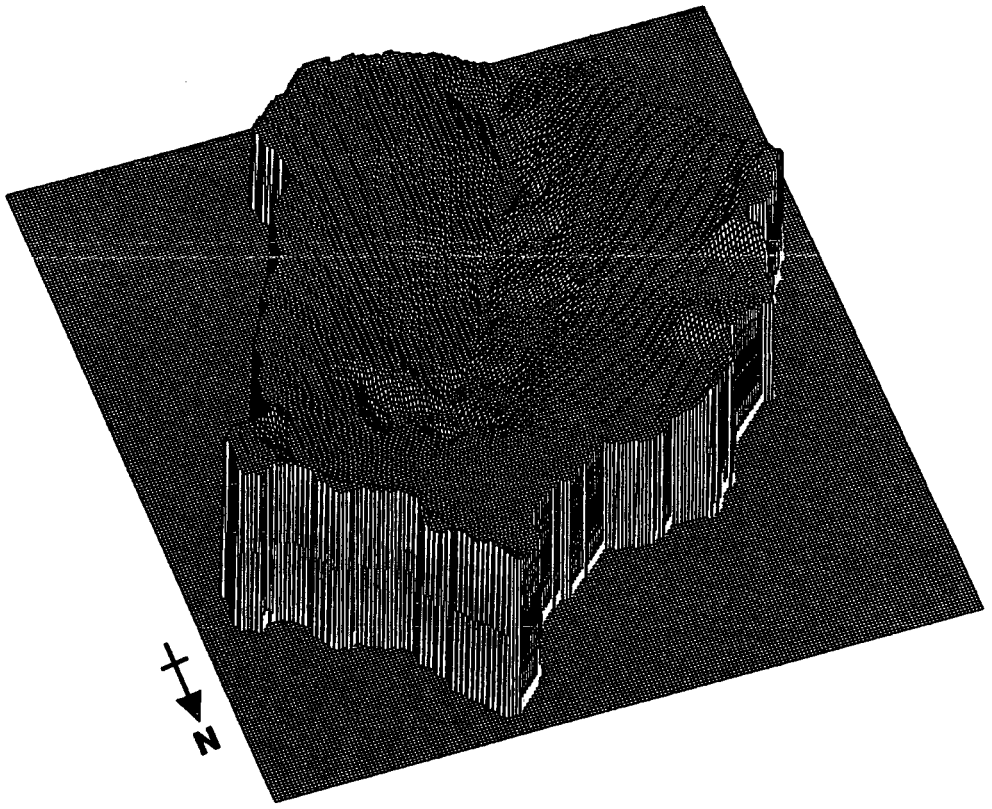

Figure 6.17: Booro - Borotou, Ivory Coast, W. Africa

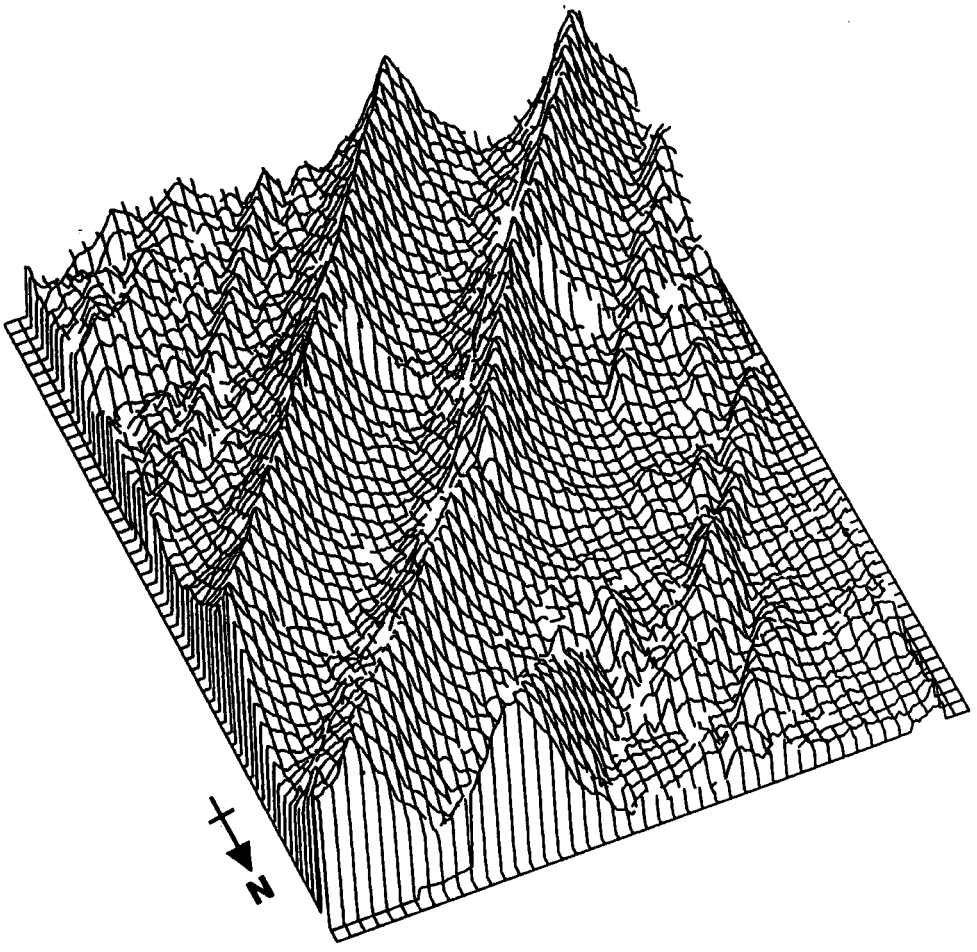

Figure 6.18: Aughwick, Appalachian Mountains, Pennsylvania, USA.

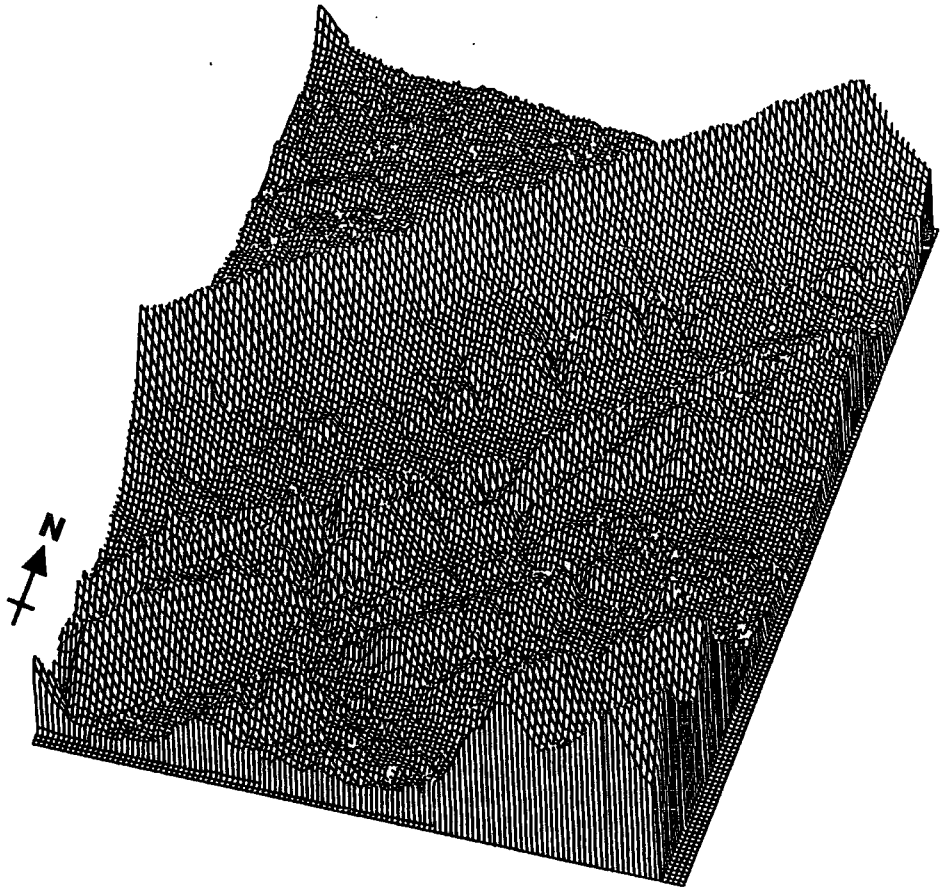

Figure 6.19: Belleville, Appalachian Mountains, Pennsylvania, USA.

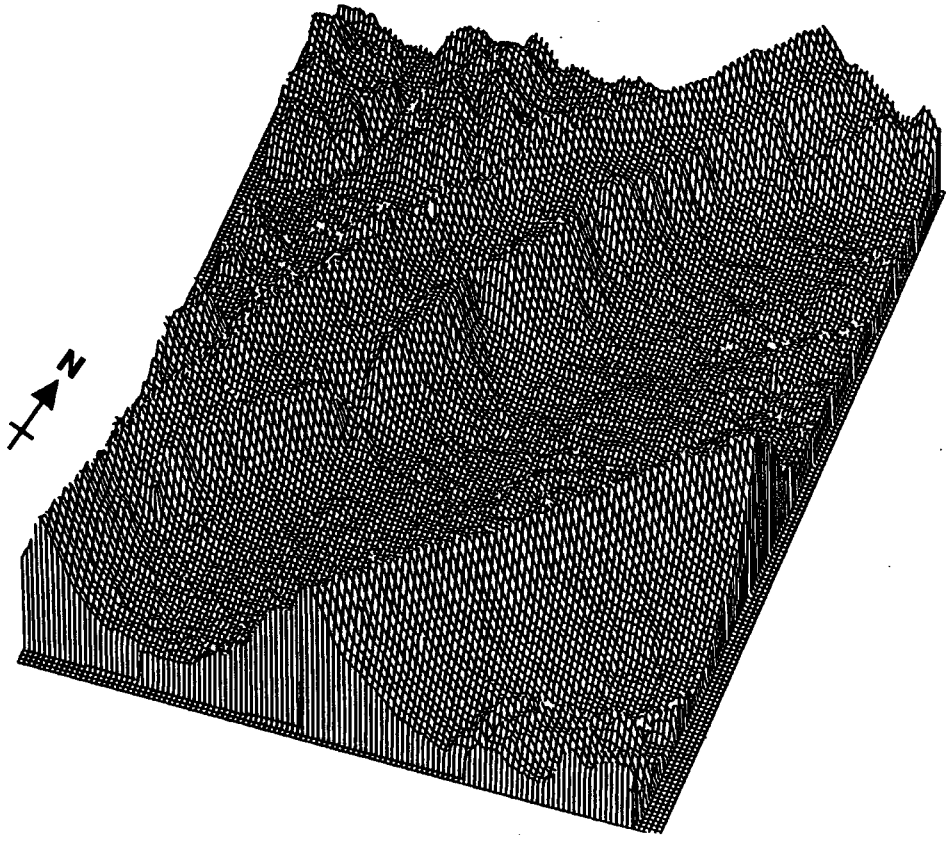

Figure 6.20: Allenville, Appalachian Mountains, Pennsylvania, USA.

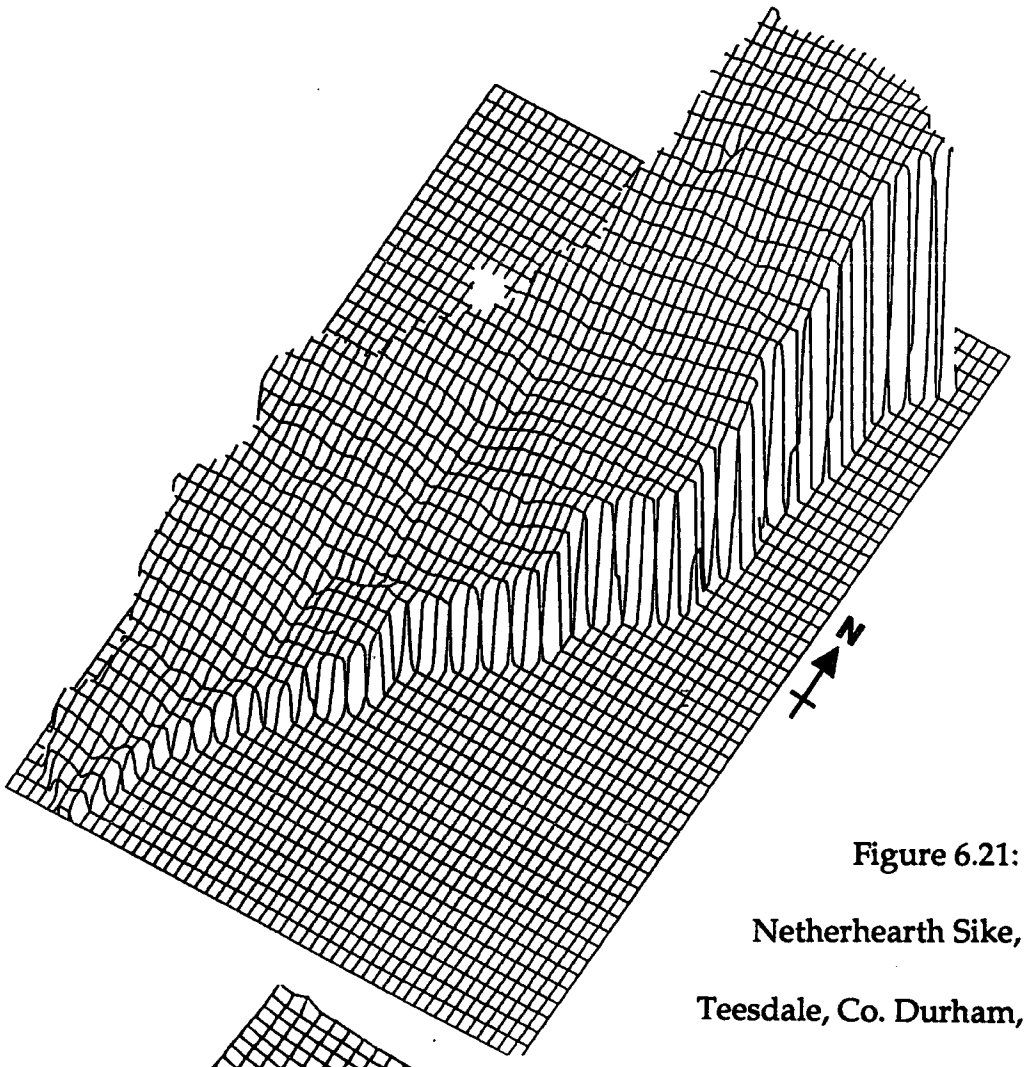

Figure 6.21:

Netherhearth Sike,

Teesdale, Co. Durham,

England.

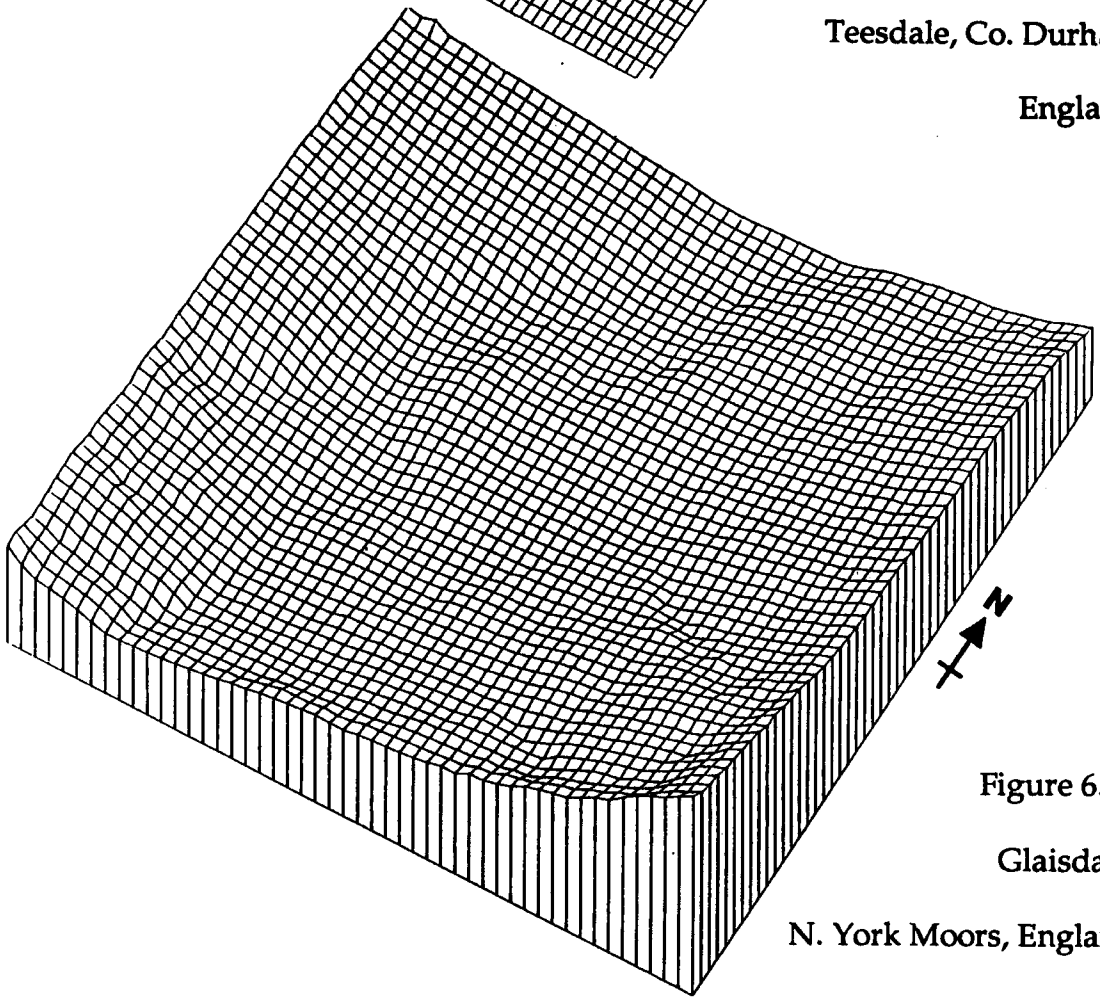

Figure 6.22:

Glaisdale,

N. York Moors, England.

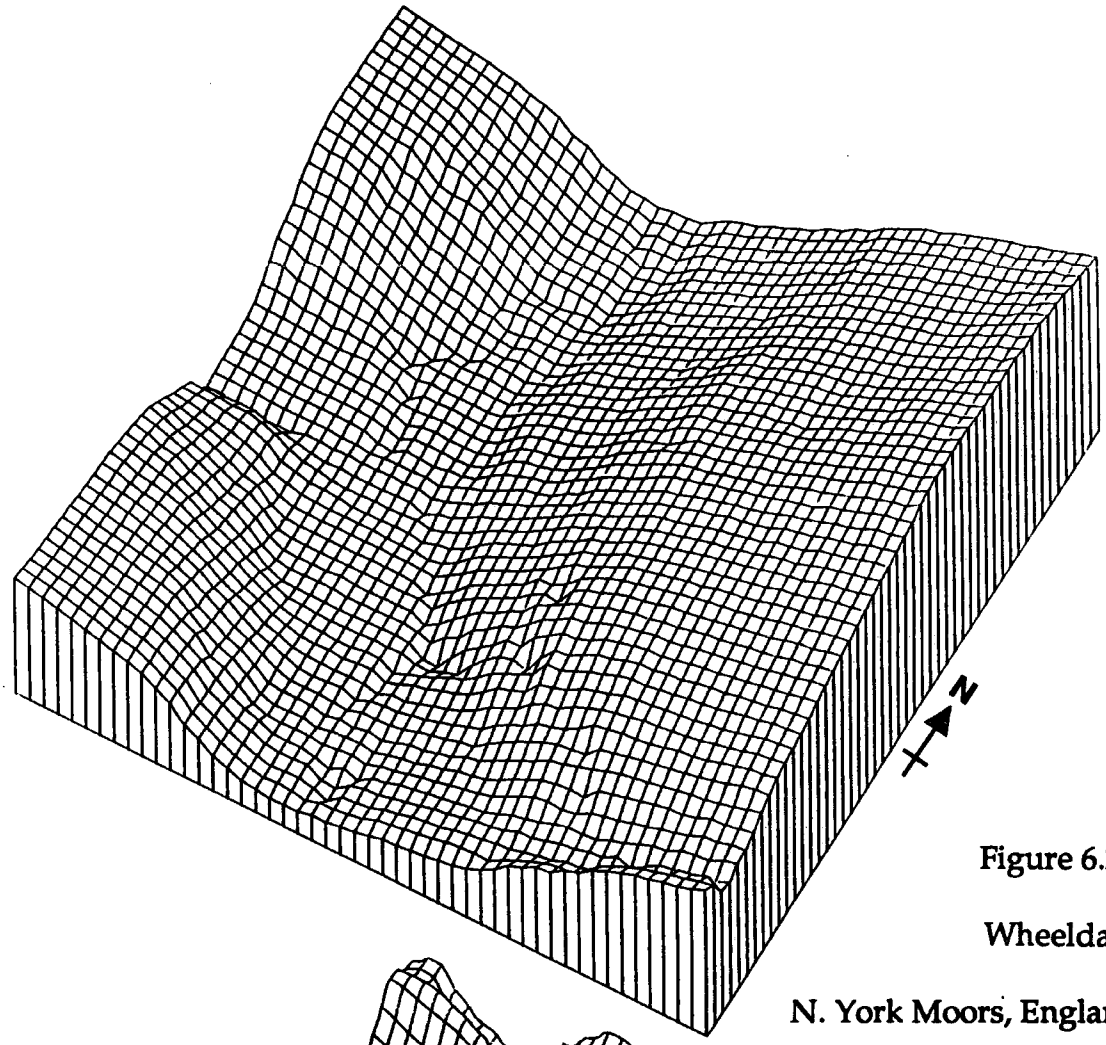

Figure 6.23:

Wheeldale,

N. York Moors, England.

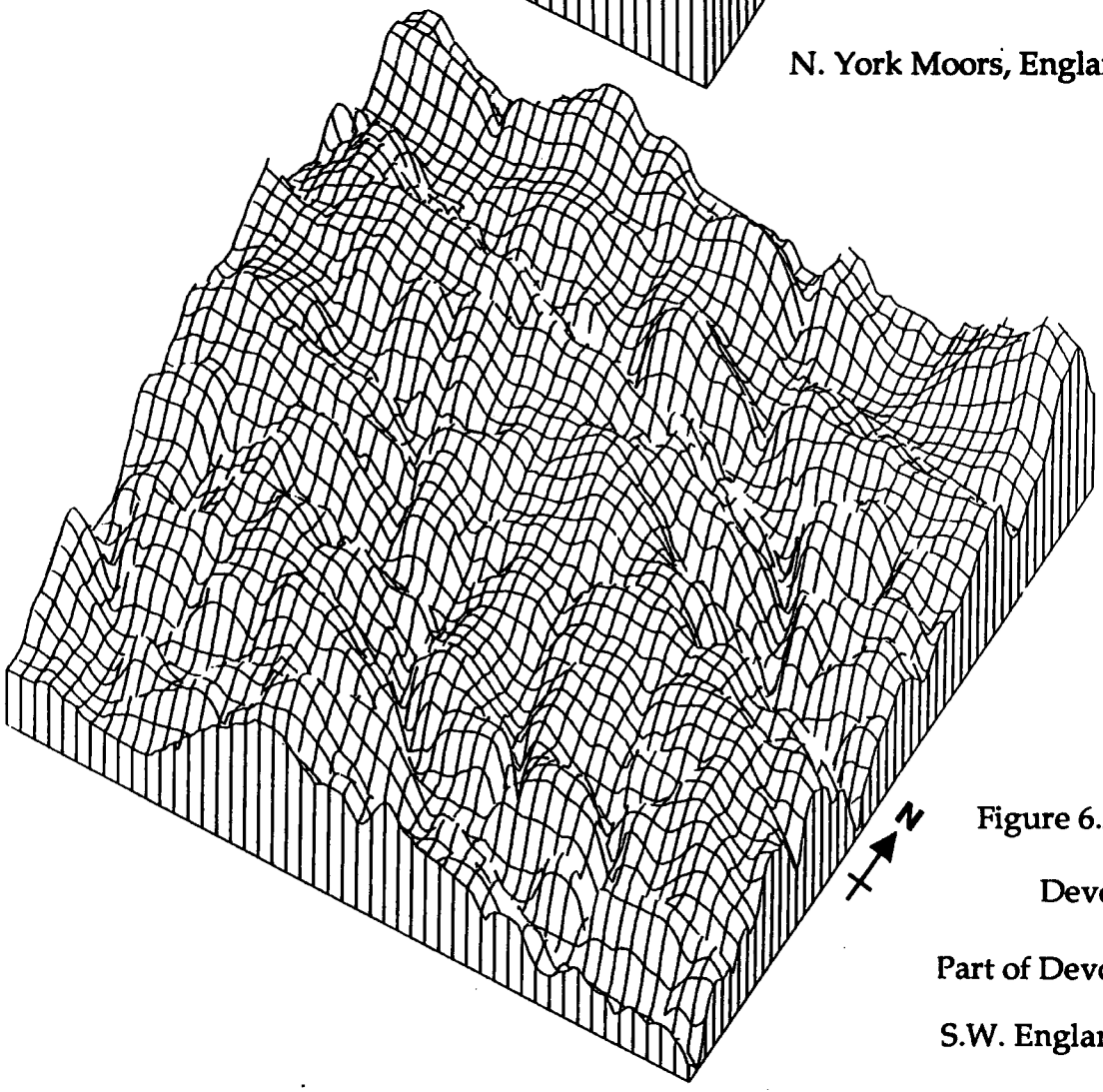

Figure 6.24:

Devon,

Part of Devon,

S.W. England.

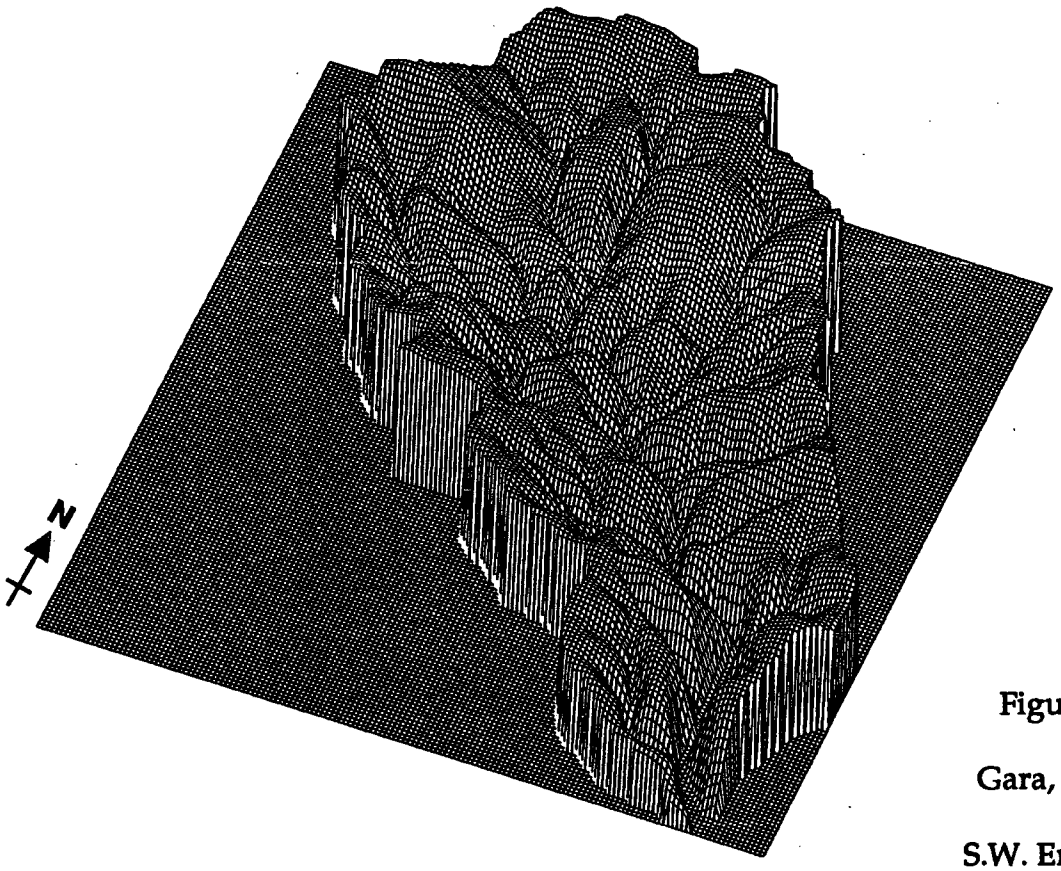

Figure 6.25:

Gara, Devon,

S.W. England.

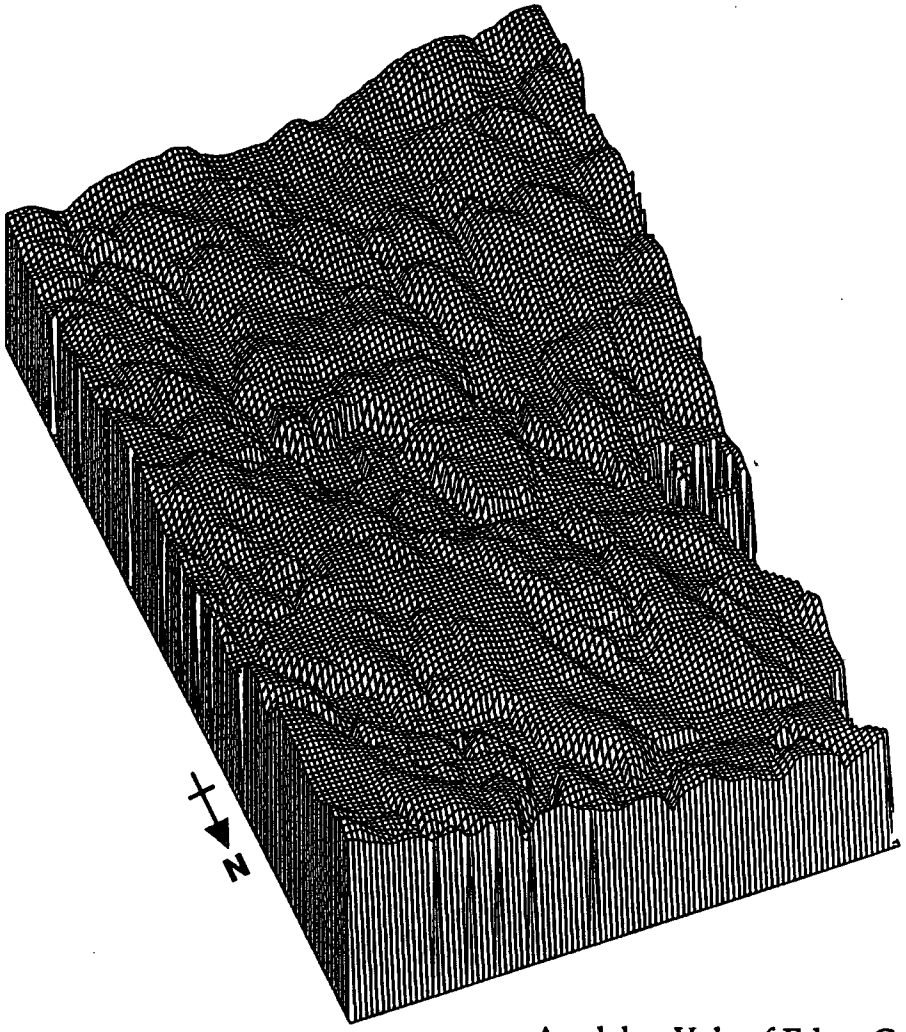

Figure 6.26:

Appleby, Vale of Eden, Cumbria, England.

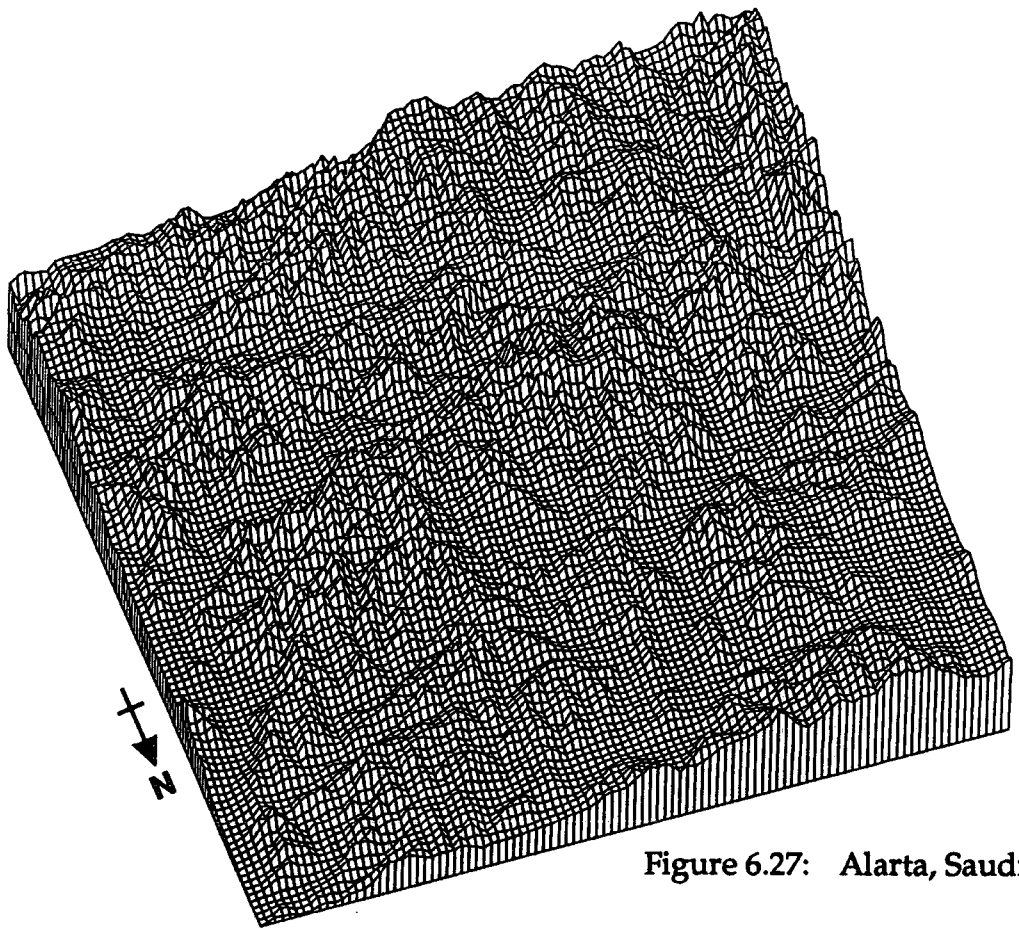

Figure 6.27: Alarta, Saudi Arabia.

6.3 Results of non-directional 60 distance variogram analysis.

Table 6.2 presents the results of the least-squares linear regressions on the variograms for 60 distances, in order of decreasing fractal dimension, *D*. The r^2 values associated with the regressions again suggest that the relationships between log variance and log distance for these real landsurfaces are indeed linear. This would suggest that the surfaces are scaling over the relatively narrow range of scales investigated. However the argument used in Chapter 5 about r^2 being very high for perfect, but non-linear monotonic relationships still applies for these surfaces. Visual reference to the scatterplots of the variograms (Appendix 3) and to the plots of residuals produced by the linear regressions indicate that most of the surfaces yield a slightly convex relationship. However when considering *D* as an index of surfaces roughness the order in which it ranks the areas would seem to correspond generally with that of surfaces roughness given by a visual ranking of the perspective block diagrams (figures 6.1-6.27). This is particularly so when considering the amount of dissection of each surface (regardless of process). ALARTA and AIGOUAL would immediately appear roughest when considering sharp features: summits, cols, V-shaped valleys. Nevertheless APPLEBY and DEVON, although possessing rounded summits and valley floors, are quite dissected with what would probably be high drainage densities.

Table 6.2 60 distance variogram results and rescaled range results

DEM	Variogram Method			Rescaled Range Method			Difference in D Between Methods
	D	R^2	SE	D	R^2	SE	
WIND	2.5760	0.9500	0.4760				
ALARTA	2.5740	0.9570	0.0114	2.4240	0.9930	0.0275	0.1500
ST. PAUL	2.4770	0.9720	0.0436				
APPLEBY	2.4430	0.9810	0.0378				
DEVON	2.4410	0.9810	0.0387	2.3280	0.9840	0.0464	0.1130
AIGOUAL	2.4290	0.9820	0.0384				
KEARY	2.3690	0.9860	0.0365	2.2530	0.9960	0.0236	0.1160
TORRIDON	2.3680	0.9910	0.0300	2.1970	0.9930	0.0329	0.1710
REUNION	2.3670	0.9980	0.0124				
GARA	2.3540	0.9780	0.0472				
NUPUR	2.3110	0.9850	0.0415	2.1810	0.9920	0.0303	0.1300
GALLOWAY	2.3060	0.9850	0.0422	2.2620	0.9820	0.0569	0.0440
MONTOIRE	2.2810	0.9870	0.0403	2.1980	0.9940	0.0303	0.0830
DUMFRIES	2.2730	0.9960	0.0237	2.2790	0.9920	0.0408	-0.0060
THVERA	2.2600	0.9920	0.0336	2.1640	0.9930	0.0350	0.0960
AUGHWICK	2.1850	0.9990	0.0104				
BELLE	2.1790	0.9990	0.0147				
ALLEN	2.1650	0.9990	0.0121				
UINTA	2.1590	0.9900	0.0133				
PUY	2.1540	0.9960	0.0262	2.1510	0.9980	0.0245	0.0030
CANIGOU	2.1460	0.9980	0.0194	2.0790	0.9970	0.0262	0.0670
DEVOLUY	2.1430	0.9980	0.0206	2.1340	0.9940	0.0368	0.0090
GLAISDALE	2.1430	0.9970	0.0216	2.0270	0.9990	0.0118	0.1160
BOORO	2.1360	0.9990	0.0126				
NETHER	2.1120	0.9980	0.0198				
WHEELDALE	2.0950	0.9960	0.0764				

Excluding Devoluy the four areas which yield the lowest fractal dimension would also seem to be the four smoothest surfaces visually although the exact order in which they would fall cannot really be judged by eye.

GALLOWAY and DUMFRIES are visually similar surfaces and do possess similar fractal dimensions. NUPUR and MONTOIRE are also very similar to one another visually and the positions of all four of these surfaces in Table 6.2 would seem appropriate. It is the DEMs representing mountain areas, on either side of these in Table 6.2, which are somewhat less understandable. THVERA looks at least as rough as TORRIDON and KEARY. AUGHWICK also appears rougher from its perspective block diagram than its estimated fractal dimension suggests. WIND certainly does not look like the roughest surface.

The unexpectedly high fractal dimension of WIND can be easily explained. It is the surface which yields the variogram exhibiting the greatest convexity. WIND has a

200m grid mesh, the second coarsest used in this study, and as a result variance is considered for larger distances than in other DEMs when only 60 distances are studied. This means that if the landsurface is not perfectly scaling and the relationship between log variance and log distance is convex, least-squares regression for a scale range from 200m to 2828m will produce a lower gradient and therefore a higher fractal dimension than least-squares regression of the same relationship for a scale range of 100m to 1414m.

It is therefore interesting to note that the 11 surfaces with the lowest fractal dimension also have grid mesh sizes of less than 100m, while the 15 surfaces which yield the highest estimates of *D* all have grid mesh sizes of 100m or greater except for APPLEBY, AIGOUAL, MONTOIRE, GARA and ST. PAUL (fig. 6.28). The least-squares regression statistics of r^2 and standard error follow a similar, if only slightly more complicated, pattern indicating greater convexity in the DEMs with larger grid mesh and higher fractal dimensions.

Figure 6.28 Fractal dimension vs. grid mesh of DEMs.

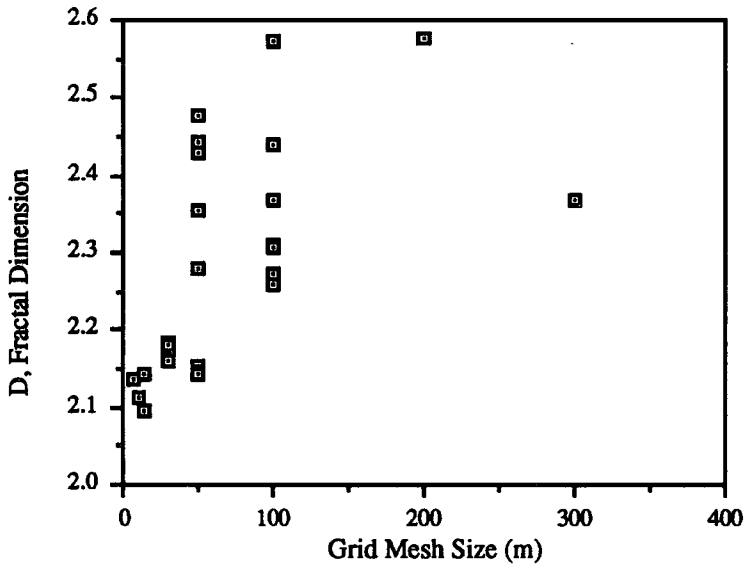

Indeed visually this pattern can be detected in the scatterplots themselves. An exception to this is ALARTA, whose variogram is predominantly straight until slight convexity at the distal end. The variogram from KEARY is also noteworthy. It is slightly convex to about 1km ($\log_{10}$ is 3), where the variogram becomes slightly concave, returning to the original gradient of the trend at about 1585m ($\log_{10}$ is 3.2).

The convexity present in the variogram of La Porge over the 60 distances makes least-squares linear regression of the variogram pointless. Looking at the structure of the curve in the variogram would seem to hold more chance of possible explanation and this surface will be considered more fully in a later section.

All of this evidence suggests that the estimated fractal dimension of a real landsurface, even when used as a simple index of surface roughness has definite limitations. One of these limitations may be the fact that different methods of estimating fractal dimension may produce different results particularly when the surface being studied may not have all the properties of a fractional Brownian surface. The next section compares the results obtained by another method, rescaled range analysis. The problem of the convexity of most of the variograms and of what may happen at longer distances in the variograms will be returned to in section 6.5.

6.4 Rescaled Range Analysis results

As was described in Chapter 5, when the rescaled range analysis of the simulated fractal surfaces was discussed, the analysis of a surface held as a DEM can only go up to a certain distance. This distance is the length of the outer perimeter of the DEM. After this, neighbouring points are used to calculate rescaled range. As a result only the linear parts of the rescaled range against distance plots were used in the least-squares regressions and to estimate fractal dimension. In most cases this was 15 or 16 observations. The fractal dimensions estimated from these observations are presented along with the non-directional 60 distance variogram results in Table 6.2. Also presented are the r^2 and standard error values for the regressions as well as the difference between the variogram fractal dimensions and the rescaled range fractal dimensions.

The algorithm for calculating the rescaled range values for the different distances, as described in Chapter 4, 'spirals' around the DEM towards its centre. When measuring the mean and the cumulative departures from it the series must be continuous, with an altitude value at each interval in the series. Therefore, the algorithm cannot deal with irregularly shaped DEMs which are padded with a value for missing data. This means that Table 6.2 shows a lack of results for several irregularly shaped models. Only nineteen real surfaces are therefore studied using rescaled range analysis.

The values of D calculated by the rescaled range method are in general lower than the values obtained when using the variogram method (fig. 6.29). The smallest difference between variogram fractal dimension and rescaled range fractal dimension is 0.003 for the Puy de Dôme area. The largest difference is 0.171 for Torridon. The average difference is however 0.085 which, as the simulated surfaces have shown, would probably be a visible difference in the roughness of two surfaces represented as perspective block diagrams. There is only one surface which gives a rescaled range analysis D value greater than its variogram fractal dimension: Dumfries gives a difference of only -0.006.

Figure 6.29 D from variogram method vs. D from R/S method.

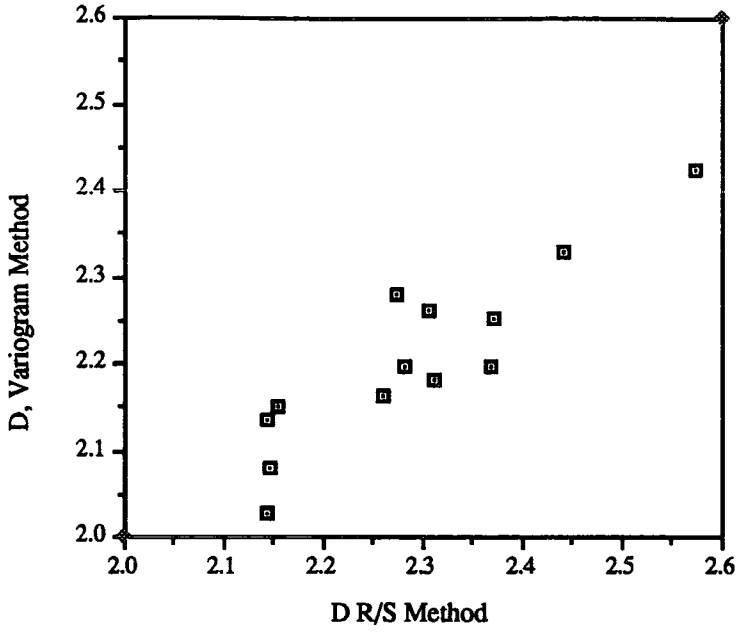

The order of the surfaces when ranked using the rescaled range D values is not quite the same as the order given by the variogram fractal dimensions. The rougher surfaces fall into a similar order, as do the smoother surfaces, but some of the surfaces in the middle of the rankings are further out of place. Similar surfaces such as Galloway and Dumfries have fractal dimensions calculated from the rescaled range analysis which are closer together than they were using the variogram method, although by the former method Dumfries is supposed to be very slightly rougher than Galloway as opposed to the reverse for the latter method. In addition, surfaces are supposed to be very slightly rougher than Keary, Torridon, Nupur and Montoire.

Montoire is also out of order, having a higher fractal dimension than Torridon and Nupur. However Torridon, Nupur, Thvera and Le Puy keep in their order as regards to each other. At the smooth end of the order rescaled range analysis of Canigou yields a very much smoother fractal dimension than its variogram counterpart. It is therefore true to say that it is surfaces such as Galloway, Dumfries, Montoire and Canigou that have the most effect on the different orders of the two sets of estimated fractal dimensions.

A clue to why this might be so is given by the fact that Galloway and Dumfries are both elongated rectangular DEMs. The rescaled range analysis algorithm works by spiralling through the DEM in a clockwise manner, first row followed by last column and so on. This means that the rescaled range is being considered for a profile which takes in only two directions. Certainly in the case of Dumfries, where the long axis of the DEM cuts across the valleys of the area at right angles, the rescaled range analysis is being dominated by that direction. As a result the fractal dimension estimated from this

method is actually very slightly higher than the fractal dimension estimated from the variogram of the area, which is more multi-directional.

This raises the question, how much does this directional limitation of the rescaled range analysis method affect the estimated fractal dimensions of the other DEMs. Torridon is the DEM which has the largest difference in fractal dimension estimates between the variogram and rescaled range methods. If its perspective block diagram is looked at (fig. 6.1) the track of the spiral can be visualized.

It starts in the northwest corner progressing along the relatively low lying northern edge of the DEM. It then follows the eastern edge encountering its first major feature of terrain at the southeastern corner and then encountering another relatively important feature in the southwest corner before returning towards its starting point. If this track is mentally continued it will follow along the length of the major ridges rather than across them, except in the cases of the ridge at the centre of the DEM and the ridge running northwest-southeast on the western side of the DEM. The maximum and minimum deviation from the mean of the increments in the calculation of the rescaled range for each segment will therefore not take into consideration the steepest sides of most of the ridges in the DEM, which are taken into consideration by the variogram algorithm. The fractal dimension given by the rescaled range analysis program is therefore lower than that given by the variogram method.

The much smaller differences in fractal dimensions yielded by the two methods when considering surfaces such as Le Puy and Devoluy are also understandable when this problem of direction is taken into consideration. In the case of Le Puy the main landscape features appear reasonably symmetrical in a central belt across the DEM and therefore affect the measurements in each method in rather similar ways. For Devoluy the dominant landform is in the centre of the DEM, while other smaller features are distributed from perpendicular to parallel to the path of the profile used in the rescaled range analysis algorithm. This means that segments along the profile sample most of the gradients of slope present in the surface, as does the variogram program.

From this evidence, the variogram method appears preferable to the rescaled range method. The variogram method is a more two dimensional method and can treat the surfaces without directional bias.

6.5 Results of non-directional long distance variogram analysis.

The variograms for longer distance ranges fall into three basic categories: those that produce straight plots; those that are often convex but sometimes nearly straight up to a maximum variance; and those that have a series of maxima and minima.

The immediate explanation that comes to mind for the surfaces which produce straight variograms is that they are completely self-similar. However in Chapter 5 the variograms for the simulated fractal surfaces showed that many fractal surfaces may produce a variogram with a maximum value of variance. This is due to the fact that the simulated surfaces are of limited area and as a result must have a local relief value. The reason why no maximum is reached in the variograms of these surfaces must lie in the shape of the surfaces themselves.

It was seen in Chapter 5 that a maximum variance can be reached if the highest feature of the surface is somewhere in the middle of the DEM while the lowest features are around the edges of the surface or vice versa. This is generally not the case for the landsurfaces yielding variograms that do not reach a turning point. In this study they are Uinta, Glaisdale, Booro Borotou, Netherhearth Sike and Wheeldale which all have simple slopes.

The latter three surfaces are all parts of, or entire, drainage basins. Glaisdale and Wheeldale are both square DEMs with the same number of rows and columns. The first row of each matrix is the upstream part of the basin while the last row is further downstream. The actual thalweg lines run roughly parallel to the column direction. The longest distance sampled to produce the variograms (Appendix 3) is about the width of the DEM. This means that the variance for that distance includes diagonal distances from the lowest part of the matrix to the highest part of the matrix and as a result the variance does not fall off.

The Booro Borotou and Netherhearth Sike catchments are orientated diagonally across the matrix containing them. Again the largest possible variance therefore corresponds to the largest possible distances and although averaging of variance measurements in different directions is being performed, the orientation of all of these catchments is such that variance continues to increase with distance over the whole variogram.

Uinta's continually increasing variance is less easily explained. However it can still be seen from figure 6.8 that there is substantial difference in altitude between diagonally opposite corners, leading to an upward trend to the north.

All of these surfaces are unusual cases of the kind of surfaces whose variograms eventually show a decrease in variance with increasing distance. The surfaces in this study which reach a single maximum variance are Wind River, St. Paul, Gara, Reunion, Nupur, Galloway, Dumfries, Le Puy and Devoluy.

The distance at which maximum variance occurs can be easily explained in the cases of Le Puy and Devoluy. In these examples the highest ground is in the centre of

the matrices, the lower ground towards the corners. As a result, at a distance of about half the width of these square matrices, the variance of each reaches a maximum value.

For Nupur, Galloway and Dumfries the topography appears slightly more complicated. However the principle of a maximum relief being present in an area which leads to a maximum variance value in its variogram remains the same. The east side of the Dumfries DEM is at all points lower than the west side and the maximum altitude attained in this DEM is at about the centre of the west side. As a result the maximum variance recorded on its variogram is reached before the maximum distance over which variance is sampled.

Galloway's highest point is in the northwest while its lowest point is clearly in the valley in the extreme south. The relief of the area in geomorphometric terms (Mark, 1975) would therefore be measured between these two points which are separated by a distance nearing the maximum distance at which variance has been sampled. The maximum variance on the variogram is reached at a distance of 7km, not however at the length which separates the minimum and maximum altitudes. The reason that the maximum variance is at a somewhat shorter distance than the distance responsible for the relief of the surface is the averaging of the variance measurements for each distance. The most rapid changes over distance in elevation are in the valleys of the southern part of the matrix. Much of the rest of the surface is at the level reached at the top of these steep slopes. Averaging of the variances measured from both areas brings the distance at which maximum variance occurs down, away from the distance at which the relief is measured.

Nupur is the most complicated of all of these surfaces to explain. Some effect of the averaging of variance for each distance must again be responsible for a maximum value of variance being attained within the maximum distance sampled. However the general appearance of the Nupur surface, with several cirques and troughs, would have suggested that it might display the third kind of variogram behaviour which must be discussed here.

Ten of the surfaces studied have more than one local maxima and minima displayed in their variograms. These are Devon, Mont Aigoual, Torridon, Montoire, Thvera, Aughwick, Allenville, Belleville, Le Porge and Canigou. Of these surfaces the relationship shown in the variogram for Thvera reveals the most about the landsurface from which it is derived. The DEM of Thvera covers an area of 104km^2.

Its variogram has a local maximum at a distance of about 2800m ($\log_{10}$ is 3.45). Variance then decreases to a minimum where points are separated by a distance of 5600m ($\log_{10}$ is 3.74). The next maximum is at 8400m ($\log_{10}$ is 3.92) and another minimum may be present at 11200m ($\log_{10}$ is 4.05). The obvious explanation of these

maxima and minima is periodicity in the spacing between valleys and ridges. In the case of Thvera, 2.8km would be somewhere near an average value for the distance between thalweg and interfluve.

Torridon (Appendix 3)also produces this sort of effect with an average value for distance between thalweg and interfluve of about 1.7km. The fact that these apparent periodicities are not true mathematical periods but just characteristic scales of valley sizes in these areas is borne out by the lack of any definite period in the minima and maxima of the other variograms with more than one maximum. It must be noted that the characteristic scales are dominant enough to show through the isotropic nature of the sampling carried out to produce these variograms. Visually, Aughwick would be the surface most expected to yield some periodicity in relation to its ridge and valley topography. However it can be seen from figure 6.18 that the valleys, although parallel to one another, are of different widths. Likewise, for Montoire, Devon and Mont Aigoual, the irregular spacing of maxima and minima must be the result of the dominant length of slope in the DEM being revealed by the averaging process of calculating variance over different distances.

The first maximum in the variogram of Le Porge occurs at 280m ($\log_{10}$ is 2.45). This is likely to correspond to the slopes of the coastal dunes of the area. A minimum is found at 630m ($\log_{10}$ is 2.8). The variogram then displays another maximum and minimum at distances beyond 4km.

In the case of some of the variograms a widening of scatter at their distal ends obscures any quantifiable interpretation of their structure. Intuitively some widening of scatter is likely to occur with most surfaces. The concept of having a maximum variance, related to the concept of relief, at somewhere beyond half the width of the DEM points to the fact that there will often be a much wider range of possible differences in altitude between points separated by greater distances. For shorter distances the sampled variances are likely to be within a much narrower range, leading to less scatter at the proximal end of the plot. If there are characteristic scale ranges for features in the landsurfaces there might well be wider scatter where the scale ranges are larger than the characteristic scale ranges. This could be the reason for the widening of scatter in the variograms calculated from the DEMs of Appleby, Galloway, Dumfries, Canigou, Netherhearth Sike, and Wheeldale.

Two of the surfaces already mentioned, Mont Aigoual and Montoire, as well as Alarta and Keary, may show signs of a step or kink in their variograms. It is these surfaces which may be of most interest in comparison with some of the results obtained by other workers finding two different values of D for different distance ranges for one surface (Mark and Aronson, 1984; Roy et al., 1987; Culling and Datko, 1986).

Mark and Aronson's (1984) analysis of 17 areas produced only one variogram which seemed visually self-similar, Shadow Mountain, Colorado. One of the remaining areas, Aughwick, seemed to have no straight segment. Mark and Aronson's scatterplot of Aughwick (fig. 6.30a) is not dissimilar to the scatterplot produced by FASTFRAC (Appendix 3). They speculated that the Aughwick plot demonstrates the periodicity of fold mountains with troughs of similar height at 3.5, 7, and 11km, corresponding to lags of one, two and three ridges or valleys. The sampling pattern and scatter of the FASTFRAC variogram of Aughwick do not allow such estimation of the period of these valley spacings. However Mark and Aronson's findings clearly echo the results in this study of surfaces such as Thvera. The major difference in these two studies is that Aughwick was the only surface which they interpreted as having no 'straight' segment. In this study least-squares regression has been performed on the variance values for shorter distances and an evaluation of its fractal dimension has been made on the basis of this part of the relationship. As has been explained previously, Aughwick produces a reasonably typical variogram. Six other surfaces produce variograms with several maxima and minima. This has been explained by the fact that there are several dominating features in the surface instead of a single feature which may produce a single maximum or in the case of Glaisdale a variogram reaching no maximum.

This discussion of the different interpretations in this study compared with Mark and Aronson's work may cast some light on why this study has only produced four variograms which show any evidence of a step between straight segments. Mark and Aronson suggested that fifteen of their sample areas produced straight segments divided by distinct breaks of slope in the variograms. Roy et al. (1987), in their study of part of the White Mountains at the border of Quebec, Maine and New Hampshire, also produced a variogram with what they perceived as a distinct break of slope (fig 6.30b). However it could be seen as a variogram which is approaching a maximum variance.

Montoire is probably the variogram in this study which is most similar to those described by Mark and Aronson. The break of slope in the variogram at about 1km ($\log_{10} = 3$ in Appendix 3) probably represents the length of the steep slopes of the incised meanders. After this the slope of the variogram is more gentle up to about 3.16km ($\log_{10}$ is 3.5). If the slope of this segment of the variogram was used to calculate a fractal dimension it would give a much higher value for D than the previous segment. Altitude differences at this scale are alternating between small negative differences and small positive differences. This alternation is what is detected in a true fractal surface (as in Chapter 5) at all scales, if the surface has a fractal dimension higher than 2.5. However, this gentle segment is followed by another steeper section in the variogram caused by sampling between points positioned in different meanders but at quite different positions on their respective slopes.

Figure 6.30 *Variogram produced by: (a) Mark and Aronson (1984) for DEMs in the Ridge and Valley Province, Pennsylvania and by : (b) Roy et al. (1987) for Moose Bog, Quebec/New England border.*

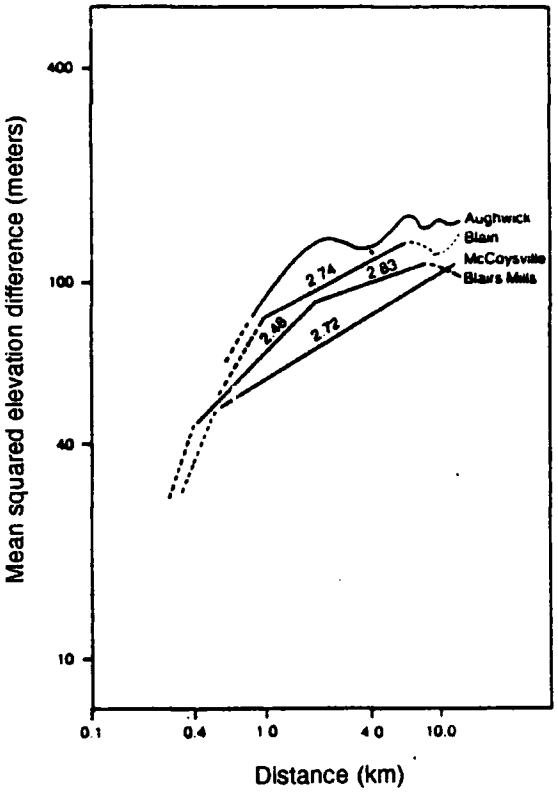

(a)

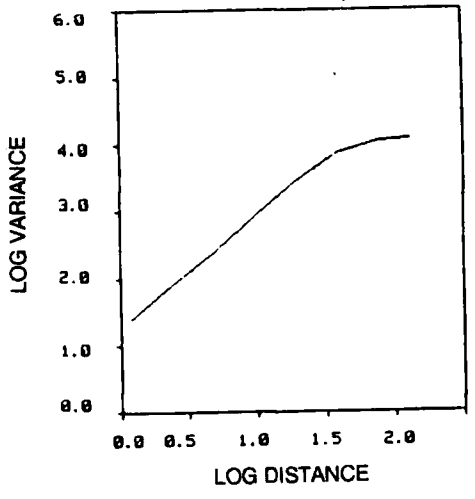

(b)

In fact the step in the variogram is therefore caused by the same process which causes the apparent periodicity in DEMs such as Thvera. The effect on the variance caused by the slopes of the meanders has not been strong enough in the averaging of variances at those distances to produce a local maximum and have only produced what amounts to a kink in the variogram.

In the cases of the Mont Aigoual region and the Keary and Nosebag basins, there are no features dominant enough in their effect on the average variance for certain distances to produce maxima and minima. As a result the trend in the variogram passes convexly through the scale range where this effect is happening, and concavely into the scale range where the sampling of different positions within slopes in different valleys is again occurring.

Alarta produces a very different kind of step. In its variogram there is a gentle segment to start with followed by a much steeper segment at about 1.58km ($\log_{10}$ is 3.2). Over the shorter scale range it may be more closely related to the generated fractal surfaces with D greater than 2.5. The surface is very rough at this scale giving some degree of antipersistence. However, more structure comes into the surfaces with a more regular drainage pattern after 1.58km. It is still irregular enough to give no sign of an average valley spacing. Perhaps in this variogram there are two different fractal zones.

It would seem from the discussion so far that the fractal model breaks down over a very limited scale range in most cases. Valleys in each area where maxima and minima or breaks in slope are present in the variograms seem to have a characteristic scale range of slope lengths. However, the reasons for the existence of some type of linear relationship in many of the variograms (particularly those such as Uinta and Booro Borotou where the variograms are linear over all distance; Mont Aigoual and Keary where there are only slight kinks in the variogram; and of course Alarta where there are two very straight segments) must be investigated further by looking at the possible influences of the surfaces being anisotropic and also the effect of subdividing the areas.

6.6 Results for directional variograms.

The analysis performed to ascertain the effect of anisotropic properties of real landsurfaces was the same process of analysis used in Chapter 5 to study the possibility of simulated fractal surfaces being anisotropic. The only difference which immediately arises is that the directions being considered have a geographical context.

First, separate variograms for a small range of distances (10) are calculated for the east-west, north-south, northwest- southeast and northeast-southwest directions.

These are of course the directions which are given by the rows, columns and diagonals of a square matrix. Obviously if the DEM is rectangular the two diagonal directions will not be northwest-southeast and northeast-southwest but for ease of discussion the terminology mentioned above will be used. Secondly, the same process is carried out to produce variograms of these directions including a larger scale range.

Table 6.3 summarises the least-squares regression results of the small scale variograms. In general all the variograms are linear or near linear, with slight convexity, similar to the non-directional variograms for the surfaces. The most interesting feature of Table 6.3 is the variation in fractal dimension with direction for each landsurface studied. Variations of 0.1 between D values for different directions are common, for example Keary, Thvera, and Wheeldale. This immediately suggests that some of the surfaces are clearly anisotropic as far as variance is concerned.

A further hypothesis would be that the fractal dimension obtained when treating the surface as isotropic (Table 6.2) is an average value taking into account the variations in topography among different directions. The mean fractal dimension for each landsurface calculated from the D values of each direction, together with the difference between it and the fractal dimension from Table 6.2, is given in Table 6.3. It can be seen from these that, although there exist quite major differences between the fractal dimensions for individual directions, the average value is indeed very close to the value obtained when treating the surface as a whole. The absolute average difference is only 0.027, with all but one of the landsurfaces, Canigou, yielding a difference no greater than 0.05.

It must be noted that all but six of the landsurfaces' mean fractal dimensions calculated from the four different directions are slightly less than the fractal dimensions from Table 6.2. This is probably due to the effect of using the variance calculated in only four directions as opposed to the much more exhaustive direction sampling performed when the surface is treated as a whole.

As discussed in sections 6.3 and 6.5, various structures in the variograms can lead to convexity in the relationship between variance and distance and this in turn affects the values of D obtained from different portions of a slightly convex variogram.

As a result this section will deal with the differences in D for different directions, at the same time as considering the variograms produced using the longer scale ranges so that any reference to a fractal dimension can be qualified by any structures found in the more complex part of the variogram.

Table 6.3

	E–W			N–S			NW–SE			NE–SW				
	D	R^2	SE	D	R^2	SE	D	R^2	SE	D	R^2	SE	$\bar{D}$	$\bar{D}-D_{6.2}$
TORRIDON	2.2830	0.9930	0.0397	2.3370	0.9990	0.0163	2.3820	0.9950	0.0304	2.3810	0.9900	0.0423	2.3460	-0.0220
KEARY	2.3080	0.9920	0.0427	2.2920	0.9900	0.0485	2.5450	0.9160	0.0927	2.2380	0.9990	0.0180	2.3460	-0.0230
WIND	2.4720	0.9730	0.0599	2.5330	0.9640	0.0605	2.6250	0.8720	0.0972	2.5120	0.9930	0.0283	2.5360	-0.0400
NUPUR	2.2160	0.9950	0.0373	2.2750	0.9900	0.0494	2.3610	0.9780	0.0650	2.2650	0.9910	0.0468	2.2790	-0.0320
THVERA	2.2210	0.9950	0.0369	2.1770	0.9970	0.0281	2.2320	0.9940	0.0395	2.3120	0.9870	0.0529	2.2360	-0.0240
DUMFRIES	2.1680	0.9990	0.0128	2.2830	0.9950	0.0353	2.2580	0.9990	0.0146	2.2890	0.9930	0.0414	2.2500	-0.0230
GALLOWAY	2.2170	0.9970	0.0298	2.2300	0.9960	0.0329	2.2640	0.9960	0.0304	2.3590	0.9740	0.0700	2.2680	-0.0380
UINTA	2.1310	0.9980	0.0277	2.1650	0.9990	0.0142	2.1980	0.9980	0.0220	2.1780	0.9980	0.0265	2.1700	0.0110
DEVOLUY	2.1060	0.9980	0.0237	2.1100	0.9980	0.0256	2.1400	0.9970	0.0303	2.1440	0.9980	0.0263	2.1250	-0.0180
CANIGOU	2.2110	0.9920	0.0522	2.2040	0.9940	0.0462	2.2900	0.9850	0.0648	2.2830	0.9790	0.0798	2.2470	0.1010
AIGOUAL	2.3430	0.9890	0.0479	2.3830	0.9870	0.0485	2.4330	0.9830	0.0467	2.0423	0.9890	0.0414	2.3960	-0.0335
MONTOIRE	2.2000	0.9940	0.0417	2.2170	0.9910	0.0548	2.2960	0.9850	0.0578	2.2680	0.9910	0.0459	2.2450	-0.0360
LE PUY	2.1600	0.9940	0.0423	2.0760	0.9990	0.0193	2.1480	0.9970	0.0320	2.1560	0.9950	0.0396	2.1350	-0.0190
REUNION	2.3290	0.9990	0.0158	2.3620	0.9960	0.0267	2.3210	1.0000	0.0085	2.4110	0.9980	0.0194	2.3560	-0.0106
ST PAUL	2.4010	0.9780	0.0600	2.3900	0.9810	0.0566	2.5390	0.9760	0.0492	2.4120	0.9870	0.0463	2.4360	-0.0410
BOORO	2.0670	0.9990	0.0142	2.0910	0.9990	0.0204	2.0840	1.0000	0.0135	2.1390	0.9980	0.0227	2.0950	-0.0407
AUGHWICK	2.1120	0.9990	0.0203	2.2180	0.9980	0.0258	2.1790	0.9990	0.0190	2.3450	0.9960	0.0290	2.2040	0.0190
BELL	2.1470	1.0000	0.0050	2.1360	1.0000	0.0116	2.1520	0.9990	0.0165	2.3120	0.9970	0.0256	2.1870	0.0080
ALLEN	2.1230	1.0000	0.0067	2.1200	1.0000	0.0094	2.1260	0.9940	0.0155	2.2520	0.9990	0.0126	2.1550	-0.0100
NETH	2.2020	1.0000	0.0112	2.0640	1.0000	0.0019	2.1800	1.0000	0.0056	2.0680	1.0000	0.0019	2.1290	0.0170
GLAIS	2.1270	0.9990	0.0205	2.1530	1.0000	0.0033	2.1200	1.0000	0.0127	2.1980	0.9970	0.0290	2.1500	0.0070
WHEELDALE	2.0490	1.0000	0.0042	2.1690	1.0000	0.0125	2.1040	1.0000	0.0029	2.0780	1.0000	0.0071	2.1000	-0.0050
DEVON	2.3750	0.9870	0.0481	2.3770	0.9840	0.0535	2.5020	0.9760	0.0531	2.4000	0.9850	0.0494	2.4140	-0.0275
GARA	2.2500	0.9900	0.0519	2.3050	0.9840	0.0600	2.3680	0.9760	0.0665	2.3340	0.9840	0.0569	2.3140	-0.0398
APPLEBY	2.3890	0.9840	0.0527	2.3620	0.9890	0.0463	2.4320	0.9800	0.0553	2.4420	0.9880	0.0424	2.4060	-0.0370
ALARTA	2.5730	0.9920	0.0266	2.5500	0.0996	0.0196	2.6530	0.9860	0.0281	2.5010	0.9980	0.0157	2.5690	-0.0050

Directional variogram results for real landsurfaces

All the types of structure which were discussed for the non-directional variograms can be detected in the directional variograms. However, for a particular landsurface the variograms for different directions may show up different types of structure. This leads to a classification into three groups, mainly to give order to the discussion, based on the types of structures found in the four variograms of each landsurface. There are those surfaces which produce variograms that either are slightly convex or reach one maximum. Included in this group are DEMs such as, Wind, Galloway, and Wheeldale. A second group includes , for example, Torridon, Nupur, Thvera, Canigou, Devoluy, and Aughwick. These surfaces produce four variograms all showing at least one maximum and minimum. The final group includes all those surfaces which produce variograms with a mixture of steps, maxima and minima. This mixture of features can occur either within one variogram or between the variograms for different directions. Examples of DEMs which fall into this group are: Aigoual, Alarta, Dumfries, Keary, Appleby, Montoire, Le Puy, and Uinta.

Looking in more detail at the first group, there are two prominent effects, for example in the variograms for Wind River. The variogram for the northwest-southeast direction reaches a maximum value followed by a decrease in variance, while all three other directions do not. The variogram for the northeast-southwest direction is much more linear than the others. This is a result of the dominant feature in the surface being elongated in a northeast-southwest direction. Therefore maximum variance is reached first by the variogram for the direction perpendicular to it while the direction parallel to the elongation produces a more linear variogram as no maximum variance is being approached. The east-west and north-south variograms sample the dominant landscape feature obliquely, thus producing more convex variograms which do not quite reach a maximum.

Galloway's four variograms each show different amounts of convexity. The most convex is the northeast-southwest variogram. This is the direction which is most closely aligned along the aspect of the slopes with the steepest gradients. In the case of Wheeldale, the lowest fractal dimension is produced by the variogram in the east-west direction. The highest in the north-south direction. It can be seen from the perspective block diagram of Wheeldale (fig. 6.23) that two small tributaries enter the main valley, one from the east the other from the west. The north-south variogram reflects the rougher profiles which are encountered when sampling in the north-south direction, caused by the tributary channels. Sampling in the east-west direction does not encounter the gradients associated with these tributaries.

The second group of surfaces is one level of complexity up from the first group. In this group maxima and minima occur in different numbers and at different points within the variograms of an area depending on direction sampled. For instance, in the

case of Torridon there are three ridges orientated roughly north-south. On the east-west variogram for Torridon there are three maxima confirming the effect of these ridges. The other directions sampled only produce one or two maxima depending on whether they cut across parts of these ridges as well as the east-west orientated ridges of Beinn Eighe and Beinn Alligin. Nupur produces four variograms revealing structure similar to Torridon. Valley or ridge spacing is slightly different in each direction and the effect of certain valleys or ridges are missed completely by sampling variance parallel to their contours, allowing one variogram to only have one maximum and one minimum while another variogram has three maxima and two minima.

In the case of Thvera, where the variogram which represents the surface with no preferred directional bias gives maxima and minima spaced very regularly, the directional variograms show maxima and minima at different positions and spaced less regularly. The northwest-southeast variogram produces the most regular spacing between maxima and minima. Canigou also follows the same kind of pattern as displayed by Thvera and Nupur, valley spacing being detected by each variogram but because of direction being sampled, valley spacings are all slightly different.

The behaviour of the variograms produced from Devoluy are slightly less complicated and the structure in each direction can be visually related back to the perspective block diagram in figure 6.9. The clearest maximum and minimum are on the east-west variogram. In it, the high ground in the centre of the matrix is detected along with the river valley on the east side of the DEM. In all the other directions the variograms only reach a clear maximum. A clear minimum followed by another increase in variance cannot be clearly detected.

Finally for this group, Aughwick shows obvious anisotropic effects. All directions except northeast-southwest show signs of maxima and minima in their variograms representing the ridge and valley topography. However, northeast-southwest is parallel to the ridges and valleys and so the variogram for this direction is straight to about 6.3km before reaching a maximum variance.

The third group for discussion includes all those landsurfaces that produce variograms with kinks and turning points. Dumfries, which produced a non-directional variogram which was convex up to a maximum variance, produces two directional variograms with kinks. Northeast-southwest and north-south both have a convex to concave to convex kink. The variogram for the east-west direction is convex, while the northwest-southeast variogram is almost straight up to a slightly convex distal end. The north-south and northeast-southwest direction obviously cut across the grain of the surface slightly more than the other two directions giving higher fractal dimensions and the step around about the length of the steeper slopes of the valleys. The east-west and

northwest-southeast directions are orientated more closely along the grain and as a result give variograms approaching a single maximum value and showing no other structure.

The Mont Aigoual area is much larger and more complicated than the Dumfries area. All of the directional variograms show a kink or break of slope. However, the most insignificant break of slope can be seen on the north-south variogram. The northeast-southwest variogram also shows a very weak break of slope. The strongest kink is found on the east-west variogram at about 1260m ($\log_{10}$ is 3.1). The northwest-southeast variogram also shows this sort of kink but it is situated nearer 630m ($\log_{10}$ is 2.8). Although the perspective block diagram in figure 6.11 shows a seemingly rough surface there does seem to be a north-south trend to many of the valleys. It may be the effect of some of the smaller valleys that trend in this direction which produces the stronger kink in the east-west and northwest-southeast variograms. The slight kinks in the other two variograms do suggest that there must be some smaller valleys perpendicular to the direction of sampling.

Alarta produced a non-directional variogram which steepened after a break in slope, unlike any other variogram in the study. In the case of its directional variograms, all except one show a similar pattern. The break of slope is at about 1km in the east-west and north-south variograms and at about 1585m ($\log_{10}$ is 3.2) in the northeast-southwest variogram. The variogram for the northwest-southeast direction is actually convex and reaches a maximum variance before it falls off at about 6310m ($\log_{10}$ is 3.8). In this direction two of the more clearly defined valleys seem to be crossed as well as the belt of higher ground running northeast-southwest between these two valleys. In the first three variograms mentioned it would seem that high frequency roughness is present in all these directions up to about 1km to 1.5km. Underneath this roughness the drainage pattern has more gentle trends which leads to a steepening of the variograms. Furthermore the high frequency roughness seems to be present in all directions except northeast-southwest.

Keary's larger scale range directional variograms follow an apparently similar pattern to those of Alarta: two of them show a kink, while one is straight and the other shows signs of a maximum and a minimum. One of Keary's shorter scale variograms, the northwest-southeast variogram, shows a break of slope at about 790m ($\log_{10}$ is 2.9). The direction perpendicular to this northeast-southwest looks almost completely straight. The remaining two variograms are slightly convex. The pattern in both the smaller and larger scale variograms is easily explained. The main valleys and ridges in the Keary DEM trends northeast-southwest. This leads to a linear variogram which reaches no maximum. Perpendicular to this, the northwest-southeast variogram shows up the ridge and valley spacing by producing a convex variogram with a break of slope

followed eventually by maxima and minima. The kinks in the variograms for the other two directions are produced by the averaging process, being only partially affected by the valley spacing.

Appleby produces some of the most interesting directional variogram results. All of the larger distance variograms show some structure. The northeast-southwest variogram is convex until a maximum at 1410m ($\log_{10}$ is 3.15), then a minimum at 2510m ($\log_{10}$ is 3.4) and finally another maximum at 3980m ($\log_{10}$ is 3.6). This variogram samples across the major valleys in the DEM and also along the minor axes of the drumlins. The spacing of the maxima and minima in this variogram would suggest that the effect of the valleys dominate over the effect of the drumlins. The direction perpendicular to this, northwest-southeast, has a kink at 500m ($\log_{10}$ is 2.7) and then another at 2510m ($\log_{10}$ is 3.4). The first kink must surely be the effect on the variance of the drumlins' long axes which are orientated in this direction. The east-west variogram is slightly more difficult to interpret. It starts off showing a slightly convex relationship until between 500m and 790m ($\log_{10}$ is 2.7 and $\log_{10}$ is 2.9) where it seems to straighten out until about 1410m ($\log_{10}$ is 3.15) where there is a slight kink. The first kink in this variogram is related to the size and spacing of the drumlins, the second one is related to do with the underlying drainage pattern. The north-south variogram is simpler, it is convex until a local maxima at about 2240m ($\log_{10}$ is 3.35) which must again be the effect of the spacing of the major valleys in the area. This surface's geomorphometry must be affected by its drainage pattern and its drumlins which makes it relatively easy to study with a view to looking at the size distribution of one particular landform. As a result this surface will be studied more closely in Chapter 8.

In the case of Montoire, the northwest-southeast variogram almost reaches a plateau at 1260m ($\log_{10}$ is 3.1), followed by rather confusing scatter beyond 5010m ($\log_{10}$ is 3.7). This plateau is reached instead of a local maximum because only part of the incised meanders are orientated perpendicular to this direction. The north-south variogram is similar except that it reaches a maximum at 5620m ($\log_{10}$ is 3.75). The northeast-southwest variogram reaches a maximum at 3980m ($\log_{10}$ is 3.6). While the east-west variogram reaches a maximum at 5010m ($\log_{10}$ is 3.7).

Le Puy is another surface which shows clearly anisotropic variance. The north-south variogram is convex until a maximum at 5010m ($\log_{10}$ is 3.7). This variogram is produced by sampling across the central east-west belt of volcanic plugs. As a result the maximum is at half the width of the width of the matrix. The northwest-southeast variogram samples obliquely across this belt and thus produces a variogram with a maximum at about 6310m ($\log_{10}$ is 3.8). The east-west and northwest-southeast variograms show a maximum and a minimum possibly related to the two channels through the belt of volcanic plugs. All the variograms would seem to show some sort of

kink at between 1km and 1260m ($\log_{10}$ is 3 and $\log_{10}$ is 3.1). This is probably related to the spacing of the plugs themselves. The averaging process of the sampling again leads to a slight kink, as opposed to a local maximum.

Uinta produces two of the straightest variograms in the whole study. The north-south and northwest-southeast variograms are very straight because they detect the northwest-southeast trend in altitude. The northeast-southwest variogram reaches a maximum at about 6310m ($\log_{10}$ is 3.8). The east-west variogram has a kink at 3980m ($\log_{10}$ is 3.6). Clearly the latter two variograms are produced by sampling across the ridges and valleys of the surface. The main valley runs nearly along the main northwest-southeast diagonal of the DEM. The east-west sampling of this will, again as a result of averaging, produce a kink at a shorter distance than the maximum found in the variogram perpendicular to this valley. The other two directions would appear to be self-affine. Indeed for shorter scale ranges all the directions show the terrain to be self-affine.

From this discussion it would seem that the fractional Brownian model breaks down on the basis that all of the surfaces studied show some signs of anisotropy. However, some of the surfaces have produced quite linear directional variograms over a reasonable range of scales, suggesting that some profiles of terrain may well be considered as self affine. It now remains in this chapter to observe how fractal dimension and the concept of self-affinity hold when the areas represented by the DEMs are divided into subareas.

6.7 Variogram results for the analysis of subareas.

From the evidence studied so far, it would seem likely that the DEMs will yield variograms showing different structures and different fractal dimensions from subarea to subarea. In section 6.4 it was shown how a dominant feature in the centre of a DEM surrounded by lower or higher ground at the edges of the matrix can lead to a variogram with a maximum variance followed by decreasing variance with distance. The relationship may also become convex as it approaches the maximum variance. This behaviour will of course be expected in the subarea variograms as, for example, one subarea may be dominated by a central hill, even though the variogram for the whole area may have shown near periodic behaviour. Likewise it was also shown that a characteristic slope length for an area may show up as a series of maxima or minima on the variogram. The combinations of these structures found in the directional variograms also suggest that there may be some discrepancy between subarea results and whole area results.

Nevertheless all the DEMs were run through a program to divide them into nine near equally sized subarea DEMs. These subareas were then run through FASTFRAC to obtain both 60 distance variograms and larger scale range variograms, as was explained in Chapter 4.

The results for the 60 distance variograms are presented in Table 6.4. In it the fractal dimension, r^2, and standard error values calculated from the least-squares regression of the 60 distance variograms for each of the subareas are given. Table 6.4 gives the mean, the standard deviation and the range of the subarea fractal dimensions for each DEM, as well as the difference between the mean fractal dimension of the subareas and the fractal dimension of the surface as a whole.

As can be seen from Table 6.4 some subareas have no information given for them. This is a result of the DEMs in question representing irregularly shaped areas which are padded out by missing data values to form matrices. If there is a large percentage of missing values in a subarea it is obviously unfeasible to calculate a meaningful variogram.

Perhaps the most dramatic results are the values for the ranges of subarea fractal dimensions. None is below 0.1. The smallest range, 0.119, is for the Mont Aigoual region. The highest is 0.612 for Galloway. This finding immediately opposes the concept of self-affinity and self-similarity. If a surface was self-affine, a subarea from that surface would be expected to yield the same fractal dimension as the whole surface. The standard deviation values merely agree with the range results.

However to take Galloway as an extreme example is unjustifiable. If reference is made to the r^2 values for the subareas of Galloway it can be seen that two of the subareas have r^2 lower than 0.9. This is a pointer to the fact that the variograms for these subareas are confused by a wide scatter. If the range is recalculated, ignoring these two outliers, a value of 0.378 is obtained, which is of course still very high.

Three other surfaces have r^2 values for subareas below 0.9. In the case of Wind, the variograms in question reach a maximum followed by a decrease in variance with distance. This is also the case for the Keary and Dumfries DEMs. When all of their summary statistics have been recalculated the surface showing the largest range of fractal dimensions yielded by its subarea variograms becomes Uinta, with a range of 0.469. The revised statistics are given in Table 6.4.

Table 6.4 Variogram results for subareas of DEMs

	1/9			2/9			3/9			4/9			5/9		
	D	r^2	SE	D	r^2	SE	D	r^2	SE	D	r^2	SE	D	r^2	SE
Torridon	2.264	0.986	0.0432	2.253	0.997	0.0194	2.208	0.999	0.0035	2.311	0.976	0.0536	2.275	0.983	0.0471
Keary	2.327	0.990	0.0328	2.566	0.752	0.1226	2.414	0.774	0.1557	2.519	0.733	0.1426	2.282	0.993	0.0372
Wind	2.712	0.615	0.1122	2.459	0.962	0.0532				2.547	0.975	0.0357	2.661	0.814	0.0800
Nupur	2.429	0.975	0.0450	2.435	0.958	0.0586	2.204	0.992	0.0356	2.304	0.981	0.0475	2.353	0.964	0.0620
Thvera	2.315	0.984	0.0428	2.216	0.966	0.0727	2.262	0.997	0.0213	2.288	0.992	0.0370	2.214	0.995	0.0283
Dumfries	2.283	0.997	0.0185	2.238	0.999	0.0093	2.734	0.527	0.1241	2.296	0.977	0.0535	2.174	0.995	0.0284
Galloway	2.149	0.998	0.0185	2.340	0.994	0.0250	2.723	0.828	0.0622	2.361	0.961	0.0633	2.287	0.986	0.0410
Uinta	2.183	0.999	0.0111	2.122	0.999	0.0112	1.940	0.984	0.0656	1.721	0.942	0.1570	1.753	0.961	0.1244
Devoluy	2.251	0.988	0.0403	2.178	0.995	0.0288	2.131	0.997	0.0236	2.170	0.996	0.0266	2.184	0.992	0.0351
Canigou	2.151	0.997	0.0220	2.221	0.992	0.0342	2.561	0.903	0.1506	2.135	0.996	0.0269	2.159	0.999	0.0149
Aigoual	2.487	0.977	0.0387	2.413	0.984	0.0366	2.496	0.985	0.0303	2.377	0.986	0.0363	2.446	0.979	0.4000
Montoire	2.295	0.983	0.0456	2.265	0.991	0.0339	2.439	0.946	0.0660	2.412	0.952	0.0646	2.294	0.987	0.0398
Puy	2.234	0.985	0.0461	2.135	0.991	0.0395	2.232	0.990	0.0385	2.099	0.998	0.0208	2.221	0.987	0.0446
St. Paul	2.582	0.976	0.0320	2.270	0.956	0.0766	2.235	0.998	0.0185	2.328	0.967	0.0614			
Booro	2.232	0.985	0.0463	2.095	0.978	0.0671	2.163	0.991	0.0403	2.123	0.996	0.0264	2.143	0.997	0.0213
Aughwick	2.207	0.997	0.0217	2.247	0.995	0.0264	2.231	0.998	0.0157	2.400	0.992	0.0260	2.186	0.988	0.0441
Belleville	2.227	0.995	0.0271	2.286	0.998	0.0161	2.088	0.995	0.0326	2.113	1.000	0.0081	2.108	0.996	0.0288
Allenville	2.131	0.999	0.0134	2.151	0.999	0.0103	2.069	0.999	0.0110	2.176	0.998	0.0170	2.131	1.000	0.0087
Nether				2.049	0.995	0.0319	2.055	0.992	0.0430	2.161	0.991	0.0384	2.159	0.999	0.0076
Glaisdale	2.121	0.983	0.0568	2.164	0.994	0.0324	2.045	0.997	0.0272	2.448	0.955	0.0900	2.083	0.999	0.0152
Wheeldale	2.077	0.996	0.0306	2.035	0.975	0.0762	2.049	0.969	0.0831	2.271	0.987	0.0416	2.045	0.921	0.1374
Devon	2.307	0.992	0.0307	2.508	0.917	0.0724	2.399	0.973	0.0494	2.448	0.982	0.0363	2.545	0.957	0.0477
Gara	2.151	0.997	0.0216	2.349	0.980	0.0460	2.184	0.996	0.0254	2.391	0.944	0.0732	2.412	0.968	0.0523
Appleby	2.407	0.993	0.0250	2.387	0.998	0.0174	2.414	0.986	0.0341	2.379	0.995	0.0212	2.420	0.986	0.0341
Alarta	2.504	0.997	0.0123	2.554	0.993	0.0188	2.522	0.995	0.0175	2.578	0.990	0.0207	2.492	0.995	0.0179

Table 6.4 continued

	6/9			7/9			8/9			9/9						
	D	r^2	SE	D	r^2	SE	D	r^2	SE	D	r^2	SE	$\bar{D}$	D_0	$\bar{D}-D_{6.2}$	Range
Torridon	2.176	0.993	0.0339	2.399	0.994	0.0234	2.394	0.989	0.0309	2.458	0.981	0.0376	2.304	0.089	-0.064	0.282
Keary	2.377	0.978	0.0462	2.672	0.709	0.1035	2.494	0.949	0.0576	2.394	0.988	0.0328	2.449	0.117	0.080	0.390
Wind	2.433	0.812	0.1346				2.414	0.837	0.1273	2.432	0.973	0.0468	2.523	0.112	-0.053	0.298
Nupur	2.256	0.993	0.0312	2.344	0.966	0.0612	2.245	0.986	0.0444	2.456	0.939	0.0685	2.336	0.086	0.025	0.252
Thvera	2.276	0.989	0.0376	2.283	0.993	0.0230	2.220	0.992	0.0347	2.166	0.999	0.0160	2.249	0.045	-0.011	0.149
Dumfries	2.724	0.830	0.0615	2.425	0.957	0.0594	2.255	0.998	0.0141	2.649	0.818	0.0815	2.419	0.210	0.146	0.560
Galloway	2.527	0.932	0.0631	2.324	0.985	0.0399	2.274	0.977	0.0551	2.761	0.613	0.0935	2.416	0.197	0.110	0.612
Uinta	1.893	0.979	0.0801	2.190	0.999	0.0125	2.127	0.999	0.0118	2.176	0.994	0.0323	2.012	0.178	-0.147	0.469
Devoluy	2.106	0.999	0.0136	2.186	0.995	0.0275	2.082	0.989	0.0486	2.180	0.995	0.0292	2.163	0.047	0.020	0.169
Canigou	2.099	1.000	0.0086	2.141	0.998	0.0183	2.166	0.997	0.0233	2.129	0.998	0.0205	2.196	0.141	0.050	0.462
Aigoual	2.435	0.982	0.0374	2.413	0.983	0.0379	2.484	0.975	0.0403	2.494	0.986	0.0296	2.449	0.041	0.020	0.119
Montoire	2.304	0.982	0.0459	2.123	0.997	0.0254	2.266	0.991	0.0353	2.258	0.993	0.0304	2.295	0.086	0.014	0.316
Puy	2.179	0.995	0.0294	2.202	0.995	0.0275	2.142	0.996	0.0268	2.129	0.998	0.0178	2.175	0.047	0.021	0.135
St. Paul	2.460	0.962	0.0526	2.329	0.988	0.0369							2.367	0.130	0.110	0.350
Booro	2.099	0.993	0.0360	2.073	0.999	0.0141	2.075	0.984	0.0582	1.962	0.988	0.0561	2.107	0.074	-0.029	0.159
Aughwick	2.221	0.999	0.0123	2.110	1.000	0.0092	2.116	0.999	0.0143	2.245	0.998	0.0146	2.218	0.080	0.033	0.290
Belleville	2.265	0.989	0.0383	2.233	0.994	0.0293	2.293	0.998	0.0156	2.291	0.995	0.0245	2.212	0.085	0.032	0.205
Allenville	2.405	0.988	0.0319	2.126	0.999	0.0137	2.128	0.999	0.0100	2.200	0.999	0.0134	2.169	0.096	0.004	0.336
Nether	2.083	0.991	0.0455	2.207	0.999	0.0128	2.075	0.988	0.0505				2.113	0.057	0.001	0.158
Glaisdale	2.075	0.981	0.0631	2.161	0.995	0.0304	2.082	0.999	0.0091	2.088	0.996	0.0271	2.141	0.115	-0.002	0.403
Wheeldale	2.038	0.983	0.0629	2.028	0.994	0.0367	2.135	0.995	0.0299	2.139	0.995	0.0158	2.091	0.075	-0.004	0.243
Devon	2.423	0.986	0.0334	2.449	0.984	0.0351	2.587	0.928	0.0566	2.494	0.969	0.0443	2.494	0.790	0.045	0.280
Gara	2.386	0.967	0.0561				2.168	0.990	0.0408	2.341	0.975	0.0523	2.298	0.110	-0.056	0.261
Appleby	2.448	0.985	0.0332	2.348	0.980	0.0459	2.511	0.939	0.0613	2.463	0.963	0.0521	2.420	0.049	-0.023	0.163
Alarta	2.606	0.986	0.0230	2.668	0.974	0.0265	2.609	0.989	0.0203	2.656	0.975	0.0272	2.577	0.060	-0.017	0.176

As in the case of the fractal dimensions of the directional variograms, the fractal dimensions of the subareas generally have a mean value close to that of the fractal dimension of the surface when it is investigated as a whole. The average difference between the mean fractal dimension of the subarea for a DEM and the fractal dimension of the DEM as a whole is 0.031.

The separate longer-scale variograms show the whole range of structures described in the earlier sections of this chapter. Rather than describing each of the 243 possible subareas' larger-scale variograms in detail only a selection of DEMs will be discussed in depth here. It would seem sensible to discuss the DEM which gives the most variation in subarea fractal dimensions, along with the DEM with the least variation and, also another surface from somewhere in the middle of this range. This means that the surfaces chosen on the basis of range of subarea fractal dimension are Uinta,Nupur, and Mont Aigoual.

However, along with these it would seem sensible to discuss some of the surfaces that have been most interesting in the earlier sections of this chapter: Alarta being perhaps the closest to a real fractal surface studied; Wheeldale, as it is one of the smoothest surfaces in the study; Aughwick, because of its link to the previous work performed by Mark and Aronson (1984).

Looking first at the results for Uinta it can be seen immediately that something peculiar is happening as far as the fractal dimensions are concerned. The third, fourth, fifth and sixth subareas produce 60 distance variograms which give fractal dimensions of below 2, the Euclidean dimension of a plane. For the remaining subareas the order of decreasing roughness, according to their estimated fractal dimensions, is subarea 7 followed by 1,9,8 and 2. Although all the variograms that yield D lower than 2.0 have r^2 values better than 0.9, they do have wide scatter and have higher standard errors than most other regressions so far (0.157 in the case of subarea 4), which must be enough to throw the estimates of D below 2.

A better reflection of what is producing this order of fractal dimensions is obtained by referring to the longer scale range variograms. The first subarea is in the northwest corner of the DEM. In its variogram (Appendix 3) the general trend is very straight. There is however a widening of scatter and signs of a maximum at 1990m ($\log_{10}$ is 3.3). The value of D, 2.183, is quite believable for this subarea. The second subarea produces a somewhat similar variogram. The scatter widens at about 1km ($\log_{10}$ is 3) after which there are possibly signs of a kink at about 2510m ($\log_{10}$ is 3.4). This subarea certainly looks smoother than the first subarea and has a correspondingly lower fractal dimension.

It is with the third subarea that confusion is met. The cloud of scatter does follow a very linear trend; however its distribution must be such that it yields the spurious fractal dimension of 1.940 . The fourth, fifth and sixth subareas all produce this wide scatter. The seventh and eighth subareas give reasonable fractal dimensions, and subarea nine, although possessing a wide scatter, is linear throughout and gives a sensible fractal dimension.

In the case of Nupur none of the fractal dimensions is below 2.0. It would be very difficult to put the subareas visually into order of fractal dimension or roughness. However there are still quite large differences in fractal dimension between certain subareas and it would be expected that this would be visible in the subarea perspective block diagrams of Nupur given in Figure 6.31. If the subarea variogram r^2 values are put in order, from lowest to highest, the order is identical to the subareas ordered by fractal dimension, highest to lowest. The differences in subarea fractal dimension are therefore partly due to the curvature of the variograms.

The subareas of the Aigoual DEM have a range of 0.119. The supposedly roughest subarea according to estimated fractal dimension is in the northeastern corner while the smoothest subarea is the west-central portion of the DEM. The reason for this is not visually obvious. It suggests that in certain situations a 0.1 difference in fractal dimension between two surfaces may not be easily detected visually.

The order of *D* for Alarta's subareas is partially related to the convexity of the variograms but may also be a true effect of roughness. Subareas 7 and 9 have the lowest r^2 values, clearly the most convex variograms, and have the highest fractal dimensions. After this the order might seem sensible, each of the other subareas showing more of the main drainage channels which are much smoother than the other features of the area.

The subarea variograms for longer distances looked at in conjunction with the shorter range variograms give added insight. For subareas 7 and 9 the variograms are convex up to 1260m ($\log_{10}$ is 3.1) and 1km ($\log_{10}$ is 3.0) respectively, then there are kinks at which the variograms become concave and steepen. In the other cases most of the variograms are straight or slightly concave before they become steeper. The variogram for the first subarea shows the best formed structure. The short distance part of the variogram is quite straight, then convexity is reached at about 1260m ($\log_{10}$ is 3.1) until the variogram steepens again at about 1990m ($\log_{10}$ is 3.3). All of these structures seem to detect some change in the way the landsurfaces' variances behave at around about 1km to 1.5km, probably the average slope length of the area. This corresponds to what was discovered earlier in the case of its overall variogram and its directional variograms.

Figure 6.31 *Nupur subareas 1–3*

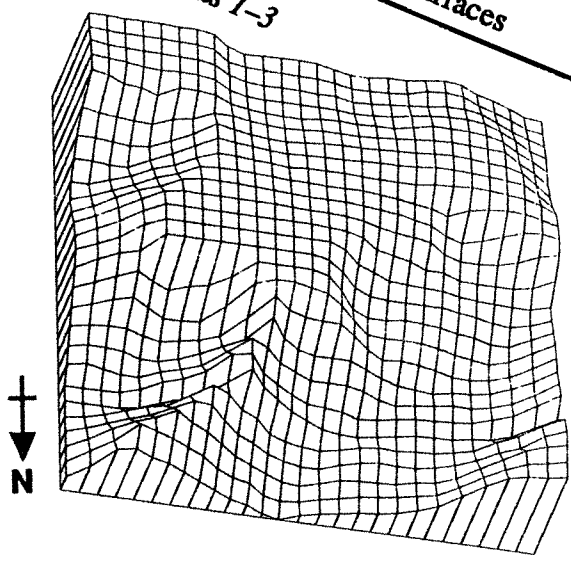

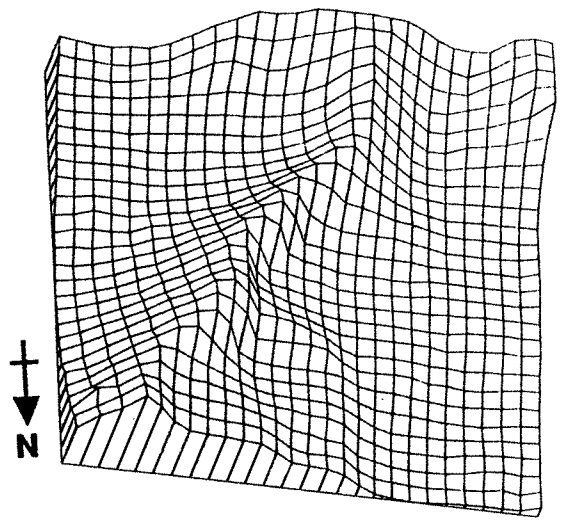

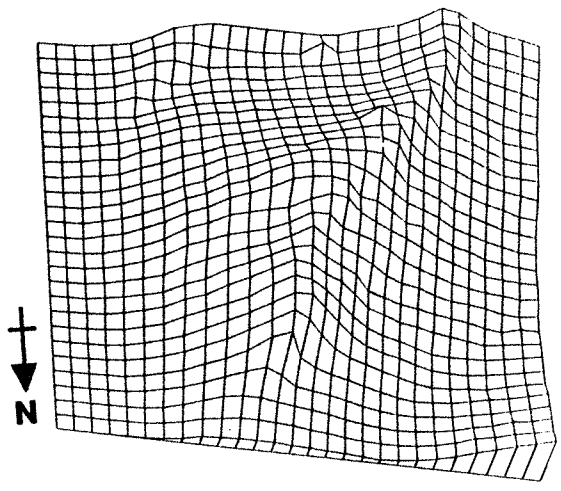

Figure 6.31 (continued)

Nupur subareas 4–6

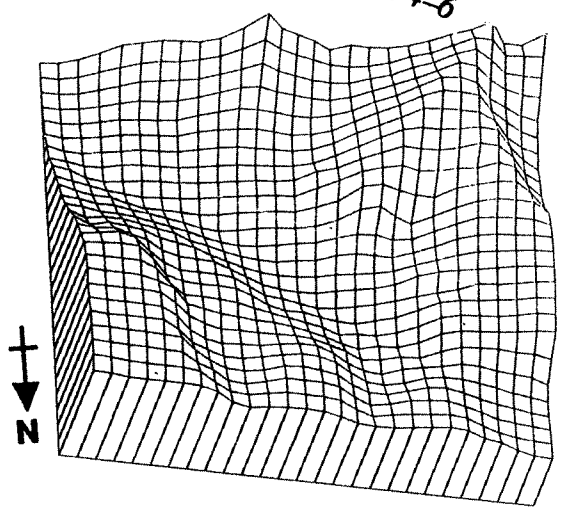

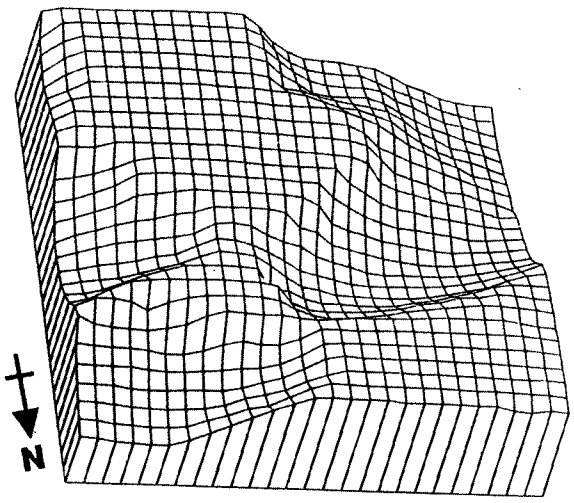

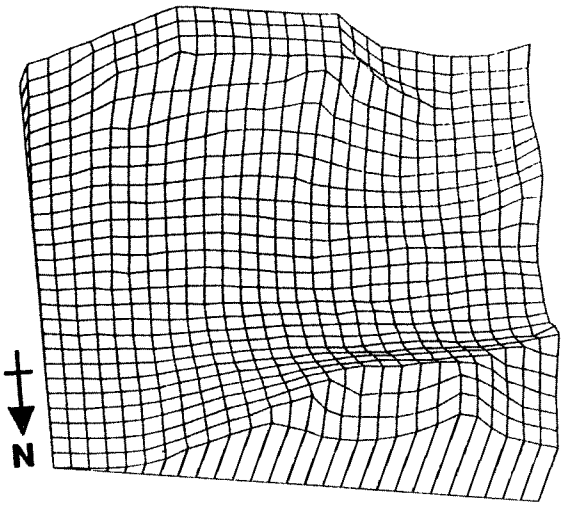

Figure 6.31 (continued) *Nupur subareas 7–9*

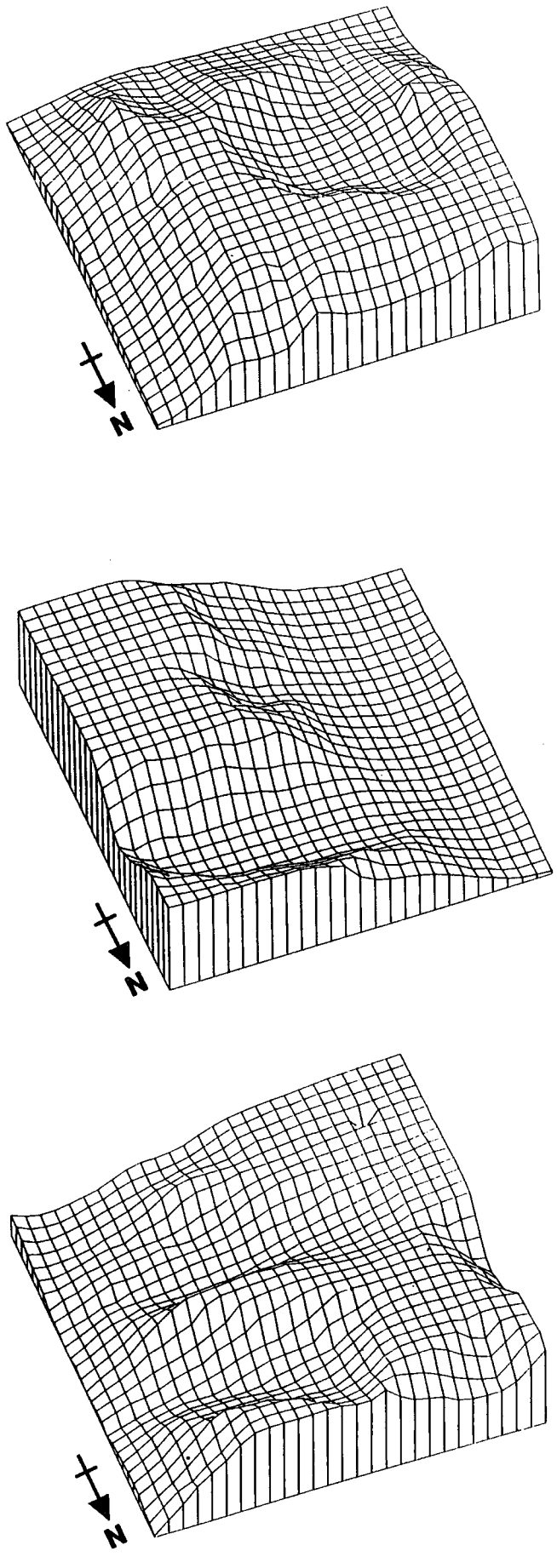

The order of fractal dimensions for Wheeldale can, to a certain degree, be judged visually from its perspective block diagram (fig. 6.23). Certainly the roughest three ninths can be picked out. They are the western central subarea, the southeastern corner and the south central subarea. After this it becomes more difficult; however all the dimensions estimated from these remaining subareas fall into a range of 0.049. In the case of this high resolution surface it would seem that the fractal model can still break down at these smaller scales.

Aughwick produces the most easily interpretable results of all the DEMs discussed so far. The order of the subareas according to their fractal dimensions is visually very plausible. Subarea 4 contains two ridges which seem to be disturbed by faulting across them; it is the subarea with the highest value of D. Likewise the next highest values of D are found for subareas 2 and 9 which seem to contain less regular structure than the subareas dominated by one ridge and its slopes such as subareas 5,8 and 7. It is interesting to note that not all the larger distance subarea variograms produce similar patterns to those found in the overall variogram result of Mark and Aronson (1984). Subarea 3 would appear to have a break of slope at about 1260m ($\log_{10}$ is 3.1). Subarea 4 has a kink starting at 630m ($\log_{10}$ is 2.8) and subarea 9 has a less obvious kink at the same distance. These variograms must be detecting a large area of slopes shorter than the slopes of the major ridges.

6.8 Conclusions

This chapter has used two methods to investigate the concepts of self-affinity and self-similarity when applied to the form of real landsurfaces. In the process of doing so estimates of the fractal dimension for each of the surfaces have been calculated by both methods. Although the orders in which the two methods estimated fractal dimensions place the surfaces are believable if D is thought of as an index of surface roughness, they are not in agreement with one another. The rescaled range analysis method gives, in general, a lower value of D than the variogram method as implemented in FASTFRAC.

The disagreement between the results of the two methods begins to cast doubts on how close the real surfaces are to fractional Brownian surfaces. More serious doubt is raised by the curvature of most of the 60 distance variograms. When the analysis is extended to longer scale ranges this curvature gives way in many cases to a decrease in variance with distance or maxima, minima and steps in the variance indicative of characteristic slope lengths in the area. Therefore at a scale of around 2 to 3km the fractal model seems to break down in most cases. Perhaps surfaces such as Keary, Uinta and Alarta show behaviour which could be looked upon as fractal.

The break down of the fractal model as it is applied to real landsurfaces is apparent not only in the scale at which characteristic slope lengths may be encountered. It is also apparent in the fact that the roughness of real landsurfaces can be concentrated in certain directions, that is it is anisotropic. The variance of fractal Brownian surfaces is on the contrary isotropic. Indeed some of the difference between the rescaled range analysis results and the variogram results are due to the rescaled range analysis being limited to only two orientations (north-south and east-west) while the variogram for the surface as a whole takes into account all of the anisotropic distribution of roughness of the surfaces.

The most simple of introductions to the concept of self-similarity describes the irregularity at one scale being similar to the irregularity of any part of the whole looked at in greater detail. The subarea analysis of the DEMs shows that in all cases the subareas may have quite different properties to those of the whole area and as a result the range of different fractal dimensions within subareas of a surface can be large.

Overall, therefore, this chapter has drawn attention to the fact that, as expected from a geomorphological viewpoint, landsurfaces are in general not similar to fractional Brownian surfaces. It has not however proven that the concept of fractal dimension is of no use as a device to classify the roughness of a surface against some simulated standard. The next chapter will therefore investigate the relationship between fractal dimension and some other, more traditional geomorphometric indices. It will also try to ascertain some of the geomorphometric properties of simulated fractal surfaces.

Chapter 7: The Geomorphometry of Simulated and Real Landsurfaces.

7.1 Introduction

The previous chapter has shown that the real landsurfaces studied fail to fit the fractional Brownian model. They seldom show signs of self-similarity over a wide scale range. The areas covered by the DEMs generally comprise subareas of differing degrees of roughness, if not of totally different topographies. Likewise the apparent orientation of features in the landsurfaces seems in many cases to be anisotropic.

It would therefore seem sensible to find out what geomorphometric properties real landsurfaces may have that make the fractal model break down. This initially involves studying the general geomorphometry of the real landsurfaces. This may point at features of landsurface form which are immediately at odds with the fractal model. However, further to this study of the geomorphometry of real landsurfaces, it would also be of interest to look at the general geomorphometry of the simulated fractal landsurfaces discussed in Chapter 5. A study of this nature would allow comparison of the real and simulated landsurfaces to indicate what aspects of geomorphometry are not found in simulations of surfaces and to point to the less realistic features of fractal simulations of terrain.

Although the fractal Brownian model was seen to break down in the investigation of the last chapter, the fractal dimension, D, calculated from the straight segments of the variograms, may still be of use as an additional geomorphometric variable providing information about surface roughness. As a result it is of interest to see how fractal dimension agrees with other more traditional indicators of roughness found in geomorphometry.

This chapter will therefore first elaborate on the concepts of geomorphometry that were introduced in Chapter 1 and discuss how the various geomorphometric parameters to be used in this chapter are calculated. The results of these calculations for real surfaces will then be discussed, followed by a similar discussion of the geomorphometry of the simulated fractal surfaces. The relationships between the range of geomorphometric variables used and the fractal dimensions of the simulated landsurfaces will then be studied. Finally, the same range of variables will be correlated with the fractal dimensions of real landsurfaces.

7.2 Geomorphometry

The analysis in this chapter will use tried and discussed techniques. These techniques will however be applied to new simulated surfaces as well as the more traditional DEMs. It is therefore necessary to give some discussion of the field of general geomorphometry (Evans, 1972) as well as the specific approach taken in this study.

As discussed in Chapter 1, general geomorphometry studies the overall properties of landsurfaces rather than subjectively dividing the surface into a number of different landforms. Mark (1975) gives a review of most of the parameters which have been used in the attempts to characterise landsurfaces. Many of these date back to a period when computers were not used to store topographic surfaces in order to *"perform detailed quantitative analysis of land surface form"* (Mark, 1975, p.165). Without the aid of computers, these parameters needed to be more easily calculated; notably the parameters of local relief, grain and texture can be readily obtained from contour maps. The concepts which they investigate have already been encountered when studying the variogram results. Since then, even personal computers have obtained the necessary capabilities to process representations of landsurfaces held as DEMs. As a result many workers have turned to calculating the first and second derivatives of altitude, certainly for mapping purposes but also to investigate, in more detail, some of the concepts mentioned above (Evans, 1980; Depraetere, 1989; O'Neill and Mark, 1987).

The first derivative of altitude is slope. Slope, a vector quantity, can be resolved into two components. The vertical component is gradient, often incompletely termed by itself as 'slope'. Evans describes gradient as *"the maximum rate of change of altitude (z) with horizontal displacement"* (Evans, 1981, p.31).

The second component of slope is the horizontal component and is mentioned in the literature using various terms such as exposure and aspect. Aspect is the term chosen here as it has fewer possible meanings in the context of the subject of this thesis. Aspect is the azimuth in which the gradient is found.

The second derivative of altitude, curvature, also has two components. Again, one is the vertical component while the other is the horizontal component. The former is referred to by Evans (1979) as the profile convexity. This is the rate of change of gradient in the direction given by the aspect. The horizontal component of curvature is plan convexity. It is the rate of change of aspect, in other words, the curvature of a contour line. The term convexity is applied because it points to the fact that curvature

can be either positive or negative. Positive curvature is convexity, while negative curvature is concavity (Evans, 1981).

In this study a program originally written for I.S.Evans (1979;1980) by Margaret Young (1978) was readily available to calculate these attributes. The program uses a single pass of the entire DEM to calculate estimated altitude, gradient, profile convexity, plan convexity and aspect, along with descriptive and moment statistics for each of the first terrain attributes and vector statistics for aspect. In addition to these calculations, Pearson's product correlation coefficients between the first four attributes are calculated and details of extreme points and points with zero slope are recorded.

Operations within the program are as follows. Only three rows of the DEM being processed are held at any time during the program's run. A pass is made along these three rows using a 3 by 3 window of points centred, in turn, on each point of the middle row, except obviously for the extreme right and left hand points. For each window a six parameter quadratic equation is fitted which allows estimated altitude and its four derivative attributes to be calculated. When one row of attributes has been calculated another row of the DEM is read in and the window passes along the next row, and so on.

During the process the relevant summations are made to calculate the moment statistics both for the entire number of cases calculated and for the cases with non-zero gradient only. At the same time the vector measurements for aspect, the correlation coefficients, and the locations of the extreme values are calculated and recorded.

Clearly the size of the grid mesh used in the DEM will have an effect on the gradient calculated (Evans, 1975; Evans, 1979). For example a cliff with a gradient of 90 degrees will not be detected in the DEM and a lower gradient will be calculated between points on either side of the cliff separated by the grid mesh difference. Profile convexity will be similarly affected by grid mesh size. These sampling effects must be taken into account when looking at the resulting statistics.

The moment statistics calculated for altitude and its derivatives can be very useful descriptors of the form and roughness of landsurfaces. Evans (1981) briefly suggests that the moment statistics, when used in conjunction with histograms of the attributes, are preferable to their quartile alternatives and also to any of the order statistics found in sedimentology. The most detailed description of the meaning of each statistic for each attribute, in terms of landscape, is given in Evans (1979). However a short summary will be provided here.

Mean altitude merely gives a general description of the elevation of the area being studied. Standard deviation of altitude give an indication of the variability of

elevation in an area. It therefore gives similar information to the older notion of relief. While Mark (1975) prefers the range, Evans (1972) suggests that the standard deviation of altitude is more stable. Skewness of altitude indicates whether there is a tail of high altitudes (positive skew) or a tail of low altitudes (negative skew). Evans (1979) gives an area containing a plateau as an example of a landsurface which would yield high negative skew, while an area including an inselberg would produce high positive skew.

Mean gradient indicates the roughness of the landsurface being considered. However, if a particular value of mean gradient is to be understood fully it is useful to consider it in the context of the grid mesh size of the DEM, as well as in comparison with other surfaces of differing roughness. Standard deviation of gradient considered along with mean gradient gives a description of the distribution of slopes in the DEM area. If the standard deviation is high it suggests contrasted topography such as inselbergs or a glaciated mountain area. Skewness of gradient for areas studied previously has varied from near zero to high positive skew. Steep, fluvially, dissected areas may be near Gaussian (Strahler, 1950; Evans, 1979,1981). In general steep slopes have a low frequency.

The frequency distributions for profile convexity of an area can be quite informative about an area's topography. Mean profile convexity should be near zero as convexities are generally balanced by concavities (Evans, 1979), ridges are balanced by valleys. The standard deviation of profile convexity is an indicator of the 'magnitude' of the profile curvature within a surface (Evans, 1979). That is the higher the standard deviation the more extreme convexities and concavities present in the surface. This can, again, be seen as a measure of roughness in the surface. The skewness of profile convexity for a surface that was composed completely of sine waves would of course be zero. However many real landsurfaces tend to have a small number of very high convexities while the area taken up by concavities in a DEM is likely to be higher and less extreme than that for convexities. This leads to positive skew. Evans has found this in many DEMs of glaciated mountain areas, some of which are studied in this work (Evans, 1979; Evans, 1981).

The moment statistics for plan convexity can be considered in a similar manner to the statistics for profile convexity. Means are again generally near zero. Standard deviation is a measure of the magnitude of plan curvature. Skewness should behave similarly to the skewness of profile convexity; however it is often quite sensitive to error in the original DEM (Evans, 1979) and may not give a good representation of what is happening in the actual landsurface as opposed to the model.

These moment statistics would appear to be the most interesting when comparing fractal dimension considered as a geomorphometric index with the

derivatives of altitude. Evans (1984) in an extensive study of the interrelationships of the various statistics obtained from the derivatives of altitude produced by the program described above tried to answer this question: *"at the most general level: what properties are important in distinguishing one part of the surface from another?"* His aim was to provide understanding of a range of surface properties from which subsets could be selected for any particular terrain analysis purpose. A list of five main variables and a further four key variables was produced. This highlights the importance of, in the order given by Evans: mean gradient; skewness of altitude; standard deviation of plan convexity; weighted vector strength modulo 180 degrees; weighted vector strength modulo 360 degrees; vector strength modulo 90 degrees; standard deviation of gradient; skewness of profile convexity; and the correlation between altitude and profile convexity.

When looking at fractal dimension as a possible index of surface roughness the first three of these variables are of definite interest. When considering whether landsurfaces are anisotropic one of the vector strengths of aspect would be interesting to study. Reference in this study will therefore be made to gradient-weighted aspect and its strength. The gradient weighting is of particular relevance when considering anisotropy as far as roughness is concerned. The aspect of a gentle slope is given less weight than that of a steep slope. Standard deviation of gradient and skewness of profile convexity are clearly important. The correlation of altitude with profile convexity may also be of interest. As well as real landsurfaces this study is looking at simulated fractal surfaces and so most of the other statistics will be included in the discussion. Therefore along with these key variables will be: standard deviation of profile convexity; skewness of gradient; mean and standard deviation of altitude; and the correlation between altitude and gradient.

7.3 The geomorphometry of the real landsurfaces.

With these considerations in mind it is now possible to look at the geomorphometry of the real landsurfaces studied. Table 7.1 presents the key variables discussed above for each of the 27 DEMs. Firstly the distributions of the statistics calculated for the derivatives of altitude, obtained from the sample of landsurfaces studied, can be discussed.

Mean altitudes of the DEMs range from 3662m in the case of the Wind River Mountains, Wyoming to 17.5m for the DEM of the littoral area Le Porge, West France. Mean altitude serves to describe the general elevation of the area studied. Little can be stated about this statistic for each DEM.

Table 7.1 Geomorphometric statistics for real landsurfaces

	D	ALT1	ALT2	ALT3	GRAD1	GRAD2	GRAD3	PROF2	PROF3	PLAN2	PLAN3	ALT.GRAD	ALT.PROF
Torridon	2.368	445.100	152.600	0.728	14.741	11.087	1.013	7.729	1.471	58	-14.796	0.547	0.302
Keary	2.369	1648.400	429.600	-0.381	32.563	11.827	-0.296	15.231	0.702	81	2.080	0.036	0.231
Wind	2.576	3662.100	208.200	-0.365	20.557	10.217	0.322	8.166	1.023	44	4.890	0.103	0.469
Nupar	2.311	439.300	197.600	-0.239	21.586	12.438	0.197	11.375	1.604	52	2.264	0.049	0.469
Thvera	2.260	881.400	229.600	-0.540	21.366	10.506	0.122	10.130	6.338	60	6.338	0.119	0.346
Dumfries	2.273	158.400	74.100	0.802	3.883	3.186	1.549	3.079	-0.797	122	-1.161	0.542	0.150
Galloway	2.306	160.500	49.500	-0.385	3.739	3.303	1.802	3.091	-0.505	190	-6.666	-0.348	0.260
Uinta	2.159	2615.700	143.200	-0.108	6.073	4.165	1.183	9.580	0.208	193	-0.703	0.174	0.058
Devoluy	2.143	1234.700	258.200	0.672	17.421	9.992	0.333	9.393	0.208	3776	-198.877	0.413	0.204
Canigou	2.146	2087.400	392.100	-0.486	28.584	11.930	0.310	13.892	2.145	90	-15.797	0.102	0.213
Aigoual	2.429	606.500	321.000	0.419	28.707	16.265	0.020	33.981	-0.399	249	15.369	0.159	0.187
Montoire	2.281	103.200	22.900	-0.180	2.571	3.056	2.298	4.118	-0.369	1341	-196.669	0.013	0.305
Le Puy	2.154	914.600	113.500	0.500	7.068	6.446	1.829	4.730	0.369	56	-1.512	0.495	0.144
Le Porge	*	17.500	4.800	1.262	1.380	1.818	1.612	2.891	0.330	1256897	-188.660	0.459	0.361
Reunion	2.366	901.300	647.300	0.491	12.875	10.255	1.596	3.799	-0.486	26	-5.649	0.335	0.810
St. Paul	2.477	114.400	58.400	0.575	14.312	12.291	1.632	21.280	2.064	86	2.075	0.105	0.172
Booro Borotou	2.136	449.400	9.700	0.055	3.283	2.183	2.087	16.015	-0.362	247	-6.220	-0.092	0.082
Auchwick	2.185	1080.300	361.000	0.727	33.518	15.121	-0.370	54.910	-1.027	405	36.235	0.512	0.120
Belleville	2.181	907.900	309.500	1.195	26.754	14.965	0.422	48.863	0.026	454	-4.020	0.517	0.107
Allenville	2.165	11.50.5	345.900	0.948	28.204	15.364	0.336	45.917	0.049	409	1.094	0.466	0.109
Netherhearth Sike	2.112	645.200	49.800	0.486	5.948	3.099	0.640	28.322	-0.675	597	2.150	0.074	0.039
Glaisdale	2.143	180.900	17.700	0.923	7.425	3.632	0.702	15.769	-0.262	188	-9.762	0.720	0.020
Wheeldale	2.095	164.300	22.000	0.411	8.465	4.184	0.161	29.066	-1.478	363	-4.566	0.170	0.132
Devon	2.441	166.900	22.100	0.033	2.628	1.591	1.043	2.419	-0.856	99	0.195	-0.212	0.310
Gara	2.354	120.616	39.600	-0.398	7.404	4.550	1.158	9.619	-1.879	158.193	-18.053	-0.493	0.346
Appleby	2.443	152.300	21.000	0.222	4.026	2.995	1.359	8.592	-0.448	160	-8.840	-0.038	0.249
Alarta	2.574	854.900	39.500	0.006	2.669	1.550	0.987	2.987	0.696	127	0.370	0.206	0.126

D *Fractal Dimension*
ALT 1 *Mean Estimated Altitude*
ALT 2 *Standard Deviation of Altitude*
ALT 3 *Skew of Altitude*
GRAD1 *Mean Gradient*
GRAD2 *Standard Gradient*
GRAD3 *Skew of Gradient*
PROF2 *Standard Deviation of Profile Convexity*
PROF3 *Skew of Profile of Convexity*
PLAN2 *Standard Deviation of Plan Convexity*
PLAN3 *Skew of Plan of Convexity*
ALT.GRAD *Correlation between Altitude and Gradient*
ALT.PROF *Correlation between Altitude and Profile Convexity*

Standard deviation of altitude qualifies each DEM's mean altitude figure. The variation of altitude around the mean value for the area indicates the extent of the range in altitude for an area. Reunion has the largest standard deviation, 647.3m and range in altitude, though not the highest mean altitude. The smallest standard deviation of altitude is for Le Porge which has both the smallest mean and range. Many of the lower lying areas have, as would be expected, lower standard deviations. Glaisdale and Wheeldale for instance are both small areas of drainage basins and are quite low lying with respect to the sample in this study, with little range in altitude. Booro Borotou is also a small drainage basin covering a fairly small area Fand although it is at a much higher average altitude it has a narrow range of altitude and low standard deviation. Uinta and Alarta are examples of areas which are at a high average altitude but have small standard deviations and ranges.

The skewness of altitude for the DEMs ranges from -0.54 for Thvera to 1.262 for Le Porge. The latter is a typical example of an area which would be expected to have high positive skewness of altitude and its skew is one of the statistics which best characterise it. Le Porge is a generally flat low-lying area which is perturbed at one side by coastal dunes. The summits of these dunes gives a tail of high altitudes to the overall altitude distribution, the bulk of which lies at lower altitudes. Torridon shows a similar effect except that instead of dunes the tail of high altitudes is provided by mountain ridges isolated from one another by wide glacial troughs.

The three Appalachian mountain areas, Aughwick, Belleville and Allenville, are also classic examples of landsurfaces which will give highly positive skewed distributions. In their cases ridges are very narrow in comparison with the distance between the talwegs they separate. Furthermore, all the ridges are at similar altitudes, as are valleys. High positive skewness of altitude is therefore an important characteristic of ridge and valley topography.

The reason for high positive skew in the case of Dumfries is the two contrasting topographies caused by two different lithologies. The lower altitudes of the Permian and Carboniferous sequences to the south dominate the dissected Silurian and Ordovician uplands to the north. At a smaller scale high positive skew in the case of Glaisdale can be explained by reference to two slopes in the DEM. The higher northwest and southeast corners provide the tail of high altitudes needed to produce the positive skew.

Evans (1979) suggests plateau areas as examples of landscapes which would yield high negative skew of altitude. In the sample here, however, it is a glaciated mountain area which gives the highest negative skew of altitude. The two deepest glacial troughs in the Thvera area are substantially deeper than the other troughs and cirques in the area. They are therefore responsible for a tail of low values in the altitude

distribution. Similar situations occur in the DEMs of Keary, Wind and Canigou. However, as would be expected of a plateau area, Nupur has negatively skewed altitude, but because of the extent of glacial dissection the negative skew is less than for the surfaces previously mentioned.

Galloway has a dominant area of upland dissected by several deep troughs and as a result has negative skew. Gara is similar and gives a very similar value for skewness of altitude. The other DEMs have either low positive or negative skew. In some cases the physical causes of the direction of the skew can be seen. However the failure of these features to dominate the altitude distribution can often also be seen as high or low areas balancing the distribution.

As previously mentioned care must be taken when looking at statistics involving gradient,when differing sizes of grid mesh are used in different DEMs. This also applies to all subsequent derivatives to be dealt with here. In this study three grid mesh sizes are the most common. The U.S.G.S. DEMs are at a 30m resolution, while the French and two of the British DEMs, Gara and Appleby, are at 50m resolution. A resolution of 100m is common to many of the earlier DEMs studied previously in Durham. Outside of these three main mesh sizes are: Booro Borotou (7m); Netherhearth Sike (10m); Wheeldale and Glaisdale (15m); Wind (200m); and Reunion (300m).

The highest mean gradient, 33.5°, is found for a 30m mesh DEM, Aughwick. However, Keary, a 100m resolution DEM has a mean of 32.6°, while Wind, with a resolution of 200m, has a mean of 20.6°. All of these means are high, allowing for the resolution of the model they came from. Certainly Keary must be considered to have a higher mean than Aughwick given differing resolutions – however, whether the mean of Wind is higher is more difficult to say. For this sample of surfaces the following generalisations seem to apply: DEMs of mountain areas which have large enough altitude ranges to include complete mountains have mean gradients over 12°, regardless of grid mesh. Lowland areas have mean gradients of below 10°.

Evans (1979) suggests that high standard deviation of gradient is an indication of contrasted topography, giving a wide spread of different gradients from gentle to steep. Again in this sample many of the mountain areas give higher standard deviations of gradient, generally greater than 10°. Lower areas with a more homogeneous set of slope forms seem to give standard deviations of gradient lower than 10°. The usefulness of the standard deviation of gradient as a distinguishing characteristic of particular types of landsurface will become more apparent when the statistical characteristics of individual surfaces studied here are discussed.

Skewness of gradient helps to reveal the predominance of steeper or gentler slopes in an area. In this sample skewness ranges from 2.298 for Montoire to -0.296 for

Keary. All but two of the gradient distributions have positive values for skewness and most of these are noticeably, if not strongly, skewed. The results agree with most other studies of gradient, finding most areas to have either Gaussian distributions of gradient or else positively skewed distributions (O'Neill and Mark, 1987). In the case of Montoire the reason for its high positive skew of gradient is immediately apparent. The steep slopes of the incised meanders cover only a small area in comparison with the gentle slopes of the valley floor and surrounding surface. The DEM Aigoual has the gradient distribution which is nearest Gaussian. In this mountainous example there are enough steep slopes to balance the more gentle slopes of the limited valley floors.

The first important moment statistic for the derivative, profile convexity, is the standard deviation. Mean profile convexity is always near zero, as expected, in the sample of DEMs in this study. Standard deviation of profile convexity ranges from 54.9°/100m for Aughwick, with a grid mesh of 30m, to 2.419°/100m for Devon, with a grid mesh of 100m. All the ridge and valley DEMs from Pennsylvania have high standard deviations even when grid mesh is taken into account (Uinta, for instance, has a standard deviation of 9.58°/100m and also has a 30m mesh). Reference to the perspective block diagrams of Chapter 6 (fig. 6.18-6.20) shows that there are several long ridges of high convexity in each, while each of the valleys is clearly concave. The amount of curvature in these areas is therefore of significance. Curvature in areas such as Dumfries, Galloway, Montoire, Le Porge and Devon is much less sharp leading to lower standard deviations.

Skewness of profile convexity ranges from 2.252 for Thvera to -2.372 for Gara. Positive skewness of profile convexity is likely where there is more area of concavity in a surface than of convexity. Thvera and all the other typical glaciated mountain areas have wide and concave glacial troughs, while ridges and arêtes separating these troughs are highly convex and narrow, thus producing a negatively skewed distribution. Gara, Devon, Montoire, Dumfries and Galloway on the other hand have gently convex hills which dominate the profile convexity distribution leaving a tail of higher concavities where the valley floors become the steeper slopes of the lower valley sides.

As was the case for profile convexity, the mean plan convexities for each of the DEMs are near to zero (certainly in relation to the ranges of each of the distributions). Le Porge has the highest standard deviation of plan convexity of this sample (1,256,897°/100m). Although this value is much too high and must be the result of outliers in the distribution caused by data error, the area would still be expected to have the highest value. The reason for this is visually immediately apparent. The coastal dunes of this area are the smallest clearly defined landforms encountered in the study. There is a large number of these convex features. Therefore within a very small distance contours are changing direction very rapidly, thus giving a wide range of plan convexity

and concavity. Reunion produces the lowest standard deviation of plan convexity, 26.4°/100m. The overall island is a convex feature but it achieves its shape over a long enough distance to keep convexities small.

Eleven of the DEMs yield positive skewness of plan convexity while sixteen exhibit negative skew. It is difficult to explain the extreme negative and positive values of skewness of plan convexity for this sample. Devoluy has the maximum negative skew -198.9 suggesting that there is more plan convexity than plan concavity. Certainly the dominant synclinal feature of the DEM shows some convexity as do the many spurs entering the main valley of the DEM. However it is difficult to perceive any obvious dominance of convexity over concavity. Aughwick with a skewness of 36.2 is the highest positive value. The linearity of ridges and valleys in this DEM does not bring to mind plan curvature at all and again the dominance of plan concavities is not visually obvious.

In many of the more moderately skewed examples the reasons for positive or negative skew can be seen more clearly. The glaciated mountains Keary, Wind, Nupur and Thvera all have positive skewness caused by the concavities of glacial cirques. Dumfries, Galloway and Le Puy with their convex hills and Appleby with its drumlins have definite negative skewness of plan convexity.

Looking briefly at the gradient weighted vector strength of aspect, it can be seen that most of the surfaces yield low strengths. The highest values are obtained for the DEMs which are sections of drainage basins. The means are in the direction of the main channels. Booro Borotou, Netherhearth Sike, Glaisdale and Wheeldale all fall into this category. The lowest strength is not surprisingly found in the case of Reunion Island. As a an island it has similar slopes in every direction.

Of the Pearson's correlation coefficients between pairs of derivatives, the correlations between estimated altitude and gradient, and between estimated altitude and profile convexity, are the highest encountered. Glaisdale yields the highest correlation coefficient for estimated altitude and gradient, 0.72. This is caused by the simple form of the DEM's valley sides. The limited parts of the valley sides which are represented steepen with estimated altitude therefore producing this high correlation coefficient. As the areas under consideration become more complex in form the correlation coefficients become lower. In the case of Torridon which yields the second highest correlation coefficient, 0.547, the same principle applies as in the example of Glaisdale. Glacial trough floor gradients are low, followed by steep mountain sides. However the convexity of the ridges leads to more gentle slopes along the ridge tops, which brings down the correlation coefficient.

Montoire has the lowest correlation coefficient for estimated altitude and gradient, 0.013. This results from the fact that although there are gentle slopes on the valley floor and steeper slopes climbing out of the valley, there are further extensive gentle slopes above the main channel meanders. Thus no relationship between altitude and gradient is suggested by the resulting correlation coefficient. In fact the relationship between these variables for some idealised slope profiles could be considered almost S-shaped. Keary, a glaciated mountain area, yields the second lowest correlation coefficient for these variables (0.036). In it and other mountain DEMs with low correlation coefficients such as Wind, Nupur, Thvera, Canigou and Aigoual, the steep slopes' absolute positions in terms of altitude vary over the areas of the DEMs, and although gentler slopes may be in the valleys and steeper slopes on the valley sides, different valleys and valley sides have different altitudes, resulting in these low coefficients.

These are the reasons for most of the high and low positive correlations. In the cases of Gara, Galloway, and Devon the correlation coefficients are noticeably negative. In the case of Galloway the majority of gentle slopes are in fact on ridges, only a minority of gentle slopes make up the valley floors. The steeper slopes are therefore generally at lower levels than most of the gentle slopes. A negative correlation coefficient of -0.348 results. Similar situations occur in Gara and Devon.

The other pair of variables producing noticeably high correlation coefficients are estimated altitude and profile convexity. The relationship between altitude and profile convexity follows logically from the relationship between altitude and gradient. Having stated that the relationship between altitude and gradient can be S-shaped, given an area considered a valley bottom to a ridge top, the valley bottom possesses the greatest concavity, while the straight steep slopes of the valley side have near zero curvature and the ridge tops have the greatest convexity, giving a positive relationship between altitude and profile convexity. Of course many of the DEMs cover several valleys complicating the altitude part of the relationship while some, as was mentioned in the case of Glaisdale, only include the valley bottom sections of the drainage basin, thus limiting the amount of convexity associated with interfluves. Wind and Nupur have the joint highest correlation coefficient between the variables, estimated altitude and profile convexity, 0.469, for exactly the reasons suggested above. There are no negative correlation coefficients.

7.4 The geomorphometric characteristics of different landsurface types.

As a prelude to categorising the DEMs on the basis of their geomorphometry, a summary of the characteristics of each DEM will be made. This will proceed in the order in which the DEMs were introduced in Chapter 5.

The first important characteristic of Torridon is its high positive skew of altitude, caused by the much larger width of glacial troughs compared with ridges. In agreement with this is the positive skew of gradient, lower gradients in the dominant troughs, steeper slopes on the mountain sides. These values of skewness are consistent with the high (in terms of this study) positive correlation coefficient for estimated altitude and gradient, and also with the reasonably high coefficient between altitude and profile convexity. Moment statistics for profile convexity are not extreme: positive skew however corresponds to the large concave glacial troughs and the narrower convex ridges. Plan curvatures are small indicating the elongated peaks and their overall convex form.

Keary's high standard deviation of altitude identifies this area as mountainous. Very high average gradient indicates the roughness and mountainous nature of the area. The correspondingly high standard deviation of gradient hints at the contrasted topography of glaciated mountains. Skewness of altitude being negative suggests that there may be a lower river channel or glacial trough that adds a tail of low altitudes to the distribution and indeed there is a flood plain in the northeast of the area. Profile convexity is positively skewed, in agreement with the curvature of cirques. The positive correlation between altitude and profile convexity is just noticeable. This weak correlation, considering the glaciated mountain nature of the DEM, the negative skew of altitude and the strength of the vector mean of aspect reveal that the area's slopes trend towards the northeast.

Wind River also has high standard deviation of altitude, again classing it as a high mountain area. Low negative skew of altitude again indicates the area trends towards the lower extreme. High mean and standard deviation of gradient indicates the contrasted topography of glaciated mountains. Positive skew of profile convexity corresponds to glacial erosion of cirque forms and troughs. Fairly low standard deviation of profile convexity is caused by the dominance of straight steep slopes. Plan convexity has high positive skew, again related to the form of cirques.

In the case of Nupur the high standard deviation indicates the mountainous nature of the DEM. The high standard deviation of gradient indicates the contrasted topography of glaciated mountains. Skewness of altitude is slightly negative. This is caused by the fact that Nupur is a plateau which is dissected by glacial troughs. Therefore, rather than the narrow ridges associated with many glaciated mountain areas, there are reasonably large areas at high altitude. Profile convexity and plan convexity are both positively skewed corresponding to cirque forms of the area.

Thvera has reasonably high standard deviation consistent with the range of altitude associated with mountain areas. Negative skew of altitude is caused by the two

deepest glacial troughs of the surface. High mean and standard deviation of gradient corresponds with the mountainous topography. Profile convexity is positively skewed because of the concavity of glacial troughs. Likewise plan convexity has high positive skew because of the cirques in the DEM.

Dumfries has a much smaller standard deviation of altitude compared with the mountain areas discussed above. High positive skew of altitude shows the effect of the lowland to the south. Mean of gradient is low with a corresponding high positive skew. The area to the south is formed by gentle slopes while at the top of the steeper slopes of the hills to the north more gentle slopes are found. The standard deviation of gradient is however high in relation to the mean. This is due to the contrast in topography between the lowlands to the south and the uplands to the north. Profile convexity is negatively skewed due to the convexity of the hills in the DEM. The surface has a strong negative skew for plan convexity. This is the result of the convexity of the spurs of the upland adjoining the lowland. These are not balanced by the concavity of valley heads which are not included in the DEM. There is a relatively high correlation for the variables altitude and gradient.

Galloway again has negative skew of altitude. In this case most of the area is upland and only a few rivers dissect it deeply. A low mean of gradient reflects the small area taken up by the steep slopes of the river valleys. As in the case of Dumfries gradient has high positive skew and plan convexity is once more negatively skewed. Profile convexity has high negative skew due to the convexity of the hills in the area and the relatively small area of concavity in the valley bottoms. The vector strength of aspect is noticeable and can be visually perceived from the block diagram (fig. 6.7). The correlation for altitude and gradient is negative, the steepest slopes being in the river valleys of the lower part of the DEM.

Uinta has the second highest mean altitude of the areas studied. It has a small standard deviation reflecting the small range in altitude. Low mean gradient with a low standard deviation indicates that the area is dominated by gentle slopes, this is the foothill zone of the mountains. Skewness of gradient is positive and high, the few steepest slopes can be clearly seen in figure 6.8. There is little profile curvature. Plan convexity has negative skew suggesting more convexity than concavity.

Devoluy has high mean and standard deviation of altitude, as expected for a mountain area. Skewness of altitude is highly positive. Clearly a tail of high altitudes is provided by the dominant synclinal mountain. Mean of gradient is suitably high for a mountain area, while its standard deviation is low due to the homogeneous form of the surface with many slopes of similar gradient. Positive skew agrees in this case with the skewness of altitude. The distribution of profile convexity for Devoluy is near normal

with only moderate standard deviation. The standard deviation of plan convexity is very large and the associated high negative skew is difficult to explain. Plan convexity does not look that dominant.

Canigou has the high mean and standard deviation of altitude of a mountainous area. The low negative skew is caused by the low lying valley in the north east corner. High mean and standard deviation of gradient also indicate the mountainous nature of the surface. The high positive skew of profile convexity is in keeping with the other glaciated mountains looked at so far. The high negative skew of plan convexity is however atypical of the glaciated mountains dominated by cirques. Many of the forms that might be cirques in the diagram of Canigou (fig. 6.10) possibly have quite low curvature while the spurs between them are reasonably wide and more strongly curved, convexly. This is perhaps the only explanation for this negative skew.

Mont Aigoual is thought to be an unglaciated mountain area. Its high mean and standard deviation of altitude identify it as a mountain area. The skewness of altitude is noticeably positive as would be expected of sharp peaks rising from flatter, lower lying areas to the northwest, northeast and southwest. As with other mountain areas the mean gradient is high. Standard deviation is also high but in this case this may be caused by the contrast between the flatter areas in the corners and the main mountainous area. Profile convexity has a high negative skew. The valleys are V-shaped rather than the broader more slowly concave troughs and cirques of the glaciated mountains. Plan convexity has a high positive skew.

Montoire has a low mean altitude with small standard deviation, reflecting its lowland position and relief. The mean and standard deviation of gradient are both very low indicating the gentle valley floors and low plateau areas. Gradient is positively and highly skewed. The tail of high gradient values of the distribution is provided by the steep meander sides. Profile convexity has noticeably negative skew: the convexity of the slopes at the top of, and above, the incised meanders dominates the distribution. The high negative skew of plan convexity must also be due to the convex nature of the undulations of the area, rather than the meanders themselves, as the curvature of one valley side should be approximately balanced by the other side. There is understandably a noticeable correlation for altitude and profile convexity.

For Le Puy the standard deviation is somewhere in the middle of the range of the sample of surfaces studied here. The high positive skew of altitude is caused by the volcanic peaks providing a tail of high altitudes to the distribution. Mean gradient is correspondingly low, while standard deviation is reasonably large for the range. This is due to the contrast between the steep slopes of the volcanic necks and the overall gentle slopes of the surrounding area. High positive skew of gradient follows from this. Profile

convexities are generally gentle. Plan convexity has high negative skew due to the convex shape of the volcanic plugs. There is a noticeable correlation between altitude and gradient obviously caused by the fact that the steeper slopes are on the sides of the volcanic plugs while the majority of low gradients are on the surrounding flatter area.

Le Porge has the lowest mean and standard deviation of altitude of the sample. It also has the highest positive skew of altitude. The dunes of this area act like the volcanic necks of Le Puy. Mean gradient is also the lowest of the study while standard deviation is also very low. Gradient in this DEM is limited by the angle of repose of the sediment making up the dunes and also smoothing caused by short steep slopes not being measured because of the grid mesh size. High positive skew is again inevitable as in Le Puy. Profile curvature is generally gentle. Standard deviation of plan convexity however is by far the highest in the study due, as previously mentioned, both error and the dunes being small convex landforms. This also leads to the very high positive skew of plan convexity.

Reunion Island has the highest altitude standard deviation of all the areas studied. It does of course range from sea level to volcanic peaks. Positive skew of altitude is due to the distorted but still basically conical slope of the island. The mean gradient is high given the mesh size of the DEM. This is probably related to the volcanic growth of the island. It is also positively skewed. Profile curvature is gentle but has noticeably negative skew due to the convex ridge of the island. Plan convexity is, as expected, for an island negatively skewed. There is a noticeable correlation between altitude and gradient.

In the case of St. Paul, standard deviation of altitude is relatively high in comparison to the mean. Clearly, as an island, the surface rises from sea level to the ridge of the volcanic crater visible in Figure 6. Skewness of altitude is high and positive, the ridge providing the tail of higher altitudes for the distribution. Mean gradient is reasonably steep, while the standard deviation of the distribution is quite high. The very steep inner slopes of the cauldera must raise the mean somewhat, and also must provide part of the tail of high gradients leading to the high positive skew of gradient.. Profile curvature is strong, and is accompanied by high positive skew. The slopes of the volcano are clearly concave. Plan convexity is also positively skewed, the reason for this being the strong concavities of the crater and some of the cliff lined bays of the island.

Booro Borotou has low standard deviation of altitude reflecting the low relief of the area. Mean gradient is low, as is gradient's standard deviation. Again this DEM shows high positive skew of gradient. There are only a few areas of steeper slopes towards the side of the drainage basin and near the actual channel, the rest of the area is

taken up by gentler slopes. Negative skew of profile convexity indicates that apart from the area between the steep slopes near the channel, slopes are convex. The shape of the drainage basin assures high negative plan convexity. Vector strength of aspect is reasonably strong because the basin drains in one resultant direction.

The ridge and valley topography of Aughwick displays the high mean and standard deviation of altitude associated with the mountain areas already studied. The sharp ridges and concave valleys ensure positive skew of altitude . The area has high mean and standard deviation of gradient; steep slopes up to the ridges are balanced by lower gradients in the valleys. Skewness is therefore low. High standard deviation of profile convexity is related to the almost constant change of gradient with altitude. Negative skew of profile convexity results from concave valleys being broader than convex ridges. High positive skew of plan convexity is difficult to explain and may be due to the quality of the DEM. There is a high correlation between gradient and altitude.

The altitude distributions of Belleville and Allenville are similar to that of Aughwick. In fact, they have higher positive skew. The means and standard deviations of gradient are again high. Skewness of gradient is however positive suggesting greater influence of the valley floor slopes than in Aughwick. Standard deviations of profile convexity are high indicating the magnitude of the valley concavities and the ridge convexities. Skews are low suggesting that convexities and concavities occupy similar portions of the DEMs surface. Plan convexities also have high standard deviations in the case of Belleville with high negative skew, but in the case of Allenville with positive skew. Once more the correlations between altitude and gradient are high.

Netherhearth Sike has a fairly low standard deviation of altitude as a result of the small range in altitude of the drainage basin. It has positive skew of altitude and gradient as a result of the much steeper upstream part of the DEM. Most of the rest of the DEM is lower lying with gentler slopes. Standard deviation and mean of gradient are both low, and the topography is very homogeneous. Profile convexity is negatively skewed suggesting that the steeper slope to the north of the DEM is convex as are the slopes out of the stream channel. Plan curvatures are very gentle. The vector strength of aspect is the highest in the sample due to the fact that the DEM is really a portion of one north facing slope of Teesdale (Bell, 1983).

Glaisdale has an even lower standard deviation of altitude, reflecting the DEM's small area and altitude range. High positive skew of altitude is caused by the small area of valley side on the western edge of the model. Mean gradient is low, as is standard deviation, while skew is positive reflecting the steeper slopes of the west side and southeast corner of the DEM. Standard deviation of profile convexity is relatively high, and most of the slopes are curved. Plan convexity has high negative skew indicating

that the contours of the valley sides are convex. There is a high correlation between altitude and gradient.

Once again, Wheeldale is another DEM with low standard deviation of altitude. For similar reasons to Glaisdale it also has positively skewed altitude. Mean and standard deviation of gradient are quite low. However skew of gradient is also low, the steeper slopes of the west side of the matrix balancing the gentler slopes of the rest of the matrix. Profile convexity and plan convexity are negatively skewed; again the slopes are convex both horizontally and vertically.

Devon has a low standard deviation of altitude reflecting the small range of altitude in the area. Altitude has however a near Gaussian distribution. The mean of gradient is very low, and the distribution has high positive skew. The steep slopes are the valley sides which take up much less area than the interfluves and the valley floors. In agreement with this, profile convexity is negatively skewed. Plan convexity is not surprisingly, nearly Gaussian. Also in agreement with the profile convexity and gradient distributions is the relatively high correlation between altitude and profile convexity.

Gara has certain similarities to Devon. Altitude is negatively skewed. Mean and standard deviation of gradient are quite high. Skewness of gradient is positive and along with high standard deviation indicates contrasted topography of the higher gentle plateau surface being dissected by steep valleys. Profile convexity has high negative skew due to the large area of convex slopes at the top of the valleys and on the plateau. Plan convexity is also negatively skewed. Both gradient and profile convexity are highly correlated with altitude.

Appleby has low mean and standard deviation of altitude. Gradient also has a low mean and standard deviation. However there is high positive skew of gradient corresponding to the large area covered by gentle slopes between and on top of drumlins. Profile convexity and plan convexity, as would be expected for an area of drumlins, have negative skew.

Alarta has a low standard deviation of altitude. Mean gradient is very low as is standard deviation of gradient. It has relatively high positive skew, the channel floors of the DEM covering more than the steeper slopes. Alarata has low standard deviation of profile convexity which is positively skewed. The slopes in the DEM are reasonably straight but there must be a larger area taken up by concave valley floor to valley side slopes than convex summits. Positive skew of plan convexity indicates that there is slightly more concavity of contours than there is convexity.

Clearly from this DEM by DEM discussion, similarities in the geomorphometry of certain areas emerge. As a result, many of the surfaces can be grouped together into categories based on the geomorphometric statistics discussed.

The glaciated mountain areas are one group which share certain characteristics. They have high mean and standard deviation of altitude and gradient, identifying them as mountainous. The cirque and trough forms result in positively skewed profile and, usually, plan convexity. Torridon, Keary, Wind, Nupur, Thvera and Canigou display either all or most of these properties.

'Dissected lowland or upland areas' is a very loose grouping. It would include much of the non-mountainous area of Britain. The dissection could be that found in the mature stages of a river course or glaciated lowland or upland. The geomorphometric characteristics are: moderate standard deviation of altitude; high positive skew of gradient; low to negative skew of profile convexity; and often negative skew of plan convexity. DEMs falling into this class would be Montoire, Devon, Gara, Appleby, Dumfries and Galloway.

Clearly the ridge and valley topography of the Appalachian mountain DEMs, Aughwick, Belleville and Allenville, gives rise to certain geomorphometric characteristics. High mean and standard deviation of altitude, as in all mountains, is present. High mean and standard deviation of gradient are also common to all mountain areas. Skewness of altitude is highly positive. Skew of gradient is either low or positive. Profile convexity has high standard deviation and there is high (for geomorphometry) correlation between altitude and gradient.

The other category that several DEMs in this study fall into is determined by the small scale at which terrain is being studied. The high resolution DEMs representing parts of, or small drainage basins can be grouped together. This group tends to have: low standard deviation of altitude; positive skew of altitude; positive skew of gradient; negative skew of profile convexity; and high strength of vector mean of aspect. Booro Borotou, Netherhearth Sike, Wheeldale and Glaisdale are all DEMs in this category.

These are loose groupings which could be more carefully defined given a larger sample of landsurfaces. Reunion, St. Paul, Uinta, Aigoual, Devoluy, Le Puy, Le Porge and Alarta are all unique in this study. It could be foreseen however that Aigoual would probably have typical statistics for a non-glaciated mountain range, while Le Porge might be typical of coastal dunes. This study of the form of real landsurfaces shows that, although complex, many of the landsurfaces show a certain order in the form of the characteristic geomorphometric statistics which they yield. This by itself does not go far in answering the question of why these surfaces do not demonstrate perfect fractal

properties. It is therefore necessary to look at the geomorphometry of fractal surfaces to identify any major difference between real and simulated surfaces.

7.5 The geomorphometry of fractal surfaces.

One of the major purposes of looking at the geomorphometry of simulated fractal surfaces is to see how their geomorphometry changes with changing fractal dimension. The geomorphometric characteristics of simulated surfaces produced by FRACSIM.FOR cannot be directly compared because with each run the process used produces surfaces, with possibly widely varying 'altitude' ranges (altitude is an artificial term here and used to associate the z-value produced by the process with the real world concept of altitude).

To allow comparison of surfaces, the altitude range of each surface was scaled to between 0 and 1. Furthermore to allow the geomorphometric values of the simulated surfaces to be more comparable to the kind of values found in real landsurfaces each rescaled altitude was multiplied by 500. Thus the eventual range of each simulated surface becomes 0 to 500, allowing comparison with real surfaces with an altitude range of 500m. To continue in making the values of the simulated surfaces' geomorphometry comparable to real landsurfaces, an arbitrary grid mesh of 50m was used when running the simulated surfaces through the terrain analysis program.

As expected for surfaces that are produced by a process which produces a specified degree of irregularity and roughness, there are several relationships immediately evident between fractal dimension and geomorphometric variables. In order to look more closely at these relationships the Pearson's correlation coefficients between fractal dimension and each of the geomorphometric variables were calculated. The geomorphometric statistics for each simulated surface are presented in Table 7.2. The correlation coefficients are presented in Table 7.3, (a) and (b). One set of correlation coefficients is calculated using all the surfaces' results (Table 7.3a), while another set has been calculated without the influence of the two most common outliers, surfaces with fractal dimension 2.9 and 3.0. The reason for this will soon become apparent.

Mean estimated altitude for the surfaces ranges from 393 to 229. Clearly the ranges are all similar. However it must be remembered that estimated altitude is calculated from 3x3 neighbourhoods of values in the models. The estimated altitude is therefore a smoothed version of the original altitude values. There is no real relationship between fractal dimension and mean estimated altitude.

Table 7.2 Geomorphometric statistics for simulated surfaces

D	ALT 1	ALT 2	ALT 3	GRAD 1	GRAD 2	GRAD 3	PROF 2	PROF 3	PLAN 2	PLAN 3	ALT. GRAD	ALT. PROF
3.0	393	7.977	0.729	4.388	3.551	3.344	22.819	-0.214	1023.7	61.454	-0.026	0.449
2.9	232	21.518	0.116	9.864	5.933	1.193	39.942	0.207	561.3	4.481	-0.08	0.395
2.8	229	70.882	0.118	22.122	11.167	0.408	69.182	0.032	461.2	-1.325	-0.002	0.273
2.7	258	75.668	0.035	21.163	10.94	0.514	58.682	-0.027	452.4	3.701	-0.072	0.249
2.6	260	93.492	0.159	15.15	8.25	0.698	39.598	0.015	361.6	-1.09	-0.111	0.147
2.5	232	104.685	0.242	16.02	8.848	0.693	37.473	-0.021	311.5	2.463	0.021	0.136
2.4	243	96.098	0.019	17.743	9.304	0.522	33.634	0.044	336.88	17.48	-0.109	0.171
2.3	249	107.952	0.051	9.704	5.386	0.732	18.209	0.007	259.3	8.002	0.034	0.076
2.2	251	112.712	0.088	12.506	7.011	0.76	17.312	0.024	194.34	1.899	0.067	0.133
2.1	259	132.008	0.008	9.214	5.355	0.877	11.19	0.021	158.95	-6.427	0.012	0.086
2.0	292	121.637	0.349	5.314	2.649	0.791	3.568	0.057	64.53	2.801	-0.13	0.07

D *Fractal Dimension*
ALT 1 *Mean Estimated Altitude*
ALT 2 *Standard Deviation of Altitude*
ALT 3 *Skew of Altitude*
GRAD1 *Mean Gradient*
GRAD2 *Standard Gradient*
GRAD3 *Skew of Gradient*
PROF2 *Standard Deviation of Profile Convexity*
PROF3 *Skew of Profile of Convexity*
PLAN2 *Standard Deviation of Plan Convexity*
PLAN3 *Skew of Plan of Convexity*
ALT.GRAD *Correlation between Altitude and Gradient*
ALT.PROF *Correlation between Altitude and Profile Convexity*

Table 7.3(a) Correlations for all simulated surfaces

	D	ALT 1	ALT 2	ALT 3	GRAD 1	GRAD 2	GRAD 3	PROF 2	PROF 3	PLAN 2	PLAN 3	ALT. G
ALT 1	0.237											
ALT 2	-0.916	-0.443										
ALT 3	0.362	0.879	-0.529									
GRAD 1	0.239	-0.623	0.101	-0.564								
GRAD 2	0.312	0.593	0.032	0.532	0.992							
GRAD 3	0.468	0.900	-0.678	0.862	-0.634	-0.566						
PROF 2	0.686	-0.370	-0.396	-0.236	0.843	0.861	-0.270					
PROF 3	-0.211	-0.757	0.184	-0.650	0.153	0.113	-0.629	0.085				
PLAN 2	0.892	0.615	-0.929	0.639	-0.097	-0.015	0.796	0.348	-0.510			
PLAN 3	0.487	0.855	-0.659	0.800	-0.419	-0.362	0.899	-0.142	-0.704	0.811		
ALT. G	-0.120	-0.113	0.181	-0.101	-0.002	0.039	0.041	-0.098	-0.245	-0.054	-0.050	
ALT. P	0.908	0.428	-0.980	0.495	-0.034	0.037	0.659	0.439	-0.197	0.922	0.630	-0.136

Table 7.3(b) Correlations for simulated surfaces except for outliers

	D	ALT 1	ALT 2	ALT 3	GRAD 1	GRAD 2	GRAD 3	PROF 2	PROF 3	PLAN 2	PLAN 3	ALT. G
ALT 1	-0.623											
ALT 2	-0.943	0.489										
ALT 3	-0.204	0.408	0.178									
GRAD 1	0.928	-0.687	-0.909	-0.352								
GRAD 2	0.919	-0.725	-0.875	-0.386	0.994							
GRAD 3	-0.835	0.539	0.937	0.215	-0.895	-0.849						
PROF 2	0.978	-0.610	-0.952	-0.215	0.958	0.938	-0.890					
PROF 3	-0.479	0.376	0.309	0.216	-0.405	-0.458	0.109	-0.410				
PLAN 2	0.979	-0.656	-0.938	-0.372	0.952	0.948	-0.861	0.962	-0.482			
PLAN 3	0.016	-0.137	-0.190	-0.169	0.149	0.132	-0.368	-0.003	0.139	0.137		
ALT. G	-0.068	-0.534	0.190	-0.306	-0.032	0.024	0.213	-0.069	-0.335	-0.060	-0.292	
ALT. P	0.877	-0.514	-0.922	-0.274	0.950	0.920	-0.911	0.950	-0.266	0.883	0.033	-0.093

D *Fractal Dimension*
ALT 1 *Mean Estimated Altitude*
ALT 2 *Standard Deviation of Altitude*
ALT 3 *Skew of Altitude*
GRAD1 *Mean Gradient*
GRAD2 *Standard Gradient*
GRAD3 *Skew of Gradient*
PROF2 *Standard Deviation of Profile Convexity*
PROF3 *Skew of Profile of Convexity*
PLAN2 *Standard Deviation of Plan Convexity*
PLAN3 *Skew of Plan of Convexity*
ALT.G *Correlation between Altitude and Gradient*
ALT.P *Correlation between Altitude and Profile Convexity*

Standard deviation of estimated altitude is however closely related to fractal dimension. A correlation of -0.916 is obtained. As fractal dimension becomes smaller, that is the surfaces becomes smoother, standard deviation of altitude becomes larger. In the case of a fractal surface with fractal dimension 2.9, for instance, there are very few slopes formed by more than three grid points. The surface is formed from alternating pits and peaks. The faulting process used to create the surface ensures that it is unusual for the same point to be uplifted or displaced downward by several iterations. As a result the surface alternates up and down closely about the mean altitude. The resulting standard deviation is therefore small. For a fractal surface of 2.1 however trends have developed in the surface. Long slopes occur due to the shape of the perturbations used in the generation process. Therefore, altitude becomes more widely spread about the mean and the surface yields a high standard deviation.

Skewness of altitude is generally low. There is a high negative skew for the surface with fractal dimension 3.0. This is because of the smoothing the surface goes through when estimated altitude is calculated. Reference to the perspective block diagram of this surface (fig. 5.12) reveals several large upward and downward spikes. The smoothing effect is particularly great on these extremes. The most extreme spike is downward and the removal by the smoothing process of this and possibly other outliers in the distribution is enough to give this negative skew and to push up the mean. Many of the other geomorphometric statistics are influenced by this smoothing effect and the two surfaces with the highest fractal dimensions, 3.0 and 2.9, are consistently seen as outliers in the distributions of the statistics for the sample of simulated surfaces.

The surface with fractal dimension 2.0 has a noticeable positive skew. From Figure 5.2 this can be seen to result from the slight hump in the DEM left by one of the more extreme faults in the generation process. This slight perturbation of an otherwise smooth surface would probably have disappeared if the generation process had included more iterations.

The correlation between mean gradient and fractal dimension, if the two roughest surfaces are omitted from the calculations, is 0.928. Generally steeper slopes are associated with rougher surfaces of higher fractal dimension. Standard deviation of gradient declines with fractal dimension. The correlation without the influence of the two roughest surfaces is 0.919. Skewness of gradient is quite highly positively skewed in all cases. When the surfaces with fractal dimension 2.9 and 3.0 are set aside there is a correlation of -0.835 between skewness of gradient and fractal dimension. Fewer areas of lower gradient are found in the rougher surfaces.

Standard deviation of profile convexity is also highly correlated with fractal dimension. A correlation of 0.686 with all the surfaces included, rises to 0.978 when the

two roughest surfaces are omitted. Clearly profile curvature is more extreme for the rougher surfaces. Interestingly skewness of profile curvature is always low.

A similarly high correlation, 0.979, is obtained between fractal dimension and standard deviation of plan convexity (0.892 if all surfaces are included in calculations). The rougher surfaces can be seen from the perspective block diagrams to have a much greater degree of plan convexity. Skewness of plan convexity is always high, and it is negative for only two surfaces, the surfaces with fractal dimensions 2.6 and 2.1. The large ranges of plan convexity for the fractal surfaces and the generally high standard deviation of altitude hint at the fact that extreme values of convexity or concavity can lead to high skew.

Of the correlations between derivatives of altitude, the variables altitude and profile convexity produced the highest. The surfaces with the highest correlation between these variables are in fact the two which have been outliers in most of the other distributions. For similar reasons to those given for real landsurfaces none of these correlations are particularly high: however they do vary consistently with fractal dimension. When all surfaces are included the correlation coefficient between fractal dimension and the correlation between altitude and profile convexity is 0.908. The alternation between peaks and pits in the rough surfaces with peak convexities and pit concavities occurring in two different bands of altitude separated by a band of altitude containing straight slopes results in the higher correlation than in the smoother surfaces where the altitudes of convexities and concavities vary more.

Strength of vector mean of aspect increases with decreasing fractal dimension. This is because the smoother the surfaces the more dominant certain faults in the generation process become leading to trends in the direction of slopes in the surface.

7.6 Differences in geomorphometry between real and simulated surfaces.

Having described the basic geomorphometric properties of fractal surfaces of different fractal dimension, it is now possible to begin identifying the fundamental differences between the geomorphometry of real landsurfaces and the geomorphometry of fractal surfaces. As an aid to this the correlations between the geomorphometric statistics of the real landsurfaces were also calculated. As previously mentioned many of the geomorphometric statistics calculated are partially dependent on grid mesh size. As a result correlation coefficients were also calculated for the statistic of DEMs with grid mesh size of 30-50m and 100-200m. They are presented in Tables 7.4-7.6.

Table 7.4 Correlations for all real surfaces

	D	ALT 1	ALT 2	ALT 3	GRAD 1	GRAD 2	GRAD 3	PROF 2	PROF 3	PLAN 2	PLAN 3	ALT. G
ALT 1	0.070											
ALT 2	-0.019	0.454										
ALT 3	-0.305	-0.336	-0.021									
GRAD 1	-0.030	0.418	0.750	-0.076								
GRAD 2	0.035	0.312	0.740	0.062	0.935							
GRAD 3	0.066	-0.388	-0.472	0.087	-0.778	-0.617						
PROF 2	-0.351	0.041	0.317	0.370	0.635	0.613	-0.535					
PROF 3	0.114	0.038	0.161	-0.282	0.231	0.244	-0.190	-0.209				
PLAN 2	-0.299	0.188	-0.202	0.367	-0.239	0.244	0.200	-0.178	0.008			
PLAN3	0.160	0.174	0.198	0.177	0.287	0.258	-0.310	0.328	0.058	-0.530		
ALT. G	-0.324	0.052	0.214	0.766	0.109	0.176	-0.109	0.210	0.112	0.184	-0.090	
ALT. P	0.540	0.082	0.001	-0.452	0.123	0.139	-0.075	0.391	0.295	0.244	-0.238	-0.401

Table 7.5 Correlations for real surfaces: grid meshes 30–50m

	D	ALT 1	ALT 2	ALT 3	GRAD 1	GRAD 2	GRAD 3	PROF 2	PROF 3	PLAN 2	PLAN 3	ALT. G
ALT 1	-0.722											
ALT 2	-0.509	0.563										
ALT 3	-0.141	-0.282	0.087									
GRAD 1	-0.193	0.289	0.912	0.083								
GRAD 2	-0.036	0.158	0.816	0.191	0.950							
GRAD 3	0.240	-0.408	-0.891	-0.120	-0.898	-0.799						
PROF 2	-0.082	0.080	0.700	0.384	0.839	0.849	-0.713					
PROF 3	-0.109	0.258	0.069	0.077	-0.081	-0.021	0.179	-0.252				
PLAN 2	-0.296	-0.326	-0.387	0.446	-0.401	-0.445	0.271	-0.307	0.069			
PLAN 3	0.162	0.290	0.412	-0.094	0.518	0.544	-0.403	0.574	-0.019	-0.501		
ALT. G	-0.595	0.207	0.347	0.782	0.135	0.152	-0.159	0.283	0.323	0.241	-0.054	
ALT. P	0.462	-0.633	-0.525	-0.240	-0.358	-0.414	0.333	-0.473	-0.291	0.497	-0.575	-0.554

Table 7.6 Correlations for real surfaces: grid meshes 100–200m

	D	ALT 1	ALT 2	ALT 3	GRAD 1	GRAD 2	GRAD 3	PROF 2	PROF 3	PLAN 2	PLAN 3	ALT. G
ALT 1	0.598											
ALT 2	-0.149	0.489										
ALT 3	-0.099	-0.410	-0.403									
GRAD 1	-0.130	0.524	0.970	-0.449								
GRAD 2	-0.218	0.415	0.822	-0.268	0.919							
GRAD 3	-0.091	-0.538	-0.857	0.530	-0.905	-0.769						
PROF 2	-0.206	0.395	0.961	-0.420	0.986	0.911	-0.893					
PROF 3	-0.263	0.154	0.410	-0.405	0.507	0.563	-0.563	0.500				
PLAN 2	-0.122	-0.485	-0.556	0.058	-0.688	-0.772	0.762	-0.648	-0.524			
PLAN 3	0.151	0.453	0.324	-0.626	0.345	0.114	-0.585	0.301	0.353	-0.293		
ALT. G	-0.057	0.001	0.069	0.745	0.054	0.209	0.009	0.059	0.138	-0.375	-0.271	
ALT. P	0.024	0.435	0.284	-0.431	0.489	0.636	-0.472	0.432	0.348	-0.652	0.267	-0.246

D	*Fractal Dimension*	PROF2	*Standard Deviation of Profile Convexity*
ALT 1	*Mean Estimated Altitude*	PROF3	*Skew of Profile of Convexity*
ALT 2	*Standard Deviation of Altitude*	PLAN2	*Standard Deviation of Plan Convexity*
ALT 3	*Skew of Altitude*	PLAN3	*Skew of Plan of Convexity*
GRAD1	*Mean Gradient*	ALT.G	*Correlation between Altitude and Gradient*
GRAD2	*Standard Gradient*	ALT.P	*Correlation between Altitude and Profile Convexity*
GRAD3	*Skew of Gradient*		

Clearly mean estimated altitude for the simulated surfaces was made to be realistic and the associated standard deviations of altitude are well within a plausible range, given the range of altitude. For real landsurfaces altitude is often strongly skewed while in these simulated fractal surfaces there is no skew of altitude. The positive skewness of altitude in real landsurfaces is of particular interest in this study.

In general positive skewness of altitude is caused by a landform or landforms rising above a more extensive lower lying area. This is immediately at odds with the fractal view of similar irregularities occurring at all scales. The fact that landforms of widely differing scales can produce high positive skew is rather ironic. The large synclinal mountain feature of Devoluy, the widely separated mountains of Torridon, the ridges of Aughwick, Belleville, and Allenville are all large scale examples of landforms producing high positive skew. The volcanic plugs of Le Puy are at a smaller scale while the dunes of Le Porge are the smallest of all.

Although the mean gradients of the simulated surfaces are within reason in comparison with possible real surfaces, the nature of their decline with fractal dimension is not echoed in reality. Rather the real surfaces split into two groups: high mean gradient, generally in mountain areas; and much lower mean gradient found in upland and lowland areas. Indeed the correlations between the estimated fractal dimensions of the real landsurfaces and their mean gradients are very low (-0.03 for calculations including all surfaces, -0.13 for the 100-200m mesh surfaces and -0.193 for surfaces with meshes of 30-50m)

In the case of standard deviation of gradient the simulated surfaces again produce a range of values similar to that of the real landsurfaces. Once more the correlation between gradient standard deviation and fractal dimension for the real landsurfaces is much lower than for the simulated surfaces (0.035 for all surfaces, -0.218 for the 100m to 200m grids and -0.036 for the 30-50m grids).

Skewness of gradient for simulated surfaces, although always positive is never as high as the highest positive skew of the real landsurfaces. Neither does the skew of simulated surfaces become as small as for the real landsurfaces. This is again caused by effects of scale in geomorphology. For instance none of the simulated surfaces have steep-sided valley slopes within an area of much more gentle slopes such as is found in Galloway, Montoire or Devon. The irregularity, of an otherwise smooth surface, caused by features of the drainage network at one scale, have no equivalent irregularities when scale is changed: this is clearly evidence against the suggestion that real landsurfaces can be considered fractional Brownian surfaces. The correlations between fractal dimension and the skewness of gradient for real landsurfaces are all low, unlike the

strong negative correlation found between the same variable for simulated fractal surfaces.

Once again the actual values produced by real landsurfaces and simulated surfaces for standard deviation of profile convexity are similar. This is of course partly due to the ranges of altitude being calibrated to range from 0 to 500. Perhaps the values for the rougher simulated surfaces are too high to be found in real landsurfaces, certainly in the landsurface types looked at in this study. Yet again the real landsurfaces show no signs of a relationship between fractal dimension and profile curvature. The highest correlation coefficient is -0.351, obtained when all the surfaces are included in the calculations. If any relevance was put on this figure it would have to be noted that it suggests that magnitude of plan curvature decreases as the surface becomes rougher. This is unlike the situation for simulated surfaces where there is an increase in the magnitude of curvature with an increase in fractal dimension.

Skewness of profile convexity reveals the largest discrepancies between real and fractal surfaces as far as profile convexity is concerned. The lack of skew in the case of the simulated surfaces contrasts with the high positive and negative skews found in the case of real landsurfaces. Once again it is the forms of certain sets of landforms caused by certain sets of geomorphic processes which produce these skewed distributions of profile convexity. The concave glacial troughs and cirques of the glaciated mountain area of Thvera for example lead to very high positive skew of profile convexity. The convex drumlins of Appleby lead to negative skew in its case. Angle of bedding and rock type itself play an important part in the way the hills in the Dumfries DEM have been eroded into gently convex forms that push the distribution of profile convexity to a negative skew. Fractal surfaces on the other hand have pits balanced by peaks, ridges balanced by valleys.

As for profile convexity, the standard deviations of plan convexity for fractal surfaces would not be seen as abnormal for real landsurfaces, although this is expected because of the imposed altitude range. Once again the differences become apparent when the correlations between fractal dimension and standard deviation of plan convexity for real and fractal surfaces are compared. The high positive correlation of the simulated surfaces is replaced by very weak correlations for the real surfaces (-0.299 when all surfaces are used, -0.122 for the 100-200m grids and 0.162 for the 30-50m grids).

Skewness of plan convexity for real surfaces was shown earlier to be related, yet again, to the shapes of the landforms created by certain processes. In the case of simulated fractal surfaces, although there is mainly positive skew, there seems to be no link between skew and fractal dimension.

The one statistic looked at in this approach to geomorphometry where there is agreement between fractal and real landsurfaces is the correlation between altitude and profile convexity which is not surprisingly high.

7.7 Conclusions.

Geomorphometric analysis, involving the derivatives of altitude calculated from a gridded DEM, allows detailed examination of landsurface form. When a real landsurfaces is studied by this method certain statistics are often found to be particularly characteristic of the landsurface form. The value of a particular characteristic statistic is often caused by forms which have been discussed by geomorphologist as particular landforms.

Even with the small number of landsurfaces studied here, some classification of the surfaces can be made on the basis of their geomorphometric statistics. For instance the glaciated mountain areas become a clear grouping because of the influence on their statistics of glacial cirque and trough forms.

The simulated fractal surfaces cannot be classified in this manner. Instead many of the geomorphometric statistics for the fractal surfaces have a close relationship to the fractal dimension of the surfaces. Correlations between geomorphometric statistics and fractal dimension for real landsurfaces are, however, all poor.

Although the simulated surfaces are generated by the superimposition of planes with only one shape, the form of the plane on the geomorphometric statistics has nothing like the effect produced by landform types in real surfaces.on the statistics The combined effects of landforms on the geomorphometric statistics of landsurfaces are much more complicated than the effect of the superimposition of planes in the fractal surfaces. Their effect on the fractal dimensions estimated from landsurfaces is also much more complicated and as a result correlations between geomorphometric statistics and fractal dimension for real landsurfaces are low.

The geomorphometry of fractal surfaces is therefore markedly different to that of real landsurfaces. Some of the differences arise from the effects of landforms. Some of these effects are related to the scale of these landforms. The next chapter looks briefly at the scale of certain landforms.

Chapter 8: The Scale of Some Specific Landforms.

8.1 Introduction.

The findings of the last chapter support the traditional approach of geomorphologists of subdividing landsurfaces into landforms. For example, chapter 7 showed that there are certain geomorphometric characteristics common to most of the glaciated mountain landsurfaces studied. The domination of concave curvatures in these surfaces results from the presence in these areas of glacial cirques and troughs. These geomorphometric characteristics are absent in simulated fractional Brownian surfaces. Support for the traditional approach is further strengthened by the evidence given by the variograms. They suggest that real landsurfaces cannot be considered as irregular fractal surfaces when distances of kilometers are being considered.

The difference in the geomorphometric characteristics of landsurface types and the behaviour of the variograms for complete areas, subareas and separate directions, indicate that landsurfaces have definite order to their complexity. This order would appear to be much greater than the self-affine irregularity of fractional Brownian surfaces. However, could a surface be made up of a landform type which occurs at a wide enough range of scales to produce fractal behaviour be envisaged?

This possibility would seem remote to most geomorphologists. They would place most landforms in a more narrow scale range in accordance to the scale at which the processes thought to create them operate. Although most landsurfaces are not made up of only one landform type, there are examples in this study of surfaces which are dominated by one landform type. The DEM of the drumlinised area around Appleby, Cumbria was created mainly because of the domination of the area by drumlins. The Le Porge area is almost flat except for the belt of coastal dunes which make this surface of interest. Le Puy is also dominated by one landform type, volcanic peaks.

It would therefore seem appropriate to analyse the landforms within these surfaces to find out over what scale range they exist in these particular areas. This will not prove that no landforms can occur over a wide range of scale, but if these landforms do not exist over a wide scale range it is yet more empirical evidence in support of the more traditional geomorphological view of landforms.

This chapter will review approaches towards identifying and studying the size distributions of landforms. On the basis of this discussion, methods to isolate drumlins, dunes and volcanic peaks from the three surfaces mentioned above will be developed and various aspects of the size of individual landforms will be studied.

8.2 Possible approaches to identifying landforms.

Evans (1985) describes the study of the morphometry of landforms as specific geomorphometry. Due to the landform-based studies of many geomorphologists, there is a vast body of work studying the morphology of landforms, often trying to relate form to process. Some of this work has studied the distributions of various size parameters.

The properties of these distributions of landforms may reveal stronger influences on a landsurface at one particular scale compared with at a larger or smaller scale. One example of a landform type which would be suspected of having more influence on a landsurface over a limited scale range would be the glacial cirque. Cirques can certainly be seen to have an effect on the geomorphometric statistics of the glaciated mountain areas studied in chapter 7. Much work has been done on the morphometry of cirques. As a result, the cirque as a landform has been carefully defined by the B.G.R.G. (Evans and Cox, 1974).

Studies, such as that by Bennett (1990) of the cirques of Snowdonia, suggest that cirques in particular areas have quite limited size distributions. Bennet (1990) finds that cirque amplitude as well as having a limited distribution, possess bimodality which can be related to how well defined the cirque form is. Evans (1990) believes the Lake District cirques fall into quite a clearly definable scale range. Evidence such as this would therefore suggest that many landforms do not occur at a wide enough scale range to fit conceptually with the fractal model.

Clearly there are some common problems encountered when studying any landform. One of the immediate problems encountered in the study of individual landforms is the level of subjectivity which may be involved in deciding what is a particular landform and what is not. Evans (1985) in his discussion of the stages of specific geomorphometric analysis mentions several stages where subjectivity creeps in.

Firstly in the conceptualization of landform types, geomorphologists call similar landforms by different names: *"Landforms such as tors, bornhardts, inselbergs, castle-kopjes and perched blocks overlap and grade into each other confusingly, as defined by different geomorphologists"* (Evans, 1985, p.2). This problem may be associated with scale, certain groups of landforms could conceivably be a continuous group of basically the same form at different scales. Sandwaves, megaripples, and ripple marks might be one example of this.In Evans' second stage of analysis there are again dangers of subjectivity. The development of an operational definition for a particular landform type needs to be precise enough to allow consideration of not only textbook examples, but also of the much more marginal cases.

The third stage of Evans discussion is the stage of delimiting the landform from the surrounding landsurface. It will become clearer during the course of this discussion that this is perhaps the most difficult of all stages in analysing landforms in which to be objective. Once these three stages of analysis are complete the further stages are much less of a problem as far as subjectivity is concerned. It is perhaps convenient in the light of the difficulties of the first three stages that this study has so far kept away from specific geomorphometry for as Evans (1985, p.4) warns: *"if delimitation of landforms cannot be completed, we must resort instead to general geomorphometry"*.

If some form of specific geomorphometry is to be performed in this study the first three stages of Evans discussion must be carefully considered and as much avoidance of subjective decisions as possible should be taken. In recent years one possible aid to objectivity in this kind of analysis is perhaps emerging. With the increase in the availability and use of DEMs many algorithms have been developed to automatically delineate features such as ridges and valleys in order to identify drainage basins (Douglas, 1986; Jensen and Dominigue, 1988; Riazanoff et al., 1988; Zhang et al., 1990). This work has encouraged geomorphologists to try to automatically delineate landforms (Dikau, 1989).

Although the process of developing such algorithms and testing them is sufficient subject matter for a whole thesis, it would seem sensible to explore the possibility of using some of the simpler algorithms already available to extract the dominant landforms of the three surfaces chosen. Of these surfaces only Appleby was created specifically for this part of the study. However, the usefulness of Le Porge to this part of the study became apparent when the behaviour of its variogram indicated that the dunes of the area were the smallest landforms encountered and that the rest of the surface is not complicated by other landforms. The reason for the inclusion of Le Puy are similar to those of Le Porge, although the dominant landforms are much larger.

There are several reasons for choosing the drumlinised area around Appleby for study. Clearly there has been a large amount of study into drumlins. The study of the form of drumlins has been used to attempt to explain the processes responsible for their development. Form, as a clue to process, has been important in the case of drumlins as subglacial processes are difficult to examine. As this study is about the scale free or scale bound nature of landsurfaces, a landform type which has had its shape so carefully studied would seem to be a suitable subject for enquiry into the fractal nature of individual landforms.

The particular area of drumlins chosen has been studied several time before (Hollingworth, 1931; Rose and Letzer, 1977; Whiteman, 1981; Evans, 1985). Any interpretation of form in this area can therefore be compared to existing results. Rose

and Letzer (1977) describe how the drumlins of the area overlap and are superimposed on top of one another. The possibility of superimposition of smaller drumlins on top of larger drumlins would at first seem to be in agreement with the concept of the landsurface appearing similar from what ever scale it is viewed.

The last reason for choosing the area around Appleby was the availability of 1:10000 scale O.S. maps of the area which represent the topography by means of a 5m contour interval. As the discussion in chapter 3 suggests, this resolution is really the minimum requirement for the creation of a DEM to represent drumlins at a 50m grid mesh.

8.3 Methods of automating the extraction of landsurface features from DEMs.

Douglas (1986) has provided a useful review of many of the earlier methods used to extract topographic features from DEMs. His discussion is aimed at finding the best method to select information-rich lines which can be used as a means by which to reduce the computer storage from the large amount required for gridded DEMs. This new, more compact DEM, it was hoped, would retain as much of the important terrain information as possible.

Perhaps the most promising methods of extracting features such as hills and basins are methods which use the calculation of slope lines. The development of algorithms to derive accurate slope lines is, in itself, a major task and has attracted quite an amount of study (Bell, 1983; Douglas 1986). If slope lines are traced from the summits in a DEM, a skeletal network of slope lines will represent 'hills', in the sense of an area of divergent flow from one summit point. Points not on the slope lines can be the starting points for slope lines traced upwards towards the existing slope lines, once they meet an existing slope line the point being studied is identified as belonging to a particular summit. This process allows each point in a DEM to be allocated to a summit therefore identifying individual hills in the model. The process can be reversed in an attempt to find basins. The drawback of this method is that it takes a large amount of computing, every point must have some form of slope line traced, at least a short distance, from it.

Two of the simplest and most effective methods which Douglas discusses for the automation of ridge and channel extraction are local procedures. Local procedures use 3x3 windows to identify points with certain properties which lead to the identification of ridge and channel points.

One is a method first discussed by Jensen (1985). It looks for V-shaped in local profiles of three points. If a 3x3 window is studied two orthogonal and two diagonal profiles can be tested as well as the three points that form the triangles between two

adjacent corners and the central point of the window. If a V exists in one of these profiles, the point at the apex of the V is a channel point. This method produces complicated clouds of points which lie in valley bottoms. If A-shaped relationships between the sets of three points were flagged instead of V-shaped ones, this algorithm could be used to identify ridge-type points.

The other local method mentioned by Douglas (1986) is to identify every point in a DEM that is not a ridge point and flag them, thus revealing the ridge points as unflagged. Similarly, channel points can be identified by flagging every point which is not in a channel. The method of identifying non-ridge points is simple. The lowest corner of every 3×3 neighbourhood cannot be on a ridge and because the window moves over every point, inside the edge rows and columns, non-ridge points are the lowest points in a window at some stage in the pass of the DEM. This method also leaves clouds of points representing ridges or valleys. However the clouds can be thinned by various algorithms (Douglas, 1986). Clearly both of these methods are much less computing-intensive than the slope line methods.

In the case of trying to extract drumlins form a DEM it is necessary to identify their boundaries, which theoretically will be predominantly channel-type points. Therefore adaptations of these algorithms to identify channel points were written in Fortran to test on the Appleby DEM of this study.

A Jensen type method was first attempted. However, this method looked for changes in the direction of slope in only the two orthogonal directions. To achieve this two passes of the DEM were carried out; one down the DEM and the other across. If, after a downward slope a channel point was found, it was flagged. As well as this a test for level sections followed by an up-slope was performed, and if such a level section was found all of the points forming it were flagged as channel points. As can be seen from Figure 8.1, a bitmap of part of the Appleby area, the process leaves quite thick clouds of points in channel-type areas. The areas left unflagged can, in some instances, be seen to be drumlin shaped. However, complete boundaries are only visible for a few drumlin shapes.

The true Jensen method was also attempted, using all the possible profiles and point relationships possible in the 3×3 window. Each of the different relationships was given a different flag so that the shape of the surface at that point was recorded. Such identification of different shapes in the landsurfaces is of continuing interest to geomorphologists such as Dikau (1989) demonstrates. The clouds from this attempt were very thick and complex and attempting to identify the boundaries of the drumlins by complicated cloud thinning algorithms would not necessarily find the real boundaries of the drumlins.

Figure 8.1 *Bitmap of Appleby DEM.*

1 = Channel point flagged in one direction
2 = Channel point flagged in two directions

A more important problem is following even thinned out suspected channel lines around a complete drumlin, even after thinning.The method of flagging non-channel points is easily programmed. Again the major problem is to follow the cloud of points around complete drumlins. Complete drumlin shapes do emerge but often the shape of the surrounding cloud of points suggests that there may be two or more adjacent or superimposed drumlins present.None of these approaches would therefore seem appropriate for the task of objectively identifying drumlins from the Appleby surface. This is because, like most other landforms, drumlins are not all 'perfect' examples in a 'typical' situation. Although some of the drumlin boundaries are in channels, other boundaries are merely breaks of slope between the side of one drumlin and the side of another drumlin on top of which the other drumlin is superimposed.

Such breaks of slope can be automatically found using the derivatives of altitude, particularly gradient, aspect and profile convexity. Once again various combinations of these detect some limited parts of drumlin boundaries; however complete boundaries were absent. The reason for the failure of these attempts is once again that drumlins and other hill forms are not bounded by changes from profile convexity to profile concavity or changes in aspect of 180 degrees, instead they are bounded by breaks of slope in the map of profile curvature. Only the use of certain 'threshold' values of gradient or curvatures will detect a particular boundary; experimenting to find which threshold values are the most common would take a long time and would also require some knowledge of the real boundary to test the correctness of the thresholds.

As in the case of manual creation of DEMs, the human interpretation of maps and displays of DEMs involves complex intelligent decision making using all of the available information in a particular situation. It has not yet been possible to make computer programs to mimic these decision making processes and such a task would be very sizeable.

8.4 The analysis of the distribution of landforms.

From the above study it appears that some human decisions about what is a drumlin and what is not will have to be made. There is still one way that such decisions can initially be lead by an automatic process. Most of the summits in the Appleby, Le Porge and Le Puy surfaces will be the summits of the landforms of interest in those particular surfaces. It is a simple task to automatically identify summit points using a computer. As well as this once the summits have been identified there is some automatic analysis of the distribution of the landforms which can be preformed.

Given the availability of the original source maps for the Appleby DEM, the first surface analysed was Appleby. Problems with using the automatic extraction of the summits could therefore be gauged before studying the other two surfaces. First a Fortran program was written which simply moved a 3x3 window over the DEM testing for pits, and filling them; and plain points and flagging them. A test for points where all eight neighbouring points were lower is carried out. If the latter condition was found it was flagged as a summit. The program then calculated the national grid coordinate of the summit so that these could be checked against the original maps.

The process detected 89 summit points. Checking the output grid coordinates with the maps of the area revealed that only 53 of these are situated on drumlins. Of the summits on the drumlins, eight are what would be considered superimposed drumlins. During the process of checking the summit coordinates with the maps it was noticed that for several drumlins there were two or even three summits on the same drumlin. The shape of the highest contours on these drumlins were in agreement with the multiple summits. However, it would be impossible working at the map and DEM scale to determine if the summits are on superimposed drumlins, and which summit is the summit of the drumlin on which the others are superimposed.

The first problem immediately apparent from the process is that not all drumlins identifiable on the map have produced a summit detectable by this method from the DEM. This may be caused by the way that the DEM is at a 1m height resolution and some of the drumlins have broad tops. The test used to find summits only checks for single summit points. Therefore the test was change to consider points whose neighbours were either less than or equal to them. This produced a set of 1057 points. Clearly in many cases here a plain of points represents the drumlin tops. Thinning of these plains to only one point would be possible however the point left for each plain would not necessarily be the real summit.

A second smaller problem also appears when comparing the detected summits and the map. A small number of the summits are likely to be errors in the DEM. The most obvious errors can be detected on the floor of the Eden valley. Summits in these areas where the contours give no indication of the likelihood of a summit must be suspected of being artificial; particularly in the light of the findings of chapter 3 which found the worst errors in the Appleby DEM to be on the Eden valley flood plain.

Identifying summit points in the case of the Appleby model therefore proves to be a difficult task to automate. Perhaps in this case general geomorphometry is more appropriate to this study and certainly the variogram approaches of chapter 6 would appear to have been strongly influenced by the drumlin forms.

However, the same method has much more success with the simpler hill forms of Le Puy and Le Porge. In the case of Le Puy, when the simple test for summits is used 68 summits are detected. Most of these are in the central volcanic peak area of the surface. Likewise, for Le Porge, when the simple test for summits is applied 309 points are detected. They are almost all coastal dune summits.

Two simple pieces of analysis which reveal something about the size distribution and the spatial distribution of the landforms in these two French surfaces can easily be derived from the program which searches for summit points. The altitude of each dune, in the case of Le Porge, and each volcanic peak, in the case of Le Puy were written to files. As both surfaces appear to lack any obvious trend in the overall altitude of the area, the altitude distributions of the two landforms can be studied quite easily.

The second piece of analysis is only slightly more complicated. The distance between each summit point and its nearest neighbour can be found by searching in concentric squares outward from the summit point under investigation until another summit is met. The distances between them can then be calculated and recorded. It may be possible to relate these distributions back to the variograms of the area, thus linking the landforms present in these landsurfaces, directly to the lack of self-affine behaviour demonstrated in the variograms.

Figures 8.2 and 8.3 are histograms of the altitude distributions of the summits extracted from Le Porge and Le Puy, respectively. The histogram for Le Porge has had 52 outliers, caused by missing altitude values at the inland edge of the DEM, removed, leaving 257 summits. Although the histogram for Le Porge would appear bimodal, the distribution has a very narrow range, 46m. The mean altitude of the summits is 24.91m, while the standard deviation is only 8.46m. The mean is noticeably higher than the mean of estimated altitude calculated in chapter 7 (17.5m). This is particularly so when the effect of the area of higher ground inland from the dunes on the mean of estimated altitude is considered (fig. 6.14). This difference suggests that the dunes are, as would be expected, a distinct group of landforms with summit altitudes in a narrow range. Similar, smaller or larger landforms, are not present in the surface. It is clear from these statistics that this set of landforms falls within a very narrow scale range. If the dunes were to be responsible for any self-affinity in the landsurface they are from, it could only be over such a limited range.

The histogram of summit altitude for Le Puy shows the mode to be around 1100m, while the mean is 1002m. The standard deviation of the distribution is 149.8m and the range of the distribution is 725.2m. In this case the mean of estimated altitude for the entire surface is 914.6m, only 87.4m less than the mean of the summit altitudes.

Therefore, although the distribution of summits would seem to suggest that the peaks in this area are another set of distinct landforms, reference to the altitude statistics for the overall surface suggest that summits are found at a wide range of altitudes given the relief of the landsurface. If reference is made to figure 6.13, smaller hills can be seen in the south of the area, as well as the larger volcanic peaks in the central belt of the DEM. The distribution of the summit altitudes of these, combined with the distribution of the larger peaks produces the distribution presented in the histogram. These peaks cannot on the basis of altitude distribution be considered as a set of distinct landforms, even though on the basis of lithology, plutonic and geomorphological process they would be grouped together as similar landforms.

Figure 8.4 is a histogram of the distribution of distance between neighbouring summits, for the Le Porge area. It shows the strong positive skew to the distribution, which pulls the mean up to the value of 301m. 169 of the summits are separated by distances of less than 300m. Once more the dunes can be seen as a set of landforms with a dominant spacing of about 200-400m. If the variograms for Le Porge, calculated in chapter 6, are referred to ,the kink which prohibited a fractal dimension being estimated over any sizeable range of distance, is between 250m and 315m . It is, therefore, definitely the spacing of the dunes which causes the break down of the fractal Brownian model demonstrated by the curvilinear variogram.

Although the distribution of distances between summits for Le Puy is also positively skewed, the skew is not nearly as extreme as in the case of Le Porge (fig. 8.5). The distribution is also bimodal with one mode at 200m and another at 1.2km. Some of the more isolated summits which must contribute to the second mode can be spotted in figure 6.13 as conical peaks rising from the general level of the surface. However, neither of these modes, nor the mean summit spacing of 538m can be related back to the non-directional long distance variogram of chapter 6. In it, the variogram is slightly convex up to a maximum variance somewhere around 5-6km. This shows that, unlike the dunes of Le Porge, the peaks of Le Puy have a wide enough variety of heights and spacing that they do not have an obvious average slope length and therefore do not show up as a break of slope on the variogram. The break of slope on the variogram at around 5-6km is caused by the fact that the highest peaks are all situated across the centre of the DEM, as discussed in chapter 6. The peaks of the Le Puy area, considered as a set of landforms on there own, are not, therefore, responsible for a break down of the fractal model. It is only when the peaks are placed in their wider surroundings, where there is less relief, that the fractal model must be rejected.

Figure 8.2 Histogram of summit altitude: Le Porge

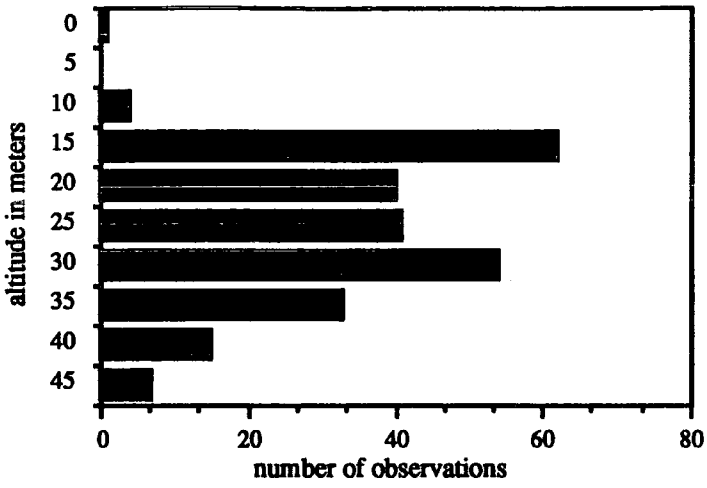

Figure 8.3 Histogram of summit altitude: Le Puy

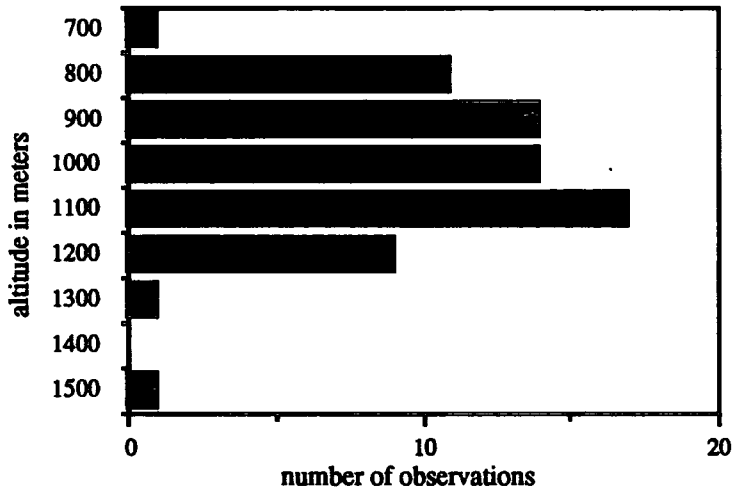

Figure 8.4 Histogram of summit spacing: Le Porge

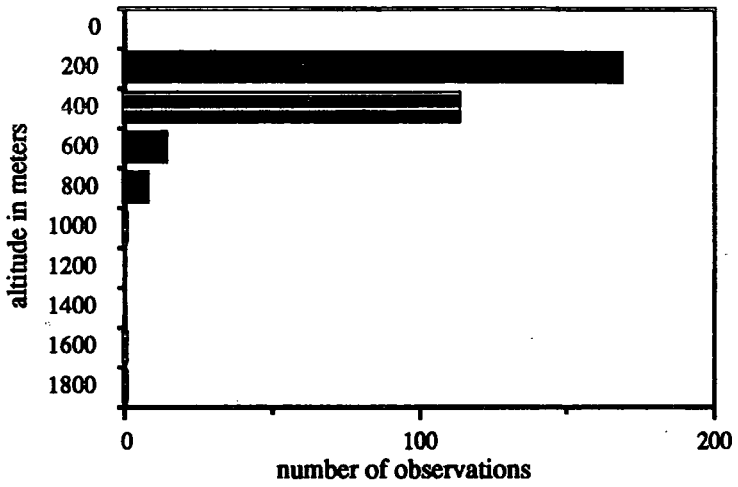

Figure 8.5 Histogram of summit spacing: Le Puy

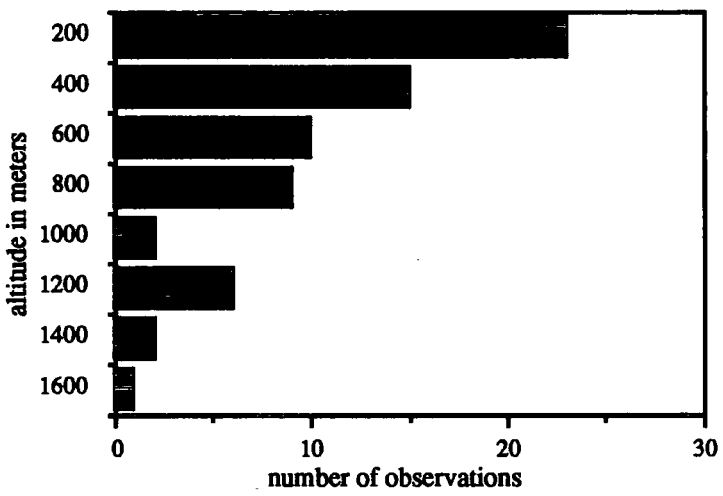

8.5 Conclusions.

This chapter has tried to approach the question of how the geomorphological practice of delimiting landforms from landsurfaces might fit with the fractal concepts of self-similarity and self-affinity. If the distributions related to the size of the dominant landform of a surface are very limited, it would be expected that the fractal idea of self-affinity would break down at around the mean size of the dominant landform type. However, if that landform type were to occur at a wide range of sizes, the concept of studying the surface at one scale and finding the same forms as at a different scale, might hold.

One difficulty of studying the scale of landform types is that they may have been somewhat subjectively defined by geomorphologist who are more interested in the processes that have made a particular landform, than the range of sizes at which they are found; a few well formed examples may prove of more use in simplifying process than a large and complicated sample. Recent attempts to automate the detection of landsurface features from DEMs may be leading to the possibility of making landform delimitation more objective. As a result, attempts were made to automatically identify the drumlins from the Appleby DEM. Several previously proposed algorithms for ridge and channel line extraction were attempted. However, they were not successful in completely delimiting one type of landform, rather they identified probable channel lines which do not fully delimit the drumlin forms.

In a further attempt to extract some information about the drumlins from the DEM, the summit points of the surface were identified. These were of little direct use for the study of the Appleby drumlins. The method was of more use when applied to the coastal dunes of Le Porge and the volcanic peaks of Le Puy. The altitude distributions of the summit points revealed the homogeneity of the set of landforms. The limited size distribution of the summit spacing also supported this. The mean summit spacing was found to be very close to the first break of slope in the areas variogram. This directly related the break down of the fractal model with summit spacing and average slope length.

The distributions obtained for the summits of the Le Puy area did not challenge the concept of self-affinity. However their limited spatial distribution results in the break down of any possible self-affine behaviour at distances around 5 to 6km.

The detailed study of landforms, therefore, still relies on some intelligent interpretation of the landsurface by a human operator. Limited size distributions of the landforms can prevent any possibility of treating the landsurface as a self-affine fractal. While the joint investigation of landform size frequency distributions and the variograms calculated from the surfaces in which they are present can be related to explain one another and the possible fractal form of a surface.

Chapter 9: Conclusions

Fractal geometry has been developed as a new stochastic modelling tool by mathematicians. It is suggested that it might have applications within geomorphology. This thesis has attempted to assess, whether or not, the fractal model, used as a stochastic model of landsurface form, can be of use in the process of seeking further explanation in geomorphology. Furthermore, any measure of its use must be in relation to the explanation already achieved in geomorphology by existing, and often more physically based models.

Theory in geomorphology already appreciates the complexity of landsurface form. However, the approach in geomorphology has generally been to isolate separate landforms, or facets of the landsurface, to study in an attempt to order and explain the complexity. This has resulted in considerable study at the "landscape scale" (Mark, 1980). It is at this scale, tens of metres to kilometres, that proponents of the fractal model (Mandelbrot, 1982) have envisaged the use of fractal geometry in geomorphology.

Fractal geometry at this scale treats the landsurface as an irregular collection of irregular shapes. Advocates of the fractal model argue that order can be brought to this irregularity, because the irregularity has certain scaling properties. This concept developed from the observation that a segment of a coastline, studied at high resolution, may visually resemble the entire coastline viewed at lower resolution. Likewise, it was suggested that parts of a landsurface, viewed at high resolution, resemble the larger area of terrain from which they are taken, viewed at lower resolution. The link between these observations and fractal geometry was made because Mandelbrot (1975) identified a set of mathematical processes, fractional Brownian noises, which produce curves and surfaces with the above visual properties, but which also show strict self-affine behaviour in the statistical sense. As a result, it is suggested that the roughness of landsurfaces at low resolution, is statistically the same as the roughness existing in the surface at a much higher resolution, when that roughness undergoes a scale related transformation.

Therefore, the argument for applying fractal geometry to the study of landsurfaces at the landscape scale, has predominantly arisen from the visual similarities between real landsurfaces and simulated surfaces, produced using fractional Brownian processes. Very little empirical study of landsurfaces, for evidence of self-affine behaviour, was carried out before the argument for applying fractal geometry to this area of study was proposed.

As far as the implications for geomorphometry are concerned, the most important property of fractal geometry is the self-affine nature of the irregularity in fractional Brownian surfaces. The self-affine nature of a fractional Brownian surface is described by its fractal dimension, and, as a result, it is this parameter which would be of most relevance to any use of fractal geometry in the field of geomorphometry. Indeed, if landsurfaces were self-affine fractal Brownian surfaces then their fractal dimensions would become a very important geomorphometric parameters.

The usefulness of the concepts of self-affine form, and its associated fractal dimension, to geomorphometry, is proportional to how accurately the fractal model reflects reality. The fractal Brownian model would be at its most powerful if all its properties were present in real landsurfaces. It rapidly loses usefulness if it is diluted and "tweaked" to fit reality. The most likely dilution of the fractal model would seem to be the placing of limits on the scale range over which self-affine behaviour should be expected. For example, if this scale range was large, from the resolution of part of an individual mountain to the entire mountain range, the fractional Brownian model would still be of great potential. If, on the other hand, the model was to be applied to the study of individual slopes, and it was found that the landsurface is only self-affine over part of the length of an entire slope, the model becomes almost useless.

Another dilution of the pure fractal model suggests that surfaces be anisotropic, possessing different degrees of irregularity in different directions. The irregularity of simulated fractal surfaces should have the same self-affine behaviour in any direction. The fractal model might still be of descriptive use if real surfaces had clearly identifiable self-affine behaviour, of differing fractal dimension, in different directions. However, application of the fractal model would immediately become much more complex.

In this thesis, an attempt has been made, to find how accurately the fractal model fits reality at the landscape scale. As well as the reasons already given for focusing at the landscape scale, the availability of data at this scale, in the form of digital elevation models (DEMs), and the increasing interest in use and development of such models, has also been of consideration. DEMs have, therefore, been the data source used in this study.

The creation of a DEM of drumlins in the vale of Eden, illustrates the difficulties involved in accurately modelling the form of the landsurface. The problems encountered in producing the Appleby DEM should serve as a warning to those about to use DEMs, particularly those which have come into their hands from a "black box" production method, even when the DEMs are produced by a national mapping agency. Much work must still be done in the areas of producing DEMs and also assessing their

accuracy. It seems that manually interpolated DEMs, still seem to be more accurate than those interpolated using semi-automated or automated techniques. This is because of the very complicated decision making process which a human interpolator can bring to bear on elevation data. A process which has not been sufficiently well mimicked by computer algorithms.

This project required that many of the existing approaches to assessing the quality of DEM data were applied in this study. Indeed, it is error in DEMs and the lack of rigorously defined and codable rules for delimiting individual landforms, which hindered attempts to automatically extract sets of landforms. The inclusion of manually produced DEMs in this study serves to reassure that data error had no detrimental effect on the other methods used. Manually interpolated DEMs are seen to yield comparable results with the poorer quality semi-automatically derived models.

Several methods designed to test real landsurfaces for the properties found in fractal Brownian surfaces have been considered. The best, and most flexible of these has proved to be the variogram method. There are several reasons supporting this conclusion. To start with, it would seem sensible when dealing with a phenomenon normally considered at a topological dimension of 2, to study it using a 2-dimensional technique. Mandelbrot (1975,1982) claims that a contour, profile or subarea, of a particular surface will exhibit the same self- affine behaviour as the surface when considered as a whole. However, if these assertions are to be verified, it is useful to have an overall picture of the surfaces fractal behaviour, against which to consider more limited measurements.

There are also certain disadvantages of using one- dimensional techniques. Automated, one dimensional, algorithms based on the Richardson (1961) walking dividers technique are usually based on only a small number of step lengths and line length measurements. Methods of analyzing the linearity of the resulting log-log output are, therefore, susceptible to deviations of the data from a straight line relationship. Furthermore, the variogram method and the rescaled range analysis method allow a larger scale range to be considered. Finding sufficient long contours, on which to run a walking dividers program, over a sensible range of altitudes for the area is another limiting factor, and one which does not lend itself easily to automation. Furthermore, the work of Goodchild (1982) makes it necessary, as he found that fractal dimension seems to vary with altitude. This amounts to the first inconsistency between the fractal model and reality.

Although, a two dimensional walking dividers method has been proposed, it has definite theoretical failing. Clarke's 1986 method is not a true two-dimensional extension of any walking dividers algorithm, and to perform a tiling of a DEM, in a true

walking dividers fashion would be an extremely complicated procedure. If achieved , such a method would still face the disadvantage of a small number of tile area and surface area measurements.

The variogram method also proved to be more use than the rescaled range method. The extension of the approach taken to analyse geophysical time series, rescaled range analysis, to consider an "unravelled" landsurface is not a true two-dimensional technique. This was emphasised when the effect of sampling the landsurface was considered. The effect of some of the landforms in DEMs was not considered by this method at all, because of their anisotropic spatial distribution. This resulted in lower estimated fractal dimension values than those produced by the variogram method.

The major advantage of the variogram method, as implemented in FASTFRAC, over all the methods considered is its flexibility. All nodes in the grid of a gridded DEM become potential data points. FASTFRAC allows the altitude variance to be measured in every possible direction within a DEM, using points which are row, column and diagonal neighbours. Of course, this is a very computer intensive task, but this study has shown that enough information can be obtained for the variogram from only a relatively small sample of the available data. Unlike the implementations of Mark and Aronson (1984) and Roy et al. (1987), the structured sampling technique used in FASTFRAC allows control over the proportion of any particular set of row, column or diagonal relationships between points being used to calculate variance. Therefore, it can be easily adapted to calculate altitude variance in a surface, in one particular directions.

One further advantage of the variogram method, is that the variograms produced are relatively simple to relate to the surfaces from which they are calculated. The effect of increased distance on expected elevation difference can be visually related to the surfaces being studied. This is particularly true when altitude variance in individual directions is being considered.

The major conclusions about the fractal nature of landsurfaces made in this study are, therefore, based on the analysis of surfaces using the variogram technique as implemented in FASTFRAC. The reliability of this technique is illustrated by its application to simulated fractal Brownian surfaces generated by a well defined algorithm. The variograms produced by FASTFRAC for these surfaces reveal that the approach does produce estimates of the surfaces fractal dimensions, which are close to the fractal dimension used to generate the surfaces. For surfaces produced by the shear displacement method, the estimated fractal dimensions deviate by less than 0.05 from the fractal dimensions input to the generation program. Differences of this order would be difficult to discern visually. However, the benefit of studying the residuals from the

regression of points in the variograms was revealed as it allowed the detection of curvature in the variograms. The convex curvature for variograms of simulated surfaces with fractal dimension of 2.5 and below, and the concave nature of variograms with fractal dimensions of greater than 2.5, implied that a higher density of faults than the 500 used for these surfaces should be used to make the surfaces truly fully self-affine.

As expected, the directional variogram results for the simulated surfaces all produced values of D which are close to the input value of D. The roughness in simulated fractional Brownian surfaces is, therefore, isotropic.

Visual inspection of the fractal surfaces shows that simulated surfaces with low fractal dimensions, of around 2.0 to 2.3, bear resemblance to real landsurfaces. However, at fractal dimensions of greater than 2.3, the simulated surfaces look much rougher than any of the landsurfaces considered in this study. Beyond a basic physical resemblance, the quantitative analysis of this study reveals that the real landsurfaces studied are very different to the simulated fractal surfaces.

In the cases of all 27 landsurfaces considered in this study, the variograms produced from them show that reality does not exhibit the self-affine behaviour suggested by the fractal Brownian model. Variograms for the entire surfaces, for larger distance ranges, all reveal some form of non-linear structure, except for the high resolution DEMs which are of small sections of drainage basins. These high resolution DEMs all yield low fractal dimensions. In general, the breaks in slope in the variograms appear from approximately 1km to about 2km. Often there are several local maxima and minima of altitude variance. The structure in all of these variograms can be related back to the forms seen to be present in the landsurfaces. Most often the breaks of slope are caused by valley spacing. Altitude variance increases as points from different relative positions within slopes are considered. However, altitude variance begins to decrease when points from the same relative positions within slopes are considered. This behaviour shows up as near periodic maxima and minima of variance in the variograms. On the basis of this evidence, the fractal model breaks down in reality when distance ranges greater than the average slope length in an area are considered.

Investigation of residuals, from regression of the shorter distance parts of the variograms, reveal convex curvature in most of the variograms. As was explained in the case of the Wind River DEM, if the relationship between log (altitude variance) and log (distance) is convex, then least- squares regression of the longer distance section of the variogram would produce a higher fractal dimension than the portion of the variogram for the smaller distances. Therefore, due to the different grid mesh sizes of DEMs and the convex shape of the variograms, the descriptive power of the parameter D become severely limited. As a result, the order given to the landsurfaces in this study, although

approximately correct when considering surface roughness, is not purely an order of surfaces on the basis of their roughness.

The convexity found at the smaller distance end of the variograms may also indicate the lack of fit of the fractal Brownian model to landsurfaces at the scale of single slopes. The convexity is an effect of sampling an increasing number of points which do not reside on the same slope facet as each other, with increasing distance, and as a result, the rate of increase of variance decreases with distance. This argument is strengthened by the fact that the most linear variograms are produced from DEMs covering only simple slopes: Glaisdale; Wheeldale; Netherhearth Sike; and Booro Borotou. These surfaces also yield the lowest fractal dimensions. Indeed, even smooth surfaces sampled at a finite grid interval will produce a fractal dimension slightly above 2.0. Therefore, this study indicates that the fractal model probably breaks down at the scale of individual slopes. However, a further study of high resolution slope profiles, or DEMs like those mentioned above, would need to be carried out to investigate this more fully.

The variograms for separate directions within DEMs echo the results for entire landsurfaces. In particular the structure in the variograms for different directions succeeds in tying the forms of the variograms more closely to the landforms being sampled across in the DEM. Therefore, as well as lending weight to the argument that landsurfaces are not self-affine, certainly over scale ranges beyond the length of individual slopes, the directional variograms expose the anisotropic nature of surface roughness in real landsurfaces. This is often seen to be the result of the drainage network of the surface. Valleys are sampled across in all directions, except in the direction parallel to the valley sides. The surface is roughest when considered in the direction perpendicular to the valley sides. In general, therefore, the fractal Brownian model is not realistic in its assumptions of an isotropic distribution of irregularity.

The final failure of the fractal Brownian model to fit reality, revealed by the variogram analysis, is the way in which very different variograms are produced for subareas of any particular DEM. In a true fractal surface, the same self- affine relationship would hold for the entire area. This is clearly not the case for the DEMs used in this study. Even in areas of fairly homogeneous topography, such as in the Alarta and Devon DEMs, a wide range of variograms and, as a result, fractal dimensions, were produced. Once again most of the variograms revealed structure which could be related to the forms found in the subareas of the DEMs.

All the results from applying the adaptations of the FASTFRAC variogram approach, indicate that the fractal Brownian model does not describe landsurfaces in reality. Its assumptions about self-affine behaviour do not hold for the surfaces studied

here. These results are in some conflict with the conclusions of Mark and Aronson (1984) and Roy et al. (1987). Both of these studies suggest that variograms produced by their methods show linear segments followed by a break of slope, which is in turn followed by another linear segment. Mark and Aronson (1984) have visually assessed where these breaks of slope are, and have then fitted straight lines to the segments, calculating fractal dimension in the process. On the basis of this rather subjective process, they suggest that certain processes, acting in a certain scale range, have produced a self-affine surface over that scale range. This, they suggest, is responsible for the first linear segment of their variograms. They then suggest that the next linear segment might correspond to a different set of processes, and that beyond a certain scale threshold the landsurface has a different fractal dimension. In the case of their variograms this fractal dimension is higher than that of the first segment. Roy et al. (1987) reach a similar conclusion, although they do show that areas of different topography, within subareas of a DEM, can produce different fractal dimensions.

The evidence of this study would suggest that variograms for landsurfaces are generally convex up to a break of slope associated with average slope length, or the position of a dominant hill or valley in the area. Variograms have been produced in this study that have steep gradients, followed by a break of slope, and then have a more gentle slope, all of which is eventually followed by another steep segment. In these cases the breaks of slope can be associated with the length of slopes which are visible in the landsurfaces, but which are not dominant enough during the sampling of altitude variance to produce full turning points in the variograms. On the basis of this evidence, it must be suggested that the segments found in the variograms of Mark and Aronson, either, result from the mistaken division of a convex variogram into segments, or, more probably, that the segments are produced by slopes that are not quite dominant enough on the sample of altitude variance to produce turning points.

Culling (1986), and Culling and Datko (1986), although using a different analysis technique, suggest that landsurfaces may behave in a self-affine way, with a discernible fractal dimension, up to a certain scale, and then, beyond that scale, they have another fractal dimension. They suggest that the scale at which this change in fractal dimension occurs, is the scale at which the drainage network begins to effect the altitude distribution. The variogram results of this study would agree the drainage network does, definitely, cause a break down of the pure fractal model at a certain distance. However, the evidence of this study suggests that at scales beyond this, there is no further scaling behaviour of the landsurface, certainly not over distance of kilometres, and probably not at distances of tens of kilometres. The evidence also suggests that the landsurface may not be fractal at the level of individual slopes.

The assertion that the drainage network has a dominant effect on the variograms of the landsurfaces studied, is supported by the study of the geomorphometry of those landsurfaces. By calculating the derivatives of the altitudes in a DEM, associated with slope and the rate of change of slope, and from them calculating moment statistics, a detailed picture of the geomorphometry of an area can be revealed. When the landsurfaces in this study were analysed, they were placed into loose groupings, on the basis of their geomorphometry. The landforms responsible for the characteristic geomorphometry of these surface groupings, were often characteristics of the dominant processes which formed the areas. This was certainly the case for glaciated mountain areas, where glacial cirque and trough forms resulted in such characteristics as positively skewed profile and plan convexity. The geomorphometry of these areas are dominated by the pattern of glaciers that, at one stage, covered them. Of course, it is this pattern which is now used by the drainage network. The high positive skew of gradient, low to negative skew of profile convexity, and negative skew of plan convexity, found in the surfaces grouped together as "dissected lowland or upland areas", are obviously a result of the form of the drainage network.

These sets of geomorphometric indicators, identifying areas dominated by certain processes are not found in simulated fractional Brownian surfaces. Instead, most of their geomorphometric parameters vary strictly in accordance with their fractal dimensions. Certainly, geomorphometric indicators of roughness, such as mean and standard deviation of gradient, and standard deviation of profile and plan convexity, are all highly correlated with fractal dimension.

In these fractal surfaces, large scale irregularities are always accompanied by the appropriate number of smaller irregularities, depending on their fractal dimension. In the case of real landsurfaces, fractal dimension may be a function of the convexity of the variogram from which it is calculated. The convexity in that variogram is a result of the dominant roughness in the surface. This is often associated with the drainage network, but may also depend upon the presents of certain landforms. These roughnesses are not accompanied by other, suitably sized features at smaller and larger scales, which would produce the self-affine behaviour present in fractal surfaces. As a result, there is little correlation between the existing geomorphometric parameters calculated, and the fractal dimensions calculated, for the 27 landsurfaces in this study.

Unfortunately, due to the difficulties of extracting individual landforms from DEM representations of landsurfaces using automated techniques, this thesis has not succeeded in relating the size distribution of sets of landforms to the breaks of slope detected in the variograms. It can be seen from the distances at which the breaks of slope occur on the variograms that individual slopes which may be associated with these landforms produce the deviations in the fractal model. However, only in the

limited study of the sand dunes of Le Porge, was any sign of a limited size distribution of landforms detected. Given the size of the grid mesh in relation to the altitude and spacing of the landforms, the evidence collected cannot be considered as being particularly strong. More detailed gathering of geomorphometric information about individual sets of landforms is required before a definite link between the scale-bound size distributions of landforms, and the break down in the scale-free fractal model, can be made.

This study has shown that although real landsurfaces bear some visual resemblance to fractal Brownian surfaces, they seem to possess none of their statistical characteristics. True self-affine behaviour is not conclusively detected over any scale range, in any landsurface studied in this thesis. Furthermore, the irregularity encountered in real landsurfaces is not isotropic. This evidence implies that a fractal dimension, calculated from such a landsurface, and used as a geomorphometric parameter contains little, if any, useful information about that surface. As a result it can not be related to other existing geomorphometric parameters.

On the basis of these conclusions, the fractal Brownian model is of little use to the explanation of landsurface form in geomorphology. Fractal surfaces could be used as a stochastic input to a model which requires surfaces with certain known properties. However, any such surface could not be considered to be realistic in terms of landsurfaces found in reality. Methods for detecting fractal behaviour do provide information about the structure of form in the areas being studied. However, similar information has been collected previously, using older methods. For example, the concepts of grain and texture of topography are not new. This sort of information is traditionally linked to physically based, deterministic models, of processes which are more easily related to the structure of landsurface form. Therefore, it would seem that the stochastic approach of the fractal Brownian model, cannot better the traditional scale-bound approach of studying landforms in relation to physical processes.

Appendix 1: Important Fortran '77 Programs Listing

DEM.FOR

```
C     PROGRAM TO FIND POINTS WHERE CONTOURS CUT XY GRID AND DIAGONALS
C      SET DIMENSIONS OF ARRAYS TO HOLD PROFILES X, Y AND DIAGONALS
     AFTER
C     ROTATION THROUGH 45 DEGREES
      REAL PROX(30000,3),PROY(30000,3),SMALL(30000,3)
     1 ,PRODX(30000,3),PRODY(30000,3),OMAX,ONAX,OMAY,ONAY,
     2 YT1,YT2,XT1,XT2,SS1(30000,3),SS2(30000,3),DEM(160,100),
     3 SS3(30000,3),SS4(30000,3),GR,W1(30000,3),W2(30000,3),
     4 W3(30000,3),W4(30000,3),HT1(160,100),HT2(160,100),HT3(160,100),
     5
     HT4(160,100),WT1(160,100),WT2(160,100),WT3(160,100),WT4(160,100)
C     REAL*8 EO2BAF,XN(500),YN(500),WN(500),KN(500),WORK1(500),
C     1 WORK2(4,500),CN(500),SS
      INTEGER XX1,XX2,YY1,YY2,ICOR(1000)
C  INITIALISE COUNTS FOR EACH CONTOUR INTERSECTION WITH PROFILES
      IC=1
      ICC=1
      IS=1
      ISS=1
C  GR-ID SIZE AND VALUE FOR PI, A ANGLE IN RADIANS
      B=2.0
      GR=SQRT(B)
      PI=3.1415926
      A=PI*0.25
      E=PI*1.75
C
C  READ IN FIRST POINT FROM CO-ORDINATE FILE
C
      READ(1,2)X1,Y1,Z1
   2  FORMAT(F10.6,1X,F10.6,1X,F3.0)
C
C CALCULATE VALUES FOR ROTATED CO-ORDINATE
      XR1=(X1*COS(A))-(Y1*SIN(A))
      YR1=(Y1*COS(A))+(X1*SIN(A))
C CHECK TO SEE IF POINT LIES ON DIAGONALS IN Y DIRECTION
      IF(AMOD(XR1,GR).EQ.0)THEN
        PRODY(IS,1)=XR1
        PRODY(IS,2)=YR1
        PRODY(IS,3)=Z1
        IS=IS+1
      END IF
C CHECK TO SEE IF POINT LIES ON DIAGONALS IN X DIRECTION
      IF(AMOD(YR1,GR).EQ.0)THEN
        PRODX(ISS,1)=YR1
        PRODX(ISS,2)=XR1
        PRODX(ISS,3)=Z1
        ISS=ISS+1
      END IF
C DEALING WITH UNTRANSFORMED CO-ORDINATES
      XX1=INT(X1)
      YY1=INT(Y1)
C CHECK TO SEE IF POINT LIES ON X*N  AXIS
      IF(XX1.EQ.X1)THEN
        PROY(IC,1)=X1
        PROY(IC,2)=Y1
        PROY(IC,3)=Z1
        IC=IC+1
      END IF
```

```
C CHECK TO SEE IF POINT LIES ON Y*N  AXIS
      IF(YY1.EQ.Y1)THEN
        PROX(ICC,1)=Y1
        PROX(ICC,2)=X1
        PROX(ICC,3)=Z1
        ICC=ICC+1
      END IF
C
C BEGINS TO CHECK POINTS BESIDE EACH OTHER FOR BEING ON OPPOSITE SIDES
C OF GRID AND DIAGONAL AXES
C
      FIN=999999
      DO 1 I=1,FIN
C READ  NEXT POINT
        READ(1,2,END=3)X2,Y2,Z2
C ROTATE POINT BY PI/4 RADIANS
        XR2=(X2*COS(A))-(Y2*SIN(A))
        YR2=(Y2*COS(A))+(X2*SIN(A))
C CHECK TO SEE IF POINT LIES ON X DIAGONAL
      IF(AMOD(XR2,GR).EQ.0)THEN
        PRODY(IS,1)=XR2
        PRODY(IS,2)=YR2
        PRODY(IS,3)=Z2
        IS=IS+1
      END IF
C CHECK TO SEE IF POINT LIES ON Y DIAGONAL
      IF(AMOD(YR2,GR).EQ.0)THEN
        PRODX(ISS,1)=YR2
        PRODX(ISS,2)=XR2
        PRODX(ISS,3)=Z2
        ISS=ISS+1
      END IF
C CHECK TO SEE IF POINT LIES ON X*N  AXIS
        XX2=INT(X2)
        YY2=INT(Y2)
        IF(XX2.EQ.X2)THEN
          PROY(IC,1)=X2
          PROY(IC,2)=Y2
          PROY(IC,3)=Z2
          IC=IC+1
        END IF
C CHECK TO SEE IF POINT LIES ON Y*N  AXIS
        IF(YY2.EQ.Y2)THEN
          PROX(ICC,1)=Y2
          PROX(ICC,2)=X2
          PROX(ICC,3)=Z2
          ICC=ICC+1
        END IF
C CHECKS TO SEE IF STILL ON SAME CONTOUR
        DIFX=ABS(X1-X2)
        DIFY=ABS(Y1-Y2)
        IF(Z1.EQ.Z2.AND.DIFY.LT.2.AND.DIFX.LT.2)THEN
C TESTS FOR POINTS ON OPPOSITE SIDE OF X*N GRID AXIS
          TESTX=XX2-XX1
          IF(TESTX.EQ.1.OR.TESTX.EQ.-1)THEN
            IF(TESTX.EQ.1)THEN
              X=XX2
            ELSE
              X=XX1
            END IF
            B=(Y2-Y1)/(X2-X1)
            Y=(B*(X-X1))+Y1
            PROY(IC,1)=X
            PROY(IC,2)=Y
            PROY(IC,3)=Z1
            IC=IC+1
```

```
          END IF
C TESTS FOR POINTS ON OPPOSITE SIDE OF Y*N GRID AXIS
          TESTY=YY2-YY1
          IF(TESTY.EQ.1.OR.TESTY.EQ.-1)THEN
            IF(TESTY.EQ.1)THEN
              Y=YY2
            ELSE
              Y=YY1
            END IF
            B=(X2-X1)/(Y2-Y1)
            X=(B*(Y-Y1))+X1
            PROX(ICC,1)=Y
            PROX(ICC,2)=X
            PROX(ICC,3)=Z1
            ICC=ICC+1
          END IF
C DEAL WITH INTERSECTED DIAGONALS
C FIND MAX X
          IF(XR1.LT.0.AND.XR2.LT.0)THEN
            IF(XR1.GT.XR2)THEN
              OMAX=XR2
              ONAX=XR1
              YT1=YR2
              YT2=YR1
            ELSE
              OMAX=XR1
              ONAX=XR2
              YT1=YR1
              YT2=YR2
            END IF
            RESX=INT(OMAX/GR)
            TX1=OMAX-ONAX
            TESX=RESX*GR
            IF(TESX.LT.ONAX.AND.TX1.NE.0)THEN
              X=TESX
              B=(YT1-YT2)/(OMAX-ONAX)
              Y=(B*(X-OMAX))+YT1
              PRODY(IS,1)=X
              PRODY(IS,2)=Y
              PRODY(IS,3)=Z1
              IS=IS+1
            END IF
          ELSE
            IF(XR1.GT.XR2)THEN
              OMAX=XR1
              ONAX=XR2
              YT1=YR1
              YT2=YR2
            ELSE
              OMAX=XR2
              ONAX=XR1
              YT1=YR2
              YT2=YR1
            END IF
C TEST TO SEE IF POINTS ARE ON OPPOSITE SIDES OF A DIAGONAL (X)
            RESX=INT(OMAX/GR)
            TX1=OMAX-ONAX
            TESX=RESX*GR
            IF(TESX.GT.ONAX.AND.TX1.NE.0)THEN
              X=TESX
              B=(YT1-YT2)/(OMAX-ONAX)
              Y=(B*(X-OMAX))+YT1
              PRODY(IS,1)=X
              PRODY(IS,2)=Y
              PRODY(IS,3)=Z1
              IS=IS+1
```

```
            END IF
          END IF
          IF(YR1.GT.YR2)THEN
            OMAY=YR1
            ONAY=YR2
            XT1=XR1
            XT2=XR2
          ELSE
            OMAY=YR2
            ONAY=YR1
            XT1=XR2
            XT2=XR1
          END IF
          RESY=INT(OMAY/GR)
          TY1=OMAY-ONAY
          TESY=RESY*GR
          IF(TESY.GT.ONAY.AND.TY1.NE.0)THEN
            Y=TESY
            B=(XT1-XT2)/(OMAY-ONAY)
            X=(B*(Y-OMAY))+XT1
            PRODX(ISS,1)=Y
            PRODX(ISS,2)=X
            PRODX(ISS,3)=Z1
            ISS=ISS+1
          END IF
C FINISHED CALCULATING INTERSECTIONS
        END IF
C POINT 2 BECOMES NEW POINT 1
        XX1=XX2
        YY1=YY2
        X1=X2
        Y1=Y2
        Z1=Z2
        XR1=XR2
        YR1=YR2
   1  CONTINUE
   3  IC=IC-1
      ICC=ICC-1
      IS=IS-1
      ISS=ISS-1
      PRINT *,IC,' ',ICC,' ',IS,' ',ISS
      CALL SORT(IC,PROY)
      CALL SORT(ICC,PROX)
      CALL SORT(IS,PRODY)
      CALL SORT(ISS,PRODX)
      DO 7 K=1,4
        ICO=0
        IF(K.EQ.1)THEN
          KC=IC-1
          CALL SMSORT(KC,PROY,ICO,KO,1.0,SS1,W1)
C         IF(KO.EQ.-1)GOTO 103
          DO 8 I=1,KO
            SS1(I,1)=NINT(SS1(I,1))
            SS1(I,2)=NINT(SS1(I,2))
            W1(I,1)=SS1(I,1)
            W1(I,1)=SS1(I,2)
   8      CONTINUE
          PRINT *,'HELLO'
          CALL DEMS(KO,SS1,W1,HT1,WT1)
          PRINT *,'HELLO'
        END IF
C
        IF(K.EQ.2)THEN
          KC=ICC-1
          CALL SMSORT(KC,PROX,ICO,KO,1.0,SS2,W2)
          DO 15 I=1,KO
```

```
            TEX=SS2(I,2)
            TEY=SS2(I,1)
            SS2(I,1)=NINT(TEX)
            SS2(I,2)=NINT(TEY)
            W2(I,1)=NINT(TEX)
            W2(I,2)=NINT(TEY)
 15       CONTINUE
          CALL DEMS(KO,SS2,W2,HT2,WT2)
        END IF
        IF(K.EQ.3)THEN
          KC=ISS-1
          CALL SMSORT(KC,PRODX,ICO,KO,GR,SS3,W3)
          DO 19 I=1,KO
            ROTX=(SS3(I,2)*COS(E))-(SS3(I,1)*SIN(E))
            ROTY=(SS3(I,2)*SIN(E))+(SS3(I,1)*COS(E))
            SS3(I,1)=NINT(ROTX)
            SS3(I,2)=NINT(ROTY)
            W3(I,1)=SS3(I,1)
            W3(I,2)=SS3(I,2)
 19       CONTINUE
          CALL DEMS(KO,SS3,W3,HT3,WT3)
        END IF
        IF(K.EQ.4)THEN
          KC=IS-1
          CALL SMSORT(KC,PRODY,ICO,KO,GR,SS4,W4)
          DO 21 I=1,KO
            ROTX=(SS4(I,1)*COS(E))-(SS4(I,2)*SIN(E))
            ROTY=(SS4(I,1)*SIN(E))+(SS4(I,2)*COS(E))
            SS4(I,1)=NINT(ROTX)
            SS4(I,2)=NINT(ROTY)
            W4(I,1)=SS4(I,1)
            W4(I,2)=SS4(I,2)
 21       CONTINUE
          CALL DEMS(KO,SS4,W4,HT4,WT4)
        END IF
  7   CONTINUE
 60   FORMAT(F11.6,1X,F11.6,1X,F11.6)
C
C
C     CALCULATE FINAL DEM FROM ALTITUDES AND WEIGHTS
C
      DO 5 I=1,82
        DO 12 J=1,53
          ALT=0
          WGT=0
          IF(HT1(I,J).NE.-999)THEN
            ALT=HT1(I,J)*WT1(I,J)
            WGT=WT1(I,J)
          END IF
          IF(HT2(I,J).NE.-999)THEN
            ALT=(HT2(I,J)*WT2(I,J))+ALT
            WGT=WT2(I,J)+WGT
          END IF
          IF(HT3(I,J).NE.-999)THEN
            ALT=(HT3(I,J)*WT3(I,J))+ALT
            WGT=WT3(I,J)+WGT
          END IF
          IF(HT4(I,J).NE.-999)THEN
            ALT=(HT4(I,J)*WT4(I,J))+ALT
            WGT=WT4(I,J)+WGT
          END IF
          IF(ALT.EQ.0)ALT=-999
          IF(WGT.EQ.0)WGT=1
          DEM(I,J)=ALT/WGT
 12     CONTINUE
 5      CONTINUE
```

```
      DO 4 I=1,82
        WRITE(8,6)(DEM(I,J),J=1,53)
C       WRITE(3,6)(HT2(I,J),J=1,53)
C       WRITE(4,6)(HT3(I,J),J=1,53)
C       WRITE(5,6)(HT4(I,J),J=1,53)
C       WRITE(8,6)(HT3(I,J),J=1,53)
C       WRITE(9,6)(WT3(I,J),J=1,53)
C       WRITE(10,6)(HT4(I,J),J=1,53)
C       WRITE(11,6)(WT4(I,J),J=1,53)
    4  CONTINUE
    6  FORMAT(20F9.2/20F9.2/20F9.2/20F9.2/20F9.2)
  103  STOP
       END
C   END OF MAIN PROGRAM BLOCK
C
C   SUBROUTINES
C
       SUBROUTINE SORT(ICOUNT,DIST)
       REAL RRA,RRB,DIST(30000,3),RRC
       INTEGER IR,ICOUNT
       L=ICOUNT/2+1
       IR=ICOUNT
   10  CONTINUE
          IF(L.GT.1)THEN
             L=L-1
             RRA=DIST(L,1)
             RRB=DIST(L,2)
             RRC=DIST(L,3)
          ELSE
             RRA=DIST(IR,1)
             RRB=DIST(IR,2)
             RRC=DIST(IR,3)
             DIST(IR,1)=DIST(1,1)
             DIST(IR,2)=DIST(1,2)
             DIST(IR,3)=DIST(1,3)
             IR=IR-1
             IF(IR.EQ.1)THEN
                DIST(1,1)=RRA
                DIST(1,2)=RRB
                DIST(1,3)=RRC
                RETURN
             END IF
          END IF
          I=L
          J=L+L
   20     IF(J.LE.IR)THEN
             IF(J.LT.IR)THEN
                IF(DIST(J,1).LT.DIST(J+1,1))J=J+1
             END IF
             IF(RRA.LT.DIST(J,1))THEN
                DIST(I,1)=DIST(J,1)
                DIST(I,2)=DIST(J,2)
                DIST(I,3)=DIST(J,3)
                I=J
                J=J+J
             ELSE
                J=IR+1
             END IF
           GO TO 20
           END IF
           DIST(I,1)=RRA
           DIST(I,2)=RRB
           DIST(I,3)=RRC
         GO TO 10
         END
```

```
      SUBROUTINE SMSORT(KC,PROF,ICO,KO,DIS,SVAL,W)
      REAL PROF(30000,3),SMALL(30000,3),SVAL(30000,3)
     1 ,W(30000,3)
      REAL*8 XN(500),YN(500),KN(500),WORK1(600),
     1 CN(500),X,S
      INTEGER M,NCAP7,IFAIL,NCA,IFA,ICO,
     1 LWRK,MM
      KO=0
      KI=0
      DO 9 I=1,KC
        IF(PROF(I,1).EQ.PROF(I+1,1))THEN
          IF(ICO.EQ.0)THEN
            IFL=I
            ICO=ICO+1
            SMALL(ICO,1)=PROF(I,2)
            SMALL(ICO,2)=PROF(I,1)
            SMALL(ICO,3)=PROF(I,3)
          END IF
          ICO=ICO+1
          SMALL(ICO,1)=PROF(I+1,2)
          SMALL(ICO,2)=PROF(I+1,1)
          SMALL(ICO,3)=PROF(I+1,3)
        ELSE
          IF(ICO.GT.3)THEN
            CALL SORT(ICO,SMALL)
            ICOL=ICO+IFL-1
            KK=0
            DO 11 J=IFL,ICOL
              JJ=J-(IFL-1)
              PROF(J,1)=SMALL(JJ,2)
              PROF(J,2)=SMALL(JJ,1)
              PROF(J,3)=SMALL(JJ,3)
              IF(SMALL(JJ,1).NE.SMALL(JJ-1,1))THEN
                KK=KK+1
                XN(KK)=SMALL(JJ,1)
                YN(KK)=SMALL(JJ,3)
              END IF
 11           CONTINUE
            M=KK
            NCAP7=M+4
            LWRK=6*M+16
            IFAIL=0
            CALL E01BAF(M,XN,YN,KN,CN,NCAP7,WORK1,LWRK,IFAIL)
            DO 17 L=1,999
              IF(L.EQ.1)THEN
                U=KN(4)
                UU=AMOD(U,DIS)
                IF(UU.EQ.0.0)THEN
                  X=KN(4)
C                 XX=X
                ELSE
                  X=(INT(KN(4)/DIS)*DIS)+DIS
C                 XX=X
                END IF
                DO 22 N=1,999
                  IF(XN(N).EQ.X)THEN
                    XFL=N
                    WT=1/SQRT(DIS)
                    GOTO 23
                  END IF
                  IF(XN(N).GT.X)THEN
                    XFL=N-1
                    WA=1/SQRT(X-XN(XFL))
                    WB=1/SQRT(XN(N)-X)
                    WT=WA+WB
                    GOTO 23
```

```
                END IF
   22           CONTINUE
   23           CONTINUE
              ELSE
                X=X+DIS
                DO 24 N=XFL,999
                  IF(XN(N).EQ.X)THEN
                    XFL=N
                    WT=1/SQRT(DIS)
                    GOTO 25
                  END IF
                  IF(XN(N).GT.X)THEN
                    XFL=N-1
                    WA=1/SQRT(X-XN(XFL))
                    WB=1/SQRT(XN(N)-X)
                    WT=WA+WB
                    GOTO 25
                  END IF
   24           CONTINUE
   25           CONTINUE
              END IF
              IF(X.GT.KN(NCAP7-3).OR.X.LT.KN(4))GOTO 30
              IFA=0
              CALL E02BBF(NCAP7,KN,CN,X,S,IFA)
C       CHECK SPLINE ESTIMATE TO CHECK FOR REALISM
              IF(YN(XFL).EQ.YN(N))THEN
                V=YN(N)-S
                IF(V.GT.4)S=YN(N)-4
                IF(V.LT.-4)S=YN(N)+4
              END IF
              VV=YN(XFL)-S
              V=YN(N)-S
              IF(YN(XFL).GT.YN(N))THEN
                IF(VV.LT.-4)S=YN(XFL)+4
                IF(V.GT.4)S=YN(N)-4
              END IF
              IF(YN(XFL).LT.YN(N))THEN
                IF(VV.GT.4)S=YN(XFL)-4
                IF(V.LT.-4)S=YN(N)+4
              END IF
C
C             WRITE(5,'(F11.6,1X,F11.6)')YN(XFL),YN(N),S
C             IF(S.LT.100.OR.S.GT.200)THEN
C              IF(KI.EQ.1)THEN
C             PRINT *,XN(XFL),' ',XN(N),' ',S,' ',KO,X
C               DO 101 II=1,KK
C                 WRITE(5,'(F11.6,1X,F11.6)')XN(II),YN(II)
C                 DO 104 JJ=1,999
C                 IF(XX.GT.XN(II).AND.XX.LT.XN(II+1))THEN
C                  WRITE(5,'(F11.6)')XX
C                  XX=XX+DIS
C                 ELSE
C                   GOTO 105
C                 END IF
C104             CONTINUE
C105             CONTINUE
C101             CONTINUE
C             KO=-1
C             GOTO 102
C             ELSE
C             KI=KI+1
C             END IF
C             END IF
              KO=KO+1
              SVAL(KO,1)=PROF(J,1)
              SVAL(KO,2)=X
```

```
                SVAL(KO,3)=S
                W(KO,1)=PROF(J,1)
                W(KO,2)=X
                W(KO,3)=WT
   51           FORMAT(4F12.3,1X,I6)
   17         CONTINUE
   30         CONTINUE
            END IF
          ICO=0
          END IF
    9   CONTINUE
  102   END
C
      SUBROUTINE DEMS(KO,SSS,W,HT,WT)
      REAL SSS(30000,3),W(30000,3),HT(160,100),WT(160,100)
      INTEGER KO
      DO 16 I=1,82
        DO 18 J=1,53
          HT(I,J)=-999
          WT(I,J)=-1
   18   CONTINUE
   16   CONTINUE
        DO 26 K=1,KO
          LY=SSS(K,2)-40
          LO=(82-LY)+1
          I=LY-(LY-LO)
          J=SSS(K,1)-47
          IF(I.GE.1.AND.I.LE.82.AND.J.GE.1.AND.J.LE.53)THEN
            HT(I,J)=SSS(K,3)
            WT(I,J)=W(K,3)
          END IF
   26   CONTINUE
        END
```

FASTFRAC

```
C     ********************************************
C     PROGRAM TO CALCULATE LOG MEAN HEIGHT VARIANCE
C     FOR DIFFERENT DISTANCES
C     ********************************************
C
C       COLIN McCLEAN 1987
C
C     ******************
C     MAIN PROGRAM BLOCK
C     ******************
C
C     ****************************
C     DECLARATION OF VARIABLE TYPES
C     ****************************
      INTEGER GR,COL,ROW,L,K,HCOUNT,NCOL,NROW,
     1 NR,NC,CD(2000),NCO,NRO,INC,INCA,FIN
     1 ,FINI,START,STAR
      REAL HT(500,500),DIST(2000),HV(2000),
     1 CONV,GS
      CHARACTER FMT*107
      CHARACTER*80 TITLE
C     **********
C        INPUT
C     **********
C     READ IN TITLE FOR GIMMS PLOTS
      READ(5,'(A80)')TITLE
C
C     READ IN CONVERSION FACTOR
      READ(5,3000)CONV
 3000 FORMAT(F7.4)
C
C     READ IN NUMBER OF ROWS IN MATRIX
      READ(5,3100)NROW
 3100 FORMAT(I3)
C
C     READ IN NUMBER OF COLUMNS IN MATRIX
      READ(5,3100)NCOL
C
C     READ GRID SIZE
      READ(5,3100)GR
      READ(5,3100)IAG
      READ(5,3100)IAG
C
C     READ IN DATA FORMAT
      READ(5,4000)FMT
 4000 FORMAT(A100)
C
C     READ IN ALTITUDE MATRIX
      DO 500 I=1,NROW
        READ(10,FMT)(HT(I,J),J=1,NCOL)
  500 CONTINUE
C
C     CONVERT TO METRES
      IF(CONV.NE.1)THEN
      DO 1500 I=1,NROW
        DO 1550 J=1,NCOL
          HT(I,J)=HT(I,J)*CONV
 1550   CONTINUE
 1500 CONTINUE
      END IF
C     ****************************
C     INITIALISE CONTROL VARIABLES
```

```
C     ****************************
      NR=NROW-10
      NC=NCOL-10
      NCO=NCOL/2
      NRO=NROW/2
      HCOUNT=0
      INC=(NC-5)/10
      START=INC+5
      INCA=(NR-5)/10
      STAR=INCA+5
      LUP=1
      KUP=1
C     ****************************************
C     INITIATE LOOP CONTROLLING SMALLER DISTANCES
C     ****************************************
      DO 550 L=1,INC,LUP
        IF(L.EQ.5)LUP=2
        GS=GR*L
C     START CALCULATING HEIGHT DIFFERENCES
        COL=NCOL-L
        ROW=NROW-L
        CALL ABSOL(NROW,COL,HT,L,NCOL,ROW,HCOUNT,HV,CD
     1  ,NCO,NRO,NR)
C     CALCULATES HORIZONTAL DISTANCES
        DIST(HCOUNT)=ALOG10(GS)
C     INITIATE LOOP CONTROLLING DIAGONAL RELATIONSHIP
        DO 800 K=1,INCA,KUP
          IF(K.EQ.5)KUP=2
          CALL DIAGO(NROW,COL,NCOL,L,HT,HV,HCOUNT
     1      ,DIST,GR,GS,CD,K,NCO)
  800   CONTINUE
        DO 2500 K=STAR,NR,INCA
          CALL DIAGO(NROW,COL,NCOL,L,HT,HV,HCOUNT
     1      ,DIST,GR,GS,CD,K,NCO)
 2500   CONTINUE
  550 CONTINUE
C     ****************************************
C     INITIATE LOOP CONTROLLING LARGER DISTANCES
C     ****************************************
      DO 6000 L=START,NC,INC
        GS=GR*L
C     START CALCULATING HEIGHT DIFFERENCES
        COL=NCOL-L
        ROW=NROW-L
        CALL ABSOL(NROW,COL,HT,L,NCOL,ROW,HCOUNT,HV,CD
     1  ,NCO,NRO,NR)
        DIST(HCOUNT)=ALOG10(GS)
        DO 6100 K=1,5
          CALL DIAGO(NROW,COL,NCOL,L,HT,HV,HCOUNT
     1      ,DIST,GR,GS,CD,K,NCO)
 6100   CONTINUE
        DO 6200 K=STAR,NR,INCA
          CALL DIAGO(NROW,COL,NCOL,L,HT,HV,HCOUNT
     1      ,DIST,GR,GS,CD,K,NCO)
 6200   CONTINUE
 6000 CONTINUE
C     ******
C     OUTPUT
C     ******
C     SORT HV AND DIST BY DIST
      CALL SORT(HCOUNT,DIST,HV,CD)
      CALL AVWRIT(HCOUNT,DIST,HV,CD,TITLE)
      STOP
      END
C     ************************
C     END OF MAIN PROGRAM BLOCK
```

```
C     ************************
C
C     ****************************************************
      SUBROUTINE ABSOL(NROW,COL,HT,L,NCOL,ROW,HCOUNT,HV,CD
     1 ,NCO,NRO,NR)
C     ****************************************************
      REAL HT(500,500),HR,HV(2000)
      INTEGER CM,COL,NROW,NCOL,L,ROW,HCOUNT,CD(2000)
      INTEGER INCB,INCC,NCO,NRO,NR
        HCOUNT=HCOUNT+1
        HR=0
        CM=0
        INCB=3
        INCC=3
        IF(L.GE.NCO)INCB=1
        DO 600 I=1,NROW
          DO 650 J=1,COL,INCB
            IF(HT(I,J).NE.0.AND.HT(I,J+L).NE.0)THEN
            HR=((HT(I,J)-HT(I,J+L))**2)+HR
            CM=CM+1
            END IF
  650     CONTINUE
  600   CONTINUE
        IF(L.GT.NR)GO TO 6300
        IF(L.GE.NRO)INCC=1
        DO 700 J=1,NCOL
          DO 750 I=1,ROW,INCC
            IF(HT(I,J).NE.0.0.AND.HT(I+L,J).NE.0.0)THEN
            HR=((HT(I,J)-HT(I+L,J))**2)+HR
            CM=CM+1
            END IF
  750     CONTINUE
  700   CONTINUE
 6300   HV(HCOUNT)=ALOG10(HR/CM)
        CD(HCOUNT)=CM
        RETURN
        END
C     ********************************************
      SUBROUTINE DIAGO(NROW,COL,NCOL,L,HT,HV,HCOUNT
     1     ,DIST,GR,GS,CD,K,NCO)
C     ********************************************
      REAL HT(500,500),HV(2000),HR,DIST(2000),DDIS,GS
      INTEGER CM,DIA,COL,GR,HCOUNT,NROW,NCOL,L,CD(2000)
      INTEGER K,INCD,NCO,JJ
        HCOUNT=HCOUNT+1
        DDIS=0
        DDIS=SQRT((GS**2)+((GR*K)**2))
        DIST(HCOUNT)=ALOG10(DDIS)
        DIA=NROW-K
        HR=0
        CM=0
        INCD=3
        IF(L.GE.NCO)INCD=1
        DO 850 I=1,DIA
          DO 900 J=1,COL,INCD
            JJ=NCOL-(L+(J-1))
            IF(HT(I,J).NE.0.0.AND.HT(I+K,J+L).NE.0.0)THEN
              HR=((HT(I,J)-HT(I+K,J+L))**2)+HR
              CM=CM+1
            END IF
            IF(HT(I,NCOL+1-J).NE.0.0.AND.HT(I+K,JJ).NE.0.0)THEN
              HR=((HT(I,NCOL+1-J)-HT(I+K,JJ))**2)+HR
              CM=CM+1
            END IF
  900     CONTINUE
  850   CONTINUE
```

```
      HV(HCOUNT)=ALOG10(HR/CM)
      CD(HCOUNT)=CM
  800 CONTINUE
      RETURN
      END
C     ***********************************
      SUBROUTINE SORT(HCOUNT,DIST,HV,CD)
C     ***********************************
      REAL RRA,RRB,DIST(2000),HV(2000)
      INTEGER IR,HCOUNT,RRC,CD(2000)
      L=HCOUNT/2+1
      IR=HCOUNT
   10 CONTINUE
         IF(L.GT.1)THEN
            L=L-1
            RRA=DIST(L)
            RRB=HV(L)
            RRC=CD(L)
         ELSE
            RRA=DIST(IR)
            RRB=HV(IR)
            RRC=CD(IR)
            DIST(IR)=DIST(1)
            HV(IR)=HV(1)
            CD(IR)=CD(1)
            IR=IR-1
            IF(IR.EQ.1)THEN
               DIST(1)=RRA
               HV(1)=RRB
               CD(1)=RRC
               RETURN
            END IF
        END IF
        I=L
        J=L+L
   20   IF(J.LE.IR)THEN
           IF(J.LT.IR)THEN
              IF(DIST(J).LT.DIST(J+1))J=J+1
           END IF
           IF(RRA.LT.DIST(J))THEN
              DIST(I)=DIST(J)
              HV(I)=HV(J)
              CD(I)=CD(J)
              I=J
              J=J+J
           ELSE
              J=IR+1
           END IF
        GO TO 20
        END IF
        DIST(I)=RRA
        HV(I)=RRB
        CD(I)=RRC
      GO TO 10
      END
C     ***********************************
      SUBROUTINE AVWRIT(HCOUNT,DIST,HV,CD,TITLE)
C     ***********************************
      REAL DIST(2000),HV(2000),DUM,BVAR,SVAR
      INTEGER HCOUN,COUNT,HCOUNT,CD(2000),DUMB,KO
      CHARACTER*80 TITLE
      HCOUN=HCOUNT-1
      DUM=0
      DUMB=0
      BVAR=0.0
      SVAR=100.0
```

```
      KO=0
      COUNT=0
      DO 60 I=1,HCOUN
        IF(DIST(I).NE.DIST(I+1))THEN
          IF(DUM.NE.0)THEN
            COUNT=COUNT+1
            HV(I)=(DUM+HV(I))/COUNT
            CD(I)=DUMB+CD(I)
          END IF
          COUNT=0
          DUM=0
          DUMB=0
          SVAR=AMIN1(SVAR,HV(I))
          BVAR=AMAX1(BVAR,HV(I))
          KO=KO+1
          WRITE(13,1000)HV(I),DIST(I),CD(I)
        ELSE
          DUM=DUM+HV(I)
          DUMB=DUMB+CD(I)
          COUNT=COUNT+1
        END IF
 60   CONTINUE
1000  FORMAT(1X,F12.4,1X,F12.4,I8)
      WRITE(13,1000)HV(HCOUNT),DIST(HCOUNT),CD(HCOUNT)
      BVAR=AMAX1(BVAR,HV(HCOUNT))
      SVAR=AMIN1(SVAR,HV(HCOUNT))
      KO=KO+1
      WRITE(15,1045)KO
1045  FORMAT('*FILEIN DATAFILE ZONES=',I3,',VARS=2')
      WRITE(15,1010)SVAR,BVAR
1010  FORMAT(1X,'YMIN=',F7.4,',YMAX=',F7.4,',YUNITS=0.5')
      WRITE(15,1020)DIST(1),DIST(HCOUNT)
1020  FORMAT(1X,'XMIN=',F7.4,',XMAX=',F7.4,',XUNITS=0.2')
      WRITE(15,1030)TITLE
1030  FORMAT(1X,'TITLE=',A50)
      RETURN
      END
```

RS.FOR

```
C      PROGRAM TO PERFORM R/S ANALYSIS OF LANDSURFACES
       REAL HT(201,201),OUT(50000),MAS,MIS,MEAN,RSJ(50000)
      1 ,RSD(50000),DIST(50000),DIF(50000)
       INTEGER X,Y,FIN1,FIN2,TEST,START,STAR,FINI,FIN,GR
       CHARACTER FMT*25,TITLE*50
C  READ DATA IN
C
       READ(5,'(A50)')TITLE
C      PRINT *,'ENTER NO. OF COLUMNS:'
       READ(5,'(I3)')NCOL
C      PRINT *,'ENTER NO. OF ROWS:'
       READ(5,'(I3)')NROW
       READ(5,'(I3)')GR
C      PRINT *,'ENTER FORMAT STATEMENT IN BRACKETS:'
       READ(5,'(A25)')FMT
       DO 1 I=1,NROW
         READ(1,FMT)(HT(I,J),J=1,NCOL)
         DO 2 J=1,NCOL
 2       CONTINUE
 1     CONTINUE
C
C    spiral through dem making one string of altitudes
C
       LEN=NROW*NCOL
       FIN1=NCOL
       FIN2=NROW
       TEST=0
       Y=1
       X=0
       DO 3 I=1,LEN
         IF(TEST.EQ.0)THEN
           X=X+1
           OUT(I)=HT(Y,X)
           IF(X.EQ.FIN1)THEN
             FIN1=NCOL-(FIN1-1)
             TEST=1
           END IF
         ELSE
           IF(TEST.EQ.1)THEN
             Y=Y+1
             OUT(I)=HT(Y,X)
             IF(FIN2.EQ.Y)THEN
               FIN2=(NROW+1)-(FIN2-1)
               TEST=2
             END IF
           ELSE
             IF(TEST.EQ.2)THEN
               X=X-1
               OUT(I)=HT(Y,X)
               IF(FIN1.EQ.X)THEN
                 FIN1=NCOL-FIN1
                 TEST=3
               END IF
             ELSE
               IF(TEST.EQ.3)THEN
                 Y=Y-1
                 OUT(I)=HT(Y,X)
                 IF(FIN2.EQ.Y)THEN
                   FIN2=NROW-(FIN2-1)
                   TEST=0
                 END IF
               END IF
```

```
            END IF
          END IF
        END IF
3     CONTINUE
      PRINT *,LEN
C
C   CALCULATE INCREMENTS
C
      DO 10 I=2,LEN-1
        DIF(I-1)=OUT(I)-OUT(I-1)
 10   CONTINUE
C
C   R/S ANALYSIS
C
      IHALF=(LEN-1)/2
      KCC=0
      DO 4 I=1,4
        IF(I.EQ.1)THEN
          START=5
          FINI=10
          INC=1
        ELSE
          START=FINI*2
          FINI=FINI*10
          INC=INC*10
        END IF
        DO 5 J=START,FINI,INC
          IF(J.GT.IHALF)GOTO 100
          KCC=KCC+1
          NCALS=(LEN-1)/J
          KC=0
          RS=0
          RS2=0
          DO 6 K=1,NCALS
            KC=KC+1
            IF(K.EQ.1)THEN
              STAR=1
              FIN=J
            ELSE
              STAR=FIN+1
              FIN=FIN+J
            END IF
            SUM=0
            SUM2=0
            DO 7 L=STAR,FIN
              SUM=DIF(L)+SUM
              SUM2=(DIF(L)**2)+SUM2
 7          CONTINUE
            MEAN=SUM/J
            TERM1=J*SUM2
            TERM2=SUM*SUM
C           WRITE(3,'(F20.5,1X,F20.5)')TERM1,TERM2
            IF(TERM1.GT.TERM2)THEN
            SD=SQRT(((J*SUM2)-(SUM*SUM))/(J*(J-1)))
            MAS=0
            MIS=99999
            CSUM=0
            DO 8 M=STAR,FIN
              CSUM=(DIF(M)-MEAN)+CSUM
              MAS=AMAX1(MAS,CSUM)
              MIS=AMIN1(MIS,CSUM)
8           CONTINUE
            RS=((MAS-MIS)/SD)+RS
            RS2=((MAS-MIS)**2)+RS2
          END IF
6         CONTINUE
```

```
          RMA=0
          RMI=9999 .
          RSJ(KCC)=ALOG10(RS/NCALS)
          RSD(KCC)=SQRT(((NCALS*RS2)-(RS**2))/(NCALS*(NCALS-1)))
          O=J*GR
          DIST(KCC)=ALOG10(O)
5       CONTINUE
4     CONTINUE
C
C   OUTPUT
C
100   CONTINUE
      DO 9 I=1,KCC
        WRITE(2,'(1X,F12.4,1X,F12.4)')RSJ(I),DIST(I)
9     CONTINUE
      WRITE(3,1045)KCC
1045  FORMAT('*FILEIN DATAFILE ZONES=',I2,',VARS=2')
      WRITE(3,1010)RSJ(1),RSJ(KCC)
1010  FORMAT(1X,'YMIN=',F7.4,',YMAX=',F7.4,',YUNITS=0.5')
      WRITE(3,1020)DIST(1),DIST(KCC)
1020  FORMAT(1X,'XMIN=',F7.4,',XMAX=',F7.4,',XUINTS=0.2')
      WRITE(3,1030)TITLE
1030  FORMAT(1X,'TITLE=',A50)
      STOP
      END
```

FRACSIM.FOR

```
C       PROGRAM TO SIMULATE FRACTAL BROWNIAN
C       SURFACES BY SHEAR DISPLACEMENT METHOD
        REAL HT(100,100)
        REAL*8 G05DAF,G05DDF
        REAL XY(4)
        PI=22/7
        DO 1 I=1,100
          DO 2 J=1,100
            HT(I,J)=0
 2        CONTINUE
 1      CONTINUE
        CALL G05CCF
        DO 3 K=1,500
          DO 4 I=1,4
            XY(I)=G05DAF(1.0,100.0)
 4        CONTINUE
          IF(XY(1).NE.XY(2).AND.XY(3).NE.XY(4))THEN
          ALT=G05DDF(0.0,1.00)
          B=(XY(1)-XY(2))/(XY(3)-XY(4))
          A=XY(1)-(XY(3)*B)
          H=0.1
          DO 5 I=1,100
            DO 6 J=1,100
              Y=A+(B*J)
              X=(I-A)/B
              DIST4=Y-I
              IF(DIST4.GT.0)THEN
                DIST1=ABS(DIST4)
                DIST2=ABS(X-J)
                DIST3=SQRT((DIST2**2)+(DIST1**2))
                ANG=DIST1/DIST3
                DIST=DIST2*ANG
                HT(I,J)=HT(I,J)+(ALT*(-(DIST**(H-0.5))))
              ELSE
                IF(DIST4.LT.0)THEN
                  DIST1=ABS(DIST4)
                  DIST2=ABS(X-J)
                  DIST3=SQRT((DIST2**2)+(DIST1**2))
                  ANG=DIST1/DIST3
                  DIST=DIST2*ANG
                  HT(I,J)=HT(I,J)+(ALT*(DIST**(H-0.5)))
                END IF
              END IF
 6          CONTINUE
 5        CONTINUE
          END IF
 3      CONTINUE
        DO 7 I=1,100
          WRITE(1,'(50F12.3)')(HT(I,J),J=1,100)
 7      CONTINUE
        STOP
        END
```

Appendix 2: Variograms Calculated from Fractal Surfaces

FRACTAL 1.0: ALT.VARIANCE AGAINST DISTANCE

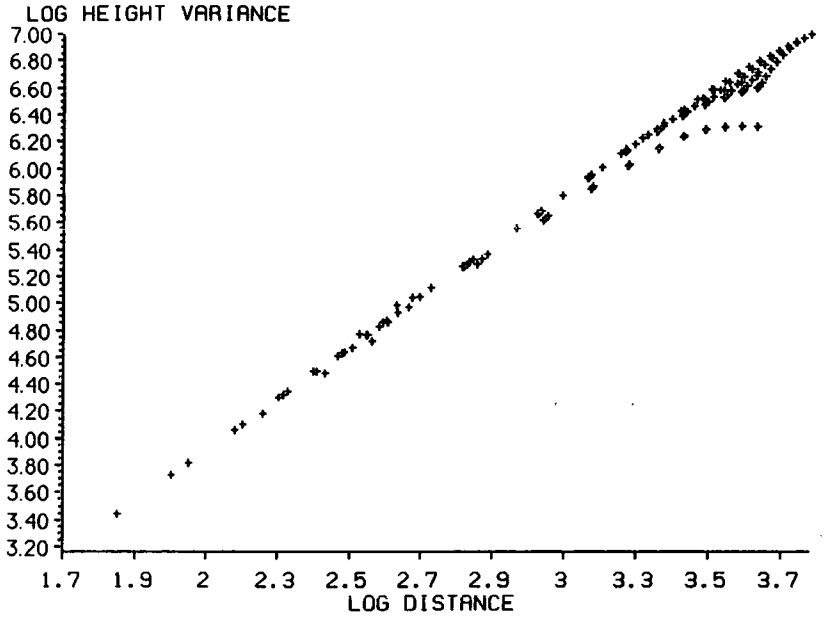

FRACTAL 1.0: ALT.VARIANCE AGAINST DISTANCE

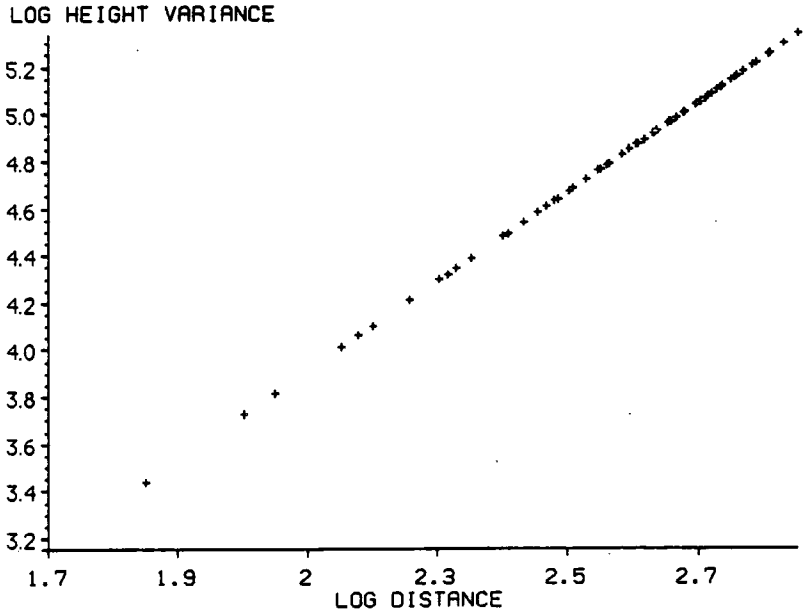

FRAC1.0: RESCALED RANGE Vs. DISTANCE

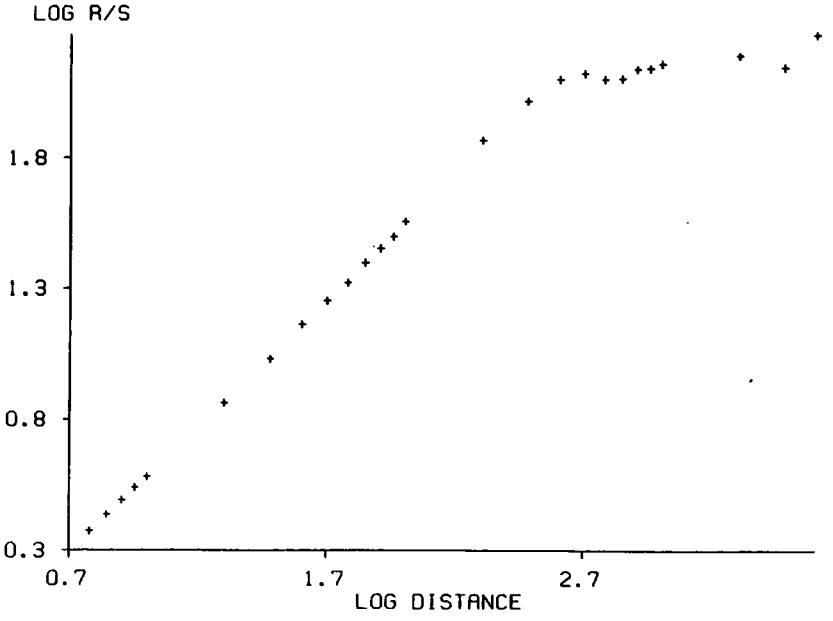

FRACTAL 0.9: ALT.VARIANCE AGAINST DISTANCE

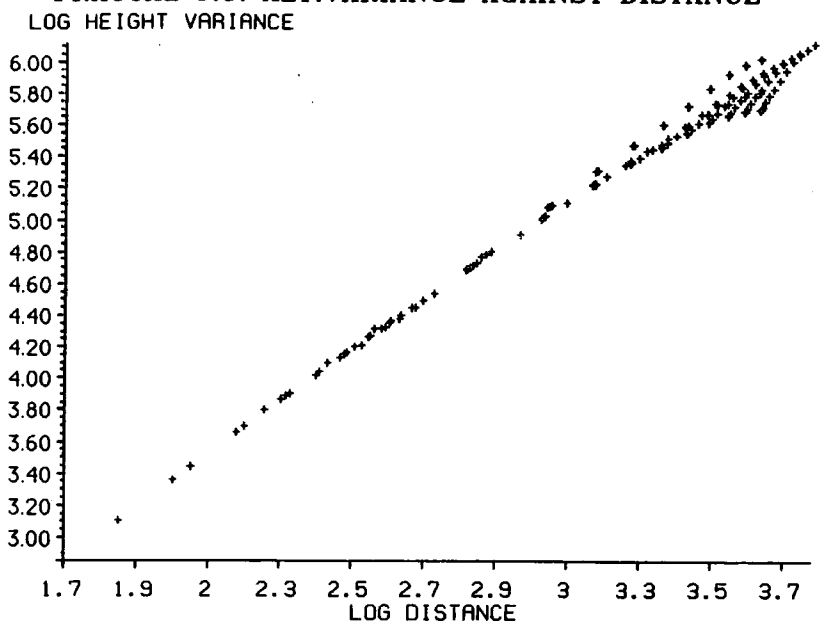

FRACTAL 0.9: ALT.VARIANCE AGAINST DISTANCE

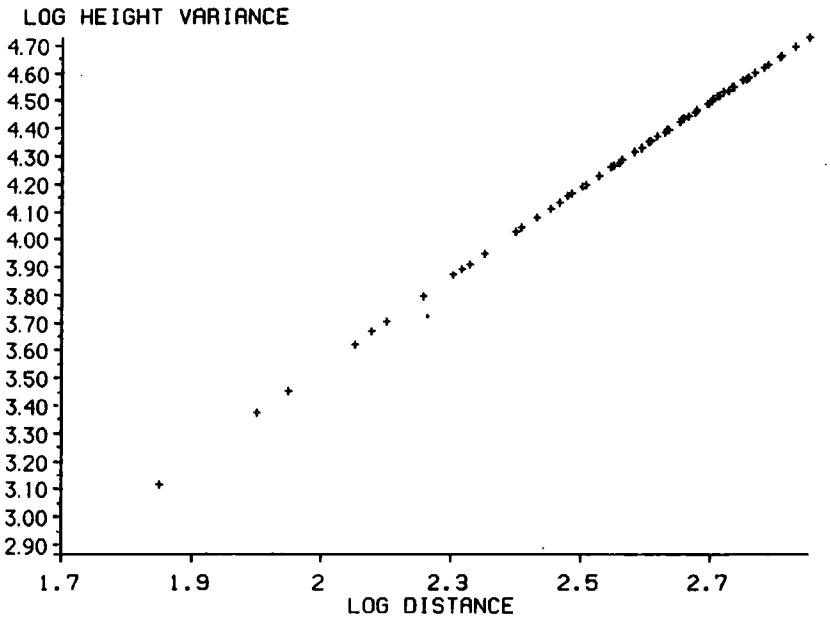

FRAC0.9: RESCALED RANGE Vs. DISTANCE

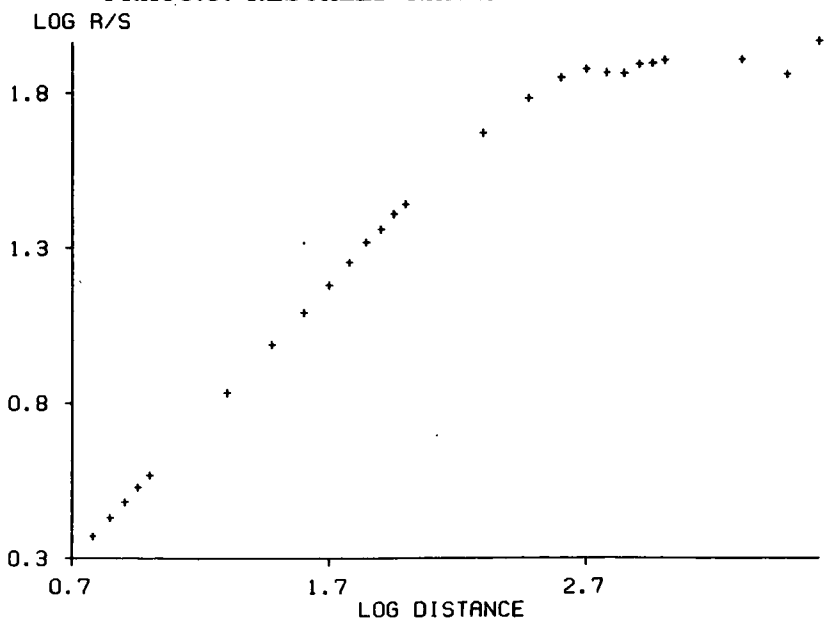

FRACTAL 0.8: ALT.VARIANCE AGAINST DISTANCE

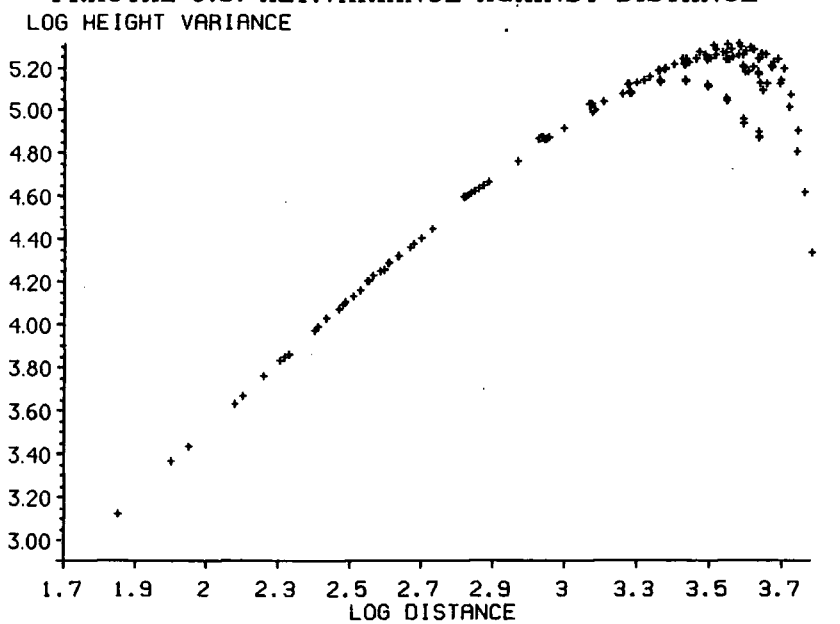

FRACTAL 0.8: ALT.VARIANCE AGAINST DISTANCE

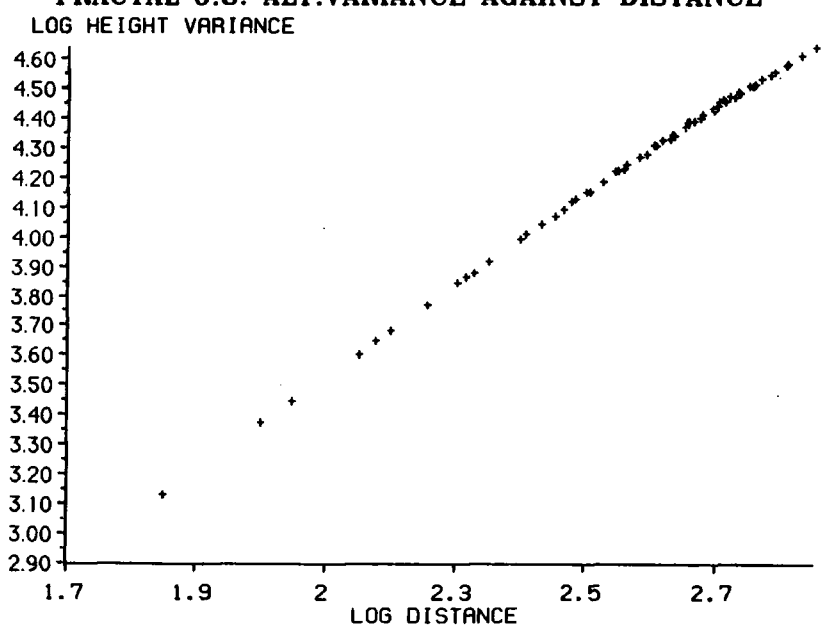

FRACO.8: RESCALED RANGE Vs. DISTANCE

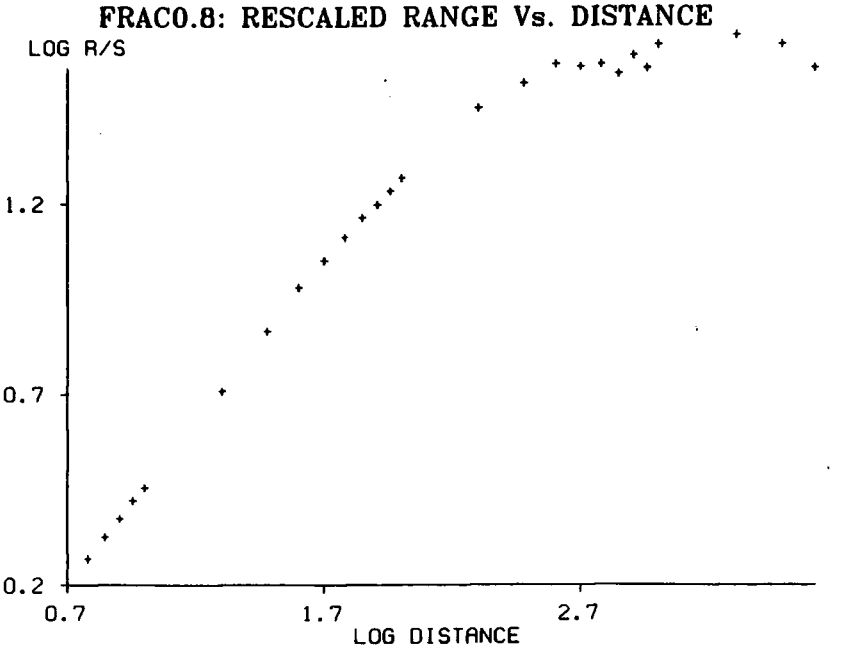

FRACTAL 0.7: ALT.VARIANCE AGAINST DISTANCE

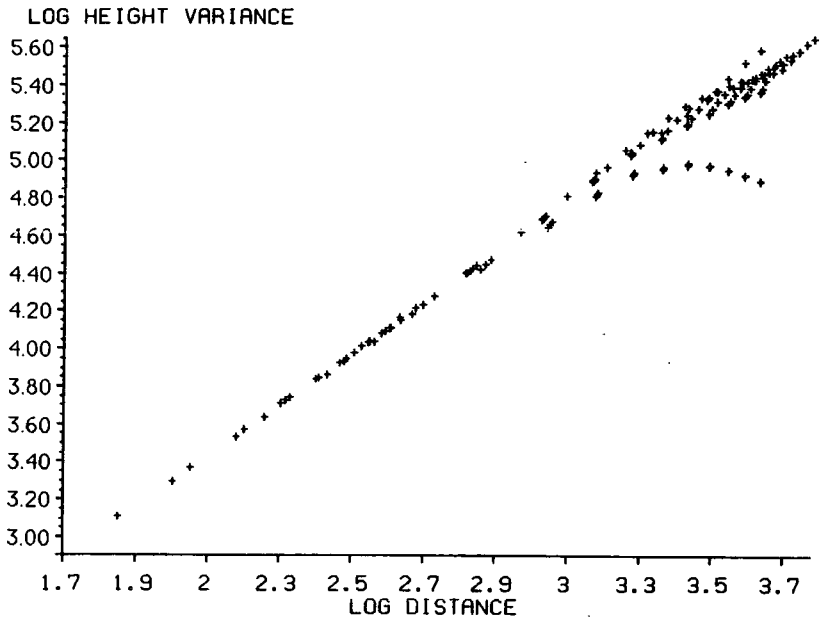

FRACTAL 0.7: ALT.VARIANCE AGAINST DISTANCE

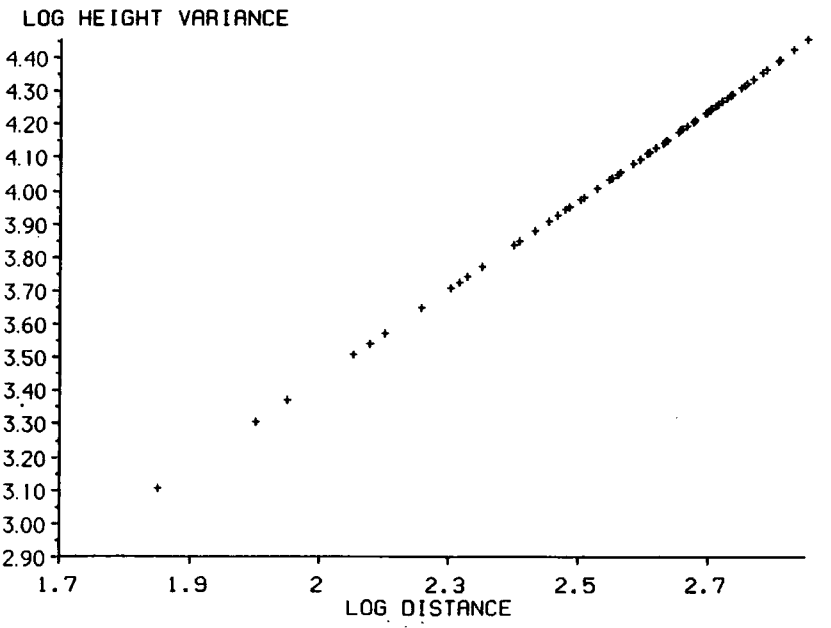

FRACO.7: RESCALED RANGE Vs. DISTANCE

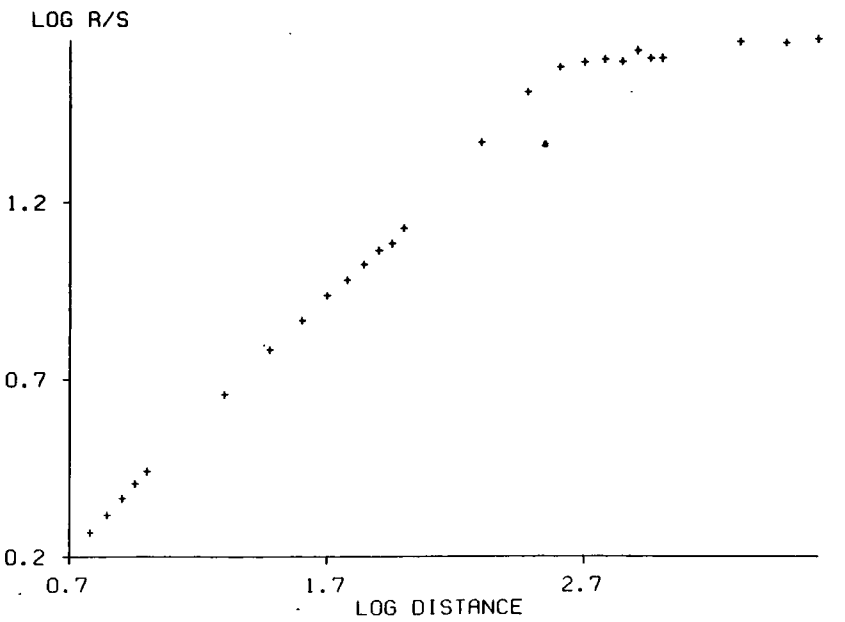

FRACTAL 0.6: ALT.VARIANCE AGAINST DISTANCE

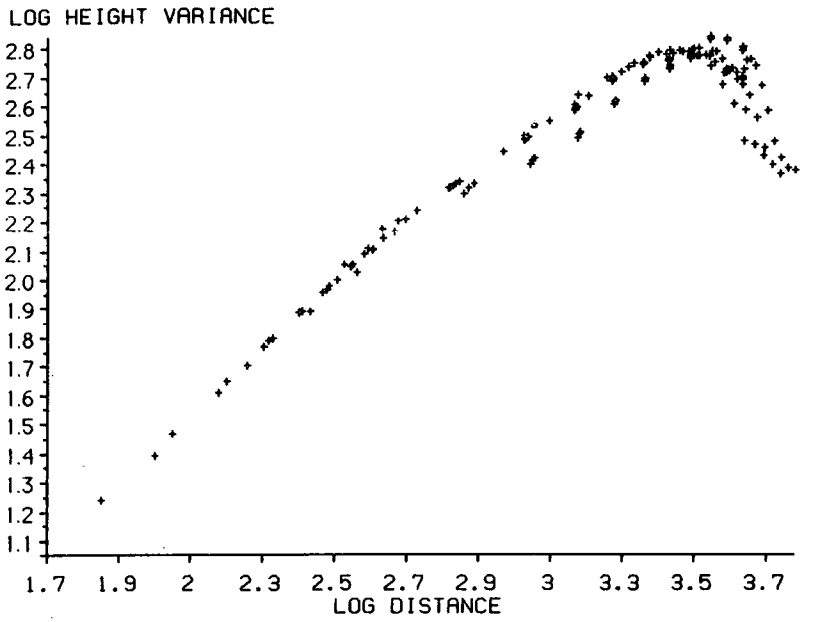

FRACTAL 0.6: ALT.VARIANCE AGAINST DISTANCE

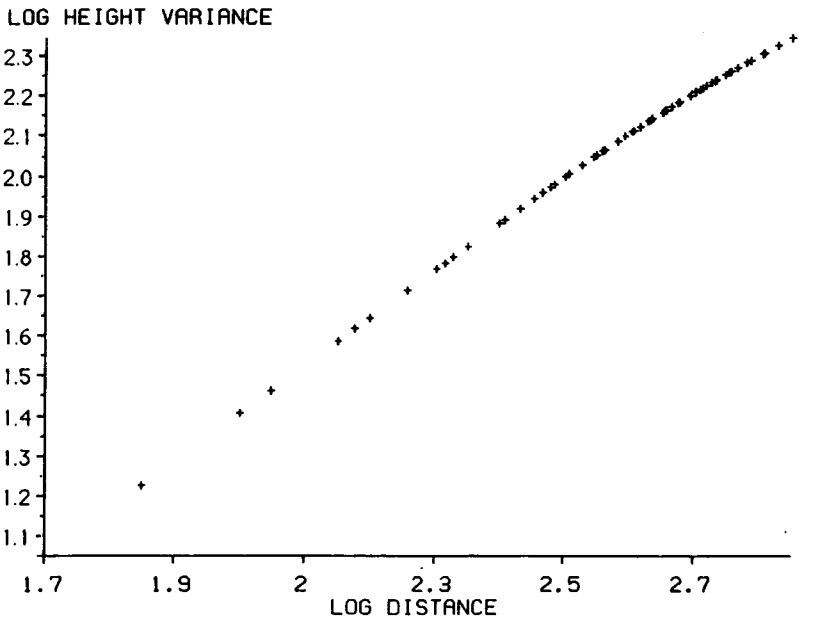

FRAC0.6: RESCALED RANGE Vs. DISTANCE

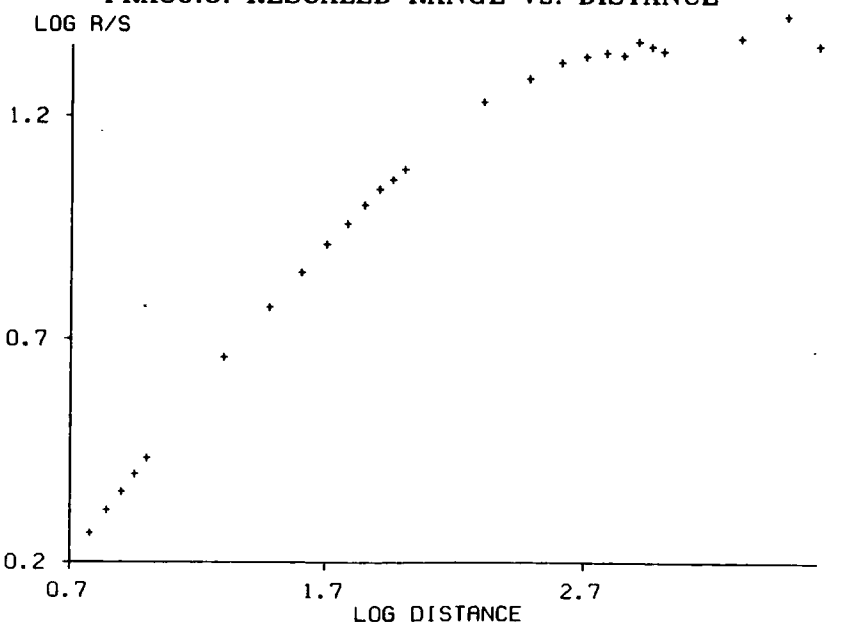

FRACTAL 0.5: ALT.VARIANCE AGAINST DISTANCE

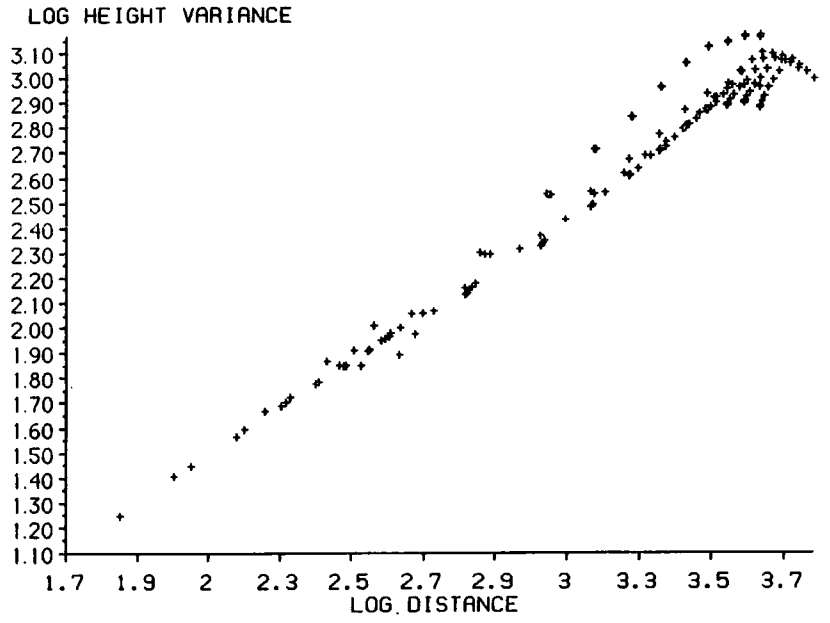

FRACTAL 0.5: ALT.VARIANCE AGAINST DISTANCE

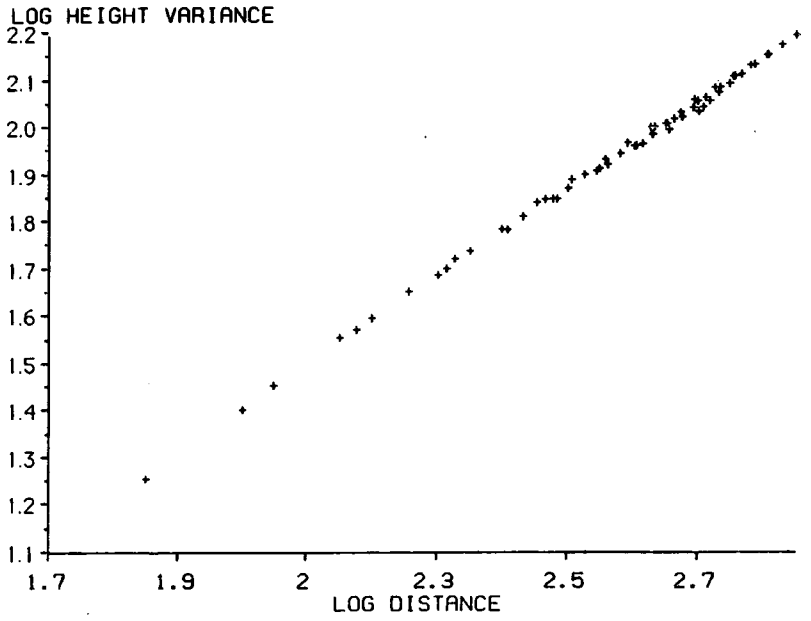

FRACO.5: RESCALED RANGE Vs. DISTANCE

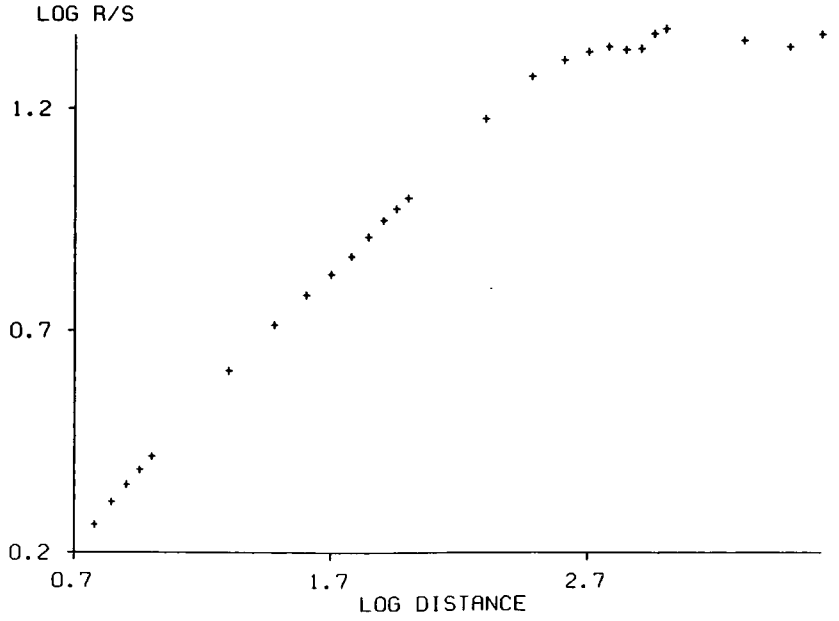

FRACTAL 0.4: ALT.VARIANCE AGAINST DISTANCE

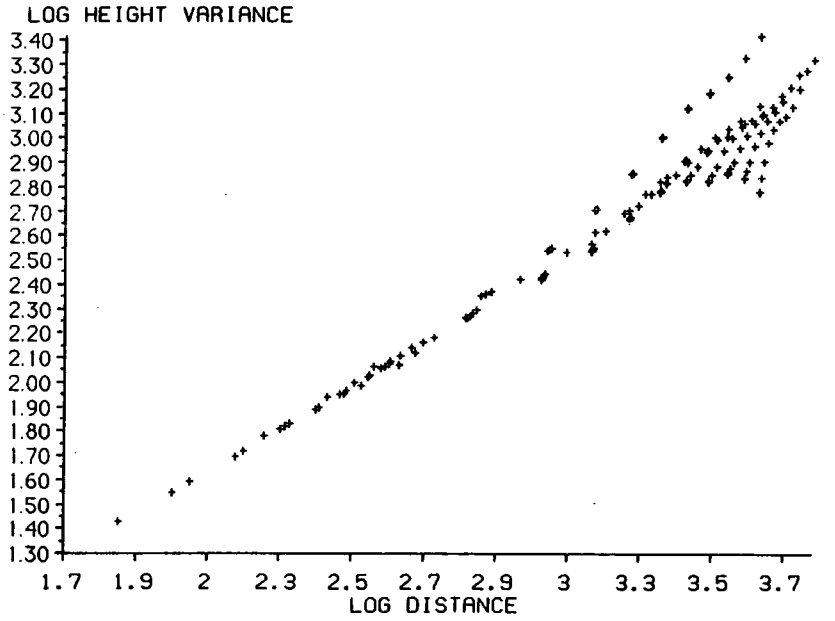

FRACTAL 0.4: ALT.VARIANCE AGAINST DISTANCE

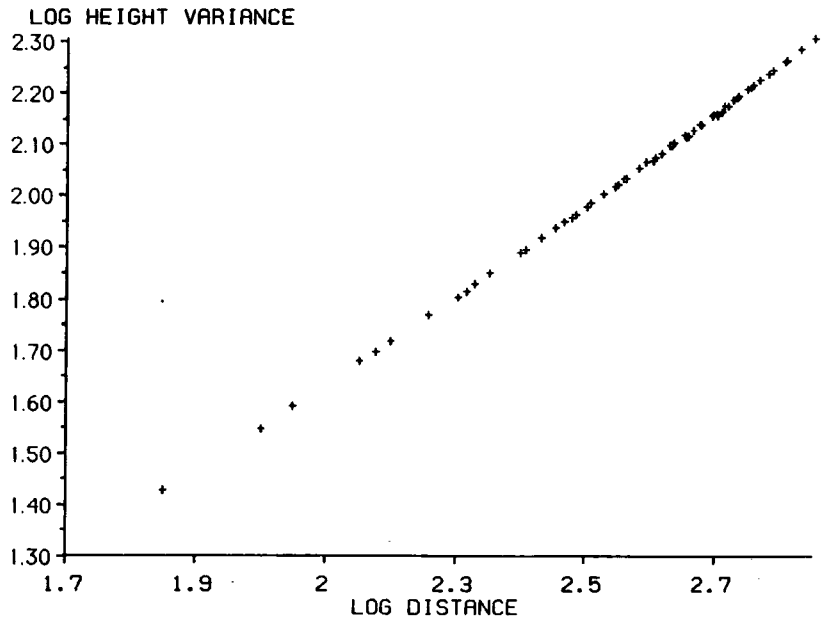

FRACO.4: RESCALED RANGE Vs. DISTANCE

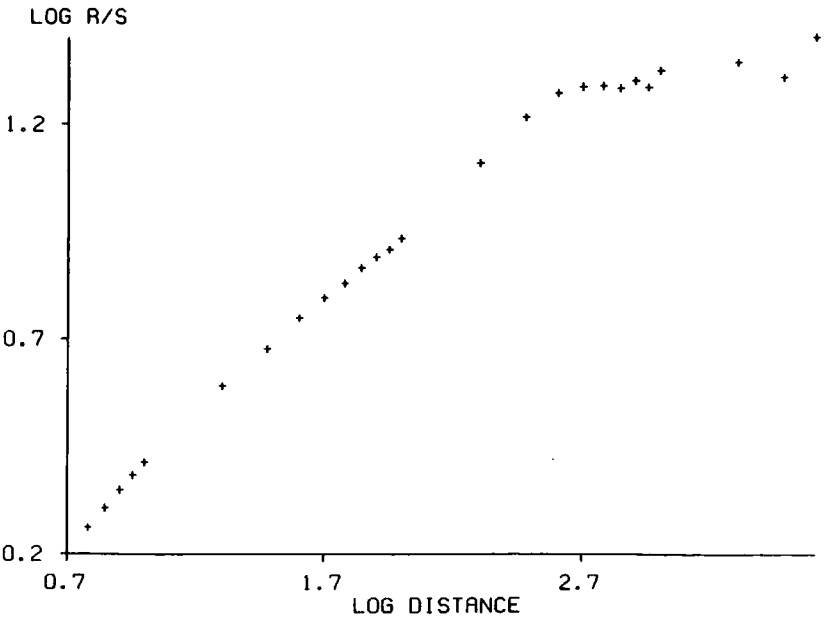

FRACTAL 0.3: ALT.VARIANCE AGAINST DISTANCE

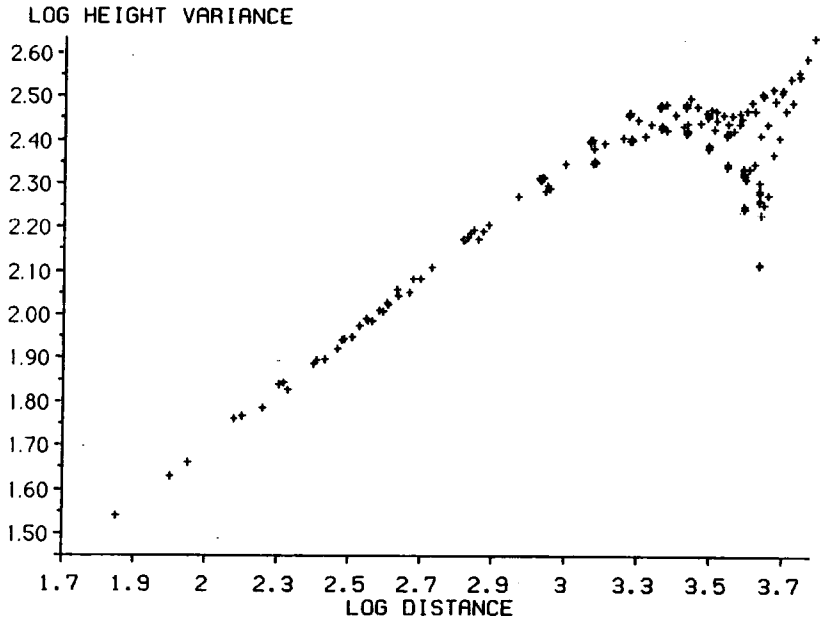

FRACTAL 0.3: ALT.VARIANCE AGAINST DISTANCE

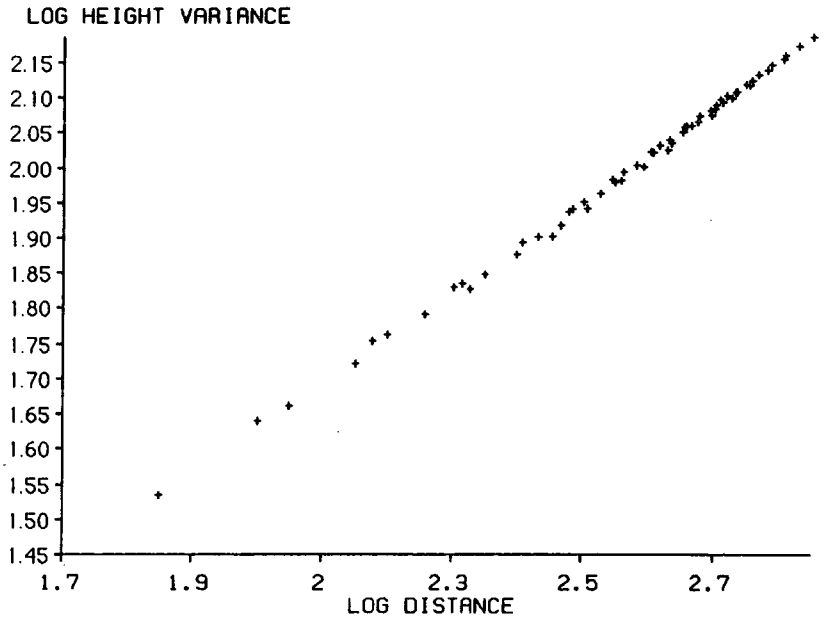

FRACO.3: RESCALED RANGE Vs. DISTANCE

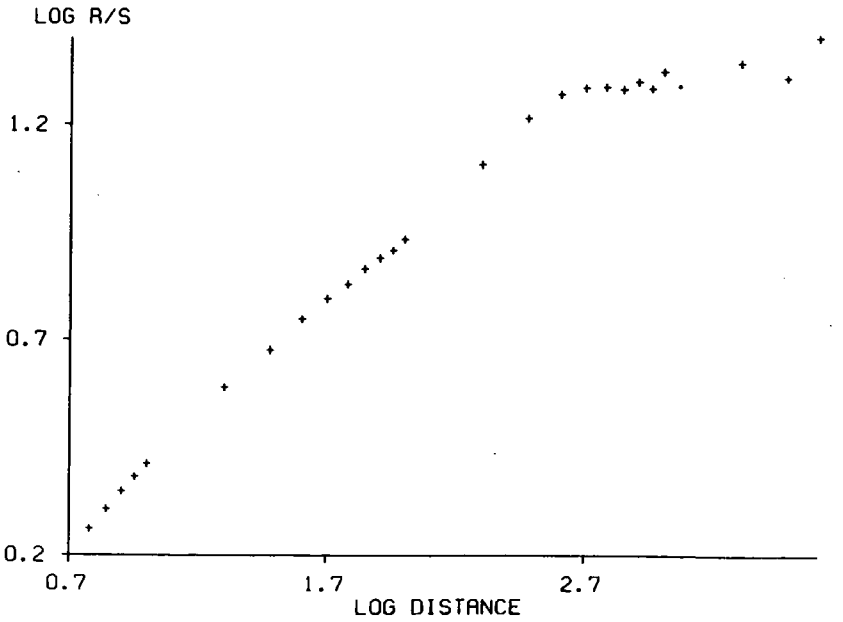

FRACTAL 0.2: ALT.VARIANCE AGAINST DISTANCE

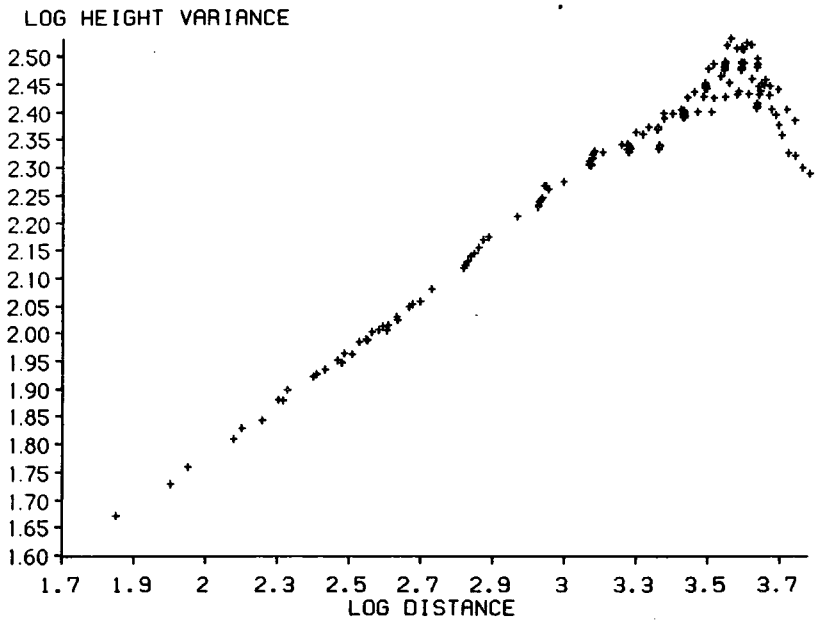

FRACTAL 0.2: ALT.VARIANCE AGAINST DISTANCE

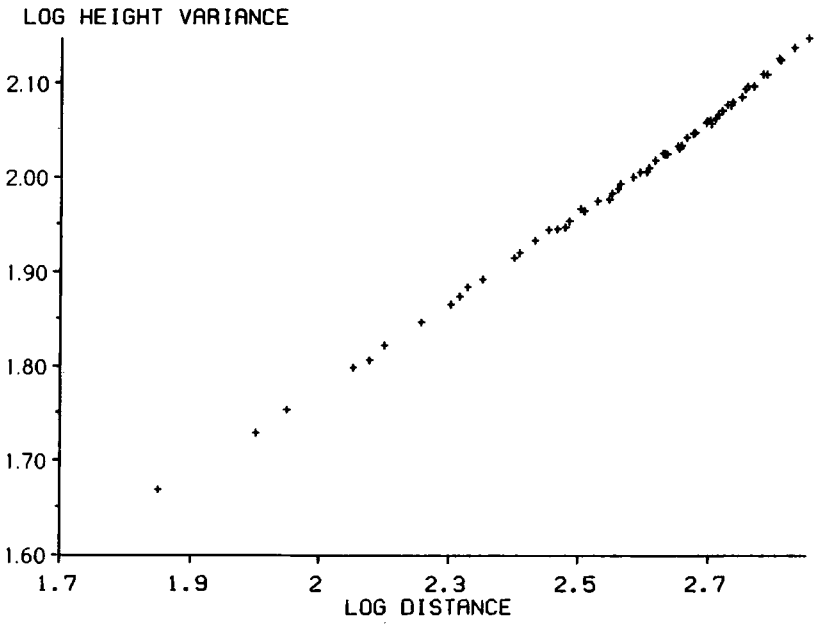

FRACO.2: RESCALED RANGE Vs. DISTANCE

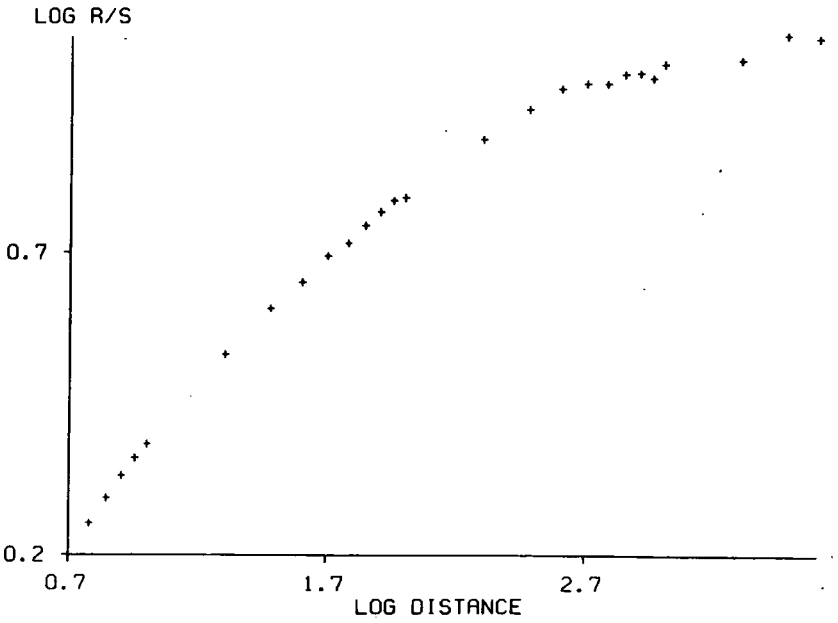

FRACTAL 0.1: ALT.VARIANCE AGAINST DISTANCE

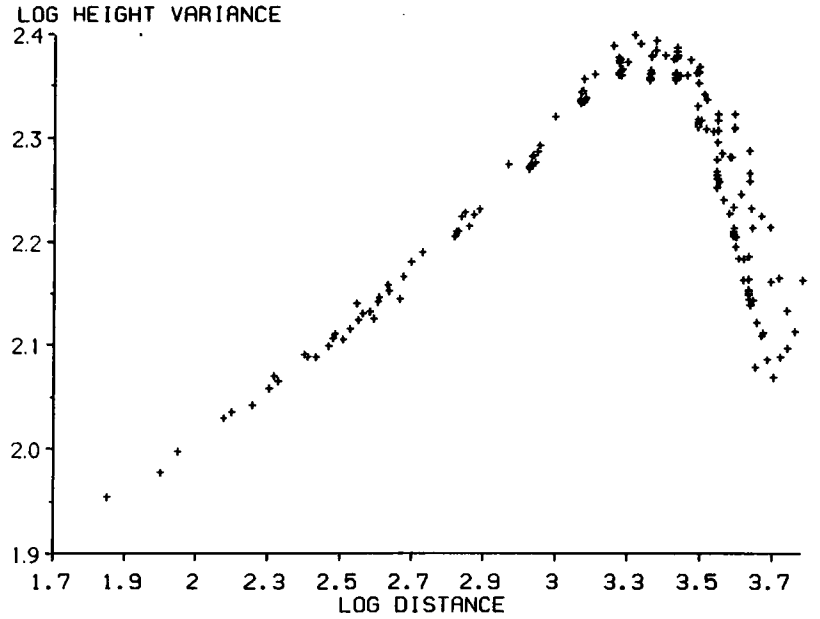

FRACTAL 0.1: ALT.VARIANCE AGAINST DISTANCE

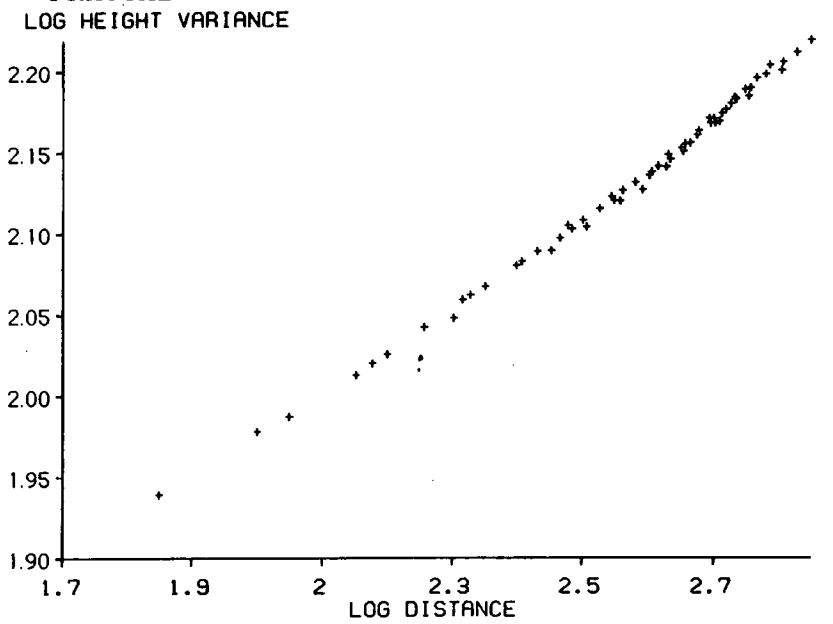

FRACO.1: RESCALED RANGE Vs. DISTANCE

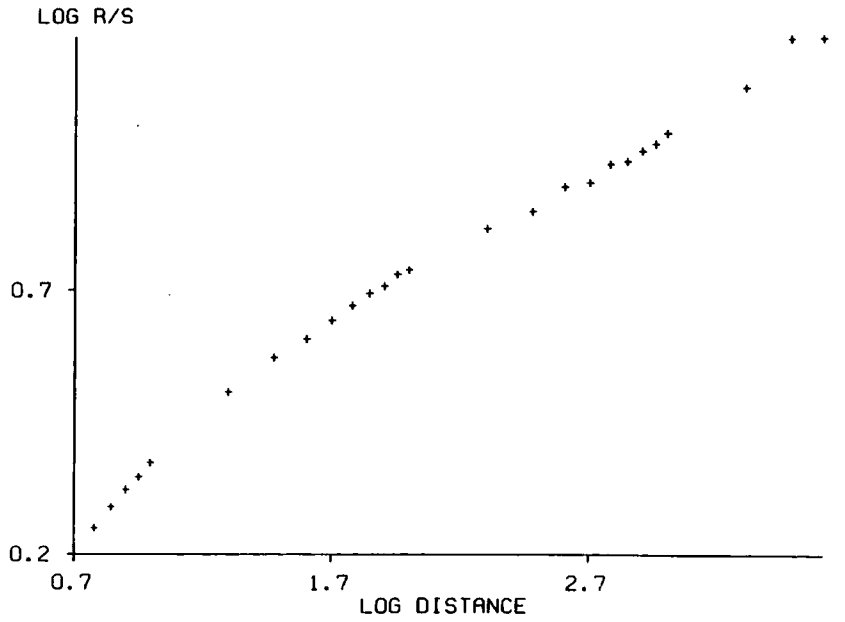

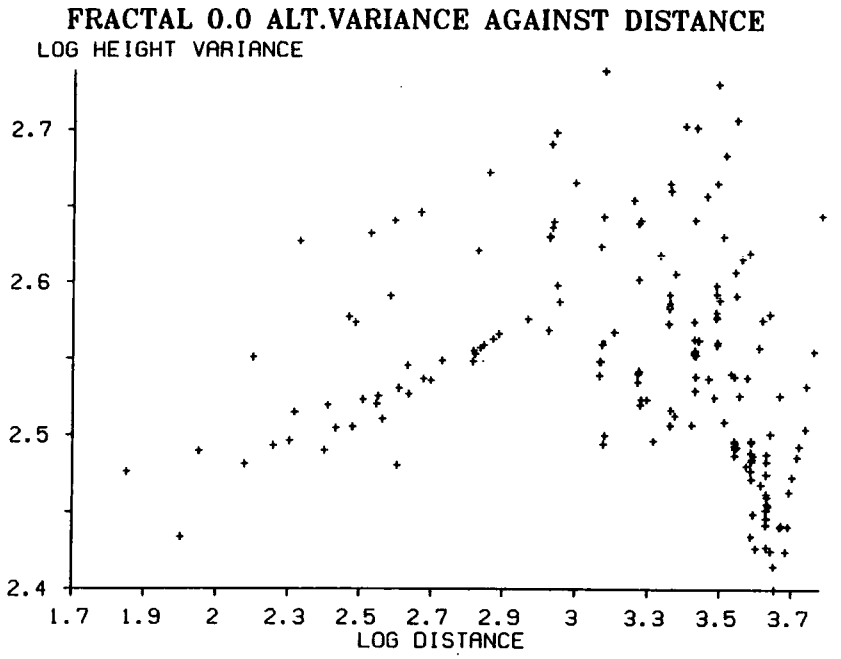
FRACTAL 0.0 ALT.VARIANCE AGAINST DISTANCE
LOG HEIGHT VARIANCE
2.7
2.6
2.5
2.4
1.7 1.9 2 2.3 2.5 2.7 2.9 3 3.3 3.5 3.7
LOG DISTANCE

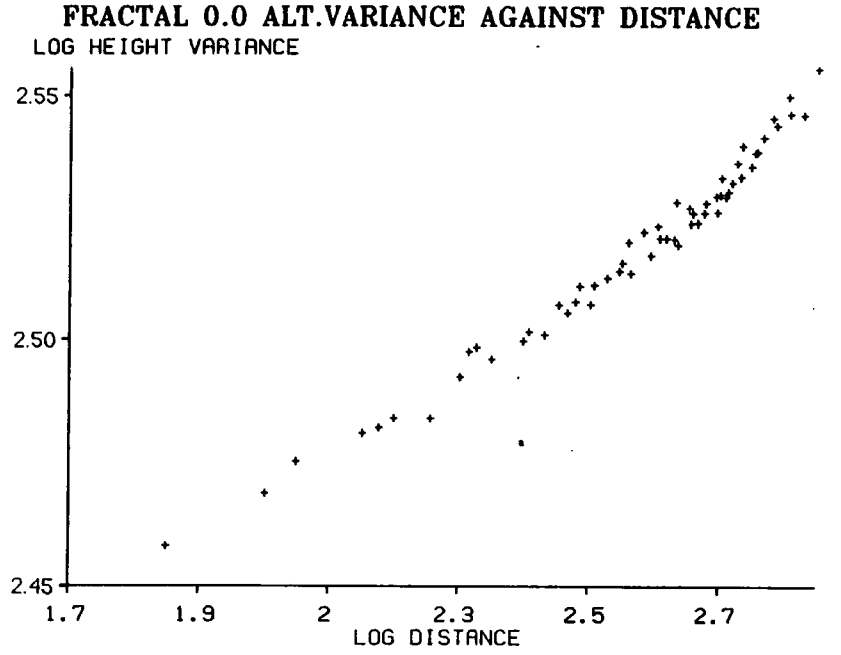
FRACTAL 0.0 ALT.VARIANCE AGAINST DISTANCE
LOG HEIGHT VARIANCE
2.55
2.50
2.45
1.7 1.9 2 2.3 2.5 2.7
LOG DISTANCE

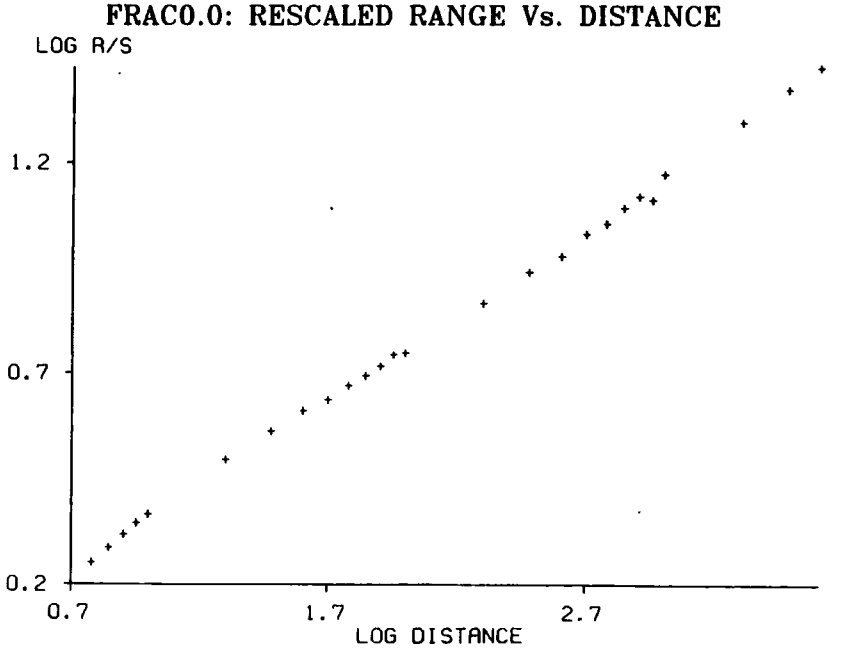
FRACO.0: RESCALED RANGE Vs. DISTANCE
LOG R/S
1.2
0.7
0.2
0.7 1.7 2.7
LOG DISTANCE

FRACTAL 1.0 E-W: ALT.VARIANCE AGAINST DISTANCE

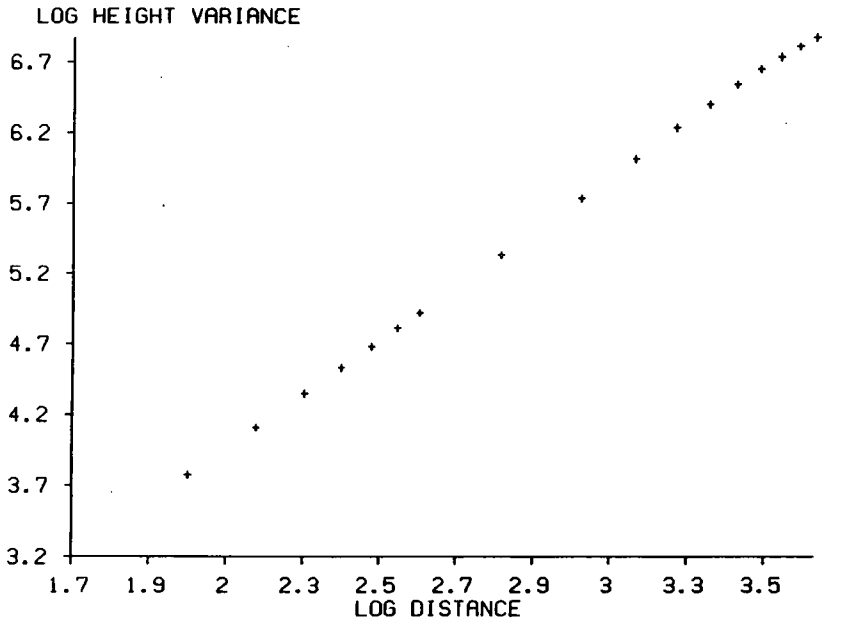

FRACTAL 1.0 N-S: ALT.VARIANCE AGAINST DISTANCE

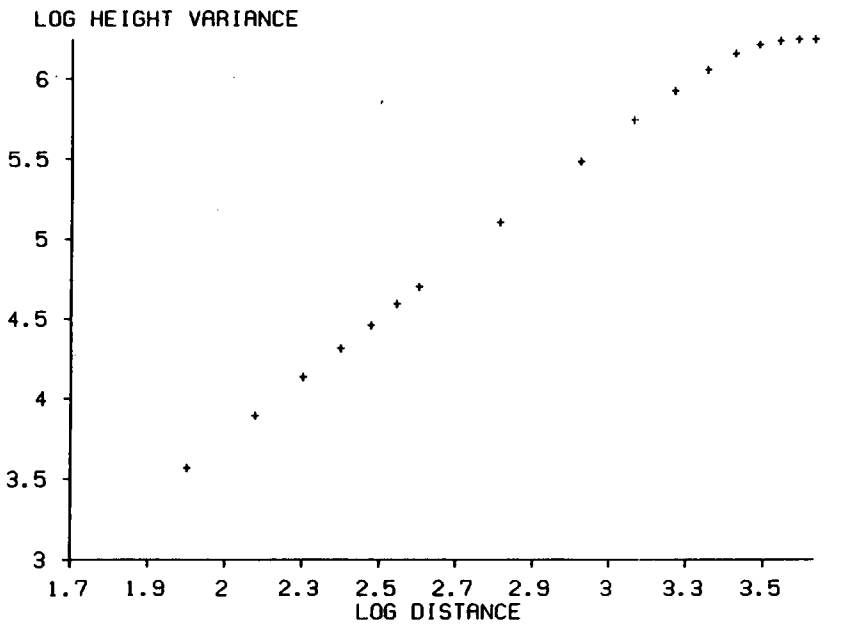

FRACTAL 1.0 NW-SE: ALT.VARIANCE AGAINST DISTANCE

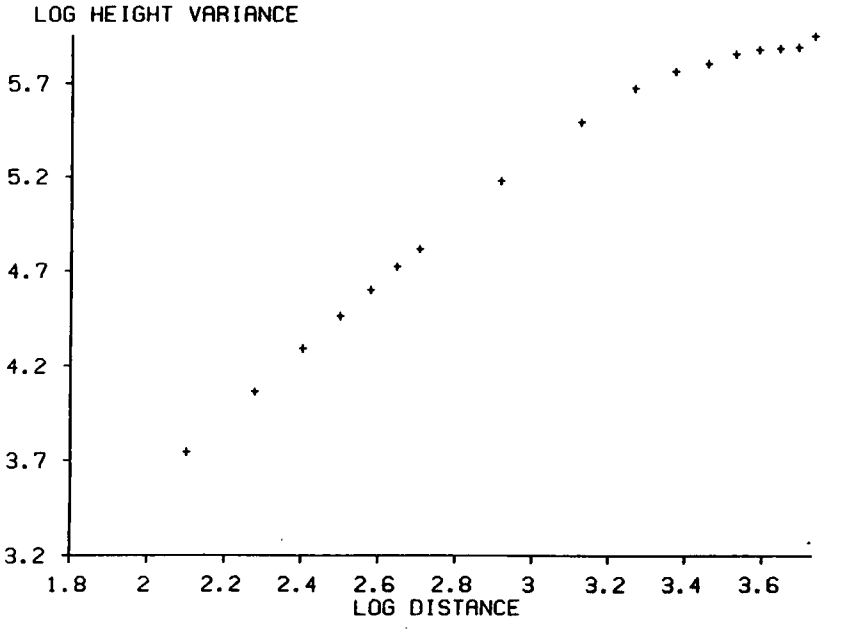

FRACTAL 1.0 NE-SW: ALT.VARIANCE AGAINST DISTANCE

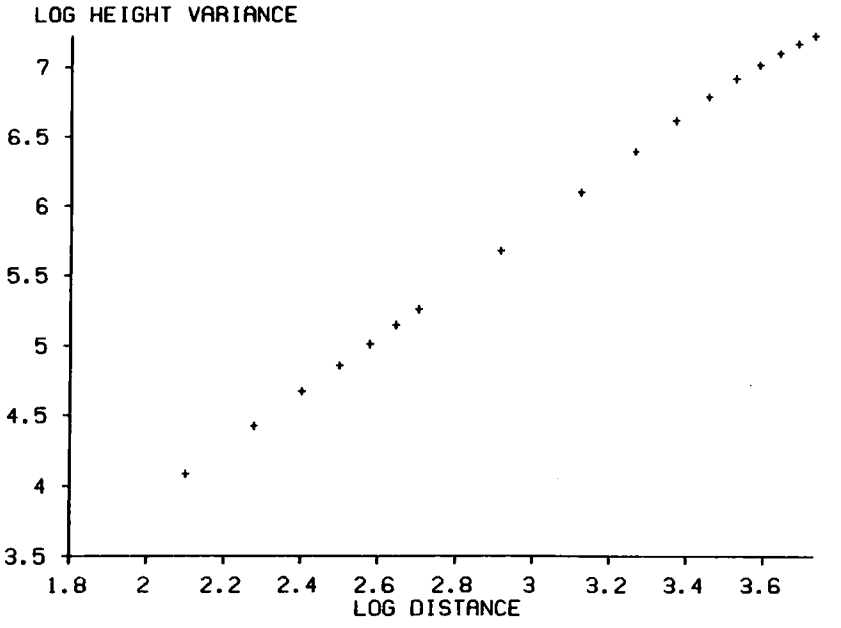

FRACTAL 0.9 E–W: ALT.VARIANCE AGAINST DISTANCE

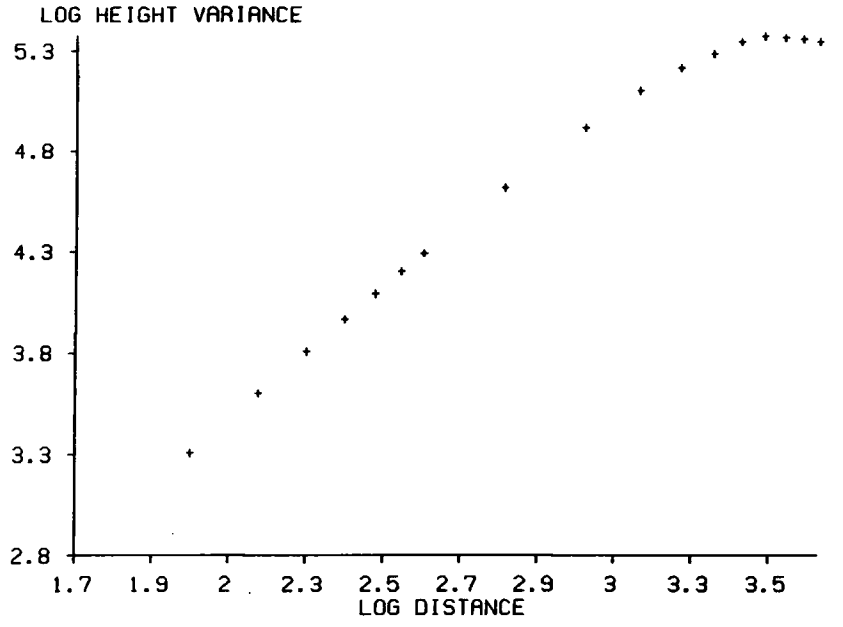

FRACTAL 0.9 N–S: ALT.VARIANCE AGAINST DISTANCE

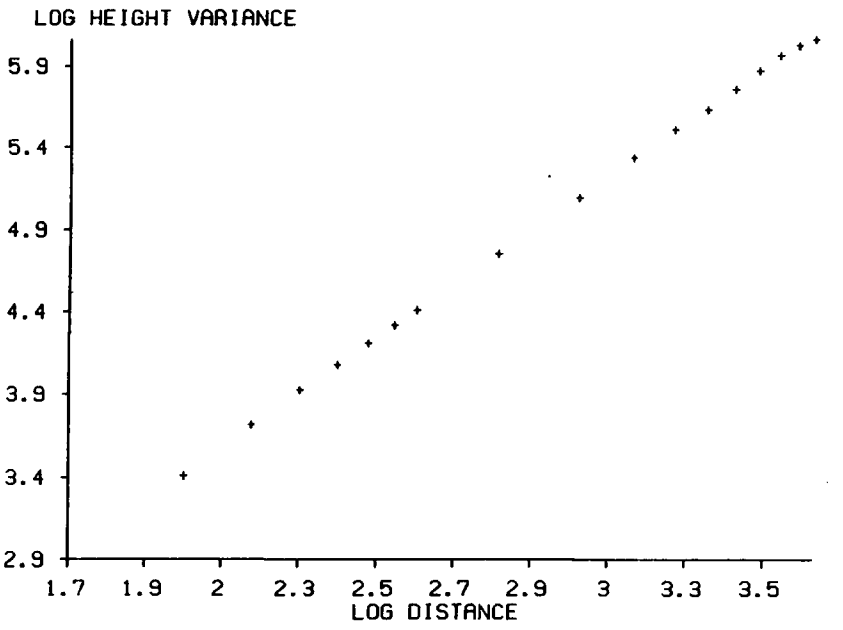

FRACTAL 0.9 NW–SE: ALT.VARIANCE AGAINST DISTANCE

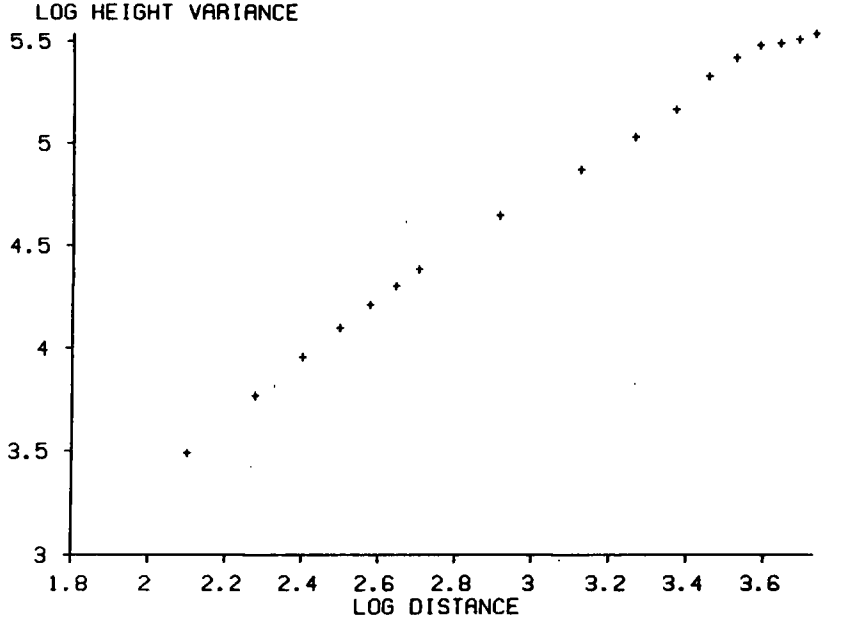

FRACTAL 0.9 NE–SW: ALT.VARIANCE AGAINST DISTANCE

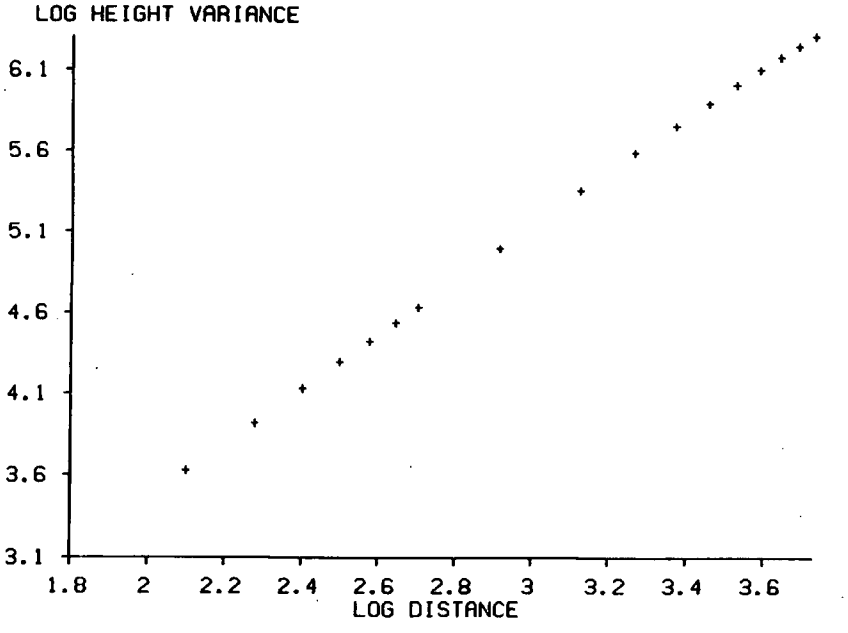

FRACTAL 0.8 E-W: ALT.VARIANCE AGAINST DISTANCE

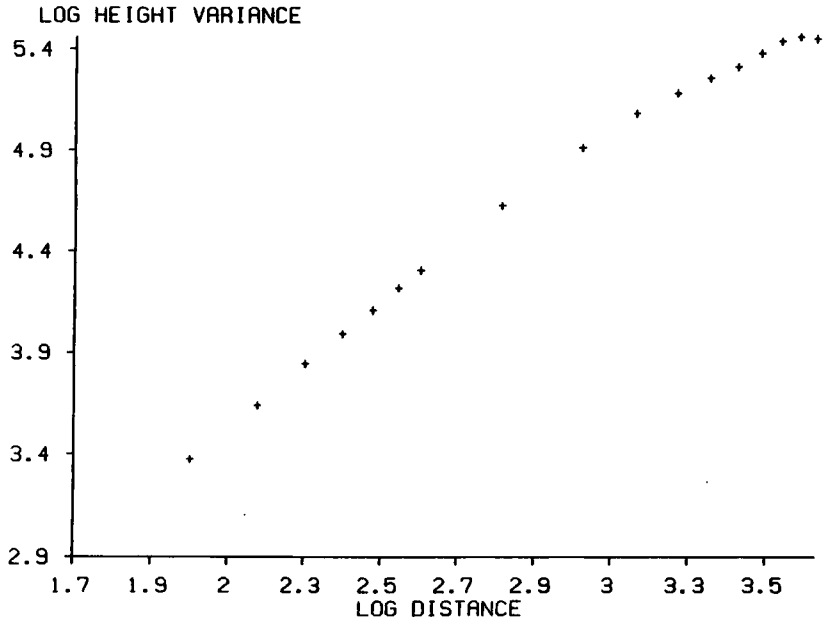

FRACTAL 0.8 N-S: ALT.VARIANCE AGAINST DISTANCE

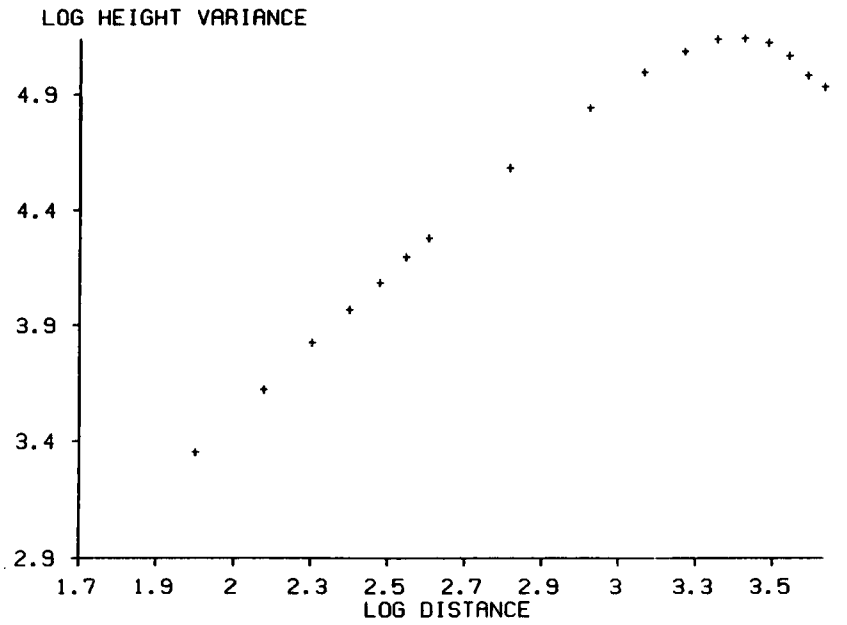

FRACTAL 0.8 NW-SE: ALT.VARIANCE AGAINST DISTANCE

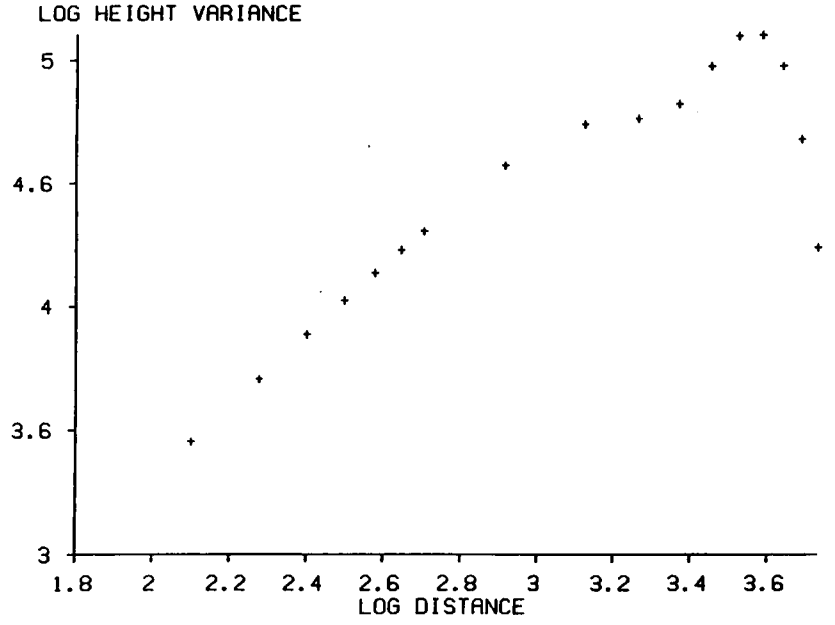

FRACTAL 0.8 NE-SW: ALT.VARIANCE AGAINST DISTANCE

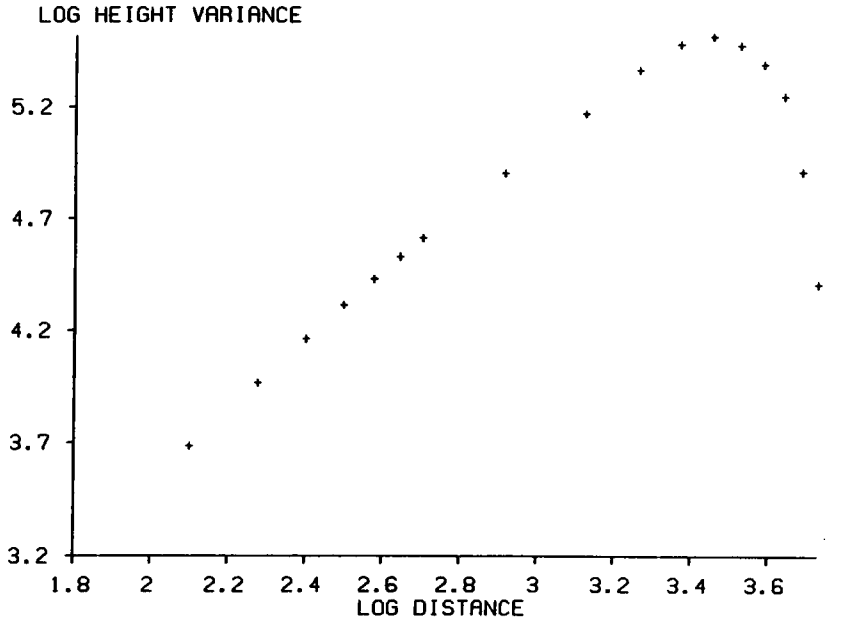

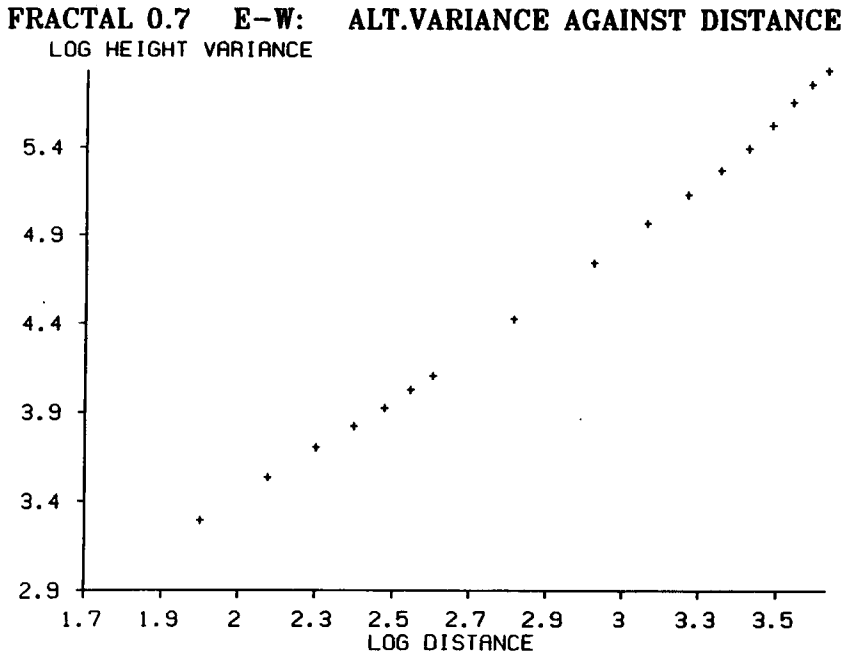
FRACTAL 0.7 E–W: ALT.VARIANCE AGAINST DISTANCE
LOG HEIGHT VARIANCE
5.4
4.9
4.4
3.9
3.4
2.9
1.7 1.9 2 2.3 2.5 2.7 2.9 3 3.3 3.5
LOG DISTANCE

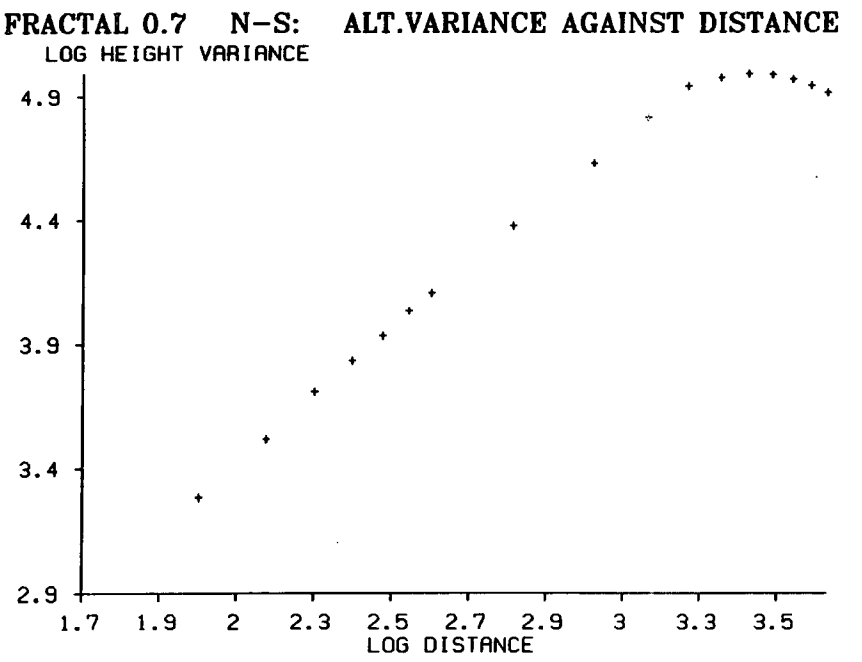
FRACTAL 0.7 N–S: ALT.VARIANCE AGAINST DISTANCE
LOG HEIGHT VARIANCE
4.9
4.4
3.9
3.4
2.9
1.7 1.9 2 2.3 2.5 2.7 2.9 3 3.3 3.5
LOG DISTANCE

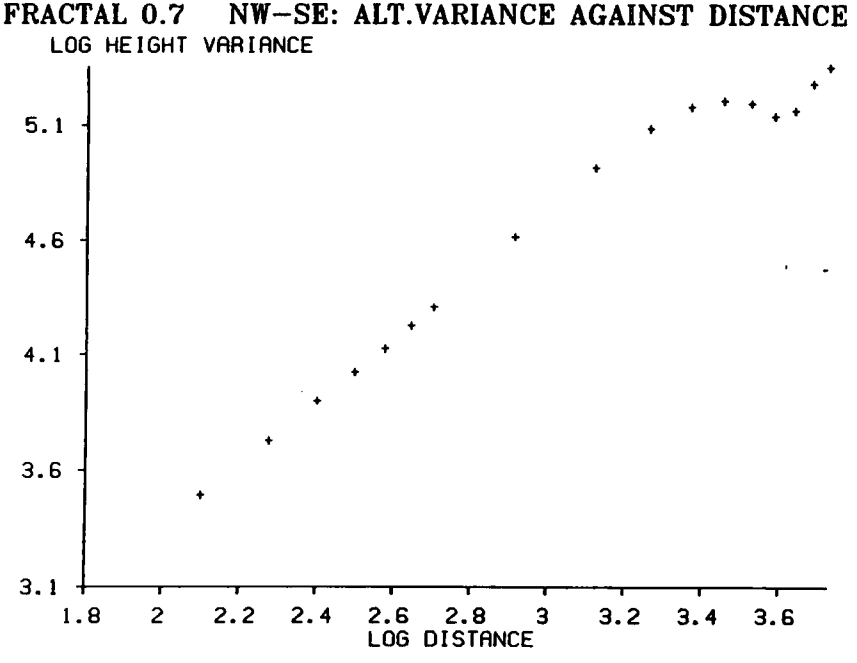
FRACTAL 0.7 NW–SE: ALT.VARIANCE AGAINST DISTANCE
LOG HEIGHT VARIANCE
5.1
4.6
4.1
3.6
3.1
1.8 2 2.2 2.4 2.6 2.8 3 3.2 3.4 3.6
LOG DISTANCE

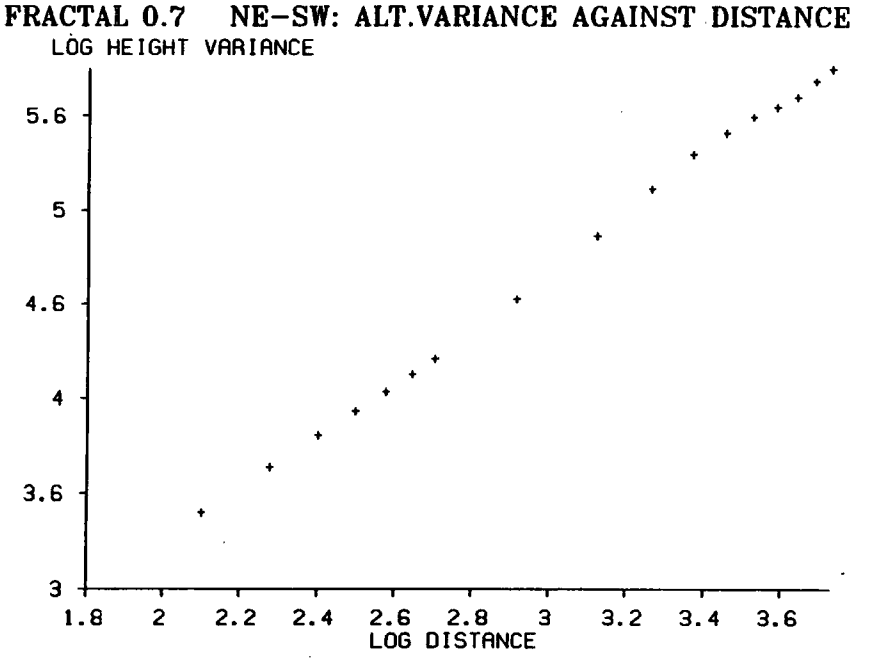
FRACTAL 0.7 NE–SW: ALT.VARIANCE AGAINST DISTANCE
LOG HEIGHT VARIANCE
5.6
5
4.6
4
3.6
3
1.8 2 2.2 2.4 2.6 2.8 3 3.2 3.4 3.6
LOG DISTANCE

FRACTAL 0.6 E–W: ALT.VARIANCE AGAINST DISTANCE

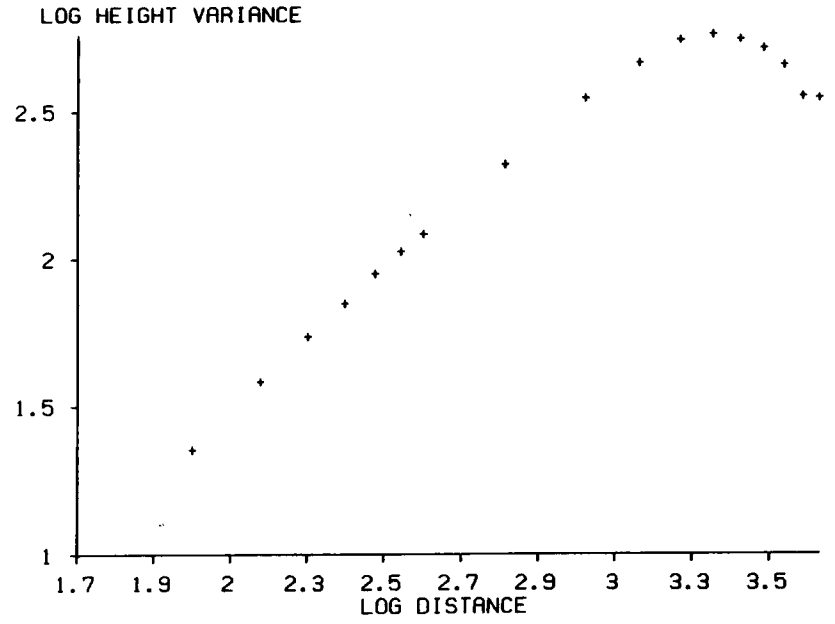

FRACTAL 0.6 N–S: ALT.VARIANCE AGAINST DISTANCE

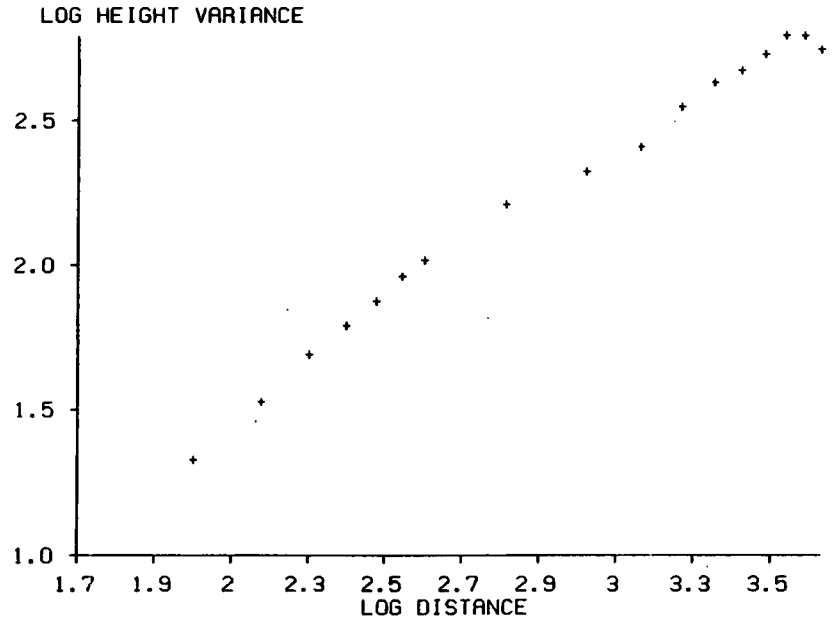

FRACTAL 0.6 NW–SE: ALT.VARIANCE AGAINST DISTANCE

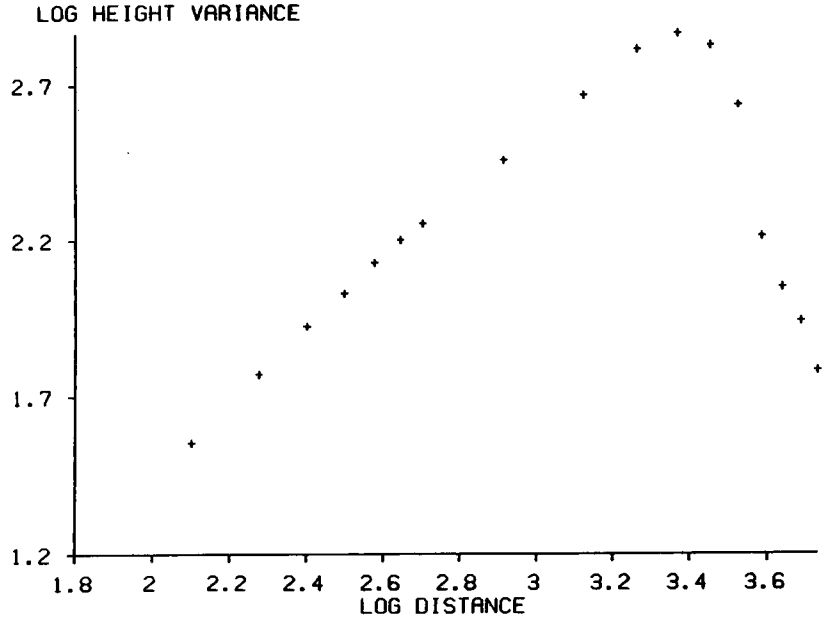

FRACTAL 0.6 NE–SW: ALT.VARIANCE AGAINST DISTANCE

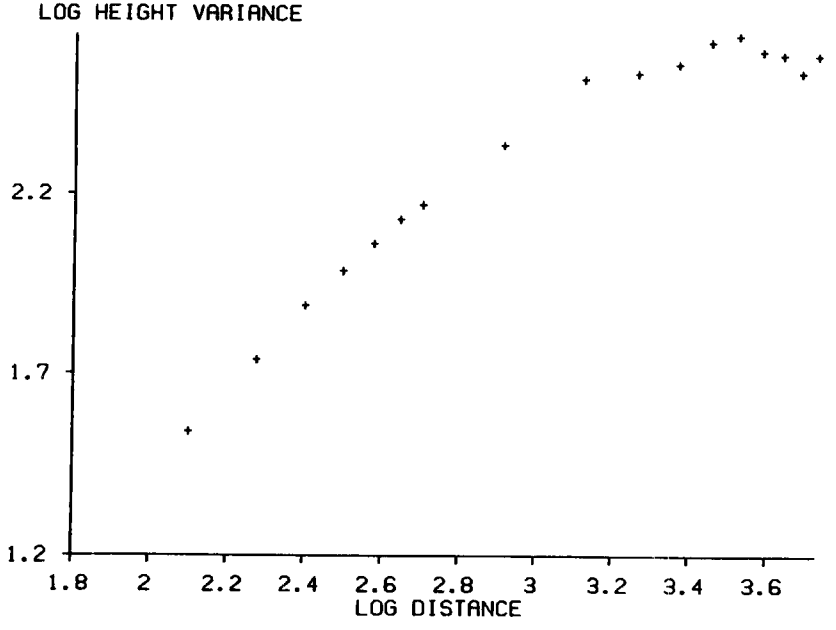

FRACTAL 0.5 E–W: ALT.VARIANCE AGAINST DISTANCE

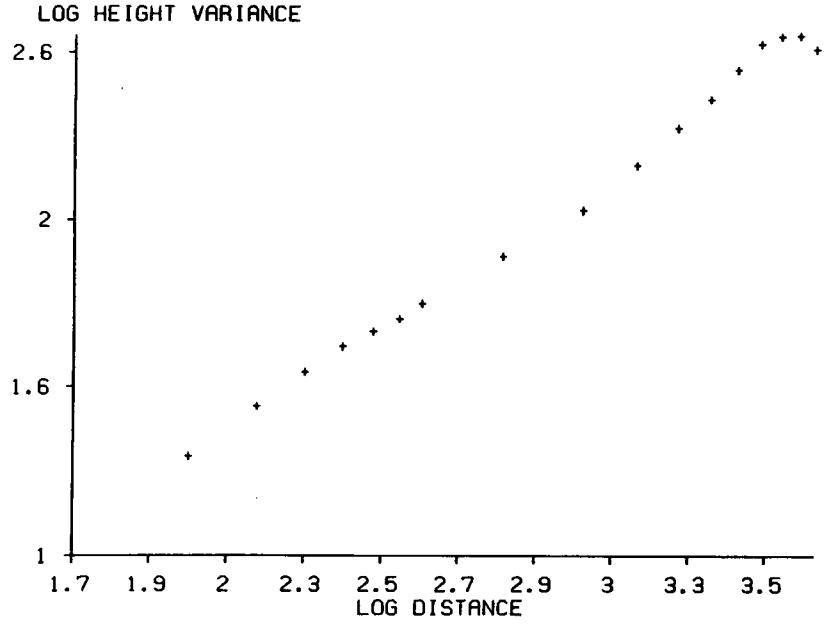

FRACTAL 0.5 N–S: ALT.VARIANCE AGAINST DISTANCE

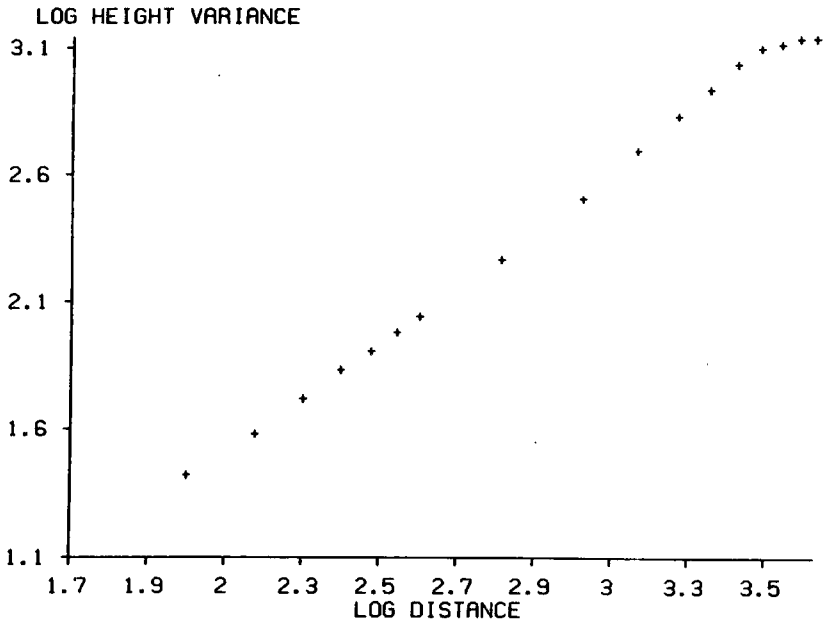

FRACTAL 0.5 NW–SE: ALT.VARIANCE AGAINST DISTANCE

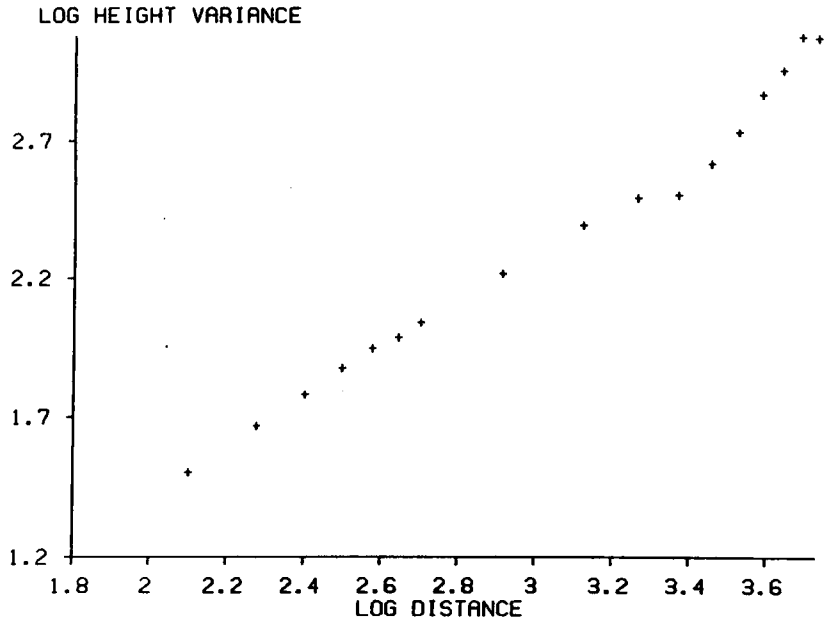

FRACTAL 0.5 NE–SW: ALT.VARIANCE AGAINST DISTANCE

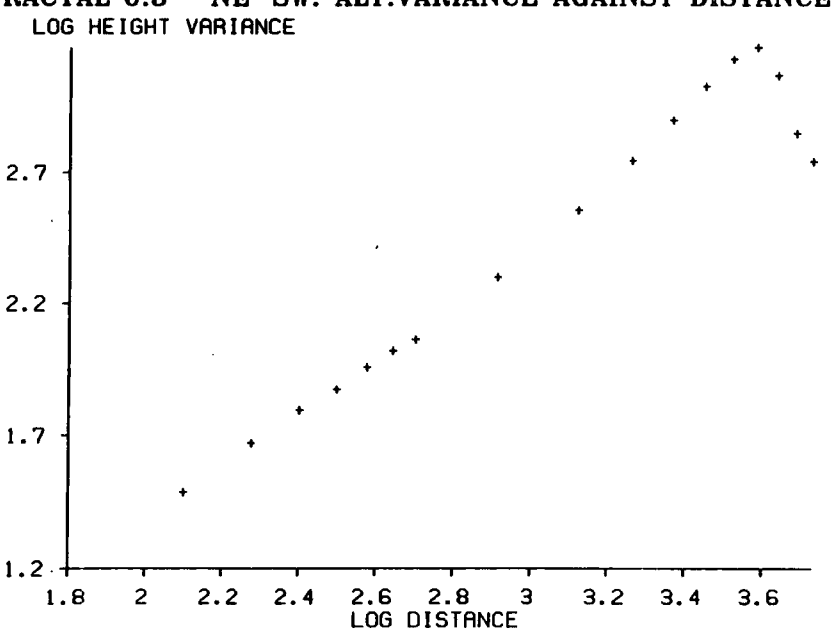

FRACTAL 0.4 E–W: ALT.VARIANCE AGAINST DISTANCE

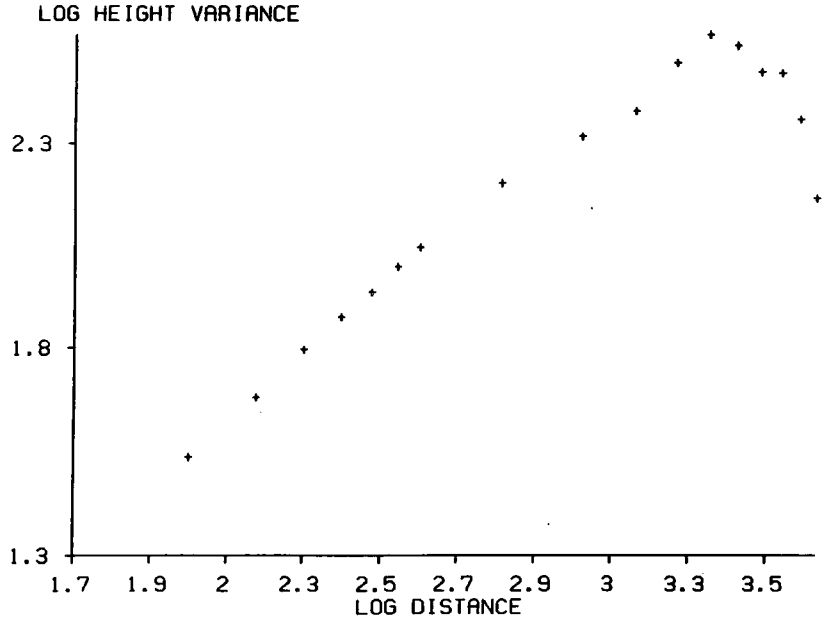

FRACTAL 0.4 N–S: ALT.VARIANCE AGAINST DISTANCE

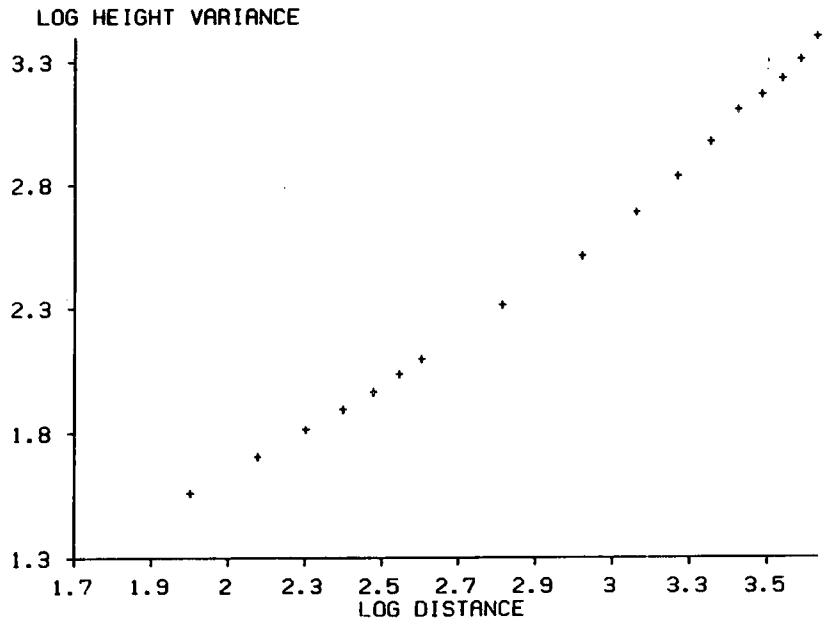

FRACTAL 0.4 NW–SE: ALT.VARIANCE AGAINST DISTANCE

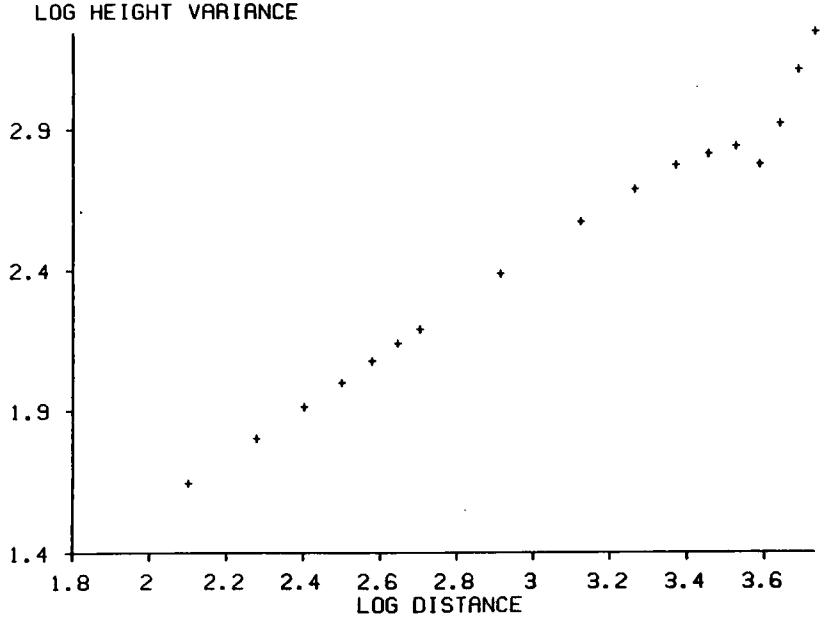

FRACTAL 0.4 NE–SW: ALT.VARIANCE AGAINST DISTANCE

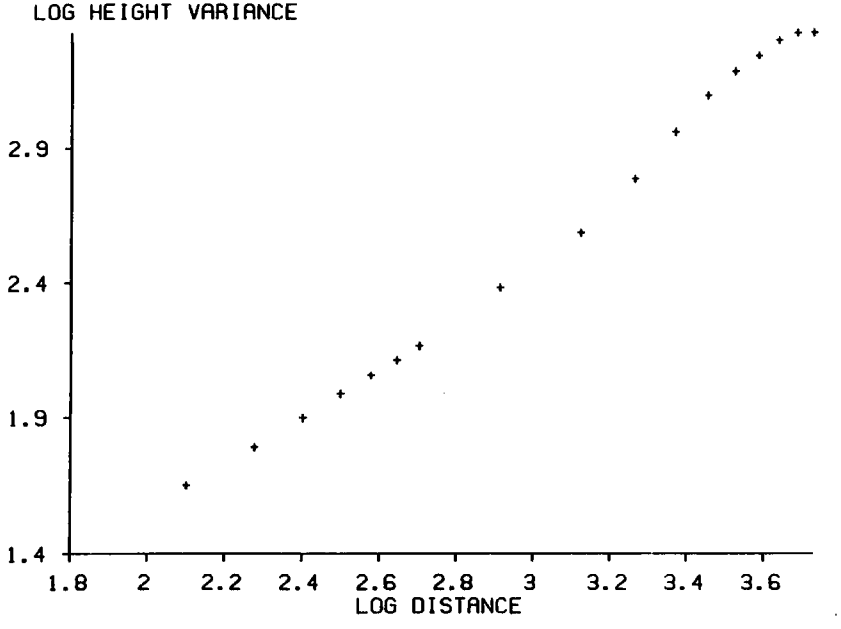

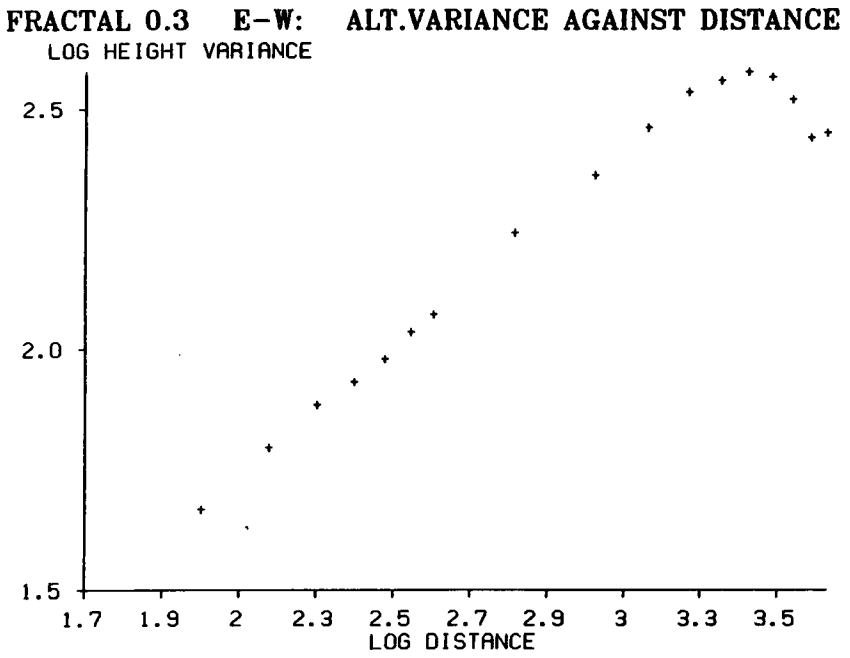
FRACTAL 0.3 E-W: ALT.VARIANCE AGAINST DISTANCE
LOG HEIGHT VARIANCE
2.5
2.0
1.5
1.7 1.9 2 2.3 2.5 2.7 2.9 3 3.3 3.5
LOG DISTANCE

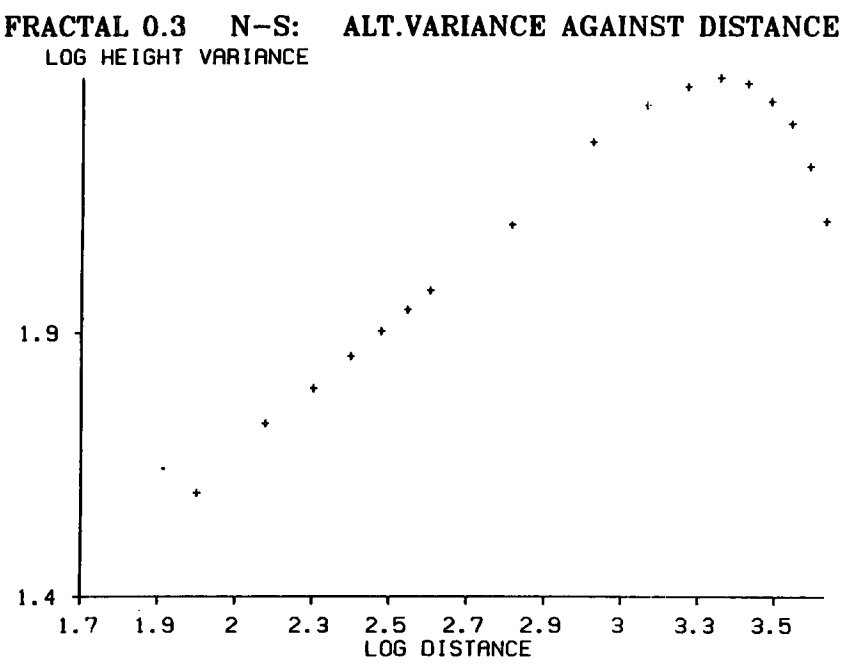
FRACTAL 0.3 N-S: ALT.VARIANCE AGAINST DISTANCE
LOG HEIGHT VARIANCE
1.9
1.4
1.7 1.9 2 2.3 2.5 2.7 2.9 3 3.3 3.5
LOG DISTANCE

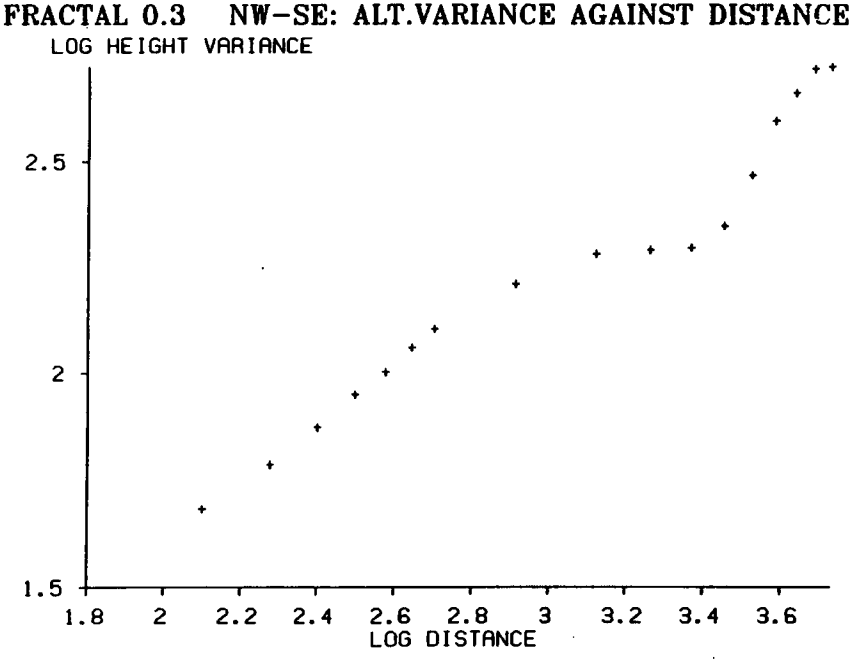
FRACTAL 0.3 NW-SE: ALT.VARIANCE AGAINST DISTANCE
LOG HEIGHT VARIANCE
2.5
2
1.5
1.8 2 2.2 2.4 2.6 2.8 3 3.2 3.4 3.6
LOG DISTANCE

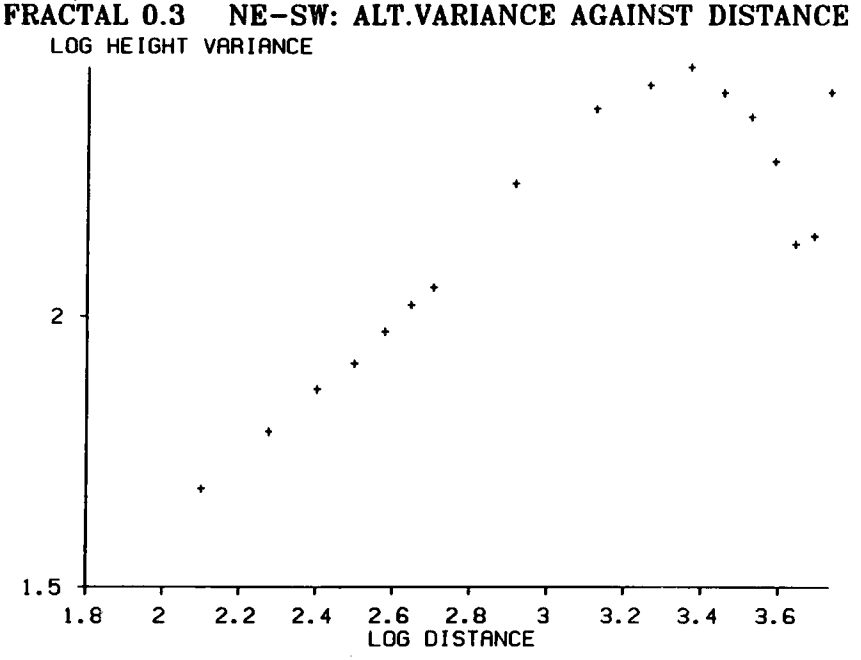
FRACTAL 0.3 NE-SW: ALT.VARIANCE AGAINST DISTANCE
LOG HEIGHT VARIANCE
2
1.5
1.8 2 2.2 2.4 2.6 2.8 3 3.2 3.4 3.6
LOG DISTANCE

FRACTAL 0.2 E–W: ALT.VARIANCE AGAINST DISTANCE

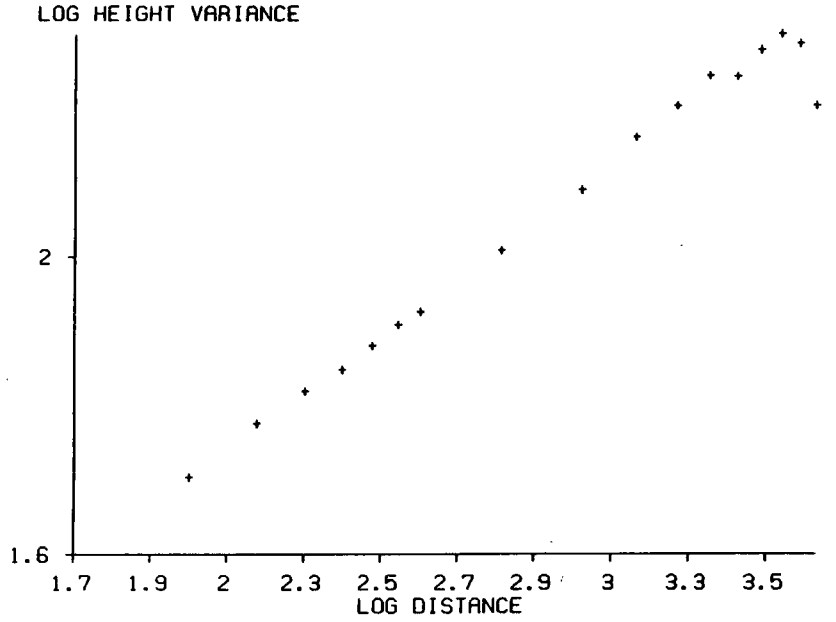

FRACTAL 0.2 N–S: ALT.VARIANCE AGAINST DISTANCE

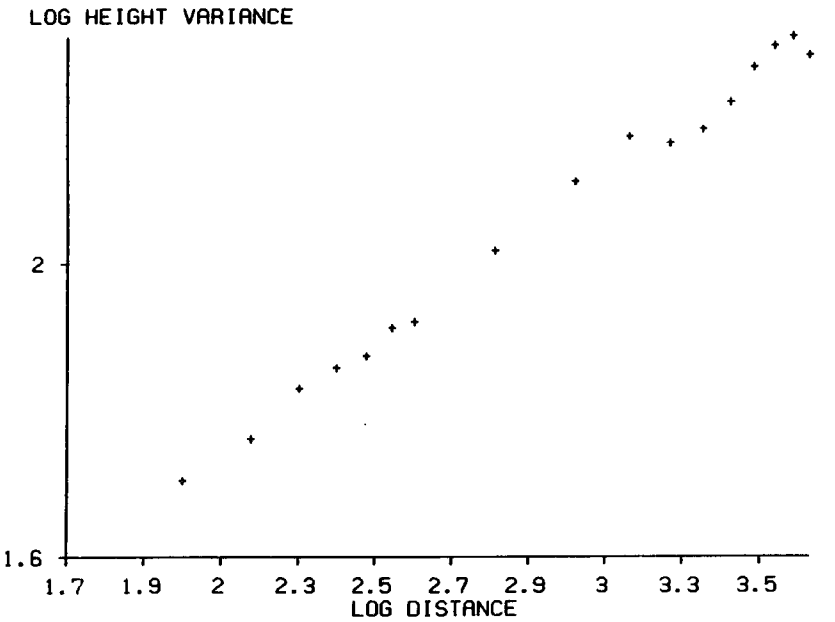

FRACTAL 0.2 NW–SE: ALT.VARIANCE AGAINST DISTANCE

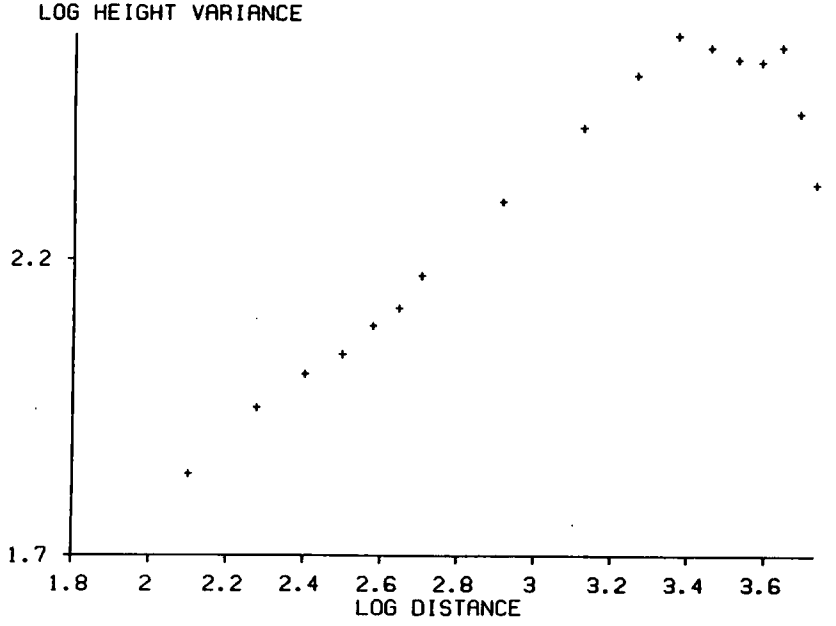

FRACTAL 0.2 NE–SW: ALT.VARIANCE AGAINST DISTANCE

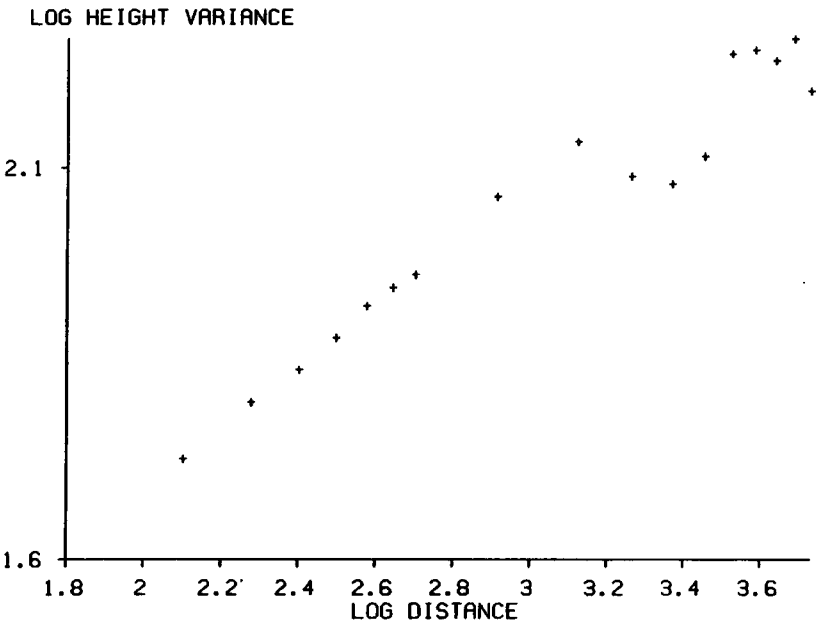

FRACTAL 0.1 E–W: ALT.VARIANCE AGAINST DISTANCE

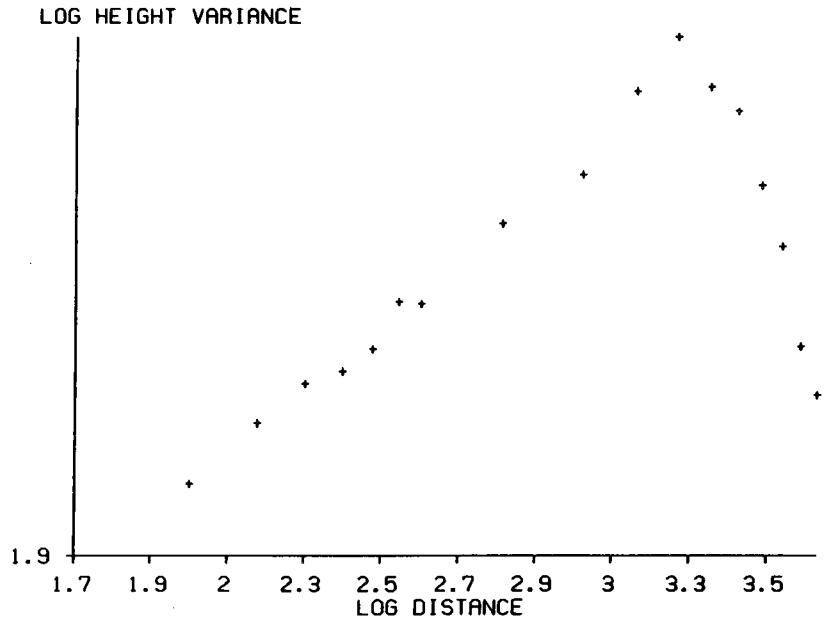

FRACTAL 0.1 N–S: ALT.VARIANCE AGAINST DISTANCE

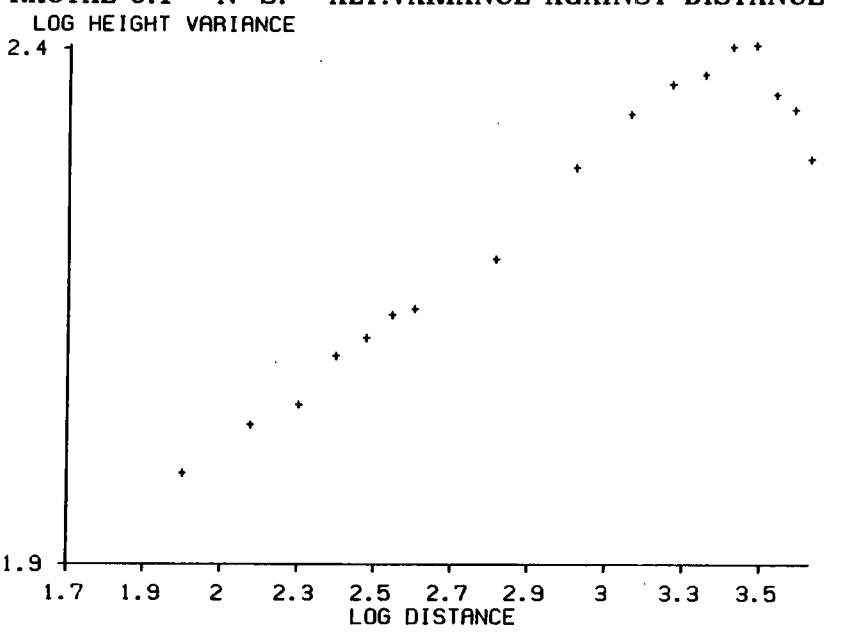

FRACTAL 0.1 NW–SE: ALT.VARIANCE AGAINST DISTANCE

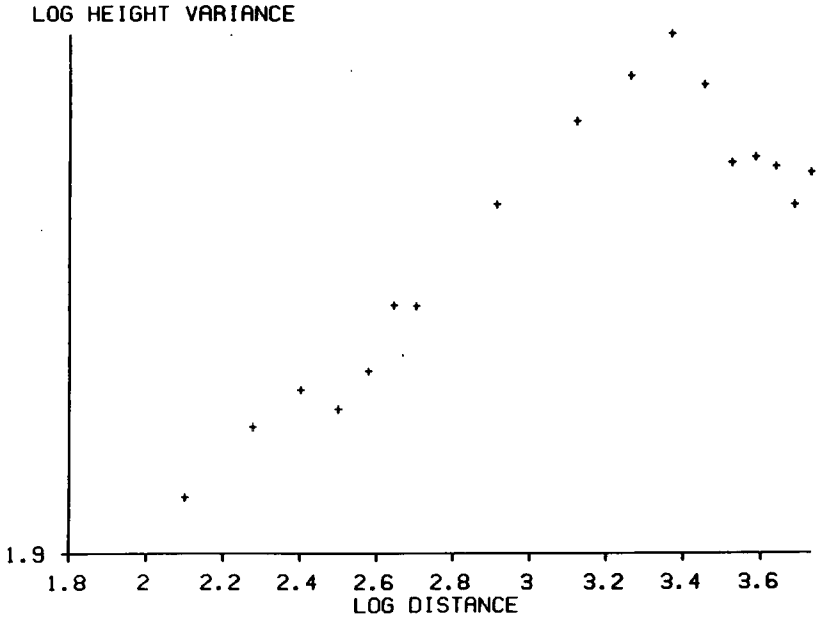

FRACTAL 0.1 NE–SW: ALT.VARIANCE AGAINST DISTANCE

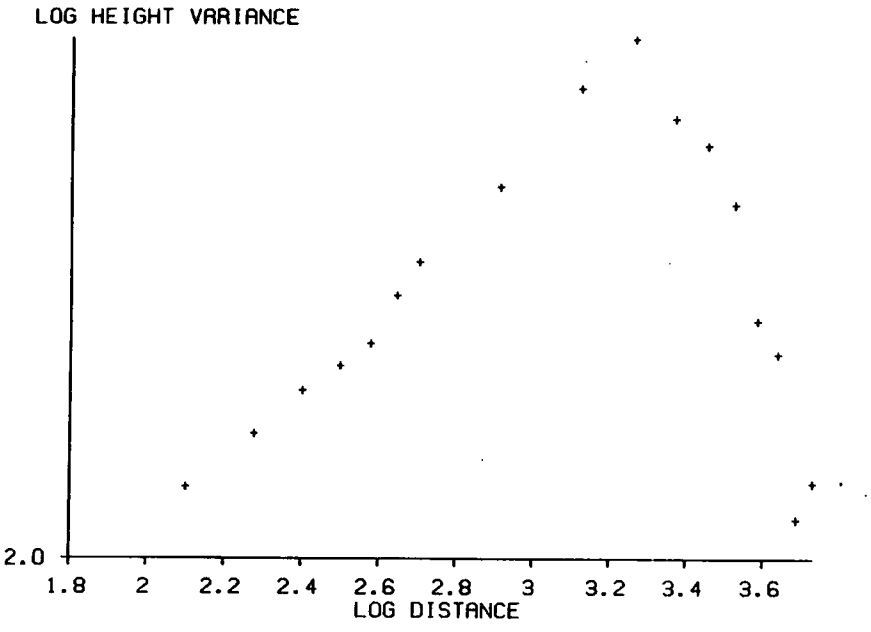

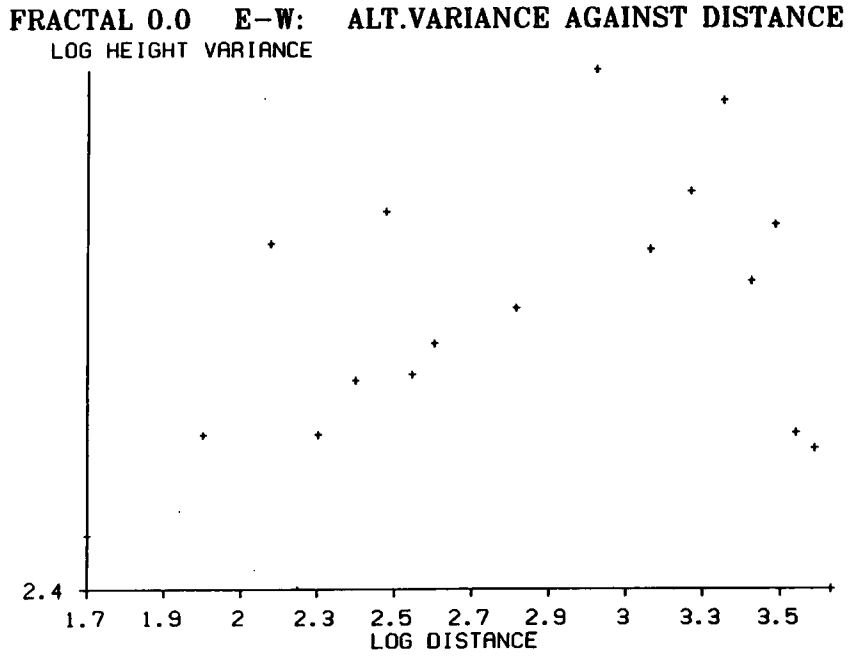
FRACTAL 0.0 E-W: ALT.VARIANCE AGAINST DISTANCE
LOG HEIGHT VARIANCE
2.4
1.7 1.9 2 2.3 2.5 2.7 2.9 3 3.3 3.5
LOG DISTANCE

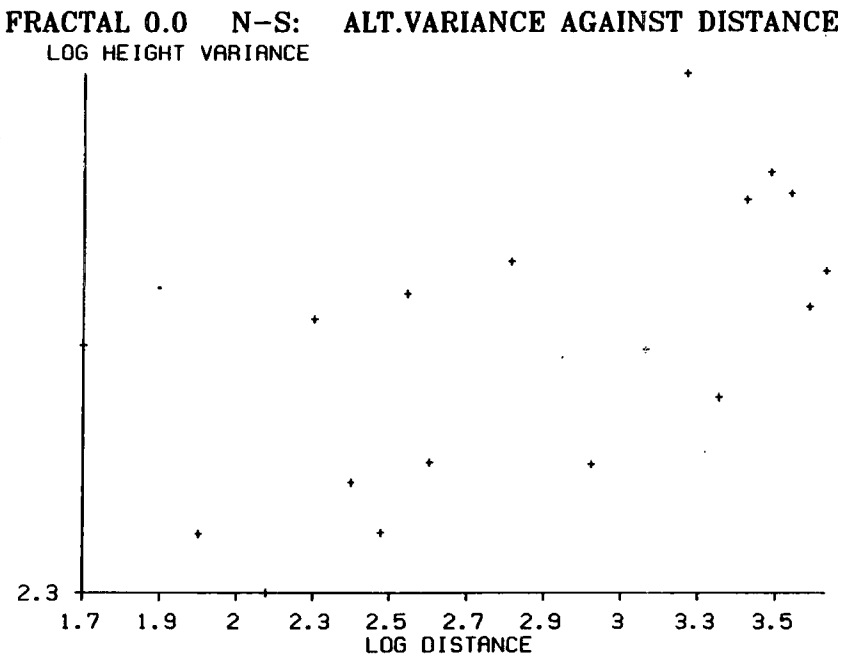
FRACTAL 0.0 N-S: ALT.VARIANCE AGAINST DISTANCE
LOG HEIGHT VARIANCE
2.3
1.7 1.9 2 2.3 2.5 2.7 2.9 3 3.3 3.5
LOG DISTANCE

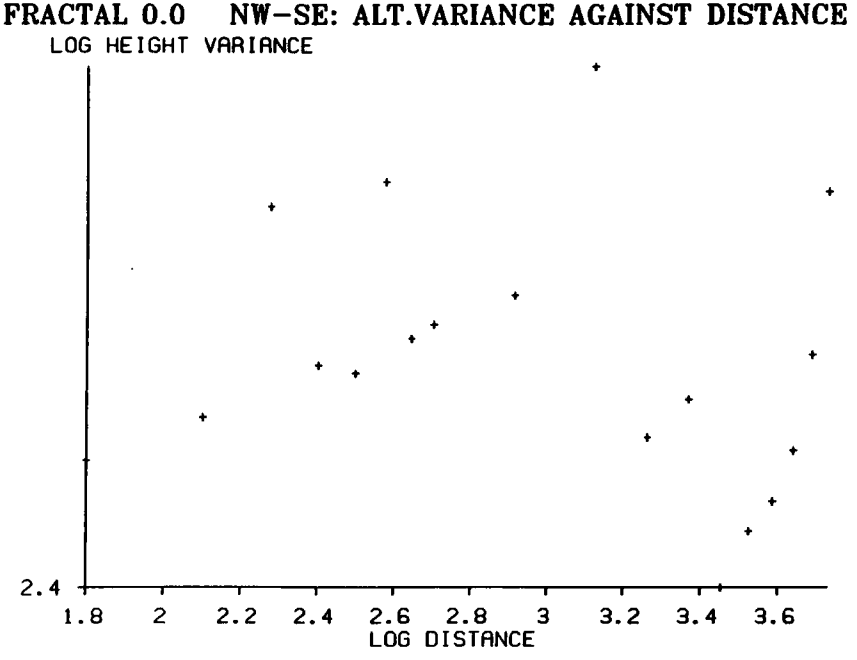
FRACTAL 0.0 NW-SE: ALT.VARIANCE AGAINST DISTANCE
LOG HEIGHT VARIANCE
2.4
1.8 2 2.2 2.4 2.6 2.8 3 3.2 3.4 3.6
LOG DISTANCE

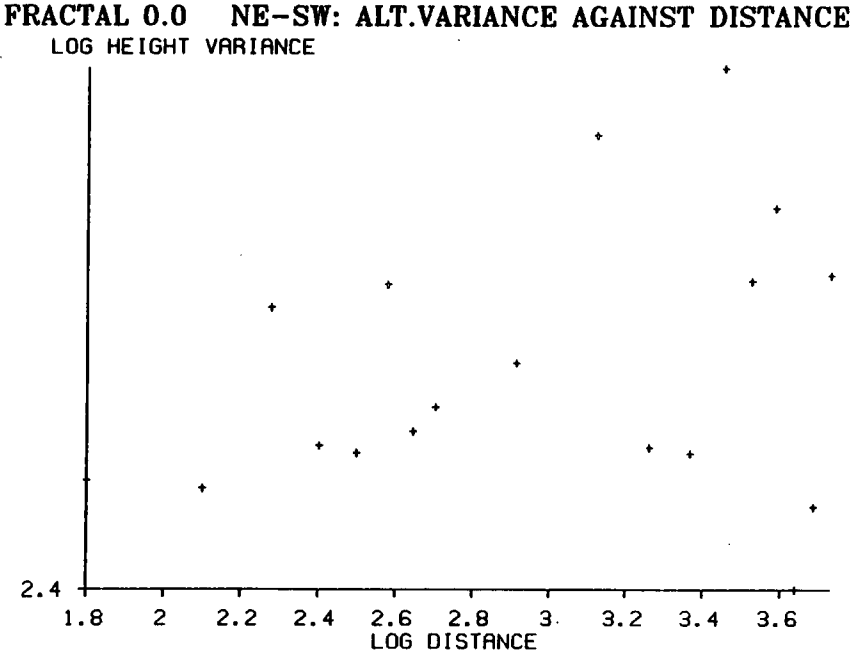
FRACTAL 0.0 NE-SW: ALT.VARIANCE AGAINST DISTANCE
LOG HEIGHT VARIANCE
2.4
1.8 2 2.2 2.4 2.6 2.8 3 3.2 3.4 3.6
LOG DISTANCE

Appendix 3: Examples of Variograms Calculated from Real Landsurfaces

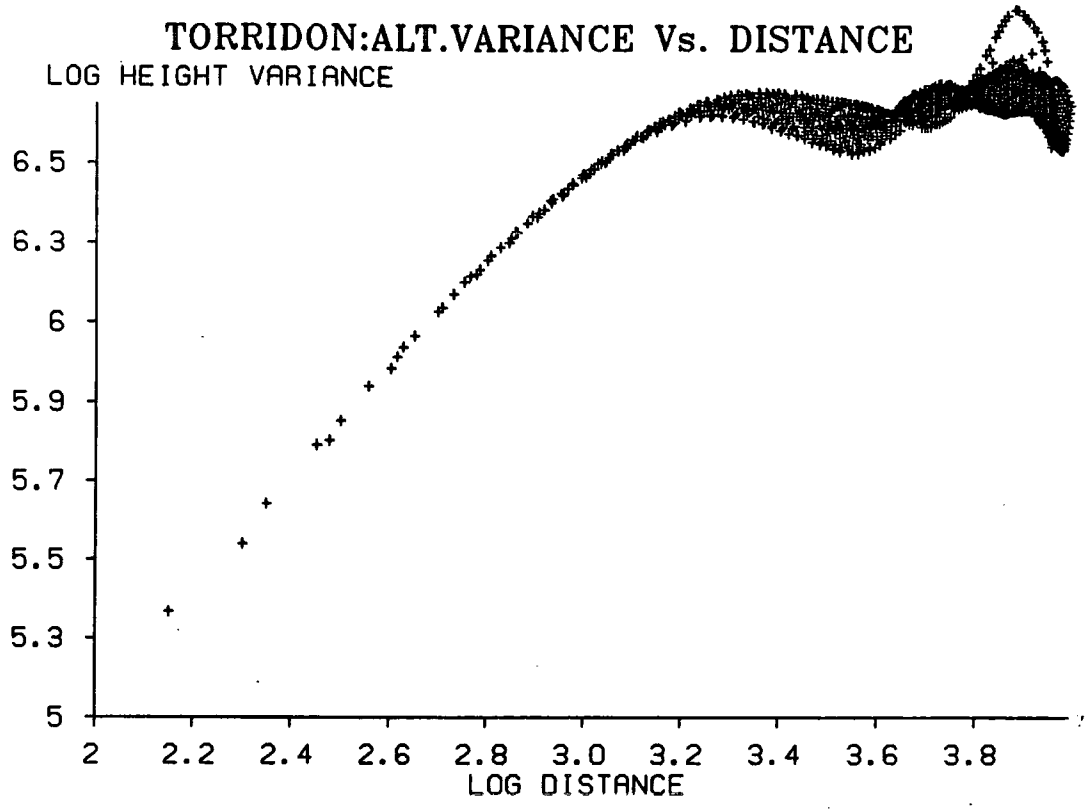
TORRIDON:ALT.VARIANCE Vs. DISTANCE
LOG HEIGHT VARIANCE
6.5
6.3
6
5.9
5.7
5.5
5.3
5
2
2.2
2.4
2.6
2.8
3.0
3.2
3.4
3.6
3.8
LOG DISTANCE

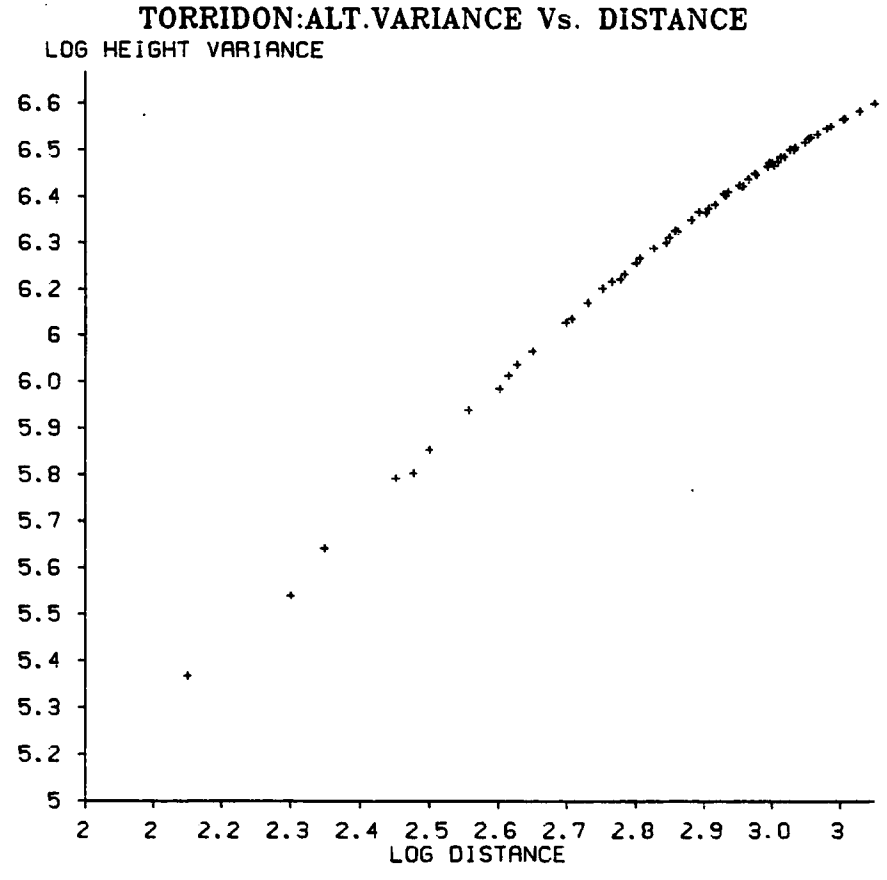
TORRIDON:ALT.VARIANCE Vs. DISTANCE
LOG HEIGHT VARIANCE
6.6
6.5
6.4
6.3
6.2
6
6.0
5.9
5.8
5.7
5.6
5.5
5.4
5.3
5.2
5
2
2
2.2
2.3
2.4
2.5
2.6
2.7
2.8
2.9
3.0
3
LOG DISTANCE

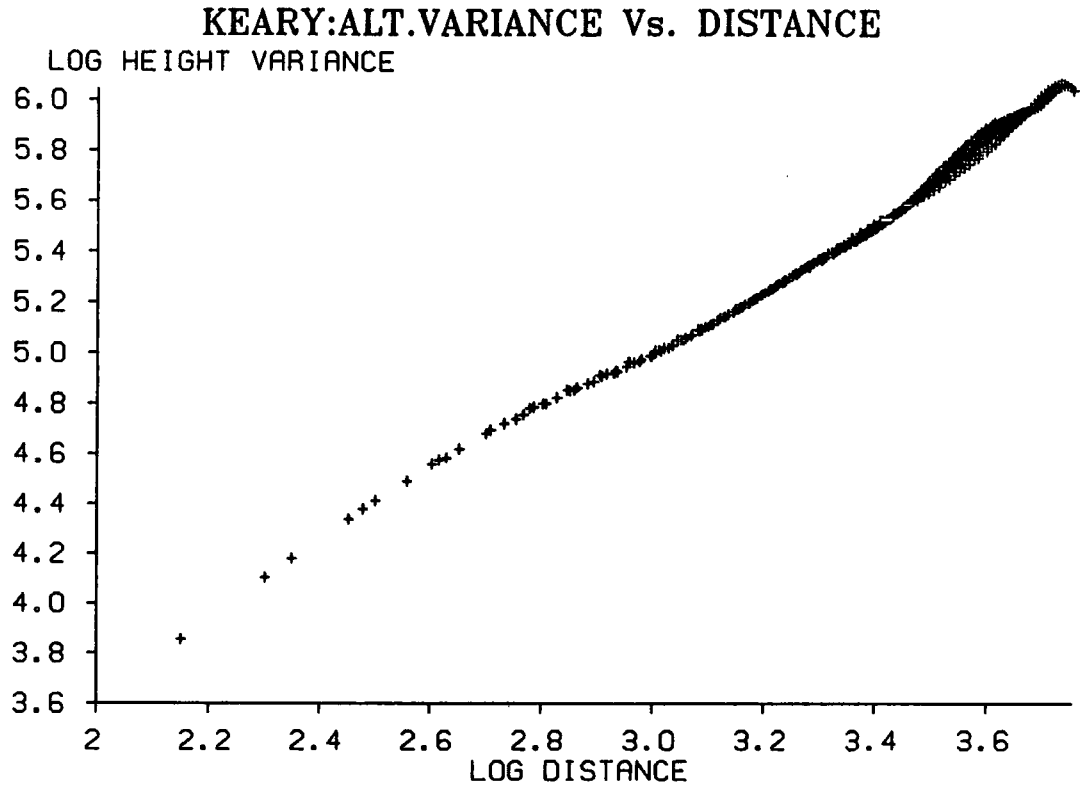
KEARY:ALT.VARIANCE Vs. DISTANCE
LOG HEIGHT VARIANCE
6.0
5.8
5.6
5.4
5.2
5.0
4.8
4.6
4.4
4.2
4.0
3.8
3.6
2
2.2
2.4
2.6
2.8
3.0
3.2
3.4
3.6
LOG DISTANCE

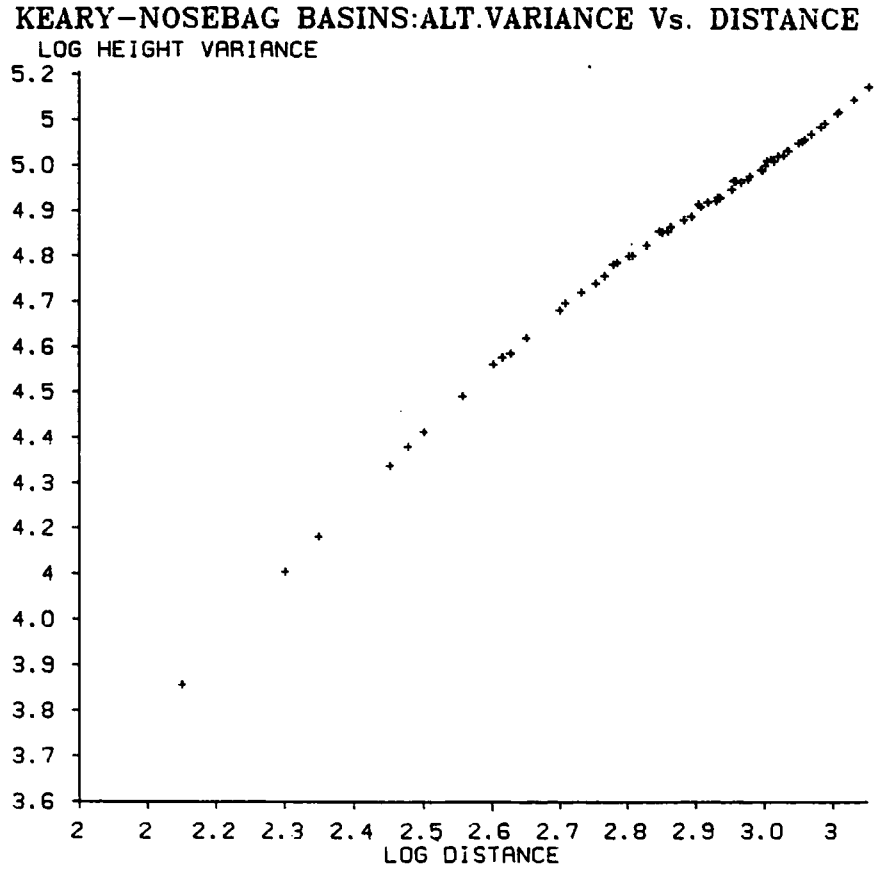
KEARY–NOSEBAG BASINS:ALT.VARIANCE Vs. DISTANCE
LOG HEIGHT VARIANCE
5.2
5
5.0
4.9
4.8
4.7
4.6
4.5
4.4
4.3
4.2
4
4.0
3.9
3.8
3.7
3.6
2
2
2.2
2.3
2.4
2.5
2.6
2.7
2.8
2.9
3.0
3
LOG DISTANCE

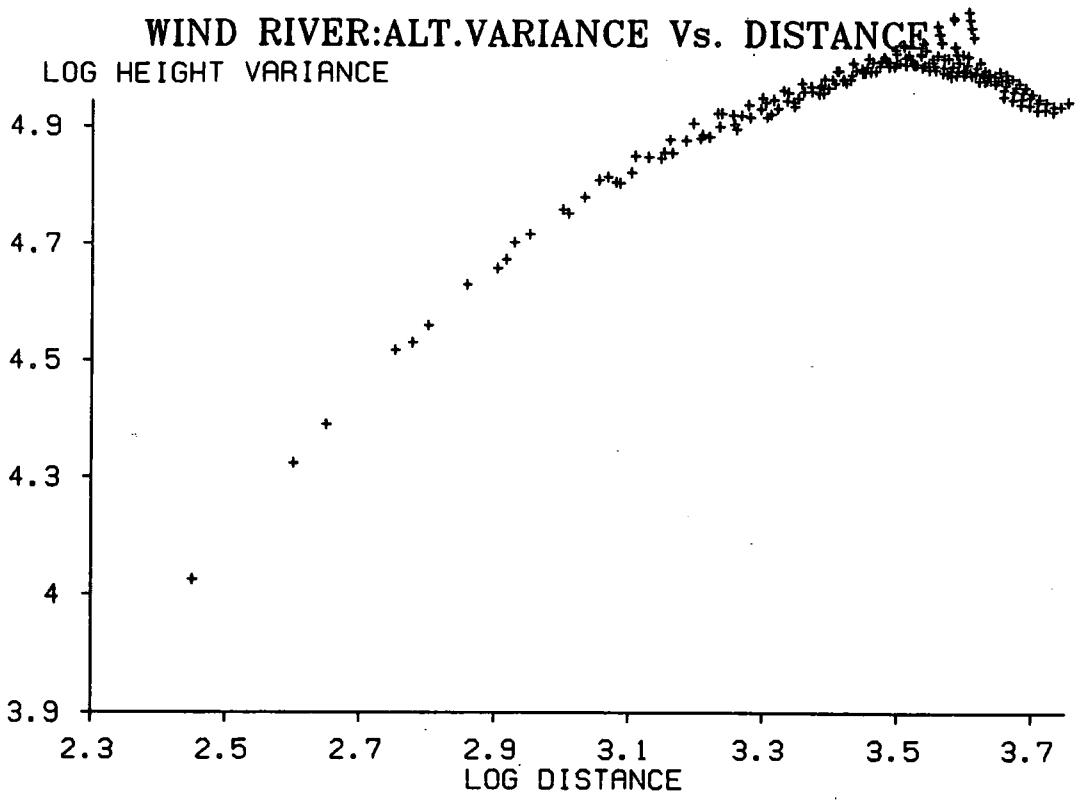
WIND RIVER:ALT.VARIANCE Vs. DISTANCE
LOG HEIGHT VARIANCE
4.9
4.7
4.5
4.3
4
3.9
2.3
2.5
2.7
2.9
3.1
3.3
3.5
3.7
LOG DISTANCE

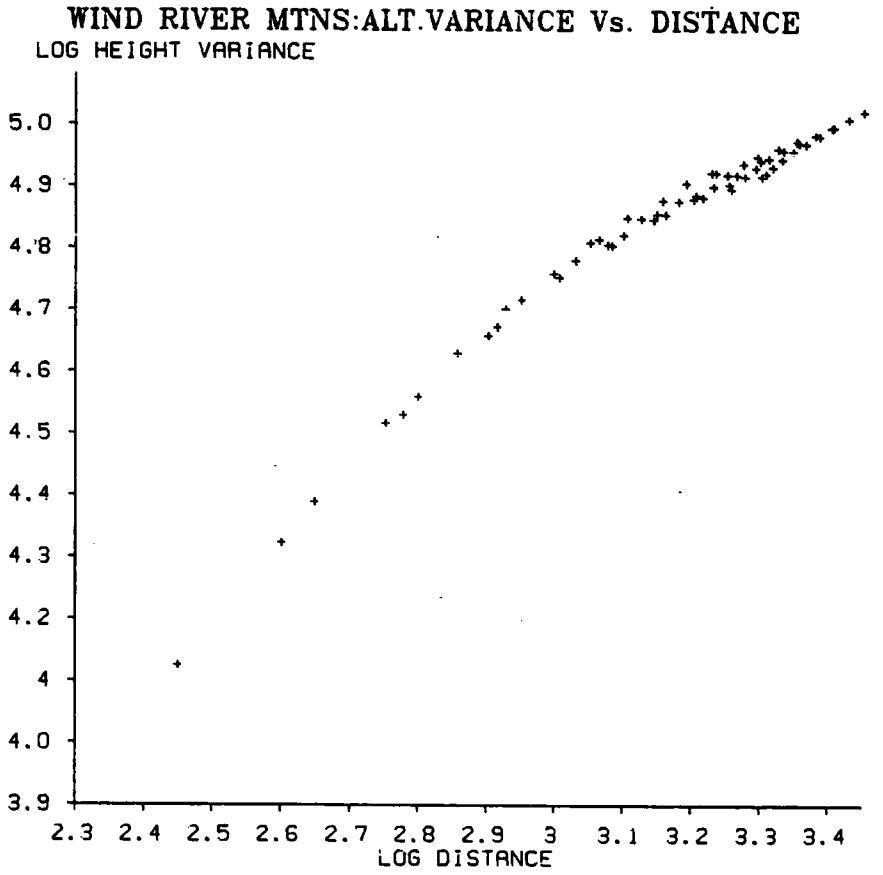
WIND RIVER MTNS:ALT.VARIANCE Vs. DISTANCE
LOG HEIGHT VARIANCE
5.0
4.9
4.8
4.7
4.6
4.5
4.4
4.3
4.2
4
4.0
3.9
2.3
2.4
2.5
2.6
2.7
2.8
2.9
3
3.1
3.2
3.3
3.4
LOG DISTANCE

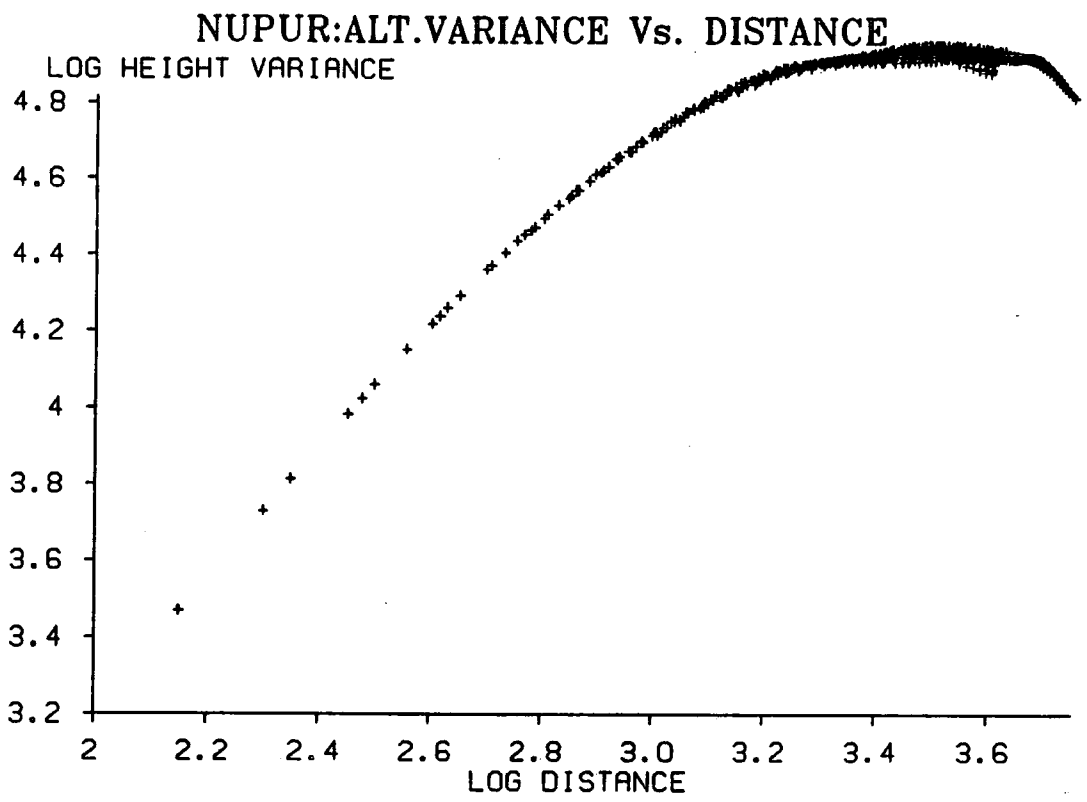
NUPUR:ALT.VARIANCE Vs. DISTANCE
LOG HEIGHT VARIANCE
4.8
4.6
4.4
4.2
4
3.8
3.6
3.4
3.2
2
2.2
2.4
2.6
2.8
3.0
3.2
3.4
3.6
LOG DISTANCE

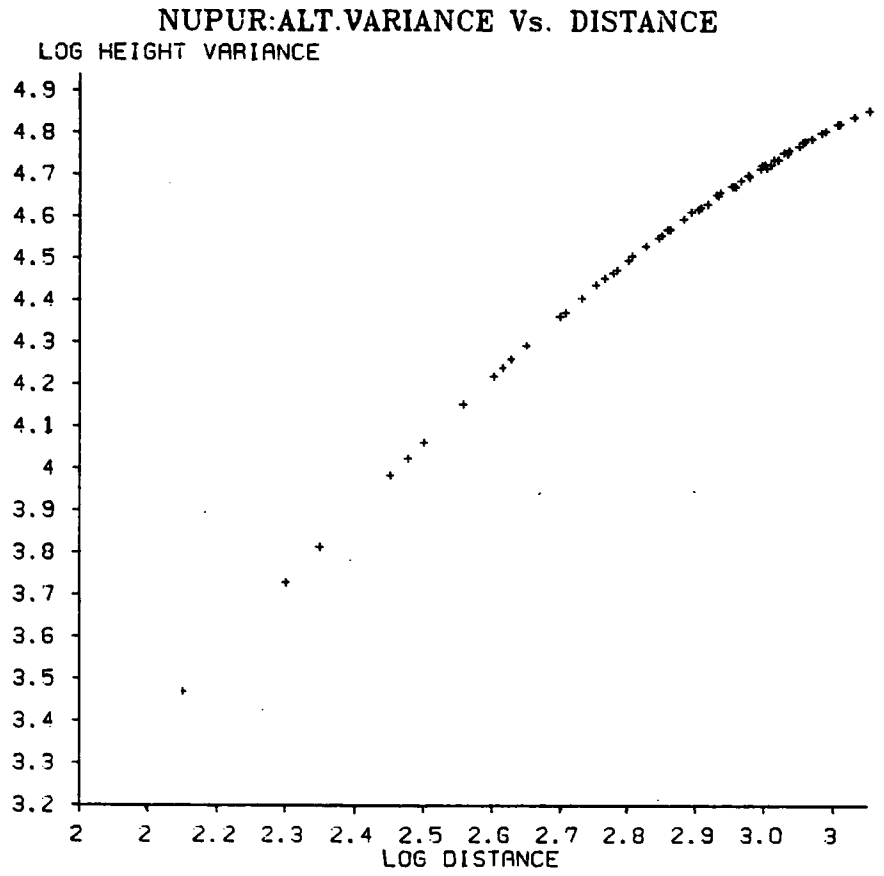
NUPUR:ALT.VARIANCE Vs. DISTANCE
LOG HEIGHT VARIANCE
4.9
4.8
4.7
4.6
4.5
4.4
4.3
4.2
4.1
4
3.9
3.8
3.7
3.6
3.5
3.4
3.3
3.2
2
2
2.2
2.3
2.4
2.5
2.6
2.7
2.8
2.9
3.0
3
LOG DISTANCE

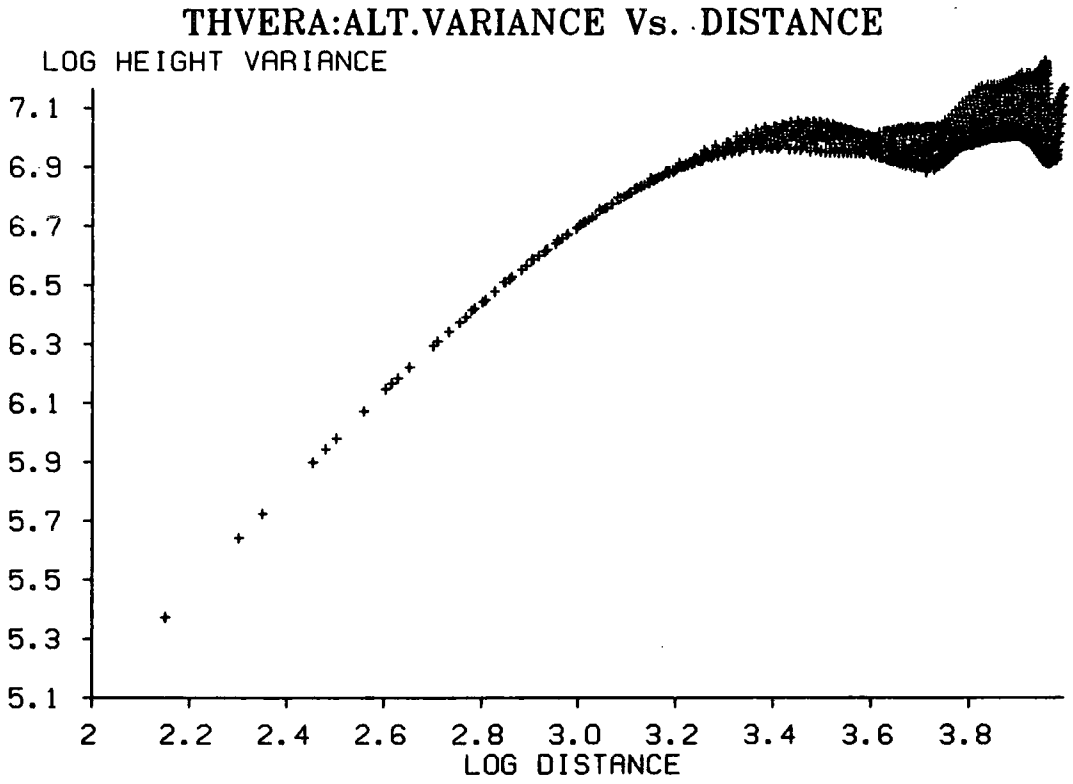
THVERA:ALT.VARIANCE Vs. DISTANCE
LOG HEIGHT VARIANCE
7.1
6.9
6.7
6.5
6.3
6.1
5.9
5.7
5.5
5.3
5.1
2
2.2
2.4
2.6
2.8
3.0
3.2
3.4
3.6
3.8
LOG DISTANCE

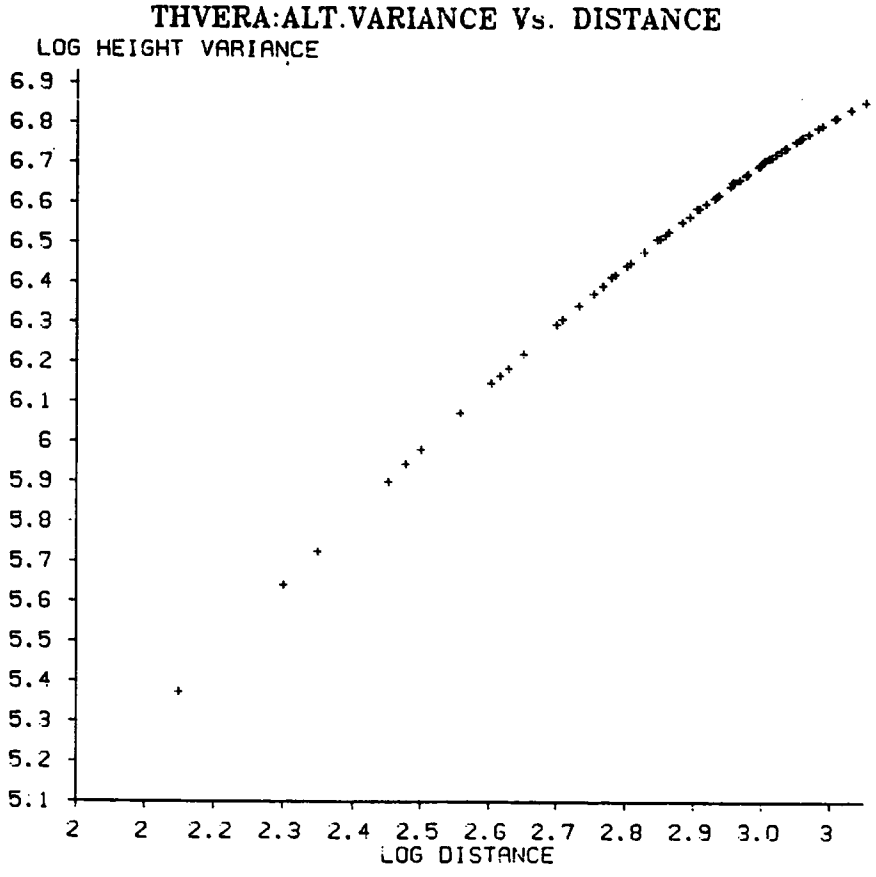
THVERA:ALT.VARIANCE Vs. DISTANCE
LOG HEIGHT VARIANCE
6.9
6.8
6.7
6.6
6.5
6.4
6.3
6.2
6.1
6
5.9
5.8
5.7
5.6
5.5
5.4
5.3
5.2
5.1
2
2
2.2
2.3
2.4
2.5
2.6
2.7
2.8
2.9
3.0
3
LOG DISTANCE

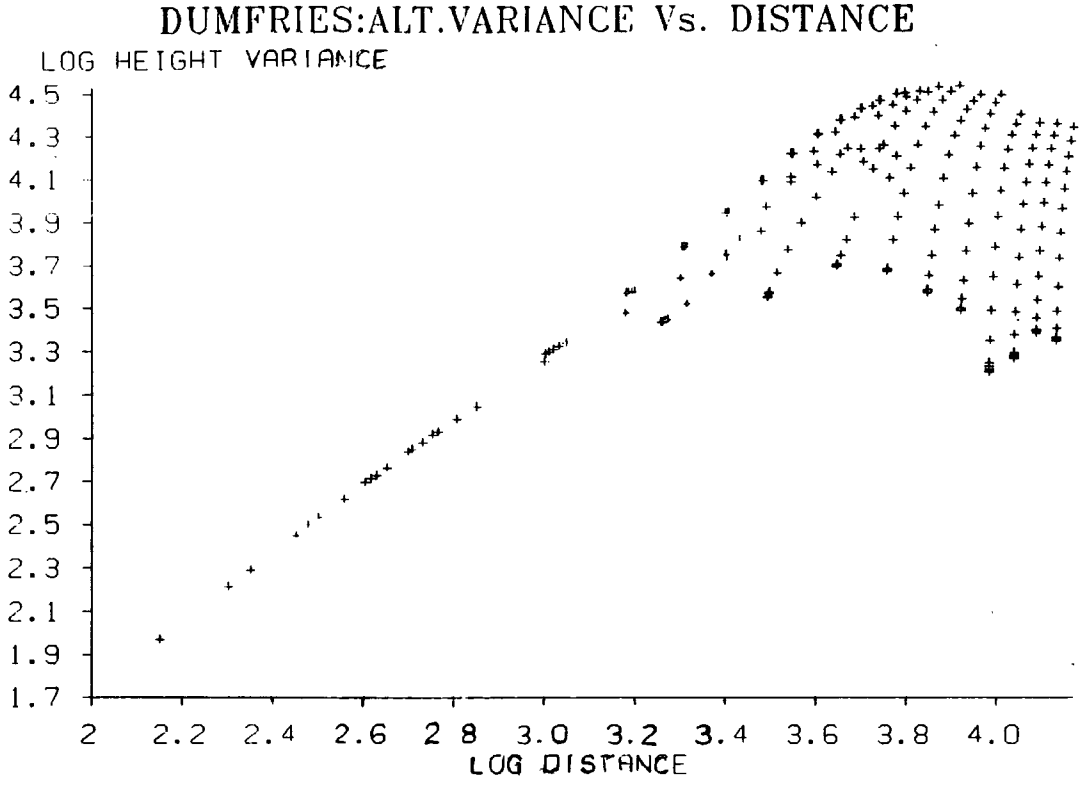
DUMFRIES:ALT.VARIANCE Vs. DISTANCE
LOG HEIGHT VARIANCE
4.5
4.3
4.1
3.9
3.7
3.5
3.3
3.1
2.9
2.7
2.5
2.3
2.1
1.9
1.7
2
2.2
2.4
2.6
2.8
3.0
3.2
3.4
3.6
3.8
4.0
LOG DISTANCE

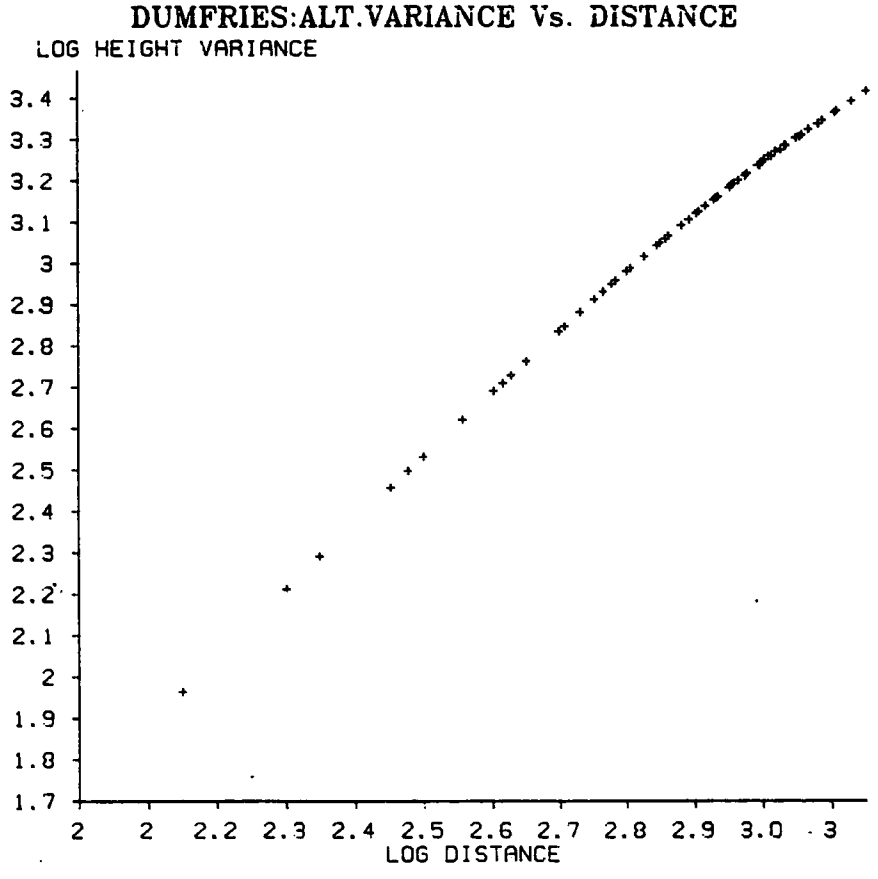
DUMFRIES:ALT.VARIANCE Vs. DISTANCE
LOG HEIGHT VARIANCE
3.4
3.3
3.2
3.1
3
2.9
2.8
2.7
2.6
2.5
2.4
2.3
2.2
2.1
2
1.9
1.8
1.7
2
2
2.2
2.3
2.4
2.5
2.6
2.7
2.8
2.9
3.0
3
LOG DISTANCE

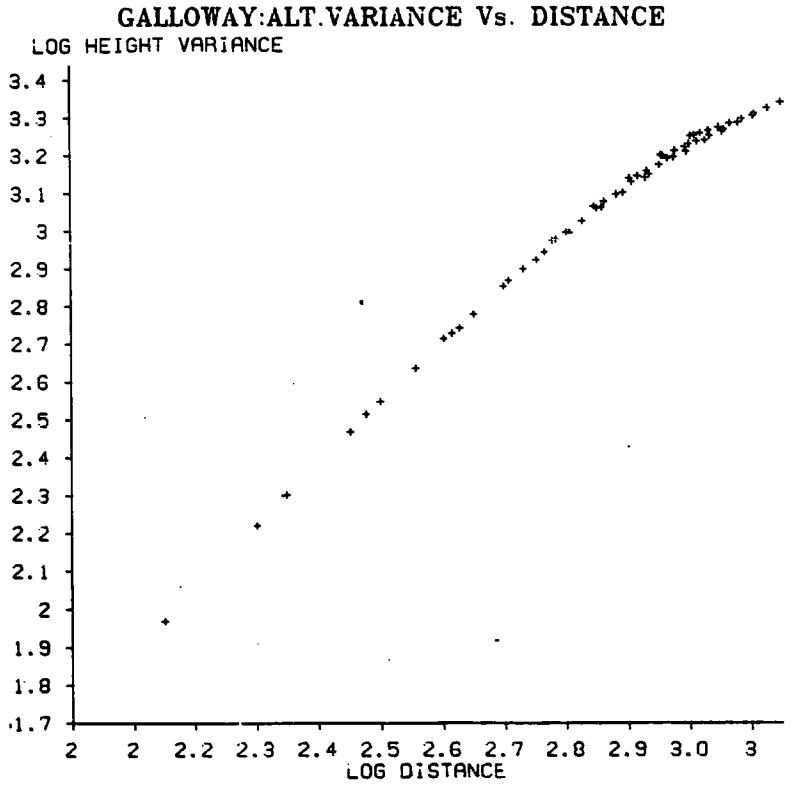
GALLOWAY:ALT.VARIANCE Vs. DISTANCE
LOG HEIGHT VARIANCE
3.4
3.3
3.2
3.1
3
2.9
2.8
2.7
2.6
2.5
2.4
2.3
2.2
2.1
2
1.9
1.8
1.7
2 2 2.2 2.3 2.4 2.5 2.6 2.7 2.8 2.9 3.0 3
LOG DISTANCE

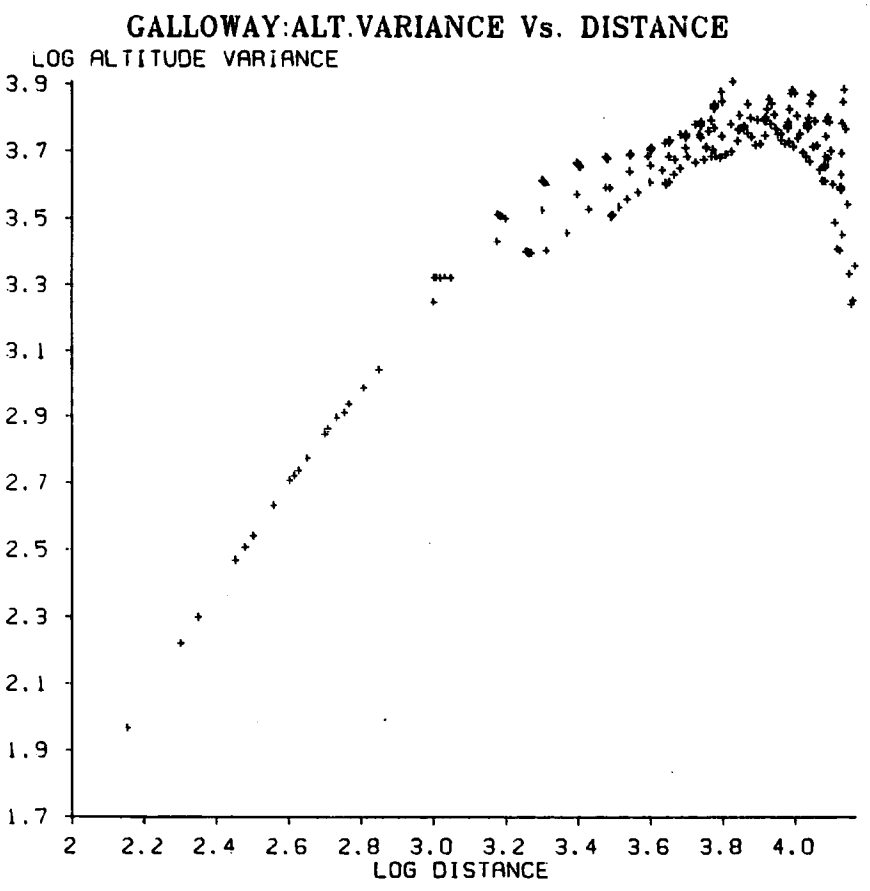
GALLOWAY:ALT.VARIANCE Vs. DISTANCE
LOG ALTITUDE VARIANCE
3.9
3.7
3.5
3.3
3.1
2.9
2.7
2.5
2.3
2.1
1.9
1.7
2 2.2 2.4 2.6 2.8 3.0 3.2 3.4 3.6 3.8 4.0
LOG DISTANCE

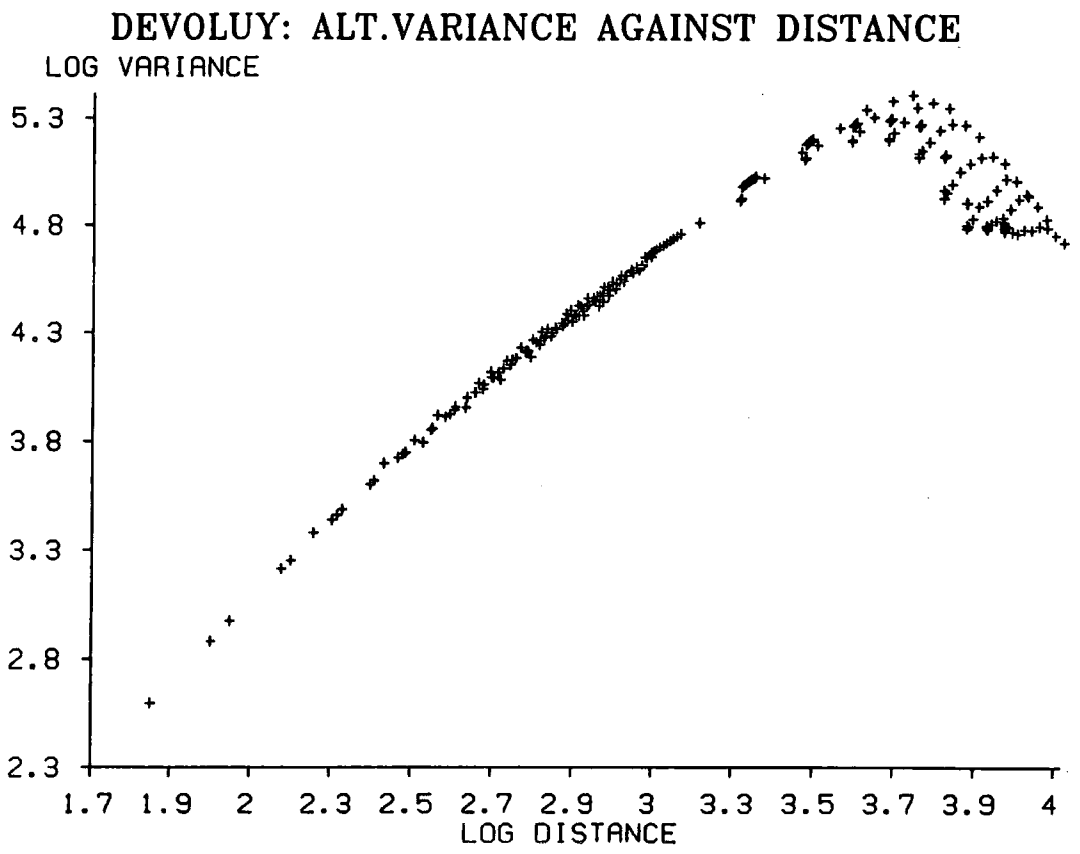
DEVOLUY: ALT.VARIANCE AGAINST DISTANCE
LOG VARIANCE
5.3
4.8
4.3
3.8
3.3
2.8
2.3
1.7 1.9 2 2.3 2.5 2.7 2.9 3 3.3 3.5 3.7 3.9 4
LOG DISTANCE

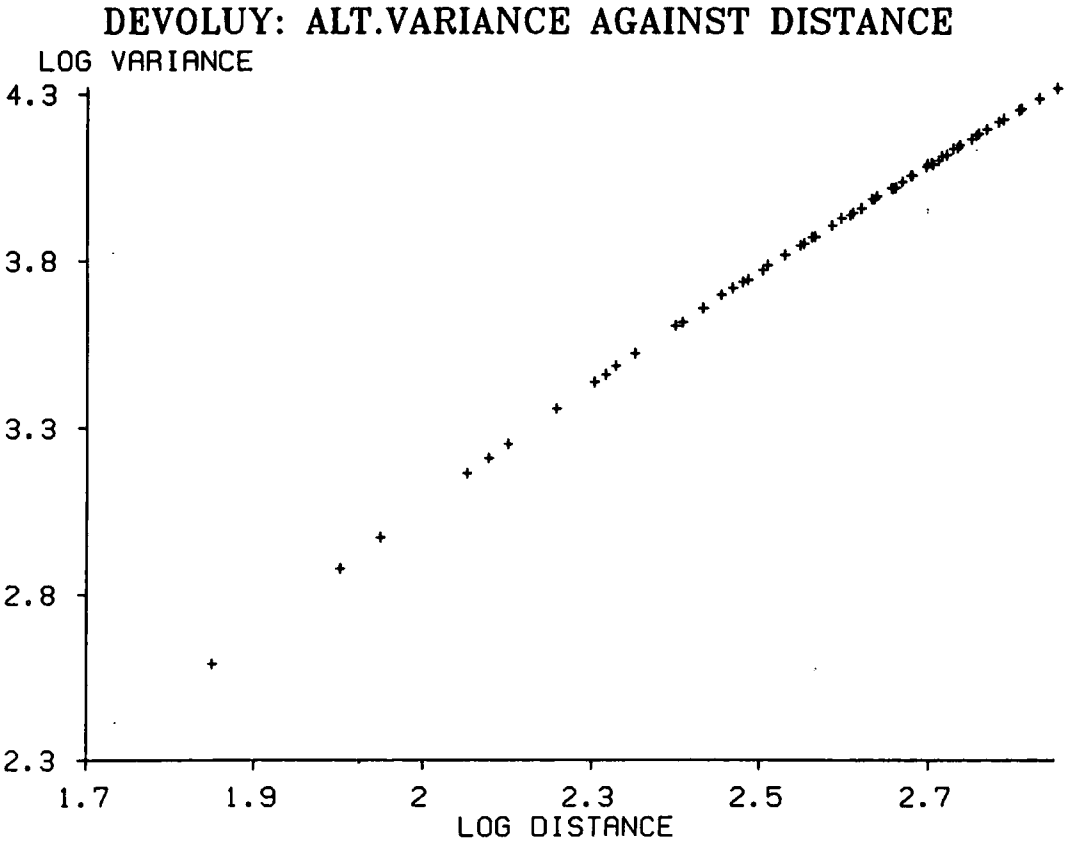
DEVOLUY: ALT.VARIANCE AGAINST DISTANCE
LOG VARIANCE
4.3
3.8
3.3
2.8
2.3
1.7 1.9 2 2.3 2.5 2.7
LOG DISTANCE

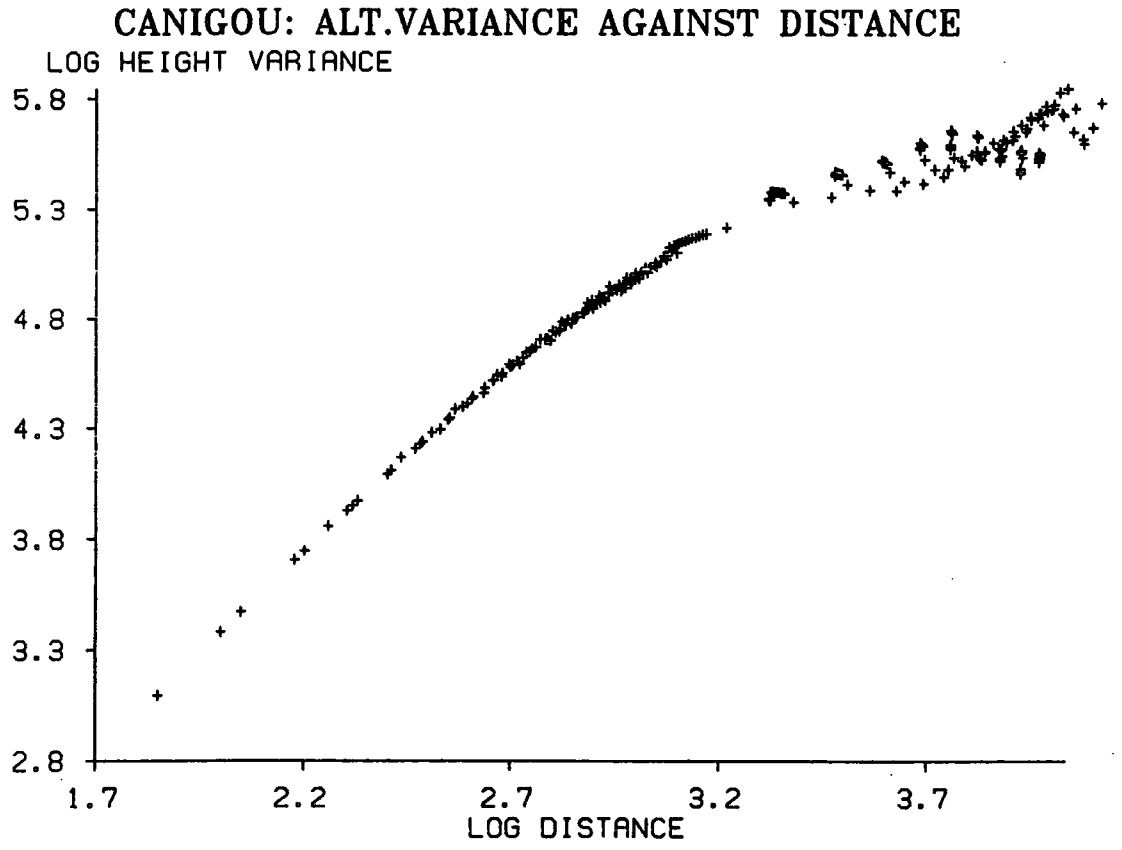
CANIGOU: ALT.VARIANCE AGAINST DISTANCE
LOG HEIGHT VARIANCE
5.8
5.3
4.8
4.3
3.8
3.3
2.8
1.7
2.2
2.7
3.2
3.7
LOG DISTANCE

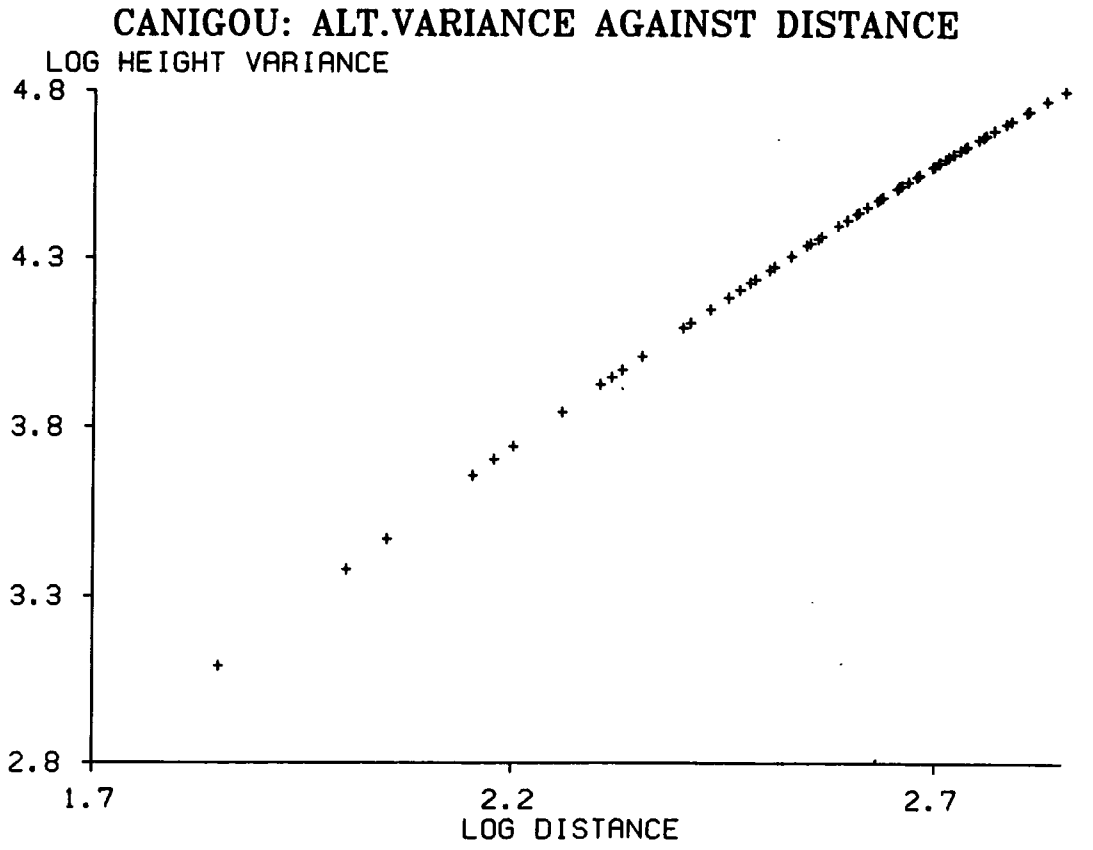
CANIGOU: ALT.VARIANCE AGAINST DISTANCE
LOG HEIGHT VARIANCE
4.8
4.3
3.8
3.3
2.8
1.7
2.2
2.7
LOG DISTANCE

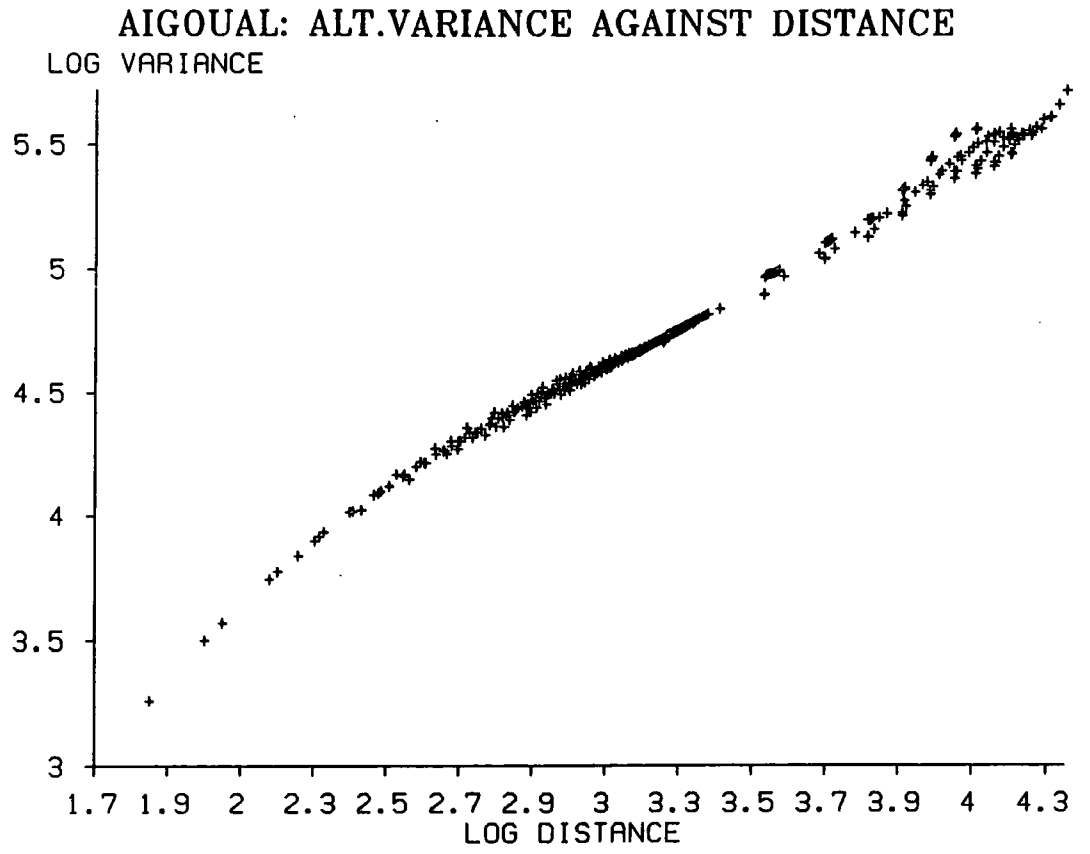
AIGOUAL: ALT.VARIANCE AGAINST DISTANCE
LOG VARIANCE
5.5
5
4.5
4
3.5
3
1.7 1.9 2 2.3 2.5 2.7 2.9 3 3.3 3.5 3.7 3.9 4 4.3
LOG DISTANCE

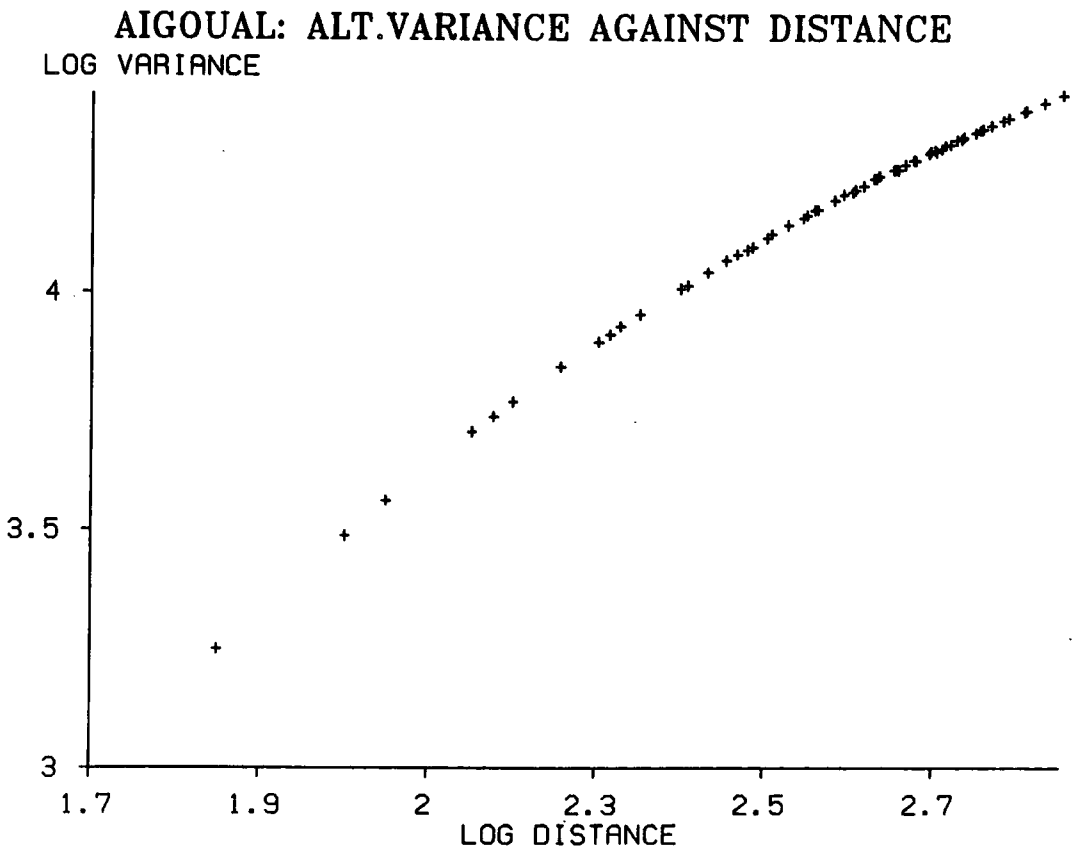
AIGOUAL: ALT.VARIANCE AGAINST DISTANCE
LOG VARIANCE
4
3.5
3
1.7 1.9 2 2.3 2.5 2.7
LOG DISTANCE

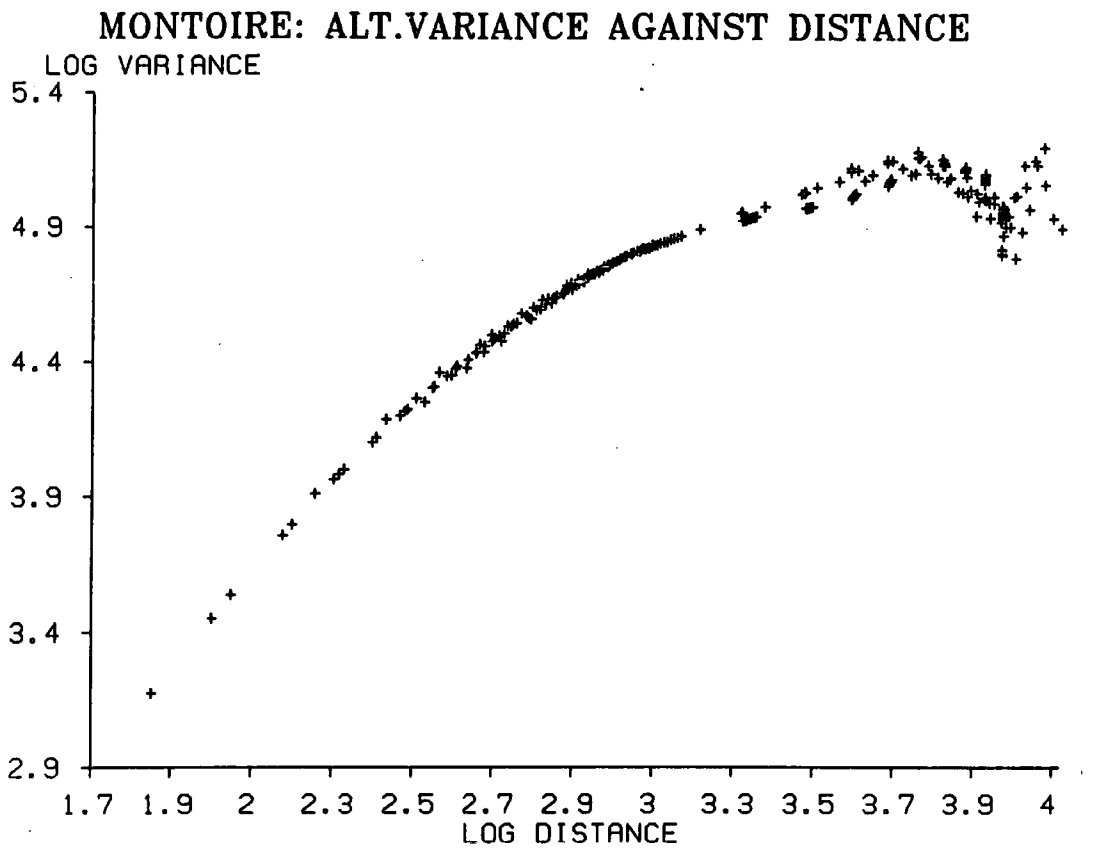
MONTOIRE: ALT.VARIANCE AGAINST DISTANCE
LOG VARIANCE
5.4
4.9
4.4
3.9
3.4
2.9
1.7 1.9 2 2.3 2.5 2.7 2.9 3 3.3 3.5 3.7 3.9 4
LOG DISTANCE

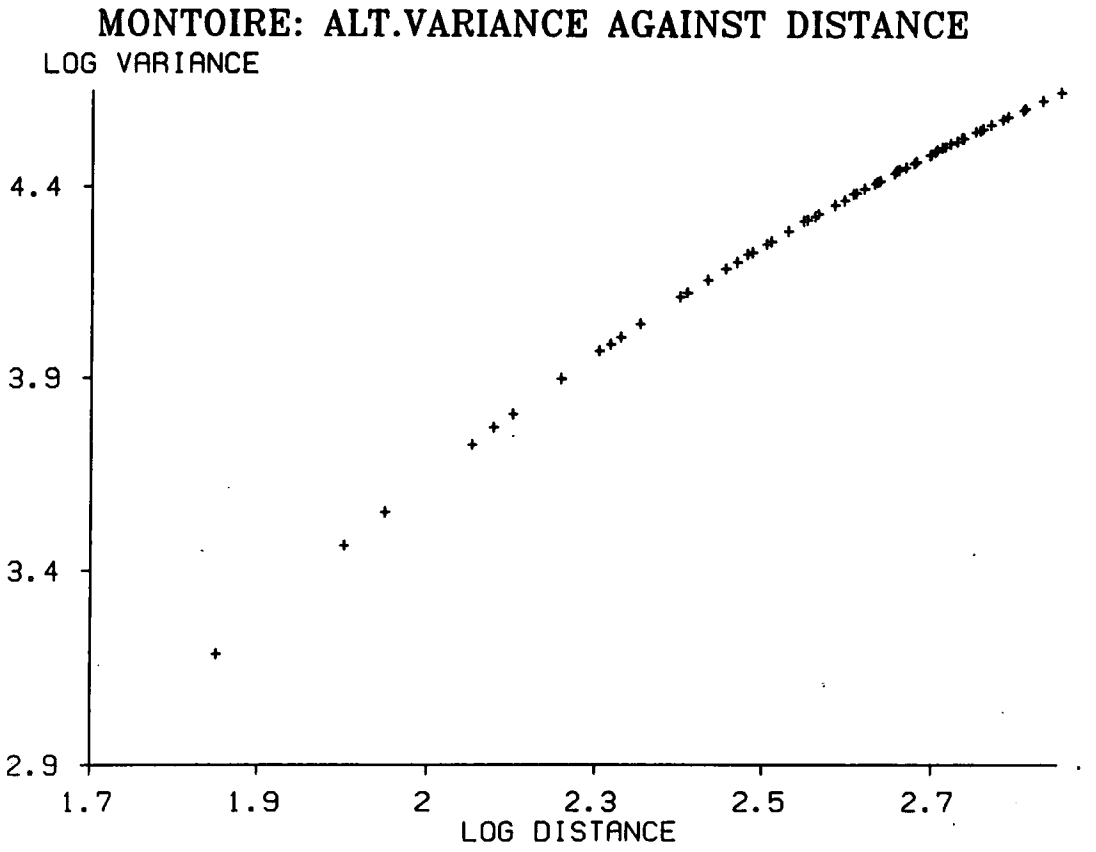
MONTOIRE: ALT.VARIANCE AGAINST DISTANCE
LOG VARIANCE
4.4
3.9
3.4
2.9
1.7 1.9 2 2.3 2.5 2.7
LOG DISTANCE

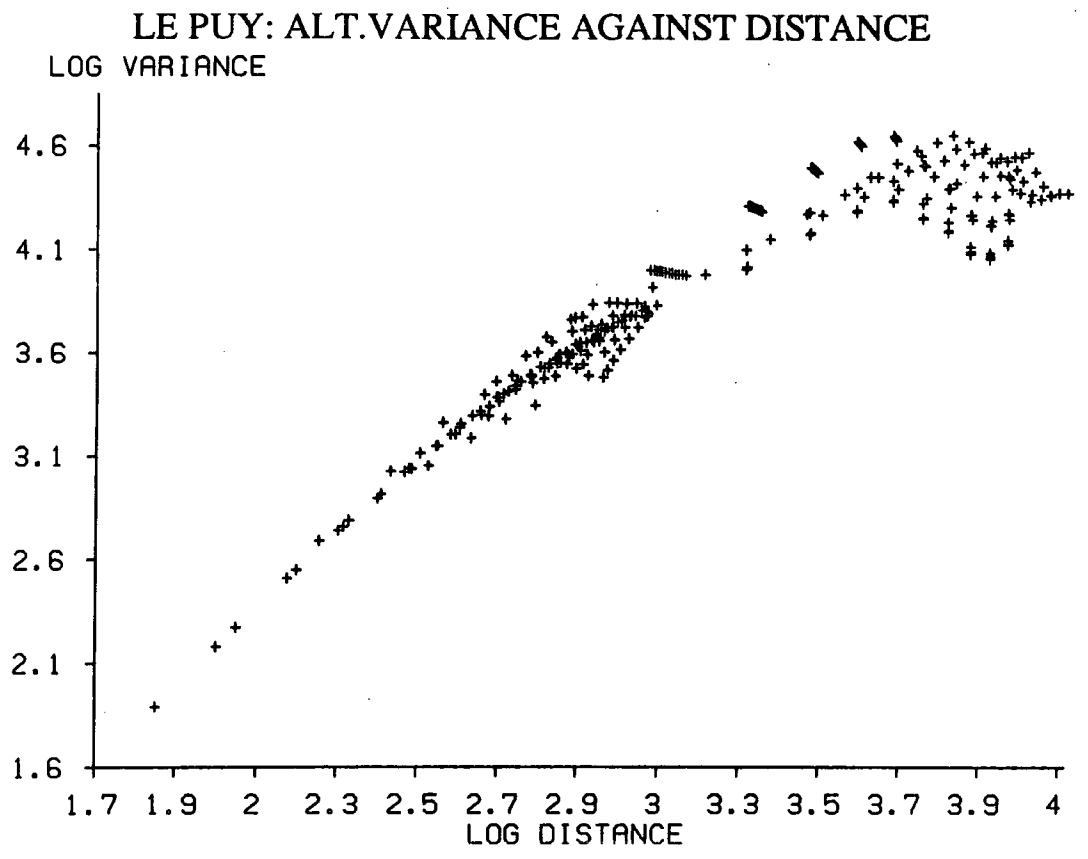
LE PUY: ALT.VARIANCE AGAINST DISTANCE
LOG VARIANCE
4.6
4.1
3.6
3.1
2.6
2.1
1.6
1.7 1.9 2 2.3 2.5 2.7 2.9 3 3.3 3.5 3.7 3.9 4
LOG DISTANCE

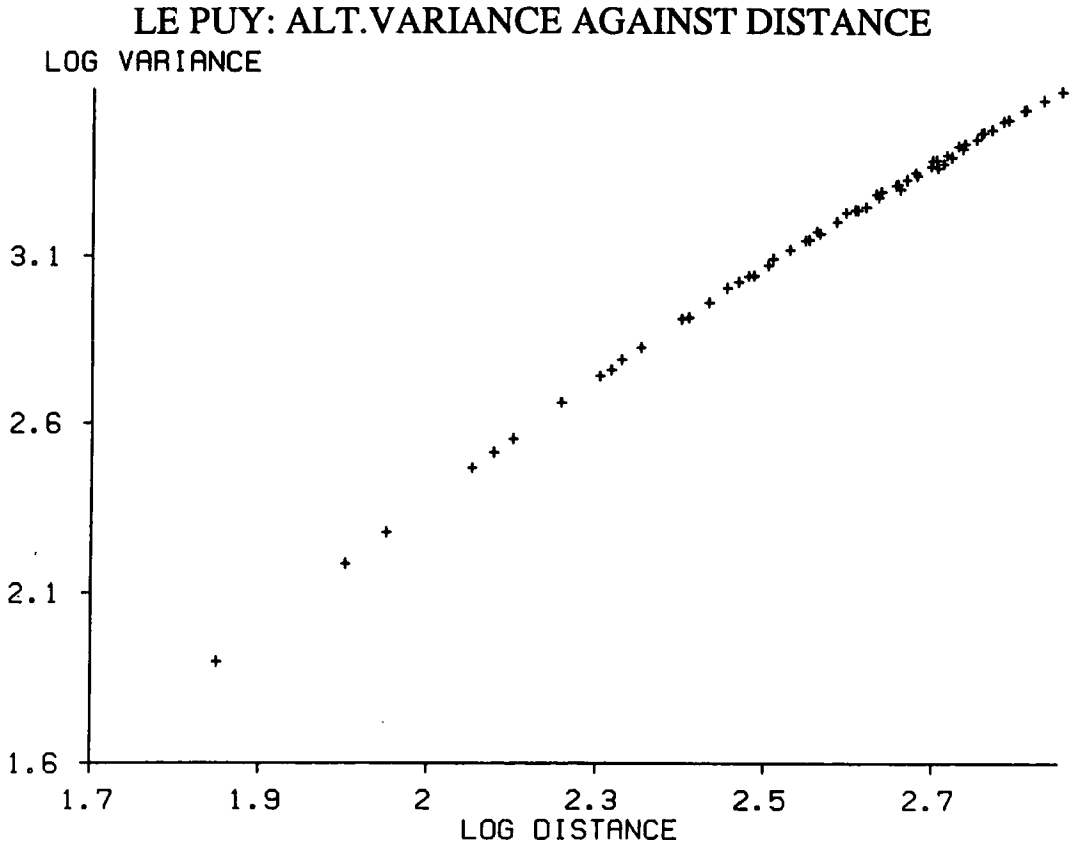
LE PUY: ALT.VARIANCE AGAINST DISTANCE
LOG VARIANCE
3.1
2.6
2.1
1.6
1.7 1.9 2 2.3 2.5 2.7
LOG DISTANCE

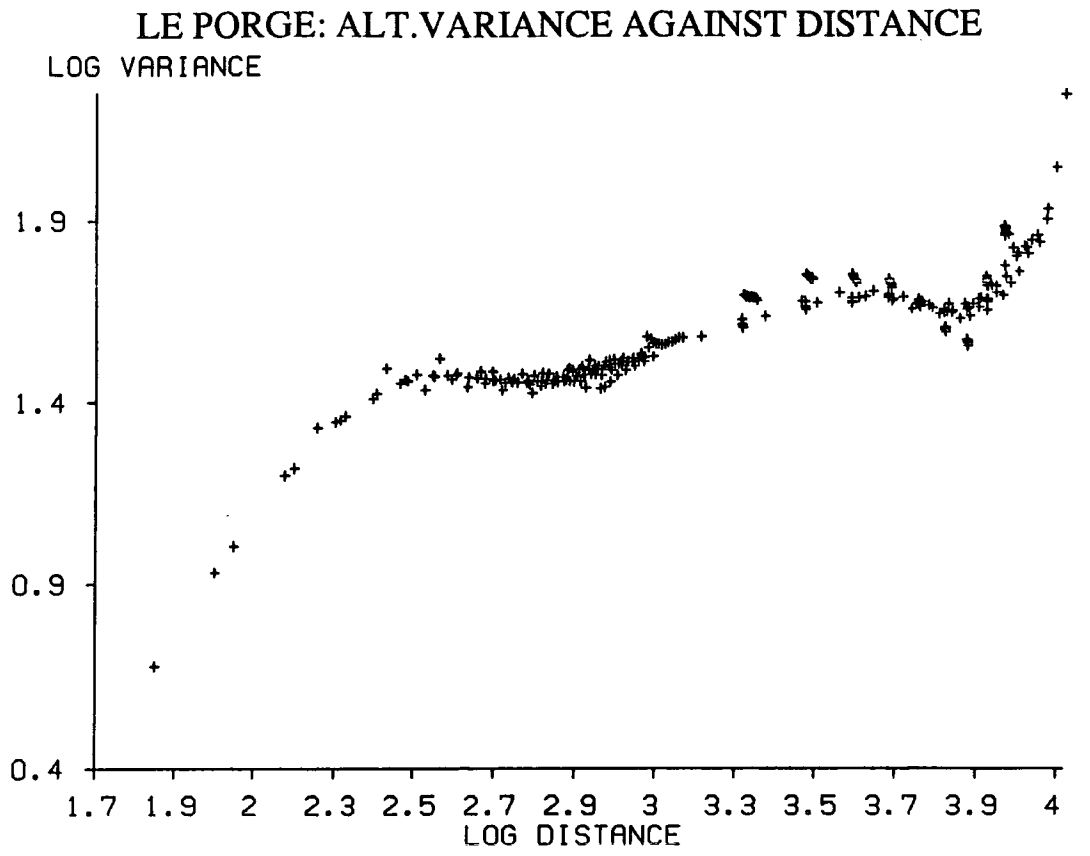
LE PORGE: ALT.VARIANCE AGAINST DISTANCE
LOG VARIANCE
1.9
1.4
0.9
0.4
1.7 1.9 2 2.3 2.5 2.7 2.9 3 3.3 3.5 3.7 3.9 4
LOG DISTANCE

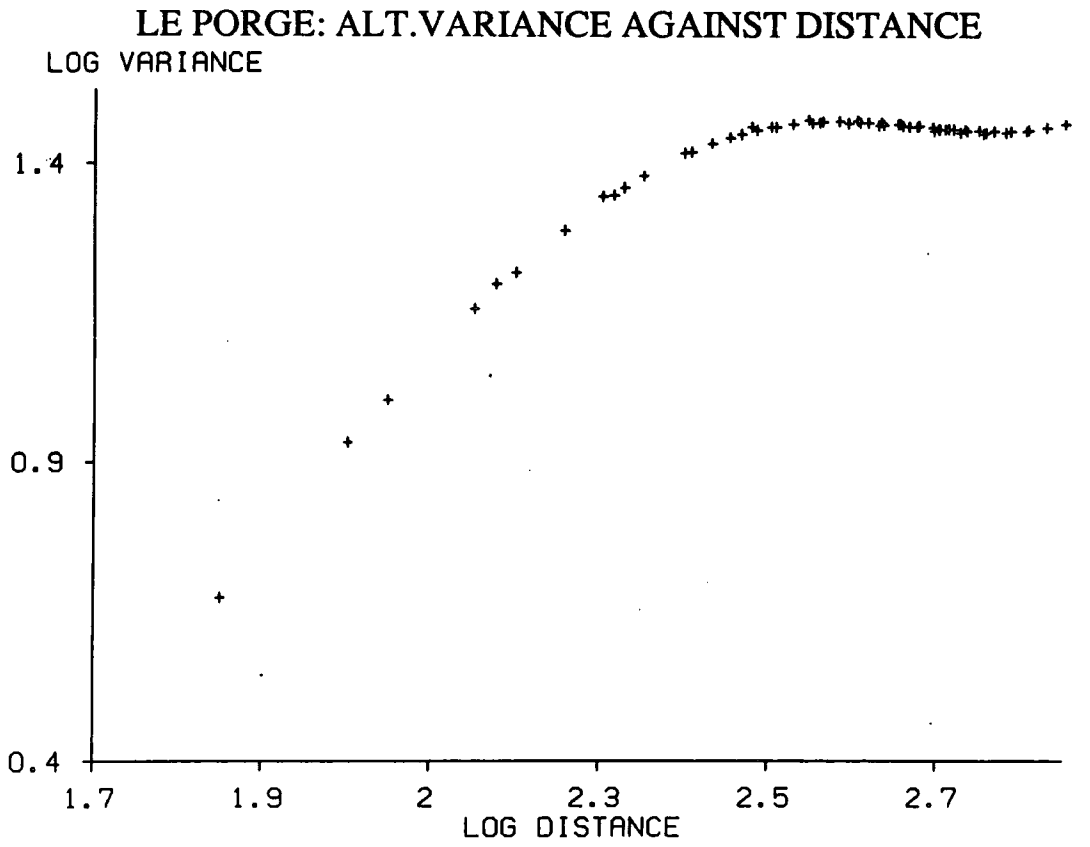
LE PORGE: ALT.VARIANCE AGAINST DISTANCE
LOG VARIANCE
1.4
0.9
0.4
1.7 1.9 2 2.3 2.5 2.7
LOG DISTANCE

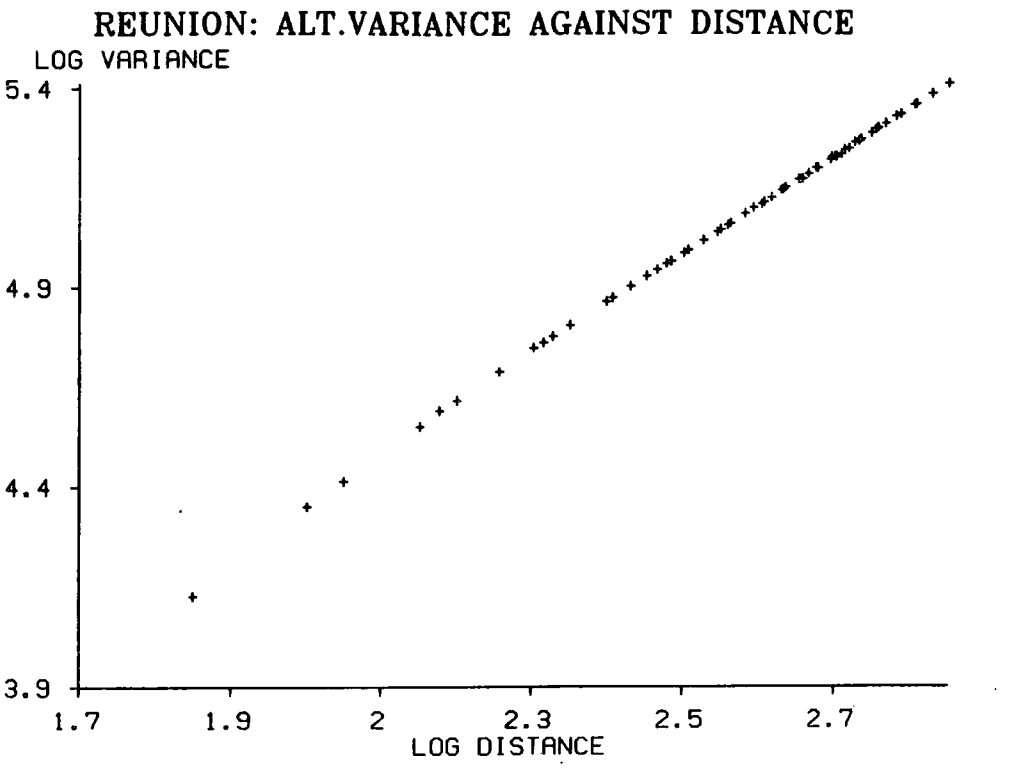
REUNION: ALT.VARIANCE AGAINST DISTANCE
LOG VARIANCE
5.4
4.9
4.4
3.9
1.7
1.9
2
2.3
2.5
2.7
LOG DISTANCE

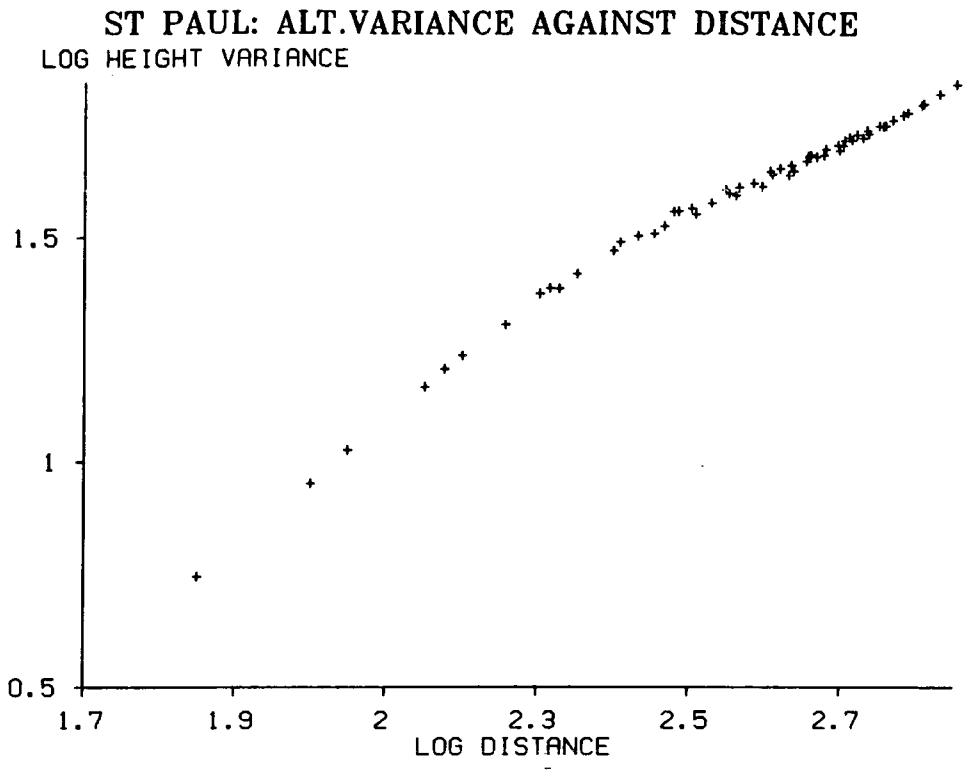
ST PAUL: ALT.VARIANCE AGAINST DISTANCE
LOG HEIGHT VARIANCE
1.5
1
0.5
1.7
1.9
2
2.3
2.5
2.7
LOG DISTANCE

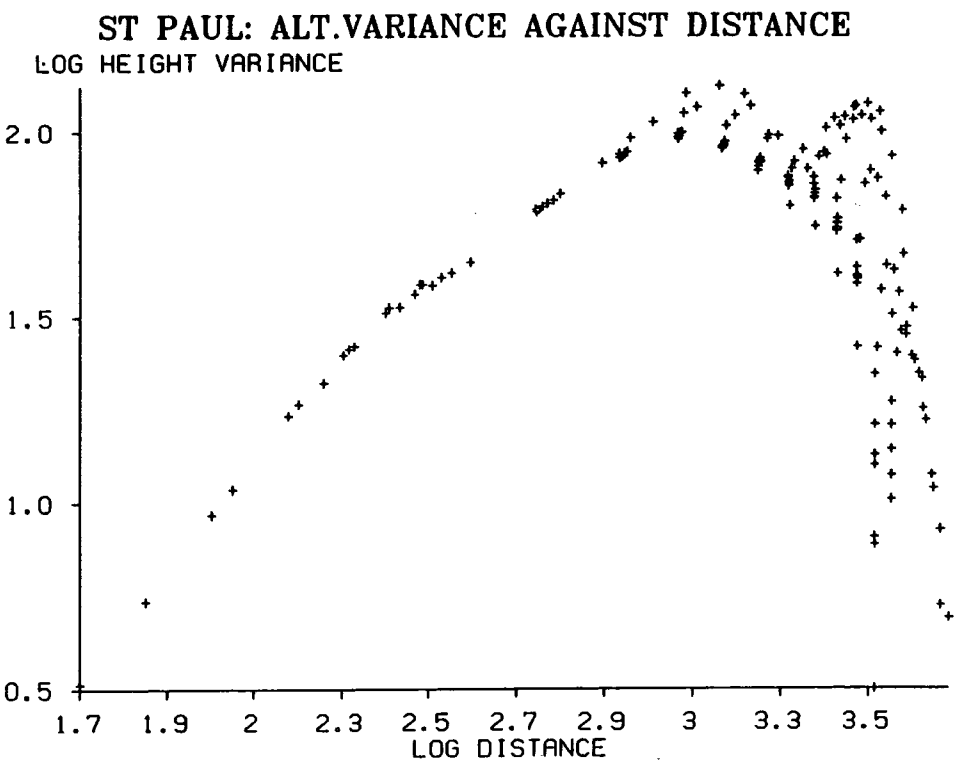
ST PAUL: ALT.VARIANCE AGAINST DISTANCE
LOG HEIGHT VARIANCE
2.0
1.5
1.0
0.5
1.7
1.9
2
2.3
2.5
2.7
2.9
3
3.3
3.5
LOG DISTANCE

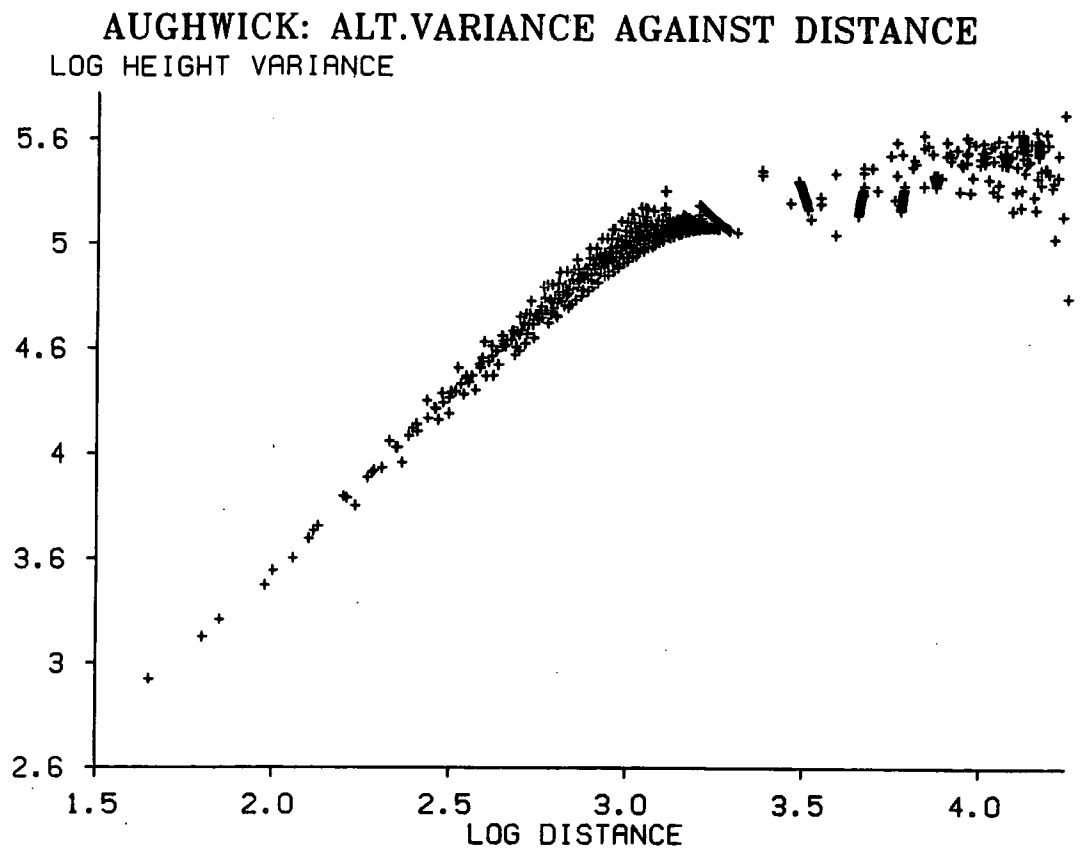
AUGHWICK: ALT.VARIANCE AGAINST DISTANCE
LOG HEIGHT VARIANCE
5.6
5
4.6
4
3.6
3
2.6
1.5
2.0
2.5
3.0
3.5
4.0
LOG DISTANCE

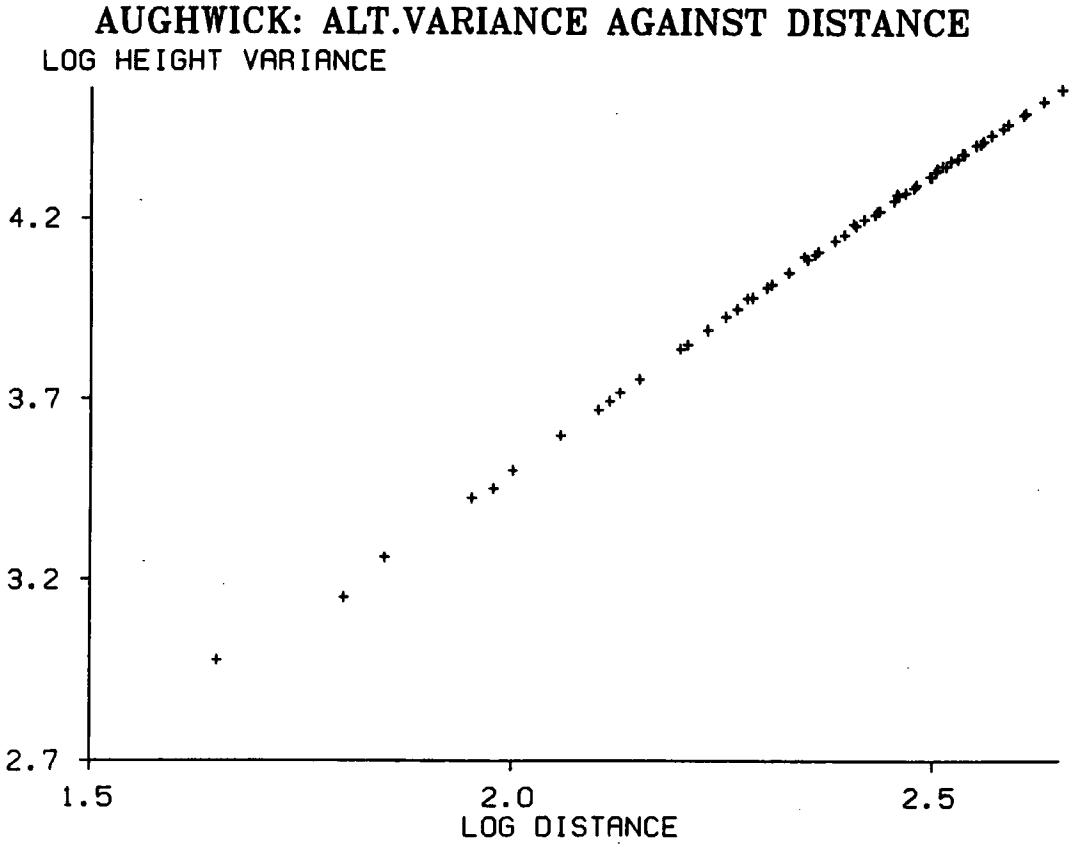
AUGHWICK: ALT.VARIANCE AGAINST DISTANCE
LOG HEIGHT VARIANCE
4.2
3.7
3.2
2.7
1.5
2.0
2.5
LOG DISTANCE

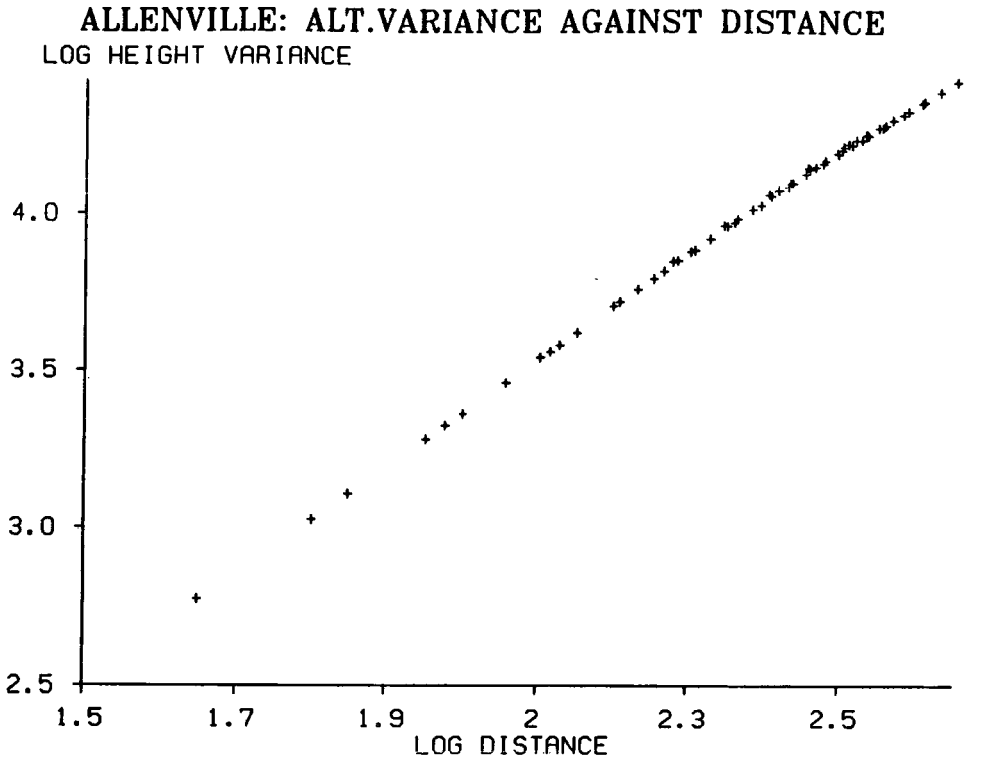
ALLENVILLE: ALT.VARIANCE AGAINST DISTANCE
LOG HEIGHT VARIANCE
4.0
3.5
3.0
2.5
1.5
1.7
1.9
2
2.3
2.5
LOG DISTANCE

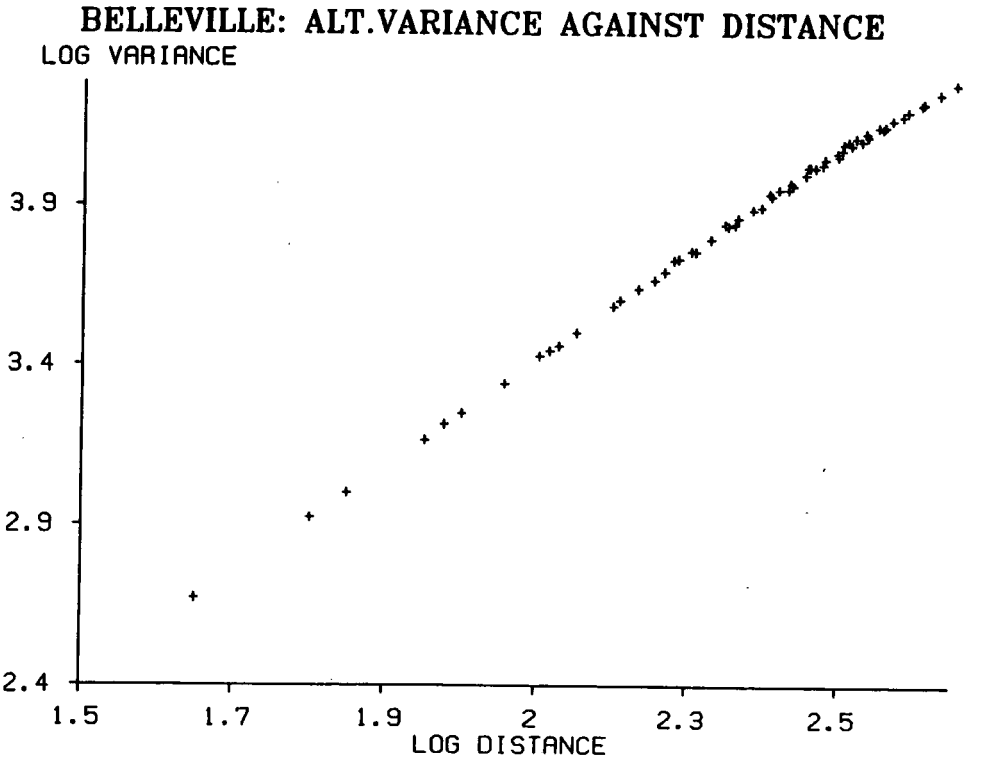
BELLEVILLE: ALT.VARIANCE AGAINST DISTANCE
LOG VARIANCE
3.9
3.4
2.9
2.4
1.5
1.7
1.9
2
2.3
2.5
LOG DISTANCE

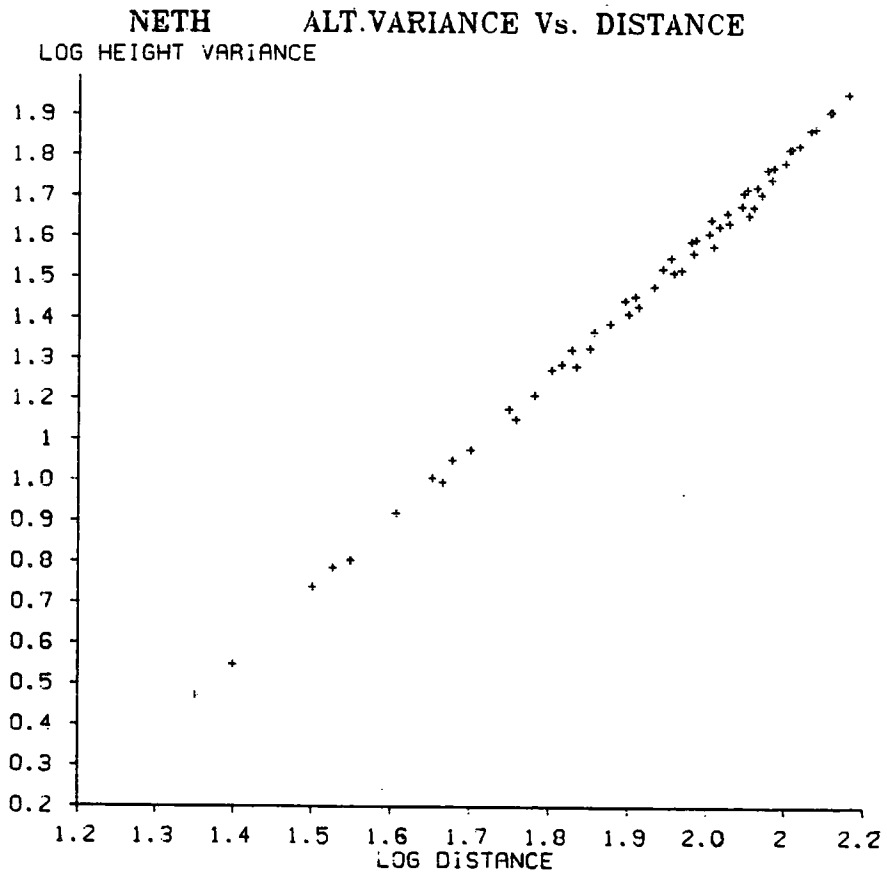
NETH ALT.VARIANCE Vs. DISTANCE
LOG HEIGHT VARIANCE
1.9
1.8
1.7
1.6
1.5
1.4
1.3
1.2
1
1.0
0.9
0.8
0.7
0.6
0.5
0.4
0.3
0.2
1.2 1.3 1.4 1.5 1.6 1.7 1.8 1.9 2.0 2 2.2
LOG DISTANCE

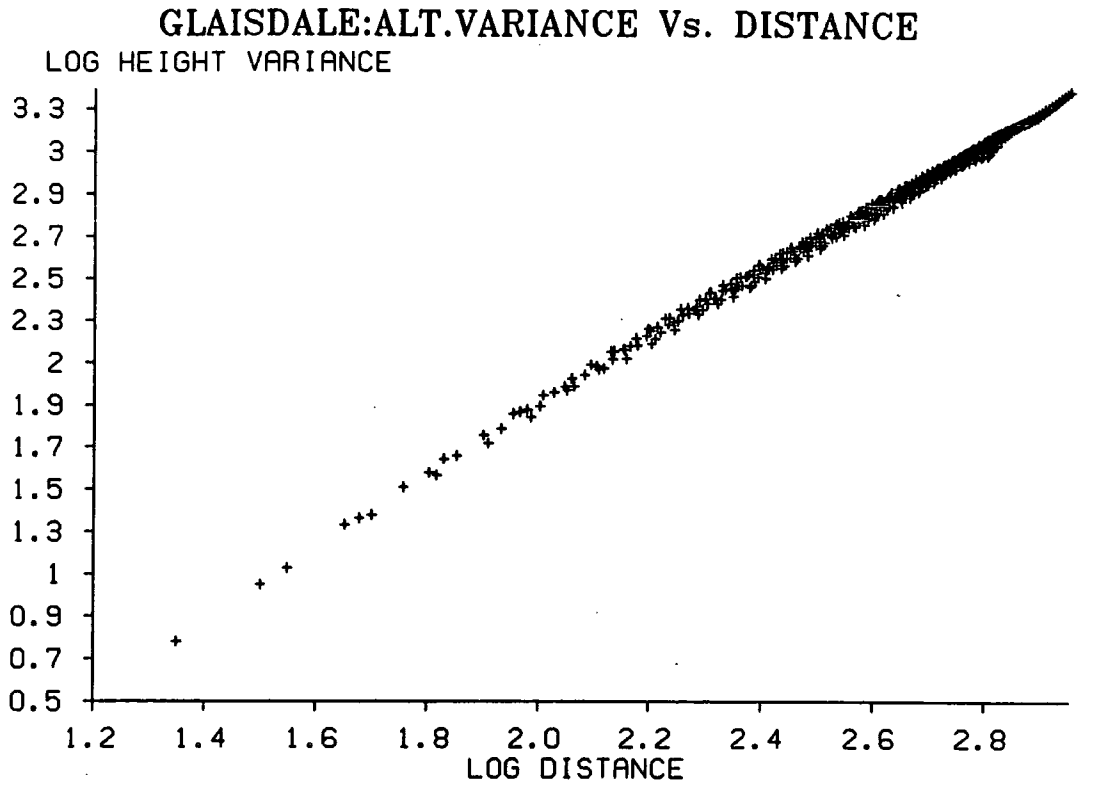
GLAISDALE:ALT.VARIANCE Vs. DISTANCE
LOG HEIGHT VARIANCE
3.3
3
2.9
2.7
2.5
2.3
2
1.9
1.7
1.5
1.3
1
0.9
0.7
0.5
1.2
1.4
1.6
1.8
2.0
2.2
2.4
2.6
2.8
LOG DISTANCE

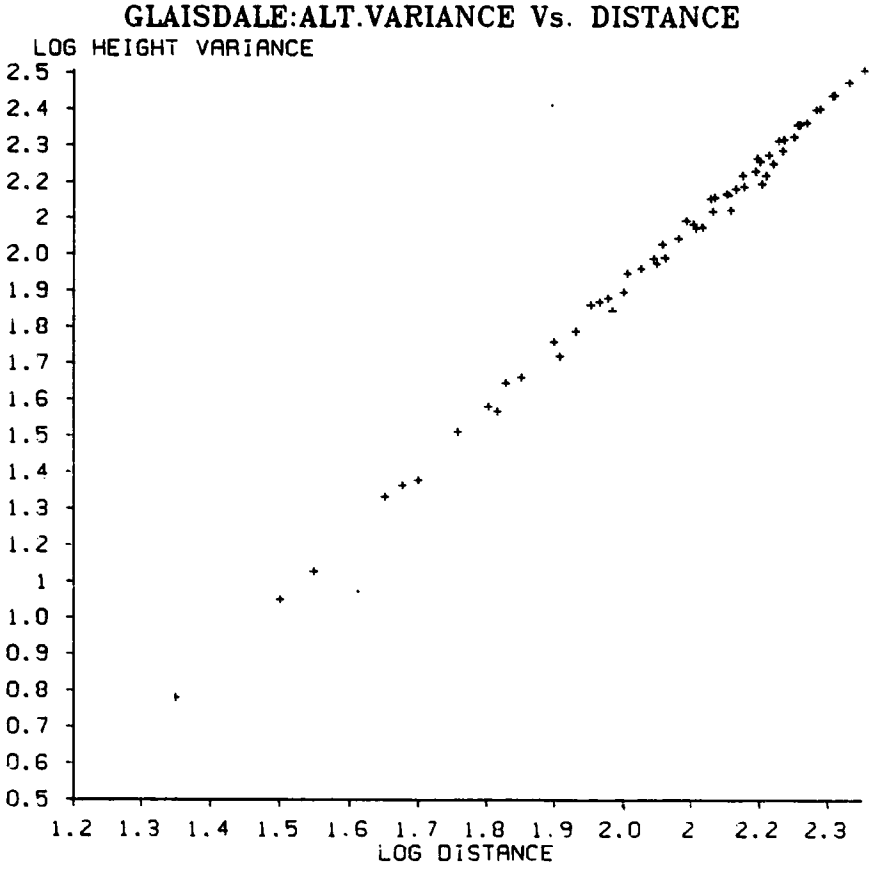
GLAISDALE:ALT.VARIANCE Vs. DISTANCE
LOG HEIGHT VARIANCE
2.5
2.4
2.3
2.2
2
2.0
1.9
1.8
1.7
1.6
1.5
1.4
1.3
1.2
1
1.0
0.9
0.8
0.7
0.6
0.5
1.2
1.3
1.4
1.5
1.6
1.7
1.8
1.9
2.0
2
2.2
2.3
LOG DISTANCE

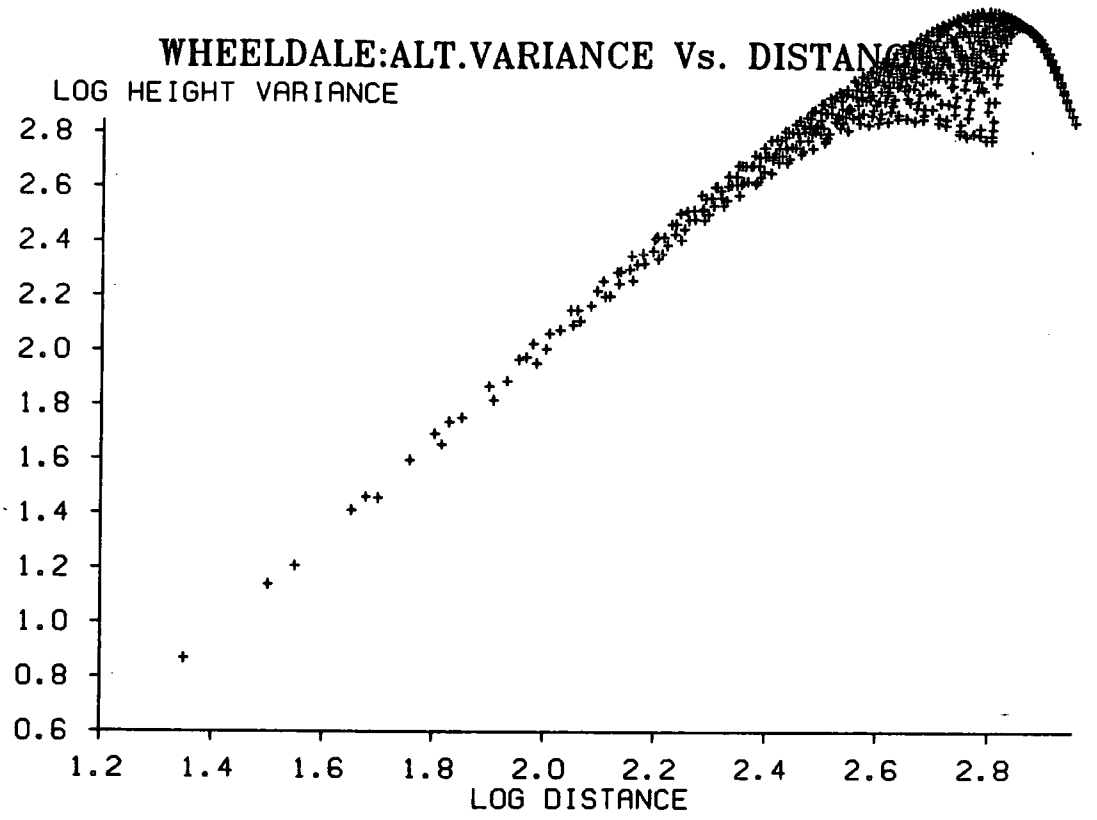
WHEELDALE:ALT.VARIANCE Vs. DISTANCE
LOG HEIGHT VARIANCE
2.8
2.6
2.4
2.2
2.0
1.8
1.6
1.4
1.2
1.0
0.8
0.6
1.2 1.4 1.6 1.8 2.0 2.2 2.4 2.6 2.8
LOG DISTANCE

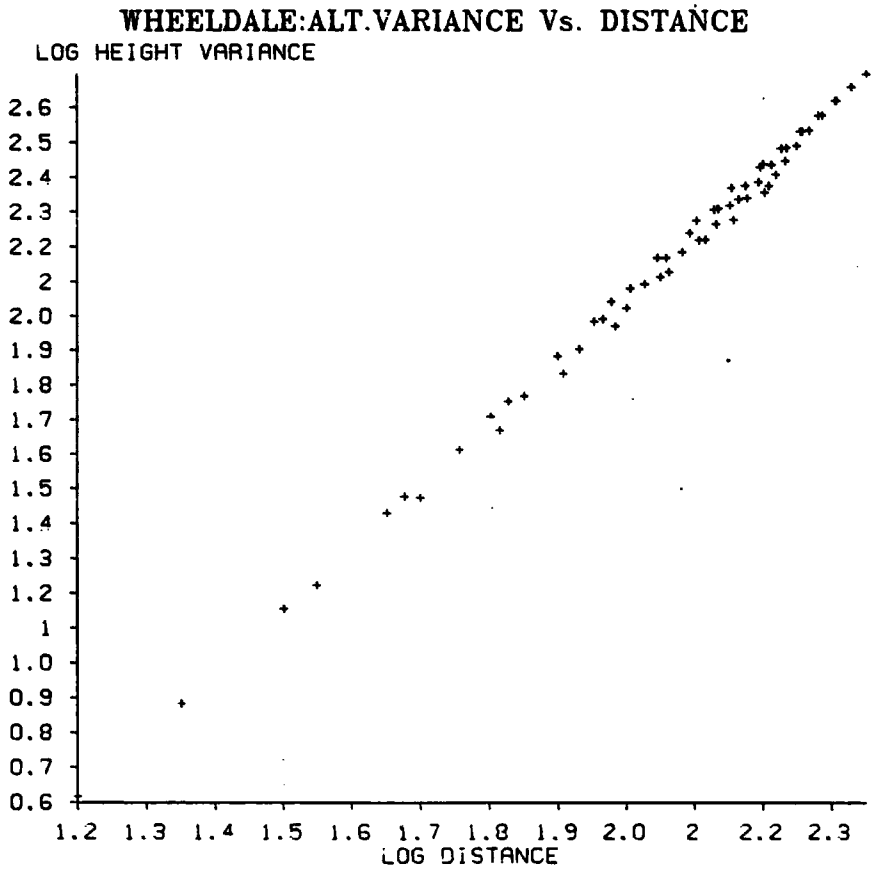
WHEELDALE:ALT.VARIANCE Vs. DISTANCE
LOG HEIGHT VARIANCE
2.6
2.5
2.4
2.3
2.2
2
2.0
1.9
1.8
1.7
1.6
1.5
1.4
1.3
1.2
1
1.0
0.9
0.8
0.7
0.6
1.2 1.3 1.4 1.5 1.6 1.7 1.8 1.9 2.0 2 2.2 2.3
LOG DISTANCE

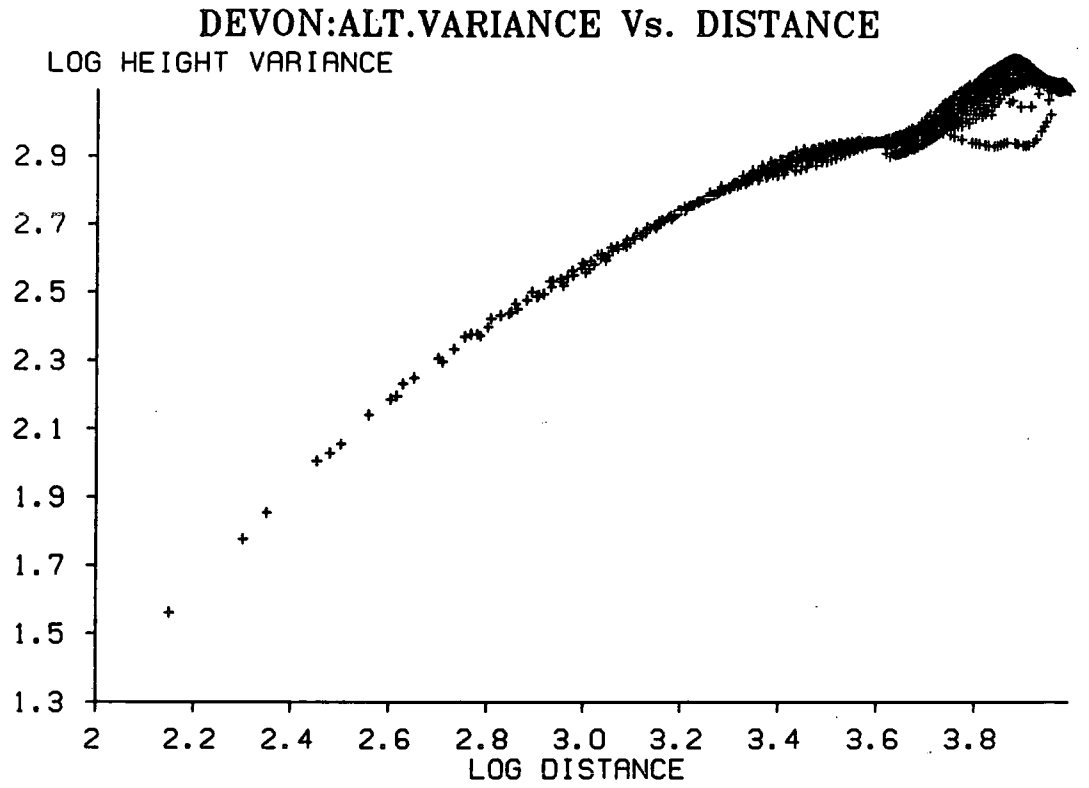
DEVON:ALT.VARIANCE Vs. DISTANCE
LOG HEIGHT VARIANCE
2.9
2.7
2.5
2.3
2.1
1.9
1.7
1.5
1.3
2
2.2
2.4
2.6
2.8
3.0
3.2
3.4
3.6
3.8
LOG DISTANCE

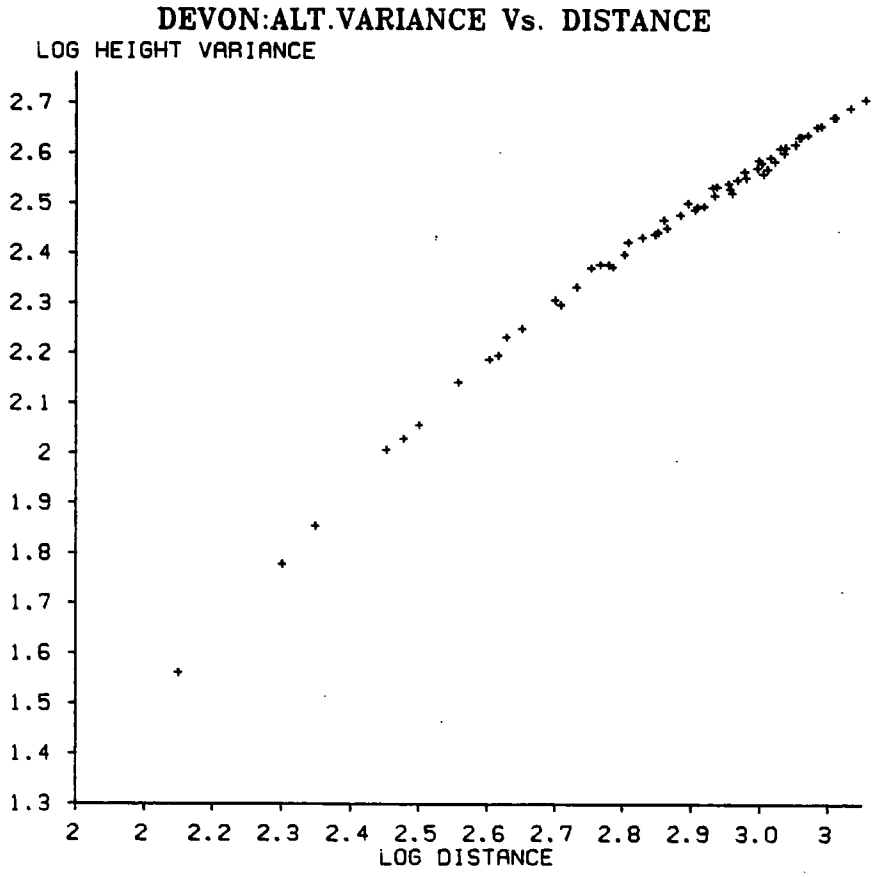
DEVON:ALT.VARIANCE Vs. DISTANCE
LOG HEIGHT VARIANCE
2.7
2.6
2.5
2.4
2.3
2.2
2.1
2
1.9
1.8
1.7
1.6
1.5
1.4
1.3
2
2
2.2
2.3
2.4
2.5
2.6
2.7
2.8
2.9
3.0
3
LOG DISTANCE

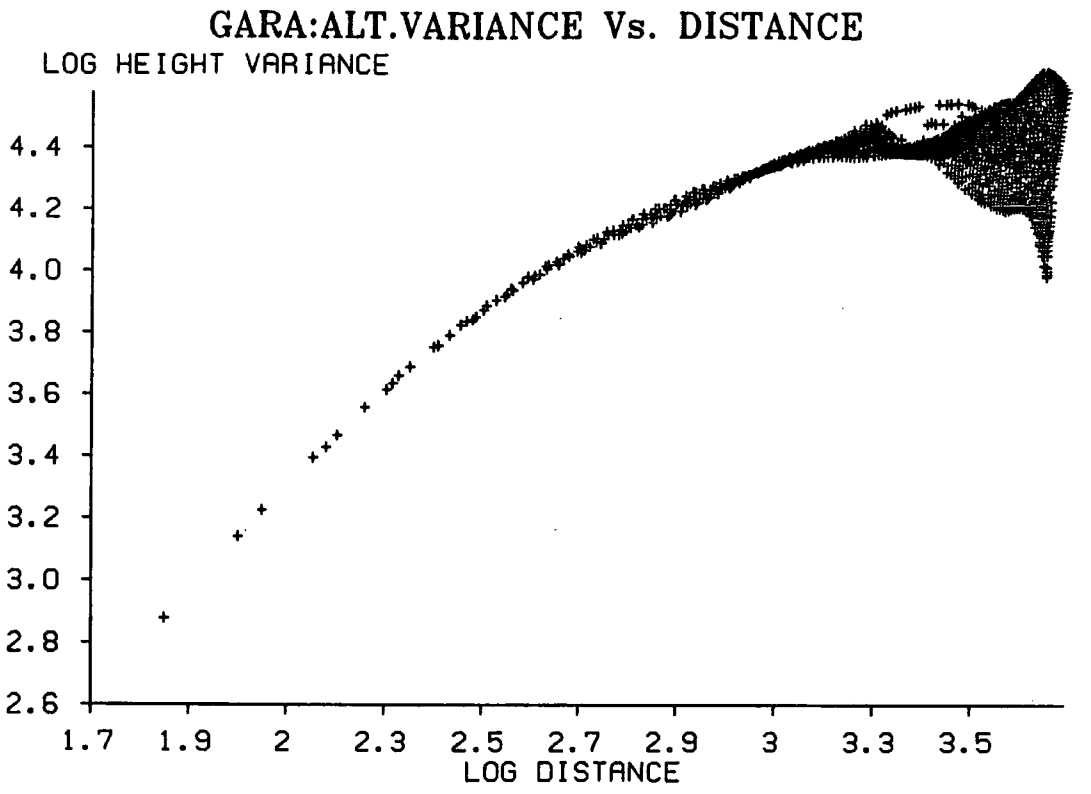
GARA:ALT.VARIANCE Vs. DISTANCE
LOG HEIGHT VARIANCE
4.4
4.2
4.0
3.8
3.6
3.4
3.2
3.0
2.8
2.6
1.7
1.9
2
2.3
2.5
2.7
2.9
3
3.3
3.5
LOG DISTANCE

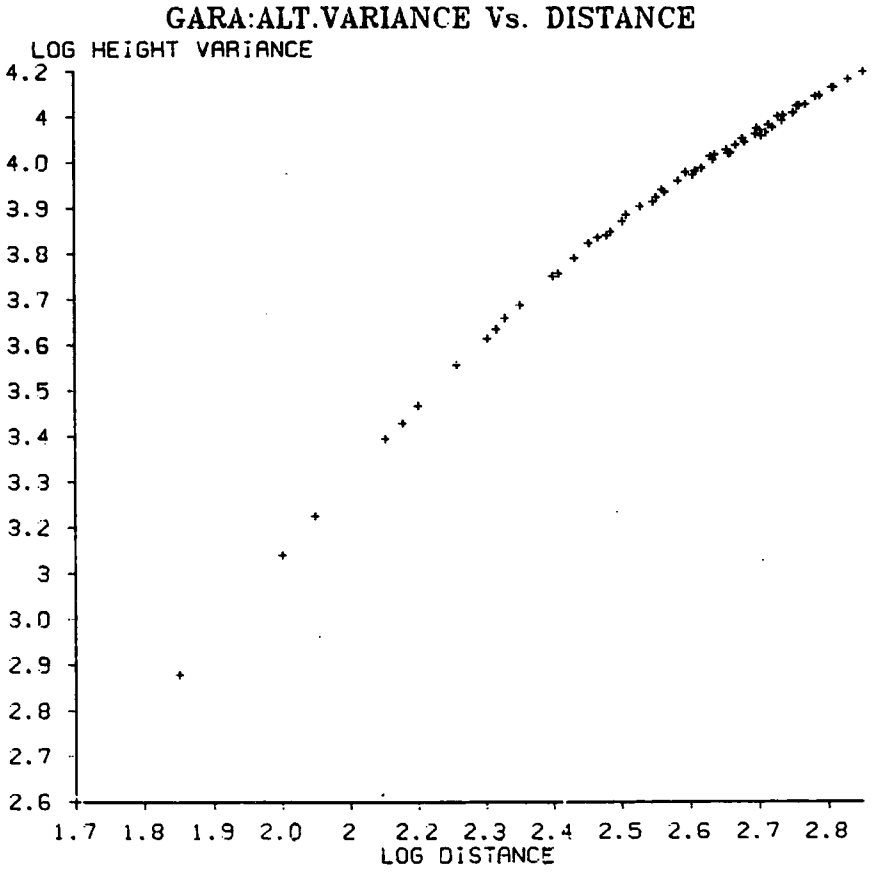
GARA:ALT.VARIANCE Vs. DISTANCE
LOG HEIGHT VARIANCE
4.2
4
4.0
3.9
3.8
3.7
3.6
3.5
3.4
3.3
3.2
3
3.0
2.9
2.8
2.7
2.6
1.7
1.8
1.9
2.0
2
2.2
2.3
2.4
2.5
2.6
2.7
2.8
LOG DISTANCE

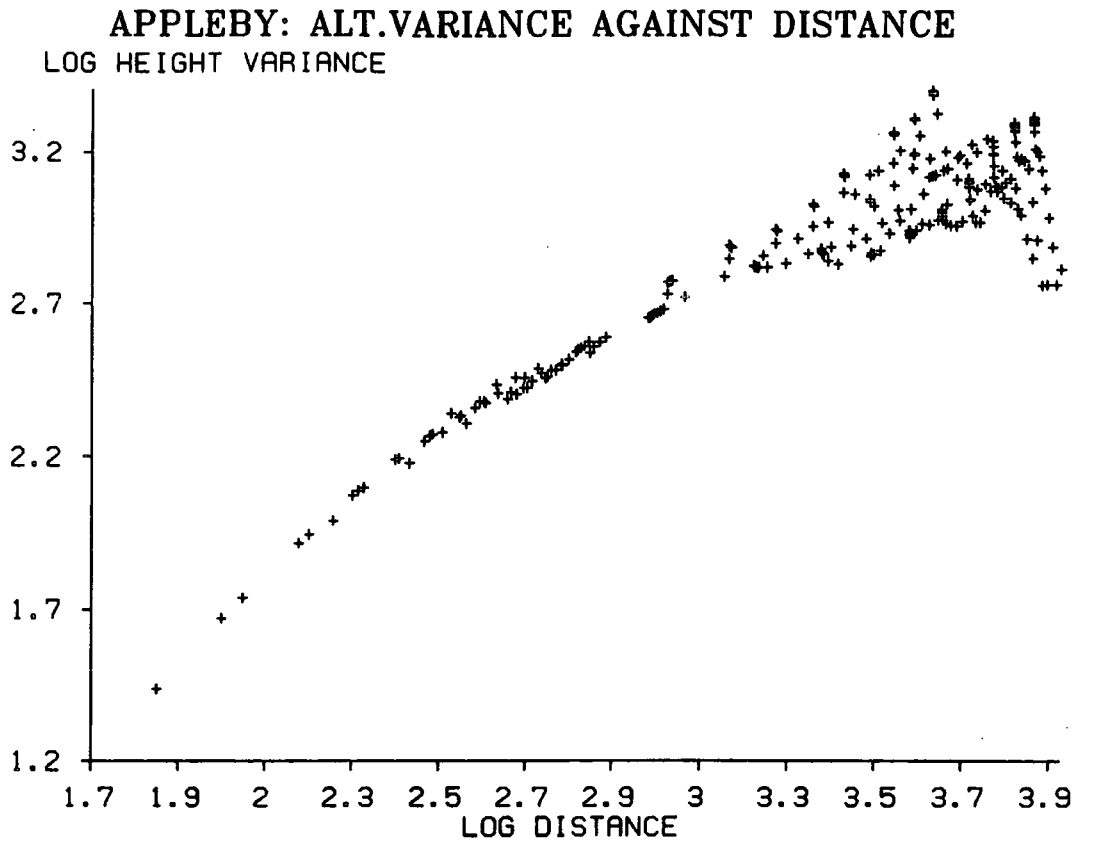
APPLEBY: ALT.VARIANCE AGAINST DISTANCE
LOG HEIGHT VARIANCE
3.2
2.7
2.2
1.7
1.2
1.7 1.9 2 2.3 2.5 2.7 2.9 3 3.3 3.5 3.7 3.9
LOG DISTANCE

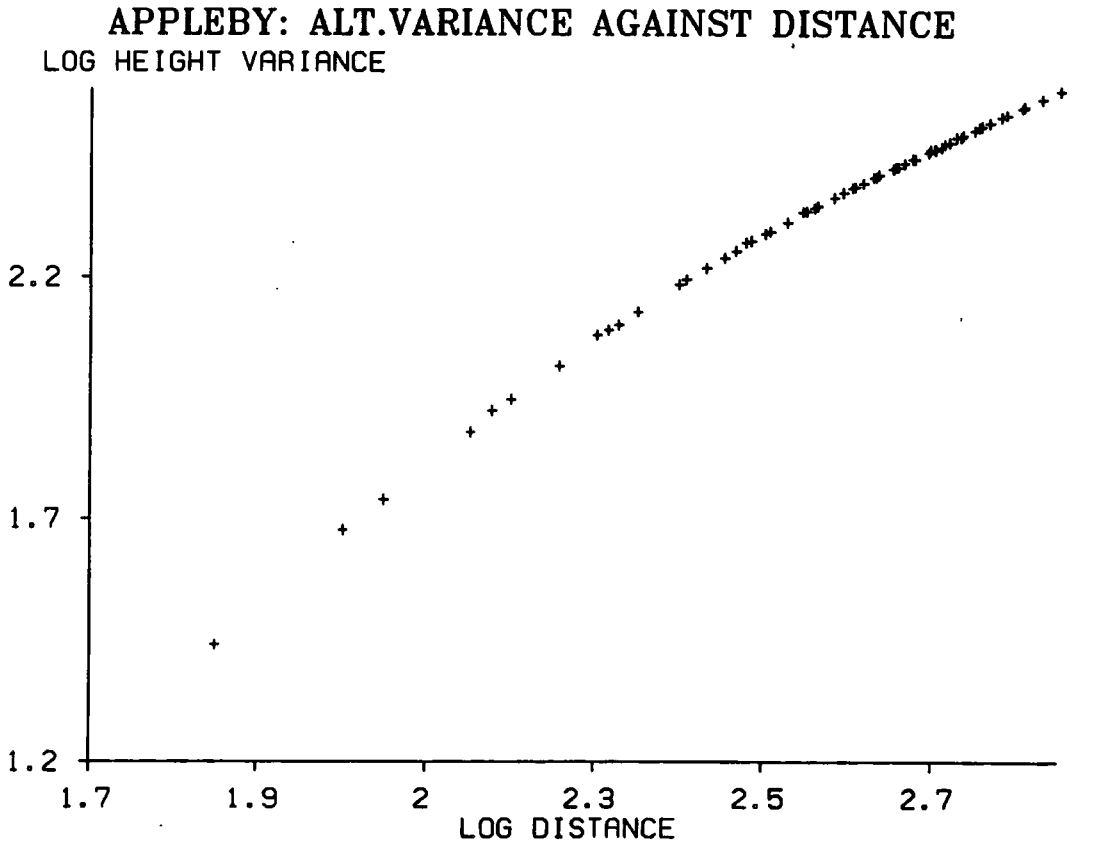
APPLEBY: ALT.VARIANCE AGAINST DISTANCE
LOG HEIGHT VARIANCE
2.2
1.7
1.2
1.7 1.9 2 2.3 2.5 2.7
LOG DISTANCE

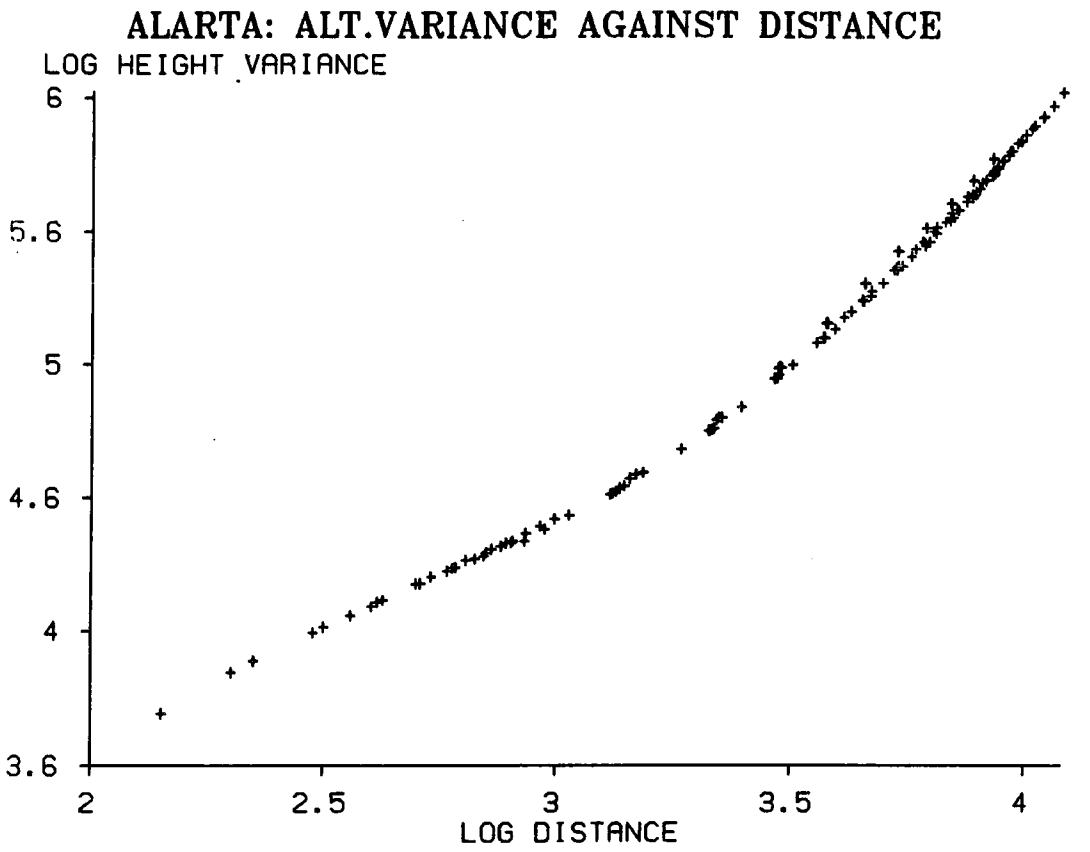
ALARTA: ALT.VARIANCE AGAINST DISTANCE
LOG HEIGHT VARIANCE
6
5.6
5
4.6
4
3.6
2
2.5
3
3.5
4
LOG DISTANCE

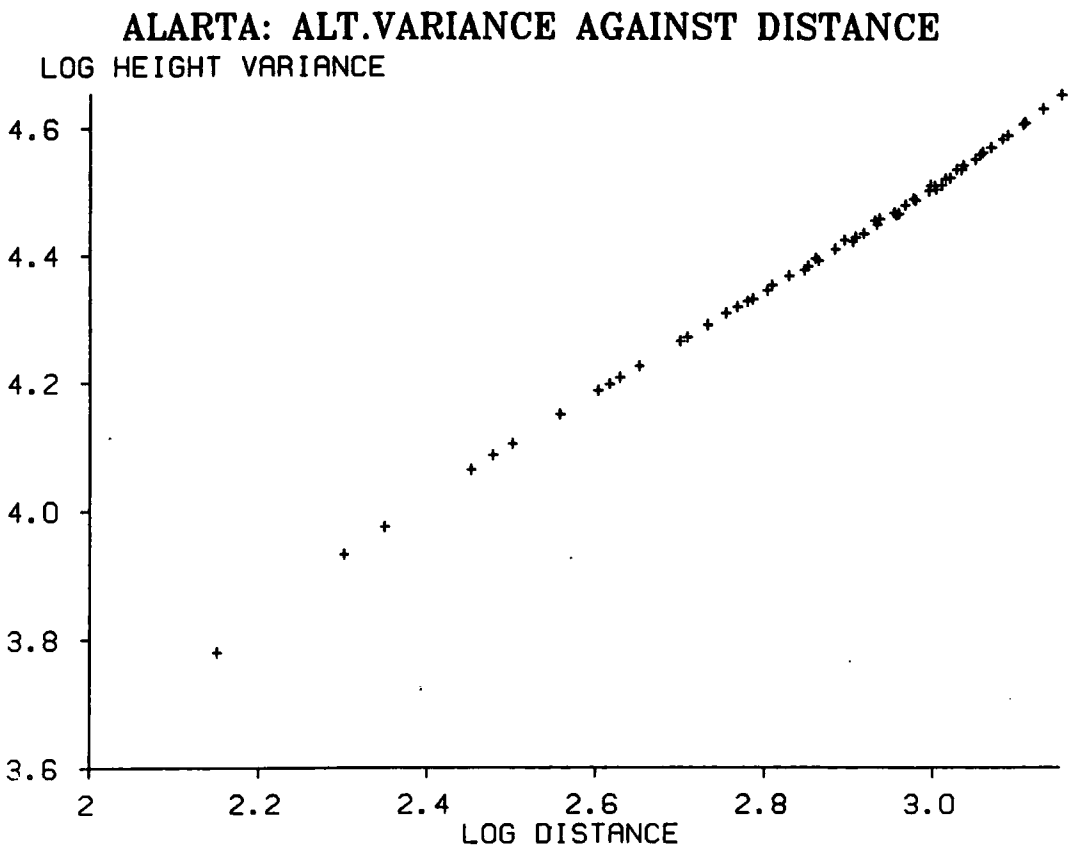
ALARTA: ALT.VARIANCE AGAINST DISTANCE
LOG HEIGHT VARIANCE
4.6
4.4
4.2
4.0
3.8
3.6
2
2.2
2.4
2.6
2.8
3.0
LOG DISTANCE

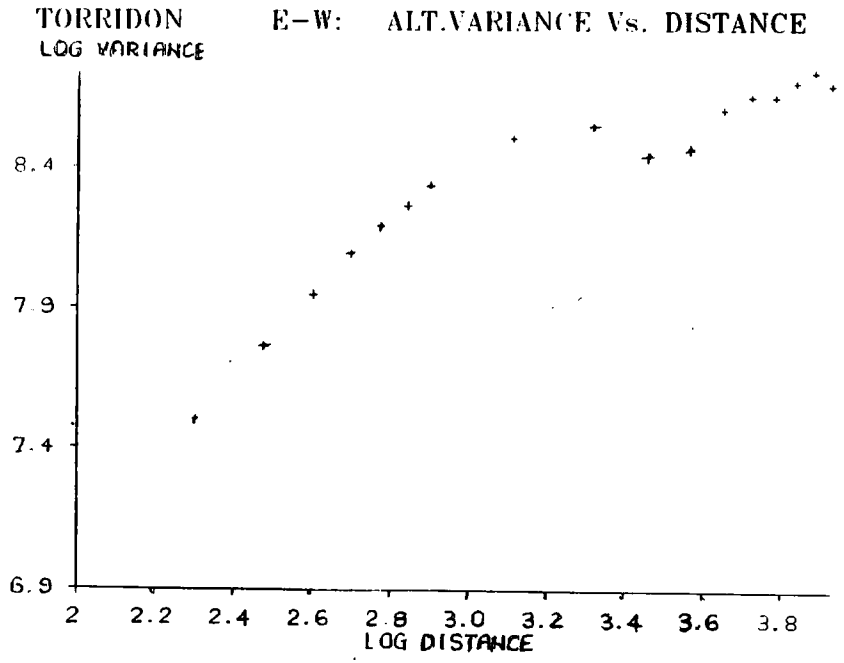
TORRIDON E–W: ALT.VARIANCE Vs. DISTANCE
LOG VARIANCE
8.4
7.9
7.4
6.9
2
2.2
2.4
2.6
2.8
3.0
3.2
3.4
3.6
3.8
LOG DISTANCE

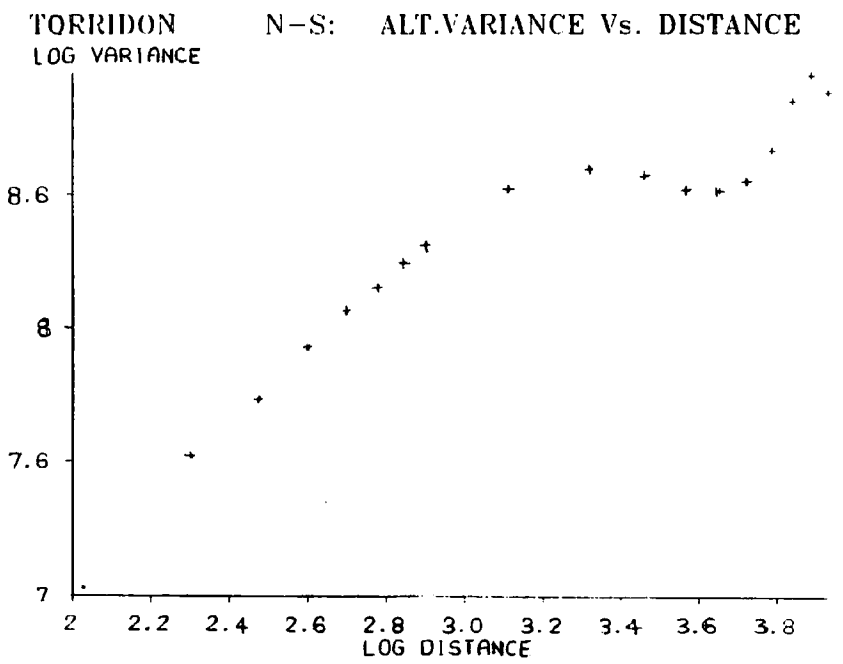
TORRIDON N–S: ALT.VARIANCE Vs. DISTANCE
LOG VARIANCE
8.6
8
7.6
7
2
2.2
2.4
2.6
2.8
3.0
3.2
3.4
3.6
3.8
LOG DISTANCE

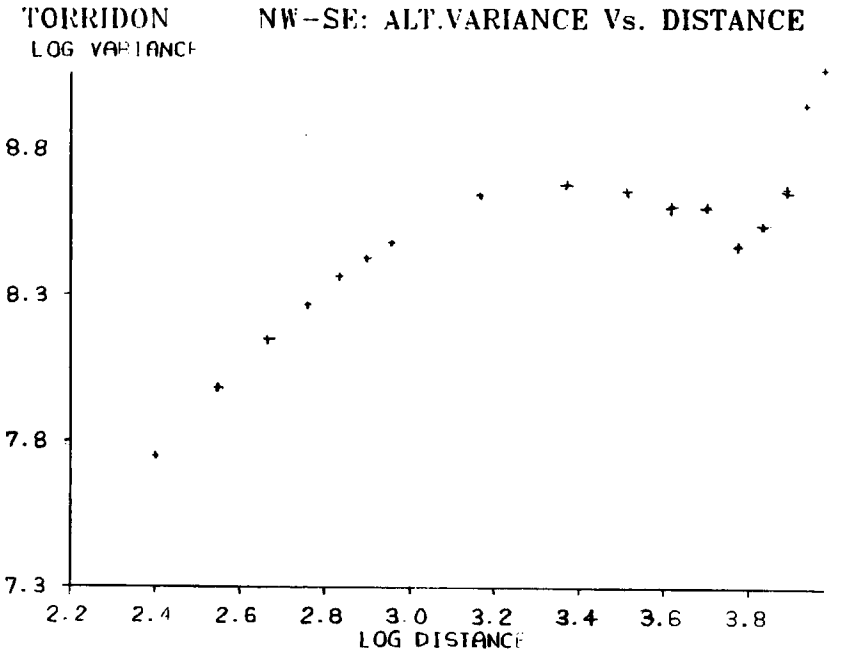
TORRIDON NW–SE: ALT.VARIANCE Vs. DISTANCE
LOG VARIANCE
8.8
8.3
7.8
7.3
2.2
2.4
2.6
2.8
3.0
3.2
3.4
3.6
3.8
LOG DISTANCE

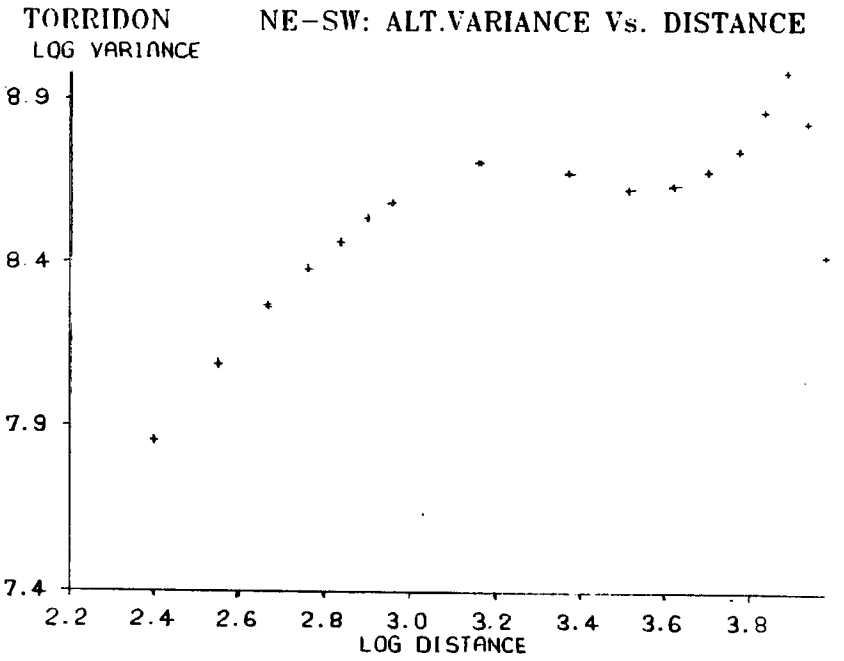
TORRIDON NE–SW: ALT.VARIANCE Vs. DISTANCE
LOG VARIANCE
8.9
8.4
7.9
7.4
2.2
2.4
2.6
2.8
3.0
3.2
3.4
3.6
3.8
LOG DISTANCE

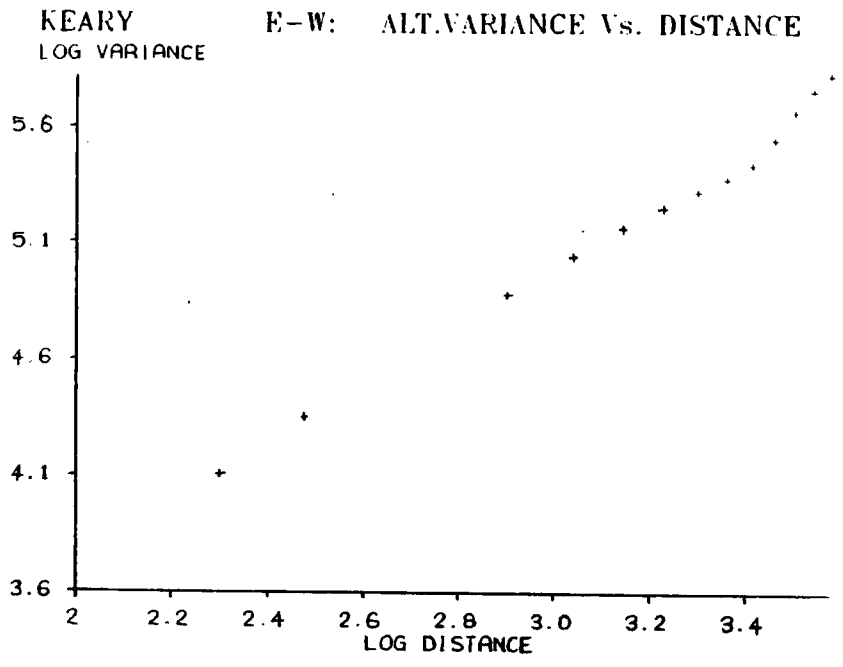
KEARY E-W: ALT.VARIANCE Vs. DISTANCE
LOG VARIANCE
5.6
5.1
4.6
4.1
3.6
2
2.2
2.4
2.6
2.8
3.0
3.2
3.4
LOG DISTANCE

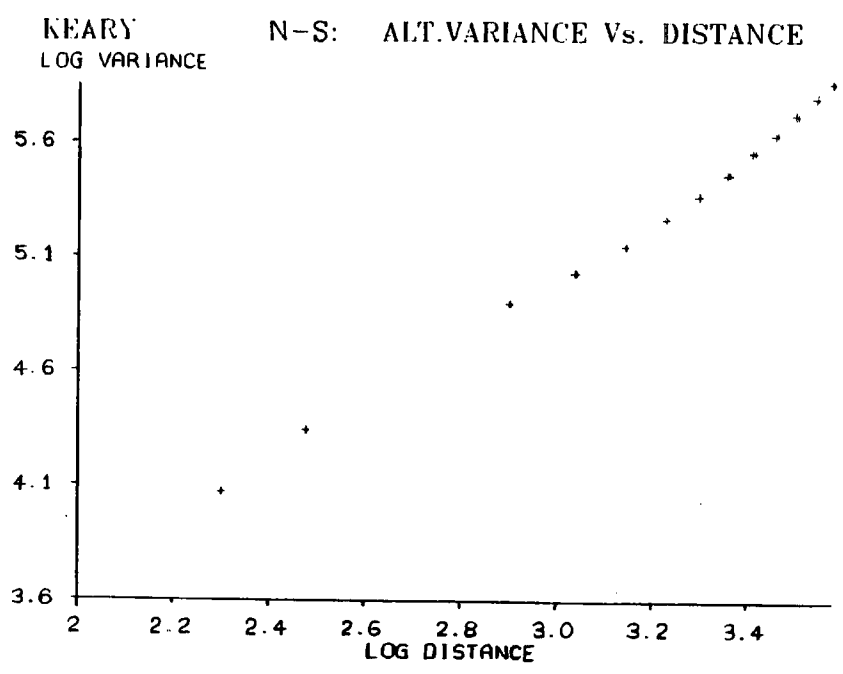
KEARY N-S: ALT.VARIANCE Vs. DISTANCE
LOG VARIANCE
5.6
5.1
4.6
4.1
3.6
2
2.2
2.4
2.6
2.8
3.0
3.2
3.4
LOG DISTANCE

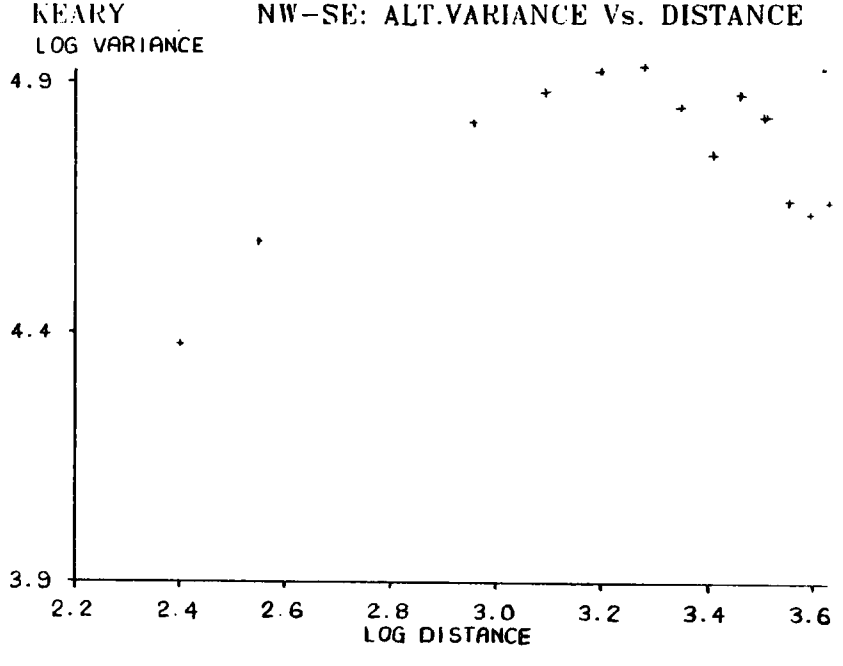
KEARY NW-SE: ALT.VARIANCE Vs. DISTANCE
LOG VARIANCE
4.9
4.4
3.9
2.2
2.4
2.6
2.8
3.0
3.2
3.4
3.6
LOG DISTANCE

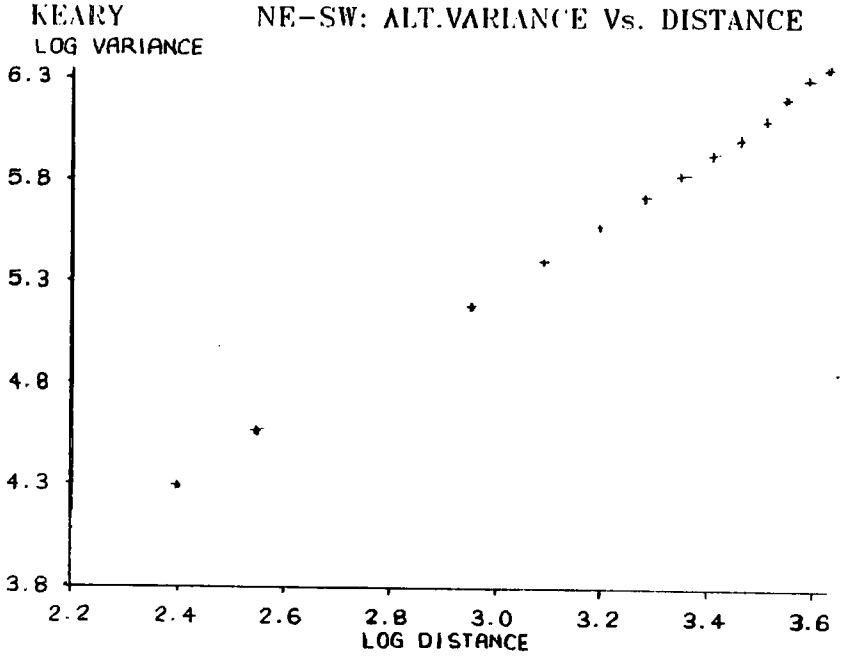
KEARY NE-SW: ALT.VARIANCE Vs. DISTANCE
LOG VARIANCE
6.3
5.8
5.3
4.8
4.3
3.8
2.2
2.4
2.6
2.8
3.0
3.2
3.4
3.6
LOG DISTANCE

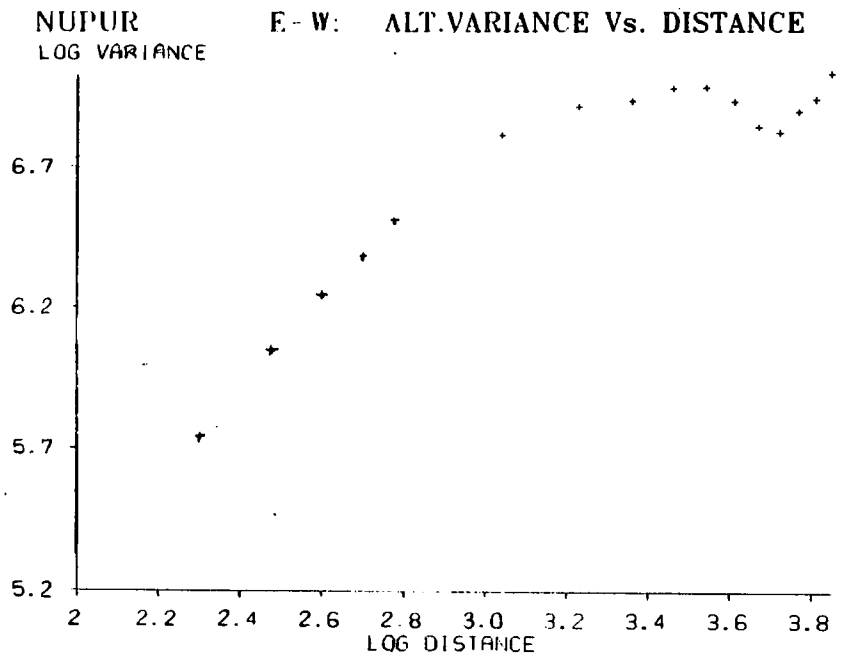
NUPUR E-W: ALT.VARIANCE Vs. DISTANCE
LOG VARIANCE
6.7
6.2
5.7
5.2
2
2.2
2.4
2.6
2.8
3.0
3.2
3.4
3.6
3.8
LOG DISTANCE

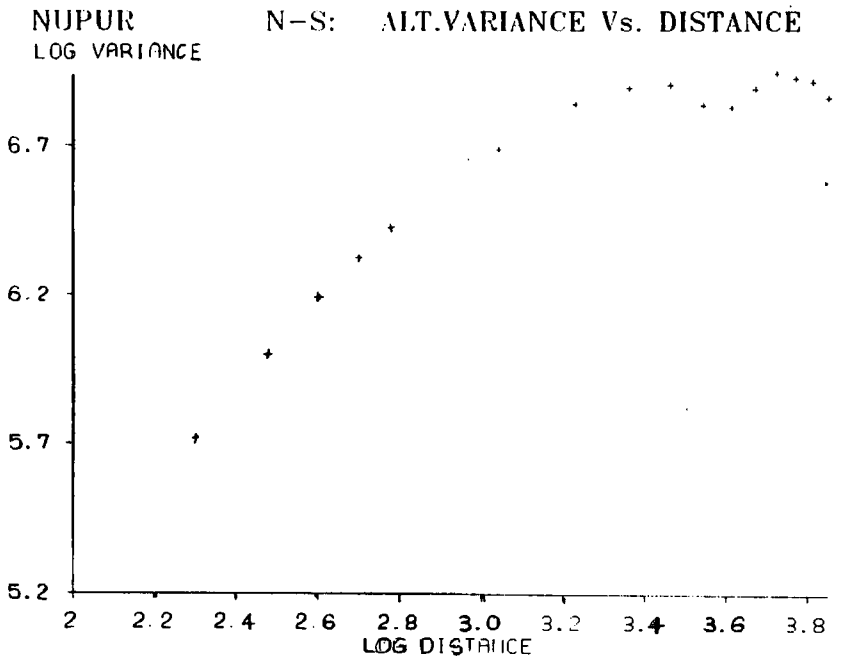
NUPUR N-S: ALT.VARIANCE Vs. DISTANCE
LOG VARIANCE
6.7
6.2
5.7
5.2
2
2.2
2.4
2.6
2.8
3.0
3.2
3.4
3.6
3.8
LOG DISTANCE

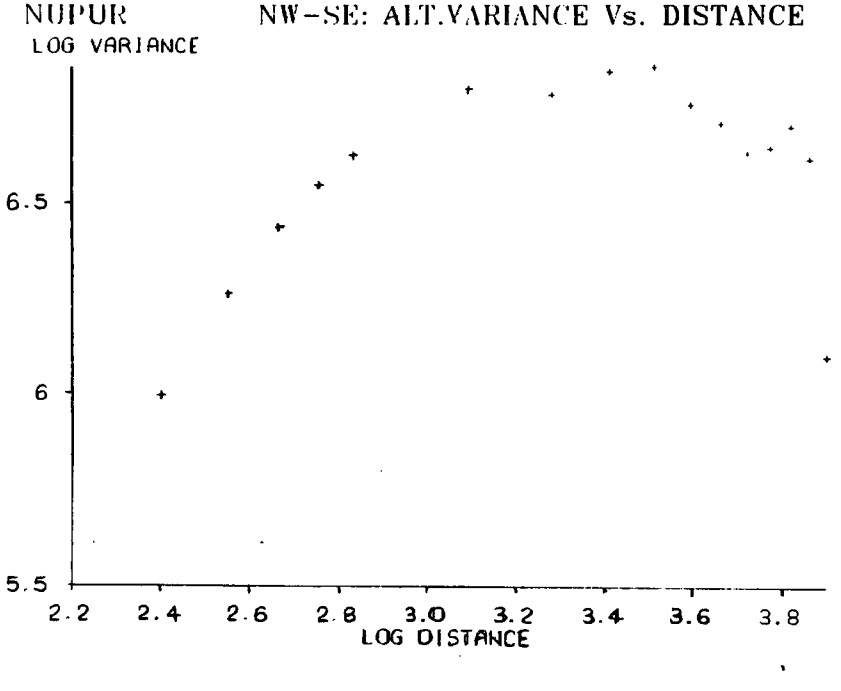
NUPUR NW-SE: ALT.VARIANCE Vs. DISTANCE
LOG VARIANCE
6.5
6
5.5
2.2
2.4
2.6
2.8
3.0
3.2
3.4
3.6
3.8
LOG DISTANCE

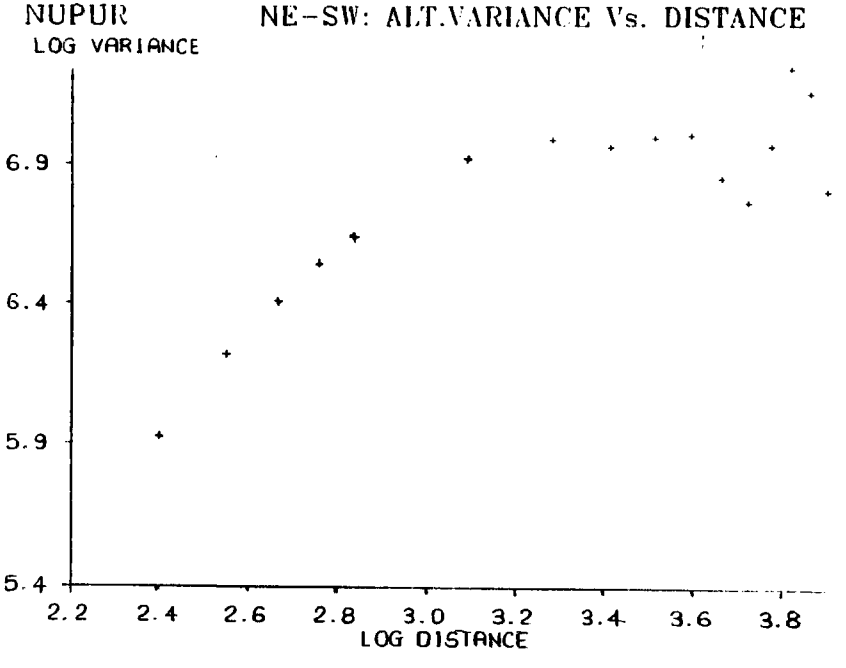
NUPUR NE-SW: ALT.VARIANCE Vs. DISTANCE
LOG VARIANCE
6.9
6.4
5.9
5.4
2.2
2.4
2.6
2.8
3.0
3.2
3.4
3.6
3.8
LOG DISTANCE

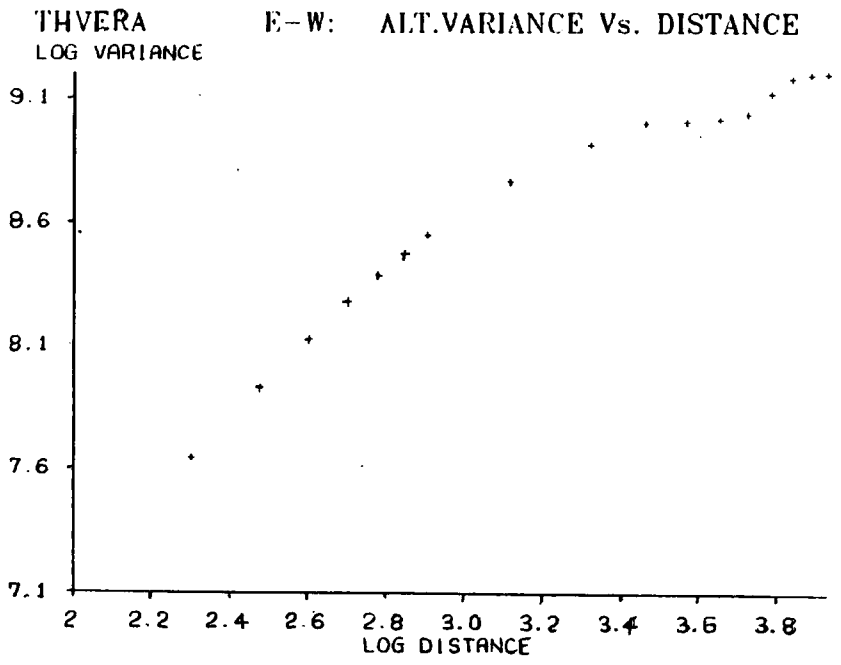
THVERA E-W: ALT.VARIANCE Vs. DISTANCE
LOG VARIANCE
9.1
8.6
8.1
7.6
7.1
2 2.2 2.4 2.6 2.8 3.0 3.2 3.4 3.6 3.8
LOG DISTANCE

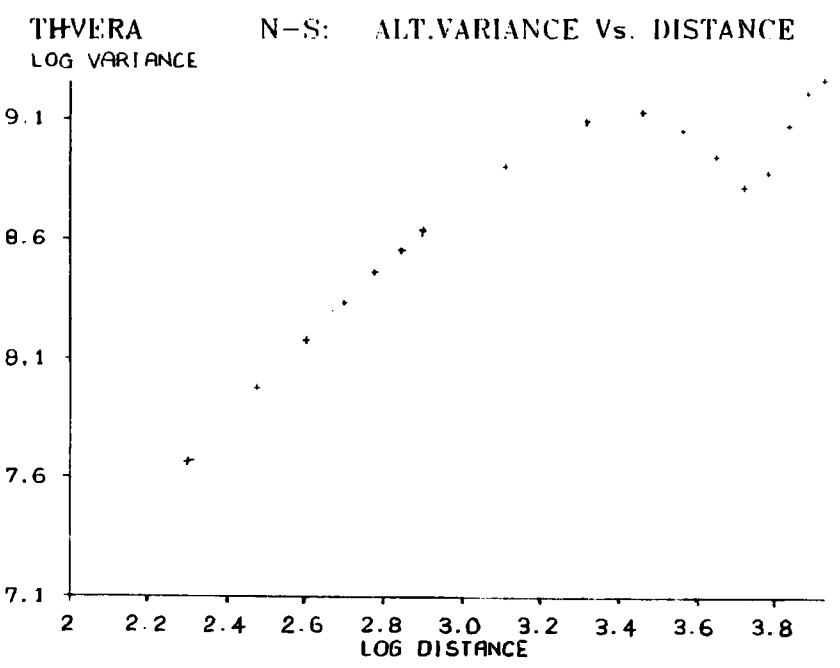
THVERA N-S: ALT.VARIANCE Vs. DISTANCE
LOG VARIANCE
9.1
8.6
8.1
7.6
7.1
2 2.2 2.4 2.6 2.8 3.0 3.2 3.4 3.6 3.8
LOG DISTANCE

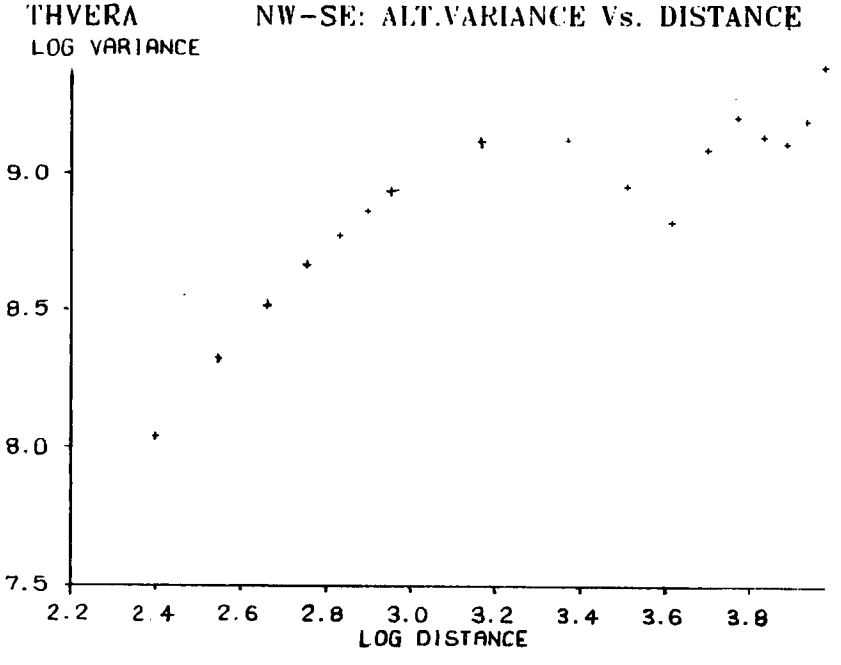
THVERA NW-SE: ALT.VARIANCE Vs. DISTANCE
LOG VARIANCE
9.0
8.5
8.0
7.5
2.2 2.4 2.6 2.8 3.0 3.2 3.4 3.6 3.8
LOG DISTANCE

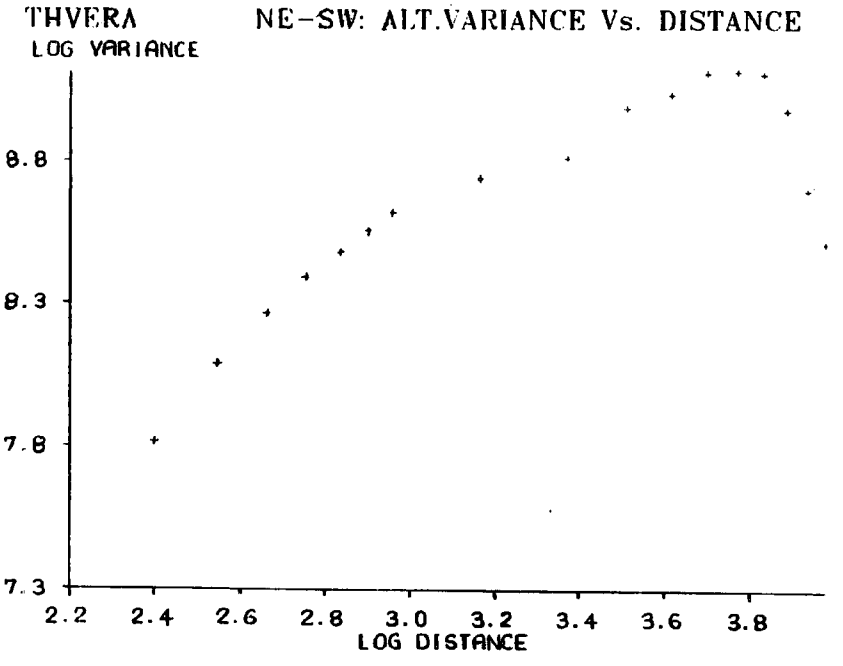
THVERA NE-SW: ALT.VARIANCE Vs. DISTANCE
LOG VARIANCE
8.8
8.3
7.8
7.3
2.2 2.4 2.6 2.8 3.0 3.2 3.4 3.6 3.8
LOG DISTANCE

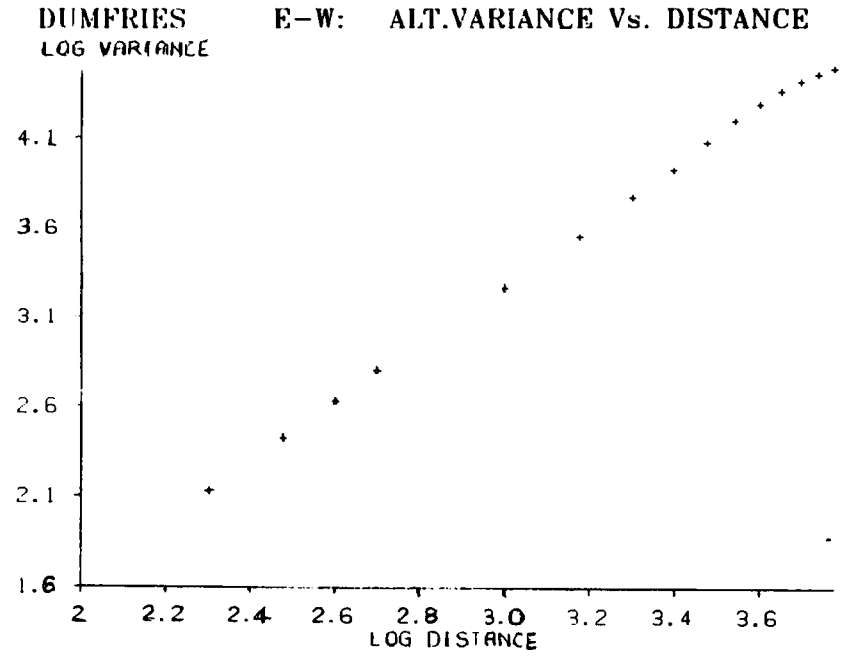
DUMFRIES E-W: ALT.VARIANCE Vs. DISTANCE
LOG VARIANCE
4.1
3.6
3.1
2.6
2.1
1.6
2 2.2 2.4 2.6 2.8 3.0 3.2 3.4 3.6
LOG DISTANCE

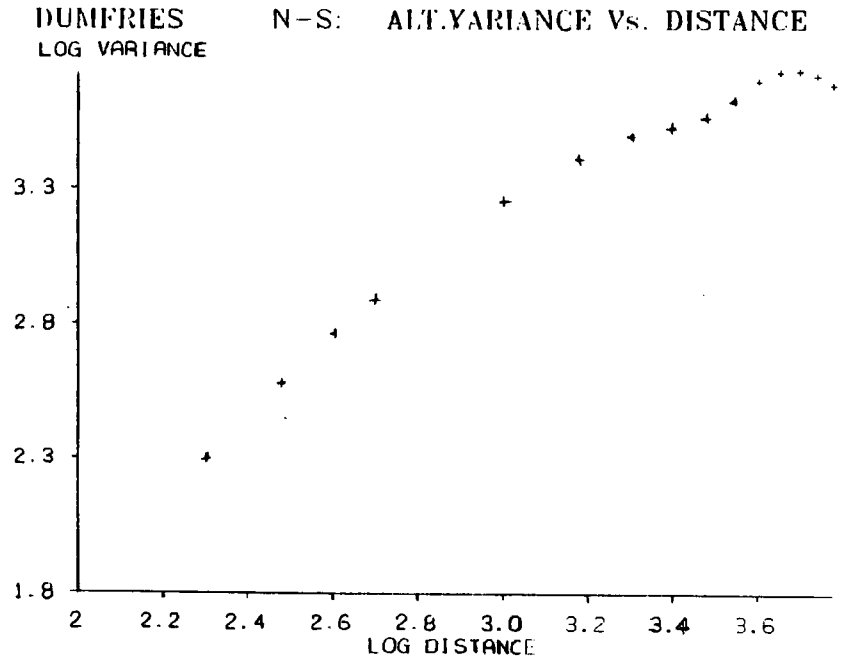
DUMFRIES N-S: ALT.VARIANCE Vs. DISTANCE
LOG VARIANCE
3.3
2.8
2.3
1.8
2 2.2 2.4 2.6 2.8 3.0 3.2 3.4 3.6
LOG DISTANCE

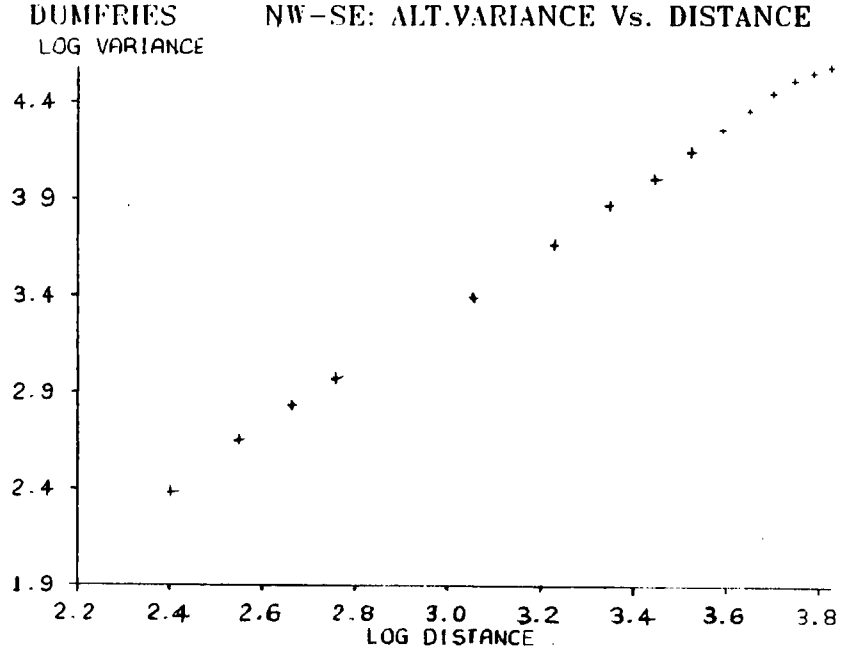
DUMFRIES NW-SE: ALT.VARIANCE Vs. DISTANCE
LOG VARIANCE
4.4
3.9
3.4
2.9
2.4
1.9
2.2 2.4 2.6 2.8 3.0 3.2 3.4 3.6 3.8
LOG DISTANCE

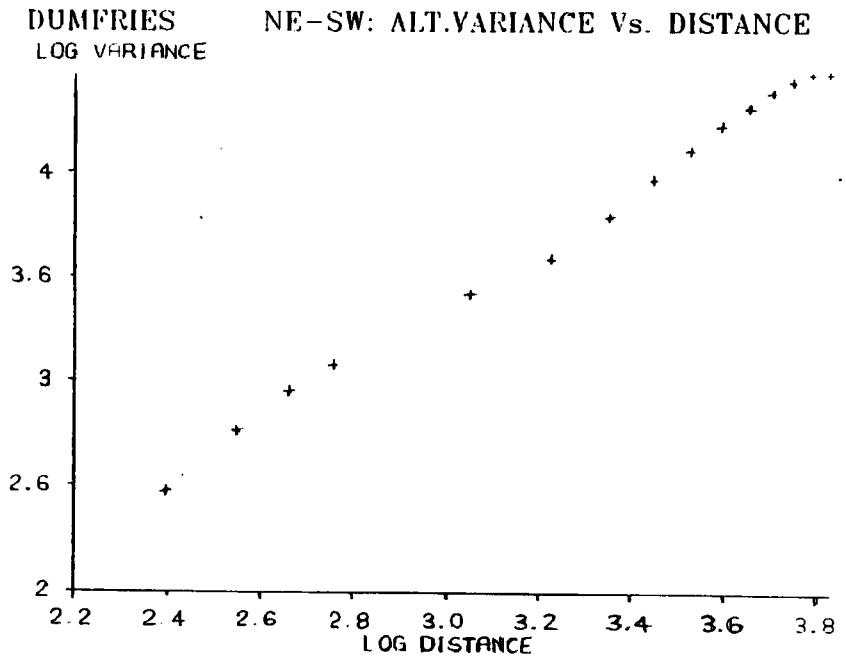
DUMFRIES NE-SW: ALT.VARIANCE Vs. DISTANCE
LOG VARIANCE
4
3.6
3
2.6
2
2.2 2.4 2.6 2.8 3.0 3.2 3.4 3.6 3.8
LOG DISTANCE

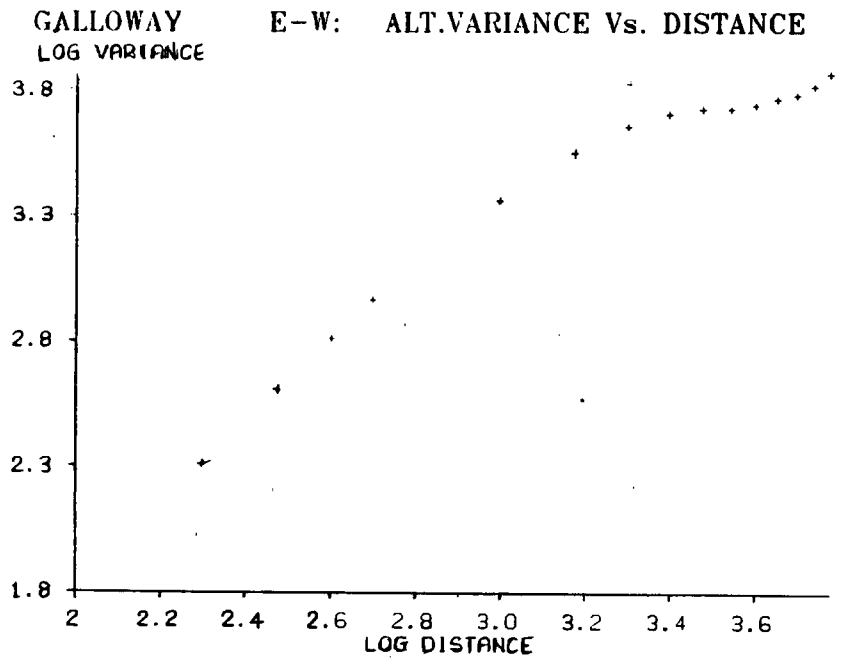
GALLOWAY E-W: ALT.VARIANCE Vs. DISTANCE
LOG VARIANCE
3.8
3.3
2.8
2.3
1.8
2
2.2
2.4
2.6
2.8
3.0
3.2
3.4
3.6
LOG DISTANCE

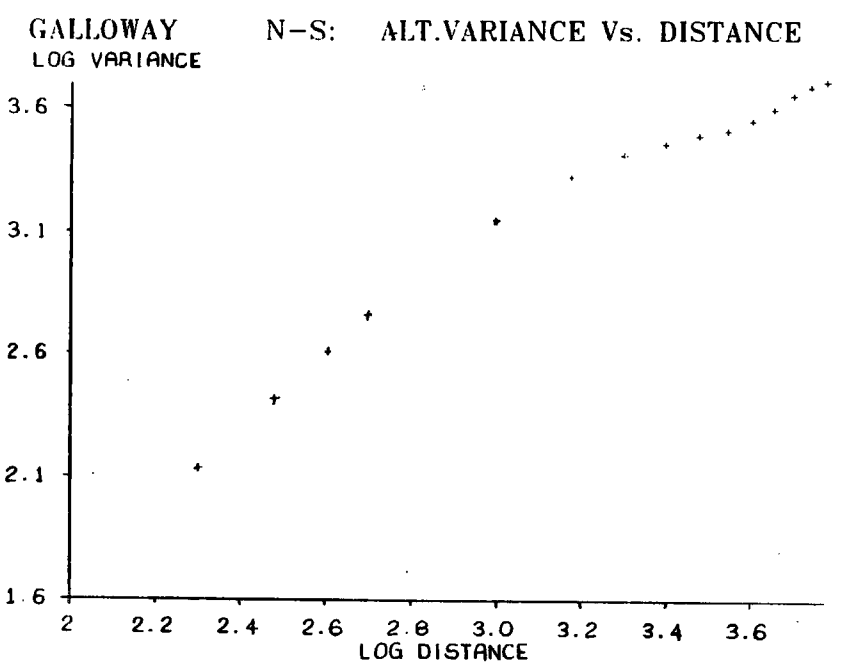
GALLOWAY N-S: ALT.VARIANCE Vs. DISTANCE
LOG VARIANCE
3.6
3.1
2.6
2.1
1.6
2
2.2
2.4
2.6
2.8
3.0
3.2
3.4
3.6
LOG DISTANCE

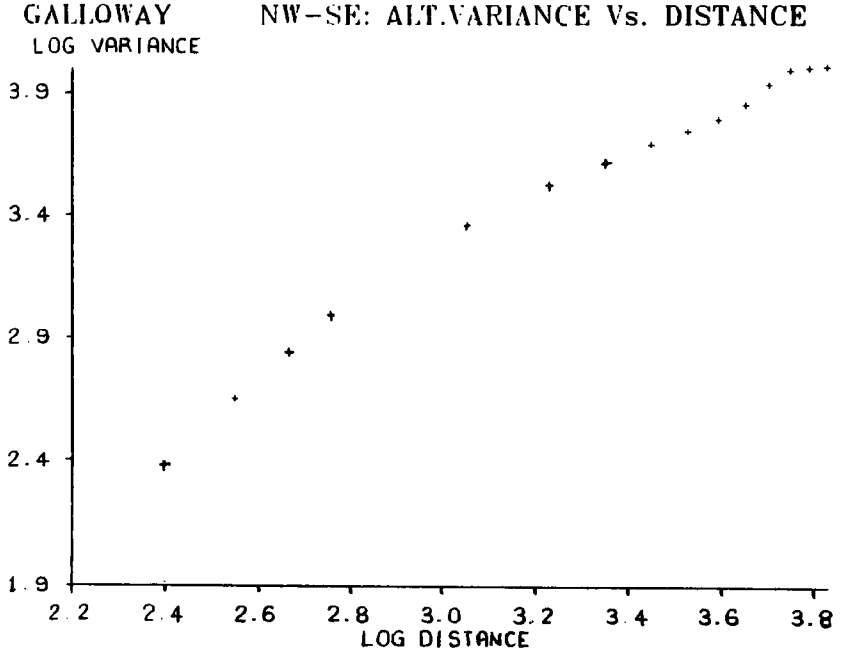
GALLOWAY NW-SE: ALT.VARIANCE Vs. DISTANCE
LOG VARIANCE
3.9
3.4
2.9
2.4
1.9
2.2
2.4
2.6
2.8
3.0
3.2
3.4
3.6
3.8
LOG DISTANCE

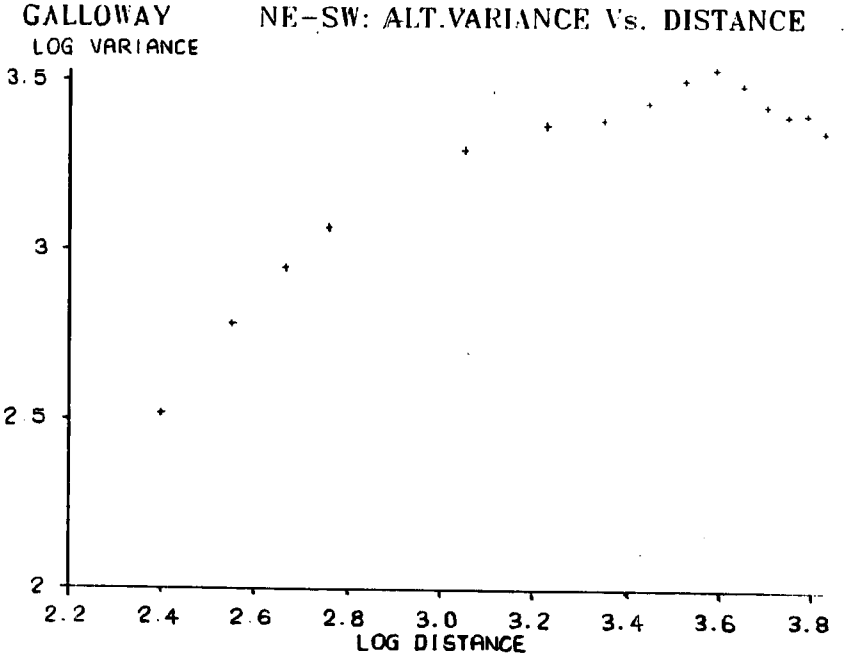
GALLOWAY NE-SW: ALT.VARIANCE Vs. DISTANCE
LOG VARIANCE
3.5
3
2.5
2
2.2
2.4
2.6
2.8
3.0
3.2
3.4
3.6
3.8
LOG DISTANCE

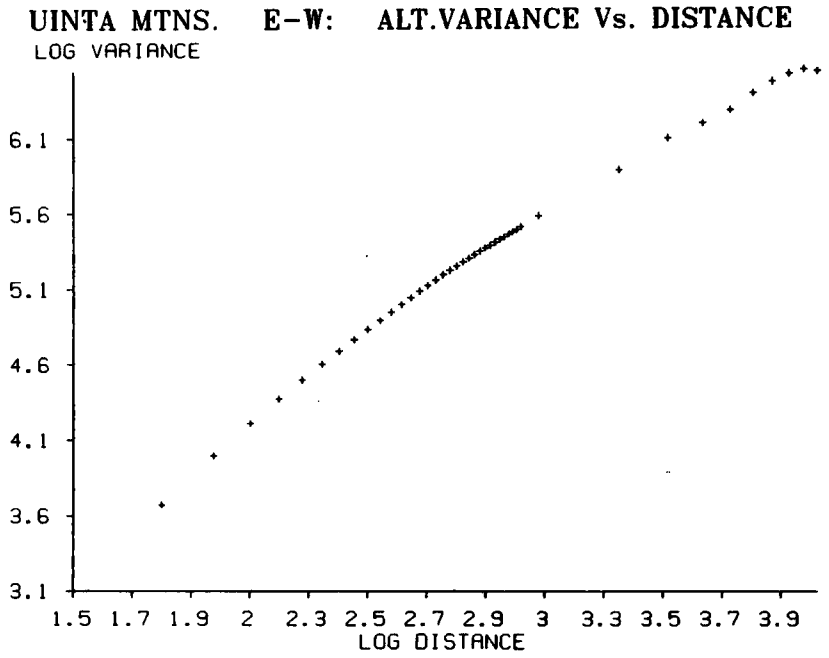
UINTA MTNS. E-W: ALT.VARIANCE Vs. DISTANCE
LOG VARIANCE
6.1
5.6
5.1
4.6
4.1
3.6
3.1
1.5 1.7 1.9 2 2.3 2.5 2.7 2.9 3 3.3 3.5 3.7 3.9
LOG DISTANCE

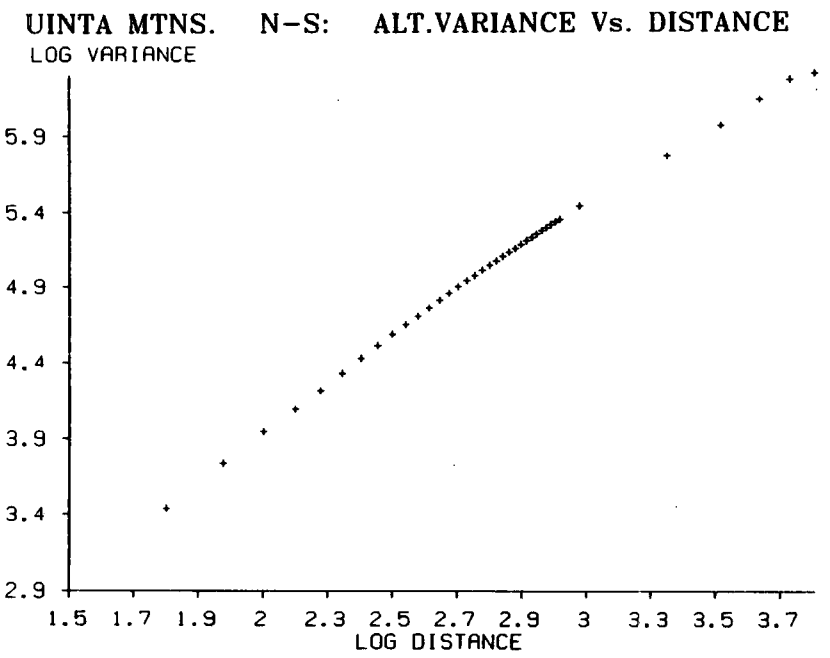
UINTA MTNS. N-S: ALT.VARIANCE Vs. DISTANCE
LOG VARIANCE
5.9
5.4
4.9
4.4
3.9
3.4
2.9
1.5 1.7 1.9 2 2.3 2.5 2.7 2.9 3 3.3 3.5 3.7
LOG DISTANCE

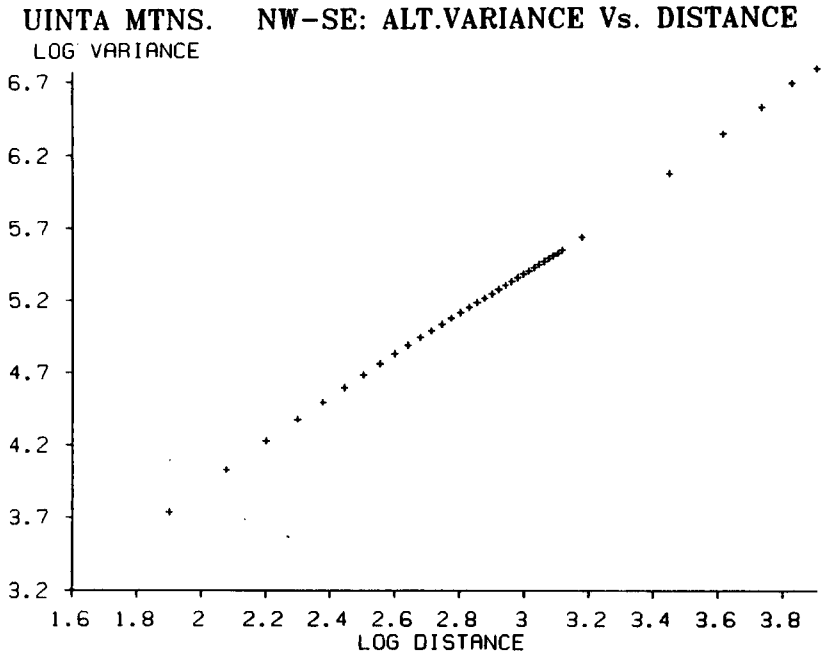
UINTA MTNS. NW-SE: ALT.VARIANCE Vs. DISTANCE
LOG VARIANCE
6.7
6.2
5.7
5.2
4.7
4.2
3.7
3.2
1.6 1.8 2 2.2 2.4 2.6 2.8 3 3.2 3.4 3.6 3.8
LOG DISTANCE

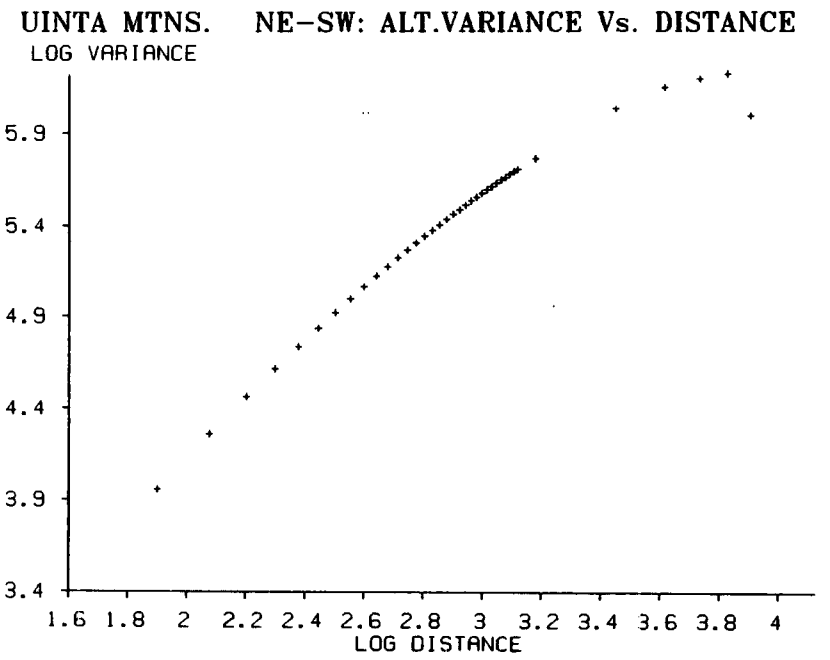
UINTA MTNS. NE-SW: ALT.VARIANCE Vs. DISTANCE
LOG VARIANCE
5.9
5.4
4.9
4.4
3.9
3.4
1.6 1.8 2 2.2 2.4 2.6 2.8 3 3.2 3.4 3.6 3.8 4
LOG DISTANCE

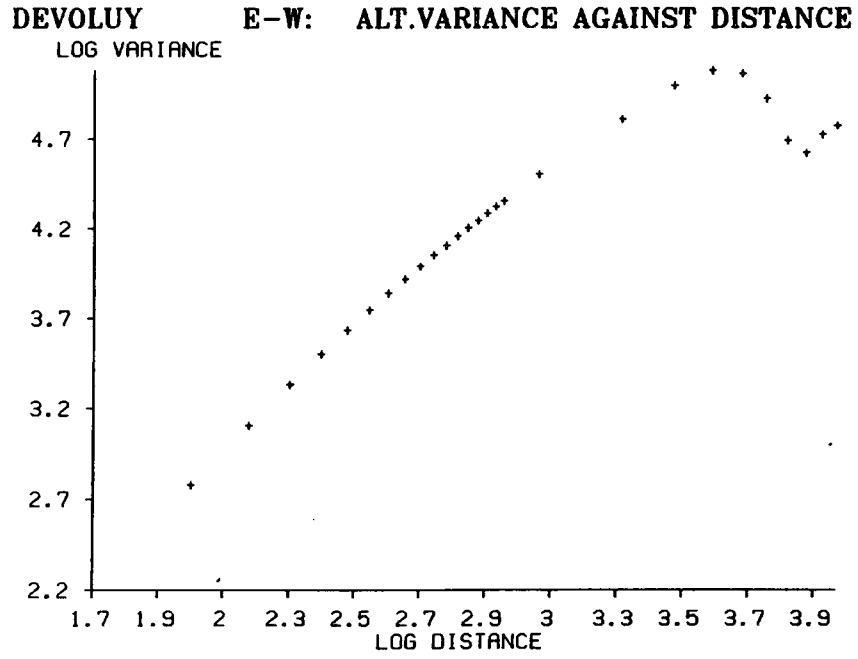
DEVOLUY E-W: ALT.VARIANCE AGAINST DISTANCE
LOG VARIANCE
4.7
4.2
3.7
3.2
2.7
2.2
1.7 1.9 2 2.3 2.5 2.7 2.9 3 3.3 3.5 3.7 3.9
LOG DISTANCE

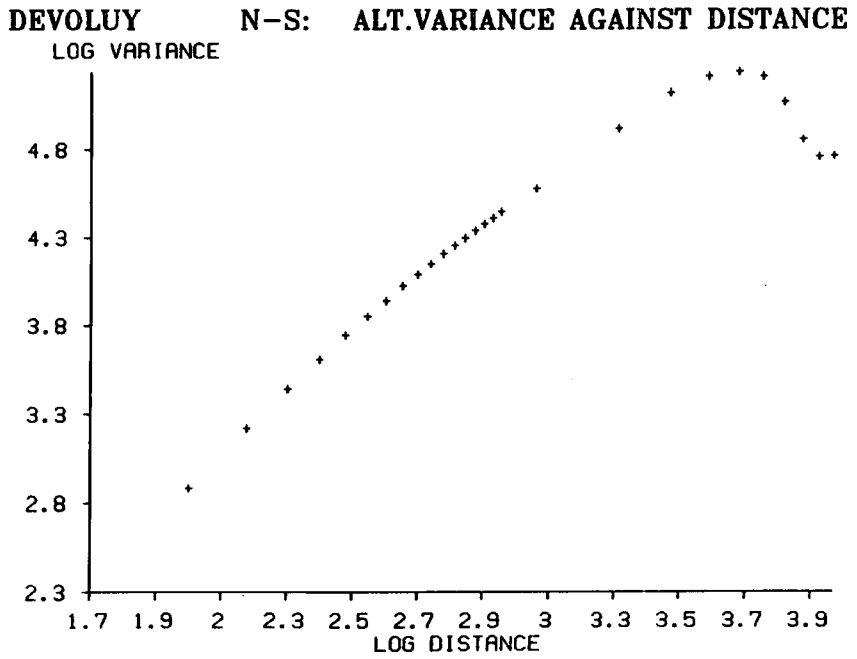
DEVOLUY N-S: ALT.VARIANCE AGAINST DISTANCE
LOG VARIANCE
4.8
4.3
3.8
3.3
2.8
2.3
1.7 1.9 2 2.3 2.5 2.7 2.9 3 3.3 3.5 3.7 3.9
LOG DISTANCE

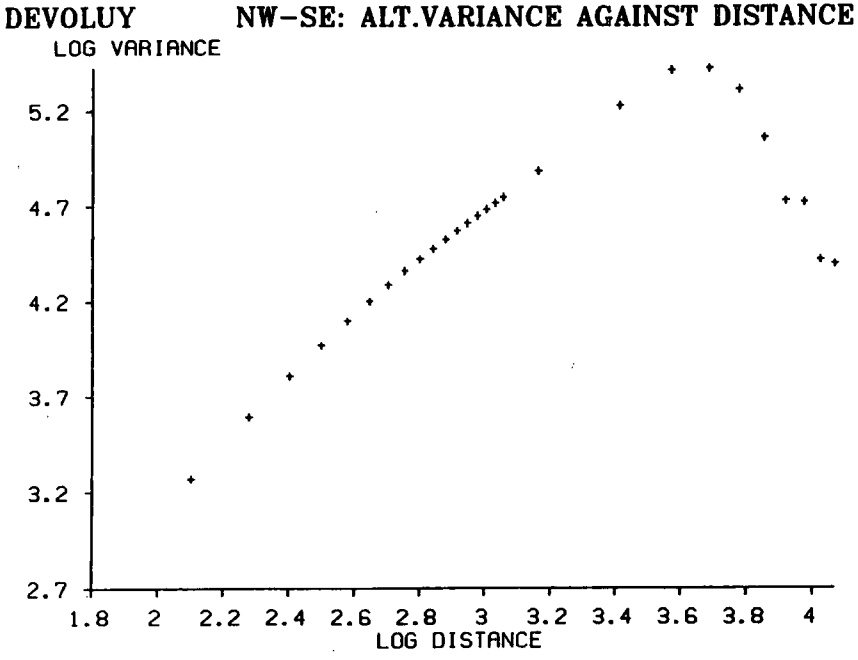
DEVOLUY NW-SE: ALT.VARIANCE AGAINST DISTANCE
LOG VARIANCE
5.2
4.7
4.2
3.7
3.2
2.7
1.8 2 2.2 2.4 2.6 2.8 3 3.2 3.4 3.6 3.8 4
LOG DISTANCE

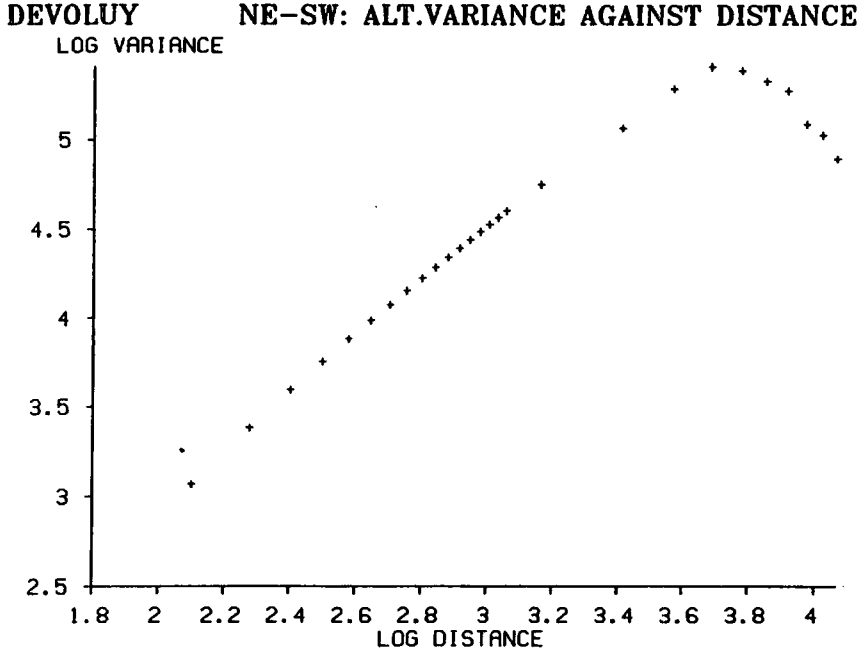
DEVOLUY NE-SW: ALT.VARIANCE AGAINST DISTANCE
LOG VARIANCE
5
4.5
4
3.5
3
2.5
1.8 2 2.2 2.4 2.6 2.8 3 3.2 3.4 3.6 3.8 4
LOG DISTANCE

CANIGOU E-W: ALT.VARIANCE AGAINST DISTANCE

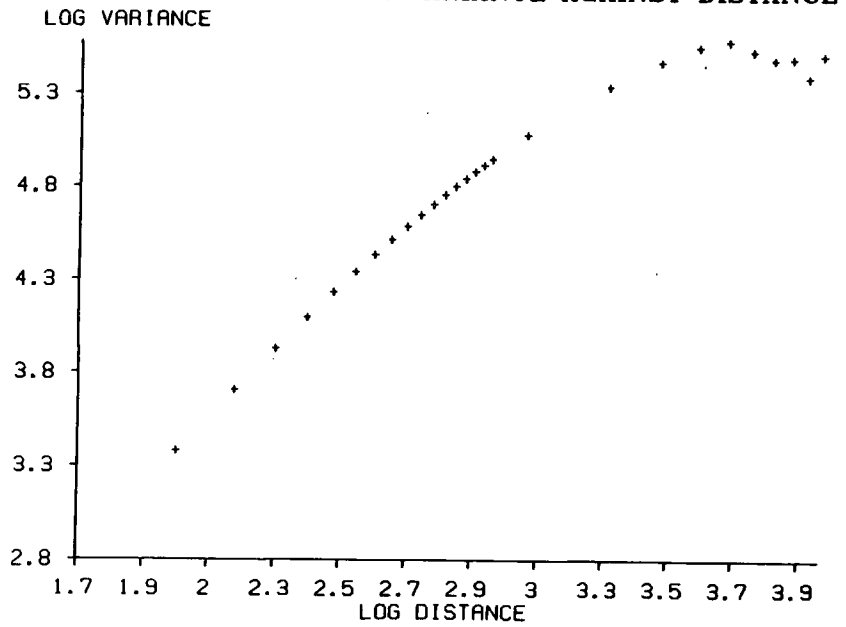

CANIGOU N-S: ALT.VARIANCE AGAINST DISTANCE

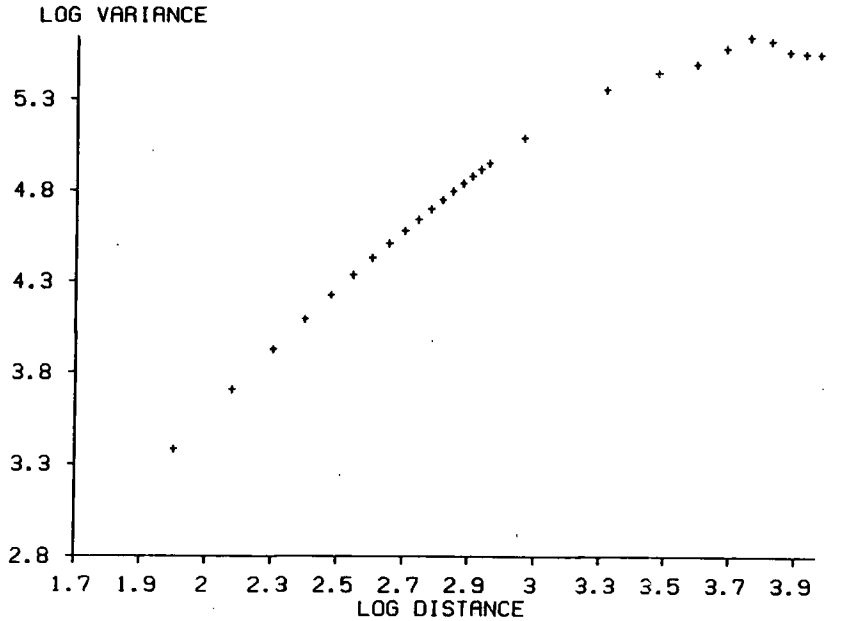

CANIGOU NW-SE: ALT.VARIANCE AGAINST DISTANCE

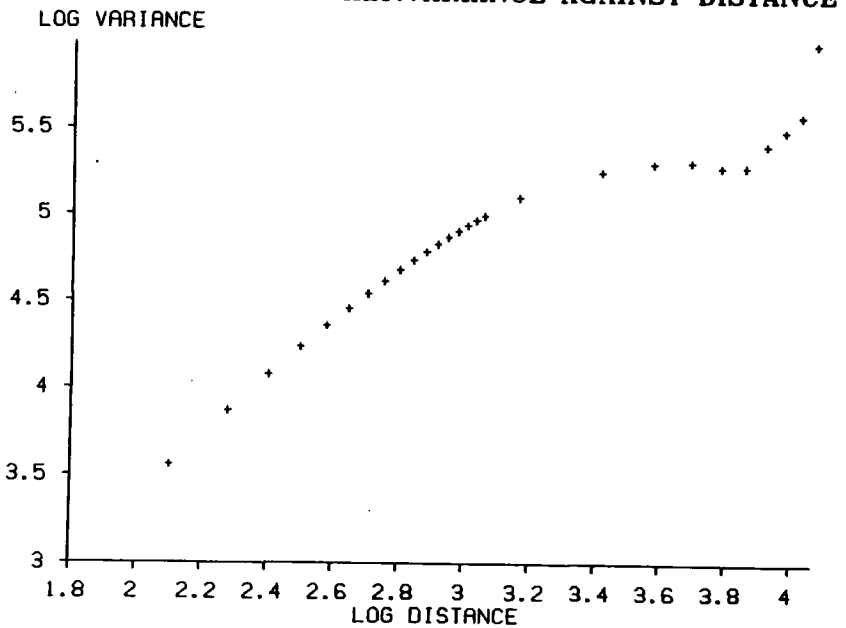

CANIGOU NE-SW: ALT.VARIANCE AGAINST DISTANCE

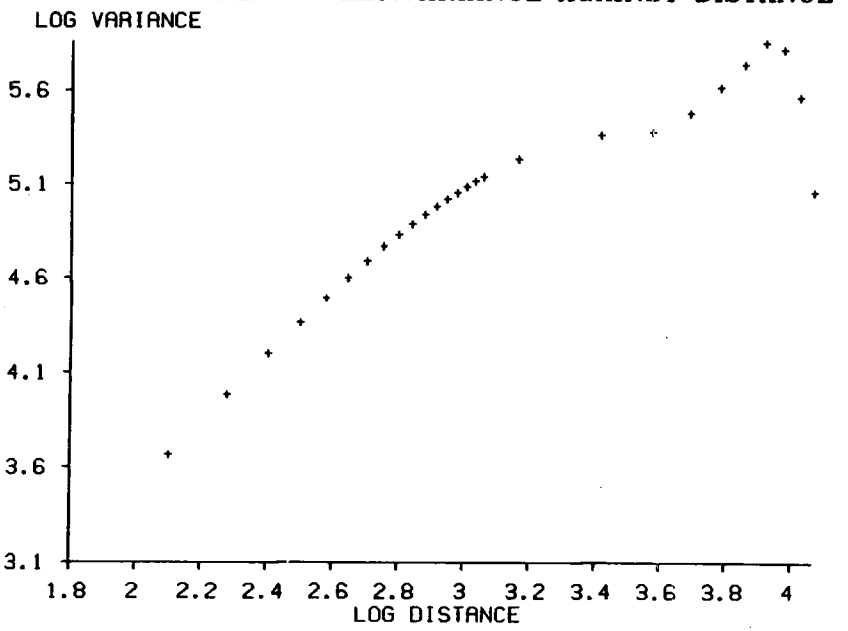

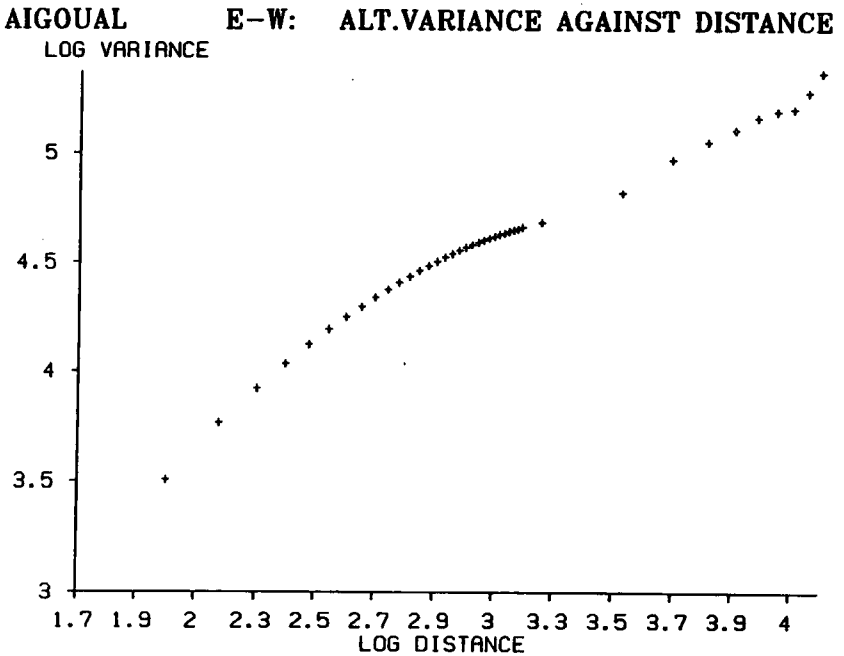
AIGOUAL E-W: ALT.VARIANCE AGAINST DISTANCE
LOG VARIANCE
5
4.5
4
3.5
3
1.7 1.9 2 2.3 2.5 2.7 2.9 3 3.3 3.5 3.7 3.9 4
LOG DISTANCE

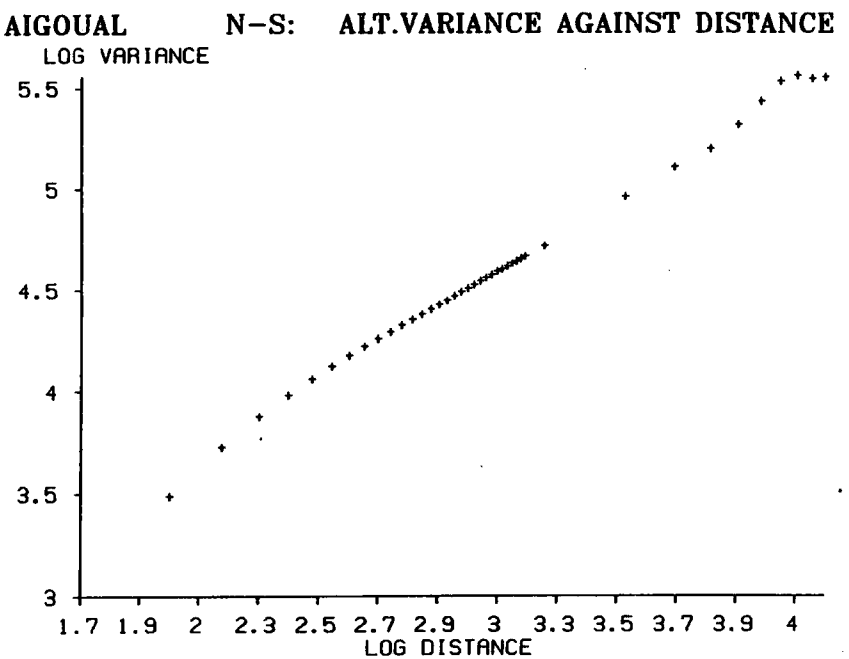
AIGOUAL N-S: ALT.VARIANCE AGAINST DISTANCE
LOG VARIANCE
5.5
5
4.5
4
3.5
3
1.7 1.9 2 2.3 2.5 2.7 2.9 3 3.3 3.5 3.7 3.9 4
LOG DISTANCE

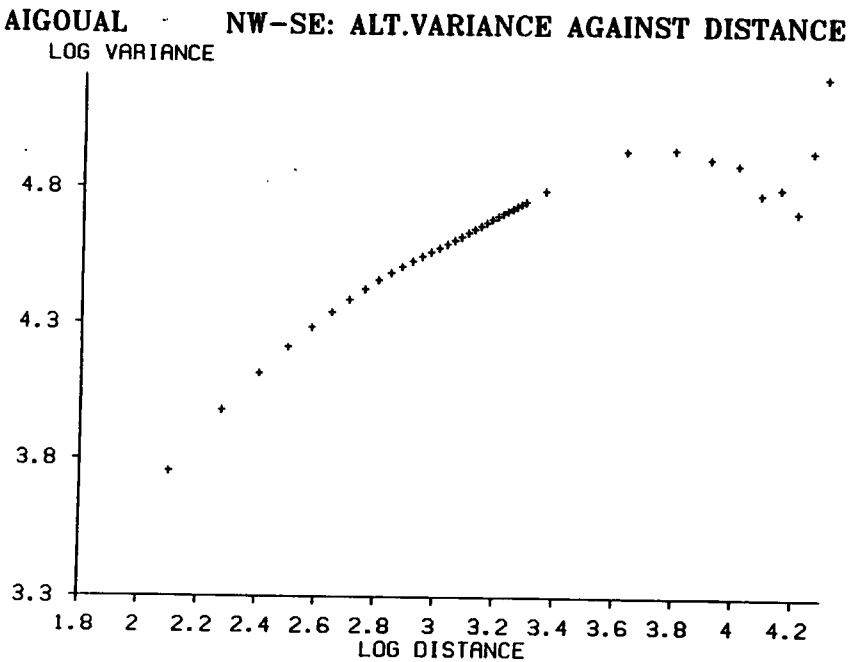
AIGOUAL NW-SE: ALT.VARIANCE AGAINST DISTANCE
LOG VARIANCE
4.8
4.3
3.8
3.3
1.8 2 2.2 2.4 2.6 2.8 3 3.2 3.4 3.6 3.8 4 4.2
LOG DISTANCE

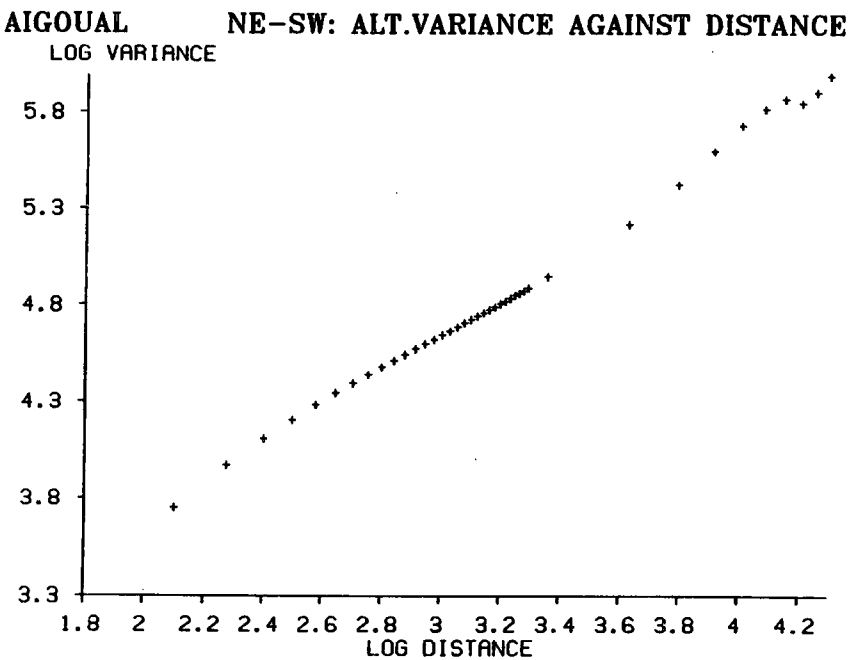
AIGOUAL NE-SW: ALT.VARIANCE AGAINST DISTANCE
LOG VARIANCE
5.8
5.3
4.8
4.3
3.8
3.3
1.8 2 2.2 2.4 2.6 2.8 3 3.2 3.4 3.6 3.8 4 4.2
LOG DISTANCE

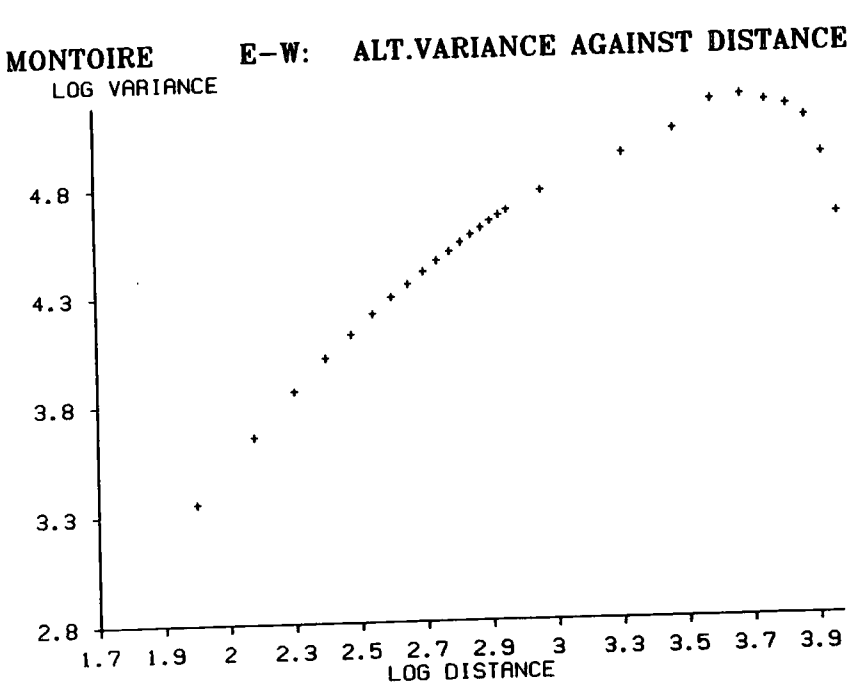
MONTOIRE E-W: ALT.VARIANCE AGAINST DISTANCE
LOG VARIANCE
4.8
4.3
3.8
3.3
2.8
1.7 1.9 2 2.3 2.5 2.7 2.9 3 3.3 3.5 3.7 3.9
LOG DISTANCE

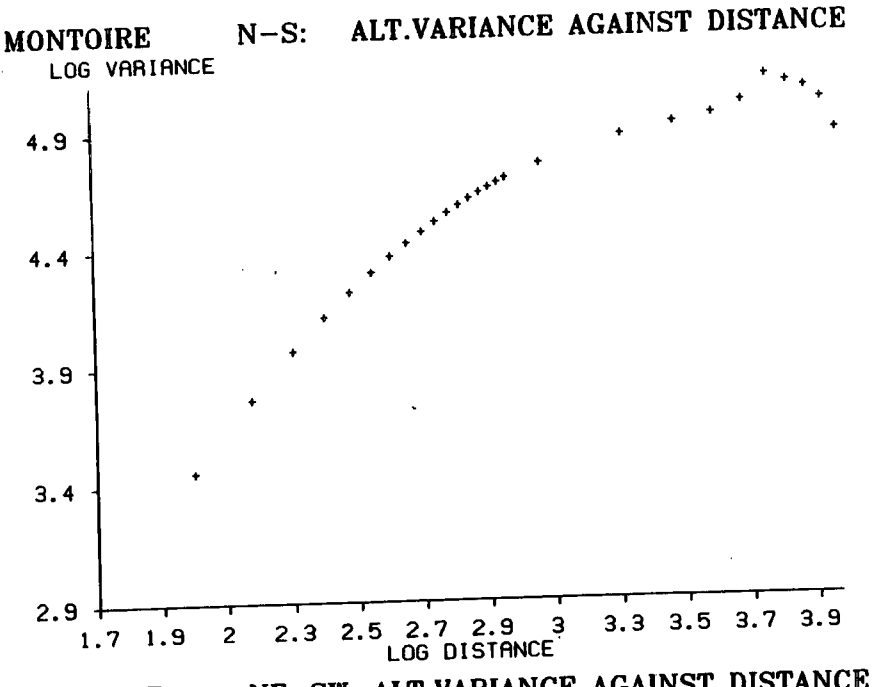
MONTOIRE N-S: ALT.VARIANCE AGAINST DISTANCE
LOG VARIANCE
4.9
4.4
3.9
3.4
2.9
1.7 1.9 2 2.3 2.5 2.7 2.9 3 3.3 3.5 3.7 3.9
LOG DISTANCE

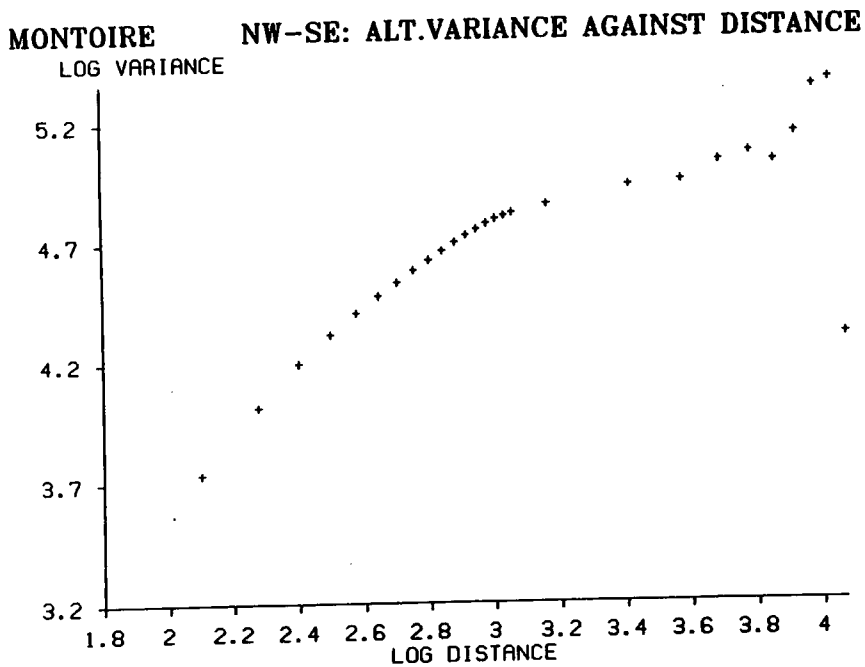
MONTOIRE NW-SE: ALT.VARIANCE AGAINST DISTANCE
LOG VARIANCE
5.2
4.7
4.2
3.7
3.2
1.8 2 2.2 2.4 2.6 2.8 3 3.2 3.4 3.6 3.8 4
LOG DISTANCE

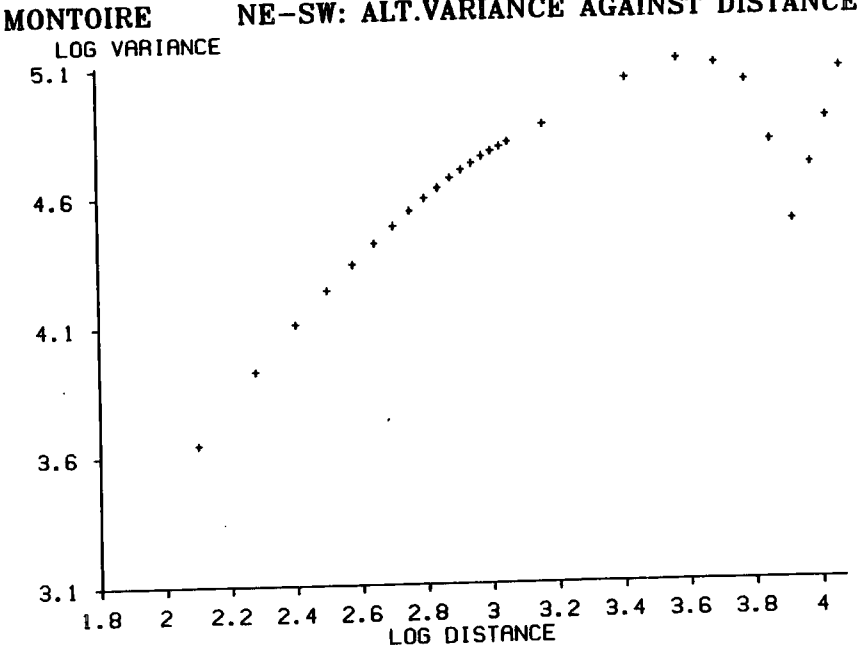
MONTOIRE NE-SW: ALT.VARIANCE AGAINST DISTANCE
LOG VARIANCE
5.1
4.6
4.1
3.6
3.1
1.8 2 2.2 2.4 2.6 2.8 3 3.2 3.4 3.6 3.8 4
LOG DISTANCE

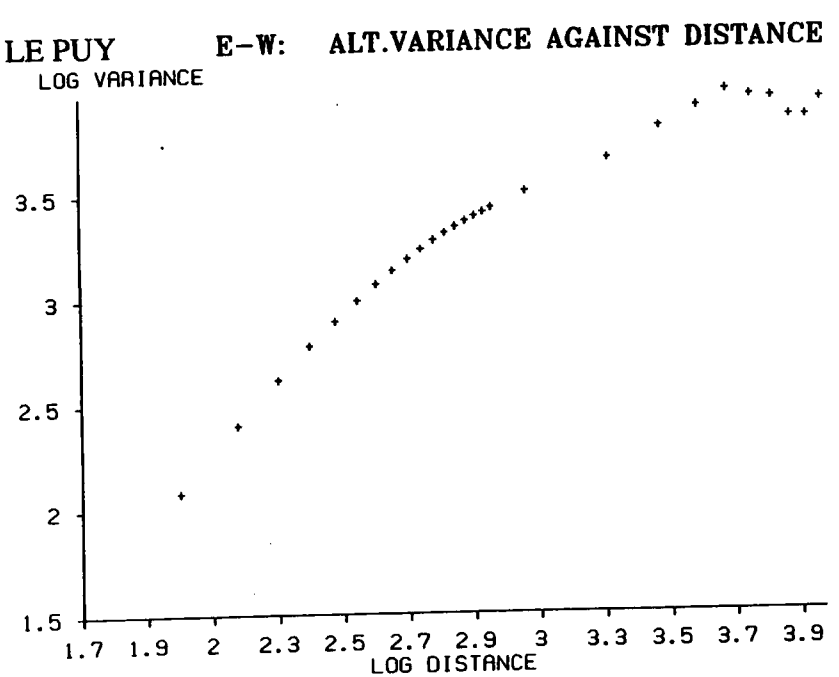
LE PUY E-W: ALT.VARIANCE AGAINST DISTANCE
LOG VARIANCE
3.5
3
2.5
2
1.5
1.7 1.9 2 2.3 2.5 2.7 2.9 3 3.3 3.5 3.7 3.9
LOG DISTANCE

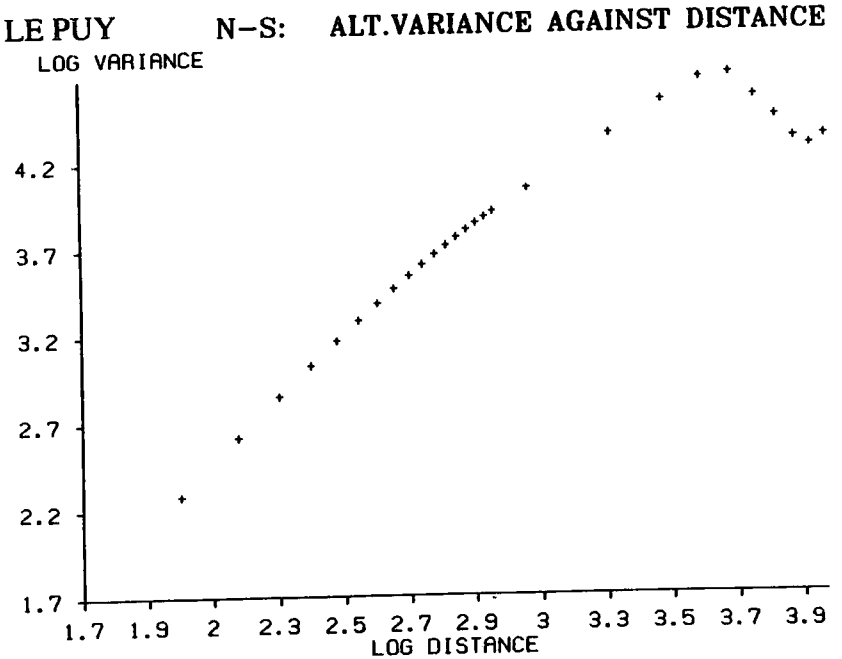
LE PUY N-S: ALT.VARIANCE AGAINST DISTANCE
LOG VARIANCE
4.2
3.7
3.2
2.7
2.2
1.7
1.7 1.9 2 2.3 2.5 2.7 2.9 3 3.3 3.5 3.7 3.9
LOG DISTANCE

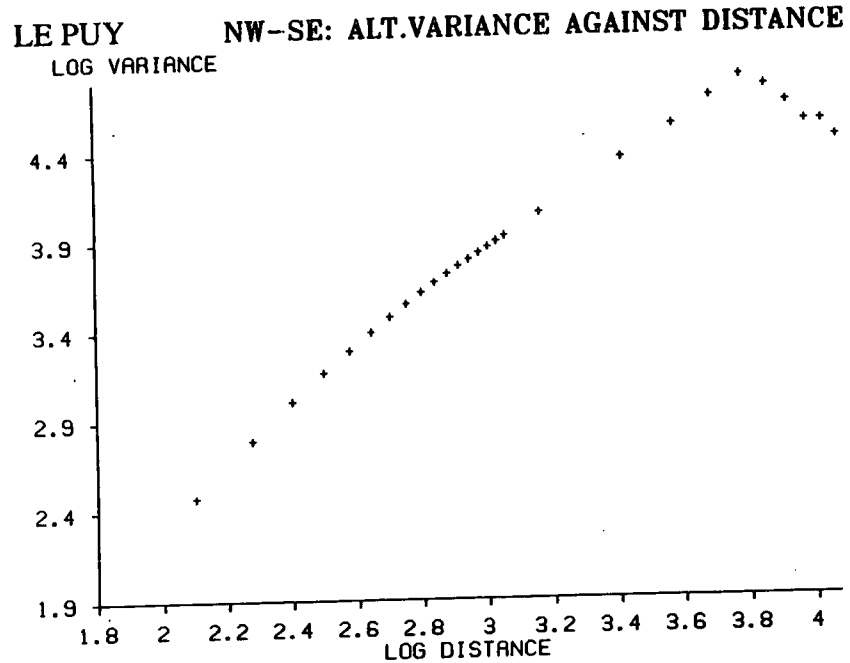
LE PUY NW-SE: ALT.VARIANCE AGAINST DISTANCE
LOG VARIANCE
4.4
3.9
3.4
2.9
2.4
1.9
1.8 2 2.2 2.4 2.6 2.8 3 3.2 3.4 3.6 3.8 4
LOG DISTANCE

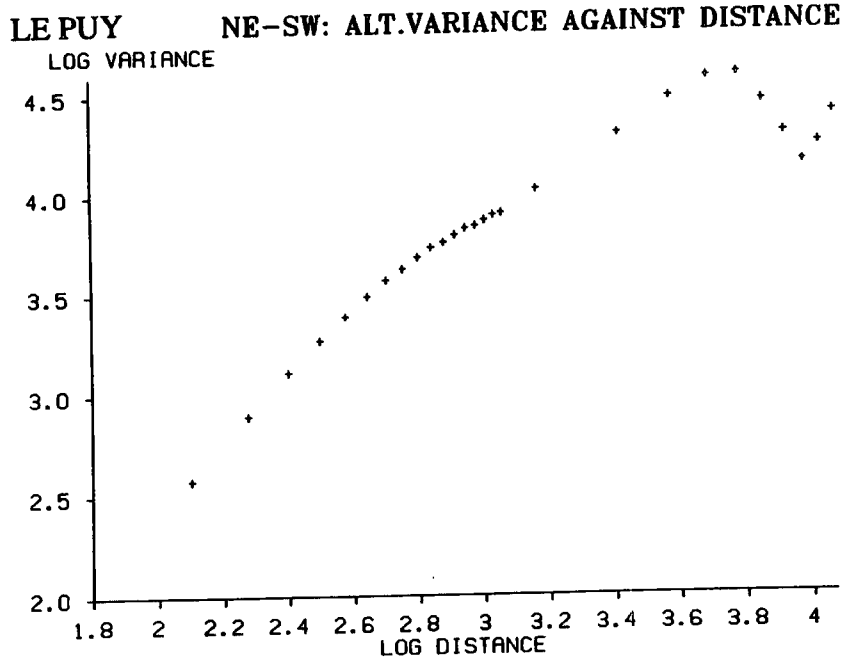
LE PUY NE-SW: ALT.VARIANCE AGAINST DISTANCE
LOG VARIANCE
4.5
4.0
3.5
3.0
2.5
2.0
1.8 2 2.2 2.4 2.6 2.8 3 3.2 3.4 3.6 3.8 4
LOG DISTANCE

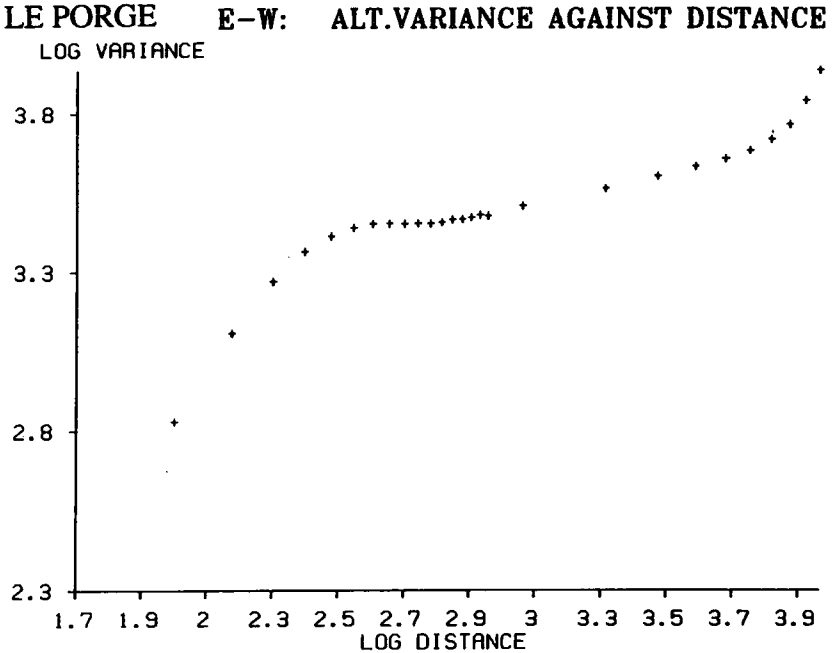
LE PORGE E-W: ALT.VARIANCE AGAINST DISTANCE
LOG VARIANCE
3.8
3.3
2.8
2.3
1.7 1.9 2 2.3 2.5 2.7 2.9 3 3.3 3.5 3.7 3.9
LOG DISTANCE

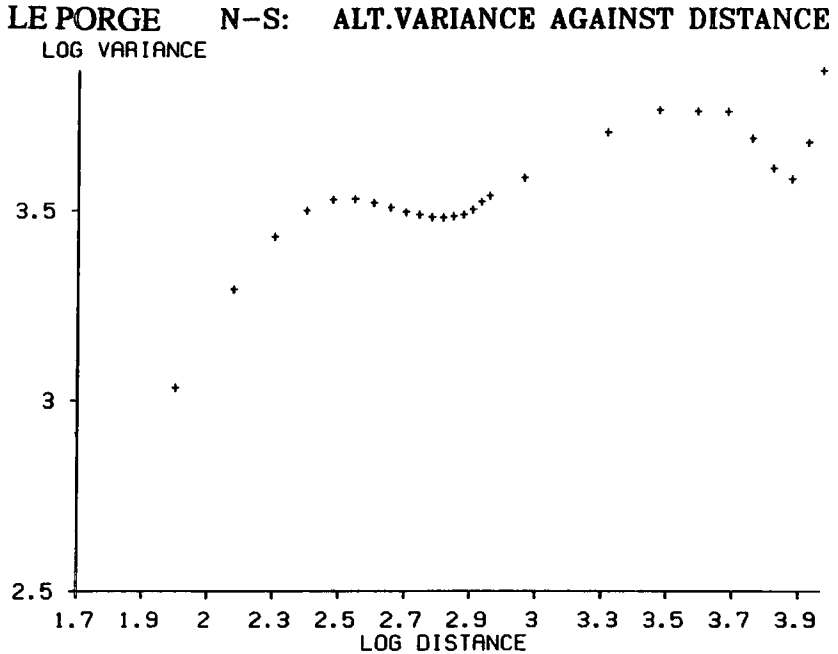
LE PORGE N-S: ALT.VARIANCE AGAINST DISTANCE
LOG VARIANCE
3.5
3
2.5
1.7 1.9 2 2.3 2.5 2.7 2.9 3 3.3 3.5 3.7 3.9
LOG DISTANCE

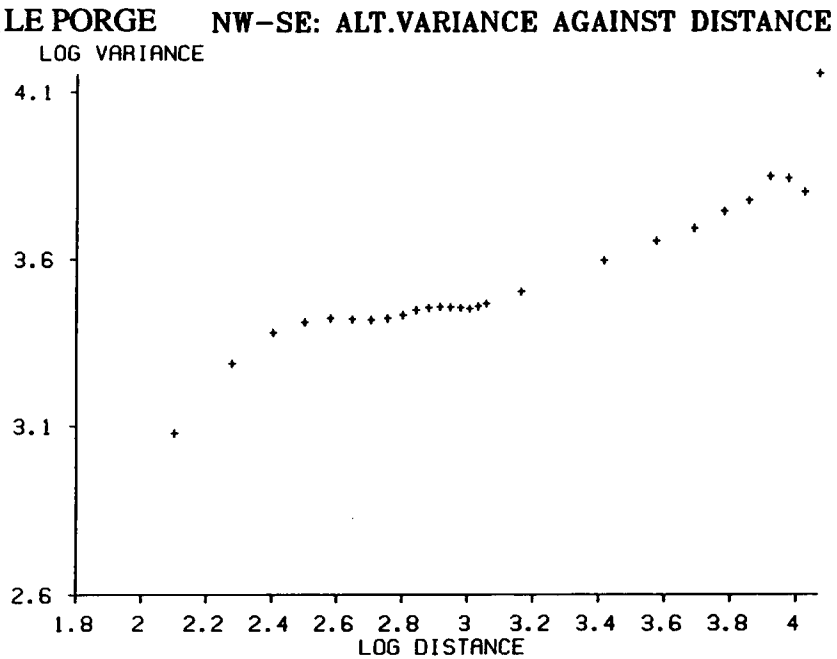
LE PORGE NW-SE: ALT.VARIANCE AGAINST DISTANCE
LOG VARIANCE
4.1
3.6
3.1
2.6
1.8 2 2.2 2.4 2.6 2.8 3 3.2 3.4 3.6 3.8 4
LOG DISTANCE

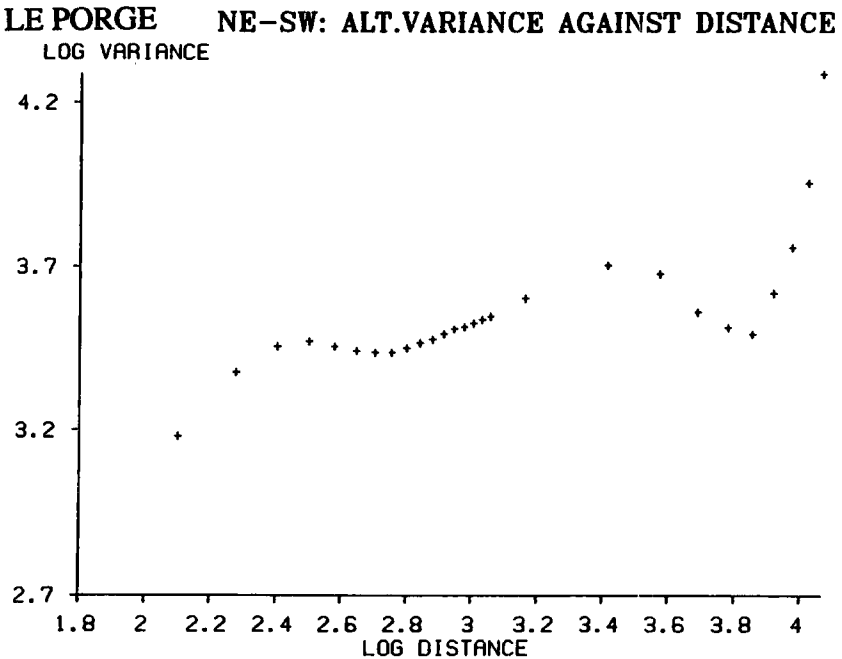
LE PORGE NE-SW: ALT.VARIANCE AGAINST DISTANCE
LOG VARIANCE
4.2
3.7
3.2
2.7
1.8 2 2.2 2.4 2.6 2.8 3 3.2 3.4 3.6 3.8 4
LOG DISTANCE

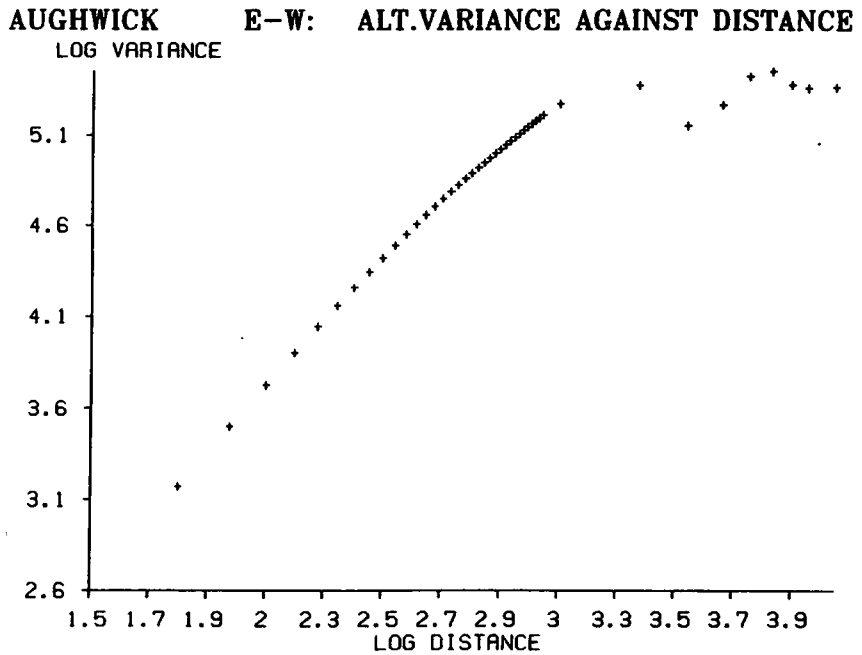
AUGHWICK E-W: ALT.VARIANCE AGAINST DISTANCE
LOG VARIANCE
5.1
4.6
4.1
3.6
3.1
2.6
1.5 1.7 1.9 2 2.3 2.5 2.7 2.9 3 3.3 3.5 3.7 3.9
LOG DISTANCE

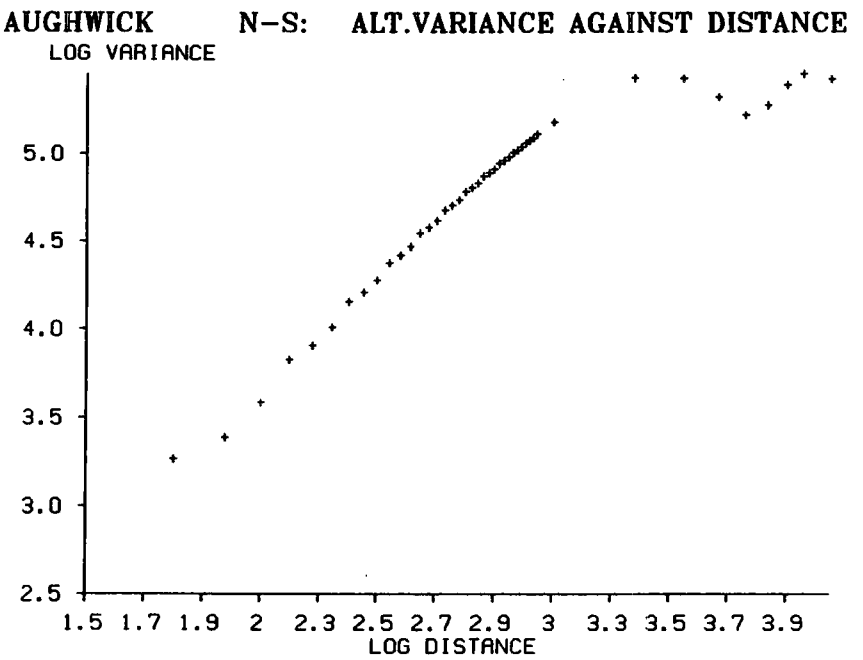
AUGHWICK N-S: ALT.VARIANCE AGAINST DISTANCE
LOG VARIANCE
5.0
4.5
4.0
3.5
3.0
2.5
1.5 1.7 1.9 2 2.3 2.5 2.7 2.9 3 3.3 3.5 3.7 3.9
LOG DISTANCE

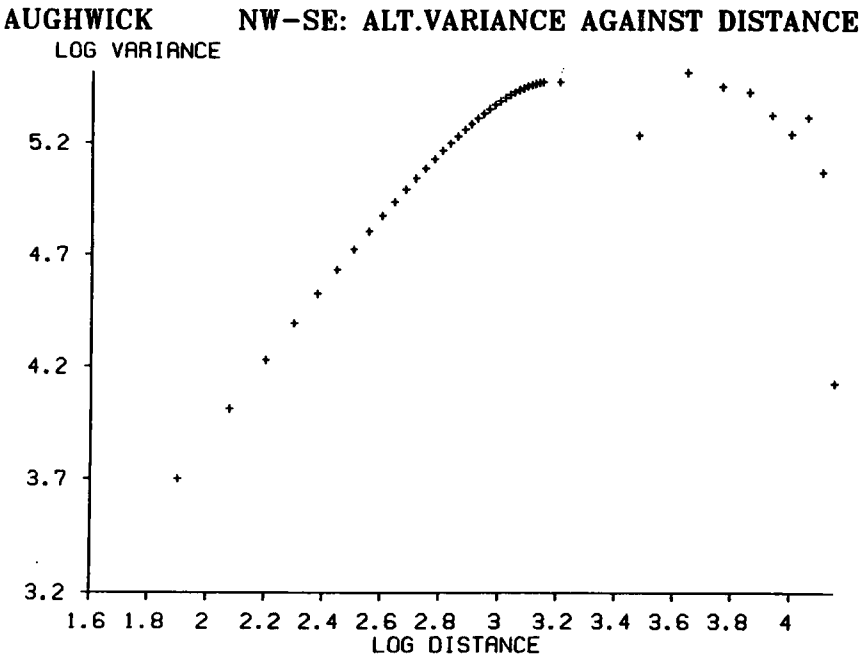
AUGHWICK NW-SE: ALT.VARIANCE AGAINST DISTANCE
LOG VARIANCE
5.2
4.7
4.2
3.7
3.2
1.6 1.8 2 2.2 2.4 2.6 2.8 3 3.2 3.4 3.6 3.8 4
LOG DISTANCE

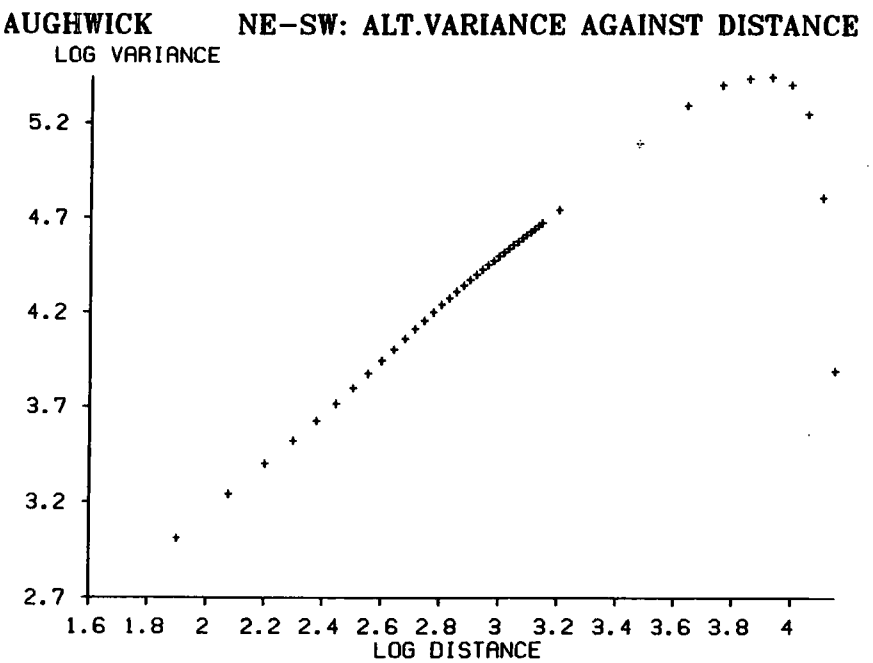
AUGHWICK NE-SW: ALT.VARIANCE AGAINST DISTANCE
LOG VARIANCE
5.2
4.7
4.2
3.7
3.2
2.7
1.6 1.8 2 2.2 2.4 2.6 2.8 3 3.2 3.4 3.6 3.8 4
LOG DISTANCE

BELLEVILLE: E–W: ALT.VARIANCE AGAINST DISTANCE

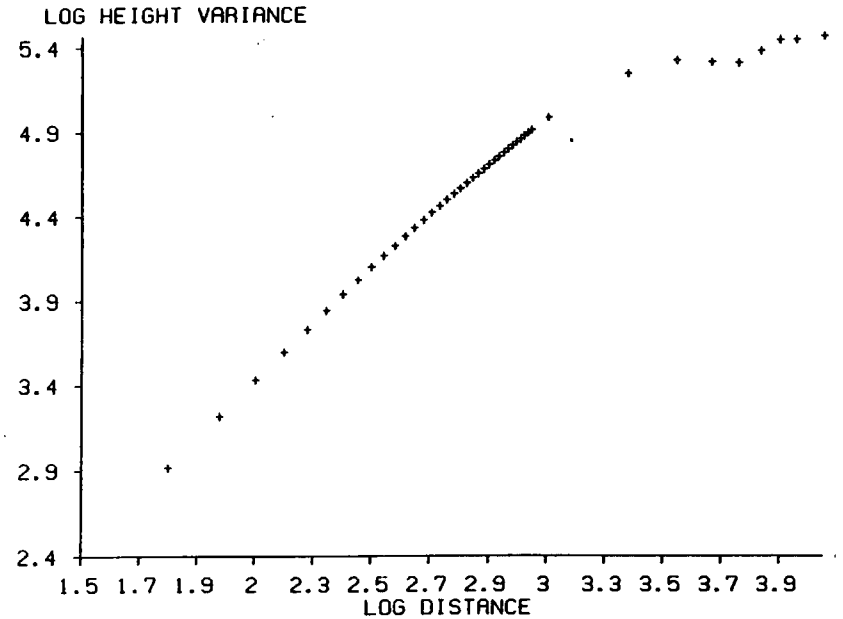

BELLEVILLE: N–S: ALT.VARIANCE AGAINST DISTANCE

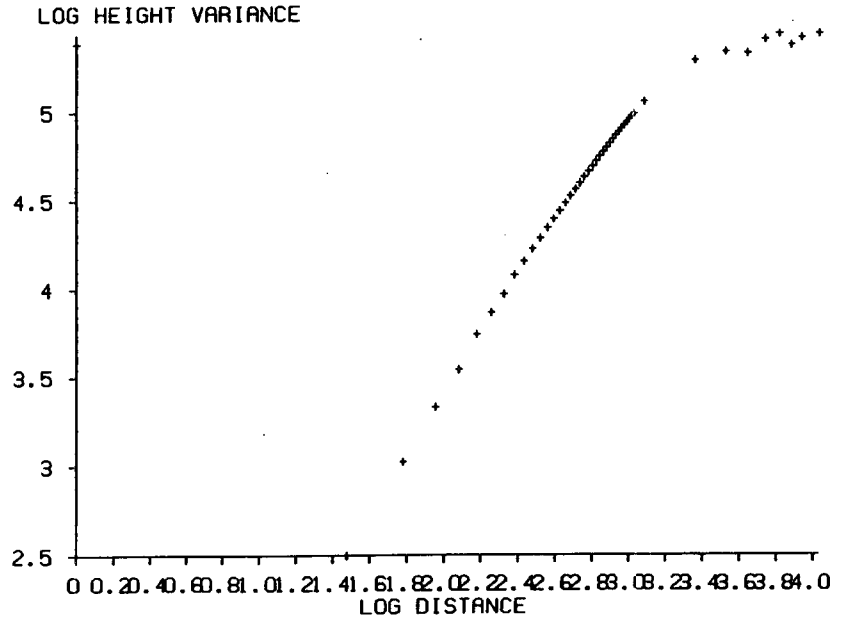

BELLEVILLE: NW–SE: ALT.VARIANCE AGAINST DISTANCE

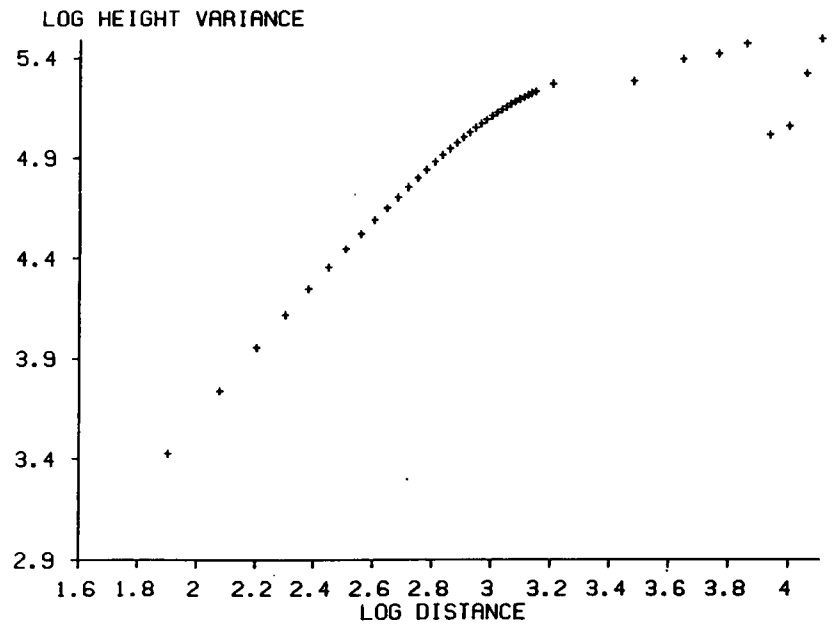

BELLEVILLE: NE–SW: ALT.VARIANCE AGAINST DISTANCE

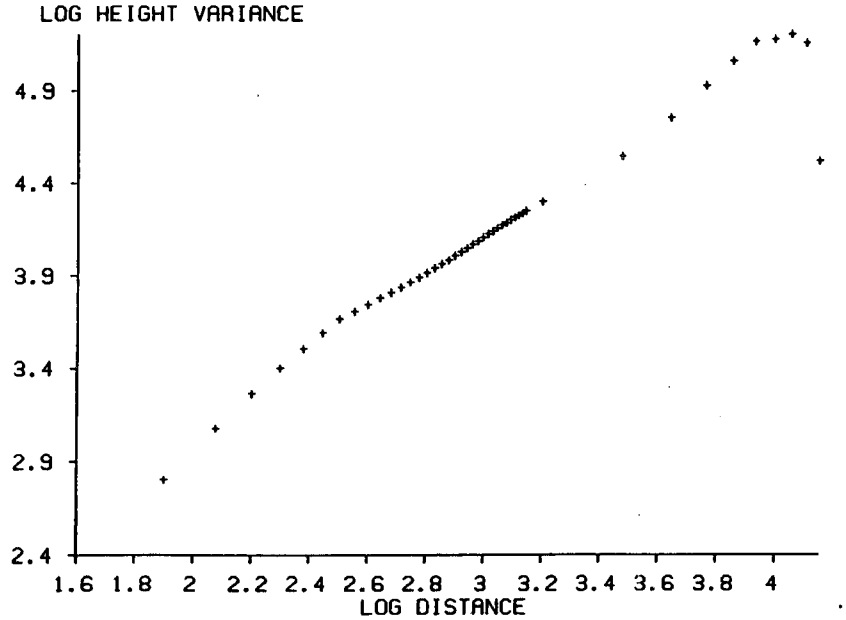

ALLENVILLE: E–W: ALT.VARIANCE AGAINST DISTANCE

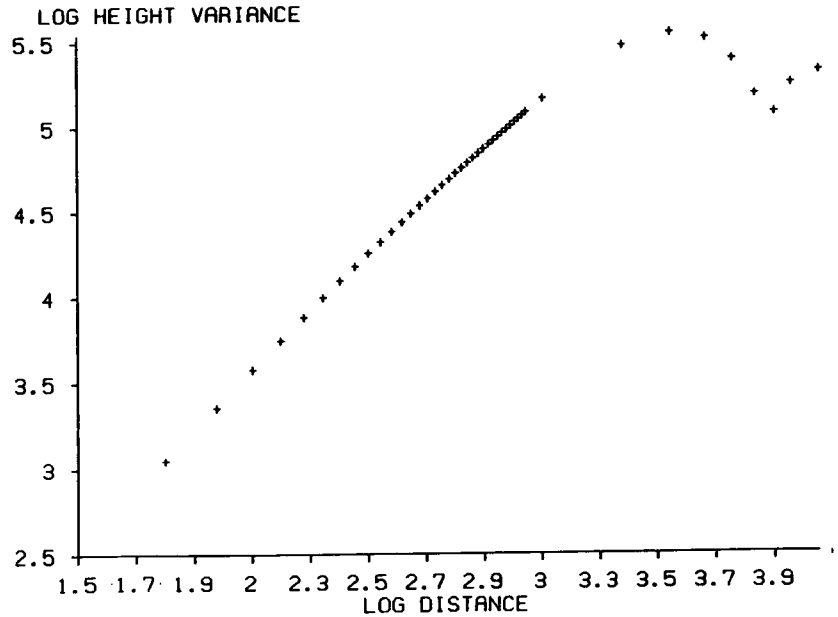

ALLENVILLE: N–S: ALT.VARIANCE AGAINST DISTANCE

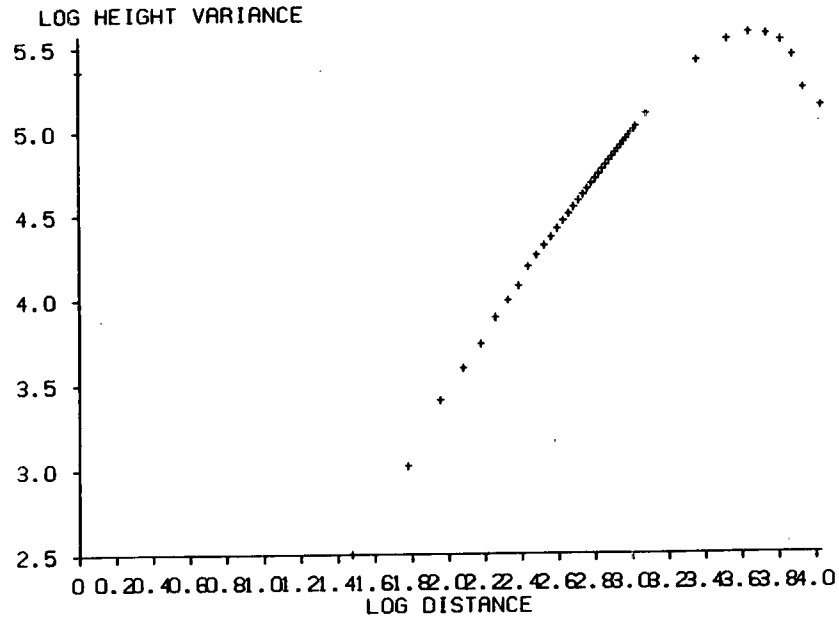

ALLENVILLE: NW–SE: ALT.VARIANCE AGAINST DISTANCE

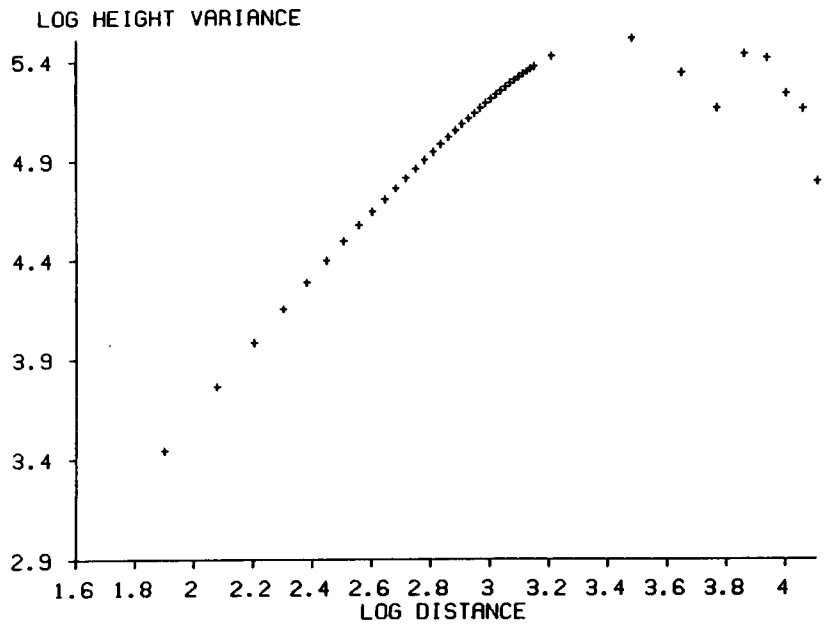

ALLENVILLE: NE–SW: ALT.VARIANCE AGAINST DISTANCE

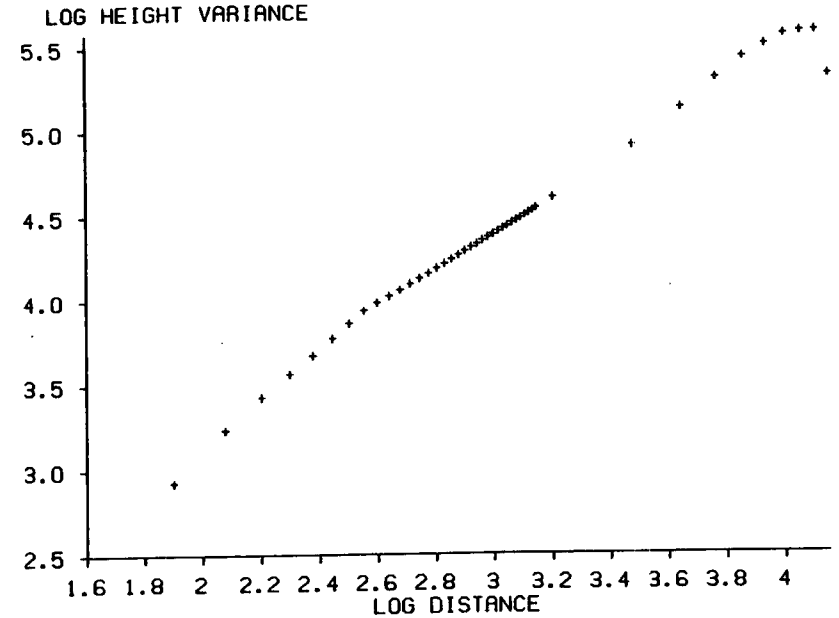

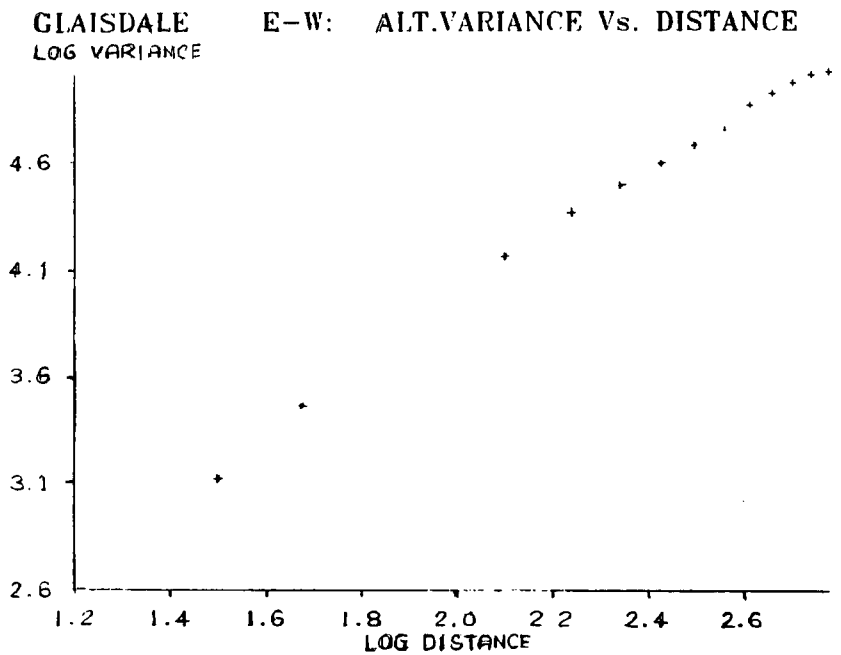
GLAISDALE E–W: ALT.VARIANCE Vs. DISTANCE
LOG VARIANCE
4.6
4.1
3.6
3.1
2.6
1.2 1.4 1.6 1.8 2.0 2.2 2.4 2.6
LOG DISTANCE

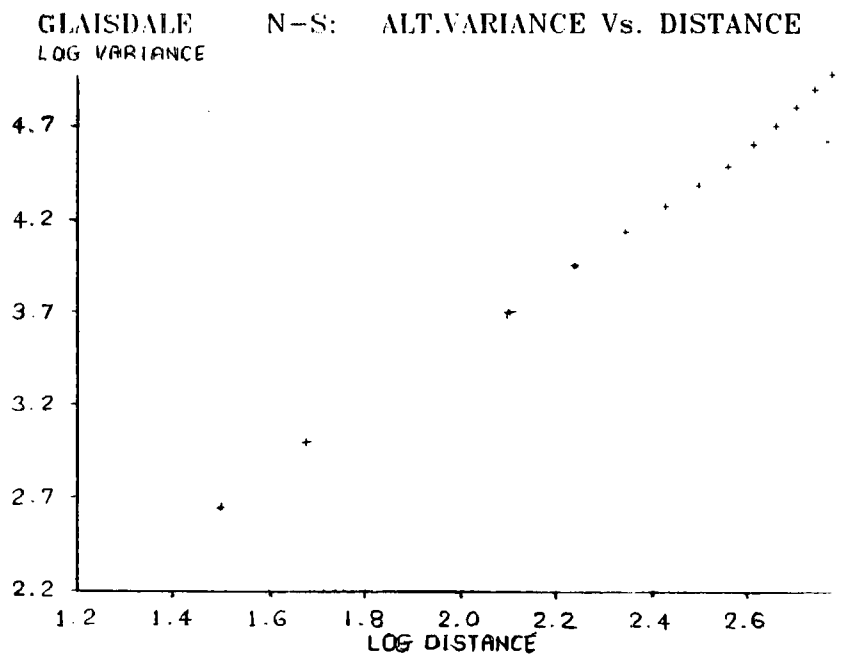
GLAISDALE N–S: ALT.VARIANCE Vs. DISTANCE
LOG VARIANCE
4.7
4.2
3.7
3.2
2.7
2.2
1.2 1.4 1.6 1.8 2.0 2.2 2.4 2.6
LOG DISTANCE

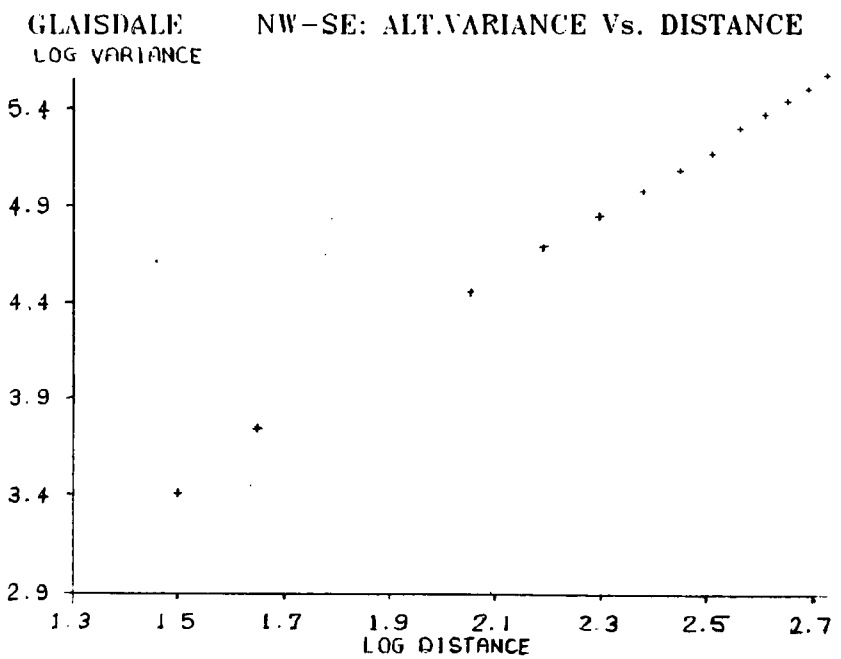
GLAISDALE NW–SE: ALT.VARIANCE Vs. DISTANCE
LOG VARIANCE
5.4
4.9
4.4
3.9
3.4
2.9
1.3 1.5 1.7 1.9 2.1 2.3 2.5 2.7
LOG DISTANCE

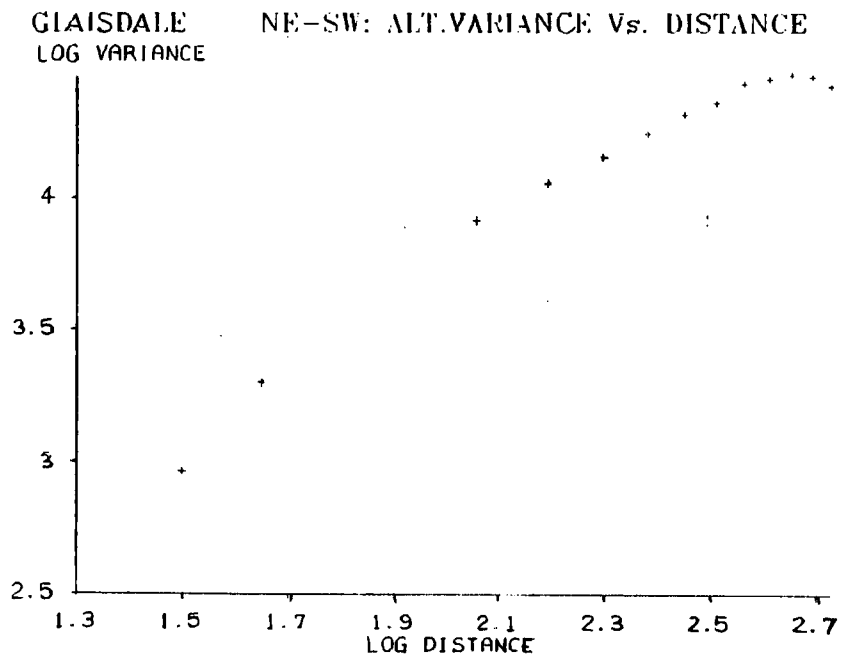
GLAISDALE NE–SW: ALT.VARIANCE Vs. DISTANCE
LOG VARIANCE
4
3.5
3
2.5
1.3 1.5 1.7 1.9 2.1 2.3 2.5 2.7
LOG DISTANCE

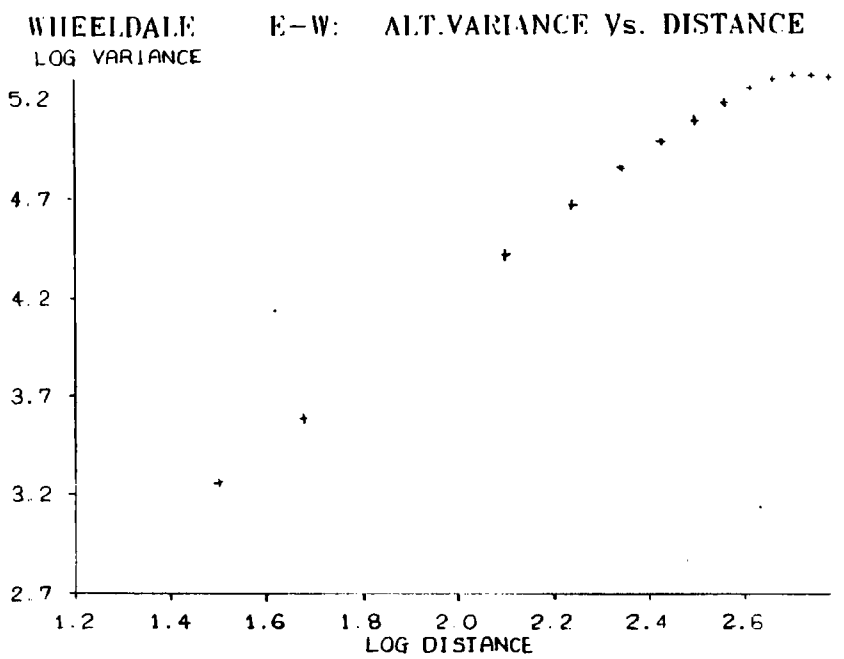
WHEELDALE E-W: ALT.VARIANCE Vs. DISTANCE
LOG VARIANCE
5.2
4.7
4.2
3.7
3.2
2.7
1.2 1.4 1.6 1.8 2.0 2.2 2.4 2.6
LOG DISTANCE

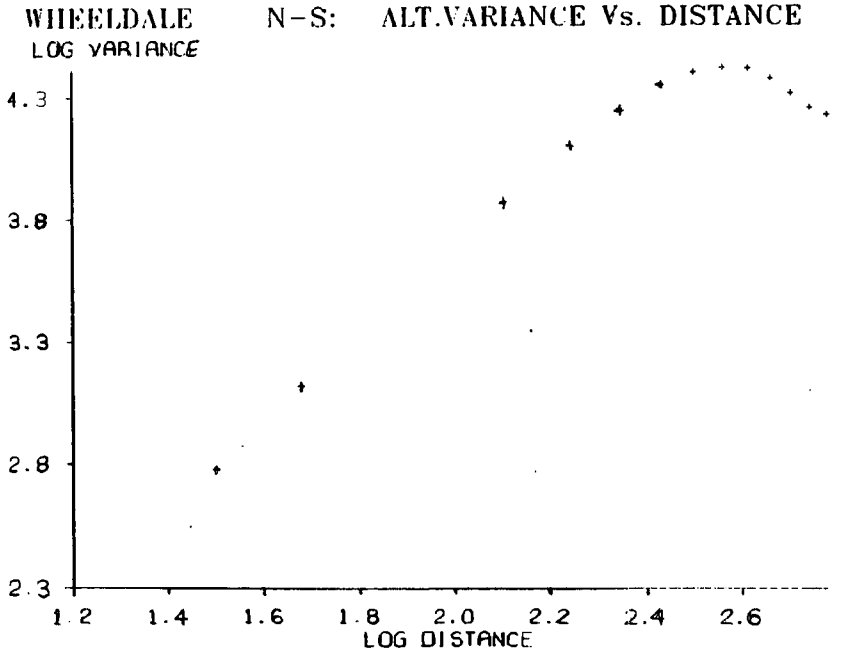
WHEELDALE N-S: ALT.VARIANCE Vs. DISTANCE
LOG VARIANCE
4.3
3.8
3.3
2.8
2.3
1.2 1.4 1.6 1.8 2.0 2.2 2.4 2.6
LOG DISTANCE

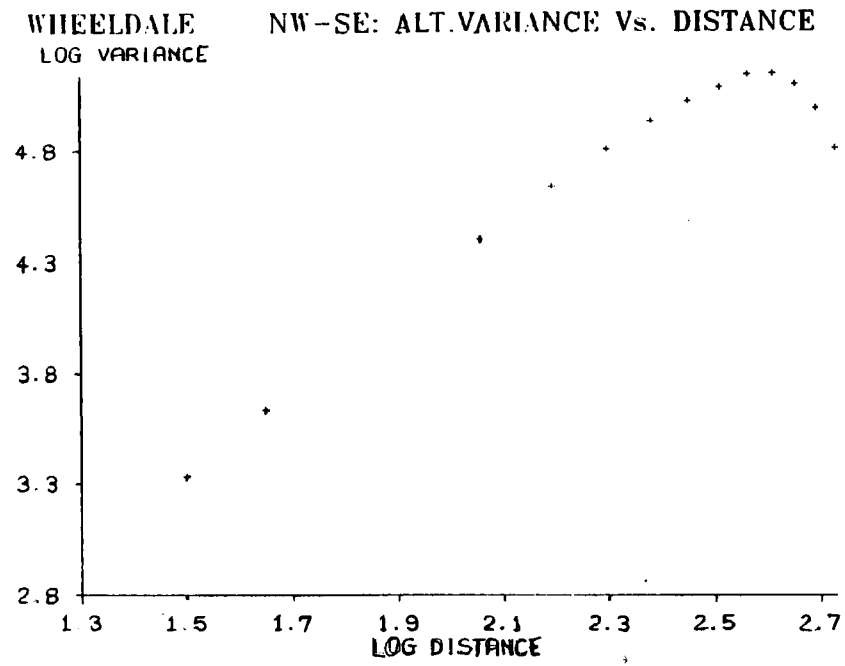
WHEELDALE NW-SE: ALT.VARIANCE Vs. DISTANCE
LOG VARIANCE
4.8
4.3
3.8
3.3
2.8
1.3 1.5 1.7 1.9 2.1 2.3 2.5 2.7
LOG DISTANCE

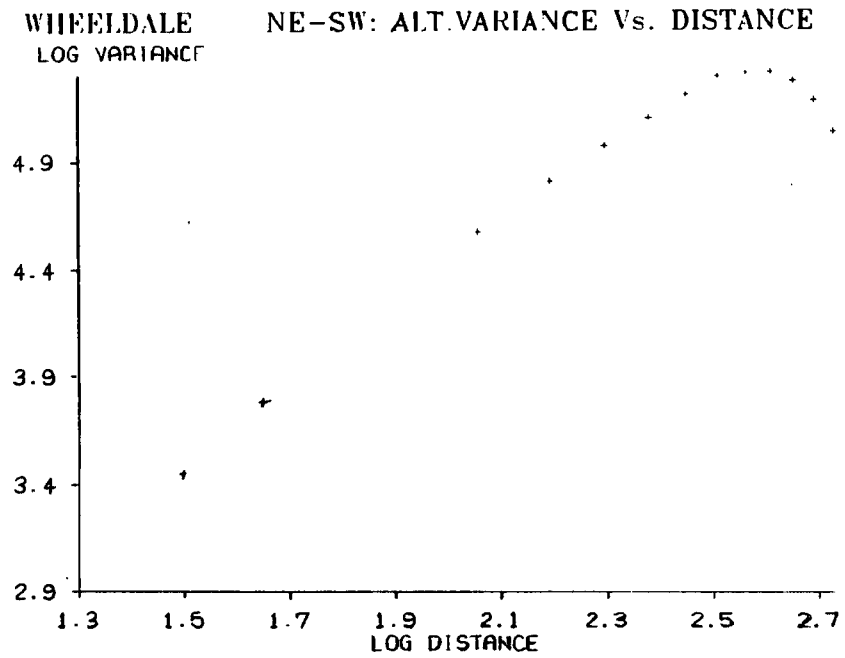
WHEELDALE NE-SW: ALT.VARIANCE Vs. DISTANCE
LOG VARIANCE
4.9
4.4
3.9
3.4
2.9
1.3 1.5 1.7 1.9 2.1 2.3 2.5 2.7
LOG DISTANCE

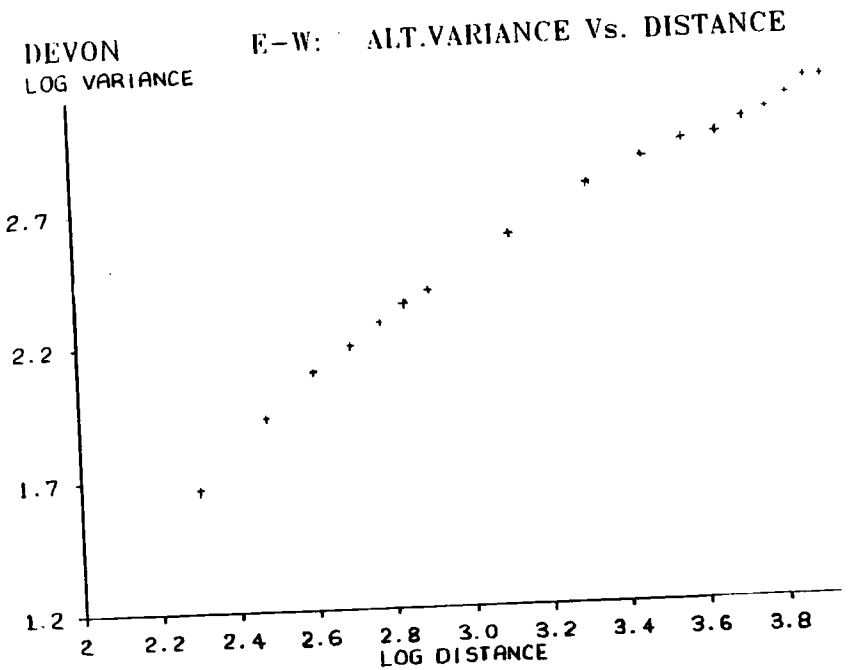
DEVON
E-W: ALT.VARIANCE Vs. DISTANCE
LOG VARIANCE
2.7
2.2
1.7
1.2
2
2.2
2.4
2.6
2.8
3.0
3.2
3.4
3.6
3.8
LOG DISTANCE

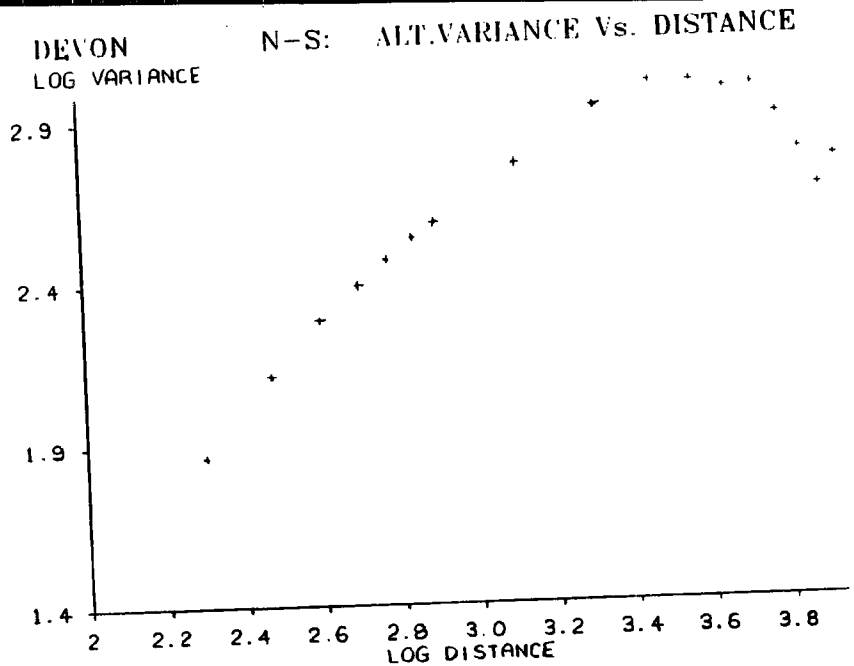
DEVON
N-S: ALT.VARIANCE Vs. DISTANCE
LOG VARIANCE
2.9
2.4
1.9
1.4
2
2.2
2.4
2.6
2.8
3.0
3.2
3.4
3.6
3.8
LOG DISTANCE

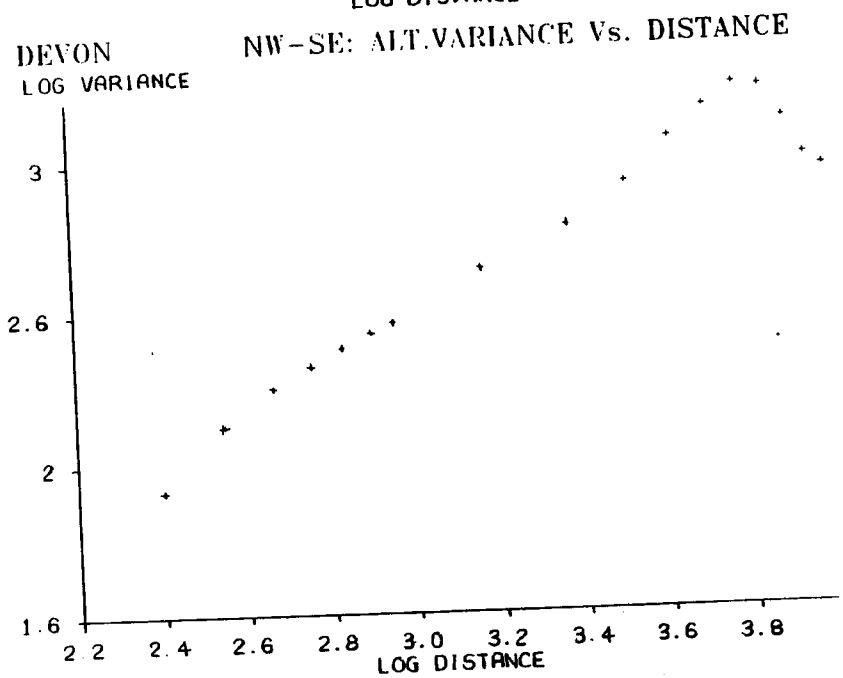
DEVON
NW-SE: ALT.VARIANCE Vs. DISTANCE
LOG VARIANCE
3
2.6
2
1.6
2.2
2.4
2.6
2.8
3.0
3.2
3.4
3.6
3.8
LOG DISTANCE

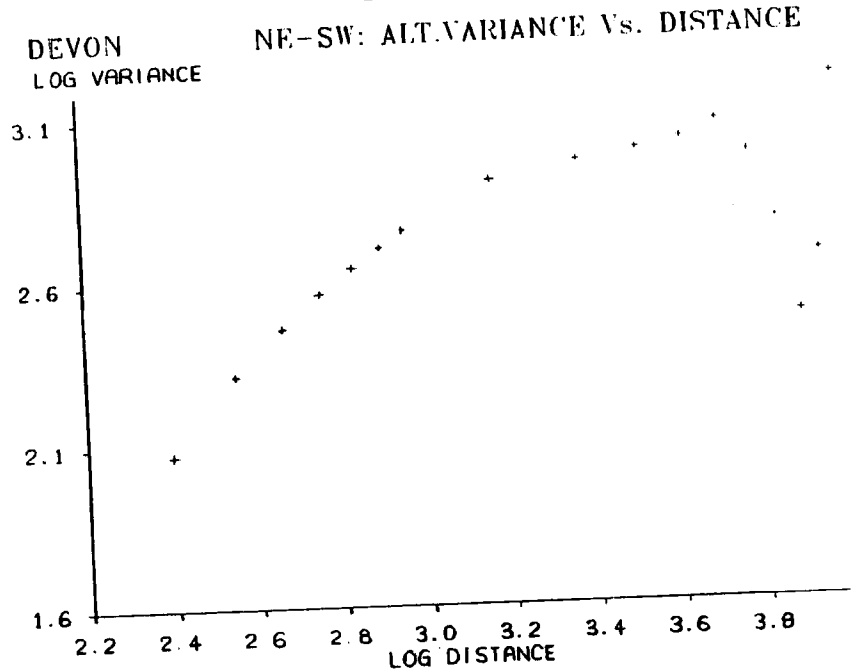
DEVON
NE-SW: ALT.VARIANCE Vs. DISTANCE
LOG VARIANCE
3.1
2.6
2.1
1.6
2.2
2.4
2.6
2.8
3.0
3.2
3.4
3.6
3.8
LOG DISTANCE

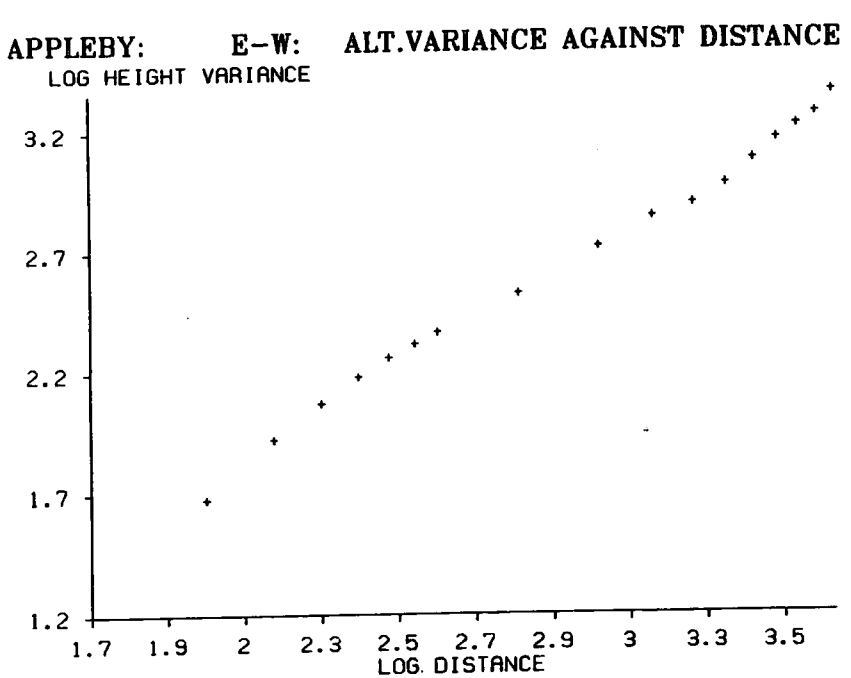
APPLEBY: E-W: ALT.VARIANCE AGAINST DISTANCE
LOG HEIGHT VARIANCE
3.2
2.7
2.2
1.7
1.2
1.7 1.9 2 2.3 2.5 2.7 2.9 3 3.3 3.5
LOG DISTANCE

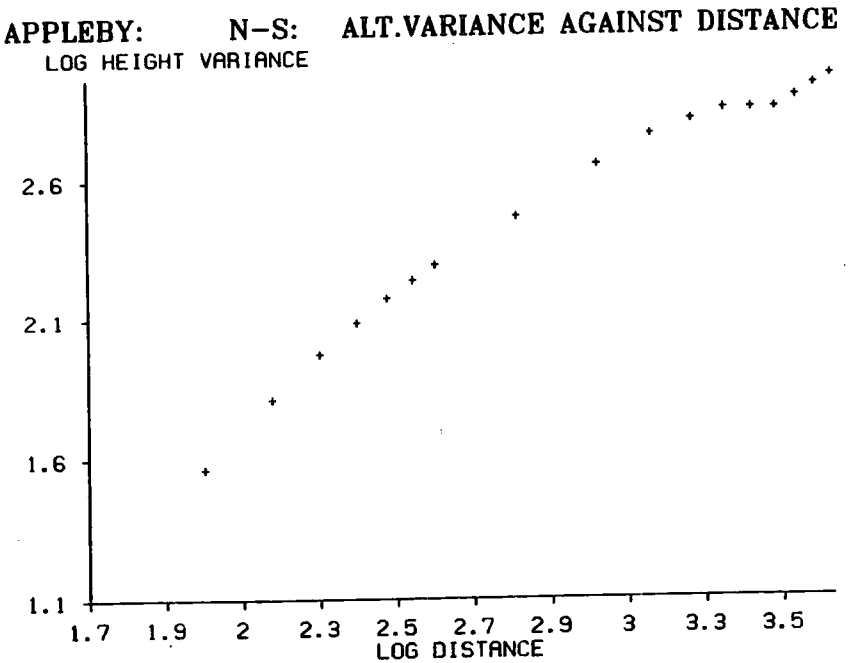
APPLEBY: N-S: ALT.VARIANCE AGAINST DISTANCE
LOG HEIGHT VARIANCE
2.6
2.1
1.6
1.1
1.7 1.9 2 2.3 2.5 2.7 2.9 3 3.3 3.5
LOG DISTANCE

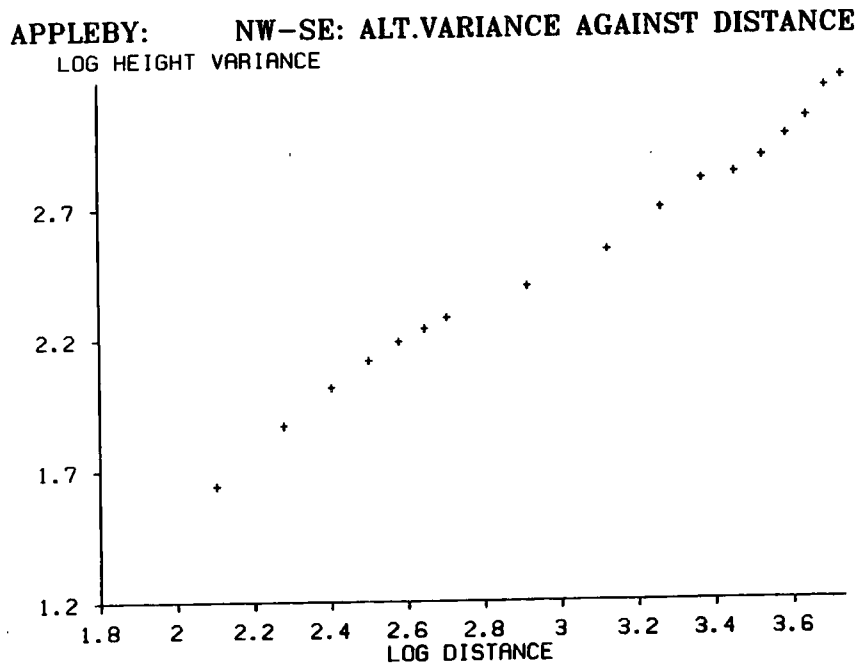
APPLEBY: NW-SE: ALT.VARIANCE AGAINST DISTANCE
LOG HEIGHT VARIANCE
2.7
2.2
1.7
1.2
1.8 2 2.2 2.4 2.6 2.8 3 3.2 3.4 3.6
LOG DISTANCE

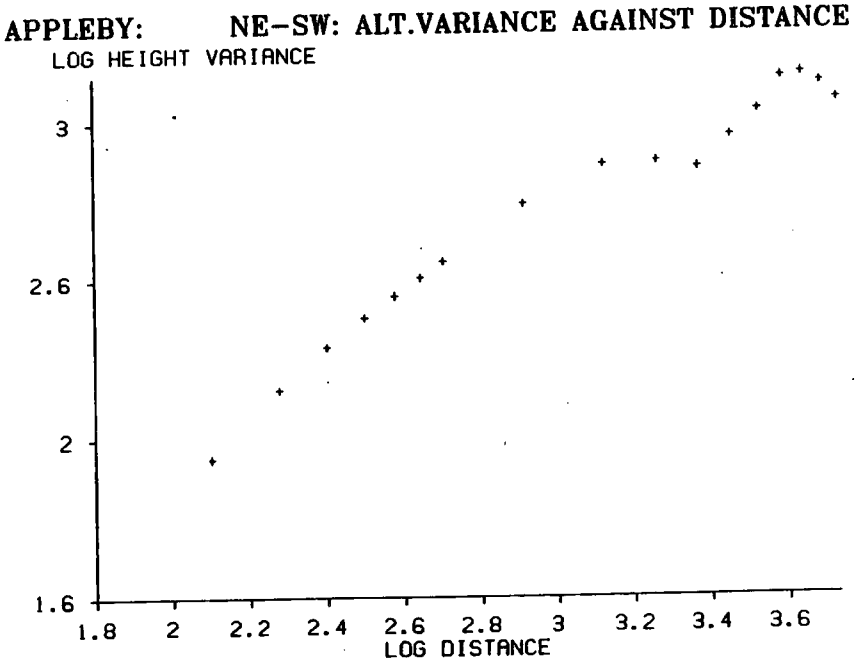
APPLEBY: NE-SW: ALT.VARIANCE AGAINST DISTANCE
LOG HEIGHT VARIANCE
3
2.6
2
1.6
1.8 2 2.2 2.4 2.6 2.8 3 3.2 3.4 3.6
LOG DISTANCE

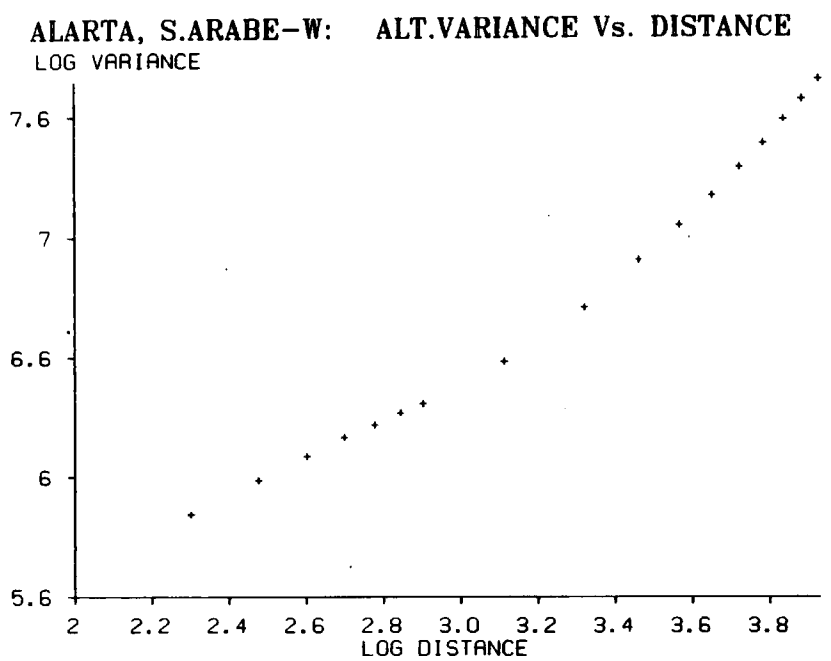
ALARTA, S.ARABE-W: ALT.VARIANCE Vs. DISTANCE
LOG VARIANCE
7.6
7
6.6
6
5.6
2
2.2
2.4
2.6
2.8
3.0
3.2
3.4
3.6
3.8
LOG DISTANCE

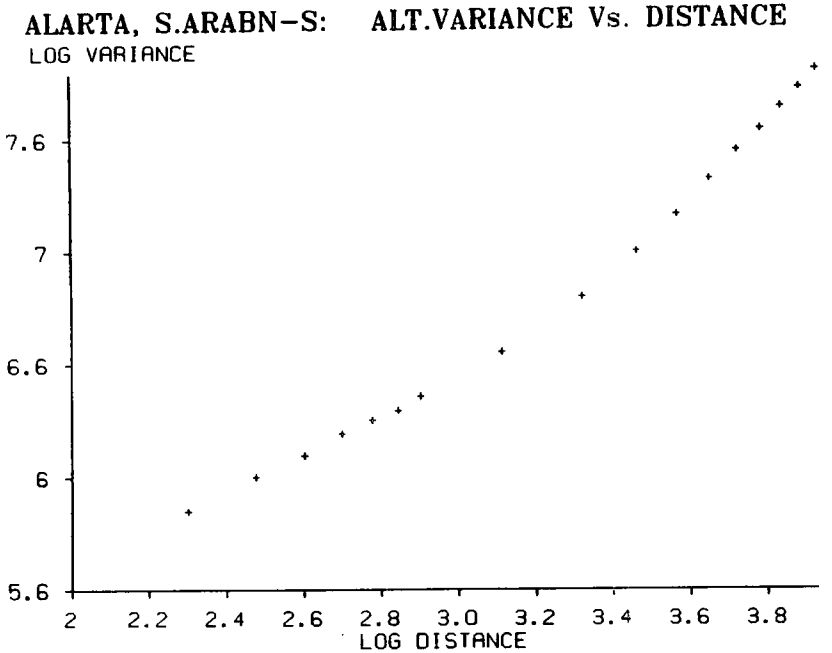
ALARTA, S.ARABN-S: ALT.VARIANCE Vs. DISTANCE
LOG VARIANCE
7.6
7
6.6
6
5.6
2
2.2
2.4
2.6
2.8
3.0
3.2
3.4
3.6
3.8
LOG DISTANCE

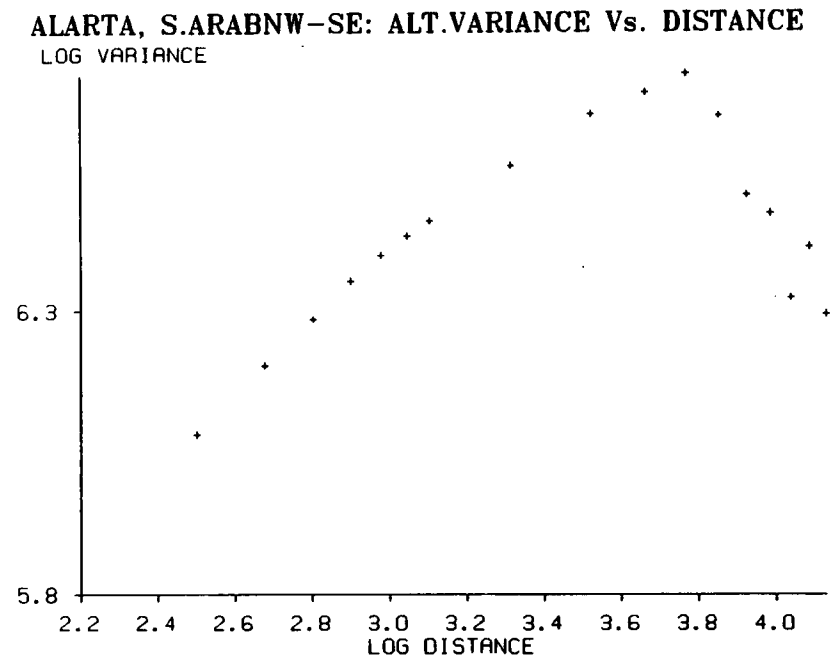
ALARTA, S.ARABNW-SE: ALT.VARIANCE Vs. DISTANCE
LOG VARIANCE
6.3
5.8
2.2
2.4
2.6
2.8
3.0
3.2
3.4
3.6
3.8
4.0
LOG DISTANCE

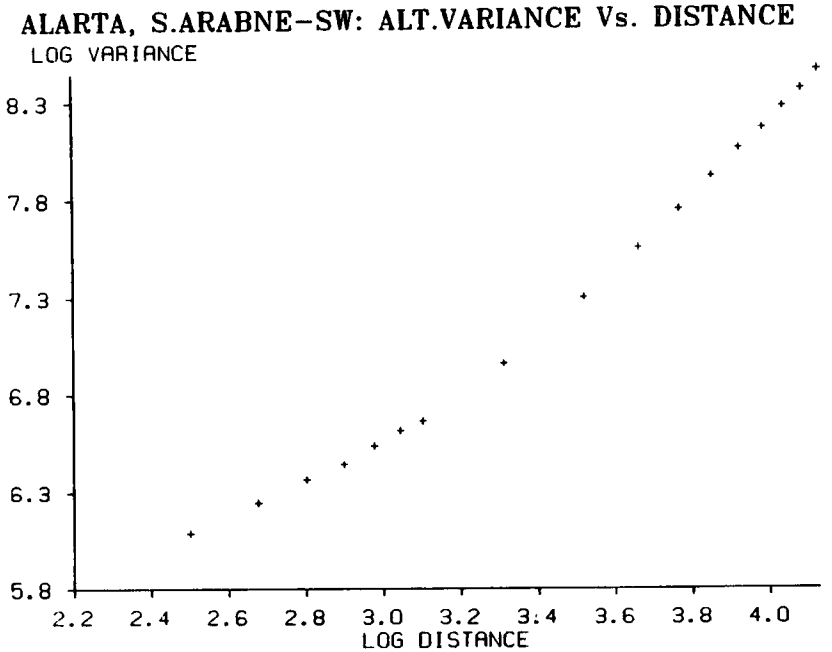
ALARTA, S.ARABNE-SW: ALT.VARIANCE Vs. DISTANCE
LOG VARIANCE
8.3
7.8
7.3
6.8
6.3
5.8
2.2
2.4
2.6
2.8
3.0
3.2
3.4
3.6
3.8
4.0
LOG DISTANCE

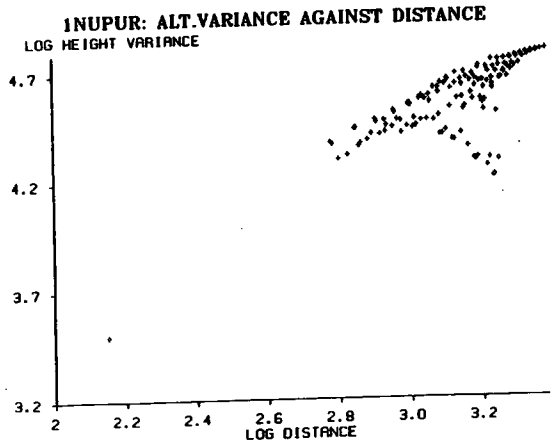
1NUPUR: ALT.VARIANCE AGAINST DISTANCE
LOG HEIGHT VARIANCE
4.7
4.2
3.7
3.2
2
2.2
2.4
2.6
2.8
3.0
3.2
LOG DISTANCE

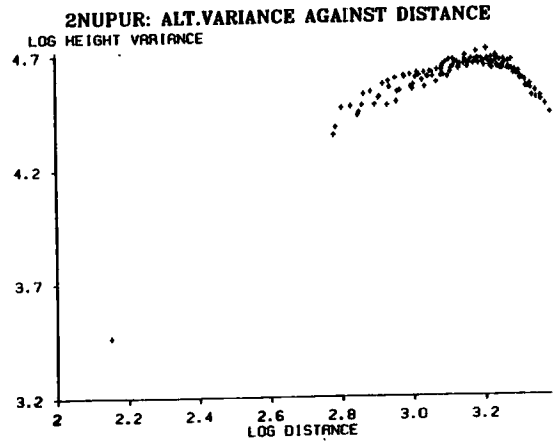
2NUPUR: ALT.VARIANCE AGAINST DISTANCE
LOG HEIGHT VARIANCE
4.7
4.2
3.7
3.2
2
2.2
2.4
2.6
2.8
3.0
3.2
LOG DISTANCE

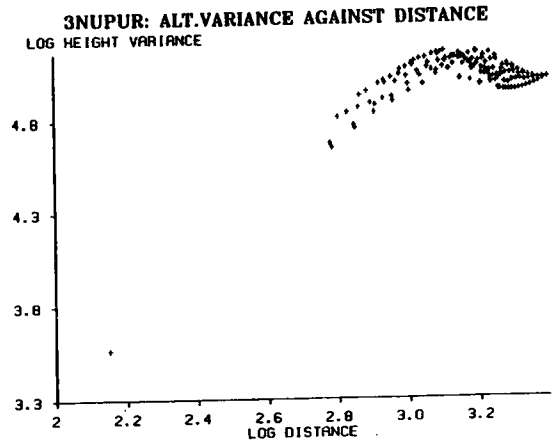
3NUPUR: ALT.VARIANCE AGAINST DISTANCE
LOG HEIGHT VARIANCE
4.8
4.3
3.8
3.3
2
2.2
2.4
2.6
2.8
3.0
3.2
LOG DISTANCE

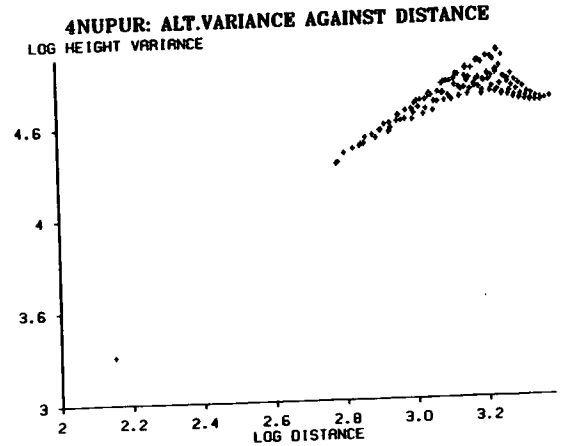
4NUPUR: ALT.VARIANCE AGAINST DISTANCE
LOG HEIGHT VARIANCE
4.6
4
3.6
3
2
2.2
2.4
2.6
2.8
3.0
3.2
LOG DISTANCE

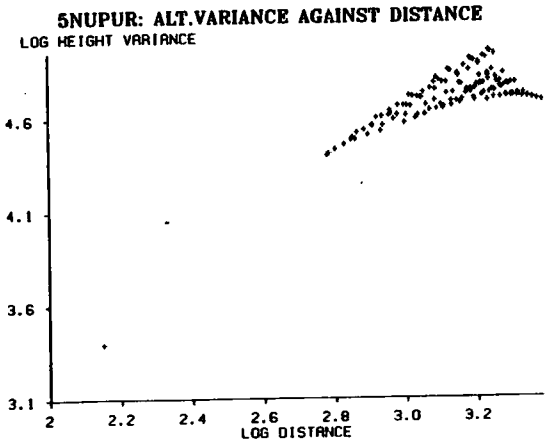
5NUPUR: ALT.VARIANCE AGAINST DISTANCE
LOG HEIGHT VARIANCE
4.6
4.1
3.6
3.1
2
2.2
2.4
2.6
2.8
3.0
3.2
LOG DISTANCE

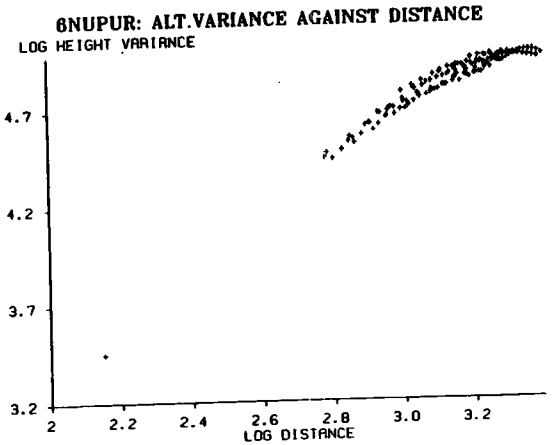
6NUPUR: ALT.VARIANCE AGAINST DISTANCE
LOG HEIGHT VARIANCE
4.7
4.2
3.7
3.2
2
2.2
2.4
2.6
2.8
3.0
3.2
LOG DISTANCE

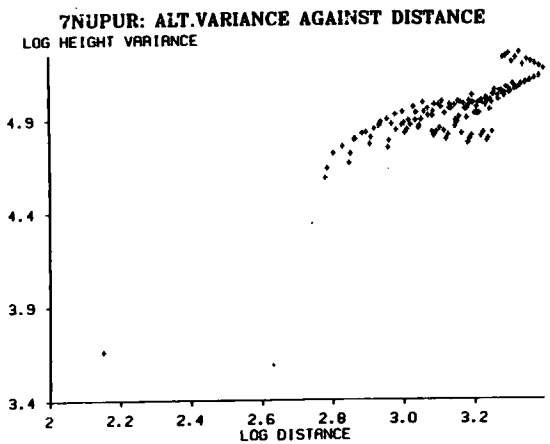
7NUPUR: ALT.VARIANCE AGAINST DISTANCE
LOG HEIGHT VARIANCE
4.9
4.4
3.9
3.4
2
2.2
2.4
2.6
2.8
3.0
3.2
LOG DISTANCE

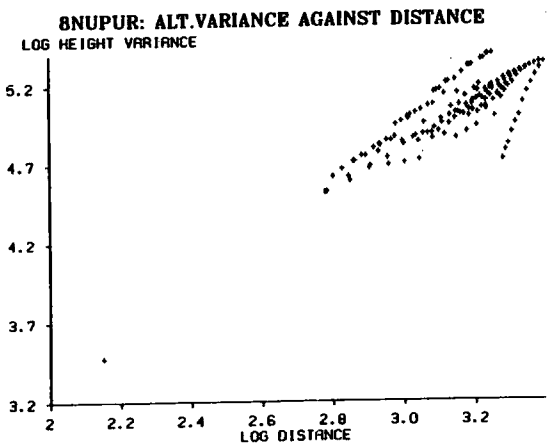
8NUPUR: ALT.VARIANCE AGAINST DISTANCE
LOG HEIGHT VARIANCE
5.2
4.7
4.2
3.7
3.2
2
2.2
2.4
2.6
2.8
3.0
3.2
LOG DISTANCE

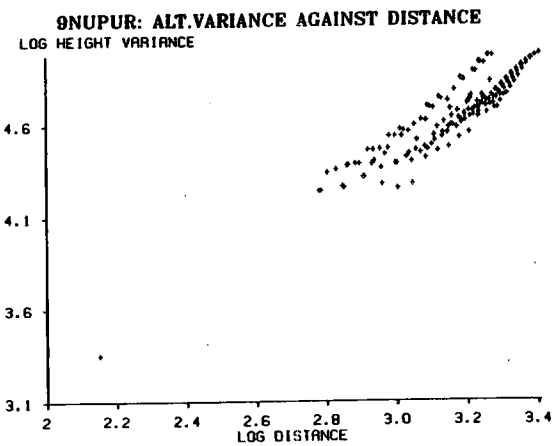
9NUPUR: ALT.VARIANCE AGAINST DISTANCE
LOG HEIGHT VARIANCE
4.6
4.1
3.6
3.1
2
2.2
2.4
2.6
2.8
3.0
3.2
3.4
LOG DISTANCE

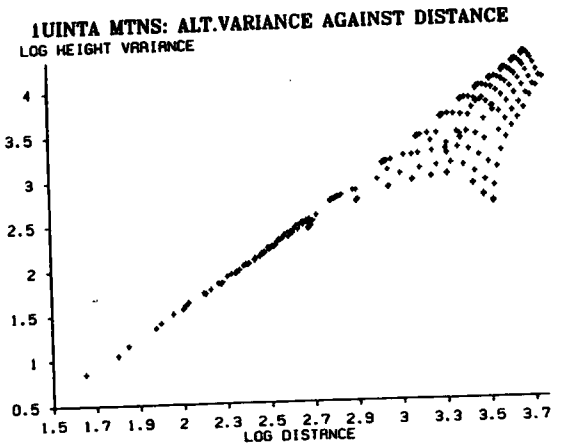
1UINTA MTNS: ALT.VARIANCE AGAINST DISTANCE
LOG HEIGHT VARIANCE
LOG DISTANCE

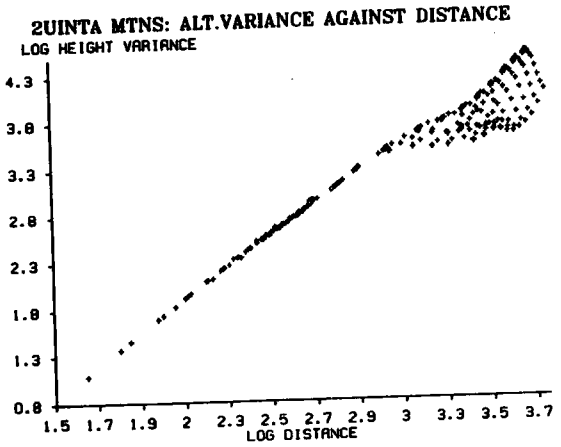
2UINTA MTNS: ALT.VARIANCE AGAINST DISTANCE
LOG HEIGHT VARIANCE
LOG DISTANCE

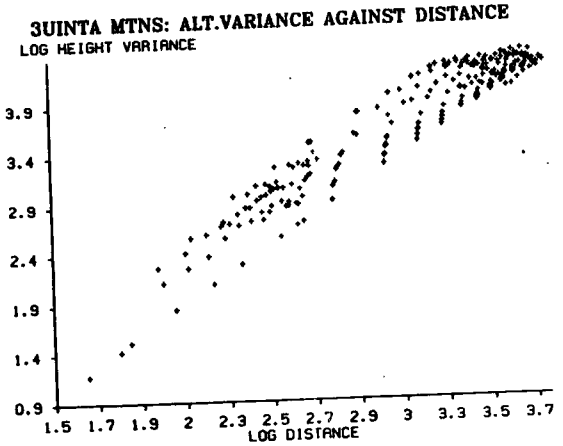
3UINTA MTNS: ALT.VARIANCE AGAINST DISTANCE
LOG HEIGHT VARIANCE
LOG DISTANCE

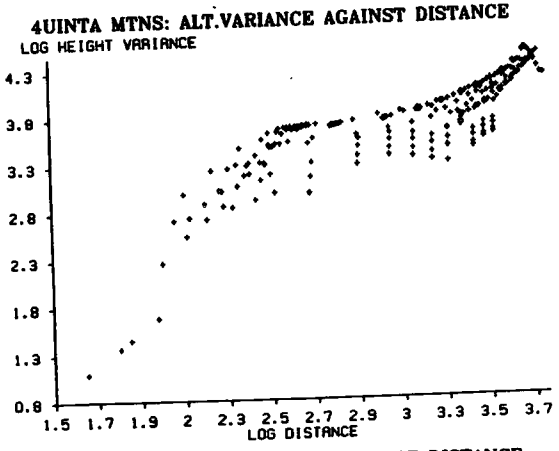
4UINTA MTNS: ALT.VARIANCE AGAINST DISTANCE
LOG HEIGHT VARIANCE
LOG DISTANCE

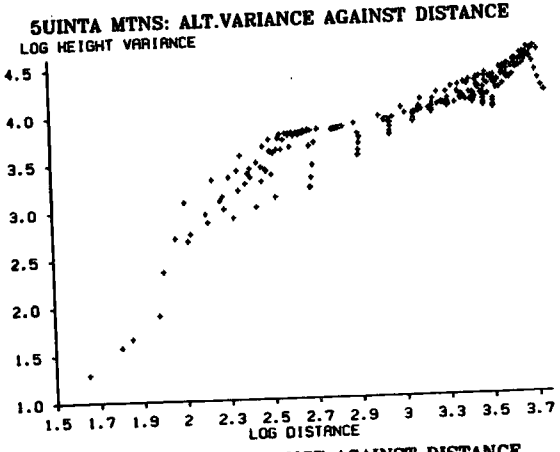
5UINTA MTNS: ALT.VARIANCE AGAINST DISTANCE
LOG HEIGHT VARIANCE
LOG DISTANCE

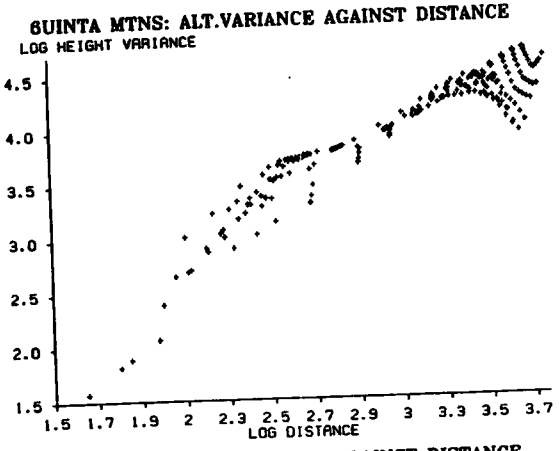
6UINTA MTNS: ALT.VARIANCE AGAINST DISTANCE
LOG HEIGHT VARIANCE
LOG DISTANCE

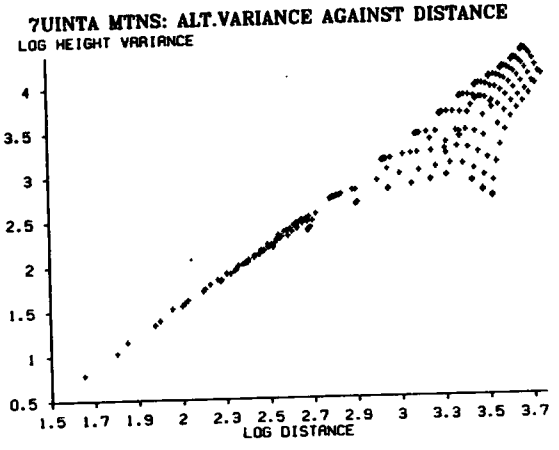
7UINTA MTNS: ALT.VARIANCE AGAINST DISTANCE
LOG HEIGHT VARIANCE
LOG DISTANCE

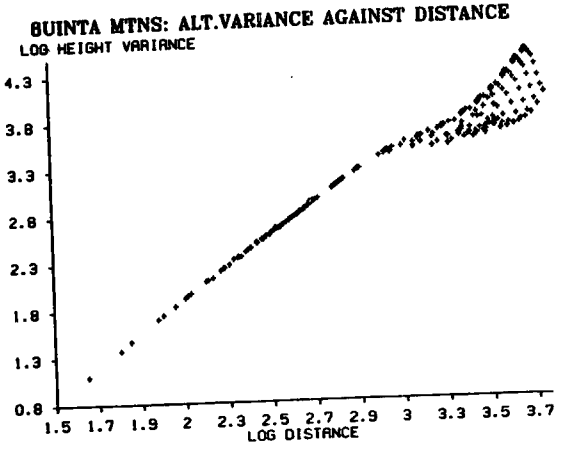
8UINTA MTNS: ALT.VARIANCE AGAINST DISTANCE
LOG HEIGHT VARIANCE
LOG DISTANCE

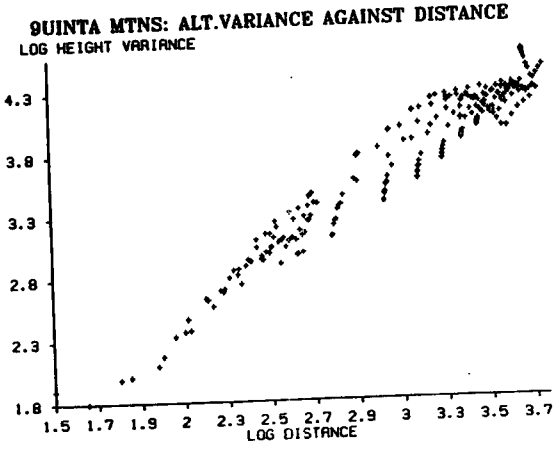
9UINTA MTNS: ALT.VARIANCE AGAINST DISTANCE
LOG HEIGHT VARIANCE
LOG DISTANCE

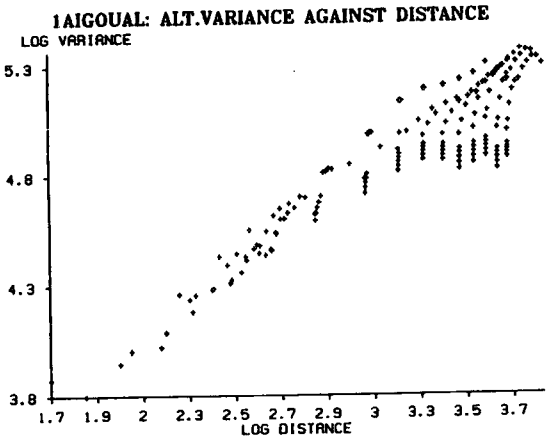
1AIGOUAL: ALT.VARIANCE AGAINST DISTANCE
LOG VARIANCE
5.3
4.8
4.3
3.8
1.7 1.9 2 2.3 2.5 2.7 2.9 3 3.3 3.5 3.7
LOG DISTANCE

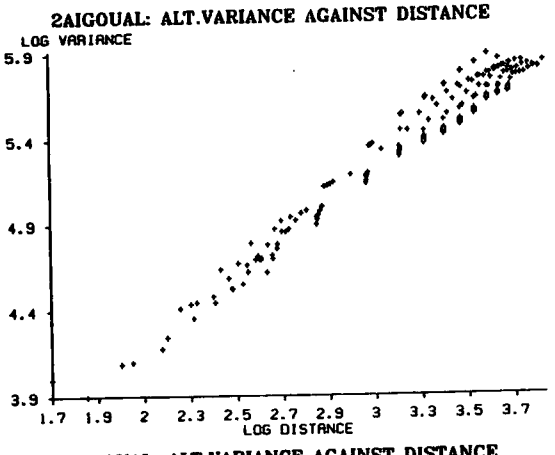
2AIGOUAL: ALT.VARIANCE AGAINST DISTANCE
LOG VARIANCE
5.9
5.4
4.9
4.4
3.9
1.7 1.9 2 2.3 2.5 2.7 2.9 3 3.3 3.5 3.7
LOG DISTANCE

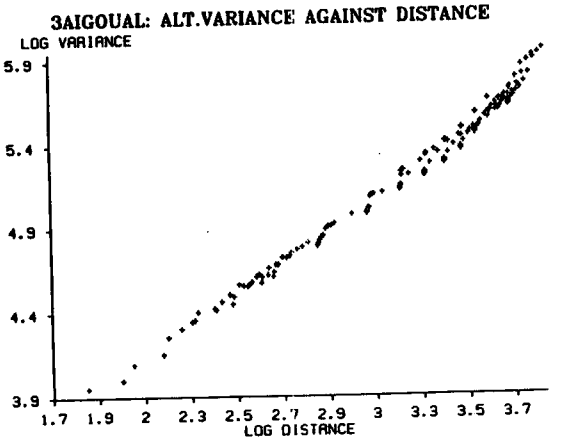
3AIGOUAL: ALT.VARIANCE AGAINST DISTANCE
LOG VARIANCE
5.9
5.4
4.9
4.4
3.9
1.7 1.9 2 2.3 2.5 2.7 2.9 3 3.3 3.5 3.7
LOG DISTANCE

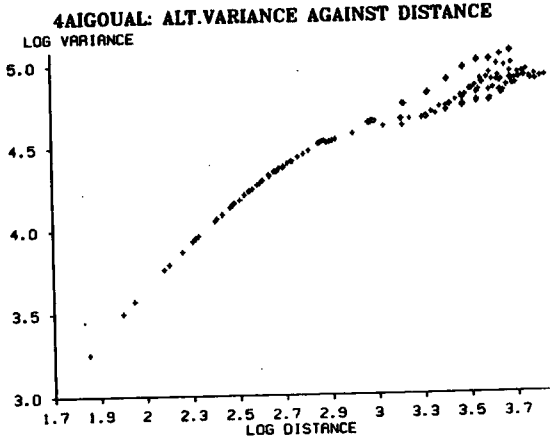
4AIGOUAL: ALT.VARIANCE AGAINST DISTANCE
LOG VARIANCE
5.0
4.5
4.0
3.5
3.0
1.7 1.9 2 2.3 2.5 2.7 2.9 3 3.3 3.5 3.7
LOG DISTANCE

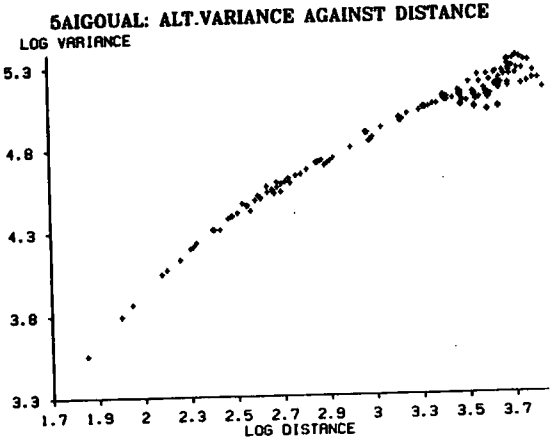
5AIGOUAL: ALT.VARIANCE AGAINST DISTANCE
LOG VARIANCE
5.3
4.8
4.3
3.8
3.3
1.7 1.9 2 2.3 2.5 2.7 2.9 3 3.3 3.5 3.7
LOG DISTANCE

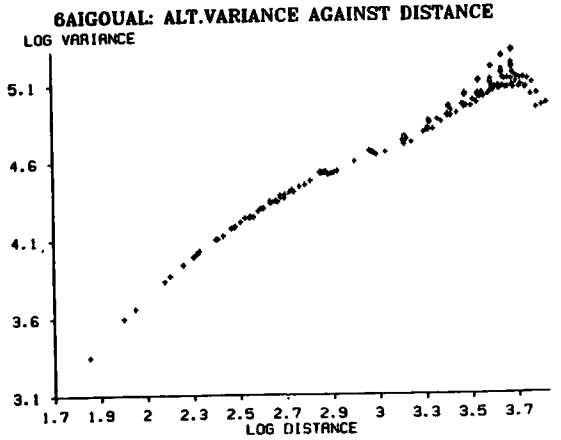
6AIGOUAL: ALT.VARIANCE AGAINST DISTANCE
LOG VARIANCE
5.1
4.6
4.1
3.6
3.1
1.7 1.9 2 2.3 2.5 2.7 2.9 3 3.3 3.5 3.7
LOG DISTANCE

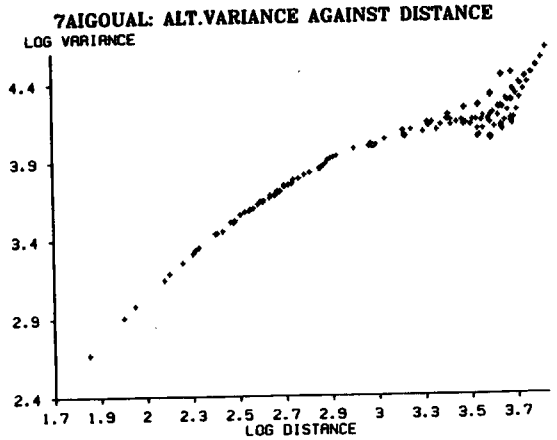
7AIGOUAL: ALT.VARIANCE AGAINST DISTANCE
LOG VARIANCE
4.4
3.9
3.4
2.9
2.4
1.7 1.9 2 2.3 2.5 2.7 2.9 3 3.3 3.5 3.7
LOG DISTANCE

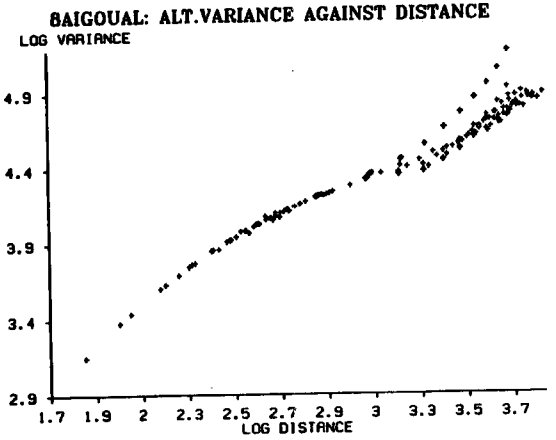
8AIGOUAL: ALT.VARIANCE AGAINST DISTANCE
LOG VARIANCE
4.9
4.4
3.9
3.4
2.9
1.7 1.9 2 2.3 2.5 2.7 2.9 3 3.3 3.5 3.7
LOG DISTANCE

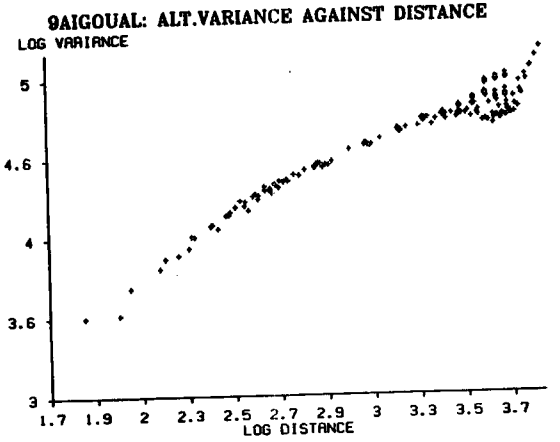
9AIGOUAL: ALT.VARIANCE AGAINST DISTANCE
LOG VARIANCE
5
4.6
4
3.6
3
1.7 1.9 2 2.3 2.5 2.7 2.9 3 3.3 3.5 3.7
LOG DISTANCE

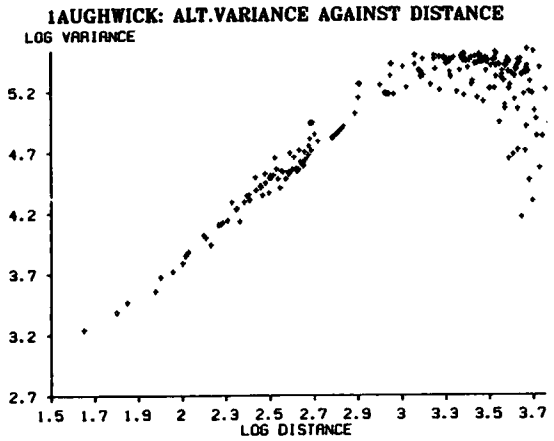
1AUGHWICK: ALT.VARIANCE AGAINST DISTANCE
LOG VARIANCE
5.2
4.7
4.2
3.7
3.2
2.7
1.5 1.7 1.9 2 2.3 2.5 2.7 2.9 3 3.3 3.5 3.7
LOG DISTANCE

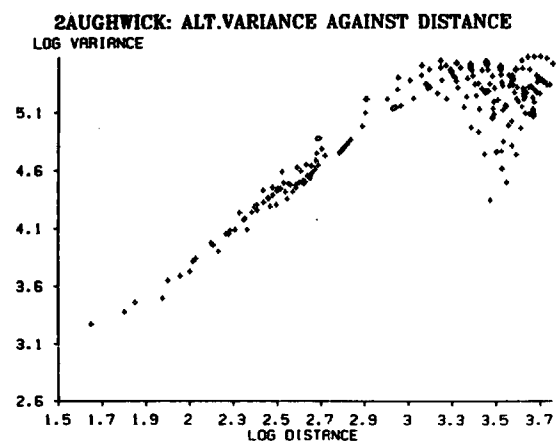
2AUGHWICK: ALT.VARIANCE AGAINST DISTANCE
LOG VARIANCE
5.1
4.6
4.1
3.6
3.1
2.6
1.5 1.7 1.9 2 2.3 2.5 2.7 2.9 3 3.3 3.5 3.7
LOG DISTANCE

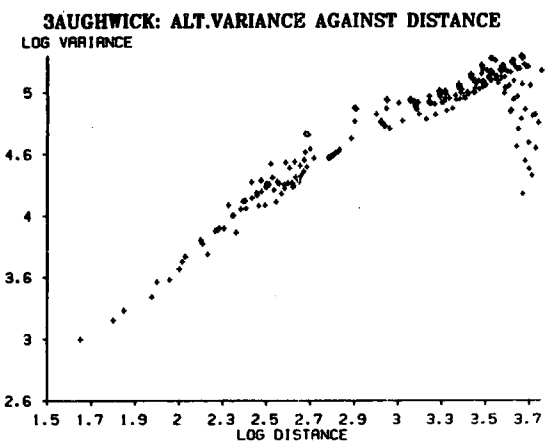
3AUGHWICK: ALT.VARIANCE AGAINST DISTANCE
LOG VARIANCE
5
4.6
4
3.6
3
2.6
1.5 1.7 1.9 2 2.3 2.5 2.7 2.9 3 3.3 3.5 3.7
LOG DISTANCE

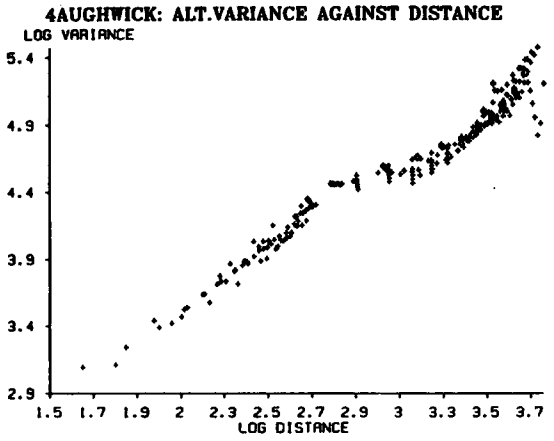
4AUGHWICK: ALT.VARIANCE AGAINST DISTANCE
LOG VARIANCE
5.4
4.9
4.4
3.9
3.4
2.9
1.5 1.7 1.9 2 2.3 2.5 2.7 2.9 3 3.3 3.5 3.7
LOG DISTANCE

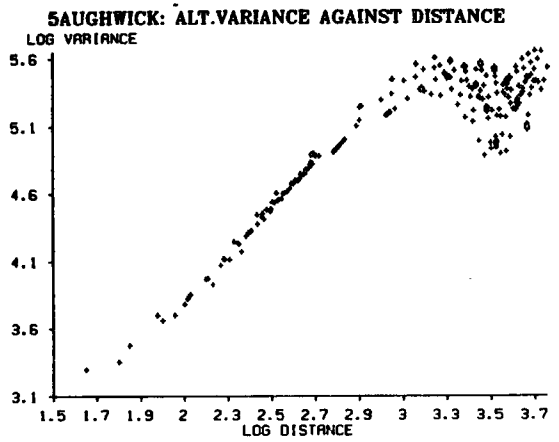
5AUGHWICK: ALT.VARIANCE AGAINST DISTANCE
LOG VARIANCE
5.6
5.1
4.6
4.1
3.6
3.1
1.5 1.7 1.9 2 2.3 2.5 2.7 2.9 3 3.3 3.5 3.7
LOG DISTANCE

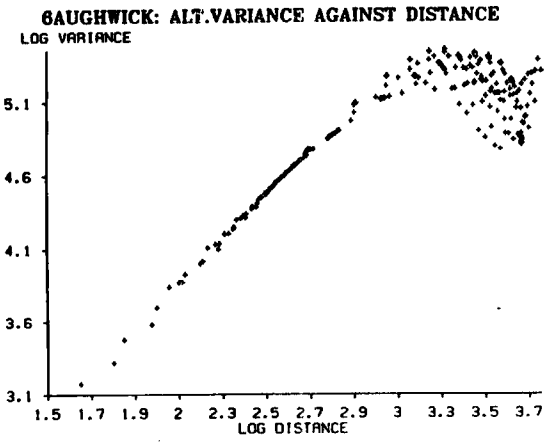
6AUGHWICK: ALT.VARIANCE AGAINST DISTANCE
LOG VARIANCE
5.1
4.6
4.1
3.6
3.1
1.5 1.7 1.9 2 2.3 2.5 2.7 2.9 3 3.3 3.5 3.7
LOG DISTANCE

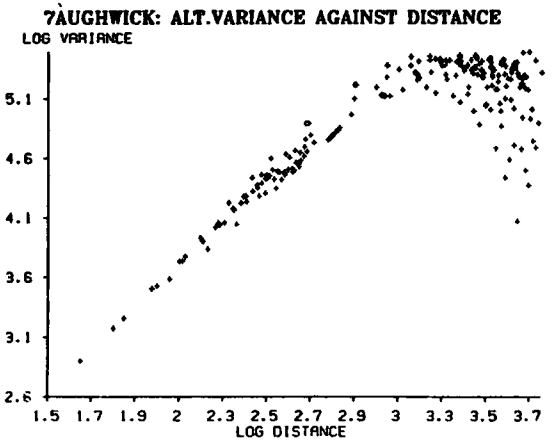
7AUGHWICK: ALT.VARIANCE AGAINST DISTANCE
LOG VARIANCE
5.1
4.6
4.1
3.6
3.1
2.6
1.5 1.7 1.9 2 2.3 2.5 2.7 2.9 3 3.3 3.5 3.7
LOG DISTANCE

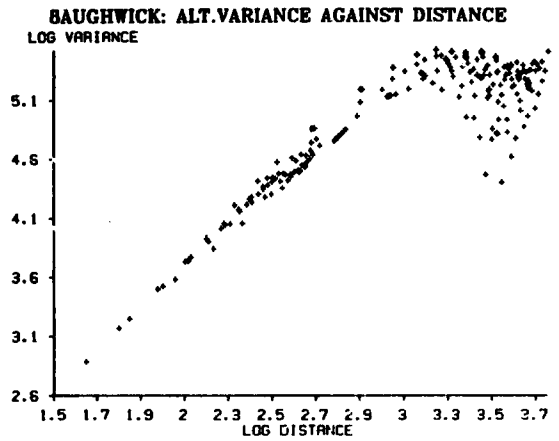
8AUGHWICK: ALT.VARIANCE AGAINST DISTANCE
LOG VARIANCE
5.1
4.6
4.1
3.6
3.1
2.6
1.5 1.7 1.9 2 2.3 2.5 2.7 2.9 3 3.3 3.5 3.7
LOG DISTANCE

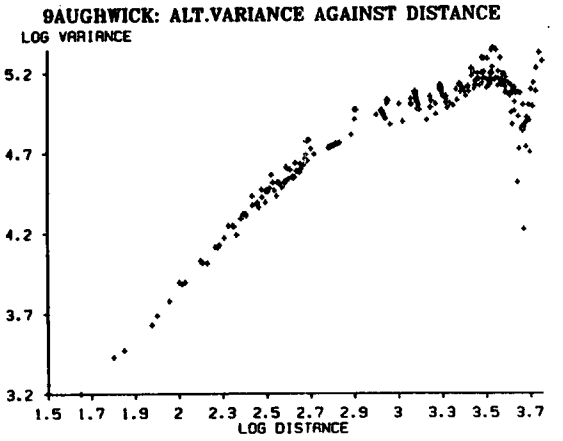
9AUGHWICK: ALT.VARIANCE AGAINST DISTANCE
LOG VARIANCE
5.2
4.7
4.2
3.7
3.2
1.5 1.7 1.9 2 2.3 2.5 2.7 2.9 3 3.3 3.5 3.7
LOG DISTANCE

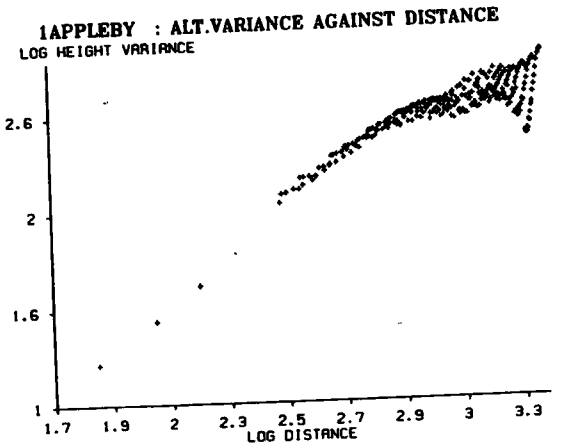
1APPLEBY : ALT.VARIANCE AGAINST DISTANCE
LOG HEIGHT VARIANCE
2.6
2
1.6
1
1.7 1.9 2 2.3 2.5 2.7 2.9 3 3.3
LOG DISTANCE

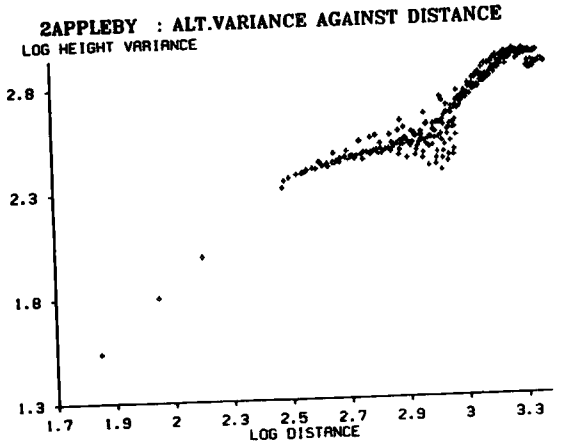
2APPLEBY : ALT.VARIANCE AGAINST DISTANCE
LOG HEIGHT VARIANCE
2.8
2.3
1.8
1.3
1.7 1.9 2 2.3 2.5 2.7 2.9 3 3.3
LOG DISTANCE

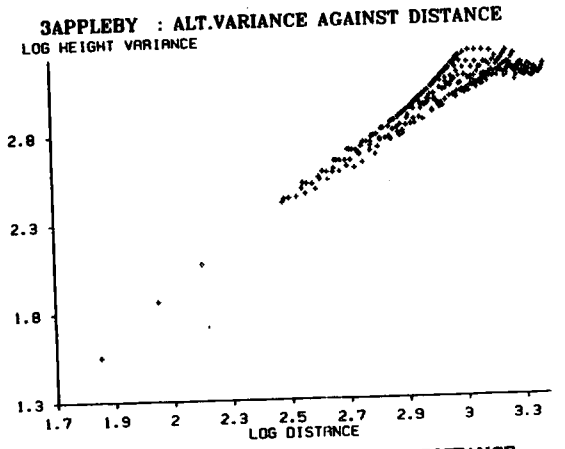
3APPLEBY : ALT.VARIANCE AGAINST DISTANCE
LOG HEIGHT VARIANCE
2.8
2.3
1.8
1.3
1.7 1.9 2 2.3 2.5 2.7 2.9 3 3.3
LOG DISTANCE

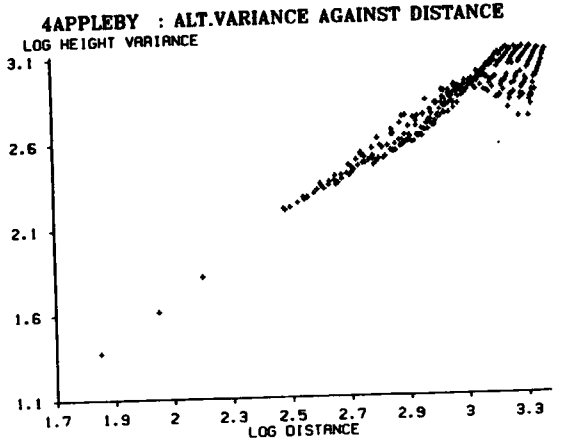
4APPLEBY : ALT.VARIANCE AGAINST DISTANCE
LOG HEIGHT VARIANCE
3.1
2.6
2.1
1.6
1.1
1.7 1.9 2 2.3 2.5 2.7 2.9 3 3.3
LOG DISTANCE

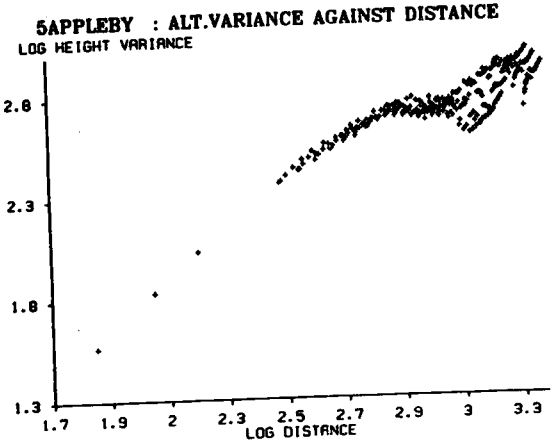
5APPLEBY : ALT.VARIANCE AGAINST DISTANCE
LOG HEIGHT VARIANCE
2.8
2.3
1.8
1.3
1.7 1.9 2 2.3 2.5 2.7 2.9 3 3.3
LOG DISTANCE

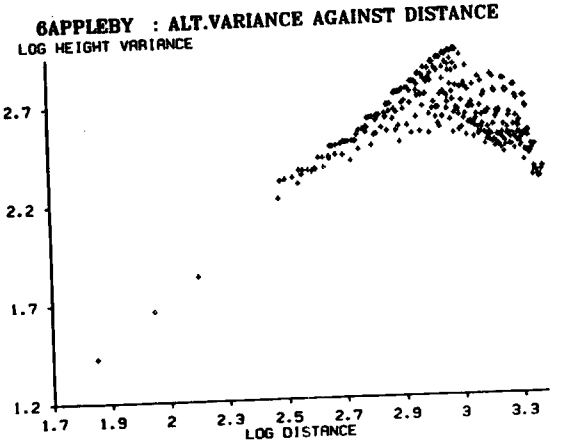
6APPLEBY : ALT.VARIANCE AGAINST DISTANCE
LOG HEIGHT VARIANCE
2.7
2.2
1.7
1.2
1.7 1.9 2 2.3 2.5 2.7 2.9 3 3.3
LOG DISTANCE

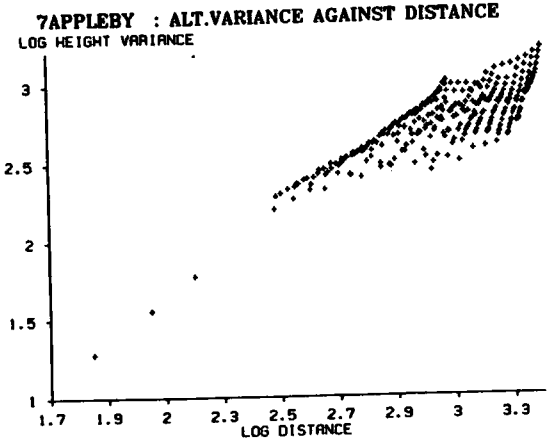
7APPLEBY : ALT.VARIANCE AGAINST DISTANCE
LOG HEIGHT VARIANCE
3
2.5
2
1.5
1
1.7 1.9 2 2.3 2.5 2.7 2.9 3 3.3
LOG DISTANCE

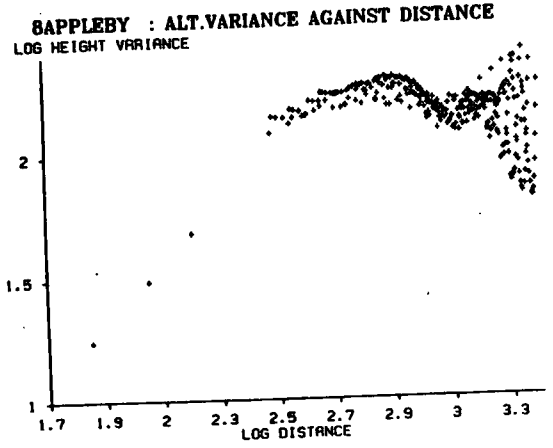
8APPLEBY : ALT.VARIANCE AGAINST DISTANCE
LOG HEIGHT VARIANCE
2
1.5
1
1.7 1.9 2 2.3 2.5 2.7 2.9 3 3.3
LOG DISTANCE

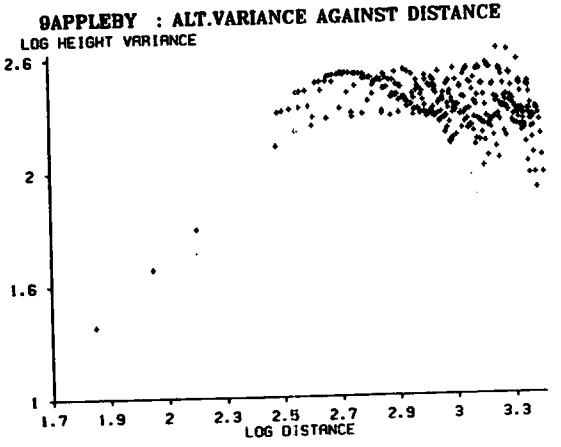
9APPLEBY : ALT.VARIANCE AGAINST DISTANCE
LOG HEIGHT VARIANCE
2.6
2
1.6
1
1.7 1.9 2 2.3 2.5 2.7 2.9 3 3.3
LOG DISTANCE

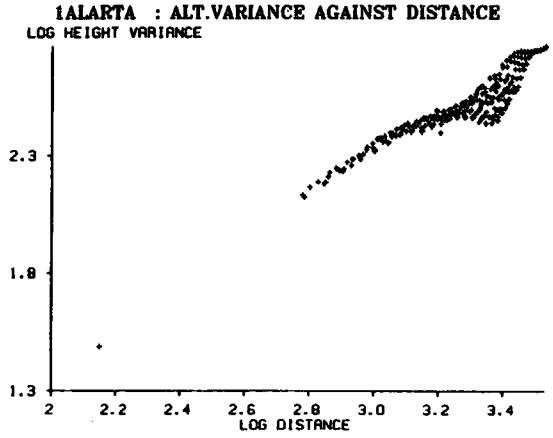
1ALARTA : ALT.VARIANCE AGAINST DISTANCE
LOG HEIGHT VARIANCE
2.3
1.8
1.3
2 2.2 2.4 2.6 2.8 3.0 3.2 3.4
LOG DISTANCE

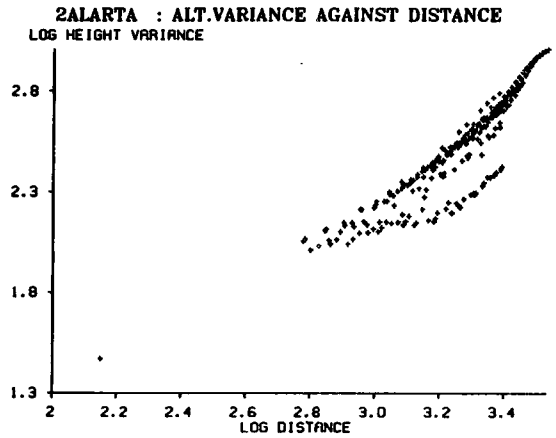
2ALARTA : ALT.VARIANCE AGAINST DISTANCE
LOG HEIGHT VARIANCE
2.8
2.3
1.8
1.3
2 2.2 2.4 2.6 2.8 3.0 3.2 3.4
LOG DISTANCE

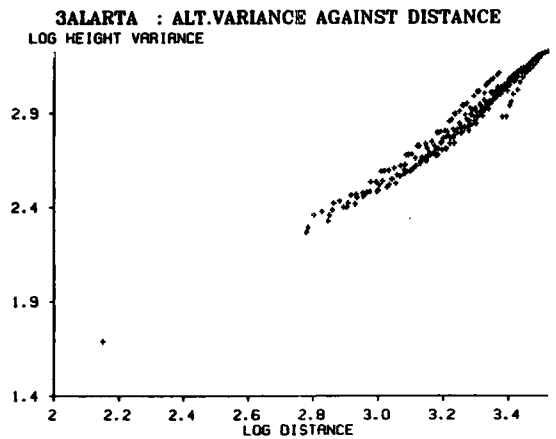
3ALARTA : ALT.VARIANCE AGAINST DISTANCE
LOG HEIGHT VARIANCE
2.9
2.4
1.9
1.4
2 2.2 2.4 2.6 2.8 3.0 3.2 3.4
LOG DISTANCE

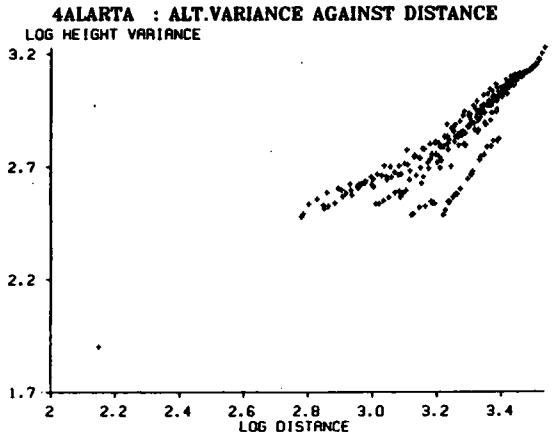
4ALARTA : ALT.VARIANCE AGAINST DISTANCE
LOG HEIGHT VARIANCE
3.2
2.7
2.2
1.7
2 2.2 2.4 2.6 2.8 3.0 3.2 3.4
LOG DISTANCE

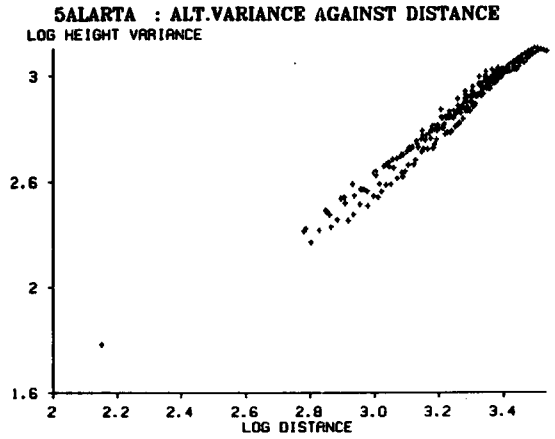
5ALARTA : ALT.VARIANCE AGAINST DISTANCE
LOG HEIGHT VARIANCE
3
2.6
2
1.6
2 2.2 2.4 2.6 2.8 3.0 3.2 3.4
LOG DISTANCE

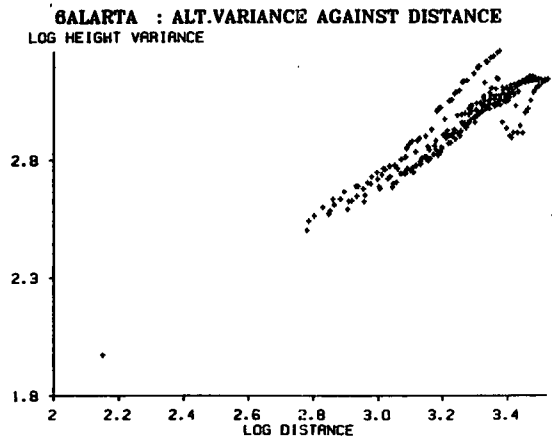
6ALARTA : ALT.VARIANCE AGAINST DISTANCE
LOG HEIGHT VARIANCE
2.8
2.3
1.8
2 2.2 2.4 2.6 2.8 3.0 3.2 3.4
LOG DISTANCE

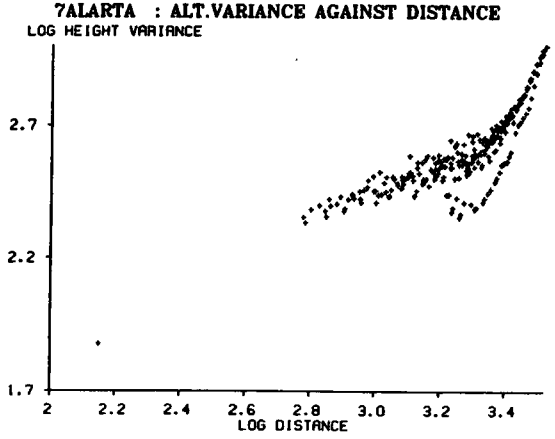
7ALARTA : ALT.VARIANCE AGAINST DISTANCE
LOG HEIGHT VARIANCE
2.7
2.2
1.7
2 2.2 2.4 2.6 2.8 3.0 3.2 3.4
LOG DISTANCE

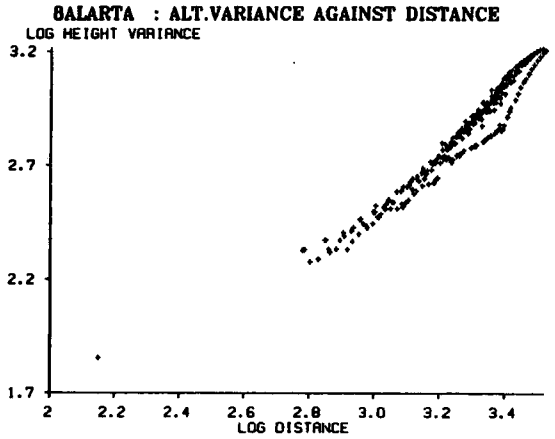
8ALARTA : ALT.VARIANCE AGAINST DISTANCE
LOG HEIGHT VARIANCE
3.2
2.7
2.2
1.7
2 2.2 2.4 2.6 2.8 3.0 3.2 3.4
LOG DISTANCE

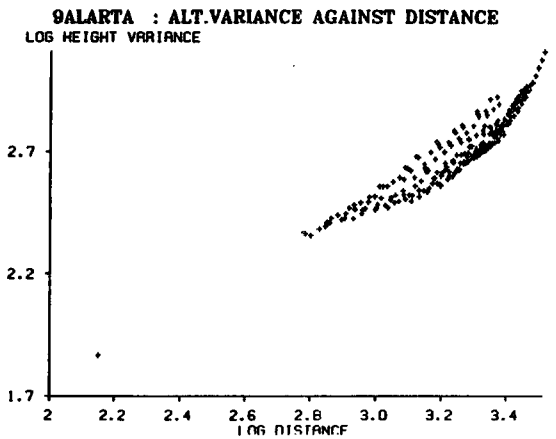
9ALARTA : ALT.VARIANCE AGAINST DISTANCE
LOG HEIGHT VARIANCE
2.7
2.2
1.7
2 2.2 2.4 2.6 2.8 3.0 3.2 3.4
LOG DISTANCE

Bibliography

Ahnert, F. (1984) Local Relief and the Height Limits of Mountain Ranges. *American Journal of Science*, v. 289, p.1035-1055.

Ayeni, O. O. (1982) Optimum sampling for Digital Terrain Models: A Trend Towards Automation . *Photogrammetric Engineering and Remote Sensing* v.48, n.11, p.1687-1694.

Barnsley, M. F. (1988) *Fractals Everywhere* . Academic Press

Bell, S. A. (1983) *Attributes of Drainage Basin Topography: An Evaluation of Profile and Altitude Matrix Approaches and Their Hydrological Relevance.* Unpublished PhD thesis, University of Durham.

Bennett, M. (1990) *The Cwms of Snowdonia: a morphometric analysis.* Research paper number 2, Dept. of Geography, Queen Mary and Westfield College, London.

Berry, M. V. and **Hannay, J. H.** (1978) Topography of Random Surfaces. *Nature* 273, p.573.

Breard, M. (1989) Pers. Comm.

Brown, S. R., Scholz, C. H. (1985) Broad Band Width Study of the Topography of Natural Rock Surfaces. *J.Geophysical Re*search. v.90, n.B14, p.12,575 - 12,582.

Bull, W. B. (1975) Allometric change in landforms. *Geol. Soc. Amer. Bull.*, v.86, p. 1489-1498.

Bull, W. B. (1977) Allometric change in landforms: reply. *Geol. Soc. Amer. Bull.*, v. 88, p.1200-1202.

Burrough, P. A. (1981) Fractal Dimension of Landscapes and other environmental data *Nature*, 294: 240-242.

Burrough, P. A. (1983) Multiscale sources of spatial variation in soil. *J. Soil Sci.* 34, p. 577-620.

Burrough, P. A. (1984) The Application of Fractal ideas to Geophysical Phenomenon *Bull. Inst. of Mathematics and its Applications* v.20, p.36-42.

Burrough, P. A. (1986) *Principles of Geographical Information Systems for Land Resources Assesment (Monographs in soil and resource survey).* Oxford Univ. Press.

Chorley, R. J. (1962) Geomorphology and general systems theory. *U.S.G.S. Prof. Paper* 500B, 10pp.

Chorley, R. J. (1967) Models in Geomorphology, In Chorley, R. J. and Haggett, P. (Eds) (1967) *Models in Geography*, Methuen and Co. Ltd.London.

Church, M. and **Mark, D. M.** (1980) On Size and Scale in Geomorphology. *Prog. Phys. Geog.* v. 4, p 342-390.

Clarke, K. C. (1986) Computation of the Fractal Dimension of Topographic Surfaces Using the Triangular Prism Surface Area Method. *Computers and Geosiences* v.12, n.5, p.713-722.

Clark, N. N. (1986) Three techniques for implementing digital Fractal Analysis of Particle Shape. *Powder Technology*, 46, p.45-52.

Cox, N. J. (1977) Allometric change in landforms: discussion. *Geol. Soc. Amer. Bull.*, v.88, p. 1199-1200.

Culling, W. E. H. (1963) Soil creep and the development of hillslopes. *Jour. Geol.* v. 71, p. 127-162.

Culling, W. E. H. (1986) On Hurst Phenomena in the Landscape. *Trans. Japanese Geomorphological Union*, v.7, n.4, p.221-243.

Culling, W. E. H., Datko, M. (1986) The Fractal Geometry of the Soil-Covered Landscape. *Earth Surface Processes and Landforms*, v.12, p.369-385.

Davis, J. C. (1986) *Statistics and Data Analysis in Geology*. John Wiley & Co.

Depraetere, C. (1989) *LAMONT Logiciel d' Application des Modeles Numeriques de Terrain: Manuel d'Utilisation*. Laboratoire d'Hydrologie, ORSTOM, Montpellier.

Dikau, R. (1989) The application of a digital relief model to landform analysis in geomorphology. In Raper, J. (1989) *Three dimensional applications in geographic information systems*. Taylor & Francis.

Douglas, D. H. (1986) Experiments to locate ridges and channels to create a new type of digital elevation model. *Cartographica* v.23, n.4, p.29-61

Doyle (1978) *Proc. DTM Symposium*. American Society of Photogrammetry. American Congress on Survey and Mapping, St. Louis, Missouri.

Evans I. S. (1985a) A new approach to drumlin morphometry. p. 119-130. In Menzies, J. and Rose, J. (1987) *Drumlin Symposium*. Proc. of the drumlin syposium, First International Conference on Geomorphology. Manchester, 1985. A.A. Balkema.

Evans, I. S. (1972) General geomorphometry, derivation of altitude and descriptive statistics. In Chorley, R. J. (Ed) *Spatial Analysis in Geomorphology*. Methuen.London

Evans, I. S. (1979) *An integrated System of Terrain Analysis and Slope Mapping* Department of Geography, University of Durham.

Evans, I. S. (1980) An Integrated System of Terrain Analysis and Slope Mapping. *Z.fur Geomorph. Suppl. Bd.* p.274-295.

Evans, I. S. (1981) General Geomorphometry. In Goudie, A et al (eds) *Geomorphological Techniques*, p.31-37. George Allen and Unwin.London

Evans, I. S. (1985) *The Morphometry of Specific Landforms* . Paper presented to 1st International Geomorph. Conference, Manchester, September.

Evans, I. S. (1990) Pers. Comm.

Evans, I.S. and Cox, N. J. (1974) Geomorphology and the operational definition of cirques. *Area*, 6, p.150-153.

Falconer, K. J. (1985) *The Geometry of Fractal Sets*. Cambridge University Press. London.

Feder, J. (1988) *Fractals* . Plenum.

Fournier, A., Fussell, P., Carpenter, L. (1982) Computer Rendering of Stochastic Models *CACM* 25.6:371-384.

Frederiksen, P, Jacobi, O., Kubik, K. (1985) A Review of current trends in terrain modelling. *ITC Journal* , 1985-2, p.101-106.

Good, I. J. (1972) Correlation for Power Functions. *Biometrics*, v. 28, p.1127-1129.

Goodchild, M. F. (1980) Fractals and the Accuracy of Geographical Measures. *J. Int. Assoc. Mathematical Geology*. 12-2: 85-98.

Goodchild, M. F. (1982) The Fractional Brownian Process as a Terrain Simulation Model. *Proceedings of 13th Annual Pittsburg Conference on Modelling and Simulation*. v 13, p.1133-1137.

Grassie, D. N. D. (1982) Contouring by computer: some observations. p. 93-116. In Rhind, D. and Adams, T. (Eds.) *British Cratographic Society Special Publication*. n. 2.

Hack, J. T. (1957) Studies of longitudinal stream profiles in Virginnia and Maryland. *U.S.G.S. Prof. Paper*. 294-B.

Hakanson, L. (1978) The Length of Closed Geomorphic Lines. *Math. Geol.* v. 10, n.2, p. 141-168.

Hentschel, H. J. E. and Procaccia, I. (1984) Relative diffusion in turbulent media: the fractal dimension of clouds. *Phy. Rev.A*, v. 29, p. 1461-1470.

Hollingworth, S. E.(1931) Glaciation of western Edenside and adjoining areas and drumlins of Edenside and the Solway basin. *Q. Jour. Geol. Soc . Lond.*, 90, p.281-359.

Hurst, H. E. (1951) Long term storage capacity of reservoirs. *Trans. Amer. Soc. Civ. Eng.*, v.116, p.770-800.

Hurst, H. E. (1956) Methods of using long term storage in reservoirs. *Proc. Inst. Civ. Eng.*, 5, p. 519-590.

Jensen, S. K. (1985) Automated derivation of hydrologic basin characteristics from digital elevation model data. *AutoCarto 7*. p.301-310.

Jenson, S.K. and Domingue, J. O. (1988) Extracting topographic structure from digital elevation data for geographic information system analysis. *Photogrammetric Engineering and Remote Sensing*, v.54, n.11, p.1593-1600.

Kaye, B. H. (1984) Multifractal Description of a Rugged Fineparticle Profile. *Particle Characterization*. v.1, p.14-21.

Kennedy, S. K., Wei-sinng Lin (1986) FRACT - a FORTRAN subroutine to calculate the variables necessary to determine the fractal dimension of closed forms *Comps. & Geosciences*. v. 12, n.5, p.705-712.

Kirkby, M. J. (1986) Modelling some influences of soil erosion, landslides and valley gradient on drainage density. *Working Paper 474, School of Geography, University of Leeds.*

Klemes, V. (1974) The Hurst Phenomenon: A Puzzle *Water Resources Research*. v. 10, n.4, p. 675-688.

Lam, N. S. N. (1983) Spatial Interpolation Methods: A Review. *The American Cartographer* v. 10, n. 2, p. 129-149.

Leopold, L. B. and Langbein, W. B. (1962) The concept of entropy in landscape evolution. *U.S.G.S. Prof. Paper* 500-A, 20pp.

Lovejoy, S. (1982) Area perimeter relation for rain and cloud areas. *Science*, 216, p. 185-187.

Lovejoy, S. and Mandelbrot, B. B. (1985) Fractal properties of rain, and a fractal model. *Tullus*, 37A, p.209-232

Lovejoy, S. and Schertzer, D. (1985) General scale invariance in the atmosphere and fractal models of rain. *Water Resources Research*. v.2, n.8, p. 1233-50.

Lovejoy, S. and Schertzer, D. (1986) Scale invariance in Climatological temperatures and the local spectral plateau. *Annales Geophysique*. Ser. B, v.9, n.4, p. 401-410.

MacEachren, A. M., Davidson, J. V. (1987) Sampling and Isometric Mapping of Continuous Geographic Surfaces. *The American Cartographer*, v. 14, n.4, p.299-320.

Mandelbrot, B. B. (1967) How long is the coast of Britain? Statistical self-similarity and Fractional dimension. *Science*, 155, p. 636-638.

Mandelbrot, B. B. (1975) Stochastic models for the Earth's relief, the shape and the fractal dimension of the coastlines, and the number-area rule for islands. *P. Nat. Acad. Sc. Am.*, v.72, n.10, p. 3825-3828.

Mandelbrot, B. B. (1977) *Fractals, Form, Chance and Dimensions*. W. H. Freeman and Co. London.

Mandelbrot, B. B. (1982) *The Fractal Geometry of Nature*. W H Freeman. London.

Mandelbrot, B. B. (1985) Self-affine fractals and fractal dimension. *Phy. Scripta*, v.32, p.257-260.

Mandelbrot, B. B. (1986) Self-affine fractal sets. p. 3-28. In Pietronero, L. and Tosatti, E. (Eds) *Fractals in Physics*. North-Holland, Amsterdam.

Mandelbrot, B. B. (1989) Fractal geometry: what is it, and what does it do? *Proc. Roy. Soc. London*. A. v.423, n.1864, p. 3-16.

Mandelbrot, B. B. and Van Ness, J. W. (1968) Fractional Brownian motions, fractional noises and applications. *S.I.A.M. Rev.*, v.10, p.422-437.

Mandelbrot, B. B. and Wallis, J. R. (1968) Noah, Joseph and operational hydrology. *Water Resources Research*, v.4, p.909-918.

Mandelbrot, B. B. and Wallis, J. R. (1969a-c) Computer experiments with fractional Gaussian noises; Parts I, II, and III. *Water Resources Research*, v.5, p. 228-267.

Mandelbrot, B. B. and Wallis, J. R. (1969d) Some long run properties of geophysical records. *Water Resources Research*, 5, p.321-340.

Mark, D. M. (1975) Geomorphometic parameters: A review and evaluation *Geografiska Annaler*, series A, v.3, p.165-177.

Mark, D. M. (1979) Topology of Ridge patterns: Randomness and Constraints. *Geol. Soc. Am. Bull.* v.90, n.1 p.164-172.

Mark, D. M. (1980) On scale of investigation in Geomorphology. *Canadian Geographer*, v. 24, p. 81-82.

Mark, D. M., Aronson, P. B. (1984) Scale-dependent factal dimensions of topographic surfaces: an empirical investigation with applications in Geomorphology and Computer Mapping. *Math. Geol.*, v.16, n. 7, p 671-683.

Mark, D. M., Church, M. (1977) On the Misuse of Regression in Earth Science. *Math. Geol.* v.9, n.1, p.63-75.

McCullagh, M. J. and Sampson, R. C. (1972) User desires and graphics capability in the academic environment. *The Cartographic Journal*. 9, p.109-122.

Menzies, J. (1979) A Review of the literature on the formation and location of drumlins *Earth Science Review*. 14:315-359.

O'Neill, M. P., Mark, D. M. (1987) On the frequency distribution of land slope. *Earth Surface Processes and Landforms*. v.12, p. 127-136.

Peitgen, H. and Saupe, D. (1988) *The Science of Fractal Images* . Springer-Verlag.

Potter, K. W. (1976) Evidence for Nonstationarity as a Physical Explanation of the Hurst Phenomenon. *Water Resource Research* ,v. 12, n.5, p. 1047-1052.

Potter, K. W. (1979) Annual Precipitation in the North East United States: Long Memory, Short Memory, or No Memory? *Water Resource Research* , p. 340-346.

Riazanoff, S.; Cervelle, B. and Chorowicz, J. (1988) Ridge and valley line extraction from digital terrain models. *Int . J. Remote Sensing,* v.9, n.6, p.1175-1183.

Richardson, L. F. (1961) The problem of contiguity. *General Systems Yearbook.* v.6, p.139-187.

Rose, J., Letzer, J. M. (1977) Superimposed Drumlins. *Journal of Glaciology*, v.18, n.80, p.471-480.

Roy, A. G., Gravel, G., Gauthier, C. (1987) Measuring the Dimension of surfaces: a review and appraisal of different methods. *Auto Carto 8*, p.68-77.

Sampson, R.J. (1978) *Surface II graphics system.* Kansas Geological Survey. Lawrence.

Sauchyn, D. J., Gardner, J. S. (1983) Morphometry of Open Rock Basins, Kananaskis area, Canadian Rocky Mountains. *Can. J. Earth Sc.*, v.20, 409-419.

Sayles, R. S. and Thomas, T. K. (1978) Surface Topography as a Nonstationery Random Process. *Nature,* 271, p.431-434.

Schwarz, H., Exner, H. E. (1980) The Implementation of the Concept of Fractal Dimensions on a semi-automatic image analyser. *Powder Technology*, v.27, p.207-213.

Shelberg, M. C., Lam, N., Moellering, H. (1983) Measuring the Fractal Dimensions of Surfaces. *Auto Carto VI v.2.* p. 319-328.

Smith, K. G. (1950) Standards of grading texture of erosional topography. *American Journal of Science*, v.248, p.655-668.

Strahler, A. N. (1950) Equilibrium theory of erosional slopes approached by frequency distribution analysis. *American Journal of Science.* , 248, p.673-696 and 800-814.

Tarboton, D. G., Bras, R. L., Rodrigues-Iturbe, I. (1988) The Fractal Nature of River Networks *Water Resources Research.* v.24, n.8, p.1317-1322.

Thornes, J. and Ferguson, R. I. (1981) Geomorphology, p.284-293. In Wrigley, N. and Bennett, R.J. (1981). *Quantitative Geography* Rutledge and Kegan Paul Ltd.

Walden, A.R. (1972) *Quantitative comparison of automatic contouring algorithms.* K.O.X. Project, Geological Research Section, Kansas Geological Survey.

Whiteman, C. A. (1981) Drumlins Around Appleby-in-Westmorland, Cumbria in Boardman, J. (ed) *Quaternary Research Association Field Guide to Eastern Cumbria*, published for Eastern Cumbria Field meeting 15-18 May 1981.

Wood, W. F. and Snell, J. B. (1960) *A Quantitative System for Classifying Landforms,* U S Department of Army, Natick, Massachusetts, Technical Report EP-124, 20.

Woronow, A. (1981) Morphometric Consistency with the Hausdorff Besicovich Dimensions. *Math.Geol.* v. 13, n.3, p.201-216.

Yoeli, P. (1986) Computer Executed Production of a Regular Grid of Height Points from Digital Contours. *American Cartographer* v. 13, n.3, p.219-229.

Young, M. (1978) *Terrain analysis: program documentation.* Durham Geomorphometry Report, Durham Univ.,Dept. of Geography.

Zhang, M.C.; Campbell, J.B. and Haralick, R.M. (1990) Automatic delineation of drainage basins within digital elevation data using the topographic primal sketch. *Math.Geol.*, v.22, n.2, p.189-209.